IAEA-TECDOC-1157

LMFR core thermohydraulics: Status and prospects

INTERNATIONAL ATOMIC ENERGY AGENCY

IAEA

June 2000

The originating Section of this publication in the IAEA was:

Nuclear Power Technological Development Section
International Atomic Energy Agency
Wagramer Strasse 5
P.O. Box 100
A-1400 Vienna, Austria

LMFR CORE THERMOHYDRAULICS: STATUS AND PROSPECTS
IAEA, VIENNA, 2000
IAEA-TECDOC-1157
ISSN 1011–4289

Printed by the IAEA in Austria
June 2000

FOREWORD

One of the fundamental steps for a successful reactor core thermohydraulic design is the capability to predict, reliably and accurately, the temperature distribution in the core assemblies. A detailed knowledge of the assembly and fuel pin thermohydraulic behaviour in the steady state and transient conditions is an indispensable prerequisite to safe and stable operation of the reactor. Considerable experimental and theoretical studies on various aspects of LMFR core thermohydraulics are necessary to acquire such knowledge.

During the last decade, there have been substantial advances in fast reactor core thermohydraulic design and operation in several countries with fast reactor programmes (notably in France, the Russian Federation, Japan, the United Kingdom, Germany and the United States of America). Chief among these has been the demonstration of reliable operation of reactor cores at a high burnup.

During the last years, some additional countries such as China, India and the Republic of Korea have launched new fast reactor programmes. International exchange of information and experience on LMFR development including core thermohydraulic design is becoming of increasing importance to these countries. It is with this focus that the IAEA convened the Technical Committee on "Methods and Codes for Calculations of Thermohydraulic Parameters for Fuel, Absorber Pins and Assemblies of LMFR's with Traditional and Burner Cores".

This meeting, which included participants from seven countries, brought together a group of international experts to review and discuss the thermohydraulic advances and design approaches providing a reliable, safe and robust reactor core, as well as to exchange the experience accumulated in different countries of using the codes for thermohydraulic calculations and to discuss the issues requiring further research and development. A total of thirty technical papers were presented by the meeting participants.

The IAEA wishes to thank all the participants of the technical committee meeting for their valuable contributions, especially A. Sorokin. The IAEA officer responsible for this publication was A. Rineiskii of the Division of Nuclear Power.

EDITORIAL NOTE

This publication has been prepared from the original material as submitted by the authors. The views expressed do not necessarily reflect those of the IAEA, the governments of the nominating Member States or the nominating organizations.

The use of particular designations of countries or territories does not imply any judgement by the publisher, the IAEA, as to the legal status of such countries or territories, of their authorities and institutions or of the delimitation of their boundaries.

The mention of names of specific companies or products (whether or not indicated as registered) does not imply any intention to infringe proprietary rights, nor should it be construed as an endorsement or recommendation on the part of the IAEA.

The authors are responsible for having obtained the necessary permission for the IAEA to reproduce, translate or use material from sources already protected by copyrights.

CONTENTS

SUMMARY

1. INTRODUCTION

The Technical Committee Meeting (TCM) on "Methods and Codes for Calculations of Thermohydraulic Parameters for Fuel, Absorber Pins and Assemblies of LMFR's with Traditional and Burner Cores" was held in Obninsk, Russian Federation from 27-31 July, 1998. This meeting was convened by the International Atomic Energy Agency (IAEA) and was hosted by the Federal Scientific Center, Institute of Physics and Power Engineering (IPPE). This meeting was organized as a forum for experts of Member States with fast reactor programmes to collectively review the present status and international progress made in LMFR's core thermohydraulics.In addition, to exchange scientific and technical information, accumulated in different countries using their codes and methods of thermohydraulic calculation, to indicate the procedures of verification of the codes available for the calculation of reactor core thermal hydraulics under steady state and transient conditions and to discuss the issues requiring further research and development.

Attendance at this TCM included twenty seven participants and fifteen observers from seven countries (China, France, India, Japan, the Republic of Korea, the Russian Federation and the United Kingdom). Thirty papers were presented by the participants on a myriad of fast reactor core thermohydraulics including thermal-hydraulic subchannel analysis, thermal-hydraulic design of LMFR core, status of the validation of codes, analytical and experimental studies on local flow blockages in subassemblies, natural convection analysis and verification for LMFR assemblies, pre-boiling and boiling transients. Each presentation was followed by general discussion and the TCM concluded with a closing session on the evaluation of future code and method development requirements and exploration of areas for LMFR core thermohydraulics.

2. STATUS OF LMFR's CORE THERMOHYDRAULICS ACTIVITIES

The subchannel (S/C) approach was developed from studies which were performed in France during the 70's and 80's. The design code CADET represents the French synthesis of this period. The aim of CADET code is to determine the Maximum Clad Temperature (MCT) thus the coolant fluid temperature for nominal and slightly deformed geometry, under forced and mixed convection (no natural convection and reversal flow) for turbulent flows. The coolant fluid temperature is calculated with the help of a thermal balance for each S/C. This equation takes into account the power distribution (axial and radial), the boundary conditions and the effect of the helical wire wrap spacer. This last effect gives transversal flows and transverse thermal couplings. These deviated flows are evaluated by correlations based on geometrical and experimental arguments. This modelling was qualified on water and sodium experiments in the framework of SuperPhenix (SPX) developments. CADET is used to design all French S/A's in reactor conditions.

A new R/D approach has just started: the 3D numerical simulation. The pins (clads, fuel pellets), the helical wire spacers and the S/Cs are represented with a refined mesh (structured meshes). Navier-Stokes equations are solved in the fluid domain, pins and wires.At present this approach is limited to a 37 pin bundle (700 Mbytes CPU size). In a first stage, these computations will be used for phenomenological thermal-hydraulic studies of new S/A concepts which are compared to those which are well known, the standard SPX S/A. It

will determine if new phenomena must be qualified and introduced into thedesign code CADET.

As far as severe accident analysis is concerned one of the tools used in CEA is the SIMMER-III (S-III) code. S-III is dedicated to the CDA analysis of LMRs. It has been accessed in the last 4 years by CEA within an international joint program with FZK and PNC. This programme includes two phases: phase 1 for individual code modelling and phase 2 for integral test calculations. CEA contributed to phase 1, with the qualification of the two-phase flow models based on air-water and steam-water experiments. CEA experience and data related to fuel freezing problems was also applied to the assessment of the freezing modelling.Following the milestone reached in 1996 for the phase 1 assessment, CEA continued the studies. Firstly, they were dedicated to the shortcomings identified during the phase 1, such as the turbulence model implementation for boiling pools, and 1D two-phase flows. Secondly, more integral experiments were calculated for phase 2, related to the following key phenomena of CDAs: expansion phase, fuel melting and propagation, fuel-coolant interactions, boiling pools,and core compaction coupled with neutronics.

A 3-D computer code development for studying the thermo-hydraulic behaviour of fuel SA is under progress in India. A porous body formulation has been adopted in which rod bundles are represented by defining volume porosity, surface permeability, distributed resistance and heat source. A cell centered collocated finite volume method is formulated for non-orthogonal meshes. Equations are written in Cartesian co-ordinates and are discretised in physical plane. First order upwind and Quick scheme as a deferred correction to the first order upwind are used for the treatment of convective fluxes, while second order central differencing is employed for diffusive fluxes. In order to avoid decoupling between pressure and velocity a special interpolation technique is used when computing the mass fluxes at cell faces. The pressure correction equation is obtained by the SIMPLE algorithm. In order to accelerate the convergence rate, the preconditioned conjugate gradient square method is used in the solution of the algebraic equations. At present 2-D version of the code has been validated against benchmark problems and experimental results for laminar flows and natural convection studies. It, also, has been applied to complex geometries like flow over a single cylinder, across banks of staggered cylinders,an eccentric cylinder placed in a cavityand natural convection studies in a porous medium. Once developed, the code will be used to define MAD in addition to investigate thermo-hydraulic behaviour of fuel SA with non-nominal geometry.

For predicting the thermo-hydraulic behaviour of totally blocked SA at the inlet, another computer code is under development. This code takes into account the presence of neighboring SA receiving full flow by the way of prescribing suitable convective boundary-conditions. The code is based on porous medium approach. This finite volume code is formulated for orthogonal meshes. Staggered grid arrangement is employed to avoid decoupling between pressure and velocity. SIMPLE algorithm is used for obtaining pressure correction equation. The code will be validated against the experimental results.

The following hydraulic experiments are under progress to validate the design and theoretical predictions

- Pressure drop and cavitation characteristics of bare SA;
- Pressure drop and cavitation characteristics of labyrinths and orifices;

- Pressure drop characteristics of SA in each zone;
- Pressure drop characteristics and Lifting force on CSR; and
- Lifting forces on fuel and blanket SA.

Water temperature is selected as 70 °C to reduce the flow rate requirement for maintaining Reynolds similarity. Temperature is maintained constant using the secondary loop consisting of heat exchanger and cooling tower. Since the flow rate through various types of SA differ widely, the water loop consists of four pumps delivering a flow ranging from 25 to 250 m^3/h at 160 mlc head. All these four pumps are connected in parallel to three test sections.

Flow is measured using an orifice flow meter and RTD are used for temperature measurement. The pressure drop across various locations of the SA is measured using Differential Pressure transmitters and the absolute pressures are measured using pressure transducers.

The development status of the detailed subchannel analysis code MATRA-LMR was assessed from the benchmark calculations with the SABRE4 and SLTHEN codes in the Republic of Korea.. The MATRA-LMR calculations for the ORNL 19-pin assembly tests and EBR-II 91-pin experiments were compared to the measurements, and to SABRE4 and SLTHEN code calculation results, respectively.

The comparison results for ORNL 19 pin tests showed that there was a good agreement between MATRA-LMR calculations and the experimental data, as shown in the axial temperature profiles. Also, the accuracy of the pressure drop models was compared for the ORNL 19-pin assembly tests. The results indicated that the CRT predictions were in good agreement with the experimental results and better than other methods. SABRE4 overmediated the temperatures at the edge and side and SLTHEN results showed higher temperatures in the internal region. The differences are found among the three codes because of the pressure drop induced by the wire wrap. In comparisons for EBR-II seven assembly problem calculations, it was observed that MATRA-LMR predicted slightly different temperatures from the other two codes by as much as 3% higher in the average exit and lower in the peak subchannel temperatures. Whereas the computational time of MATRA-LMR is 75% less than SABRE4 but is considerably larger than SLTHEN. In the application for KALIMER design, MATRA-LMR predicted just as well as the other two codes.

From all the benchmark calculations, it can be concluded that MATRA-LMR code is a reliable analysis tool for KALIMER subassembly design and performance analysis. The current version of MATRA-LMR is used only for a single subassembly analysis, but it is planned to extend in to the multi-assembly whole core calculations.

A methodology for thermal hydraulic conceptual design and performance analysis of KALIMER core was developed especially for the preliminary methodology of flow grouping and peak pin temperature calculation in detail. For preliminary steady state thermal hydraulic performance analysis, ORFCE-F60 and ORFCE-T60 modules are used for the flow grouping and the peak pin temperature calculation respectively. The major technical results for the preliminary conceptual design for KALIMER 98.03 design core are shown and compared with the results of KALIMER 97.07 design core. The number of flow groups are reduced

from 16 to 11, as is the equalized peak cladding midwall temperature from 654°C to 628°C through a core design optimization study. The comparison for the KALIMER 98.03 core design results of this preliminary calculation with SLTHEN, MATRA-LMR and SABRE4 code calculations shows that ORFCE modules can be used in the preliminary conceptual design with a sufficient margin.

At later design stages, the basic subchannel analysis will be performed with the SLTHEN code, a steady state thermal hydraulic analysis code based on the ENERGY model. The detailed subchannel analysis will be done with the MATRA-LMR code which is being developed based on COBRA-IV-I and MATRA. MATRA-LMR is now used for a single assembly analysis but will *be* extended for the multi-assembly whole core calculations.The SABRE4 code, a three dimensional subchannel code developed in the UK AEA, will be used for benchmark calculations. These three codes provide temperature maps for all pins in all assemblies and thus facilitate core-wide failure probability studies. It is expected they will form the licensing data basis and will be extensively used during preliminary and final design phases.

JNC (Japan Nuclear Fuel Cycle Development Institute) and TIT (Tokyo Institute of Technology) activities in the thermohydraulic area are as follows:

- Natural Convection Decay Heat Removal (JNC) focusing on the inter-wrapper flow multi-dimensional whole core analysis method was developed and a validation study showed good agreement with the data from a 37-pin bundle surrounded by six 7-pin bundles. Also, focus was given to the intra-subassembly transfer phenomena including mixing enhanced by the thermal plume effect in a subchannel. A function based on Richardson number was proposed to control the usage of the correlations with respect to the flow regime. The method was applied to larger pin bundles up to a 169-pin bundle and showed good agreement with experiment.

- As for the studies in the area of local fault with porous blockage (JNC), a series of water experiments with a 4 subchannel model, blocked by porous media was shown and a 3-D calculation was carried out to look into subchannel scale phenomena using a porousbody model. The computational result showed fairly good agreement with the experiment and gave information on the flow field inside the porous blockage. The information provided by the experiment and the 3-D calculation will be used to derive lumped model parameters for a subchannel analysis which will be a tool for production runs of safety assessments.

- An overview of thermohydraulic code development (JNC) was given for the single-phase flow subchannel analysis code ASFRE, a whole core analysis code ACT and a FEM code SPIRAL. The distributed resistance model (DRM) in ASFRE was explained briefly, in describes spacers and influences on momentum transfer due to the presence of the wire-spacers in a rod bundle

- General safety evaluation model (TIT) was developed which is based on a simple analytical method to predict transient temperature distributions in a metallic fuel FR. The conditions under which sodium boiling or fuel melting takes place are correlated into unique linear functions in terms of effective fuel and coolant reactivities.

- A computational fluid dynamics approach that enables the prediction of the wall shear stress distribution in a distorted rod bundle was developed (TIT). A code system COOLFD was written based on the EFD scheme and on the object-oriented programming technique that gives flexibility in generating orthogonal mesh grids. Comparison of calculated sodium temperature along the simulated fuel pins and wall shear stress were fairly good.

The large complex of experimental, theoretical and calculated work in the area of fast reactor core thermohydraulics is carried out in Russia with the purpose of supporting the operation of demonstration fast reactor BN-600, experimental reactors BOR-60 and BR-10, both development and substantiation of the reactor BN-800 project and advanced fast reactors of a higher potency.

The physical regularities of thermohydraulic processes in core and fuel subassemblies are investigated, their performances for various modes of operations are defined:

- characteristics of an interchannel exchange ;
- analytical closure relationships for subchannel wall friction, heat and mass transfer coefficients;
- flow resistance in rod assemblies.

The methods and codes for thermohydraulic calculations of fast reactor cores are created, validation calculations are carried out:

- small Reynolds k-ε model of turbulence for the calculation of flows inside fast reactor channels with complex form;
- method of approximate modeling of nonstationary temperature fields in central zones of fast reactor fuel assemblies;
- the two-fluid model of liquid metal two-phase flow in the FBR core channels;
- method of statistical calculation of fast reactor core with an account of influence of the fuel assembly form change in process of campaign and other factors;
- MIF code on base of subchannel analysis for calculation of nominal and transient conditions;
- GRIF-SM code for analysis of beyond design basis accidents on sodium cooled reactors;
- hydrodynamic module of THEHYCO-SDT code.

Large volume of calculated researches in the substantiation nominal, unnominal, transitional and emergency operation of working fast reactors core is carried out:

- temperature field formation in the system of interacting fuel subassemblies in fast reactor core;
- numerical simulation of fuel assembly thermohydraulics of fast reactors with the partial blockage of cross section under the coolant;
- 3-D thermal hydraulic analysis of transient heat removal from fast reactor core using immersed coolers.

The realization of the significant programme of experimental and theoretical researches is rated on study, first of all, of emergency conditions of core cooling: researches of liquid metal coolant boiling under conditions of heat removal, modelling of natural convection processes in a reactor tank with use of accident heat removal systems with inner

heat-exchangers, creation and study of passive devices for emergency protection based on various physical principles.

The work above drives the creation of the advanced three-dimensional codes with use of three and four-parametrical turbulence models for the analysis of transients and emergencies in core. This work is proceding.

The analysis of research into thermohydraulic condition of the fast reactor core is being conducted, the problems of advanced fast reactor thermohydraulics are defined.

The preliminary design of the China experimental fast reactor (CEFR) was completed in the early part of 1997. In the framework of thermal hydraulic design of a CEFR core, the programmes undertaken / completed are as follows:

1. Hydraulic simulation of local blockage in a CEFR fuel subassembly.

Local flow blockage in a fuel subassembly is of continuing interest in nuclear safety research as one of the hypothetical accidents of the LMFR's. Analytical work on the problem and many experimental studies have been carried out. Prediction and evaluation of the phenomena of local flow blockage have been achieved by various computer codes. It was concluded that the numerical results of the codes must be checked by experimental data.

The test section was constructed of an electrically heated CEFR core assembly with 19 fuel pins cooled by liquid sodium. The comparison of code predictions against experiments (including non-blockage and ten blockage positions) appears good. The thermal hydraulic behaviour of a fuel assembly with a 61 fuel pin blockage was calculated with a two-dimensional computer code SIMPLE-P. The results indicate that the maximum coolant temperature is 815°C when the blockage area is about 37% (54% subchannels are blocked). This means that the fuel pin cladding is not damaged and no sodium boiling takes place.

2. The development of fast reactor thermohydraulic studies for the near future consists of two parts:

2.1. Experimental Programme:

- hydraulic tests of fuel assembly pressure drop characteristics,
- coolant flow rate distribution in the core fuel subassemblies,
- transient studies of a hot pool.

2.2. Development and code validation :

- SIMPLE-P code (2D porous body model),
- FASTER code (3D porous body model),
- DHRS code (system analysis code for decay heat removal).

Research and development on fast reactor thermal-hydraulics was slowed down in the UK when funding for further fast reactor development and the EFA project was terminated by the UK government in 1993. Since then, fast reactor work has been funded by private industry. A small UK effort has been mainly devoted to the CAPRA project and innovative features and alternative coolants for EFR. The work on the CAPRA project has been mainly concerned with the development of core calculation methods and design for plutonium and minor actinide burning.

3. CONCLUSIONS AND CHALLENGES FOR THE FUTURE

From all benchmark calculations and experiments it might be concluded that there are reliable tools for steady-state thermohydraulic analysis of the conventional core design with nominal geometric parameters of the fuel assembly and nominal operational regimes. The computational method using multi-dimensional codes (e.g. CADET, AQUA, SABRE4, TEMP-M, MATRA-LMR) have been established in Member States for thermohydraulics inside the fuel assembly.

For the non-nominal conditions there are thermohydraulic issues which influence on the accuracy of prediction of the temperature distributions in the coolant, fuel and assembly structures. Such conditions may occur because of flow blockage either at the inlet of the core assembly or by local blockage within assemblies by e.g. excessive bowing or swelling. There are several types of anticipated transients without scram (ATWS) which need the advanced thermohydraulic analysis computer code.

The challenges enumerated in the following paragraphs remain.

3.1. *Off-normal conditions.* Thermohydraulic performance of fuel with non-nominal geometry and flow cross-section has received considerable attention. Once the fuel elements are distorted or local flow cross-sections are varied due to irradiation-induced or local blockages, the geometrical flow paths become very complex, making their accurate representation in calculational procedure very difficult. Some participants pointed out that subchannel analysis for distorted or blocked rod-bundle geometries can be subject to some difficulties and errors. The porous medium approach has the advantage over subchannel analysis in that the distorted and blocked geometry can be represented more accurately by varying the volume porosity and surface permeability. It was stressed that although the analysis of existing experimental results has allowed to evaluate rough thermohydraulic characteristics of the blockages, additional systematic studies are required. Also, there is a little data available related to smaller blockages. Some of the data was obtained for blocked assemblies of smooth pins. The hydrodynamic characteristics of the blockage in the weak region could be appreciably different in the case of rod-bundle with wire-wrap due to higher lateral heat and momentum exchange.

To establish a reliable evaluation method for predicting the thermal-hydraulic parameters in the subassembly with porous blockages, comprehensive development has been carried out at JNC (Japan). The fundamental water and sodium experiments have been performed to understand the phenomena in the subchannel and subassembly. It was pointed out that the developed multi-dimensional analysis gave useful information to understand blockages inside /outside interactions.

3.2. *Heterogeneous fuel assemblies.* In the Western European countries, Japan and Russia there is interest in fast "burner"-reactors (as opposed to "breeders"). The French CAPRA project is aimed at the incineration of Plutonium stocks arising from the operation of commercial thermal reactors. Each assembly of a dilute core in CAPRA reactor contains a large number of small diameter pins about two thirds of which contain fuel and the remaining one third contains empty pins. It was noted that these could give high-temperature heterogeneity in the sub-channel. On the other hand, the helical wire increase the mixing of the coolant fluid, but perturbs the clad/fluid heat transfer. These effects could be evaluated by multi-dimensional computations. The FAIDE supporting experimental programme gives

information on the velocities inside the triangular sub-channels. The exchange of information on heterogeneous fuel assembly thermohydraulics was acknowledged by many meeting participants.

3.3. *ATWS analysis.* There are several types of anticipated transients without scram (ATWS) which need careful attention. The ULOF (unprotected loss of flow) is potentially one of the most severe ATWS. The advanced tools to analyze ATWS should provide the possibility of evaluating of pre-boiling, boiling and post-failure transients including material-coolant interaction and material movement and relocation in the reactor. The thermohydraulic analysis aimed to achieve long-term coolability of the established core configuration after reactivity-initiated accident.

Several computer codes for system analysis exist in the Member States to evaluate ATWS, and two of them were discussed at the meeting.

The Russian GRIF-SM code package with the complementary CANDLE code package provides results for ULOF-type transients up to molten clad relocation. Future developments deal with coupling a transient fuel pin mechanics code package to the system and will extend the capabilities of the code system to describe material relocation phenomena after fuel pin failure or break-up.

SIMMER-III (SIII) code is developed by JNC (Japan) in cooperation with CEA (France) and FZK (Germany) to investigate postulated core disruptive accident (CDA) in LMFR. SIII is two-dimensional multiphase, multi-component fluid-dynamic code coupled with a space- and energy-dependent neutron kinetics model. It includes advanced features such as interfacial area convection and generalized heat and mass transfer. After approaching completion with experimentally qualified models SIII will allow to evaluate consequences along all stages of the CDA.

3.4. *Issues requiring further research and development:*

- LMFR with passive decay heat removal and shutdown systems, and core design with strong negative reactivity feedback;
- a benchmark exercise for 3-D numerical simulation of pin bundles;
- inter wrapper flow simulation in LMFR core;
- fuel behaviour under handling operations.

METHODS AND CODES FOR MODELING THERMOHYDRAULICS OF FAST REACTOR CORE SUBASSEMBLIES UNDER NOMINAL AND NON-NOMINAL OPERATING CONDITIONS

A.P. SOROKIN, A.D. EFANOV, Yu.S. YURIEV, A.V. ZHUKOV,
P.A. USHAKOV, G.P. BOGOSLOVSKAYA
State Scientific Center of Russian Federation,
Institute of Physics and Power Engineering,
Obninsk, Kaluga Region, Russian Federation

Abstract

The paper represents an overview of the codes developed for predicting the behavior of fast reactor core under nominal and transient operating conditions. The possibilities for solution of a wide variety of thermohydraulic issues taking into account an influence of such factors as non-regular geometry in different parts of subassembly, non-uniform length distribution of power production, subassembly deformation, coolant flow through the inter-subassembly gap, different directions of wire wrapped on fuel pins, blockages and others are demonstrated with some codes based on the porous body model.

Numerical approaches are classified on three groups: (1) local (finite-differences, finite elements, variational, thermal source and so on), (2) subchannel and (3) porous body model. Comparative analysis of the approaches (possibilities, realization, advantages and drawbacks) is presented, too. The tendencies for the further development of numerical methods and fast reactor thermohydraulic codes are analyzed.

OBJECTIVES AND GOALS OF REACTOR CORE THERMOHYDRAULIC ANALYSIS

Thermohydraulic analysis is one of the most important part among the interconnected definitions of nuclear power plant parameters, concerned with physics, thermal mechanics, theory of stress and other components (Fig.1). It covers prediction of reactor core unit behavior, determining temperature field, hydraulic characteristics, operating and maximum power of fuel subassemblies. One of the major problem facing the researcher is to show that under all operating conditions the coolant parameters and thermal mechanical characteristics of the structure fall within the ranges allowing reliable operation of reactor.

In development of the methods of thermohydraulic analysis, consideration must be given to the design, technological and physical features of fast reactor core.

Design features. Central reactor components are core and blanket built up of hexagonal subassemblies (SA) with distributed flow rate of the coolant (Fig. 2-a,b). Subassembly represents the bundle of the fuel pins arranged in triangular lattice (or in square one for reactors cooled by lead) (Fig. 2-c).

The key design features of fast reactor are the following:

- Great number of fuel pins in SA causes the dimension of fast reactor core SA to be large. Geometry of SA is combined and multiply connected
- Technological margin causes the geometrical parameter within SA to be distributed, with the distribution mentioned being of statistical character. Periphery of SA differs in geometry from the internal area.
- Wire wrap on the fuel pins lead to the coolant circulation around the pin to be complicated, helical wire wrap is favorable to the initiation of definitely directed flow streams.
- Inter-subassembly gap allows the coolant flowing between neighboring SAs.

Technological features. Among them it should be noted the following:

- Low heat capacity of liquid metal coolant causes its heating up to ~200 K.

- High thermal conductivity of liquid metal (sodium) is the reason for small "wall-liquid" temperature difference being about 5-20 K.

Physical features.

- Distribution of power production depends on the reactor core volume, type and shape of surrounding shields, number of zones, availability of blanket inserts, availability and type of reactivity controls, state of reactor with reference to the refueling moment. Thus, the features aforementioned cause a considerable non-uniformities within SA to exist .

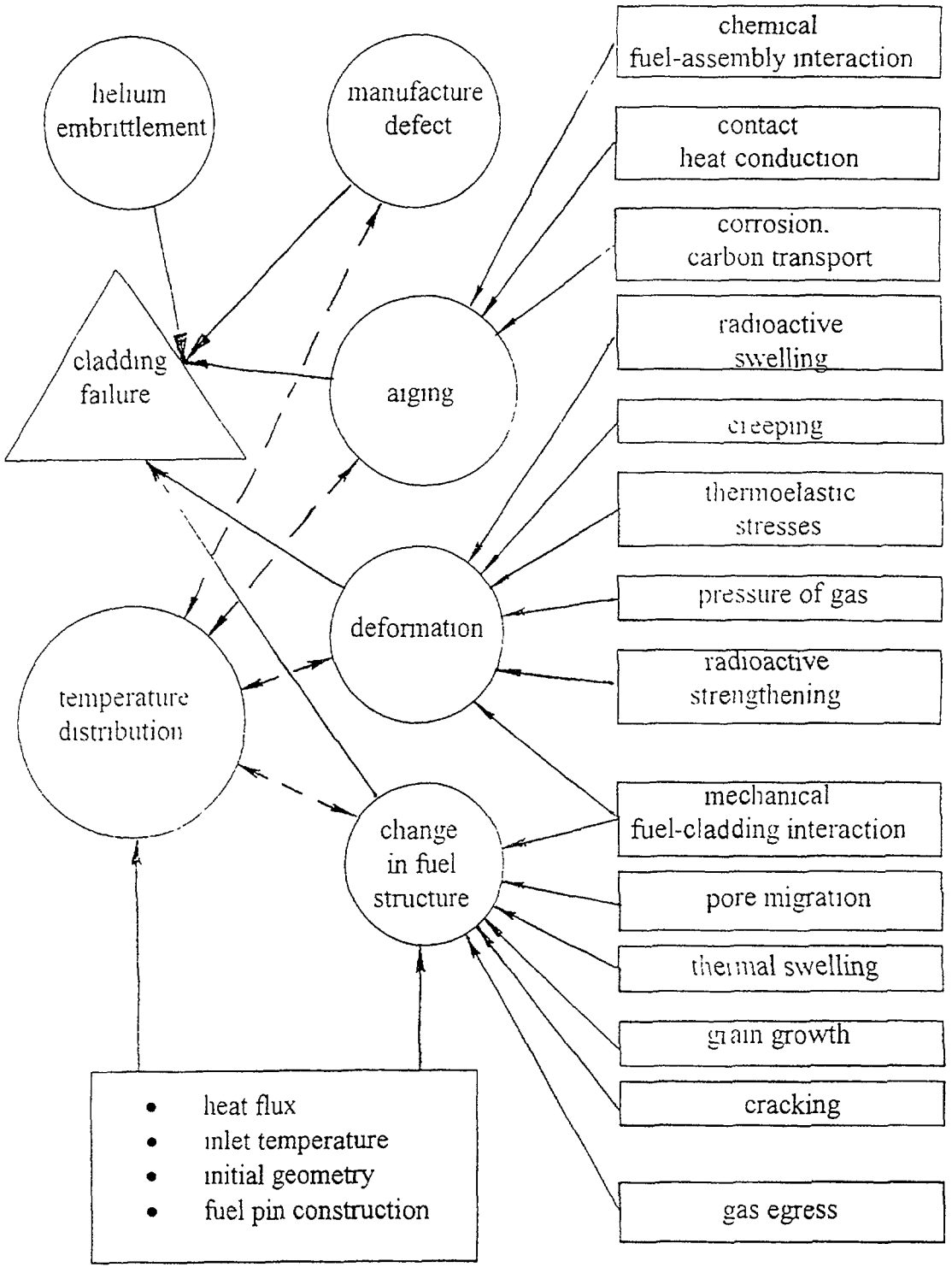

Fig.1 Temperature factor in validational of subassembly operation

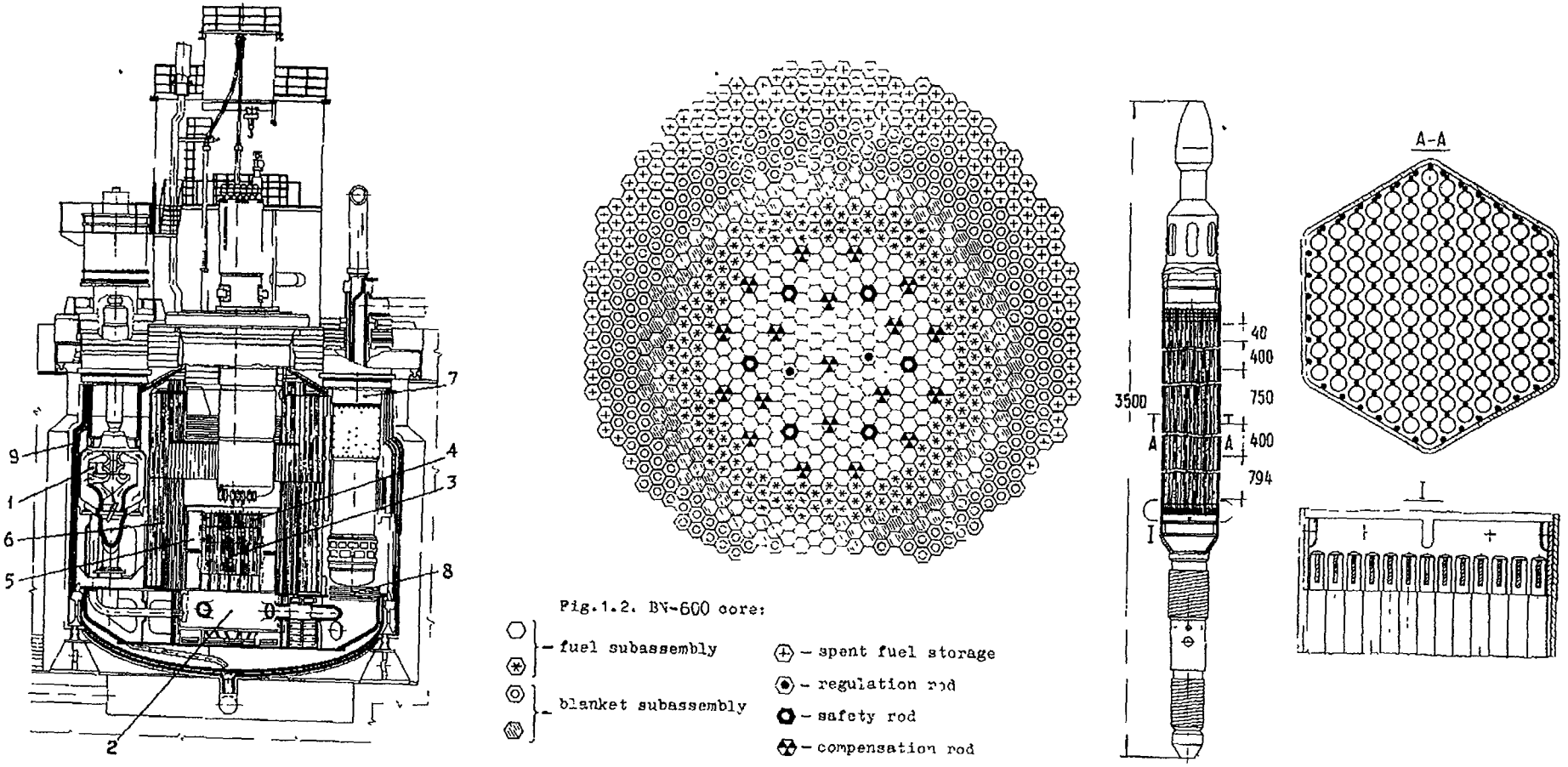

Fig. 2. Integral fast reactor BN-600 block (a), core (b), subassembly (c)

- Under high dose of radiation both hexagonal wrapper tube and pin bundles being under non-uniform temperature and neutron fields may be deformed significantly due to as radioactive effects (swelling, creeping) and thermal expansion.

In addition to validity of predicted parameters an advanced thermohydraulic analysis of reactor core SA should take into account the following specific features:

- inter-channel exchange by mass, momentum and energy;
- complicated irregular geometry, multiply connected calculation domain, number of nodes;
- influence of deformation both wrapper tube and pin bundle within SA on heat transfer characteristics and velocity disturbances;
- conjugate consideration of pin/coolant heat transfer;
- variable power production with SA length and across core and SA;
- heat transfer in the near-wrapper area, diabatic boundary conditions at the wrapper tube;
- exposure of availability of wire wrap on the fuel pin on velocity and temperature fields;
- possibility to vary thermohydraulic parameters of the core units and to optimize them;
- stochastic distribution of input parameters.

DEVELOPMENT OF METHODS AND CODES FOR PREDICTING FAST REACTOR CORE THERMOHYDRAULICS

Naturally, when analyzing hydraulics and heat transfer in fast reactor subassembly, a single channel was initially considered. In 50-s - 60-s some approaches were developed, which are analytical method by P.A.Ushakov [1], [2], method of point source by A.A.Sholochov et al [3], some later a finite differences by N.Buleev [4], A.Zhukov [5], finite elements by P. Milbauer [6], H.G. Kaiser [7], variational differences by E.Nomofilov, V.M.Trevgoda [8]. First of all, the temperature irregularities within the separated channels were investigated.

In the beginning of 60-s, so called subchannel method treating the system of interacting channels which the subassembly is divided on, was under development. It allowed consideration of influence of spatial irregularity in geometry and power production, and mainly the interchannel exchange. First codes (THINC-1[9] (USA), JOTO [10] (Japan), TEMP [12] (USSR) and others) were intended to define the location of hot channel considering the influence of periphery and variable power production of the pins. In the beginning of 70-s the set of subchannel codes simulating coolant flows in the event of availability of the spacing wire wrap on the fuel pins was created (COTEC [13], SIMPLE [13], SWEEP [14], TEMP-M [15] and others.). Conservation equations for momentum and energy were considered with approximation of invariant pressure in the given SA cross section ($P = idem$).

Stochastic distribution of one of the topical parameter defining to a large extent the temperature behavour in subassembly - that is technological margin - was realized in the codes PACT [16] and TEMP-M [15] based on Monte Carlo procedure. In terms of dispersion of coolant temperature across the subassembly, results of calculations on PACT are shown in [16]. Comparison of experimental data on coolant temperature in cross section of reactor "RAPSODIA" with predictions on code DISTAV [17], showed that pin bundle geometry was of statistical character.

Next was the development of the codes treating governing equations with different value of pressure in channels, different initial boundary conditions for steady state and transient processes (DIANA [18], HAMPO [19], COBRA II [20], FLICA III [21], CORTRAN [22] and others.). These codes were effective tools for SA thermohydraulic analysis.

A number of codes was developed with the purpose to analyze the temperature behavior in reactor core having regard to thermal interaction between adjacent subassemblies

(SUPERENERGY [23], MONICAN [24], MIF-C [25]). It was shown that inter-SA heat transfer defines temperature behaviour of considerable amount of pins. At the second half of 70-s and at the beginning of 80-s some codes were developed for predicting thermohydraulics in blockaded subassembly. Governing equations were solved as in subchannel approximation and in the framework of the porous body model. Subchannel approach was developed in such codes as COBRA-IV-I [26], TOPFRES [27], SABENA [28], a porous body model in UZU [29], COMMIX-1 [30], PORTER [31], SABRE-1 [32].

In parallel, some codes were developed in order to analyze the accidents associated with liquid metal boiling, at first in homogeneous approximation of two-phase flow, then considering the separated phases. Analysis of these codes will be presented in other paper. Overview in detail is presented in [33].

CLASSIFICATION AND BRIEF OVERVIEW

Let us take a look at the thermal hydraulic approaches applied to analysis of fuel subassemblies. Thermal hydraulic analysis of reactor subassembly implies that mass, momentum and energy conservation equations are solved together with initial and boundary conditions. Mathematical modeling of hydrodynamics and heat transfer in fast breeder reactor have been analyzed in [33-36].

Fuel pins in combination with the subassembly wrapper and displacers form the channel of complex shape with essentially variable thermal and hydraulic characteristics across the channel, that results in 3-D coolant flow. That is why, researcher fails to find thermal hydraulic characteristics with a required accuracy by the methods based on an idea of "equivalent channel" determining an average parameters of subassembly.

Three lines in thermal hydraulic analysis of pin bundle (Fig.3) can be currently recognized, with each of them having its own advantages and disadvantages:

- prediction of local velocities and temperatures in SA;
- prediction of average characteristics in the framework of the porous body model;
- prediction of lumped parameters (coolant velocities and temperatures averaged over the channel under consideration), that is subchannel analysis (Fig.4 a, b, c).

The main difficulties in application of mathematical models to thermal hydraulic analysis are the combined geometry and large length of the calculation domain.

Local methods based on the system of differential equations (in Reynolds approximation) allow the local flow characteristics to be predicted and then starting from them the integral parameters, such as friction factor, heat transfer, maximum non-uniformity of temperature at the pin cladding, to be evaluated. Moreover, the complexity of the bundle geometry (especially in the event of deformation), a tedious procedure of solution of the heat and mass transfer equations give no way of taking into account an influence of various factors on temperature behaviour in subassembly. As usual the problem is considered in general as steady state coolant flow in the bundle of smooth pins.

To find an average flow parameters on the basis of averaged momentum and energy equations with the use of Euler procedure (the porous body model and subchannel analysis) extends calculation domain, allows an influence of various factors to be taken into account. But, such a methods involve an additional procedure, from which one can define the temperature of units in subassembly structure.

The porous body model, which implies that an averaging is carried out with the greater scale, and in some cases, the vastly greater, than the size of the channel in bundle and which uses the mesh being not coincident with the bundle channels allow us to gain the less detailed solution. This method reflects an effects being much more extended than the channel in bundle, whereas subchannel analysis covers phenomena with inherent scale being equal to the

distance between the pins' axis. Thus, a porous body model describes macro parameters, and subchannel approach can be considered as macro-micro approximation in the sense that it describes macro effects in reference to the phenomena occurring in the channel, and yet describes micro effects in reference to the bundle dimension.

In spite of commonness of setting up the problem for different approaches, similarity of equations, and respective calculation procedure, there is distinction between them associated with the evaluation of the constants inherent in equations (transport factors and others). These methods are followed to be mutually relative. The use of the local methods allows the constants to be defined as input parameters for solving transport equations with averaged flow approximation.

It should be noted that in spite of a number of fundamental works (for example, [37, 38]) concerned with the derivation of governing equations the system of correct equations has not be yet written in the full form.

Analogy between equations for the model of continuos media and the porous body model allows the mathematical class of the problems to be specified and also the approximate equations to be analyzed, for example, without regard to axial diffusion, with the use of the hypothesis of isobaric cross section, and the algorithm of the problem solution to be simplified.

Strict analysis of macro-transport equations (conservation equitation) indicates that mass, momentum and heat transfer exchange in pin bundles is due to molecular, turbulent,

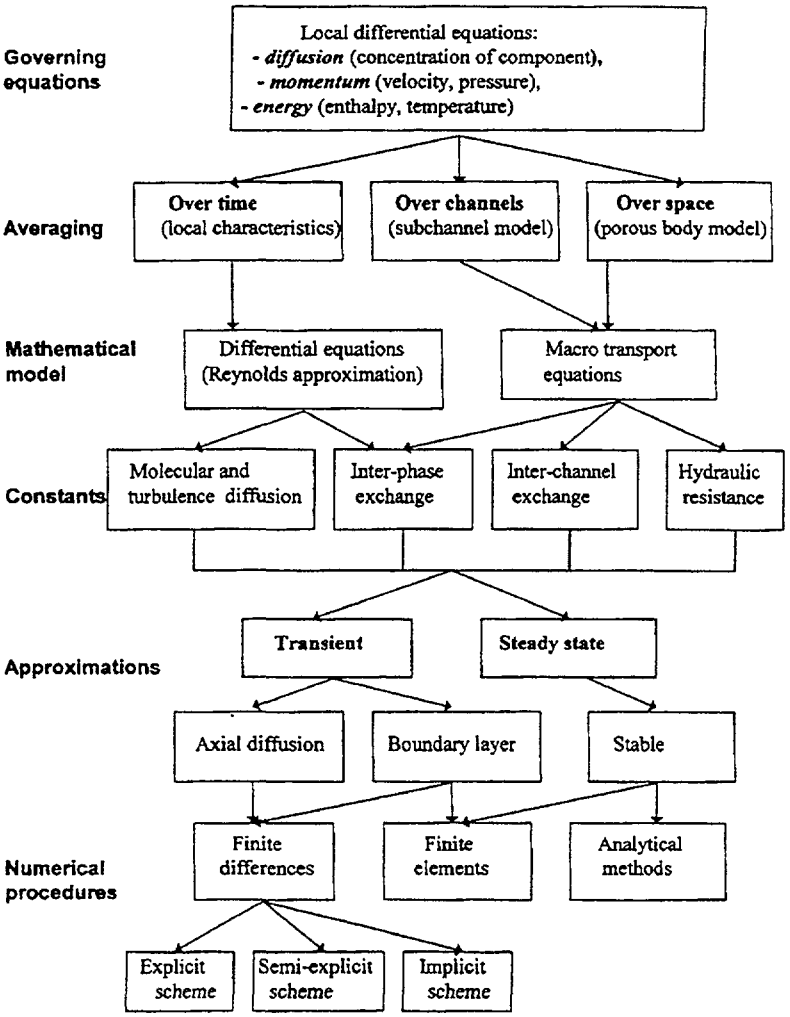

Fig. 3. Classification of approaches to thermal hydraulic analysis

convective mechanisms, as well as due to heat conduction over the pin cladding. Physics of exchange varies under influence of various factors on velocity and temperature fields (deformation, wire wrap and so on) [39].

TENDENCIES FOR DEVELOPMENT OF THERMOHYDRAULIC METHODS AND CODES

Development of thermohydraulic codes for liquid metal cooled reactors is directly related to the widening of the problems under consideration, accumulating experimental data on structure and characteristics of liquid metal flow in reactor subassembly, attempts to explain the data available, advanced numerical modeling of the equations to be solved, availability of modern advanced computers.

The data on turbulence velocity pulsations obtained by Heina J. et al [40] in experimental deformed pin bundle is that the radial distribution of axial turbulence velocity pulsations in the area between pins in deformed arrangement differ considerably from those in round tube. Near the wall the value of u'/v^* is close to the value in round tube. The value of u'/v^* increases for a number of profiles outward from the wall, having maximum in the flow core. It explains a very flat distributions of axial velocity gained in experiment (Fig. 4d). Local maximum of u'/v^* is observed in a direction toward to the channel expansion.

In the area between shifted pins, which form deformed channel, velocity turbulence pulsations in radial and azimuthal directions arise, whereas their values in the remainder of the channel follow the relationship for round tube.

The more flat velocity profile in that area of the channel formed by the shifted pins is explained by intensive transverse momentum transfer in the gap between pins. Rearrangement of velocity profile occurs due to variation of turbulence structure and energy. As a

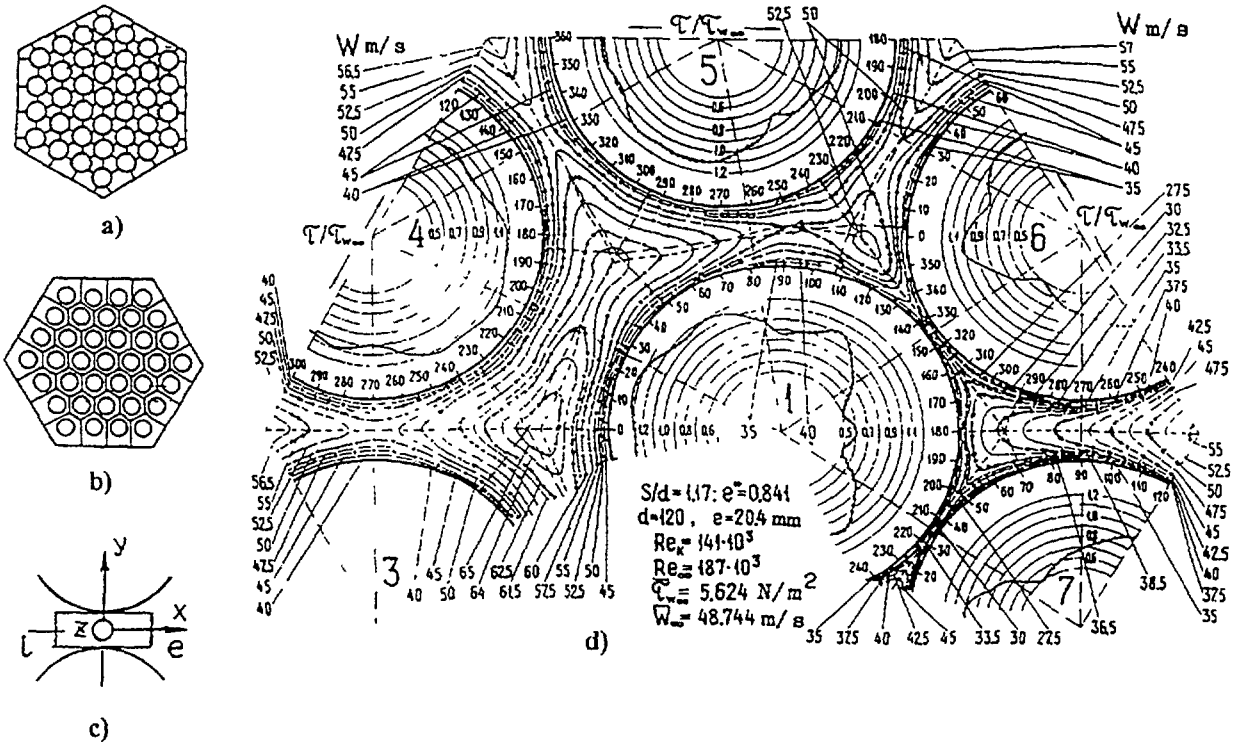

Fig. 4. Scheme of bundles with different cells (a, b) and cell in gaps (c) and shear stresses and coolant velocity in deformed bundles (d)

consequence of momentum transfer from internal area of adjacent channels a turbulence energy increases over the gaps, as well as in the space between the shifted pins.

An influence of large-scale turbulence on temperature behaviour is illustrated in [41]. General k-ε model of turbulence does not allow modeling large-scale turbulence tranfer of momentum and energy. Attempts to develop such a models were made by N.I.Buleev [41] and Y.A. Hassan [42], as well in [44] in four-parameters turbulence model.

Recently, an information on local structure of inter-channel convective exchange within bundles of wire wrapped pins has been gathered [45]. To simulate actions of wire wrap on coolant flow is based on the representation of the wrap as a forced force [46,47].

It can be marked a considerable successes in realization of finite differences, as applied to calculation of the complete subassembly area, made by Larrauri D., et al [48], Nagayoshi T., et al. [49]. Conjugate consideration of pin/liquid heat transfer is of important practical use.

In the framework of subchannel approach, it is of great importance to simulate a local structure of inter-channel exchange based on the model of mole motion [47] and to take into account a centrifugal effect in the event of longitudinal deformation of the bundle [50]. Based on the aforementioned the thermal effects predicted with MIF code for specific situations in Phenix reactor [51] may be quite considerable.

Local model of convective transfer is seemed to be very effective in the event of the counter-directional wire wraps are used (Fig.5). Analysis of influence of various factors on temperature field is demonstrated in Fig. 6.

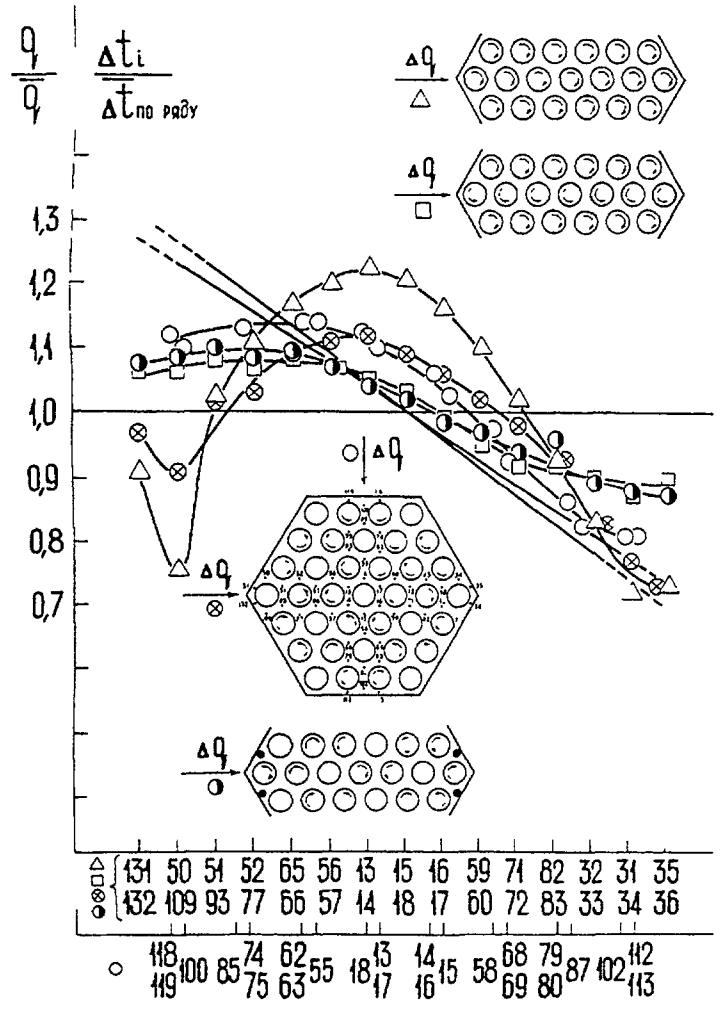

Fig. 5. Equalization of temperature fields due to counter-directional with wrap

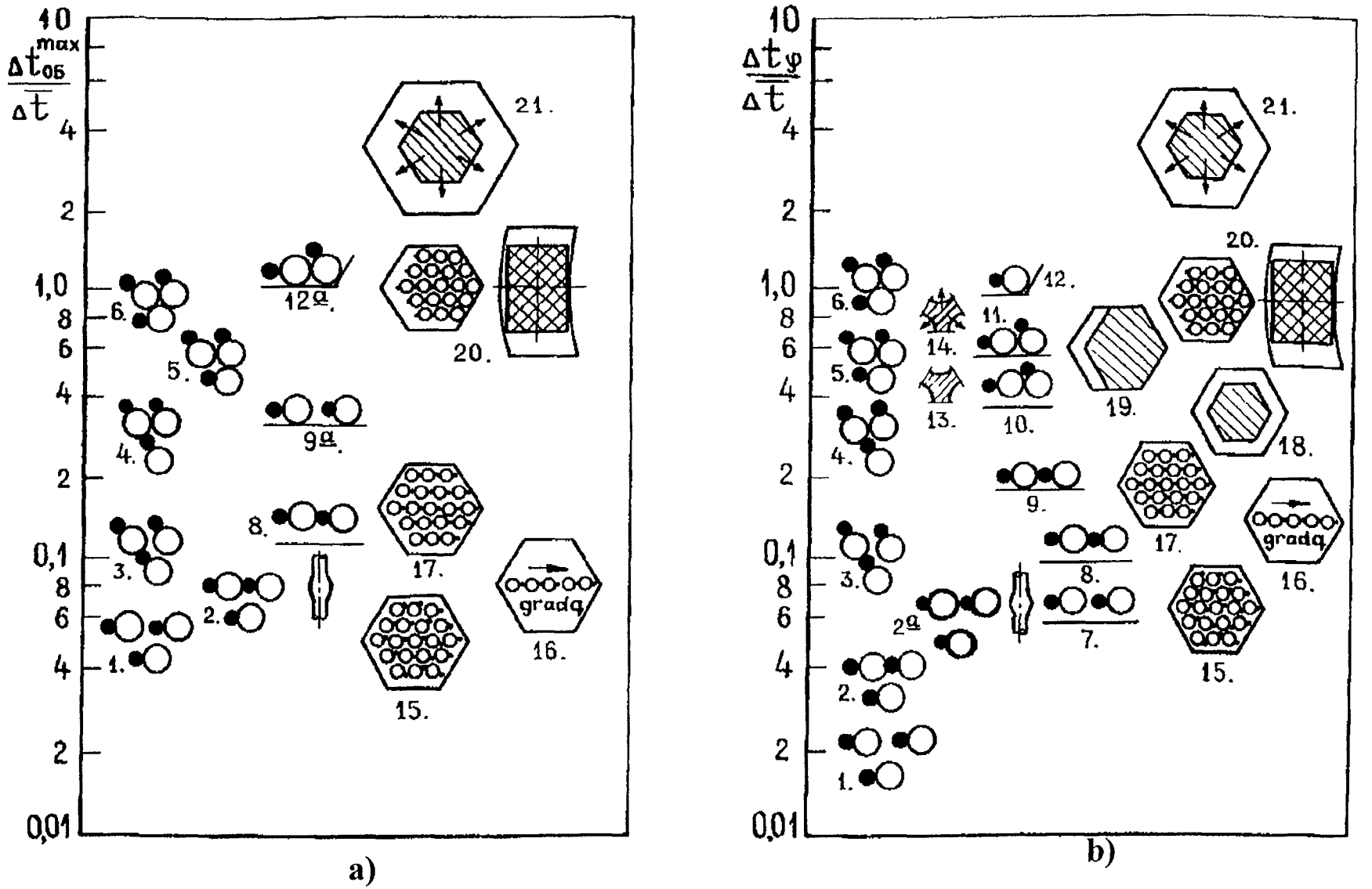

Fig. 6. Exposure of maximum temperature of fuel cladding (a) and maximum temperature non-uniformity around pins (b) to different factors

CONCLUSION

Over 60-s - 90-s in current century many codes were developed to analyze thermohydraulics in fast reactor core, which may be classified in accordance with three lines:

- prediction of local velocities and temperature in the individual subassembly;
- prediction of averaged over channel fields in subassembly and in reactor core in whole;
- prediction of averaged over volume velocity and temperature fields.

The most advanced is simulation of averaged characteristics of the flow. Recently a wide class of the problems is resolved in order to validate nominal, non-nominal and accident performance of fast reactor subassembly.

Significant experimental data were accumulated, that indicates features of exchange by mass, momentum and energy in multiply connected areas in pin bundles and gives the possibility to verify the code developed.

Advances in numerical solution of heat transfer and hydrodynamic equations, improved computer possibilities cause the progress in modeling of local characteristics in such cases as:

- deformation of the bundle;
- influence of wire wrap on coolant flow;
- solution of conjugate pin/liquid heat transfer problem.

To conclude, it should be noted that at present it is central to develop as codes for modelling of local characteristics and procedures for engineering estimations of reactor core in whole, and optimization of the core parameters for the use in the combined neutron-physical and thermohydraulic calculations.

REFERENCES

[1] NEVSTRUEVA E.I., USHAKOV P.A. Heat and Mass Transfer in Nuclear Power Plants with Reactors Cooled by Liquid Metals // Heat and Mass Transfer. M: VINITI, 1980. v.2.

[2] YEUNG M.R., WOLF L. Multi-Cell Flow Heat Transfer Analysis for Finite LMFBR Bundles // Nuclear Engineering and Design. 1980. v.62. N1-3. p.101-121.

[3] SHOLOKOV A.A., ZASORIN M.P., MINASHIN V.E., et al. Temperature Behavior in Nuclear Reactor Ful Pins. M.: Atomizdat, 1978.

[4] BULEEV N.I. Further Development of Spatial Model of Turbulence Exchange in Flow of Incompressible Liquid // Near Wall Turbulent Flow. Novosibirsk: SB AS USSR. 1975, 4.1, p.51.

[5] SIDELNIKOV V.N., ZHUKOV A.V. Calculation of Temperature Fields at the Entrance Section and Influence of Variable Power Production (Slug Flow of Coolant): Preprint IPPE-414, Obninsk, 1973.

[6] MILBAUER P. Application of Finite Elements for Calculating of Turbulent Flow in Direct non-Round Channels // Hydrodynamics and Heat Transfer in Reactor Core and Steam Generators of Fast Reactors Cooled by Sodium. Prage: CSSR, 1984, v.1, p.104-115.

[7] KAISER H.G., ZEGGEL W. Turbulent Flows in Complex Rod Bundle Geometry Numerically Predicted by the Use of Fem and Basic Turbulent Model // Nuclear Engineering and Design. 1987. V.99. N 3. p.351-363.

[8] NOMOFILIV E.V., TREVGODA V.M. Method for Calculating Velocity and Temperature Fields in Non-Standard Channels // Hydrodynamics and Heat Transfer in Reactor Core and Steam Generators of Fast Reactors Cooled by Sodium. Prage: CSSR, 1984, v.1, p.174-182.

[9] ZERNICK W., CURRIN H.B., ELYATH E., PREVITI G. THINC - A Thermal Hydraulic Interaction Code for a Semi-Open or Closed Channel // WCAP; 3704. 1962.
[10] OKAMOTO Y., HISHIDA M., AKINO N. Hydraulic Performance in Rod Bundles of Fast Reactor Fuel Pressure Drop Vibration and Mixing Coefficient // Progress in SodiumCooled Fast Reactor Engineering. Monako. IAEA / SM-130/5. 1970.
[11] BAUMANN W., HOFFMAN H. Coolant Cross Mixing of Sodium Flowing in Line through Spacer Arrangements // International Heat Transfer Seminar. Trogir. Yugoslavia, 1971.
[12] ZHUKOV A.V., MOUZANOV A.B. et al. Inter-channel Mixing in Pin Bundles // Preprint IPPE-413. Obninsk, 1973.
[13] NOVENDSTERN E.H. Mixing Model for WireWrap Fuel Assemblies // Transactions of the American Nuclear Society. 1972. Vol.15, N2.
[14] GINSBERG T. Forced-Flow Interchannel Mixing Model for Fuel Rod Assemblies Utilizing a Helical wire-Wrap Spacer System // Nucl. Engng and Design. 1972. v.22, N1.
[15] BOGOSLOVSKAYA G.P., ZHUKOV A.V., et al. Code TEMP-M for Thermohydraulic Analysis of Fast Reactor Subassembly // Preprint IPPE-1401. Obninsk, 1983.
[16] WEI J.P., STEPHEN J.D. PACT: A Probabilistic Method for Analysis of LMFBR Coolant and Cladding Temperature Distribution // Trans. American Nucl. Soc. 1976. v. 24, N1.
[17] LETEINTURIER D., CARTIER L. Theoretical and Experimental Investigations of the Thermohydraulics of Deformed Wire-Wrapped Bundles in Norman Flow Conditions // IWGFR/29. Vienna: IAEA, 1979.
[18] HIRAO S., NAKAO N. DIANA - A Fast and High Capacity Computer Code for Interchannel Coolant Mixing in Rod Arrays // Nuclear Science And Design. 1974. v.30, N3.
[19] BOWRING R.W. HAMBO - A Computer Programme for Subchannel Analysis of the Hydraulic and Burnout Characteristics of Rod Bundles (Ps.1) General Description // AEEW-R524. London, 1967.
[20] ROWE D.S. Thermal-Hydraulic Analysis for Rod Bundle Nuclear Fuel Elements // Heat Transfer Conference Paris-Versailles. 1970. v. 3. FC 7.13.
[21] PLAS E. Programme FLICA-III Pour l'Etude Thermohydraulic de Reacteurs et de Boucles d'Essees // Rep. On the France-Soviet Seminar. Moscow, 1974.
[22] KHAN E.V., George T.L., Wheeler C.L. COBRA and CORTRAN Code Thermal-Hydraulic Models for LMFBR Core Wide Temperature Distribution During a Natural Convection Transient // IWGFR / 29.1979.
[23] WOLF L., FISHER K., HERKENRATH H., et. al. Comprehensive Assessment of the Ispra BWR and PWR Subchannel Experiments and Code Analysis with Different Two-Phase Model and Solution Schemes // Nuclear Engineering and Design. 1987. v. 99, N 1.
[24] CARELI M.D., BACH C.W. Thermal-Hydraulic Analysis for CRBRP Core-Restraint Design // Transactions of the American Nuclear Society, 1975, v. 21, N 1.
[25] MARTCHUK G.I. Methods of Numerical Mathematics. Novosibirsk: Nauka, 1973.
[26] WHEELER C.L. COBRA-IV-I: An Interim Version of COBRA for Thermal-Hydraulic Analysis of Rod Bundle Fuel Elements and Cores // BNWL-1962. Battelle-Pacific Northwest Laboratories. Richland, Washington, 1976.
[27] ARAI M., HIRATA H. Numerical Calculation For Two-Phase Flow Analysis in Pin Bundles // Nuclear Engineering and Design. 1984. v. 82, N 2.

[28] NINOKATA H. Analysis of Low-heat-flux Sodium Boiling Test in a 37-Pin Bundles by the Two-Fluid Model Computer Code SABENA // Nuclear Engineering and Design. 1987, v. 97, N 2.
[29] MIYAGUCHI K. Analytical Studies on Local Flow Blockages in LMFBR Subassemblies Using the UZU Code // Nuclear Engineering and Design. 1980. v. 62. N 1-3.
[30] DOMANUS H.M., SHAN V.L., SHA W.T. Applications of the COMMIX Code Using the Porous Medium Formulation // Nuclear Engineering and Design. 1980. v. 62. N 1-3.
[31] KUMAEV B.J., LEONCHUK M.P., et al. Method of Calculations of 3D Flow in Pin Bundle // Preprint IPPEE-1733. Obninsk, 1985.
[32] MACDOUGALL J.D., LILLINGTON J.N. The SABRE Code for Fuel Rod Cluster Thermohydraulics // Nuclear Engineering and Design. 1984. v. 82, N 2-3.
[33] ZHUKOV A.V., SOROKIN A.P., et al. Interchannel Exchange in Fast Reactor Subassembly. M.: Energoatomizdat, 1991.
[34] ZHUKOV A.V., KIRILLOV P.L., et al. Thermohydraulic Calculations in Fast Reactor Subassembly Cooled by Liquid Metal. M.: Energoatomizdat, 1985.
[35] RECOMMENDATIONS FOR THERMOHYDRAULIC ANALYSIS OF FAST REACTOR CORE // RTM 1604. 008-88. State Committee on Atomic Energy. M., 1989.
[36] SHA W.T. An Overview on Rod Bundle Thermal-Hydraulic Analysis // Nuclear Engineering and Design. 1980, v. 62, N 1-3, p. 3-21.
[37] SHA W.T., CHAO B.T., SOO S.L. Porous-Media Formulation for Multti-Phase Flow with Heat Transfer // Nuclear Engineering and Design, 1984, v.82, N 2-3, p.93-106.
[38] NINOKATA H. Advances in Subchannel Analysis for Boiling Two-Phase Flows in Rod Bundles // Subchannel Analysis in Nuclear Reactors, Proceedings of the International Seminar on Subchannel Analysis (ISSCA'92), Tokyo, 1992, p.15-68.
[39] ZHUKOV A.V., SOROKIN A.P., MATJUKHIN N.M. Interchannel Exchange in Fast Reactor Subassemblies. M., Energoatomizdat, 1989.
[40] HEINA J., MANTLIK F., et al. Experimental Investigations of Hydrodynamic Characteristics at the Edge Area of Fast Reactor Subassembly. Turbulence Microstructure in Deformed Bundle // Report UJV-8981 T, Rez, CSSR, 1989.
[41] MOLLER R. TEGENA Experiment: Two-Dimensional Measurements of the Mean Temperature Fluctuations in Wall Channels of a Sodium-Cooled 4-Rod Bundles // Proceedings Fourth International Topical Meeting on Nuclear Reactor Thermohydraulics, Karlsruhe, 1989, v.2, p.1271-1278.
[42] BULEEV N.I. Spatial Turbulence Model. M., Nauka, 1989.
[43] HASSAN Y.A., BARSAMIAN H.R. Application of Large Eddy Simulation in Subchannel Analysis // Proceedings Fourth International Seminar on Subchannel ANalysis (ISSCA-4), Tokyo, 1997, p.43-52.
[44] IEVLEV V.M. Numerical Modeling of Turbulent Flow. M., Nauka, 1990.
[45] SUH K.Y., TODREAS N.E. An Experimental Correlation of Cross-Flow Pressure Drop for Triangular Array Wire-Wrapped Rod Assemblies // Nuclear Technology, 1987, v.76. N 3, p.229-240.
[46] NINOKATA H., EFFHIMIADIS A., TODREAS N.E. Distributed Resistance Modeling of Wire-Wrapped Rod Bundles // Nuclear Engineering and Design, 1984.
[47] BOGATYREV I.L., et al. Calculation Model for Reactor Subassembly Hydrodynamics // Preprint IPPE-2228, Obninsk, 1991.
[48] LARRAURI D., LEDUC Ch., et al. 3-D Simulations of Single Phase Flows in Rod Bundles with ESTET-ASTRID Code // ISSCA'4, Tokyo, 1997, p.27-42.

[49] NAGAYOSHI T., KOMATSU I. et al. Development of Prediction Method of Void Fraction Distribution in FUel Assemblies for Use in Safety Analysis // ISSCA'4, 1997, p.53-60.
[50] KAZACHKOVSKI O.D., et al. Temperature Fields in Deformed Subassemblies // Atomic Energy, 1988, v.65, N 2, p.89-97.
[51] MARBACH J. Coomportement d'un faisceau d'aigulles Phenix sour irradiation. In: Irradiation Behavior of Metallic Materials for Fast Reactor Core Components. CEA-DMECH B.P. N 2-91190, France, 1979, p.269-301

THE STATUS OF STUDIES ON FAST REACTOR CORE THERMAL HYDRAULICS AT PNC

M. NISHIMURA, H. OHSHIMA, H. KAMIDE,
K. YAMAGUCHI, A. YAMAGUCHI
O-arai Engineering Center,
Power Reactor and Nuclear Fuel Development Corporation,
O-arai, Ibaraki-ken, Japan

ABSTRACT

An outlook was addressed on investigative activities of the fast reactor core thermal-hydraulics at Power Reactor and Nuclear Fuel Development Corporation. Firstly, a computational modeling to predict flow field under natural circulation decay heat removal condition using multi-dimensional codes and its validation were presented. The validation was carried out through calculations of sodium experiments on an inter-subassembly heat transfer, a transient from forced to natural circulation and an inter-wrapper flow. Secondly, experimental and computational studies were expressed on local blockage with porous media in a fuel subassembly. Lastly, information was presented on an advanced computational code based on a subchannel analysis code. The code is under the development and extended to perform whole core simulation.

1. INTRODUCTION

An overview is presented in this paper on fast reactor core thermal-hydraulic research and development of numerical analysis methods at Power Reactor and Nuclear Fuel Development Corporation (PNC). A natural circulation decay heat removal (NCDHR) has been one of the most important issues in this R&D field. Some computational models for a 3-dimensional code have been developed to predict the core thermal-hydraulic characteristics under NCDHR conditions accurately. The development was carried out in two stages: modeling for 1) thermal-hydraulics in the subassembly[1] and 2)thermal-hydraulic interaction between inside and outside the subassembly. The code was validated through the analysis of the sodium experiments: 61-pin subassembly steady state tests, unsteady 7-subassembly sodium tests under the transitions from forced to natural circulation with/without the inter-subassembly heat transfer and steady state test on the inter-wrapper flow (convection in the gap region between the subassemblies).

A local blockage with porous media at certain subchannels inside the subassembly brings another main thermal-hydraulic issue in which the maximum cladding temperature and its appearing position are of interests. A water test with magnified, 5/1 scale, 4 subchannel bare rod bundle model has been performed and its 3-dimensional thermal-hydraulic simulation model was developed. The computational result gave insights on the flow pattern and cooling mechanism inside the porous blockage and the interaction between the blockage inside/outside flows. Sodium and water tests with 1/1 scale 37-pin subassemblies have been also performed on the local blockage. These tests pay attention on corner blockage in which two rows of subchannels were blocked by the porous media from the inner face of one side wall of the wrapper tube. Preliminarily sodium test results were obtained. And flow visualization of the water test have been performed. Some calculations using subchannel analysis code ASFRE[2] were carried out for the sodium test to predict the maximum temperature and its appearing position.

Some advanced codes for the core thermal-hydraulics are under the development. ASFER is extended to the whole core thermal-hydraulic code ACT. To calculate detailed flow field in the subchannel of the wire wrapped rod bundles, a finite element method code is also developed.

All the data from the sodium and the water experiments were used for the validations of analysis codes to develop them capable of predicting thermal-hydraulics in the real reactor.

2. NATURAL CIRCULATION DECAY HEAT REMOVAL

2.1 Development of computational model for multi-dimensional codes

2.1.1 Subassembly thermal-hydraulics

The prediction of temperature distribution in the fuel subassembly is one of the most important issues for the reactor safety assessment. Temperature distributions thus the maximum cladding temperature in the subassemblies are interactively affected by inter-subassembly heat transfer and cooling capability of an inter-wrapper flow. The inter-subchannel mixing, which is caused by wire sweeps, turbulence, and thermal plumes due to heating, is one of the most important parameters predominating temperature profiles inside the subassembly. A systematically formulated mixing correlation was constructed at MIT for the subchannel analysis to apply to all flow regimes[3],[4].

Cheng and Todreas[3] reported that under the forced convection, the mixing due to swirl flows generated by wrapped wire spacers on the pins plays key role. While the mixing induced by thermal plumes prevails, in the mixed convection flow regime. And the inter-subchannel mixing plays minor role under the natural convection condition. Because an inter-subchannel flow redistribution is predominant in determining temperature profiles inside the subassemblies. From these contexts, a threshold function was proposed to control the usage of mixing factor and enabled simulations to handle the all flow regimes continuously; forced, mixed and natural convection, appeared in the reactor transient conditions. A detailed expression of this modeling is presented in Ref.[1]. This modeling for effective diffusivity was implemented to the diffusion terms of the conservation equations in the multi-dimensional thermal hydraulic code AQUA[5]. The computational models and the code were validated through the analyses of a sodium experiments.

2.1.2 Thermal-hydraulic interactions between flows inside and outside the subassembly

The inter-wrapper flow (IWF) occurred in NCDHR is a flow of cold coolant fluid comes from direct heat exchanger (DHX) immersed into a hot plenum[6]. It penetrates into the gap regions between the subassemblies (inter-wrapper gaps) cooling the subassemblies from outside of the wrapper tube wall. Two major influences have been concerned on the IWF: 1) temperature decrease inside the subassemblies and 2) decrease in natural circulation head within the primary loop. Of course the former is a positive effect and the latter is a negative one regarding the decay heat removal capacity.

Another type of the IWF was reported[7] which was observed under forced circulation conditions. This type of the IWF is occurred by the driving force from the pressure difference between the core outlet region just below the upper internal structure (UIS) and the hot plenum. Thus the coolant dives into inter-wrapper gaps within the center region of the core outlet, turns to horizontal direction crossing through the wrapper tube bundle, goes upward in the outer region of the core and exits from the inter-wrapper gaps into the upper plenum.

The IWF occurred in NCDHR has been mainly studied at PNC recently. In this case, an adequate modeling is of importance to treat the interactions between thermal-hydraulic fields inside and outside the subassembly. Inside the subassembly, a large difference of friction force exists between interior and edge subchannels which imposes velocity difference between them. This also makes temperature in the edge subchannels lower than subassembly bulk temperature. Therefore, edge subchannel temperature should be referred to as a characteristic temperature of flow inside the subassemblies to calculate heat fluxes through the wrapper wall tubes unless a specific correlation for heat transfer were used. A square mesh model of the subassemblies was proposed to simulate the IWF, flows inside the subassembly and the hot plenum simultaneously. The interior and edge subchannels had each own mesh in this arrangement. Typical mesh arrangement of this model is presented in *FIG. 1*. This mesh simulated the 7-subassembly sodium test facility: plant dynamics test loop with direct heat exchanger (PLANDTL-DHX, see *FIG. 5*). The detail of the test facility will be addressed later.

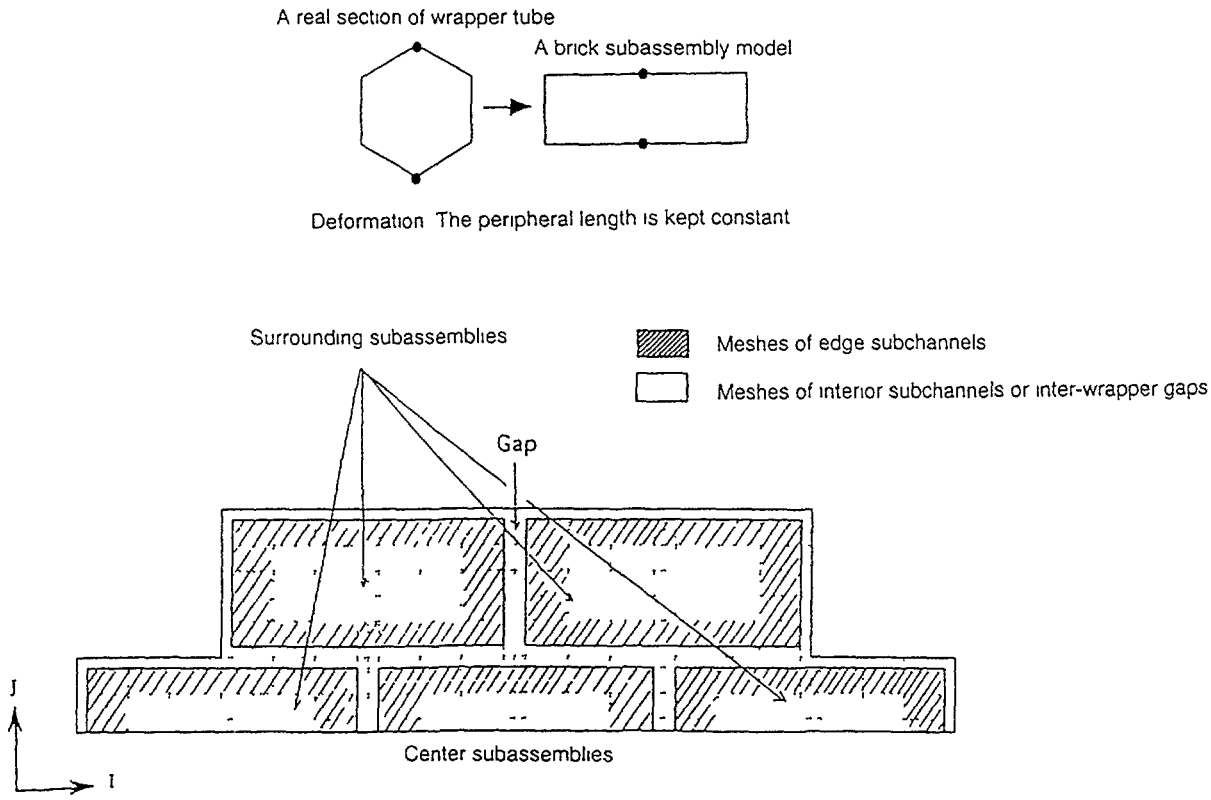

FIG 1 Brick subassembly mesh arrangement

2.2 Validation through sodium experiments

2.2.1 Inter-subassembly heat transfer

Predictive capabilities of house code AQUA was examined on temperature profiles in the subassemblies accompanied by the inter-subassembly heat transfer. The code validation was carried out through calculations of sodium experiments core component test loop (CCTL-CFR)[8] and PLANDTL-DHX. A schematic diagram of CCTL-CFR and its test section are shown in *FIG. 2*. TABLE 1 shows specifications of the test rigs simulated in the present code validation. The test section is consisted of a 61-pin bundle and two 19-pin bundles, simulating the blanket and driver subassemblies respectively. Each bundle is such bounded by solid steel slab to the others that the heat flux due to the inter-subassembly heat transfer is measurable using thermocouples enveded on the slab surfaces. A cooling channel was also equipped in 61-pin bundle behind the wrapper wall opposite to the 19-pin bundle side to provide various thermal boundary conditions simulating the inter-subassembly heat transfer.

Test conditions of CCTL-CFR used in the code validation were shown in TABLE 2. In Case-61A, the 61-pin bundle was heated by the 19-pin bundles and cooled by the cooling channel featuring heat flux crossing the 61-pin bundle. While the 61-pin bundle was under almost adiabatic wrapper wall condition in Case-61B. A staggered half pin mesh arrangement[9] were used to simulate the fuel pin bundles, in which each mesh accommodates only 1 subchannel in its horizontal cross section.

Comparisons of the experimental and numerical temperature distributions are shown in *FIG 3* The difference of temperature between the experiment and the prediction is less than 3 °C that is within the uncertainties of the measurements. In Case-61A prediction reproduced temperature gradient imposed by the heat flux crossing the 61-pin bundle from 19-pin bundle side to the cooling channel.

2.2.2 Transient from forced to natural circulation

To simulate the complex phenomena in the reactor, a core model composed of seven subassemblies was installed in the sodium test loop PLANDTL-DHX. A schematic flow diagram of

PLANDTL-DHX is shown in *FIG. 4*. The core model's horizontal cross section is illustrated in *FIG. 5*, and TABLE 1 shows specifications of it. The core model was connected to the upper plenum in which DHX of a direct reactor auxiliary cooling system (DRACS) was immersed to remove the decay heat. The inter-wrapper gaps filled with sodium were also connected to the upper plenum. The primary circuit had an intermediate heat exchanger (IHX) equipped with a primary reactor auxiliary cooling system (PRACS), a pump, and a lower plenum. Sodium coolant flow was fed by three lines respectively to the center subassembly, the three surrounding subassemblies ranging in one side, and

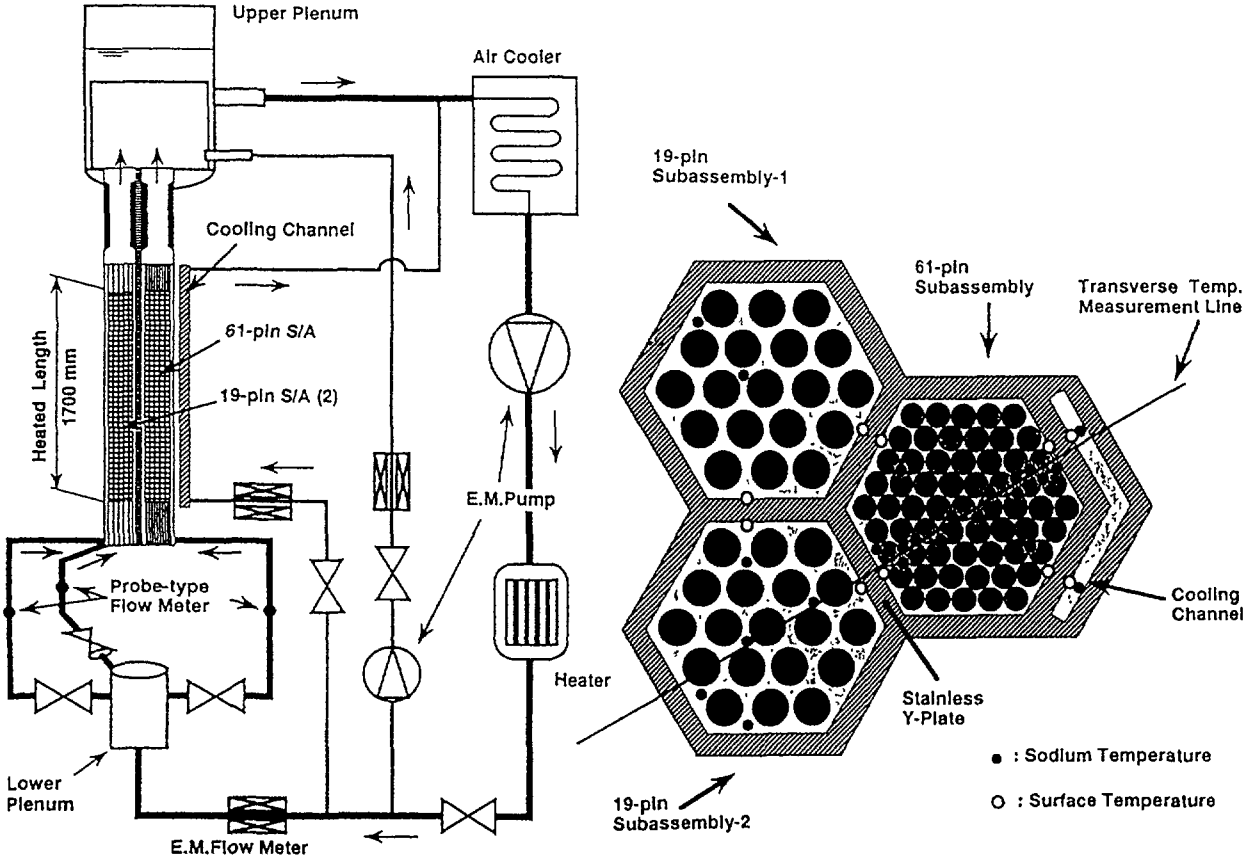

FIG. 2 Schematic diagram of core component test loop (CCTL-CFR) and its test section

TABLE 1 SPECIFICATIONS OF SODIUM TEST SUBASSEMBLIES

		CCTL-CFR		PLANDTL-DHX	
		Driver	Blanket	Center	Surrounding
Number of Subassemblies		1	2	1	6
Number of Pins		61	19	37	7
Pin Diameter	(mm)	16.0	25.0	8.3	20.8
Pin Pitch	(mm)	17.4	30.2	9.9	22.4
Spacer Wire Diameter	(mm)	1.4	5.2	1.5	1.5
Spacer Wire Lead	(mm)	200	700	165	165
Wrapper Tube Inner Flat to Flat Distance	(mm)	140.0		63.0	
Inter-wrapper Gap Width	(mm)	0		7	
Wrapper Tube Thickness	(mm)	15		4	
Heated Length	(mm)	1700		1000	
Axial Power Profile		Uniform		Chopped Cosine	

TABLE 2 TEST CONDITIONS OF CCTL-CFR

Case No.	Heater Power (KW/Ass.)		Flow Rate (ℓ/min/Ass.)			Inlet Temperature (℃)			Heat Transfer To 61pin Bundle
	61 pin Bundle	19 pin Bundle	61 pin Bundle	19 pin Bundle	COOLING CHANNEL	61 pin Bundle	19 pin Bundle	COOLING CHANNEL	
61A	14.5	33.5	10.3	13.1	1.0	251.3	252.1	247.2	heated
61B	15.3	7.8	29.4	13.5	0.0	251.2	252.2	-	isothermal

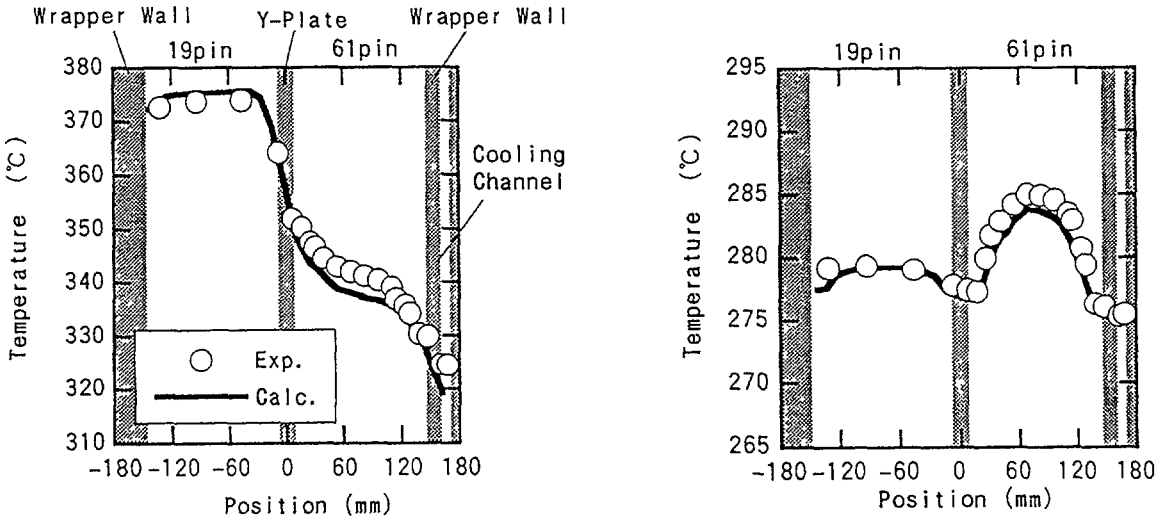

(a) Case-61A *(b) Case-61B*

FIG.3 Comparisons of temperature profiles in CCTL-CFR

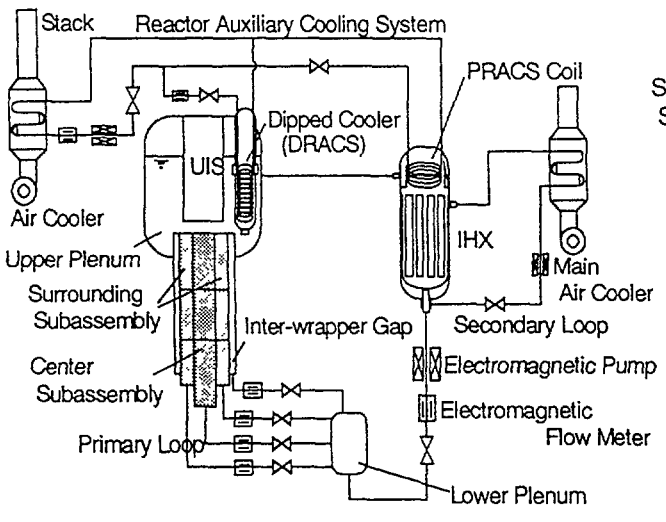

FIG. 4 Flow diagram of PLANDTL-DHX

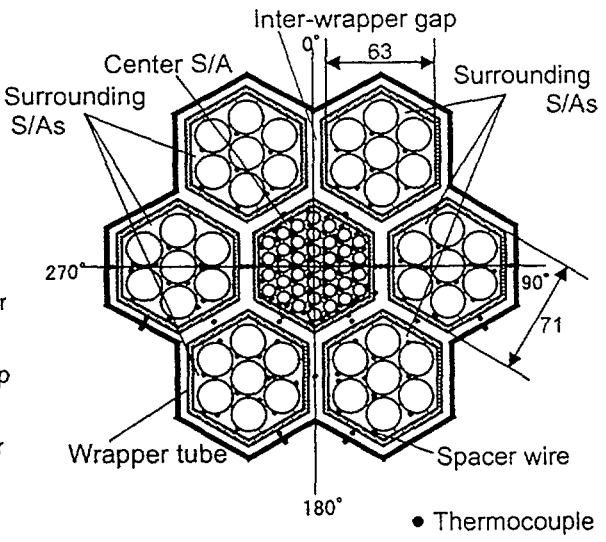

FIG.5 Horizontal cross section of the core model

the opposite side. The flow rate in each line of the three was controlled individually. The secondary circuits of the IHX and the two reactor auxiliary cooling systems had air coolers and pumps. This facility could simulate transitions from forced to NCDHR conditions in the primary and decay heat removal systems of FBRs.

The center subassembly consisted of a 37-pin bundle. And the surrounding subassemblies had 7 pin bundles in each. Every pin was heated by electrical heater. The heater pin in the center subassembly simulated a core fuel pin of a FBR in full scale. The flat to flat distance of the subassembly was about 1/2 of that of FBRs which contains 217 or 271 fuel pins. Coolant temperatures of the core model were measured by K-type thermocouples of 0.3 or 0.5 mm in diameter. The positions of thermocouples were also shown in *FIG. 5*. The signal of temperature, flow rate, and electric power of heater pins were recorded at a sampling interval of 0.096 s using a mini-computer system.

Symmetry with respect to the vertical center plane (parallel to 90°-270° line, see *FIG. 5*) of the core model was assumed on the thermal hydraulic field regarding the geometry and the boundary conditions. Again the staggered half pin mesh arrangement was applied to the core model of PLANDTL-DHX. In vertical direction, each subassembly was divided into 29 meshes for the total length of 2825 mm. And the mesh widths in the heated length were 82.5 mm or 87.5 mm. The sodium coolant in the inter-wrapper gaps were assumed to be stagnant in the calculations.

Transient behaviors in the multi subassemblies were studied under the conditions with and without inter-subassembly heat transfer. In the experiment of Case-TR43, a transient condition was given as follows. Initially, the facility was operated at 12% power and forced flow velocity corresponding to the rated condition of the real reactor. Then scram shutdown was imposed to reach 2% forced flow rate which simulated the NCDHR condition. Time trends of power and flow rates are shown in *FIG. 6*. During the transition, the flow rates and the heater powers in the all subassemblies were controlled to kept identical with each other. In this condition, therefore, no inter-subassembly heat transfer could occur.

IHX was used as a heat sink of the primary system to suppress the IWF. The IWF is also suppressed if the PRACS were applied as a heat sink. Therefore, the experiments mentioned below were characterizing NCDHR with IHXs or PRACSs.

In Case-TR49, all test conditions were set similar to that of Case-TR43 except the initial heater powers of the surrounding subassemblies. They were set lower than the center subassembly to make the surroundings outlet temperature lower by 30 °C than the center if adiabatic wrapper walls were assumed. Thus the inter-subassembly heat transfers occurred in Case-TR49.

Time trend of temperature variations are presented in *FIG. 7* at the center subchannel in the center subassembly where peak temperatures were observed. The maximum temperatures in space and time were observed at the top end of the heated section and around 150 s. in both cases. The numerical results over-predicted the maximum temperatures by 15 to 20 °C. Overall, the calculations showed good agreement with the experiments.

Figure 8 shows variations of horizontal temperature profiles at the top end of the heated section. In both cases, the prediction reproduced the change of temperature profiles well. At the start of the scram (t = 0 s), the predicted and the experimental temperature profiles are in good agreement in both cases .

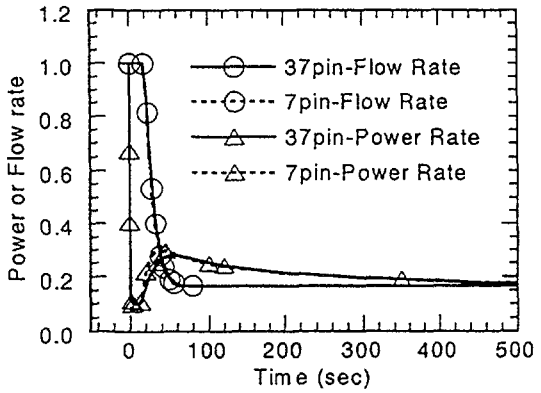

FIG. 6 Power and flow rate time trend of transition experiments

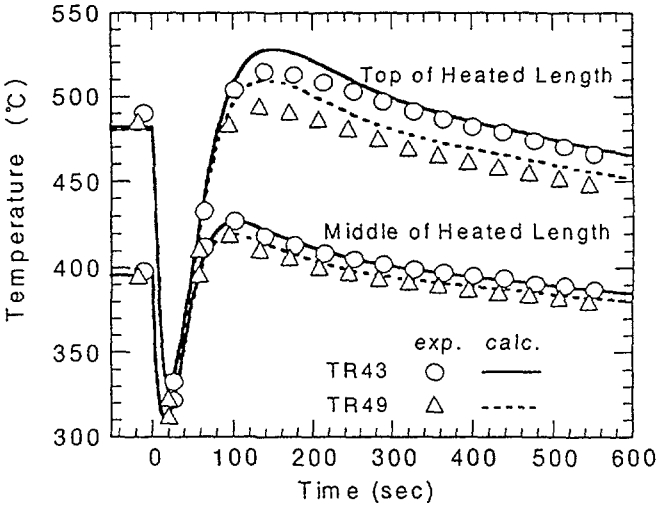

FIG.7 Time trend of temperature variations at the center subchannel in the center subassembly

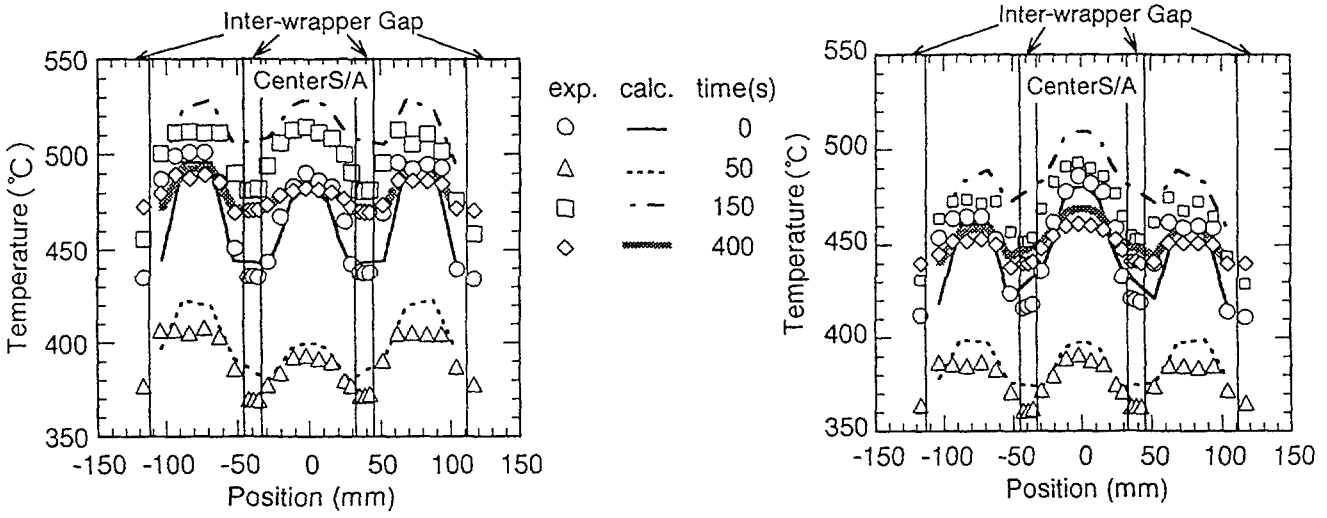

(a) Iso-temperature rise (Case-TR43) *(b) Inter-subassembly heat transfer (Case-TR49)*

FIG. 8 Variation of horizontal temperature profiles at the top end of the heated section

After 50 s from the scram, predicted temperatures were 15 to 20 °C higher than the experiments in the surrounding subassemblies. And at 150 s of both cases, the predicted maximum temperatures were over-estimated by 15 to 20 °C both in the center and the surrounding subassemblies. Temperatures in the inter-wrapper gaps also gave large deviation between the predictions and the experiments. This deviation caused the over-prediction of the maximum temperature. In the calculations, sodium in the inter-wrapper gaps was assumed to be stagnant. Although, these experimental results suggest existence of cooling effect by the IWF which was neglected in the calculations. Actually, temperature differences about 25 °C are seen between the center and outer inter-wrapper gaps at 150 s in both cases. These temperature differences may cause the IWF in reality. At 400 s, the predictions gave good agreements with the experiments of both cases.

2.2.3 Inter-wrapper flow

Some tests were performed on the IWF using PLANDTL-DHX. During first stage of the scram, i.e. the fast transient period, the IWF would show slight cooling effect as seen in the above transient tests. The cooling effect of the IWF becomes more active after the hot plenum is cooled by DHXs. Because cold coolant from the DHX penetrates into the inter-wrapper gaps. Therefore, it is important to clarify behavior of the IWF after the hot plenum is cooled: in general 1000 s after the scram and

essentially under quasi-steady states. From this point of view, we carried out the sodium test under the steady states. The 7 subassemblies were set to provide the same heater power. The DRACS removed all the thermal energy generated by the heaters except heat loss which was about 5 % of the total heater power. The test condition is listed in TABLE 3. The sampling time and its interval of temperature data acquisition were 180 s and 0.096 s respectively.

TABLE 3 CONDITIONS OF TESTS ON THE INTER-WRAPPER FLOW

Case No.	Power		Flow Rate		Inlet Temperature	Heat Sink in the Primary Loop
	(kW)	(%)	(ℓ/min/Ass.)	(%)		
I10	18.38	1.53	4.15	1.04	277.4	DHX
I05	18.38	1.52	2.06	0.52	301.9	DHX

A sector model of 180 ° was used in the calculation based on the assumption of flow field symmetry regarding geometry and boundary condition of the test section. The computational region took 7-subassembly core model and the hot plenum into account. Five of seven subassemblies were simulated by the square shaped model with their full length (see *FIG. 1*). The cross section of a subassembly was such modeled that the peripheral length of a rectangle wrapper wall in the numerical model was set equal to that of the hexagonal wrapper tube of the test rig, to simulate the heat transfer area and relative position of the subassemblies. The all subassemblies were thermally connected to the inter-wrapper gaps using the thermal structure model. In the hot plenum, the following components were modeled: DHX, UIS and outlet nozzle. For inlet boundary conditions of the primary system, the flow rate and the temperature were set at the pin bundle inlet of the subassemblies. In the DHX model, the flow rate and the inlet temperature of the secondary (i.e. auxiliary) system were provided as boundary conditions. The test condition calculated here corresponded to natural circulation flow regime. And inter-subchannel mixing plays so minor role in this flow regime, as mentioned in section 2.1.1, that no mixing correlation was used in this calculation.

Velocity fields in the vertical section of the inter-wrapper gaps are shown in *FIG. 9*. In the case of 0.5% flow rate (Case-I05), the cold coolant dived into the core barrel from the right side, went down, turned, went up and out to the hot plenum at the left side. While flow direction was entirely opposite in Case-I10. Temperature field in the core barrel was colder at the upper part and hotter at the lower part, when the IWF occurred. In such a temperature field, specific weight field of the fluid is so unstable that axially symmetrical flow was hard to be occurred unless an adequate flow shroud were installed, even the initial boundary condition was axially symmetrical. And flow direction could not be

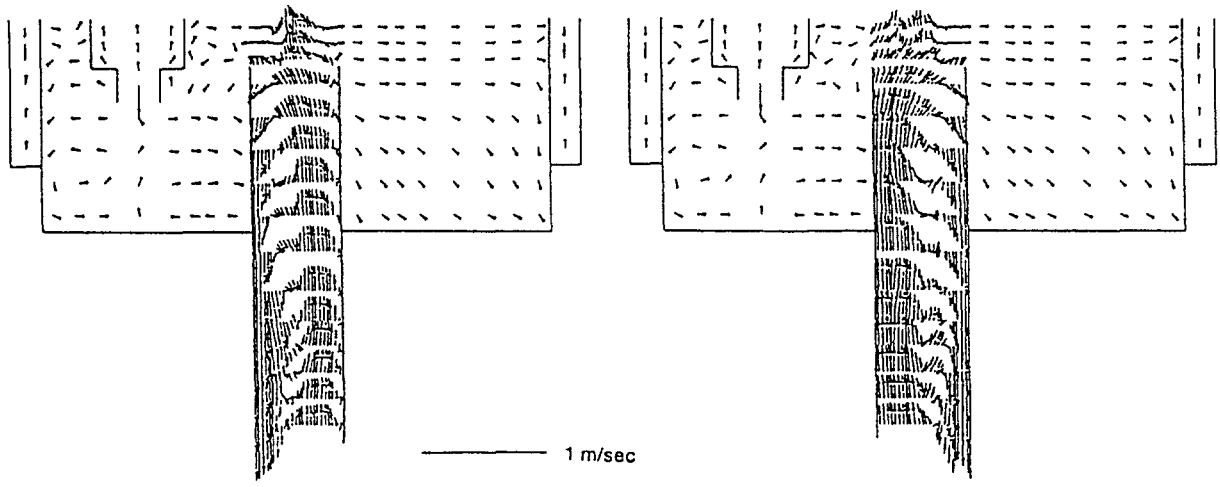

(a) Case-I10 : 1% flow rate *(b) Case105 : 0.5% flow rate*

FIG. 9 Velocity fields in the vertical section of the inter-wrapper gaps

reproduced deterministically. Figure 10 presents velocity fields in the region including the heated section. In both cases, reverse and recirculating flows were occurred inside the subassembly at the diving side of the IWF. The recirculating flow was lager in lower flow rate case. Diving depth and velocity of the IWFs were almost same in both cases. A comparison of axial temperature profile along the center subchannel in the center subassembly are shown in *FIG. 11*. Numerical data agreed well to the experiment in Case-I10. While the computation over-predicted the temperature especially in the upper part of the subassembly in Case-I05, invalidating predicted heat removal capability of the IWF. Horizontal temperature profiles at the top end of the heated section is presented in *FIG. 12*. The calculations reproduced overall features of the temperature profiles. In Case-I10, the experimental temperature was traced well by the prediction in the center subassembly. The experimental and numerical data showed differences in the outer subassemblies. However if the numerical data plots in the right and left sides of the outer subassemblies were changed, they showed fairly good agreement. In Case-I05, numerical data over-predicted the temperature. The maximum difference was seen at the left side inter-wrapper gap. This result may imply invalidity of assumption of the vertical symmetrical plane including 90° -270° line. The test section had another symmetrical plane in 120°-300° direction. Further more, in such an unstable flow field, no symmetrical plane could be expected. Therefore, strictly speaking, the IWF is essentially 3-dimensional and unsteady. This suggests the need for a time-dependent computation of full-sector core.

3. LOCAL FAULT WITH POROUS BLOCKAGES

3.1 Evaluation methods and experimental program

Local blockage issue in the subassembly is one of the most important issue of safety assessments for the fast reactor. An experimental program is under going in PNC to establish the evaluation methods for the local fault issue. The porous type blockage is assumed in the program as the most certain form of the blockage in the wire wrapped pin bundle geometry.

Computational methods have been developed to evaluate the highest temperature in the blocked subassembly. Integrity of the subassembly or the fuel pin depends strongly on the highest temperature of the structures. Two methods were developed to cover the phenomena in a subchannel scale and in a subassembly scale.

The subchannel scale phenomena inside/outside the porous blockage were calculated by a three-dimensional thermal-hydraulic analysis code, CASCADE. In the code, three-dimensional thermal conduction in a porous structure was modeled. Flow through the porous structure and heat transfer among coolant fluid, fuel pins, and porous structure were taken into account in the porous-body model.

Whole subassembly analysis was performed by an subchannel analysis code, ASFRE. It would predict the highest temperature in a blocked subassembly under actual reactor conditions. In the code, the porous blockage was also calculated by a physical model using lumped parameters of the subchannel scale, for example, an effective heat conduction coefficient. Such lumped parameters were derived from fine mesh calculations using the CASCADE code.

In the experimental program, three kinds of tests were planned in order to investigate the phenomena in a subchannel scale and in a subassembly scale. These were 4-subchannel water test, 37-pin water test, and 37-pin sodium test.

The 4-subchannel water test were carried out as a fundamental experiment to investigate the thermal-hydraulics in a porous blockage and also interaction between the inside/outside flows of the blockage. Schema of the test section is shown in *FIG. 13*. Spatial distributions of temperature and flow velocity in a porous blockage are of interests to establish a lumped model of the porous blockage and to validate the computational method of subchannel scale using the CASCADE code.

Two types of pin bundle geometry experiments were carried out using water and also sodium as working fluids. For the water and sodium experiments, the same geometry of 37-pin bundle was used. Flow field was measured in the water test. The velocity data are helpful to understand the phenomena in the sodium experiment which provides only the temperature data. These data are used to validate the subchannel analysis code, ASFRE and also the lump parameters of porous blockage.

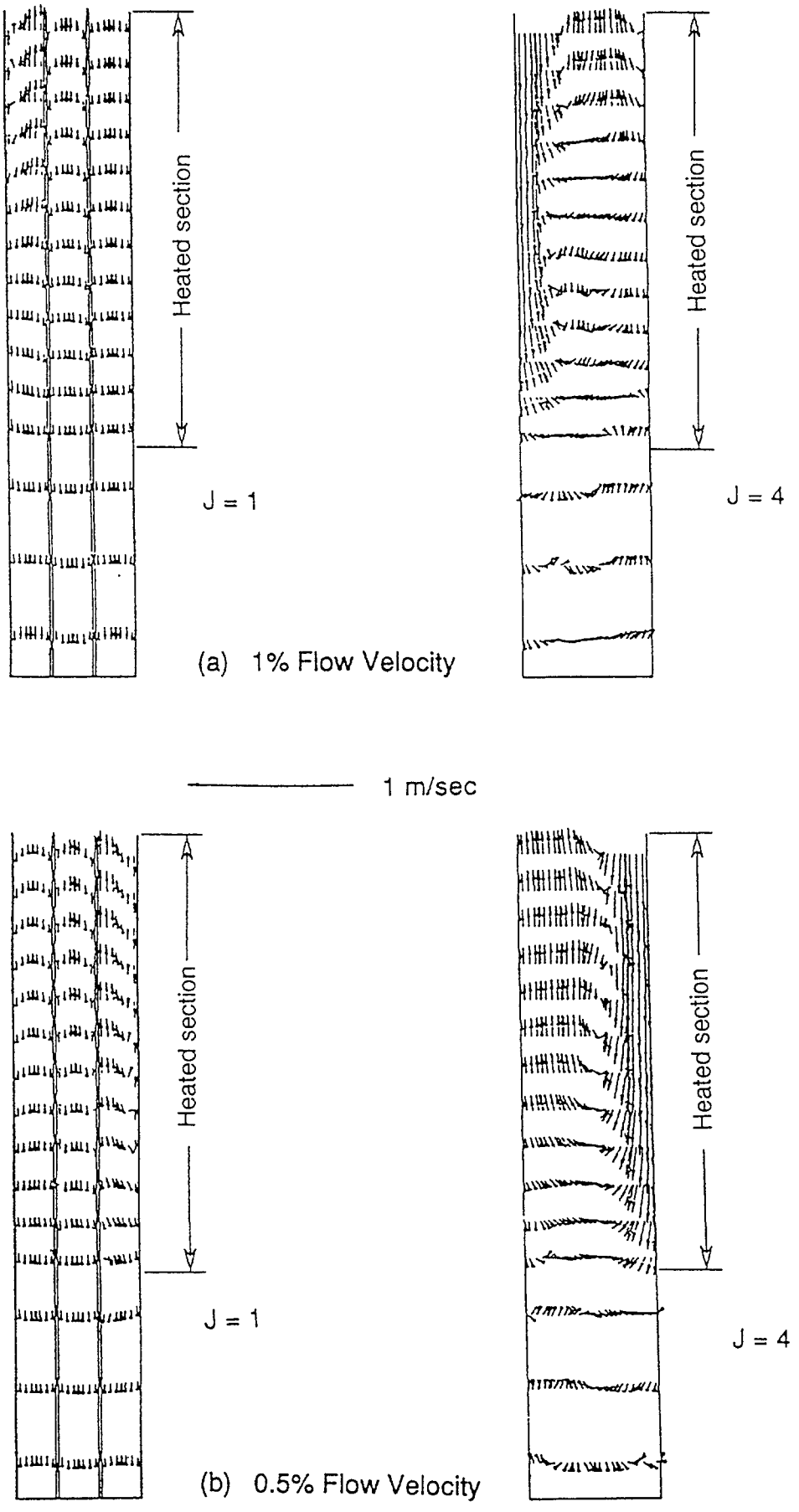

FIG. 10 Velocity fields in vertical planes at heated section of the core model

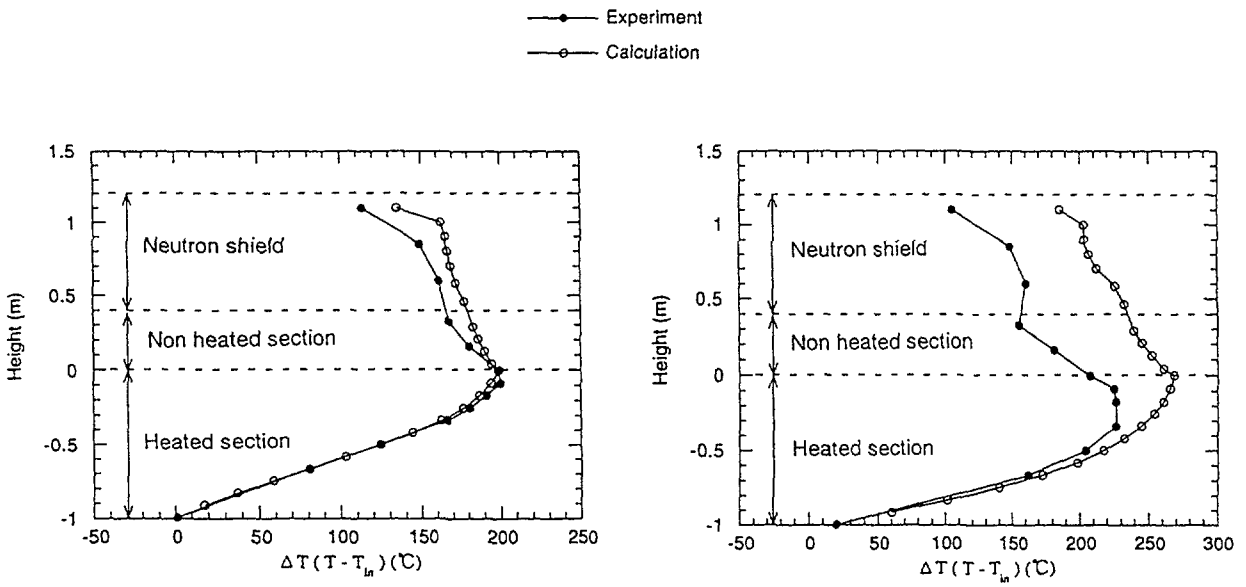

(a) Case-I10 : 1% flow rate *(b) CaseI05 : 0.5% flow rate*

FIG. 11 Comparisons of axial temperature profile along the center subchannel in the center subassembly

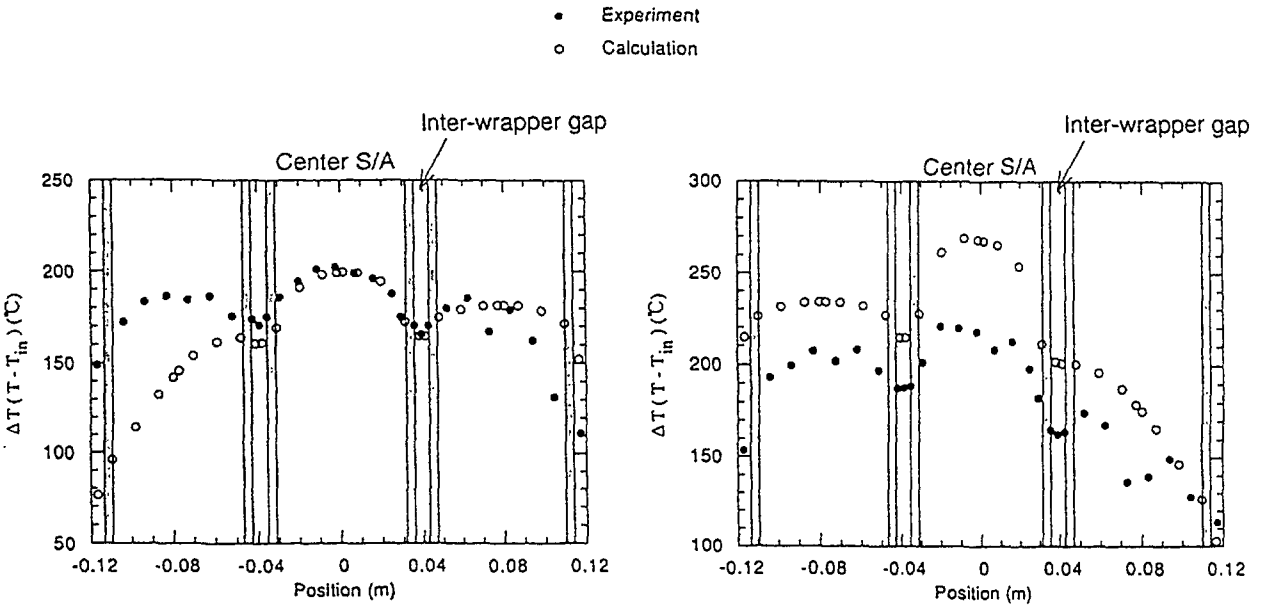

(a) Case-I10 : 1% flow rate *(b) CaseI05 : 0.5% flow rate*

FIG. 12 Horizontal temperature profiles at the top end of the heated section

3.2 Fundamental experiment

Velocity measurements in the unplugged subchannel and temperature measurements of the coolant inside/outside the blockage were made. Particular interest was the correlation between the temperature inside/outside the blockage and the flow field outside the blockage, thus revealing the heat transfer mechanism within the blockage.

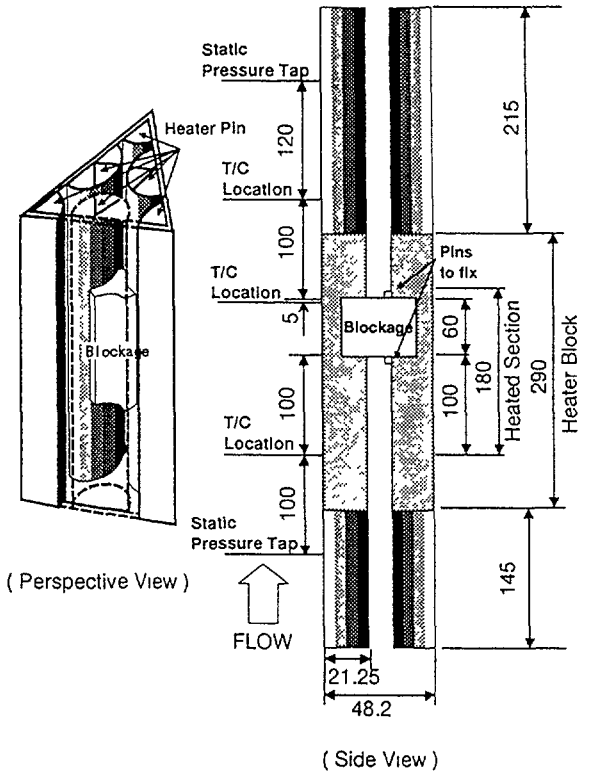

FIG. 13 Schematic view of 4-subchannel test section

In parallel, a multi-dimensional analysis modeling with CASCADE code has been developed to predict the hottest point and the maximum temperature in the subassembly. The porous blockage was modeled with porous body model introducing a volume porosity and a surface permeability of the fluid. A thermal structure model was used to calculate the heat transfer among the heater pins, the blockage and the coolant fluid. The interaction of heat transfer among these structures and the fluid was calculated by empirical correlations of wall-particles, wall-fluid, particles-fluid, and equivalent thermal conductivity of the fluid in the porous media. Turbulent and laminar calculations, i.e. calculations with and without k-ε two equation turbulence model were performed.

Comparisons of the horizontal temperature profiles are shown in *FIG. 14.* In the lower part of the blockage, the laminar calculation showed better agreement with the experiment than the turbulent one. While the turbulent calculation gave better result in the upper part. Figure 15 presents predicted distributions of temperature and flow patterns inside the porous blockage. One can see an injection into the porous media at the bottom plane. On the right hand side plane facing to the unplugged subchannel, a suction occurred in the half lower portion, and a small injection region was seen just above the suction part. Only vertical upward flow was occurred at the left hand side plane facing to the heater pin surface. The position of the maximum temperature was observed on the heater pin surface and in the blockage region. This position of hottest point implied influences of cooling due to the horizontal velocity component inside the porous media. Because temperature should rise monotonously with rise in level if only the upward axial velocity component existed. The importance of horizontal flows on the cooling was also confirmed experimentally[10]. The multi-dimensional analysis provide useful information to understand thermal-hydraulic interactions inside/outside the blockage. Nevertheless the present modeling needs more brush up in quantitative predictive capability.

3.3 Experiments with 37-pin bundles

Evaluations under the actual reactor conditions will be performed by the subchannel analyses. To validate such simulation method, pin bundle geometry experiments were planned using water and sodium as working fluids and the identical geometry of 37-pin bundle. The porous blockage is set at

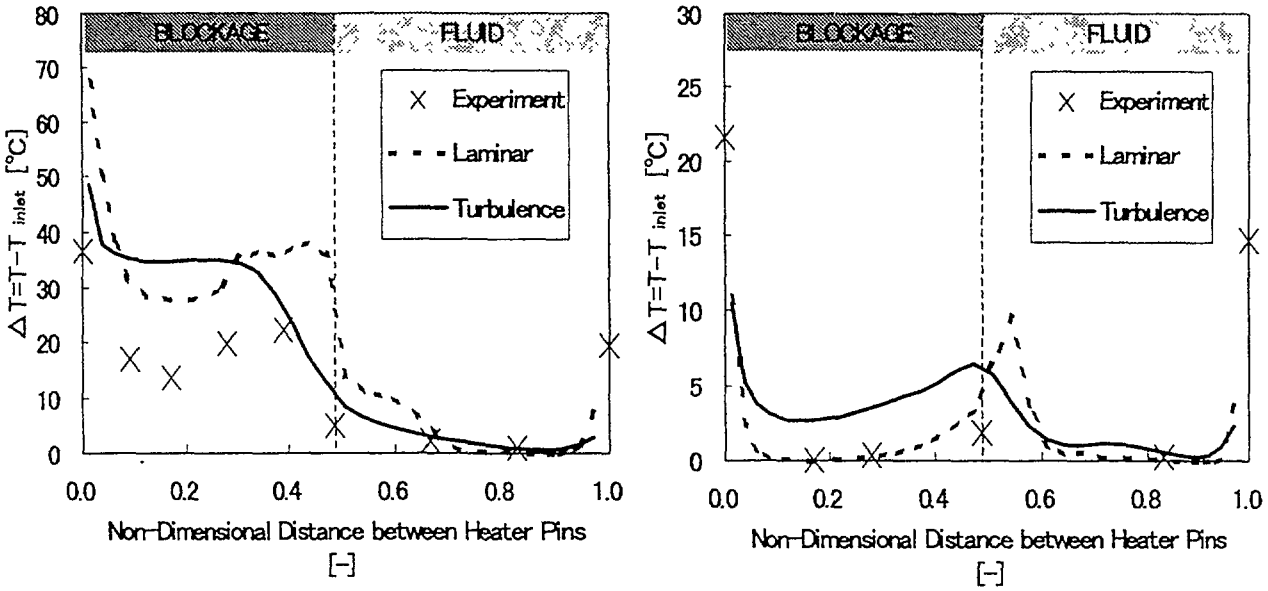

(a) Upper thermocouple location *(b) Lower thermocouple location*

FIG. 14 Comparisons of horizontal temperature profiles in 4-subchannel model

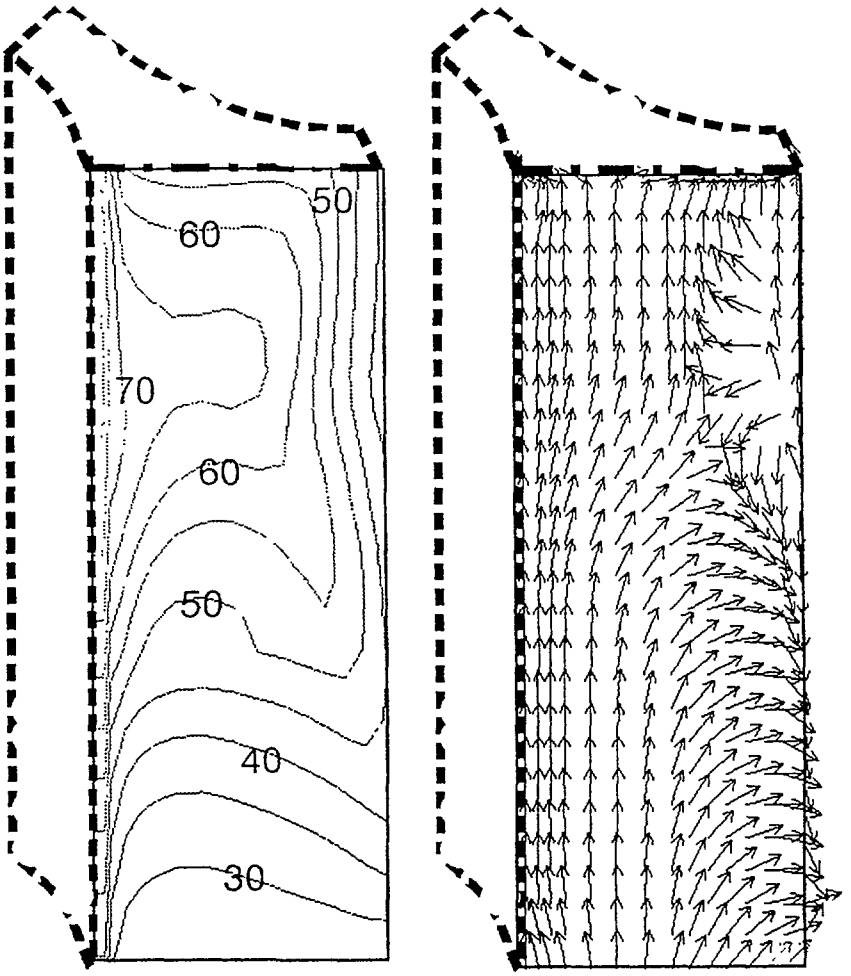

(degree centigrade) *(allows show direction only)*

(a) Contour of iso-therms *(b) Flow directions*

FIG. 15 Predicted temperature distribution and flow patterns in the porous blockage (Calculated with turbulence model)

outer most two layers of subchannels along one side of hexagonal wrapper tube. Figure 16 shows schema of the test section of sodium test. This arrangement includes a blocked subchannel surrounded by three blocked subchannel, which will have the maximum temperature due to restricted flow paths to cool the blockage.

In the water test, flow fields are measured in the subassembly, especially around the blockage, for example, a recirculation flow region downstream of the blockage. The velocity data are measured by an two-dimensional laser Doppler anemometer and ultrasonic velocity profile monitor (UVP). For fine measurements of spatial dependency, two times enlarged model is used. Influences of swirl flow due to the wrapping wires are also of interests. The wrapping wires and the blockage can be removed from the test section. The experiments are under going. The velocity data will be useful to estimate the sodium experimental results and the code validation.

The sodium test is also under going using the identical geometry of the water test with the 1/1 scale of the Japanese demonstration reactor. The wrapping wires are simulated and heated length is 0.65 m with a flat power distribution. The porous blockage is set at middle level of the heated length. The temperatures at pin surfaces covered by the blockage and the center of blocked subchannels are measured at several heights in the blockage and also in the downstream region. The experimental parameters are heater power of the simulated fuel pins and sodium flow rate in the subassembly. Preliminary tests were carried out under low power conditions. The temperature profiles including the porous blockage were successfully measured. The calculation has predicted that the maximum temperature was yielded almost upper end of the blockage. And the temperature rise from the inlet to the maximum values was essentially proportional to the ratio of heater power to flow rate. These features were also observed in the preliminary experiments.

4. ADVANCED CODES FOR CORE THERMAL-HYDRAULICS

4.1 ASFRE and SPIRAL codes - fuel subassembly thermal-hydraulics

For the design of the FBR, it is necessary to evaluate the coolant thermal-hydraulic behavior in wire-wrapped fuel-pin bundles accurately under various operational and unusual conditions, e.g. forced to natural circulation, local blockage, deformed fuel pin and so on. The simulation of thermal-hydraulics in fuel subassemblies has been generally done by using mathematically expressed empirical correlations on the basis of model parameters, i.e. engineering model. They should be determined based on experiments that reflect actual geometry and thermal-hydraulic characteristics. However,

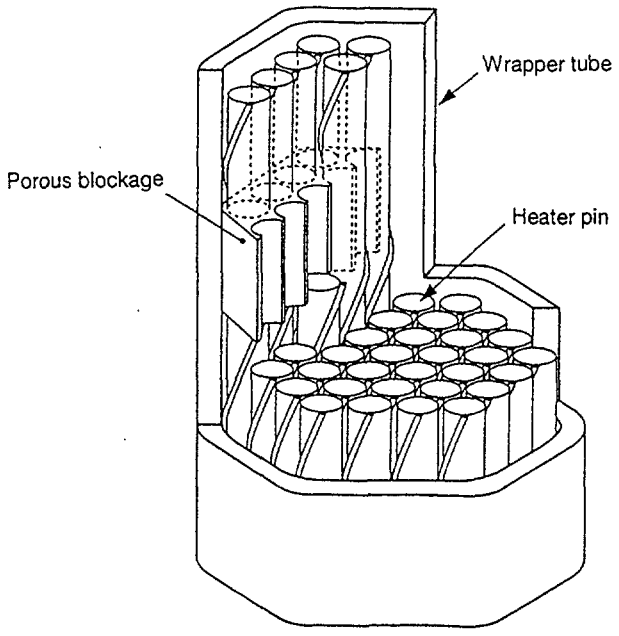

FIG. 16 Schematic test section of 37-pin sodium subassembly

measurement in sodium is not easy and the experimental cost is expensive. Direct numerical simulation could be an alternative way to determine the empirical correlation for the engineering model. From this viewpoint, two numerical methodologies are being developed and applied to the thermal-hydraulic simulation in the wire-wrapped fuel subassembly. One is a parametric method, i.e. a subchannel analysis code ASFRE that uses more empirical correlations in the physical modeling and that is applicable to large-scale fuel subassemblies such as 271-pin bundle. The other is a mechanistic numerical simulation, i.e. finite element analysis code SPIRAL that uses the least empirical correlations, if any. However, it is noted that the mechanistic approach is not feasible to solve whole 271-pin bundle fuel subassembly because of high computing cost. Therefore interactive use of the two approaches is a practical way.

ASFRE code is designed to calculate single-phase flow thermal-hydraulic phenomena in the fuel subassemblies, taking into account of the fuel pin heat conduction and heat transfer to the fluid. A triangular coordinate system is adopted in ASFRE to model the fuel bundle in accordance with the triangular pin array configuration. The finite difference equations of mass, momentum and energy conservation are derived using the standard control volume integration method based on a specific subchannel control volume. A large system of non-linear equations and the equation of state are solved based on the semi-implicit method developed Liles and Reed[11]. All equations are reduced to a set of the Newton-Raphson iteration equations in the form of a large and sparse matrix. The resulting pressure equation is solved by the Incomplete LU Decomposition Bi-Conjugate Gradient (ILUBCG) method[12]. Momentum or energy exchange between stationary solid wall and fluid and between fluids at subchannel boundaries are modeled in terms of rather simple correlations such as friction factor, wire forcing function, heat transfer coefficient, and turbulence mixing coefficients. The distributed resistance model is adopted for modeling of momentum exchange between wire-wrapped fuel pin wall and fluid[13]. The transport of momentum and energy by turbulence diffusion across the subchannel volume boundaries was considered by the effective viscosity and conductivity. ASFRE was parallelized to enhance the computational performance for large-scale pin bundle analysis. For small-size 37-pin subassembly analysis, the computation performance is found to be improved by more than 60 times of the original version on CRAY-T3D (128 processor elements).

Code verification and validation were made using the data of the following out-of-pile experiments in both sodium and water with wire-wrapped pin bundles:

1) JOYO fuel subassembly mock-up test (128-pin bundle; water) for axial pressure drop,
2) MONJU fuel subassembly mock-up test (169-pin bundle; water) for axial pressure drop and circumferential pressure distribution along wrapper tube,
3) PLANDTL test (37-pin bundle; sodium) for coolant temperature fields in nominal operation condition[14],
4) CCTL-CFR test (61-pin bundle; sodium) for coolant temperature distribution under natural circulation condition[8], and
5) Scarlet-2 test (19-pin bundle; sodium) for coolant temperature distribution under partially flow-blocked condition (porous blockage)[15].

Each calculation result showed good agreement with experimental data. Numerical and experimental pressure drops are shown in *FIG. 17*. The experimental plots were from the water tests of 128-pin (Joyo) and 169-pin (Monju) bundles. These plots were traced well by ASFRE. Figure 18 shows comparison of temperature profiles in 37-pin subassemblies of PLANDTL. One can see that the computational error was slightly larger than uncertainty of the measurement.

The finite element analysis code SPIRAL is under development for predicting local characteristics of thermal-hydraulics behavior. The flow channel is descretized using second order isoparametric elements. This code will be used to evaluate the model parameters in the empirical correlations and offer detailed data for the engineering model verification of ASFRE. The present approach aims at substituting the mock-up experiment with the computer codes regarding thermal-hydraulic prediction of FBR fuel subassembly.

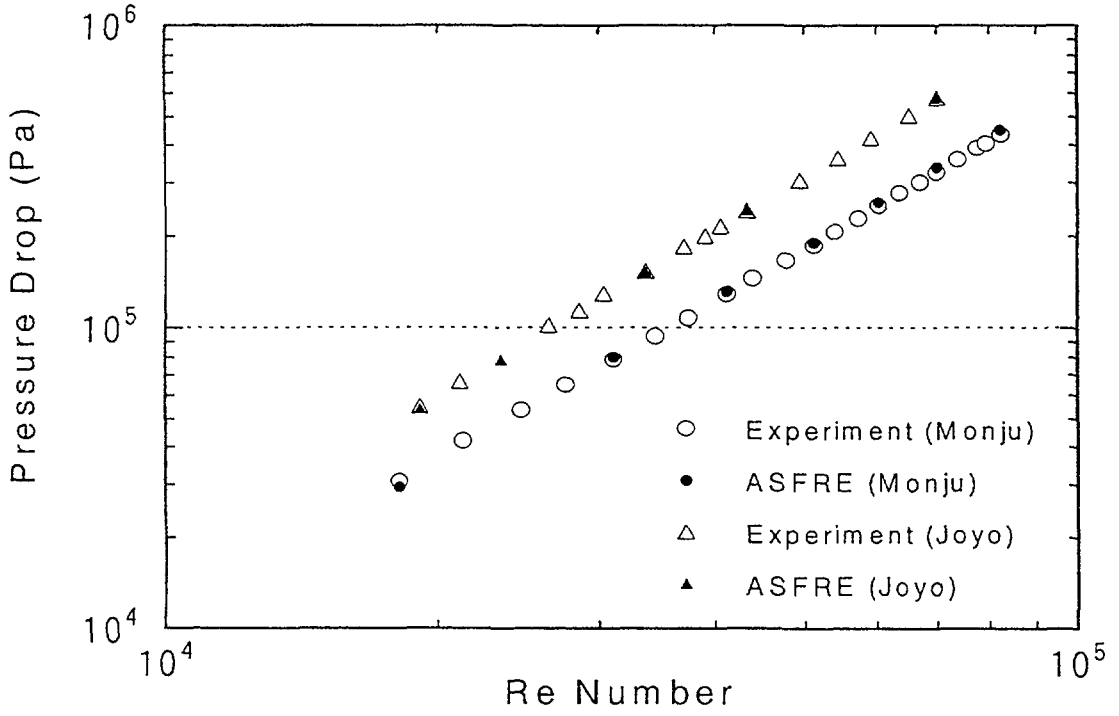

FIG. 17 Experimental and predicted pressure drop along modeled subassembly axis

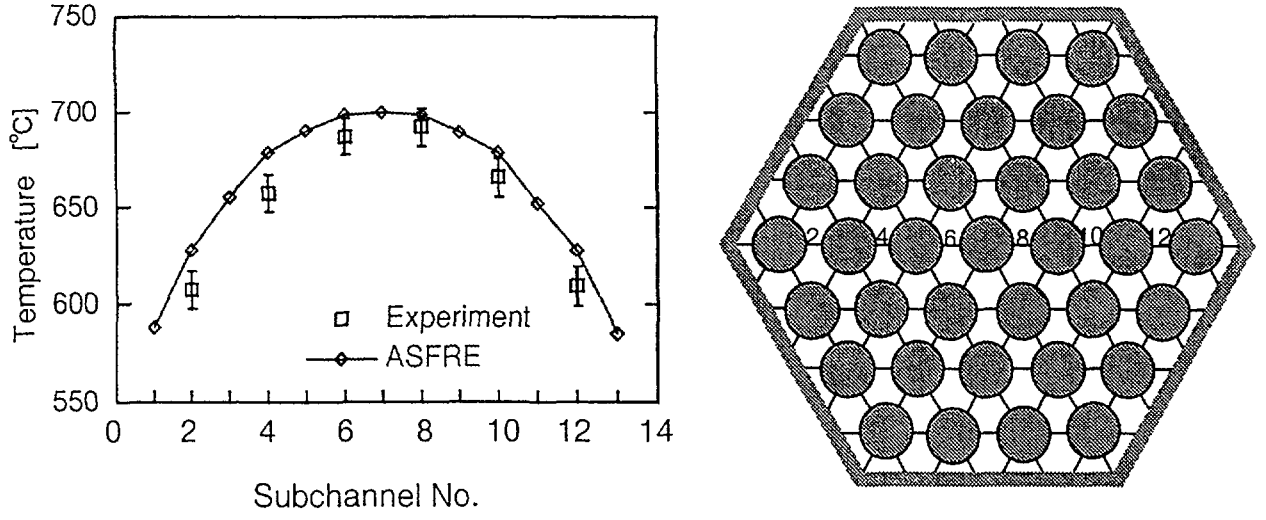

FIG. 18 Comparison of measured and predicted temperature profiles at the top end of heated section in the center subassembly of PLANDTL

4.2 Whole core thermal-hydraulic analysis code ACT

Whole core thermal-hydraulic analysis code ACT is being developed for the purpose of evaluating detailed in-core thermal hydraulic phenomena of fast reactors. For the high accurate predictive capability of the in-core thermal-hydraulics, key phenomena such as the IWF and core-plenum thermal-hydraulic interaction should be accounted for. Therefore, ACT consists of several thermal-hydraulic calculation modules related to the following regions:

1) subassemblies (fuel, blanket and control rods)
2) inter-subassembly gaps,

3) upper plenum and
4) primary heat transport system.

The subassembly module is almost equivalent to the subchannel analysis code ASFRE. The inter-subassembly gap module is used for calculating the flow and temperature fields in the gaps between the wrapper tubes (i.e. the IWF) and was also developed based on ASFRE code. The upper plenum and primary heat transport system modules are utilized to offer complicated boundary conditions to the whole-core analysis especially under natural circulation conditions with the operation of the direct reactor auxiliary coolant system. These four modules will be coupled with each other and be calculated simultaneously by using parallel computers.

The core model as the main part of ACT has been already developed by coupling the subassembly modules and the inter-subassembly gap module and it has made possible to calculate flow and temperature fields in the whole core including thermal interaction between the inner subassemblies and the inter-subassembly gaps. The coupling was made explicitly through the heat exchange on the wrapper tube outer surface from the viewpoints of flexibility to model various core geometry and program parallelization for large-scale simulation. The core model was applied to the analysis of PLANDTL-DHX sodium experiment whose test section consisted of 7 subassemblies for code verification. It was confirmed that the predicted sodium temperature distributions agreed with the measured data within the measurement error.

5. CONCLUSION

The overview was addressed on investigative activities of the fast reactor core thermal-hydraulics at PNC. The activities are mainly divided into three categories: Studies on natural circulation decay heat removal, local fault with blockage of porous media and advanced simulation codes. The status of these studies are summarized as follows.

1) Natural circulation decay heat removal
   - The numerical modeling was developed to predict thermal-hydraulic field in the subassemblies by introducing inter-subassembly mixing correlations. The modeling was validated thorough the analyses of steady and transient sodium experiment with and without inter-subassembly heat transfer. The numerical and experimental results agreed well showing that the modeling is capable of predicting the thermal-hydraulic field inside the subassembly.
   - The brick subassembly mesh arrangement was proposed to simulate the thermal interactions between inside and outside the subassemblies, especially featuring the IWF. This method could reproduce characteristics of the thermal-hydraulic field of the IWF.
2) Local fault with porous blockages
   - The strategic development has been carried out to establish a reliable evaluation method for predicting the hottest position and the highest temperature in the subassembly with porous blockages. The fundamental water test with 4-subchannel model and full-bundle with 37-pin water and sodium experiments have been performed to understand the phenomena in the subchannel scale and the subassembly scale. Also the multi-dimensional and subchannel analysis models have been developed. The multi-dimensional analysis gave useful information to understand blockage inside/outside interactions. The information from the experiments and the multi-dimensional analysis is used to derive lumped parameters and a model of porous blockage for the subchannel analysis.
3) Advanced codes for core thermal-hydraulics
   - The aims and strategies on the advanced codes development were presented. The ACT code based on subchannel code ASFRE is extended to perform whole core computation and under development to apply to the overall primary system dynamic calculation. The finite element code SPIRAL is also developed to carry out detailed simulations of the deformed bundles.

The sodium and water experiments will be performed continuously from now on to take thier advantages to develop the numerical modeling for the simulation codes. And detailed computations with the multi-dimensional codes will be also carried out to break down thermal-hydraulic phenomena

and complement the information acquired from the experiments to derive engineering models with lumped parameter for production runs of safety assessment using the codes such as ACT and ASFRE.

ACKNOWLEDGMENT

The authors are grateful to Mr. Kotake of JAPCO for useful discussion on the safety study and information on Japanese DFBR. And the authors appreciate Mr. Miyake of NDD Co. for his support for performing calculations and technicians of Joyo Sangyo Co. for their technical supports for the experiments.

REFERENCES

[1] M. Nishimura, H. Kamide, K. Hayashi and K. Momoi, "Inter-subassembly Heat Transfer During Natural Circulation Decay Heat Removal - Experimental Transient Behavior from Forced to Natural Circulation and its Multi-dimensional Analysis with Mixing Model -", Proc. of NURETH-8, Kyoto Japan, p.903, Oct. (1997).

[2] H. Ohshima and H. Ninokata, "Analysis of Thermal-Hydraulic Behavior in a Fast Reactor Fuel Subassembly with Porous Blockages," International Meeting on Advanced Reactor Safety (ARS'97), Orlando USA, (1997).

[3] Shih-Kuei Cheng, Tae Sun Ro and N. E. Todreas, "Energy Transfer Mechanism Under Mixed Convection Conditions in LMFBR Wire-Wrapped Bundles", Proc. of the 3rd Int. Topical Mtg. on Reactor Thermal Hydraulics, Newport USA, Oct. (1985).

[4] Shih-Kuei Cheng and Neil E. Todreas, "Hydrodynamic Models and Correlations For Bare and Wire-Wrapped Hexagonal Rod Bundles - Bundle Friction Factors, Subchannel Friction Factors and Mixing Parameters", Nuclear Engineering and Design, Vol. 92, pp.227-251, (1986).

[5] T. Muramatsu, "Development and application of multi-dimensional thermohydraulic code AQUA", PNC Technical Review, No. 76, Power reactor and nuclear fuel development corporation, Japan, (1990).

[6] H. Kamide, K. Hayashi and K. Momoi, "Experimental Study of Core Thermohydraulics in Fast Reactors during Transition from Forced to Natural Circulation - Influence of Inter-Wrapper Flow -", Proc. of NURETH-8, Kyoto Japan, p.922, Oct. (1997).

[7] C. Betts, M. W. Ashton, et al, "European Studies on Fast Reactor Core Interwrapper Flows", Proc. of FR'91, Kyoto Japan, p.1.15-1, Oct. (1991).

[8] H. Kamide, et al., "Inter-subassembly heat transfer during natural circulation decay heat removal of FBRs", Proc. of ICONE-3, Kyoto, Japan, S101-3, April (1995).

[9] T. S. Ro et al, "Porous Body Approach for Wire-wrapped rod bundle analysis", Proc.3rd International Topical Meeting on Nuclear Power Plant Thermal Hydraulics and Operations, Seoul, South Korea, Nov.,(1988).

[10] M. Tanaka, J. Kobayashi, T. Isozaki, M. Nishimura and H. Kamide, "An Experimental Investigation on Heat Transfer in a Subchannel with a Porous Blockage - The Influence of Flow on Temperature Distribution inside the Porous Blockage -", Proc of 5th ASME/JSME Thermal Engineering Joint Conference, (in preparation).

[11] D.R. Liles and W.H. Reed, "A Semi-Implicit Method for Two-Phase Fluid Dynamics", J. Comp. Phys., 26, 390, (1978).

[12] J.A. Meijerink and H.A. van der Vorst, "Guidelines for the Usage of Incomplete Decompositions in Solving Sets of Linear Equations as They Occur in Practical Problems", J. Comp. Phys., 44, 134, (1981).

[13] H. Ninokata, A. Efthimiadis, N. E. Todreas, "Distributed Resistance Modeling of Wire-wrapped Rod Bundles", NED, 104, pp.93-102, (1987)

[14] H. Hayafune, et al., "Out-of-Pile Experiment for Sodium Boiling in FBR Fuel Assembly", D15, 1993 Spring Mtg. of Atomic Energy Society of Japan, (1993).

[15] J. Olive and P. Jolas, "Internal Blockage in a Fissile Super-Phenix Type Subassembly: The Scarlet Experiments and Their Interpretation by The Cafca-NA3 Code", Nucl. Energy, 4, 287, (1990).

THERMAL HYDRAULIC DESIGN OF PFBR CORE

D.G. ROYCHOWDHURY, P.P. VINAYAGAM, S.C. RAVICHANDAR,
M.V. SRIDHAR RAO, G. RAVICHANDRAN, R.R. SAHU, V. PRAKASH,
S. GOVINDARAJAN, G. VAIDYANATHAN, R. PRABHAKAR, R.D. KALE,
S.C. CHETAL, S.B. BHOJE
Indira Ghandi Centre for Atomic Research,
Kalpakkam, India

Abstract

The thermal-hydraulic design of core is important in respecting temperature limits while achieving higher outlet temperature. This paper deals with the analytical process developed and implemented for analysing steady state thermal-hydraulics of PFBR core. A computer code FLONE has been developed for optimisation of flow allocation through the subassemblies(SA). By calibrating β_n (ratio between the maximum channel temperature rise and SA average temperature rise) values with SUPERENERGY code and using these values in FLONE code, prediction of average and maximum coolant temperature distribution is found to be reasonably accurate. Hence, FLONE code is very powerful design tool for core design. A computer code SAPD has been developed to calculate the pressure drop of fuel and blanket SA. Selection of spacer wire pitch depends on the pressure drop, flow-induced vibration and the mixing characteristics. A parametric study was made for optimisation of spacer wire pitch for the fuel SA.

Experimental programme with 19 pin-bundle has been undertaken to find the flow-induced vibration characteristics of fuel SA. Also, experimental programme has been undertaken on a full-scale model to find the pressure drop characteristics in unorificed SA, orifices and the lifting force on the SA.

1.0 Introduction

The primary objective of thermal-hydraulics design of the core is to ensure that adequate flow of coolant is passed through each subassembly(SA) and to determine the temperature distributions and coolant velocity distributions in the core which are inputs for structural design of core components. Methods developed for temperature distributions should be able to account for the effects of geometrical tolerances and wide ranges of operating conditions for different SA. This paper describes the various methods developed/adopted for analysing the steady state temperature distribution of PFBR core.

2.0 Coolant Flow Allocation

The power distribution in the reactor is not uniform. About 90% of the total power is generated in the fuel region, 8% in the blanket region, 0.4% in control and 0.15% in the shielding region. Again the blanket power increases with the burnup due to accumulation of fissile material while the fuel power decreases. This causes a change of radial profile from Beginning-of-life (BOL) to End-of-life (EOL). Given the total power and the average temperature rise, the total mass flow rate through the core gets fixed and this flow should be distributed to various regions such that the design criteria are met under operating conditions of individual SA. Thermal-hydraulic performance predictions for the core SA begin by calculating SA flow rates necessary to satisfy the limiting design parameters or constraints. Typical constraints are :

- the maximum cladding temperatures in the SA during steady state and transient operations must be limited to avoid premature failure;

- the maximum coolant temperature during severe transients must be limited so that wide spread coolant boiling is avoided throughout the accident and coolable geometry is maintained;
- the maximum temperature exiting the core SA and the temperature difference between the adjacent SA must be within the acceptable limits for the structural integrity of the upper core structure from thermal striping consideration;
- the maximum velocities in the SA must be limited to avoid cavitation, flow-induced vibration, erosion and corrosion problems;
- the maximum fuel, blanket, absorber temperature must be limited to avoid large scale melting during over power transients;
- the number of flow zones must be minimum for practical reasons.

The maximum cladding temperature is primarily determined by the coolant temperature rise and coolant inlet temperature. Judicious allocation of flow to each SA by orificing at the inlet of SA, makes the maximum cladding temperature in different SA nearly equal, thereby minimising the highest cladding temperature in the core for a given set of plant operating conditions. Hence, for a given total coolant flow, it is desirable to adjust the flows to the SA proportional to their power ratings to obtain the uniform outlet temperature as high as possible. Uniform outlet temperature is desirable from thermal striping considerations too. Equilibrium core rather than the first core should be taken as the basis for flow zoning[1]as

- the reactor is expected to operate at equilibrium core for more than 80% of its life time;
- at full power, the temperatures are usually lower during first-core rather than at equilibrium; and
- if necessary, operation at reduced power is possible during the initial years.

Because of different life time of fuel and blanket SA and outlet temperature of the blanket SA are not monitored, the maximum cladding temperatures in fuel and blanket SA should be set at different values. Also, the maximum cladding temperature should not exceed the maximum cladding hotspot temperatures during lifetime. While allocating the flow through each assembly, it is necessary to take into account the mixing in the SA as this factor affects the maximum temperature. Due to mixing, the average temperature of the SA improves. This can be seen from fig. 1 where temperature profiles for the central and peripheral assemblies are shown. Also, for blanket SA, where coolant flow rate is very less compared to fuel SA, inter SA heat transfer plays an important role. Hence, unless these two factors are considered while allocating the flow for a given hotspot temperature, flow through the SA will be overpredicted. Hence, a judicious estimate of these factors is necessary.

2.1 Design Criteria

1) *General*

- Power and residence time of SA shall be restricted such that the temperature difference between the two adjacent SA does not exceed 100K during its life-time;
- there shall be no cavitation even under 110% of the rated flow through the SA.

2) *Fuel SA*

- clad mid-wall hotspot temperature shall be restricted to 973K (700^{o}C) under normal operation;

3) *Blanket SA*

- clad mid-wall hotspot temperature shall be limited to 953K (680^{o}C) under normal operation.

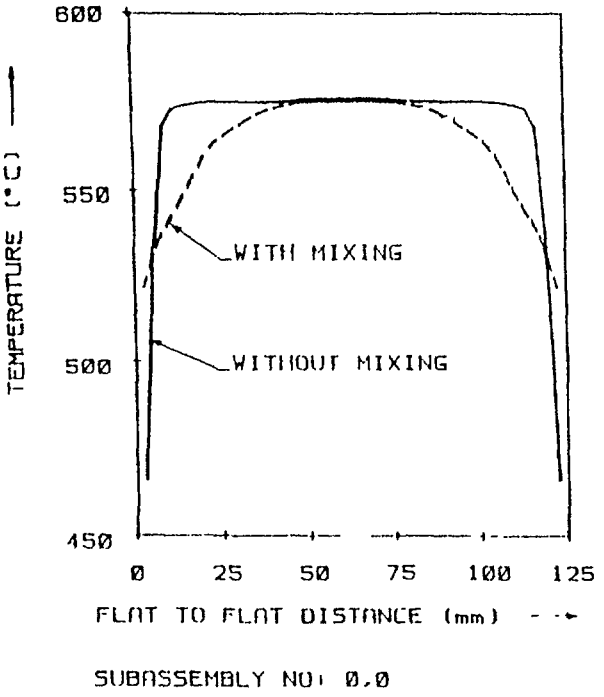

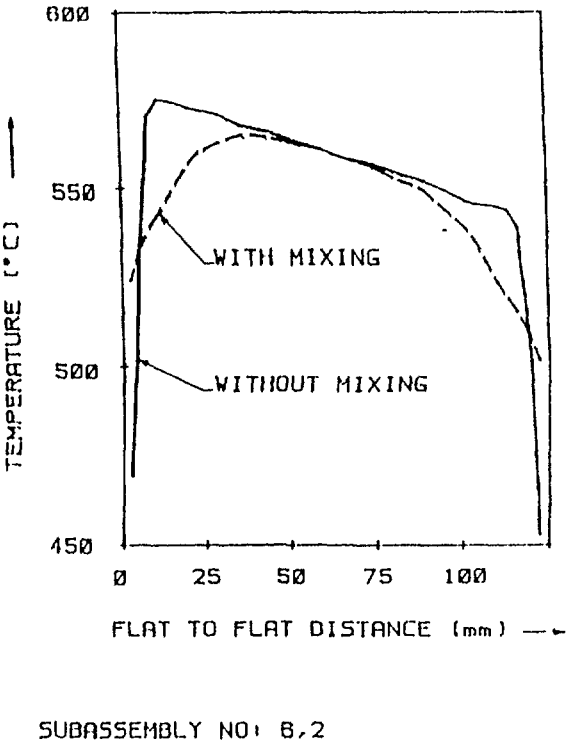

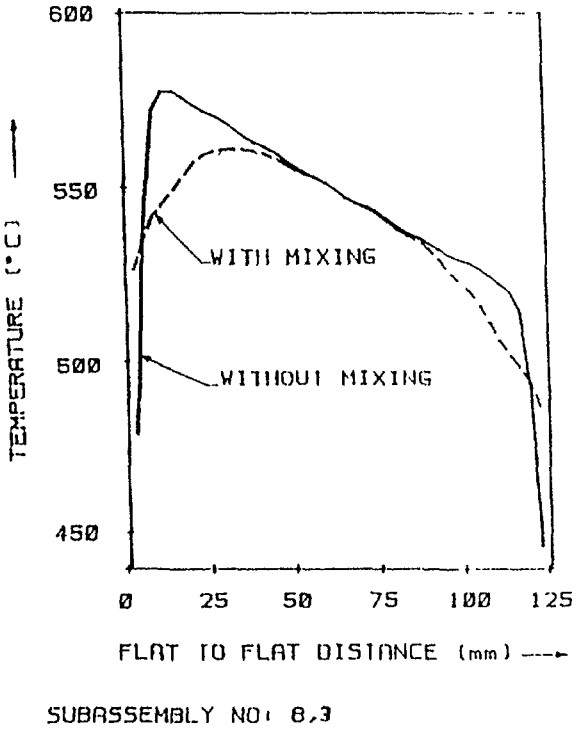

TEMPERATURE PROFILE IN THE SUB-ASSEMBLY

Fig-1

4) *CSR & DSR SA*

Flow in CSR & DSR SA shall be such that

- clad mid-wall hotspot temperature shall not exceed 953K (680°C) under normal operating conditions.
- sodium (hotspot) shall not exceed boiling point under the hypothesis that a single absorber rod is fully in the core when the reactor is operating at full power.

5) *Internal storage*

The flow in the storage locations shall be such that clad mid-wall hot spot temperature is restricted to

- 953K (680°C) under normal operating conditions;
- 1073K (800°C) under safety grade decay heat removal (SGDHR) condition.

2.2 Theoretical Background

The cladding mid-wall hotspot temperature is given by

$$T_{clad} = T_{in} + \beta_n F_{ch} \Delta T_n + \Delta T_f F_f + \frac{\Delta T_{clad}}{2} F_{cl} \qquad (1)$$

where

T_{in} = coolant inlet temperature, K
ΔT_n = average coolant temperature rise in the SA, K
β_n = ratio of maximum channel temperature rise to the average coolant temperature rise in a SA
F_{ch} = coolant hotspot factor
F_f = film hotspot factor
F_{cl} = cladding hotspot factor

For a fixed cladding mid-wall hotspot temperature the mass flow rate in each SA depends on ΔTs and hotspot factors. Once the mass flow rates in each of the SA are known, the flow zoning can be obtained by lumping the SA in such a way to satisfy

$$M = \Sigma M_n \qquad (2)$$

and

$$P = \Sigma P_n = M.\, C_P\, \Delta T \qquad (3)$$

where

P = total reactor power, W
ΔT = average coolant temperature rise in the core, K
M = total mass flow rate in the core, kg/s
P_n = maximum power of a SA
M_n = mass flow rate of a SA , kg/s
C_P = specific heat of coolant, J/kg K

2.3 Input

For fuel, the peak power of each SA is taken for deciding the mass flow rate. For blanket region, an optimisation study has been carried out to determine the blanket residence time based on design criteria.

The 30° sector of the core with peak power for fuel and blanket SA is shown in fig. 2. There are 75 positions for storage of spent fuel SA. During fuel handling operation, the maximum rated SA is put into internal storage position after 10 days after reactor shut down. The maximum decay heat power of the central SA after 10 days of shut down is 15.2 kW . While refuelling campaign is going on, if total power failure occurs, SGDHR will be in operation after 1/2 h after power failure. During this time, the core will be cooled by natural convection. So mass flow rate in storage location is based on removal of decay heat power of 15.2 kW under SGDHR condition.

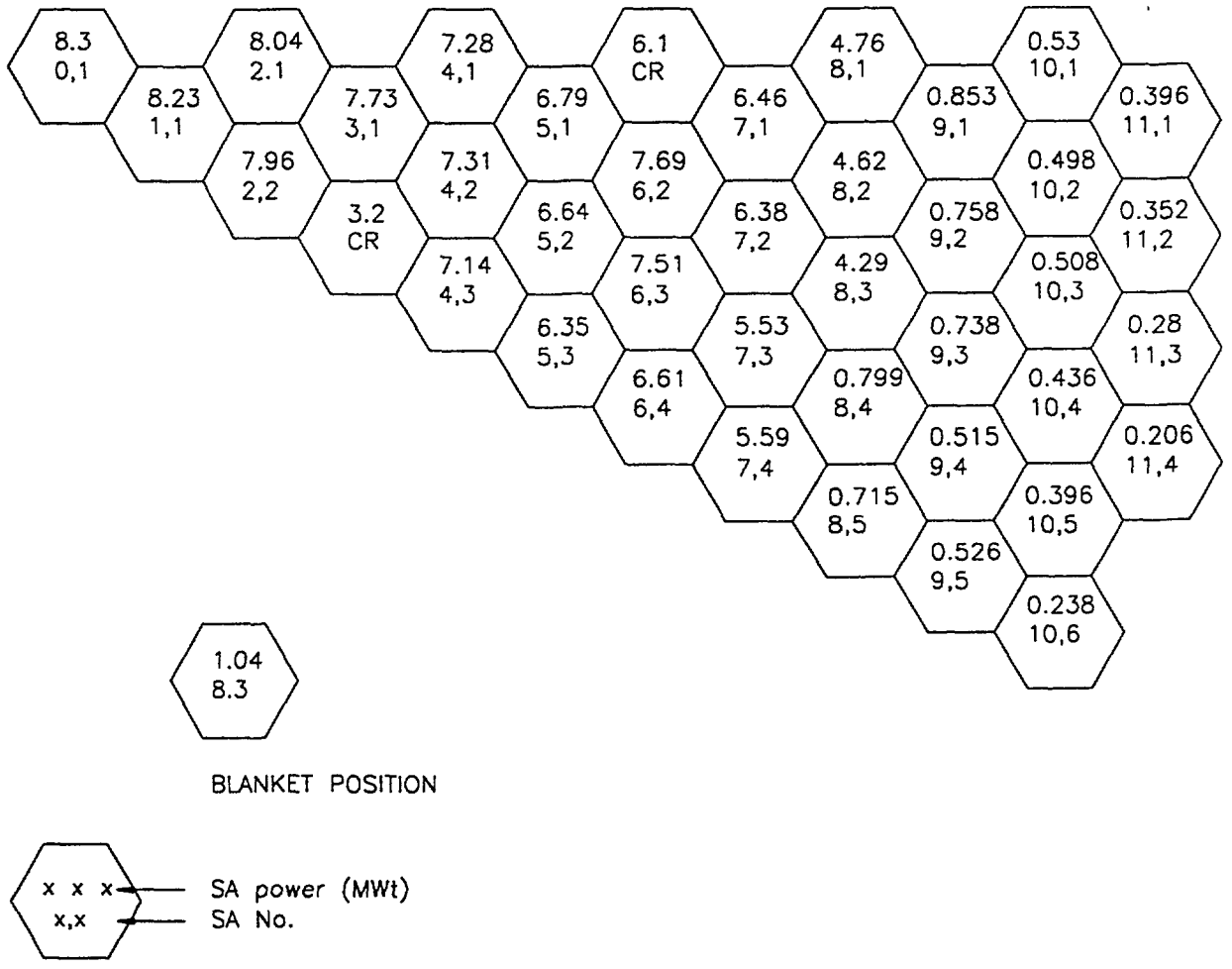

30° SECTOR OF CORE WITH PEAK POWER FOR FUEL AND BLANKET SUBASSEMBLIES

Fig.2

Uncertainty analysis has been carried out to find the hotspot factors of each type of SA. These values are given in Table - I. β_n values depend on the ratio of peak pin power to average pin power and mixing characteristics of a particular SA. These values are obtained by using **SUPERENERGY**[2] code by giving power data and a nominal flow as the input for each fuel and blanket SA. For avoiding risk of cavitation, a certain percentage of leakage flow has to be permitted through the seating of SA from the grid plate. This leakage flow is assumed to be 3% of the total flow through the core. This flow will mix with the fluid coming out of the SA at the upper plenum, thereby changing average coolant outlet temperature. Hence, the total mass flow rate through the core has been calculated in such a way that mixed mean temperature rise at the core outlet becomes 150K.

2.4 Analysis

For determining the mass flow rates in each SA a computer code **FLONE** has been developed. The flow diagram of this code is given in fig. 3.

Table- I Hot Spot Factors

Type of SA	Hot Spot Factors		
	Coolant, F_{ch}	Cladding, F_{cl}	Film, F_f
Fuel	1.2118	1.4213	2.3919
Blanket	1.3346	1.4650	5.1684
CSR & DSR	1.3209	1.5680	5.8233
Reflector & Shielding	1.3127	1.6852	5.9401
Internal storage	1.3127	1.6852	5.9401

The code starts with calculation of the minimum flow required for each SA so as not to exceed the limiting temperatures once the inputs are given. Thus for a given power generation, the limiting flow is uniquely determined for each SA. It may be noted that about 1.06 % of total SA power is generated in the upper axial blanket region. Although this power will contribute to the SA outlet temperature rise, it will not have any effect on the maximum clad mid-wall temperature.

The code then calculates the minimum mass flow rate through the core that would satisfy the temperature limits. This flow is found to be 5882.91 kg/s. However, for a reactor outlet temperature rise of 150 K and power level of 1253 MWt, flow rate is 6407 kg/s which is the available flow through the core. Thus it is possible to reduce the number of flow zones. The SA having nearly equal power are grouped together to form a flow zone and the total mass flow rate through the core for a particular flow zone scheme is compared with the available flow to decide the number of flow zones.

Also, during optimising of the number of flow zoning, it was observed that the fuel region need not always be lumped first and then the blanket region. In fact from Table- II, it can be observed that for increase in total number of flow zones from 8 to 9, benefit in increasing the number of flow zones in blanket region is better than increasing flow zones in other regions. By having 2 zones in blanket, the minimum total mass flow rate is obtained. The optimised flow zones thus obtained is shown in Table- III.

2.5 Rationalisation of Flow zones

From Table- III, it can be seen that the difference in mass flow rates between zone number 3 and 5 is very small. Since the mass flow rates through each SA are to be achieved by orificing, rationalisation of mass flow rates through the above zones becomes necessary to simplify the orifice design. After rationalisation the flow in each flow zone is shown in Table- IV. It can be seen that total mass flow rate required is 6388.83 kg/s against the available mass flow rate of 6407 kg/s. Hence, the number of flow zones has been fixed at 15. With these flow rates, temperature distributions in the core have been carried out. The power, flow and temperature distributions for BOEC are shown in figs. 4 and 5. Also the temperature rise in each zone is shown in Table V.

3.0 Orificing

For designing the orifice in each SA so that the required flow rates can be allocated, it is necessary to determine the pressure drops through each SA in each zone. For pin-bundle pressure drop, a comparison has been made with various correlations. This is shown in fig. 6. Based on this study, Cheng's correlation [3] is used as it covers a wide range of Reynolds

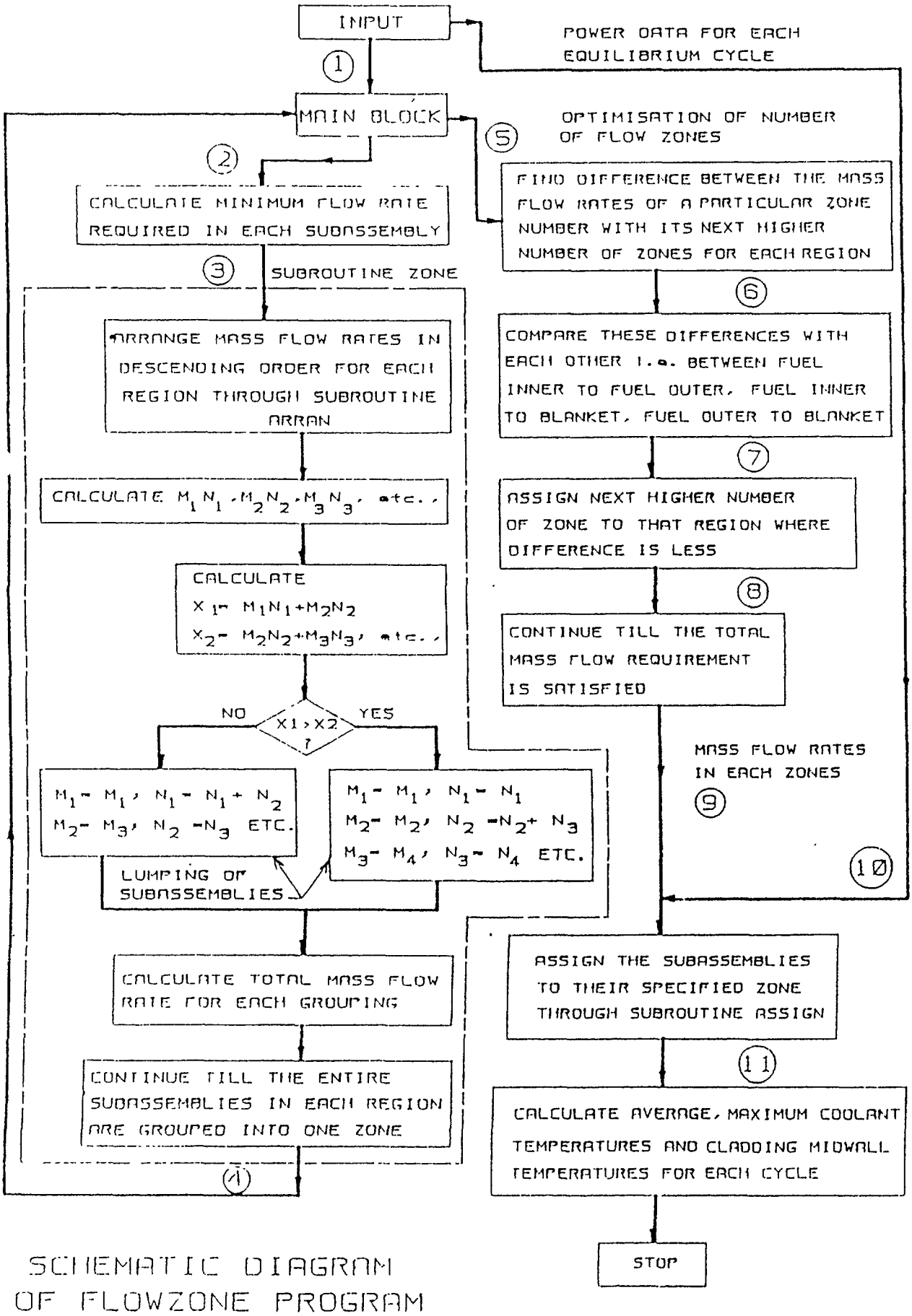

SCHEMATIC DIAGRAM OF FLOWZONE PROGRAM

Fig-3

number, pin pitch-to-diameter ratio and wire-wrap pitch-to-diameter ratio. The pressure drops in fuel and blanket SA in each zone have been calculated by a computer code **SAPD** and are shown in Table VI. Since the pressure drop in CSR&DSR, reflector and shielding SA is very small, it is felt that the entire pressure drop is to be achieved outside of the SA. However, the final design will depend on the results of hydraulic experiments.

4.0 Effect of Surface Roughness and Tolerances

The effect of tolerances is to reduce the channel area and thereby increase the pressure drop. Also, the pin-bundle pressure drop will be affected by surface roughness. Normally, these effects are taken care of through the hot spot factors. However, it was found that a

Table- II Optimisation Scheme

Total no of Flow zones	No. of Flow Zones in each region						Minimum required Flow rate to meet Design criteria (kg/s)
	Fuel		Blanket	CSR & DSR	Shielding & Reflector	Internal Storage	
	inner	outer					
8	1	2	1	1	1	1	7346.50
9	1	2	2	1	1	1	7059.15
10	2	2	2	1	1	1	6819.85
11	2	3	2	1	1	1	6628.20
12	3	3	2	1	1	1	6547.80
13	3	4	2	1	1	1	6484.75
14	3	4	3	1	1	1	6428.31
15	3	4	4	1	1	1	6385.67

Table- III Flow zoning before Rationalisation

Region	SA Type	Zone no.	Mass flow per SA (kg/s)	Total no. of SA in the zone	Total mass flow in the zone (kg/s)	Min. required flow rate to meet design criteria (kg/s)
1	Fuel inner	1	35.83	31	1110.73	6385.79
		2	31.40	24	753.60	
		3	28.72	30	861.60	
2	Fuel outer	4	34.07	24	817.68	
		5	28.80	30	864.00	
		6	25.30	18	455.40	
		7	20.82	24	499.68	
3	Blanket	8	5.46	6	32.76	
		9	4.42	54	238.68	
		10	3.18	48	152.64	
		11	2.64	78	205.92	
4	CSR &DS	12	2.55	12	30.60	
5	Reflector	13	0.3	72	21.60	
6	Shielding	14	0.3	69	20.70	
7	Storage	15	3.88	75	285.00	

reduction in the uncertainty in flow through the SA leads to a gain of 1.5 - 1.8 K in coolant temperature. Hence, a study was carried out to determine effect of tolerances on the flow through the SA as well as in the channel. For the analysis, maximum tolerance on the wrapper inside width-across-flats (WAF) and statistical variation of tolerances for 3σ deviations on 217 pin outer diameter and wire diameter was considered. The uncertainty value for flow through SA was found to be 5% . The pressure drop was found to increase by ~4%.

Table- IV Flow zoning after Rationalisation

Region	SA Type	Zone no.	Mass flow per SA (kg/s)	Total no. of SA in the zone	Total mass flow in the zone (kg/s)	Min. required flow rate to meet design criteria (kg/s)
1	Fuel inner	1	35.83	31	1110.73	6388.83
		2	31.40	24	753.60	
		3	28.80	30	864.00	
2	Fuel outer	4	34.10	24	818.40	
		5	28.80	30	864.00	
		6	25.30	18	455.40	
		7	20.82	24	499.68	
3	Blanket	8	5.46	6	32.76	
		9	4.42	54	238.68	
		10	3.18	48	152.64	
		11	2.64	78	205.92	
4	CSR &DSR	12	2.55	12	30.60	
5	Reflector	13	0.3	72	21.60	
6	Shielding	14	0.3	69	20.70	
7	Storage	15	3.88	75	285.00	

Total mass flow rate allowed for average
core outlet temperature rise of 150 K = 6407 kg/s.

Table - V Temperature distribution for BOEC

Region	Zone	Mass flow (kg/s)		Power (MWt)		Temp rise, K	
		Each zone	Total	Each zone	Total	Each zone	Total
1	1	1110.73	2728.33	243.74	609.62	173.4	176.5
	2	753.60		170.88		179.1	
	3	864.00		195.00		179.3	
2	4	818.40	2637.40	176.52	559.38	170.6	167.6
	5	864.00		186.24		179.3	
	6	455.40		91.02		157.9	
	7	499.68		105.60		167.0	
3	8	32.46	630.00	6.21	61.93	149.7	77.7
	9	238.68		32.45		107.5	
	10	152.64		13.50		69.8	
	11	205.92		9.77		37.5	

Table - VI Pressure Drop in SA

SA Type	Zone no	Mass flow (kg/s)	Bare SA pressure drop (m of Na)	Additional Pressure drop required (m of Na)
Fuel	1	35.83	58.11	0.0
	2	31.40	45.80	12.31
	3	28.80	39.19	18.92
	4	34.10	53.17	4.92
	5	28.80	39.19	18.92
	6	25.30	31.07	27.04
	7	20.82	21.98	36.11
Blanket	8	5.46	12.86	45.25
	9	4.42	8.37	49.74
	10	3.18	4.44	53.67
	11	2.64	3.04	55.07
CSR & DSR	12	2.55	0.93	57.18
Reflector	13	0.30	~ 0.0	~ 58.11
Shielding	14	0.30	~ 0.0	~ 58.11
Storage	15	3.80	1.0	57.11

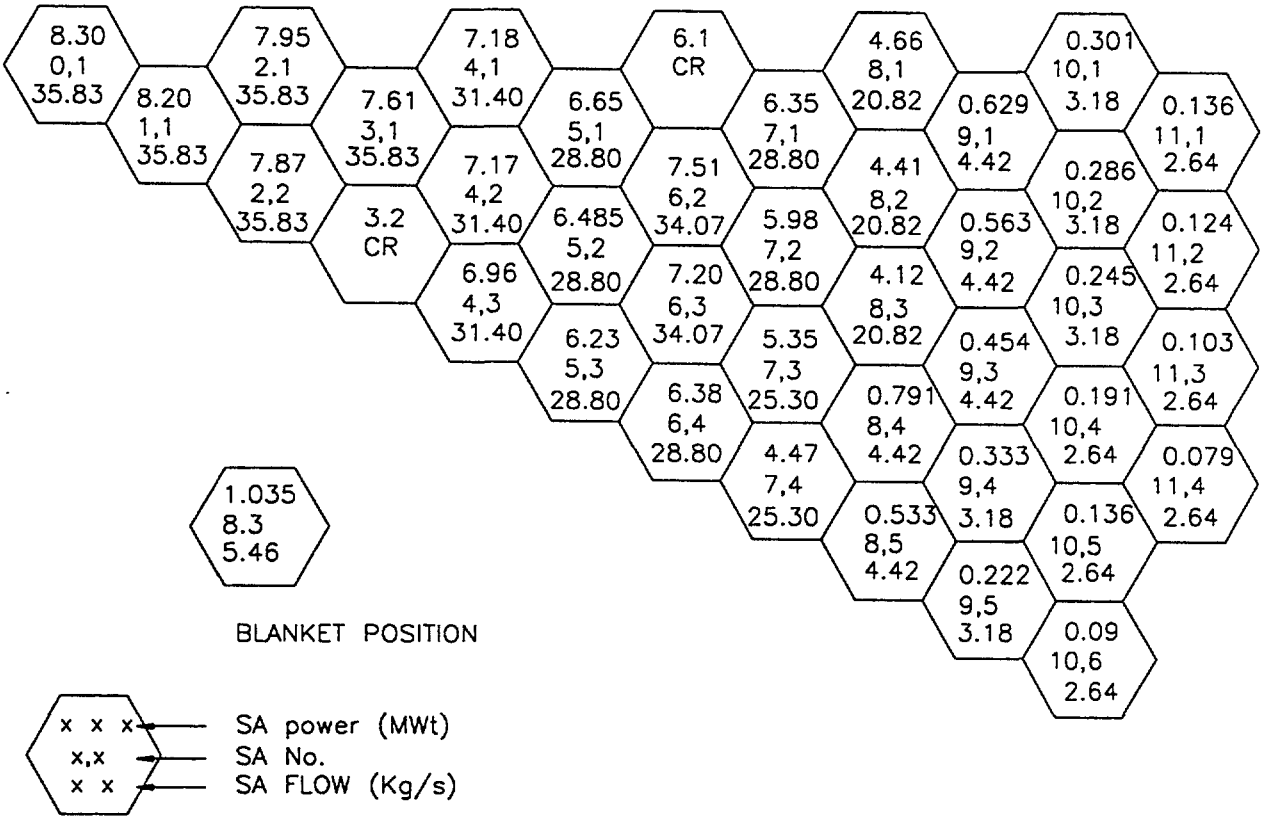

POWER AND FLOW FOR BOEC

Fig.4

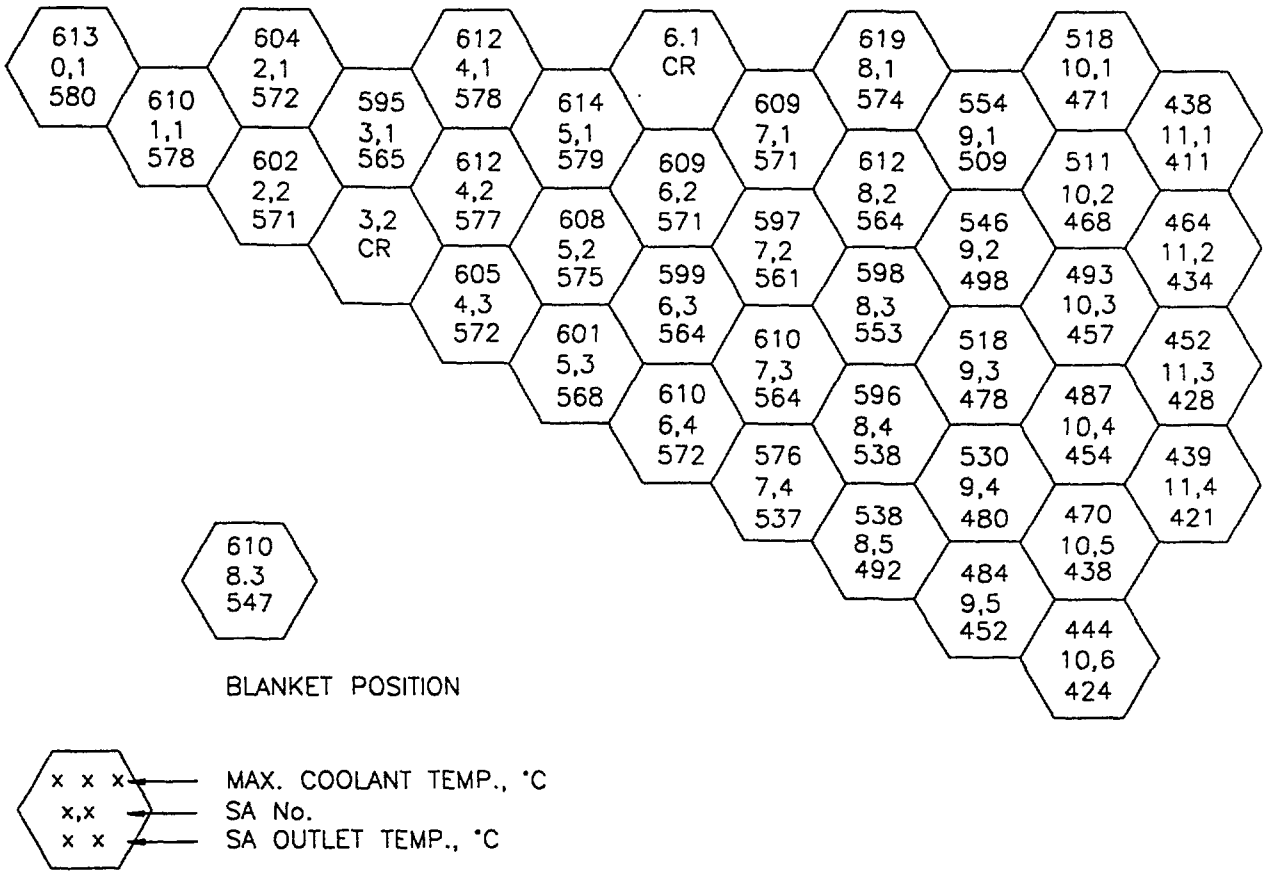

COOLANT TEMPERATURES FOR BOEC

Fig.5

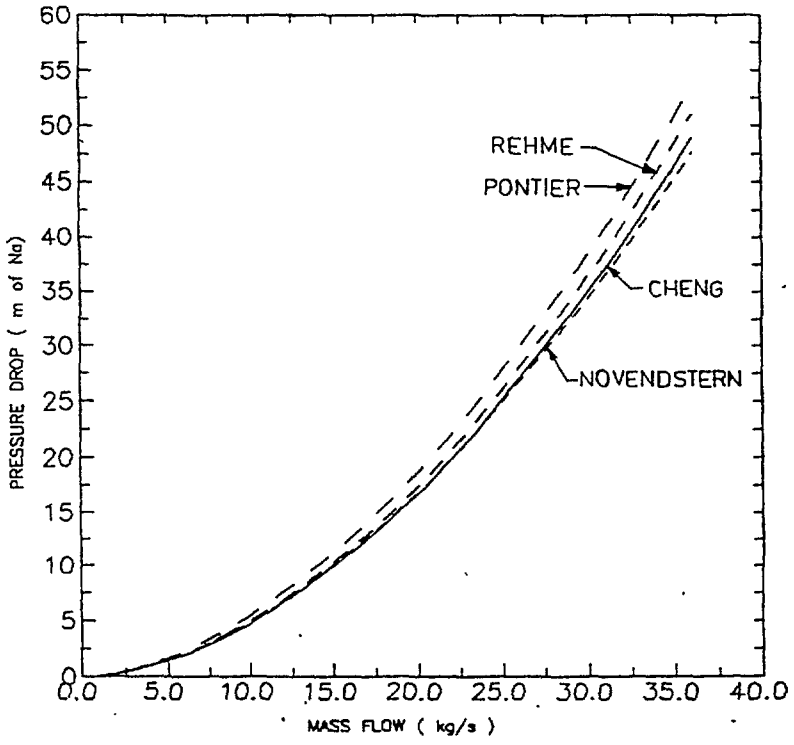

Fig. 6 – COMPARISON OF BUNDLE LOSS FOR PFBR

Normally the pressure drop correlations are based on friction correlation for smooth pipe for which the surface roughness is ~ 0.2 μm. By using Pontier's correlation [4] it was observed that the pin-bundle pressure drop for nominal geometry increases by 3.28% for increase in surface roughness from 0.2 μm to 0.6 μm. The combined effect of tolerance and surface roughness was 7.8% increase in pressure drop from the nominal configuration.

5.0 Effect of Spacer Wire Pitch

Selection of spacer wire pitch depends on the pressure drop, flow-induced vibration and the mixing characteristics. As the spacer wire pitch reduces, pressure drop increases, flow-induced vibration reduces and better mixing takes place, thereby reducing the clad mid-wall temperature. Hence, a parametric study was made for optimisation of the spacer wire pitch for the fuel SA. The study has indicated that there is practically no effect on mixing and vibration strain for wire-wrap pitches from 150 mm to 250 mm. However, the saving in pumping power because of the lower pitch is appreciable. This is shown in Table- VII.

Table VII Effect of spacer wire pitch on some SA parameters

Pitch (mm)	Bundle pressure drop (m of Na)	Clad hot spot temperature K	Pin vibration		
			Displacement x 10^{-3} (mm)	Stress (MPa)	Strain x 10^{-6}
150	49.0	~ 970	3.4	0.76	4.76
200	43.0	970	8.2	1.04	6.48
250	39.4	971	16.3	1.32	8.24

At present, top axial shield is of solid block type. However, as an alternative, Pin-bundle type may also be considered as this concept offers better homogeneity, larger B_4C volume fraction and ease of fabrication. Also, the outlet temperature of the coolant will be more uniform due to better mixing in the bundle concept. But the pressure drop for the pin-bundle concept was found to be 6.5 m of Na compared to 1.12 m of Na for solid block concept. This increase in pressure drop can be compensated by choosing wire-wrap pitch of 200 mm for the fuel SA. However, the final choice will be made after evaluation of the behaviour of the totally/partially blocked SA during natural convection.

6.0 Core Wide Temperature Distribution

Once the coolant flow allocation to each core SA has been determined, it is necessary to find out the coolant flow and temperature distributions in the core. This is required to accurately predict the clad mid-wall temperatures of all SA. For this calculation, **SUPERENERGY**[2] code was used for analysing the fuel and blanket SA as this code takes care of the inter-assembly heat transfer into account, important especially for peripheral SA(blanket).

7.0 R & D Activities

As part of the design evaluation of PFBR SA, Hydraulic and Flow Induced Vibration (FIV) studies on dummy full scale SA and on 19 pin-bundle model in water are in progress.

7.1 Flow Induced Vibration Studies on 19 Pin Model

The fuel SA of PFBR consists of 217 fuel pins wrapped with spacer wire. The sodium flow velocity in the fuel bundle region is about 7.6 m/s. The turbulent flow in the bundle region can excite vibration of fuel pins. The induced vibration leads to fretting and wear

causing failure of pin. Pin vibration amplitude decreases with decrease of spacer wire pitch. Hence, experimental studies were conducted on a 19 pin-bundle to optimise spacer wire pitch.

The model consists of 19 dummy fuel pins contained inside a hexagonal sheath and stainless steel pellets are used in place of fuel pellets. Preliminary studies were conducted with 19 pin-bundle with 6.6 mm outer diameter and 1.65 mm wire diameter and up to a maximum velocity of 9.88 m/s. The spacer wire pitch was varied from 150 to 250 mm. The test set up is shown in fig. 7. Pin vibration was measured with strain gages mounted axially on the pin outer surface which respond to bending strain. The strain gages were located at mid point of third span from bottom. Required test flow velocity was arrived at using Burgreen correlation. The experimental results were compared with the analytical results. It was concluded that for 200 mm spacer wire pitch, overall strain rate are below the permissible values from both fatigue and fretting wear consideration. With 250 mm spacer wire pitch, the measured overall

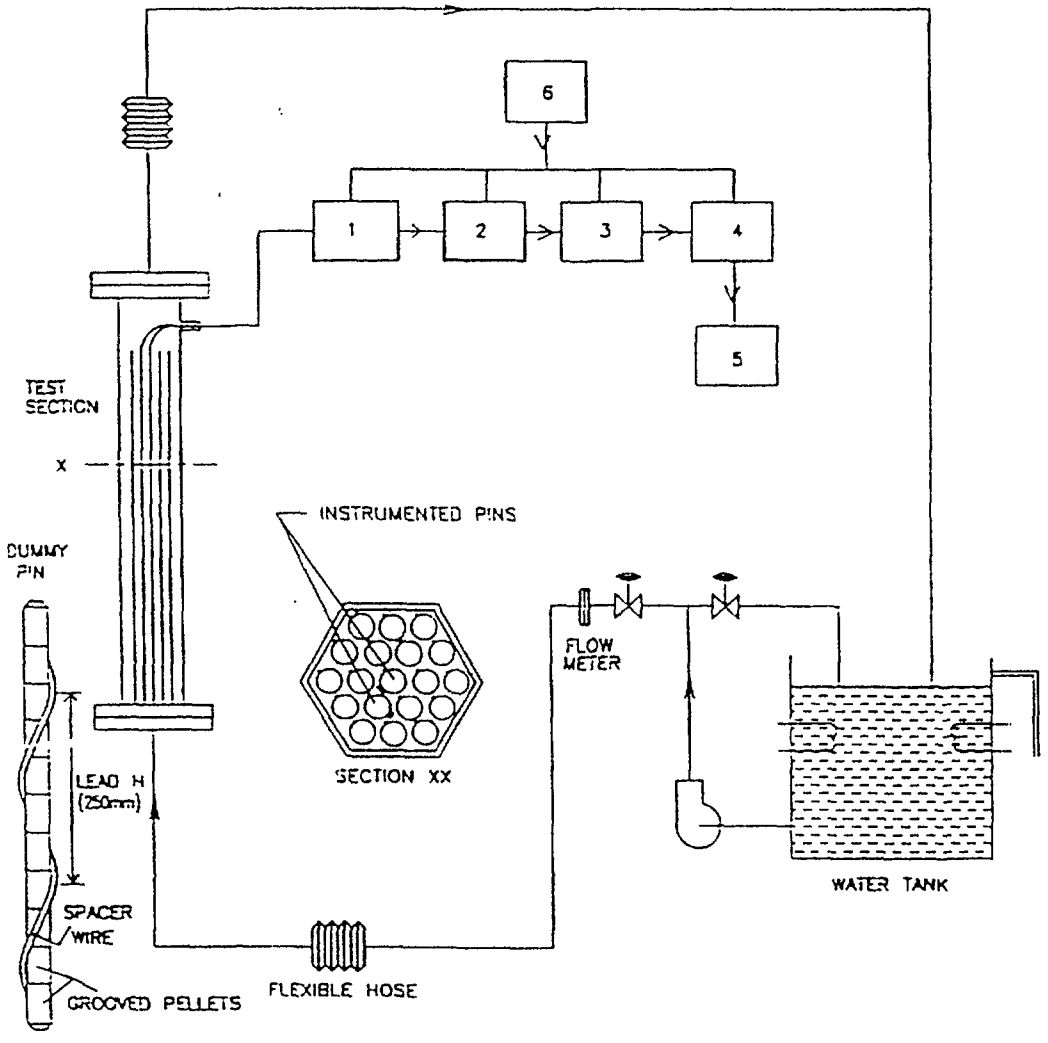

1. Conditioning amplifier 2. High pass filter 3. Low pass filter

4. Oscilloscope 5. Signal Analyzer 6. Power supply unit

Fig. 7 EXPERIMENTAL SET-UP FOR FIV TEST

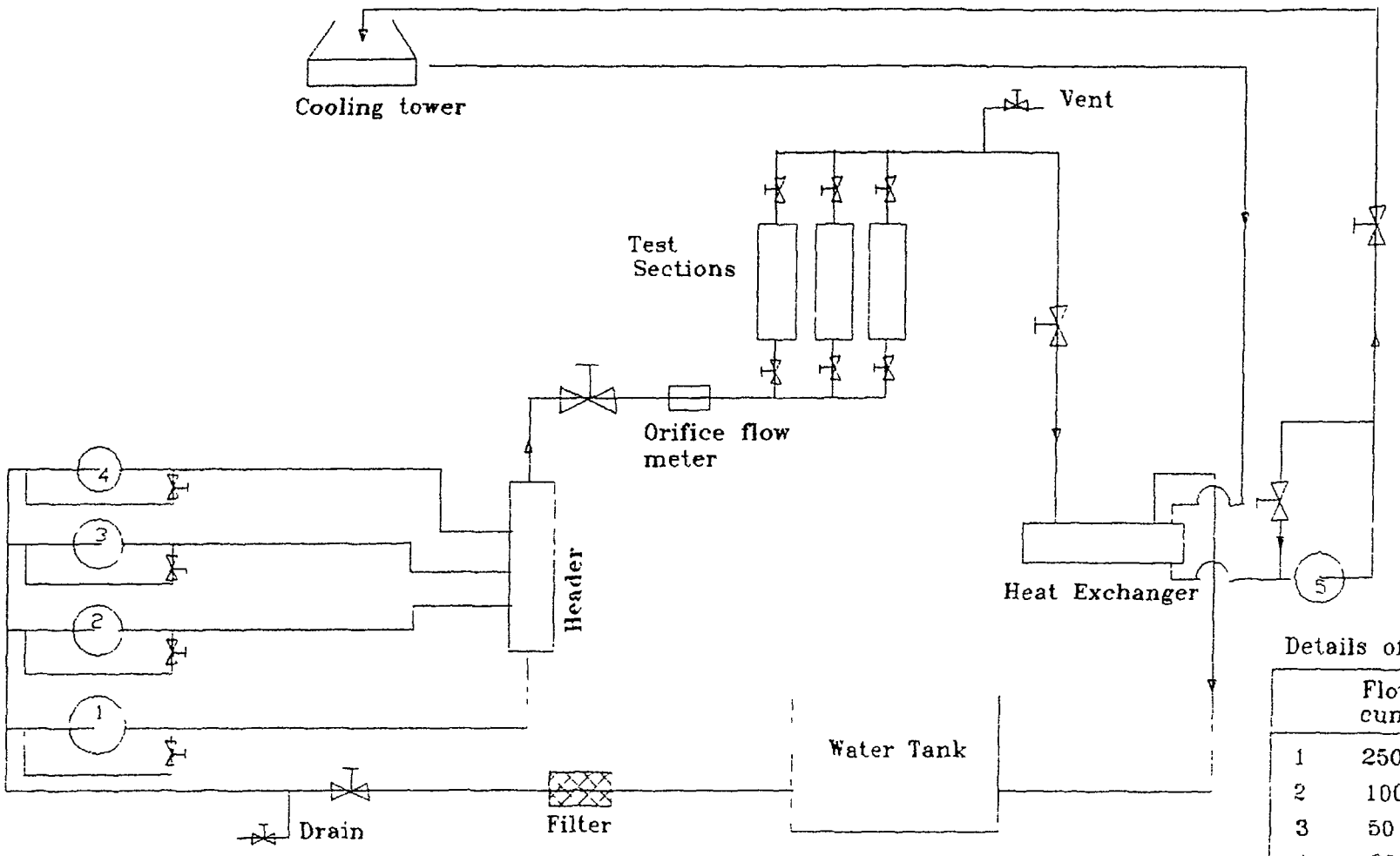

Details of pumps:

	Flow cum/h	Discharge Head (bar)
1	250	16
2	100	16
3	50	16
4	25	16
5	30	16

Fig. 8 : Schematic of PFBR Subassembly Test Rig

strain levels exceeded the permissible limits. A full scale instrumented fuel SA is being fabricated with 200 mm spacer wire pitch for qualifying the SA against FIV.

7.2 Hydraulic Studies:

The following hydraulic experiments are under progress to validate the design and theoretical predictions

- Pressure drop and cavitation characteristics of bare SA;
- Pressure drop and cavitation characteristics of labyrinths and orifices;
- Pressure drop characteristics of SA in each zone;
- Pressure drop characteristics and Lifting force on CSR; and
- Lifting forces on fuel and blanket SA.

Water temperature is selected as 70° C to reduce the flow rate requirement for maintaining Reynolds similitude. Temperature is maintained constant using the secondary loop consisting of heat exchanger and cooling tower (fig. 8). Since the flow rate through various type of SA differ widely, the water loop consists of four pumps delivering flow ranging from 25 to 250 m^3/h at 160 mlc head. All these four pumps are connected in parallel to three test sections.

Flow is measured using an orifice flow meter and RTD are used for temperature measurement. The pressure drop across various locations of the SA is measured using Differential Pressure transmitters and the absolute pressures are measured using pressure transducers.

8.0 Conclusion

Based on the optimisation and rationalisation study, the number of flow zones has been fixed at 15. Required flow through fuel SA has been calculated based upon fresh SA peak power in equilibrium core configuration. The temperature limits of 700°C for fuel clad and 680°C for blanket clad and 680°C for CSR & DSR clad have been respected in deciding the flow required. The temperature difference between adjacent coolant streams has been limited to 100°C from thermal striping considerations. Temperature distribution in core has been given for **BOEC** configuration. Pressure drops in SA are also presented. For CSR, DSR, Reflector and shielding SA the pressure drop is very low, as the flow in these SA are very small. Hence, for these SA , it is necessary to achieve the required pressure drop outside the SA.

REFERENCES

1. Tang Y.S. et al- Thermal analysis of liquid metal fast breeder reactors, Nucl. Sci. Technology series, ANS, 1978.
2. Chen B.C and Todreas N.E.- Prediction of coolant temperature field in a breeder reactor including interassembly heat transfer, COO-2245-20 TR, Rev. 1.
3. Cheng S.K. and Todreas N.E. - Hydraulic models and correlations for bare and wire wrapped hexagonal rod bundles - bundle friction factors, subchannel friction factors and mixing parameters, Nucl. Engg. and Des. 92, 227-251.
4. Pontier M. et al, Etude Des Pertes de charge dans Des faisceaux d'aiguilles, DRP/SEMTR/CAD.68.R.555,1968.
5. Novendstern E.H., Turbulent flow pressure drop for fuel rod assembly using a helical wire-wrap spacer system, Nucl. Engg. & Design, V. 22, pp 19-27, 1977.
6. Rehme K., Pressure drop correlations for fuel element spacers, Nucl. Technology, V. 17, pp 15-22, 1973.
7. Zhukov A. V. et al, Analysis of the fast reactors' fuel-rod bundle flow resistance, Atomnya Energiya, V. 60(5), pp 317-321, 1986.

METHODOLOGY FOR THERMAL HYDRAULIC CONCEPTUAL DESIGN AND PERFORMANCE ANALYSIS OF KALIMER CORE

YOUNG-GYUN KIM, WON-SEOK KIM, YOUNG-JIN KIM, CHANG-KUE PARK
Korea Atomic Energy Research Institute,
Taejon, Republic of Korea

Abstract

This paper summarizes the methodology for thermal hydraulic conceptual design and performance analysis which is used for KALIMER core, especially the preliminary methodology for flow grouping and peak pin temperature calculation in detail. And the major technical results of the conceptual design for the KALIMER 98.03 core was shown and compared with those of KALIMER 97.07 design core. The KALIMER 98.03 design core is proved to be more optimized compared to the 97.07 design core. The number of flow groups are reduced from 16 to 11, and the equalized peak cladding midwall temperature from 654℃ to 628℃. It was achieved from the nuclear and thermal hydraulic design optimization study, i.e. core power flattening and increase of radial blanket power fraction. Coolant flow distribution to the assemblies and core coolant/component temperatures should be determined in core thermal hydraulic analysis. Sodium flow is distributed to core assemblies with the overall goal of equalizing the peak cladding midwall temperatures for the peak temperature pin of each bundle, thus pin cladding damage accumulation and pin reliability. The flow grouping and the peak pin temperature calculation for the preliminary conceptual design is performed with the modules ORFCE-F60 and ORFCE-T60 respectively. The basic subchannel analysis will be performed with the SLTHEN code, and the detailed subchannel analysis will be done with the MATRA-LMR code which is under development for the K-Core system. This methodology was proved practical to KALIMER core thermal hydraulic design from the related benchmark calculation studies, and it is used to KALIMER core thermal hydraulic conceptual design.

1. INTRODUCTION

KALIMER (Korea Advanced Liquid Metal Reactor), a pool-type sodium cooled prototype reactor with thermal output of 392 MW (electric power of 150 MW), is currently under conceptual design study at KAERI. The objective of the KALIMER program is to develop an inherently and ultimately safe, environmentally friendly, proliferation-resistant and economically viable fast reactor concept. The KALIMER core is initially designed with 20% enriched U-10%Zr binary alloy metallic fuels, which generates a net negative reactivity with an inherent safety characteristics[1].

In this context, K-Core system, an integrated system of the KALIMER core design and analysis modules, is being developed in the KALIMER core design and technology development team, to provide major data links among the principal core design modules.

Core steady state thermal hydraulic performance analysis includes coolant flow distribution to the assemblies and core coolant/fuel temperature calculations. LMR core has generally configured duct assemblies with a triangular channel arrangement of fuel rods within, which made a closed circuit by themselves without any flow path between them. Thus the purpose of core thermal hydraulic design is to efficiently extract the thermal power of each assembly by distributing the appropriate sodium coolant flow.

1.1. Coolant Flow Distribution to the Assemblies

Sodium coolant flow is distributed to the assemblies with the overall goal of equalizing pin cladding damage accumulation and pin reliability. Sodium flow distributed in each assembly has to ensure the integrity of fuels and structures, and no sodium coolant boiling is allowed in both steady state and transient conditions[2,3].

In practice, initial flow grouping analysis attempts to equalize peak pin cladding midwall temperatures in all assemblies. Assuming peak fuel burnup to be equal in all assemblies, this flow grouping analysis can equalize fission gas pressure, cladding stress and damage accumulation.

Sodium flow is distributed according to the peak linear power of each assembly. The peak temperatures of the coolant assembly outlet, cladding midwall and fuel centerline are calculated in each assembly with previously distributed flows. Once the flow is distributed so as to equalize peak cladding temperatures in all assemblies, the remaining flow and thermal criteria should be checked to verify all criteria are met.

1.2. Coolant and Fuel Temperature Calculation

The key core temperature parameters are: (a) peak subchannel coolant temperature, (b) peak cladding midwall temperature, (c) peak thermal striping potential, (d) peak assembly outlet temperature, (e) peak fuel surface temperature and (f) peak fuel centerline temperature. The peak subchannel coolant temperature indicates the margin to coolant boiling. The saturation temperature of sodium at the depth of the core is greater than 950℃ with the pump pressure off and greater than 1,060℃ with the pumps on. So 950℃ is used as the conservative limit for this parameter[4].

Temperatures are computed by adding relevant temperature rises to the assembly inlet temperature. 2σ hot channel factors based on CRBR analyses are used in temperature predictions to account for core design, analysis, fabrication and operational uncertainties and variations[5].

1.3. Pressure Drop Calculation

Once the flow grouping and the peak pin temperature calculation was performed, the core pressure drop based on the fuel assembly with maximum flow, has to be calculated to see if it does not exceed the limit value. The primary pump of 0.8 MPa pressure head is used in KALIMER design. Thus the assembly bundle pressure drop has to be within 0.32 MPa with 20 % uncertainty, noting that pressure loss through the fuel element bundle and loss through the core contribute 40 and 80 % of the total reactor pressure loss, respectively[6].

Three models developed for the wire wrap rod spacing assemblies are used in bundle pressure loss calculations: (a) Novendstern model, (b) Chiu-Rohsenow-Todreas model, (c) Cheng-Todreas model[7].

1.4. Steady State Subchannel Analysis

Detailed core wide coolant temperature profiles are efficiently calculated using the simplified energy equation mixing model and the subchannel analysis method. SLTHEN code is a steady state thermal hydraulic analysis code based on the ENERGY model[8]. The efficiency of the ENERGY model in both computer storage and run time is due to the simplicity of its computational model where only the energy equations are solved, and the momentum and continuity equations are not directly included. The momentum coupling between coolant channels is indirectly taken into account using enhanced eddy diffusivity and the swirl velocity ratio with the experimental modellings developed for the wire-wrap spacing rod assemblies.

SLTHEN has a capability to calculate the multi-assembly whole core calculations. This code provide temperature maps for all pins in all assemblies and thus facilitate core wide failure probability studies.

1.5. Detailed Subchannel Analysis

The detailed subchannel analysis will be performed with MATRA-LMR code[9] which is being developed for KALIMER, and SABRE4 code[10] developed in the UK AEAT. MATRA-LMR is the detailed subchannel analysis code developed based on COBRA-IV-I[11] and MATRA[12]. MATRA-LMR solves the mass, axial and transverse momentum, and energy equations. MATRA-LMR is used for a single assembly analysis and will be extended for the multi-assembly whole core calculations. SABRE4 was initially developed for grid spacing assemblies and modified to wire wrap version. It is a three dimensional subchannel code which has good predictions especially in the blocked channel analysis.

It is expected they will form the licensing data basis and will be extensively used during preliminary and final design phases.

In this paper, the preliminary methodology for flow grouping and peak pin temperature calculation used for KALIMER core conceptual design is summarized. Figure 1 shows the overall conceptual design procedure for KALIMER core thermal hydraulics. The major technical results of the conceptual design for the KALIMER 98.03 core is shown and compared with those of KALIMER 97.07 design core. The steady state and detailed subchannel analysis methodology and the results are summarized in the other paper presented at this meeting[13].

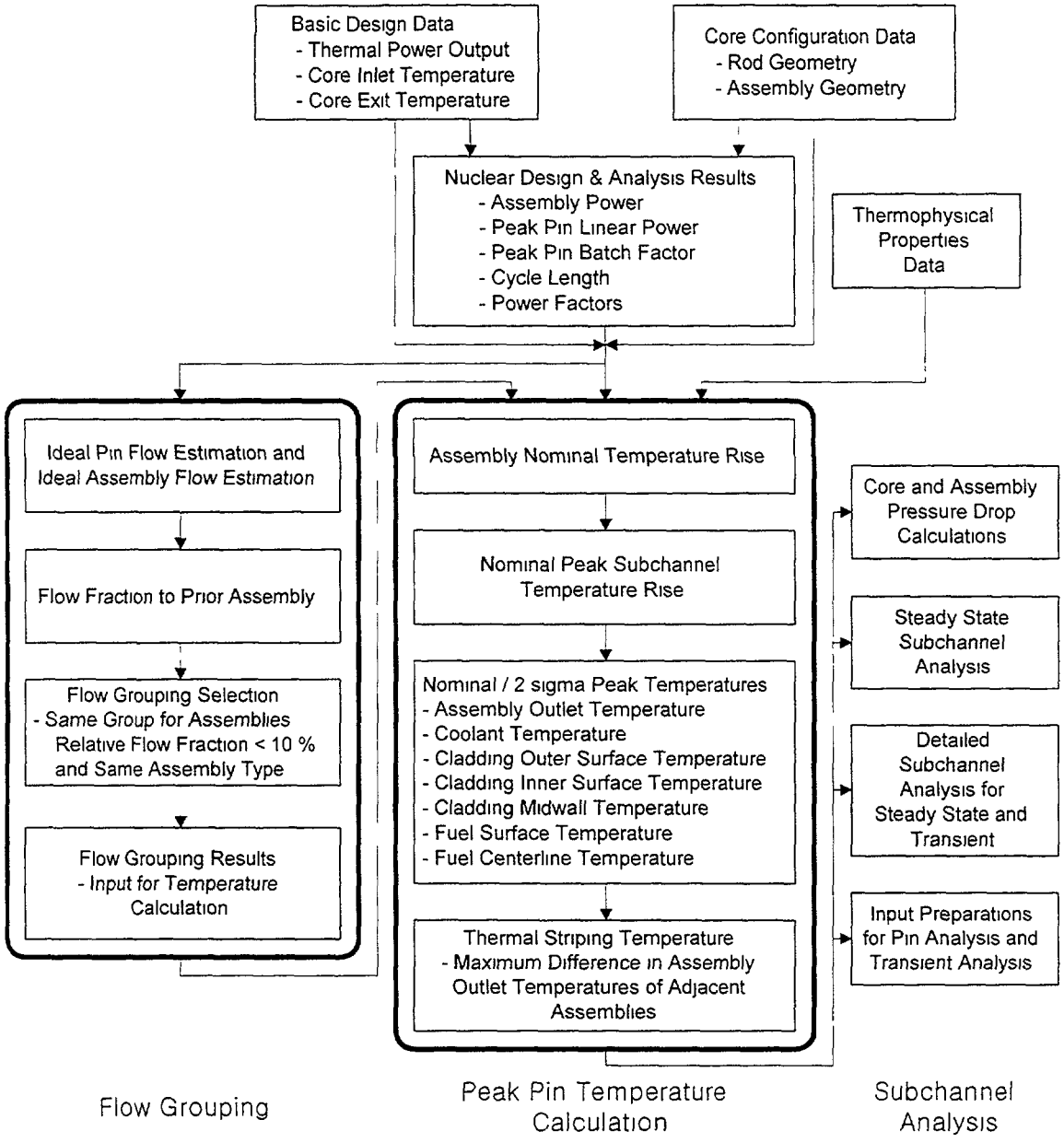

Figure 1. Conceptual Design Procedure for KALIMER Core Thermal Hydraulics

2. PRELIMINARY CONCEPTUAL DESIGN METHODOLOGY

2.1. Flow Grouping

Coolant flow controls, i.e orificing flow restrictions, are located at the inlet orificing modules into which the assemblies are inserted at the lower nosepieces end. The flow groups remain in the same core locations for the plant lifetime. Thus it is associated with a core location and not with a particular assembly. Sodium coolant flow has to be supplied to the assemblies based on the peak linear heat generation rate for their whole lifetime to ensure the structural integrity of fuels, claddings and ducts. But small flow control is not expected with this method, so flow groups are limited in number.

During the conceptual design, reflector, shield and IVS were not considered for flow grouping, because their flow rates are small and the powers do not change so significantly throughout their lifetime to complicate their detailed orificing. The orificings for the reflector, shield and IVS were determined based on an average group assembly[4,5].

Total primary loop flow is set by the core power and the desired reactor temperature rise. A small portion of flow is assumed to bypass the core by leaking around the inlet module and assembly nosepieces seal rings, and to be used for structural cooling within the reactor. In general, 1.5% of the primary loop flow is assumed to bypass the core and is thus not included in the flow distribution to the assemblies, thus which is not included in the initial flow grouping.

Every assembly in the range of about 10% power difference was put in the same group. And separate flow groups were maintained for each assembly type, even where flows were virtually identical. This gives the conservative estimations in the number of flow groups, which will be improved at further design changes, considering the non-fuel assemblies. The flow groupings for these regions will be expanded later with better gamma heating calculations into those assemblies and thus increase the total number of flow groups.

Coolant Temperature Along Pin

Maximum coolant temperature increases along the pin can be calculated from the bundle average temperature rise as follows.

Maximum subchannel coolant temperature rise, ΔT_{max}, can be expressed as

$$\Delta T_{max} = f\,\Delta T_B \tag{1}$$

where

f is the peak pin ΔT peaking factor,
ΔT_B is the bundle average temperature rise,
$_B$ is for bundle.

And the bundle average temperature rise is calculated as

$$\Delta T_B = \frac{Q_B}{\dot{m}_B\, c_P} \tag{2}$$

where

Q_B is the total heat generation in bundle,
$\dot{m}_B$ is the total mass flow rate in bundle,
c_P is the coolant specific heat.

In the equation (2), total heat generation in bundle Q_B is, from the number of pins in bundle (n) and the average heat generation from the fuel pin (q_{avg}), $Q_B = n\,q_{avg}$, and the bundle mass flow rate is

$$\dot{m}_B = \rho\, u_B\, A_B \tag{3}$$

where

ρ is the coolant density,
u_B is the bundle average velocity,
A_B is the flow area in bundle.

Substituting the above relation and equation (3) in equation (2), the bundle average temperature rise becomes

$$\Delta T_B = \frac{n\, q_{avg}}{\rho\, u_B\, A_B\, c_P} \tag{4}$$

With equation (4) and (1), the maximum subchannel coolant temperature rise becomes

$$\Delta T_{\max} = f\left[\frac{n\, q_{avg}}{\rho\, u_B\, A_B\, c_P}\right] \tag{5}$$

Otherwise, maximum subchannel coolant temperatures that rise along the pin can be also calculated in the hottest channel as

$$\Delta T_{\max} = \frac{q_C}{\dot{m}_C\, c_P} \tag{6}$$

where

q_C is the heat added to the subchannel by adjacent pins,
$\dot{m}_C$ is the subchannel mass flow rate,
c is for subchannel,

and where q_C is from 3 pins as shown in the figure below.

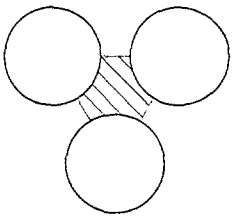

Assuming they are the hottest pins, q_C becomes

$$q_C = 3 \times \frac{q_{\max}}{6} = \frac{q_{\max}}{2}$$

and the bundle mass flow rate $\dot{m}_C$ is

$$\dot{m}_C = \rho\, u_C\, A_C$$

So the equation (6) becomes

$$\Delta T_{\max} = \frac{q_{\max}/2}{\rho\, u_C\, A_C\, c_P} \tag{7}$$

Equalizing equations (5) and (7) with the assumption of uniform density and specific heat of the coolant, the following relation is obtained

$$\Delta T_{\max} = f\left[\frac{n\, q_{avg}}{\rho\, u_B\, A_B\, c_P}\right] = \frac{q_{\max}/2}{\rho\, u_C\, A_C\, c_P} \tag{8}$$

Peak pin ΔT peaking factor, f, can be expressed, from the equation (8), as

$$f = \left(\frac{q_{\max}}{q_{avg}}\right)\left(\frac{u_B}{u_C}\right)\left(\frac{A_B}{2\, n\, A_C}\right) \tag{9}$$

Each term in the right hand side of the equation (9) has the meaning as follows

$f_P = \frac{q_{\max}}{q_{avg}}$ is the bundle radial power peaking factor, (10)

$f_v = \frac{u_B}{u_C}$ is the bundle radial split factor, (11)

$f_g = \frac{A_B}{2\, n\, A_C}$ is the geometry factor. (12)

Using these factors and the bundle average temperature rise, ΔT_B, the maximum coolant temperature rise, $\Delta T_{\max}$, can be calculated. Because temperature is directly related to power, these factors have to be considered in the flow grouping procedure, in modifying the peak pin linear power of each assembly.

2.2. Peak Pin Temperature Calculation

Temperatures are computed by adding relevant temperature rises to the assembly inlet temperature. Each temperature rise is computed from energy input, heat capacity, thermal conductivity and heat transfer coefficients. The temperature rises to be included are: (a) the coolant subchannel temperature rise from the inlet to the elevation modeled, (b) the film temperature rise between the subchannel bulk coolant and the cladding surface, (c) the cladding temperature rise, either to the midwall radius or to the inner surface, (d) the gap temperature rise between the cladding and the fuel surface and (e) the fuel temperature rise from the surface to the center[4,5].

Hot channel factors are introduced in the temperature predictions to account for core design, analysis, fabrication and operational uncertainties and variations. 2 σ uncertainty factors based on CRBR analyses were employed in the KALIMER design.

The temperatures which influence design conditions have to be checked with the limit values because they are important in the following senses. The limit to the nominal peak assembly outlet temperature is set to limit thermal aging effects and the thermal striping potential temperature is set to limit thermal fatigue effects in the UIS. The peak thermal striping potential temperature is a possible maximum difference in the assembly coolant discharge temperatures of adjacent assemblies. The maximum differences possible by combining +2 σ outlet temperatures adjacent to -2 σ are used. A limit of 190℃ is applied to this parameter to control high cycle fatigue of the permanent upper internal structures. Mixing between the core and UIS, about 1 meter above the core assembly coolant discharge reduces this temperature difference to an acceptable level for permanent structural components. These become important during transient analysis of duty cycle events and primarily serve to set maximum rates of power and temperature change during plant maneuvering. A considerable damage accumulation margin is reserved in assembly steady state structural analyses to accommodate these transients. The low powers in the control and USS assemblies require the minimum flow These assemblies have low outlet temperatures. As a result, the control assemblies and their immediate neighbors set the maximum thermal striping potential. The equalized cladding midwall temperature is limited to about 650℃ for fuel and blanket assemblies to ensure the cladding material's structural integrity. The peak fuel surface temperature is limited to 700℃ to avoid liquefaction of a low melting temperature alloy formed by inter diffusion of cladding iron and fuel uranium and plutonium. Liquefaction greatly accelerates cladding internal wastage rates and shortens pin lifetime. The peak fuel centerline temperature indicates the margin to fuel melting.

Second Row Peak Pin Modification

The peak power pin appears generally in the last row facing the core center in each assembly. But the channel area surrounding that pin is larger than the interior channels, thus it is cooled more than other pins. So the real peak temperature channel is in one row inside. This peak temperature channel factor can be considered by the linear interpolation method, as shown in the figure below.

$$f' = f\left(\frac{n-2}{n-1}\right) \tag{13}$$

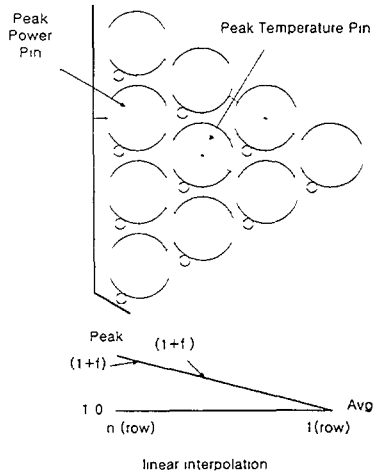

linear interpolation

pins	rows	$\left[1-\frac{1}{n-1}\right]$
271	10	0.8889
217	9	0.8750
169	8	0.8571
127	7	0.8333
91	6	0.8000
61	5	0.7500
37	4	0.6667
19	3	0.5000
7	2	0.0000

And from the equation (13), the power factor in one row inside can be obtained

$$1+f' = 1+f\left(\frac{n-2}{n-1}\right) = 1+(f_p-1)\left[1-\frac{1}{n-1}\right] \tag{14}$$

where

$1+f = f_p = q_{\max}/q_{avg}$ is the bundle radial power peaking factor.

The bracket term in the right side of the equation (14) has only the geometry dependency as shown in the table above.

Thus the linear pin power can be modified with these factors as follows

$$q'|_{row2} = \left(\frac{1+f'}{1+f}\right) q'|_{row1} = \frac{\left[1+(f_p-1)\left\{1-\frac{1}{n-1}\right\}\right]}{f_p} q'|_{row1} \tag{15}$$

Subchannel $\Delta T_{\max}$ can be modified in the same way. The peak subchannel temperature rise $\Delta T_{\max}$ is expressed in the equation (7). But the real peak temperature channel is in one row inside, so the equation (7) becomes

$$\Delta T_{\max,row2} = \frac{q_{\max}/2}{\rho\, u_C\, A_C\, c_P}\left(\frac{1+f'}{1+f}\right) \tag{16}$$

The above equation (16) can, using the equations (4), become

$$\begin{aligned}\Delta T_{\max,row2} &= \left[\Delta T_B \cdot \frac{\rho\, u_B\, A_B\, c_P}{n\, q_{avg}}\right]\cdot\frac{q_{\max}/2}{\rho\, u_C\, A_C\, c_P}\left(\frac{1+f'}{1+f}\right)\\ &= \Delta T_B\left(\frac{q_{\max}}{q_{avg}}\right)\left(\frac{u_B}{u_C}\right)\left(\frac{A_B}{2\,n\,A_C}\right)\left(\frac{1+f'}{1+f}\right)\end{aligned} \tag{17}$$

The meaning of each term in the right hand side is in the equations (10), (11), (12) and (14).

Thus, the real maximum subchannel coolant temperature rise can be obtained from the equation (17), (14) and the relation $q_{\max}/q_{avg} = f_p = 1+f$,

$$\begin{aligned}\Delta T_{\max,row2} &= \Delta T_B \cdot (f_v \cdot f_g)\cdot(1+f')\\ &= \Delta T_B \cdot FF \cdot \left[1+(f_p-1)\left\{1-\frac{1}{n-1}\right\}\right]\end{aligned} \tag{18}$$

where

$FF = f_v \cdot f_g$ is the bundle radial flow peaking factor.

Each temperature rise is recalculated in order to account for the uncertainties, i.e., design, analysis, fabrication and operational uncertainties and variations. 2σ hot channel factors based on CRBR analyses are used in KALIMER analysis.

The 2σ temperature rises are obtained from the nominal temperature rise, with the corresponding hot channel factors

$$\Delta T_{i,hcf} = \Delta T_i \cdot HCF_i \tag{19}$$

where

HCF_i is the corresponding hot channel factors for i component

3. CONCEPTUAL DESIGN CHARACTERISTICS OF KALIMER CORE

KALIMER core thermal hydraulic conceptual design was performed with the above mentioned methodology. In 97.07 design core, there were 16 flow groups and the equalized cladding midwall temperature was 654℃. Some nuclear design optimizations were done to improve the performances[14].

Table 1 and figure 2 show core configuration and the basic design data of KALIMER 98.03 design respectively. The core flow grouping and the peak pin temperature calculation results are shown in table 2 and

Table 1. Basic Design Data of KALIMER 98.03 Design Core

Core Thermal Output (MWth)	392.2
Core Electric Power (MWe)	150.0
Net Plant Thermal Efficiency (%)	38.2
Core Inlet/Out Temperature (℃)	386.2/530.0
Total Flow Rate (kg/s)	2143
Active Core Height (cm)	100.0
Core Diameter (cm)	344.73
Core Configuration	Radial Homogeneous
Number of Core Enrichment Zones	2
Feed Fuel Enrichments (w/o%) (IC/OC)	14.41/20.00
Fuel Form	U-10%Zr Binary Alloy
Refueling Interval (months)	12
Refueling Batches (Driver/Radial Blanket)	3/6
Duct Inside Flat to Flat Distance (mm)	149.8
Pins per Fuel Assembly (Driver/Radial Blanket)	271/217
Pin Outer Diameter (Driver/Radial Blanket) (mm)	7.67/12.0
Pin P/D Ratio (Driver/Radial Blanket)	1.167/1.083
Average/Peak Fuel Burnup (MWD/kg)	25.35/42.67
Avg/Peak Linear Power for Driver (BOEC) (W/cm)	160.2/208.5
Peak Fast Neutron Fluence (E>0.1 MeV) ($x10^{23}n/cm^2$)	1.399
Cladding Material	HT9

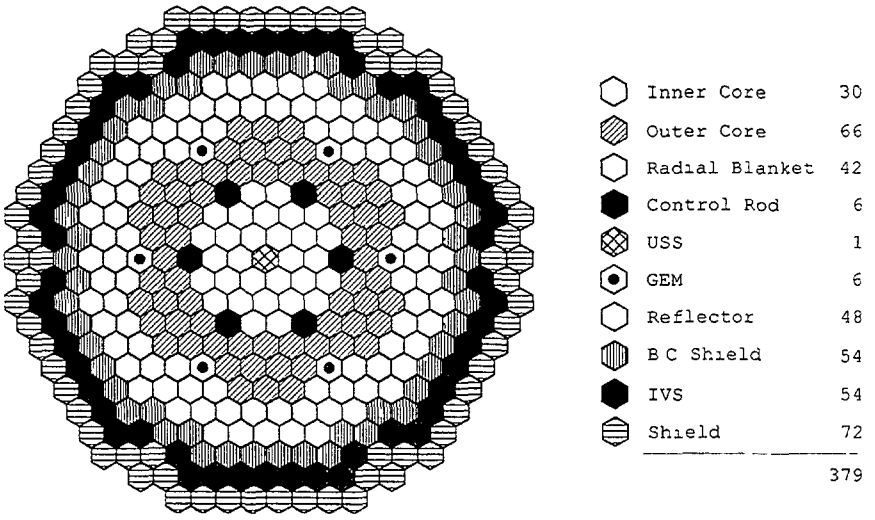

Figure 2. KALIMER 98.03 Design Core Configuration

figure 3 on the 1/6 core configuration map Table 3 shows an example of the peak pin temperature calculation results for three peak flow assemblies of inner and outer enrichment zones, and radial blankets Design data and core configuration are shown in table 5 and figure 4 respectively for KALIMER 97 07 design, and the flow grouping and the peak pin temperature calculation results in table 6 and figure 5

Both cores have the same thermal power of 392 MW (electric power of 150 MW) The core exit temperature is the same for both cores (530℃), but the core inlet temperature is increased from 361 4℃ to

Table 2 Flow Grouping and 2 σ Peak Pin Temperature Calculation Results of KALIMER 98 03 Design Core

Flow Group	Assy Type	Assy Count	Assy Flow (kg/s)	Zone Flow (%)	Assy Outlet (℃)	Thermal Striping (℃)	Cladding Midwall (℃)	Fuel Surface (℃)	Fuel Center (℃)
limit					*590*	*190*	*650*	*700*	*1000*
1	IC	6	21 6		575	160	628	635	680
2	IC	24	20 4		578	158	628	635	674
3	OC	24	23 7		571	148	628	636	691
4	OC	12	20 6		561	31	628	635	675
5	OC	12	19 2		556	78	628	634	667
6	OC	18	15 8	90	554	79	628	633	650
7	RB	12	4 6		508	78	628	632	642
8	RB	18	3 3		501	79	628	631	641
9	RB	12	2 7	7	498	71	628	631	641
10	CTL	6	3 1		397	158	-	-	-
11	USS	1	3 1	1	393	160	-	-	-
Total primary loop flow 2143 kg/s Total bypass flow 2 0 %									

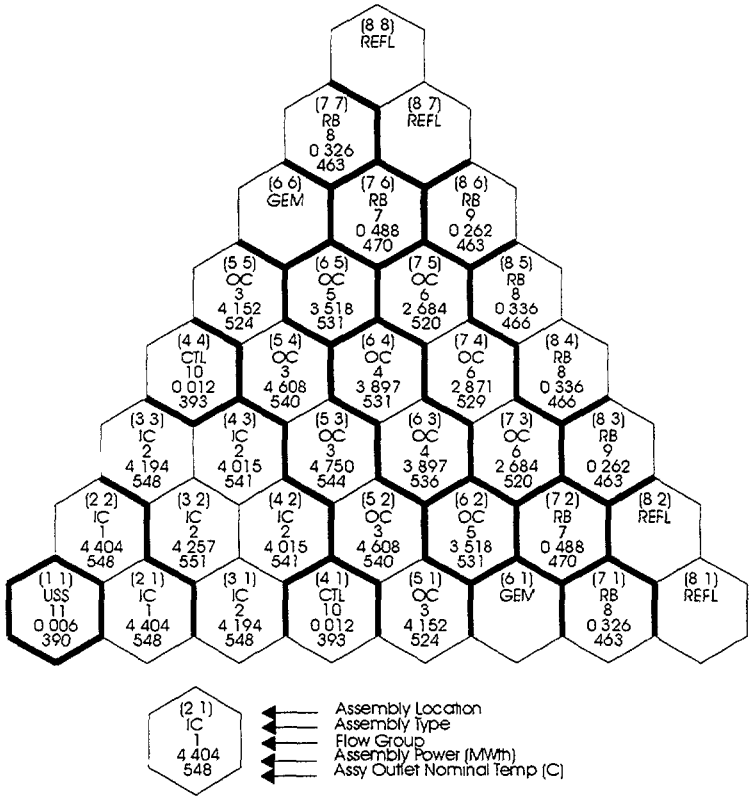

Figure 3 Flow Grouping and Temperature Calculations of KALIMER 98 03 Design Core (1/6 Core Map)

386.2℃ (the average temperature rise in the core is decreased from 168.6℃ to 143.8℃). The pin's outer radius is increased also from 7.4mm to 7.67mm and the fuel enrichment in the outer core is decreased from 15.0% to 14.4%, based on the nuclear and thermal hydraulic design optimization study[14].

Table 3. Temperature Calculation Summary Table of 98.03 Core (Example)

ASSEMBLY & GROUP MODEL DATA	Assy 1 (IC)		Assy 11 (OC)		Assy 11 (RB)	
Type & Location	F	(2,1)	F	(5,3)	RB	(7,2)
Orifice Group & Flow Rate (kg/s)	1	21.6	3	23.7	7	4.6
Inlet Temp. (℃) & Avg. Cp (J/kg-℃)	386.2	1267.8	386.2	1267.8	386.2	1267.8
Film & Gap Coefficients (kW/m^2-℃)	132.5	132.5	132.5	132.5	88.3	132.5
Pin OD & ID (mm)	7.67	6.61	7.67	6.61	12.0	10.9
Clad Thickness & Pellet OD (mm)	0.53	5.8	0.53	5.8	0.54	10.1
Adjustment For 2nd Row Pin Power	0.8889	–	0.8889		0.8333	
Power Factor: Peak Clad, Peak Fuel	0.41	0.92	0.41	0.92	0.35	0.73
Temperature Factor: Peak Clad, Peak Fuel	1	0.71	1	0.71	1	0.85
	BOL	EOL	BOL	EOL	BOL	EOL
Peak Pin W/cm, BOL & EOL	189.5	186.7	207.8	201.7	69.6	80.3
Assembly Total Power (MWth)	4.404	4.377	4.750	4.654	0.488	0.581
Bundle Radial Power Peaking Factor	1.042	1.040	1.063	1.062	1.520	1.467
Bundle Radial Flow Peaking Factor	1.13	1.13	1.13	1.13	1.21	1.21
Fuel Porosity Factor	0.5	0.7	0.5	0.7	0.5	0.7
ASSY OUTLET TEMPERATURE						
Assy T Rise Based On Core Cp (℃)	143.6	142.6	140.2	137.0	66.2	82.2
Assy Avg T Based On Core Cp (℃)	466.9	466.4	465.2	463.6	428.2	436.2
Cp (J/kg-℃)	1266.5	1266.6	1266.7	1267.0	1272.9	1271.5
Assy Nominal T Rise (℃)	143.7	142.7	140.3	137.1	65.9	81.9
Nominal Outlet Temp (℃)	547.7	546.7	544.3	541.1	469.8	485.9
Nominal Peak Subchannel T (℃)	574.5	574.0	574.8	570.9	531.2	553.7
Nominal Peak Clad Midwall T (℃)	581.0	579.5	580.9	576.8	532.5	555.2
Nominal Peak Fuel Surface T (℃)	587.0	585.3	587.4	583.2	533.6	556.5
Nominal Peak Fuel Centerline T (℃)	637.6	610.2	647.5	614.9	541.3	556.3
+2σ ASSEMBLY PEAK T (℃)						
+2σ Coolant Outlet	574.8		570.9		507.6	
+2σ Thermal Striping	160.0		26.9		78.0	
+2σ Cladding Midwall	628.5		628.6		628.1	
+2σ Fuel Surface	635.1		635.8		629.5	
+2σ Fuel Centerline	680.4		691.2		631.6	
+2σ Peak Fuel Surface At Scram	667.1		667.9		660.8	
+2σ Peak Fuel Center At Scram	718.3		730.5		663.2	

Table 4. Comparisons of the Calculation Results of KALIMER 98.03 Core

Temperature (℃) / Code	Peak Subchannel			Bundle Average		
	IC	OC	RB	IC	OC	RB
ORFCE	574.5	574.8	531.2	547.7	544.3	469.8
SLTHEN	548.2	544.6	481.9	530.0	527.0	458.9
SABRE4	565.3	561.4	485.1	533.0	530.0	462.5
MATRA-LMR	556.2	552.5	482.7	533.0	530.0	462.5

Table 5. Basic Design Data of KALIMER 97.07 Design Core

Core Thermal Output (MWth)	392.0
Core Electric Power (MWe)	150.0
Net Plant Thermal Efficiency (%)	38.3
Core Inlet/Out Temperature (℃)	361.4/530.0
Total Flow Rate (kg/s)	1824
Active Core Height (cm)	100.0
Core Diameter (cm)	344.3
Core Configuration	Radial Homogeneous
Number of Core Enrichment Zones	2
Feed Fuel Enrichments (w/o%) (IC/OC)	15.0/20.0
Fuel Form	U-10%Zr Binary Alloy
Refueling Interval (months)	12
Refueling Batches (Driver/Radial Blanket)	3/3
Duct Inside Flat to Flat Distance (mm)	149.0
Pins per Fuel Assembly (Driver/Radial Blanket)	271/217
Pin Outer Diameter (Driver/Radial Blanket) (mm)	7.4/12.0
Pin P/D Ratio (Driver/Radial Blanket)	1.189/1.083
Average/Peak Fuel Burnup (MWD/kg)	28.0/47.3
Avg/Peak Linear Power for Driver (BOEC) (W/cm)	151.9/234.6
Peak Fast Neutron Fluence (E>0.1 MeV) ($x10^{23}n/cm^2$)	1.434
Cladding Material	HT9

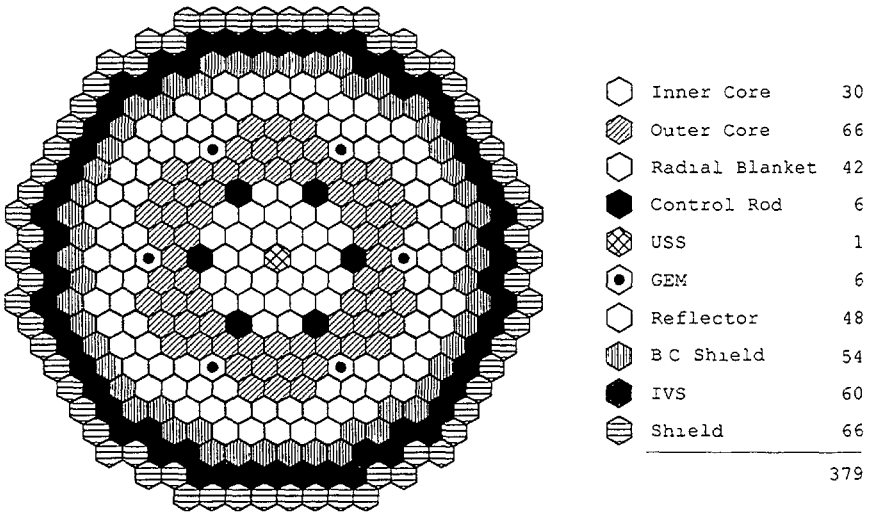

Figure 4. KALIMER 97.07 Design Core Configuration

Eleven flow groups were specified, as shown in table 2, for the present KALIMER 98.03 design core: six groups are used for fuel assemblies, the radial blanket assemblies utilize three flow groups and the six control assemblies and the USS assembly use a single flow group each. Both the control and USS assemblies have sliding rod bundles and their flow grouping is subject to a minimum flow that maintains turbulent flow cooling during a scram drop. These assemblies strongly affect thermal striping potential temperatures during conceptual design. The minimum flow was assumed to be 3.15 kg/s based on ALMR design analyses[3]. One flow group for GEMs are subject to the high pressure coolant plenum with no orificing restriction and serves as the sodium inlet and outlet connection which activates the GEM reactivity feedback upon loss of pumped flow. With the 1.5 % bypass flow, an additional 0.5% of primary flow was omitted in the conceptual design study and is reserved for the perimeter assemblies not explicitly being orificed. Thus 2.0% of primary flow is not distributed in the initial flow grouping analyses.

Table 6. Flow Grouping and 2 σ Peak Pin Temperature Calculation Results of KALIMER 97.07 Design Core

Flow Group	Assy Type	Assy Count	Assy Flow (kg/s)	Zone Flow (%)	Assy Outlet (℃)	Thermal Striping (℃)	Cladding Midwall (℃)	Fuel Surface (℃)	Fuel Center (℃)
Limit					*590*	*190*	*650*	*700*	*1000*
1	IC	6	18.4		593	190	654	663	728
2	IC	6	17.8		592	33	654	663	718
3	IC	6	17.3		591	172	654	662	713
4	IC	12	16.4		587	169	654	661	704
5	OC	18	26.2		538	116	654	663	734
6	OC	6	17.4		584	166	654	663	733
7	OC	12	16.1		579	62	654	661	711
8	OC	12	14.6		577	98	654	661	701
9	OC	6	12.5		561	101	654	660	676
10	OC	12	11.8	92	557	100	654	660	673
11	RB	12	2.0		540	98	654	657	666
12	RB	6	2.4		500	57	654	657	667
13	RB	12	2.3		493	101	654	657	666
14	RB	12	2.1	5	487	100	654	657	665
15	CTL	6	3.1		409	172	-	-	-
16	USS	1	3.1	1	385	190	-	-	-
Total primary loop flow : 1824 kg/s Total bypass flow : 2.0 %									

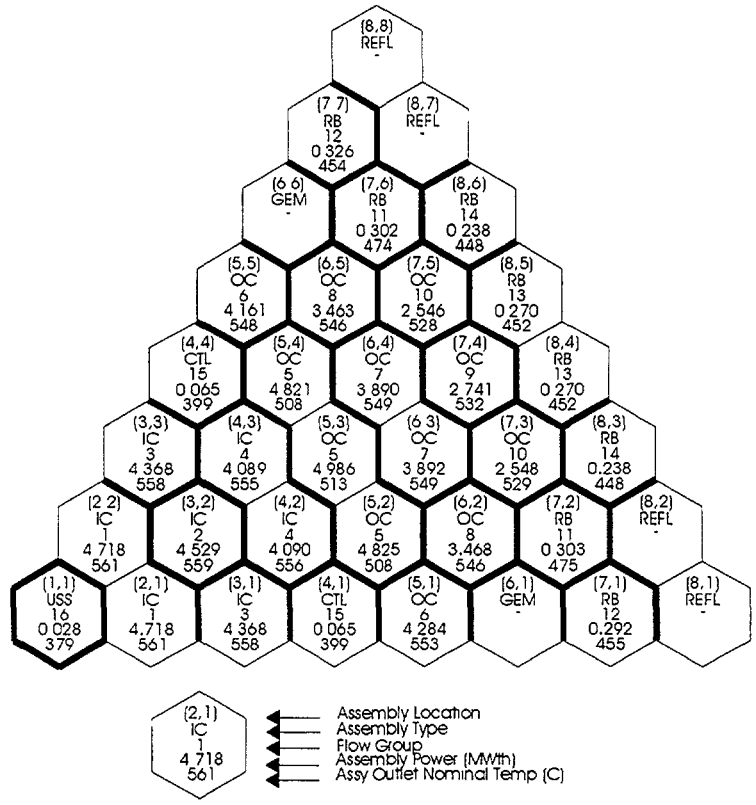

Figure 5. Flow Grouping and Temperature Calculations of KALIMER 97.07 Design Core (1/6 Core Map)

The key peak temperatures are calculated for the peak power pin of each flow group and compared to the appropriate limits in table 2 and 6. The criteria used for steady state thermal performance are the same as those for design basis events. As shown in table 2, all the criteria are met with a margin, not in the case of table 6. In the KALIMER 98.03 design core, given the core power distribution and total flow rate, the equalized cladding midwall temperature is about 628℃ for fuel and blanket assemblies which is below the limit temperature of about 650℃. The maximum $+2\sigma$ cladding temperature is limited to ensure adequate fuel lifetime. Table 3 lists some of the detailed peak pin temperature calculation results for the peak flow assemblies of inner and outer enrichment zones, and radial blankets. It shows an example of the calculation results for each assembly.

Table 4 shows the comparison for KALIMER 98.03 core design results of this preliminary calculation with SLTHEN, MATRA-LMR and SABRE4 code calculations. It is done for the nominal subchannel peak and bundle average temperatures in the peak flow assemblies of inner and outer enrichment zones, and radial blankets. Table 4 shows that ORFCE calculation can be used in the preliminary conceptual design with a sufficient margin.

In summary, the number of flow groups are reduced from 16 to 11, the equalized peak cladding midwall temperature from 654℃ to 628℃ for the KALIMER 98.03 design core. It was achieved through a core design optimization study, i.e., power flattening and radial blanket power fraction increase. The peak assembly flow rate is decreased from 26.2 kg/s to 23.7 kg/s, and thus the average flow velocity from 4.26 m/s to 4.05 m/s and the maximum bundle pressure drop from 0.21 MPa to 0.18 MPa. The KALIMER 98.03 design core is proved to be more optimized compared to the 97.07 design core.

4. CONCLUSION

A Methodology for thermal hydraulic conceptual design and performance analysis of KALIMER core is summarized, especially the preliminary methodology for flow grouping and peak pin temperature calculation in detail. For its preliminary steady state thermal hydraulic performance analysis, ORFCE-F60 and ORFCE-T60 modules are used for the flow grouping and the peak pin temperature calculation respectively. The major technical results of its preliminary conceptual design for KALIMER 98.03 design core are shown and compared with the results of KALIMER 97.07 design core. The number of flow groups are reduced from 16 to 11, as is the equalized peak cladding midwall temperature from 654℃ to 628℃ through a core design optimization study. The comparison for the KALIMER 98.03 core design results of this preliminary calculation with SLTHEN, MATRA-LMR and SABRE4 code calculations shows that ORFCE modules can be used in the preliminary conceptual design with a sufficient margin.

At later design stages, the basic subchannel analysis will be performed with the SLTHEN code, a steady state thermal hydraulic analysis code based on the ENERGY model, and the detailed subchannel analysis will be done with the MATRA-LMR code which is being developed based on COBRA-IV-I and MATRA. MATRA-LMR is now used for a single assembly analysis but will be extended for the multi-assembly whole core calculations. And SABRE4 code, a three dimensional subchannel code developed in the UK AEA, will be used as benchmark calculations. These three codes provide temperature maps for all pins in all assemblies and thus facilitate core-wide failure probability studies. It is expected they will form the licensing data basis and will be extensively used during preliminary and final design phases.

REFERENCES

[1] PARK, C.K., "Development of Korea Advanced Liquid Metal Reactor", IWGFR (1998).
[2] YOKOO, T., et al., Design Study on Metal Fuel FBR Cores, T91013, CRIEPI (1991).
[3] HAHN, D.H., et al., KAERI Concept Study, GE (1995).
[4] PARK, C.K., et al., KALIMER Design Concept Report, KAERI/TR-888/97 (1997).
[5] KIM, Y.G., et al., "Thermal Hydraulic Analysis of KALIMER 98.03 Design Core", Proceedings of KNS Spring Meeting (1998).
[6] TANG, Y.S., et al., Thermal Analysis of Liquid-Metal Faster Breeder Reactors, ANS (1978).
[7] WALTER, A.E., REYNOLDS, A.B., Fast Breeder Reactors, Pergamon Press, New York (1981).
[8] YANG, W.S., "An LMR Core Thermal Hydraulics Code Based on the ENERGY Model", Journal of KNS, Vol.29, No.5, pp.406-416 (1997).

[9] KIM, W.S., et al., "Code Development for LMR Core Thermal Hydraulic Subchannel Analysis", Proceedings of KNS Spring Meeting (1998).
[10] MacDOUGALL, J.D., LILLINGTON, J.N., "The SABRE Code for Fuel Rod Cluster Thermohydraulics", Nucl. Eng. and Des., V. 82, pp. 171-190 (1984).
[11] WHEELER, C.L., et al., COBRA-IV-I : An Interim Version of COBRA for Thermal-Hydraulic Analysis of Rod Bundle Nuclear Fuel Elements and Cores, BNWL-1662 (1976).
[12] YOO, Y.J., HWANG, D.H., "Development of Subchannel Analysis Code MATRArm alpha -version", Proceedings of KNS Autumn Meeting (1997).
[13] KIM, W.S., KIM, Y.G., "Recent Development of Subchannel Analysis Code MATRA-LMR for KALIMER Subassembly Thermal-Hydraulics", IAEA TCM, 27-31 July 1998, Obninsk, Russia (1998).
[14] KIM, Y.I., et al., "KALIMER Core Design and Analysis", Proceedings of KNS Autumn Meeting (1997).

CURRENT STATUS OF THERMOHYDRAULIC VALIDATION STUDIES AT CEA-GRENOBLE FOR THE SIMMER-III CODE

P. COSTE, S. PIGNY, R. MEIGNEN**
Commissariat à l'énergie atomique (CEA),
DRN/DTP/SMTH,
Grenoble, France

XA0055043

Abstract

SIMMER-III (SIII) is a two-dimensional, three-velocity-field, multiphase, multicomponent, Eulerian, fluid-dynamics code coupled with a space- and energy- dependent neutron kinetics model, to investigate postulated core disruptive accidents in LMFRs. It is developed by PNC, Japan. The paper makes the synthesis of the SIII assessment performed at CEA-Grenoble since 1996, which covers a large variety of multiphase flows, from two-phase flow basic modelling to LMFR accident simulation experiments with real materials. Single bubbles or droplets equilibrium radii and velocities, air/water experiments in tubes, and comparisons with the literature, are used to qualify the interfacial area convection equation and the momentum exchange functions. Using the second order differencing scheme of the Navier-Stokes equation, a turbulence model for two-phase recirculating flows is implemented. It is successfully validated on an adiabatic air/water experiment, and on the Sebulon boiling pool simulation experiment, which is a box of water internally heated, with a cover gas, and cooled at the walls. The successful calculations of the SGI experiment and of a reactor scale case contribute to the code validation for LMFR expansion phase. Besides, the large scale UO2/sodium interactions of the Termos T1 experiment, and the UO2 boiling pool laterally cooled with sodium flow at the wall of the Scarabee BF2 experiment, is also studied with SIII. Lastly, satisfying results are obtained with the calculation of the Scarabee APL3 slow pump run down without scram. It is shown that SIII is a state-of-the-art tool to simulate transient multiphase phenomena. The paper also discusses those areas, identified through these assessment calculations, which require further research and development.

1. INTRODUCTION

The advanced safety analysis computer code, SIMMER-III (SIII), has been developed to investigate postulated core disruptive accidents (CDA) in liquid-metal fast reactors (LMFR). SIII is a two-dimensional, three-velocity-field, multiphase, multicomponent, Eulerian, fluid-dynamics code coupled with a space- and energy-dependent neutron kinetics model. It includes advanced features such as interfacial area convection and generalized heat and mass transfer. After an initiation at the Los Alamos National laboratory in 1988, the SIII program has been conducted by the Power Reactor and Nuclear Development Corporation (PNC), at O-Arai, Japan, in collaboration for the assessment with the Commissariat à l' Energie Atomique (CEA), France, and the Forschungszentrum Karlsruhe (FZK), Germany. The systematic assessment program is being conducted in two steps: phase 1 for fundamental assessment and phase 2 for integral code assessment. The phase 1 was dedicated to fundamental or separate-effect of individual code models. It was achieved and compiled in 1996 [1]. It consisted in 32 problems treating the fluid convection algorithm, the flow regimes, the momentum exchange and interfacial area models, the heat and mass transfers. It demonstrated the code potential to simulate a variety of transient multiphase flows.

Many of the problems areas highlighted during the phase 1 have been partially solved since 1996. The SIMMER-III code has reached a stage which allows to study key phenomena in CDAs [2]. The CEA-Grenoble (CEA-Gre) contribution is focused on the thermohydraulics and the study of multiphase flows. Since 1996 CEA-Gre worked on basic problems related to two-phase flows, on boiling pools, and on phase 2 type integral experiments calculations. The paper presents a synthesis of these studies.

It begins with phase 1 type basic problems. Most of them are related to the qualification of the interfacial area (IFA) and momentum exchange functions (MXF) modelling, with the following calculations: academic cases of a single water droplet falling in air or a single air bubble rising in water; two phase air/water flows in tubes, prediction of the pressure drop and flow regimes.

As far as phase 2 assessment is concerned, the paper presents applications which are connected to phenomena relevant to CDA issues. The focus is on boiling pool dynamics, and fuel removal and freezing. The SIII verification on material expansion into pool was recently presented [3]. Fuel Coolant Interactions applications have been studied and presented by Morita et Al [4][2] and Teyssier et Al [5]. So these two items will be just shortly evoked in this paper.

As SIII applies to materials very different from water in a great variety of multiphase flow situations, it is not interesting to adjust the code on a particular case. Therefore the presented results are not obtained by the tuning of parameters. Most of the time only the default models and parameters are used.

**CISI Company, France

2.1. Basic SIMMER-III Fluid dynamics features

The conservation equations involving fluid mass, momentum and internal energy are solved, with an algorithm based on a time-factorization approach developed for AFDM [6], with a higher order differencing scheme. The prediction of the interfacial areas in multicomponent multiphase thermohydraulics transients is essential, because the components exchange mass, momentum, and energy mutually through them. An interfacial area convection equation is solved in a general form as proposed by Ishii [7] The source terms of the equation deal with the hydrodynamic break-up, the flashing, the turbulence-driven break-up, the nucleation, the bubbles and the droplets coalescence, the interfacial area changes due to mass transfer or the change of microscopic densities [8].

Given the extreme complexity and the large spectrum of multicomponent multiphase flows that SIII is designed to describe, it uses quite a simple flow regime map based on the volume fraction and on the entrainment fraction Er (Fig.1). Its equilibrium value E_e is derived from the Ishii and Mishima correlation [9]. Eu is the upper limit of the entrainment. α_B (resp. α_D) is constant equal to 0.3 (resp. 0.7). SIII is able to distinguish seven types of channel flow regimes In 1D and 2D: bubbly, transition, dispersed; only in 1D: interpolated, annular dispersed, slug, annular. In transition flows, the flow in a mesh is divided into two parts: a gas continuous and a liquid continuous region.

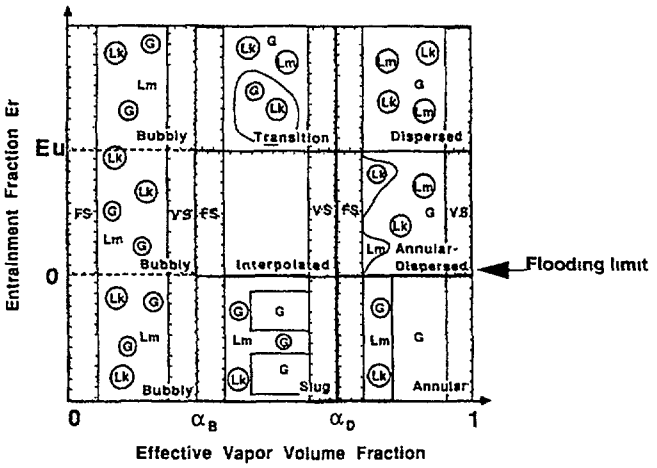

Fig.1: SIII flow regime map.

2.2. Verification of equilibrium IFA and MXF in simple cases

In the literature [10] is given reference values of the terminal speed and maximum radius of a single drop falling in air at 1 bar and 293K (9.2 m/s, r=5mm). A SIII calculation of drops falling in air until they reach their equilibrium has been performed. The result is very close to the one given by Ishii's correlation [11] but in comparison with the experimental values the drop radius is 2 times too big and the velocity 30% too low. The IFA source term due to droplets coalescence seems gives the impression of a correct order of magnitude, no more can be said because no data was referred to.

In the case of a single air bubble rising in water, the consistency with the Ishii's correlation [11] is also very good, but the consistency with experiments looking for the maximum size of a single bubble rising in stagnant water is not high because SIII does not take into account the Kelvin-Helmoltz instabilities which are the governing phenomena in this case [12].

2.3. Bubble coalescence and breakup

The Dedale experiment [13] was calculated with SIII. It consists in an experimental study of the axial development of a two-phase air-water upward bubbly flow in a vertical cylindrical pipe, in which the bubble coalescence is observed. The bubble coalescence modelling is necessary to simulate the tests. SIII coalescence term order of magnitude seems correct, with an error estimated to be around a factor 2.

The SIII models of the bubbles coalescence due to turbulence and of the turbulent breakup maximum diameter take into account the turbulence intensity u_L. There are two contributions to u_L: the liquid motion itself, sometimes called the 'true turbulence' [14], and the fluctuations velocity induced by the bubbles wakes. Both are evaluated in SIII and the maximum of these two effects is chosen. The first one is evaluated as a function of the velocity gradients, the second one is evaluated with the correlation from Theofanous and Sullivan [15]. Several bubble maximum diameter, turbulence intensity, and bubble coalescence models from the bubbly flows literature were compared with SIII. They were all published during the 90's, that is to say later than the related SIII code models [8] which are mainly coming from the AFDM code [16]. The u_L models were compared against the Serizawa et

al. experiment [17] and on Dedale [13]. Theofanous and Sullivan [15] proposed two formulas for u_L. The first one is the current SIII model. The comparison with the Dedale data shows that it is too low. On the other hand the second formula gives satisfying results. The taitel et al. [18] and the Kocamustafaogullari et al. [19] u_L models assume that u_L increases with the wall friction. It is against the Dedale data. For void fractions over 0.1 the bubble maximum diameter (d_{max}) in SIII is consistent with the Kocamustafaogullari et al. [19] model. For low void fractions below 0.08, all the models agree quite well except the SIII d_{max} which increases due to a questionable dependency on the inverse of the void fraction. If d_{max} is calculated with a turbulent break-up Weber number and the second formula of Theofanous and Sullivan, this problem does not occur and a remarkable consistency with the Blahak and Stadkte formulation [20] is obtained. The SIII current coalescence model is still up-to-date when compared to other more recent models [20][21][22], even if it overestimates the coalescence up to a factor 5 with our data deduced from the Prince and Blanch experiment [21]. Its results are improved by a factor two if the second formula of Theofanous and Sullivan is used for the turbulence intensity and if the Prince and Blanch coalescence efficiency [21] is used instead of the SIII constant collision probability equal to unity.

As the code is designed to calculate extremely complex 2D multiphase flows in the whole range of volume fractions, it can calculate situations which involve phenomena in which there remain many unknowns and limitations in the state of the art knowledge. Therefore when the verification is focused on very isolated models as described above, a high level of accuracy is not looked for, but only a consistency with all the other assumptions. Consequently the above results of section 2.2. and section 2.3. were judged satisfactory in a first step, even if a lot of work on the physics could be done to improve the models, providing that new data are available to separately assess each interfacial area source term and momentum exchange function.

2.4. Prediction of flow regimes and pressure drop in 1D two-phase flow

The LOTUS experiment [23][24] was chosen to assess SIII on these items [25]. It gives fully developed flow data under controlled conditions. This rig consists of a 31.8mm diameter vertical tube with the total length of 23m. With a constant outlet pressure of 2.39 10^5 Pa, a fixed liquid mass flow of 297 kg $m^{-2}s^{-1}$, and gas mass flowrates ranging from 2.96 to 162 kg $m^{-2}s^{-1}$, the following classical two-phase flow regimes are covered: bubbly, slug, slug/churn, churn, churn/annular, annular. The apparatus is especially dedicated to the study of the annular flow, with the measurements of the film flowrates which are used for the code entrainment model assessment.

In the bubbly, slug and churn flows, it was shown [26] that the interfacial friction can be directly expressed in terms of the drift flux model [27] coefficients. This model is commonly used for the bubbly, slug and churn flow in the LOTUS range of flowrates, pressure and diameter. A good agreement was found between the SIII gas velocity and the gas velocity predicted by the above drift flux correlation with classical correlations for the drift velocity [27] and the distribution parameter [28], as a function of J, the total superficial velocity.

The discrepancy in the liquid film flowrate prediction can be explained by the known uncertainties [24] of the Ishii and Mishima correlation for the entrainment rate [9] used in the code. The agreement with the pressure gradient is good, within 12%, when the Ueda model [29] is used. This model was implemented to take into account the turbulence effect in the liquid film for the liquid/structure friction. It improves significantly the calculation of the pressure gradient at moderate gas flowrates in annular-dispersed flows, but it requires more validation, especially with reactor materials. The same is truefor the entrainment correlation which was shown to fit earlier data with air-water only. With or without the Ueda model, the phenomenology of the flow regimes is quite well predicted. As for calculations, a «churn» case means oscillations, instabilities; a «slug» case, in a mesh with a lower size than a typical taylor bubble length, means: oscillations between annular flow and a flow with more liquid [25]. Therefore our slug flow calculations oscillate consistently with the observed phenomenology because it reproduces the experimental fact that the liquid phase flow near the wall changes from upwards to downwards and back to upwards as the Taylor bubble passes along the tube. The SIII Taylor bubble is represented as a SIII annular flow. The churny experimental runs give SIII chaotic and/or oscillatory calculations with reasonable average results. The flow stabilizing corresponding to the occurrence of the annular-dispersed flow which goes together with an increase of the pressure gradient with the gas flowrate is predicted, so that the annular dispersed flow calculations are stable.

Last, one can mention that in this study the equilibrium value of the entrainment rate was evaluated, and not the entrainment transient equation. It would be of interest to study it with a suitable experiment.

3. IMPROVEMENT OF THE BOILING POOL MODELLING

3.1. Modelling the momentum diffusion in the SIMMER-III code

The SIMMER-III code is expected to allow the correct representation of LMFBR severe accident situations, as the transition phase one. According to Bohl [30], one significant difficulty in satisfying such an expectation is the need for modelling the momentum diffusion in the direction perpendicular to the velocity. It can be represented by modelling the diffusion of mass, momentum and energy through the transport of turbulent eddies. Because reactor materials, as soon as they are in liquid form, have low viscosity, turbulence is the most important phenomenon in diffusion transport. In the absence of general turbulent flow theory, practical approaches deal with methods that are based upon simulation and modelling. The different approaches are characterized by different levels of accuracy to be reached, and by different levels of sophistication in computational models. In our approach, a statistical model is considered, for which some averaging operations are required.

3.2. Accuracy of the model and computational approach

Due to the computational approach, a certain roughness has to be expected in the modelling. Flow quantities are locally estimated with uncertainties. Our purpose cannot consist in an accurate description of phenomena, for two different reasons. First, in two phase flow computational modelling, and in view of the present day state of computational resources, physical balances have to be locally written in numerical cells the size of which is far larger than the space scale of many phenomena. Let us mention turbulent dissipation, or, in the frame of two phase flow investigations, phenomena that are related to the dispersed phase. The physical quantities of the flow are defined over each computational cell, in an averaged way, at each time step. They are reduced to discrete ones. More over, the different physical and chemical species of the flow are schematically represented, in each cell, by the mean of few volume fractions only. Some phenomena are therefore represented in an idealized way. This is true especially for LMFBR severe accident studies, where motions in the domain are described by the mean of three velocity fields only, in the present version (V2) of the SIMMER-III code.

3.3. Two dimensional calculations

Finally, an emphasis has to be lain on the fact that while turbulence phenomena are basically three dimensional ones, a rough model remains of interest, in the present version of the SIMMER-III code, where the calculation domain is a two dimensional one. The physics of turbulence can correctly be modelled, in 1D or 2D computational investigations, in some particular situations only, where the ratio between the geometrical characteristic lengths of the domain, in different space directions, keeps a value far from one. Let us mention one dimensional calculations in pipe flows, or two dimensional ones, in meteorological forecasting. One can notice that in these studies, the momentum transfer is the largest in the directions that are not directly represented in the computational investigations: the radial one, in pipe flows, due to the boundary layers close to the solid walls; the vertical direction, in meteorology, due, among other phenomena, to boundary layer, upon the soil. Characteristic times for mass, momentum and energy transfers in the ignored directions have much lower values than in the directions directly represented in the approach.

Nevertheless, in the frame of our studies, we cannot consider that the geometrical dimensions of the system are of different orders of magnitude, in the different space directions. The interest of full three dimensional calculations should be underlined. A two dimensional approach leads there to a basically rough modelling. The roughness of the model has to be compared with the level of accuracy of the code calculations themselves.

3.4. Accuracy of experimental data

Finally, one can notice that, in the experiments, we consider for the assessment of the SIMMER-III code, rarely detailed measurements are obtained, for example three dimensional ones. The level of accuracy of the turbulence model has to be compared not only with the roughness of the computational approach, but with the informations available in the literature about experimental data.

3.5. Simplicity of the modelling

In qualification experiments, fluids in the domain generally are air, water and steam. More over, the geometrical features of the domain are not time dependent. Thus experimental data or general considerations help to assess the input data. In the reactor safety analysis, one can face the problem considering the uncertainties in the knowledge of the accident scenario itself. In that case, basic calculations, with best estimated quantities, could be carried out. A simple model is defined, in which the turbulent viscosity coefficient is locally determined. In each region of the flow, it can be supposed either to keep a time constant and space uniform value, or to depend on the local average velocity value.

No transport equation is solved, to estimate the local value of the turbulent viscosity coefficient. Firstly, the approaches based upon transport equations lead to take into account local values of specific terms in the equations, the accurate determination of which would be a difficult task, for reason of roughness of the computational approach. Secondly, the validation of such a model on the basis of some qualification experiments would be of relatively low interest, in the frame of LMFBR severe accidents studies. Large uncertainties in the scenario are there expected. The modelling would have no universal character. Thirdly, the turbulence model in which transport equations are solved generally is the k-ε one. Such an approach is basically very rough. The representation of turbulent quantities is subject to important numerical damping. For example, pressure peaks are underestimated. More over, the basic assumption of the k-ε model deals with the isotropic feature of turbulent structures. Wrong results are obtained in the case where turbulence is an anisotropic phenomenon, as close to the solid walls. Let us notice that generally turbulence level is the highest close to the walls. Lastly, the need for accuracy in turbulent modelling in transition phase boiling pools of LMFBR severe accidents has to be related to other phenomena that can take place in the flows, as, for instance, two phase ones.

3.6. Local approach

Some basic assumptions are deduced from the results of some analytic experiments as the Burty [31] or the Sebulon one [32]. Above all, we consider the approach that consists in assuming that the domain is divided in three different subregions, in each of which the physics of the flow has different features. The regions are defined as follows.

a- *A quasi single phase one lies in the center of the bulk*, where the volume fraction is less than the value of a given parameter α_{go}. It is situated far from the solid walls. Although turbulence dissipation of momentum is less important in that region than close to the vertical wall, it should be correctly modelled, because in that region transit phenomena take place: momentum is there transported from the two phase region to the boundary layer one. In adiabatic situations, the characteristic length of the flow in the liquid bulk is generally given by the hydraulic diameter of the pool. In natural convection ones, it is given by the height of the pool. The importance of that quantity may be underlined, seeing the definition of the non dimensional Rayleigh number, which depends on the corresponding parameter by a power superior to one. In this region, the classical k-ε model is valid. Thus developed turbulence takes place. Turbulent quantities are there assumed to have isotropic and homogeneous properties. The general expression of the turbulent viscosity is there:

$$\mu_{t,BULK} = \rho \cdot C_\mu \cdot H \cdot \sqrt{k} \tag{1}$$

where *H* is the height of the pool. It is supposed to be the characteristic length of the flow in that region. Generally, the value of C_μ is 0.09. In the present version of the SIMMER-III code, no transport equation is solved, to determine the value of the turbulent kinetic energy *k*. It is deduced from the averaged local velocity value *U*, assuming that the ratio between fluctuating and averaged velocity *r* keeps a constant and uniform value, that is equal to 0.1. This assumption corresponds to a situation where turbulence is developed. Finally, in the quasi single phase region, the turbulent viscosity coefficient expression yields:

$$\mu_{t,BULK} = \rho \cdot C_\mu \cdot H \cdot r \cdot U \tag{2}$$

b- *In the vicinity of the solid walls, the most important phenomena deal with the boundary layers*. Since the turbulent shear stress reaches its maximum level in that region, the viscous effects there dissipate a lot of kinetic energy and tend to minimize the global kinetic energy of the liquid layer, in the domain. Locally the expression of the stress in the motion yields:

$$\tau_{local} = \mu_{local} \cdot \frac{\partial u}{\partial y} \tag{3}$$

Turbulent structures are there anisotropic, and turbulence statistical properties remain highly non homogeneous in space. The characteristic length of the flow is there given by the thickness of the boundary layer. On a computational point of view, the boundary layer thickness is generally far less than the cell size of the mesh. This involves the need for a particular approach to model it, above all in non adiabatic calculations. The boundary layer region is considered to be included in the first vertical row of computational cells, in our calculations. In the frame of our investigations, turbulent phenomena close to the solid wall are investigated via a global balance between physical effects. One can consider that for a given particle of liquid, the main motion in the tank consists approximately in two stages. First it is upward driven, due to the drag between gas and liquid phase. Second it is downward driven, in the regions that are close to the vertical walls. If turbulent phenomena reach a developed and statistically steady state regime, the global kinetic energy in the liquid phase is assumed to be dissipated in the second step of the motion, due to the shear stress in the vertical boundary layers. In most computational applications, the cell size is much larger than the boundary layer thickness. It has to be modelled with the help of the quantities that stand for the numerical variables of the calculations. The turbulent viscosity coefficient can be related to the horizontal dimension of the pool *R* and to the stress in the boundary layer as follows:

$$\tau_{BOUNDARY} = \mu_{t,BOUNDARY} \cdot \frac{U}{R} \tag{4}$$

In the previous equation, the length scale is given by the horizontal dimension of the tank, instead of the horizontal dimension of the cell. The kinetic energy is dissipated within the transit along the vertical wall, the length scale of the phenomena is given by the height of the pool. In the case where a cylindrical tank is considered, the turbulent viscosity coefficient should be written as follows:

$$\mu_{t,BOUNDARY} = \frac{1}{4} \cdot \frac{R^2 \cdot \rho \cdot U}{H} \tag{5}$$

The present approach is of interest for the analysis of recirculating flows. It may be useful to investigate the physics of boiling pools.

c- *The bubbly region*, is the region where the gas volume fraction is larger than a given value, generally 10^{-3}. The corresponding value represents the limit above which the two phase phenomena are of first importance in the flow. In some adiabatic experiments, where air is injected in the central part of a tank, water is upward driven, by the gas motion. It can therefore drive momentum to farther liquid, due to viscous effects in the continuous phase. The viscous effects that take place there tend to increase the global kinetic energy of the liquid flow. If the gas volume fraction reaches a so high value as the liquid phase becomes the dispersed one, no momentum diffusion is taken into account in the liquid in our calculations. In the bubbly region, the expression of the turbulent viscosity coefficient is deduced from the one in the recirculating quasi single phase region. The characteristic length R_{BUBBLY} is there either the bubble diameter or the radial dimension in which the bubbly regions expanses. Let us consider the equality of the shear stress between the two neighbouring regions. The expression of the turbulent viscosity in the bubbly region is given by:

$$\mu_{t,\,BUBBLY} \cdot \frac{U}{R_{BUBBLY}} = \mu_{t,\,BULK} \cdot \frac{U}{R} \qquad (6)$$

3.7. Application of turbulent model to adiabatic experiments

The investigation of the Burty experiment [31] is now carried out, with the help of the previously defined turbulence model. Air and water are considered there, in an adiabatic and recirculating flow. Motion is induced in the continuous phase by the rising of bubbles in the central part of a tank of 0.25 meter in radius and 0.3 meter in height. The air injection, at the lower part of the tank, deals with a mass flow rate of 6.6 10^{-4} $kg.s^{-1}$. In the calculations, 25 cells are involved, in the horizontal direction, and 40 in the vertical one. At the upper part of the calculation domain, the pressure is supposed to keep atmospherical values. In Fig.2, one can see first the velocity field in the liquid continuous phase, in the absence of turbulence modelling. The aspect of the velocities is not realistic: the lack of momentum dissipation lets kinetic energy accumulate at the small scales of the flow. Secondary non physical recirculations therefore take place, above all in the upper part of the flow. In figure Fig.2, too, one can see the velocity field in the liquid continuous phase, in the presence of turbulence modelling. A single eddy takes place in the liquid pool, as in the experiment. To investigate numerical results in a more accurate way, we focus at the velocity modulus profile in the radial direction of the tank, at half the height of the pool. Detailed measurements have been obtained in the experiment, and one can see in Fig.3 that numerical results are correct, at least for the great tendencies of phenomena, and even for coarse meshing

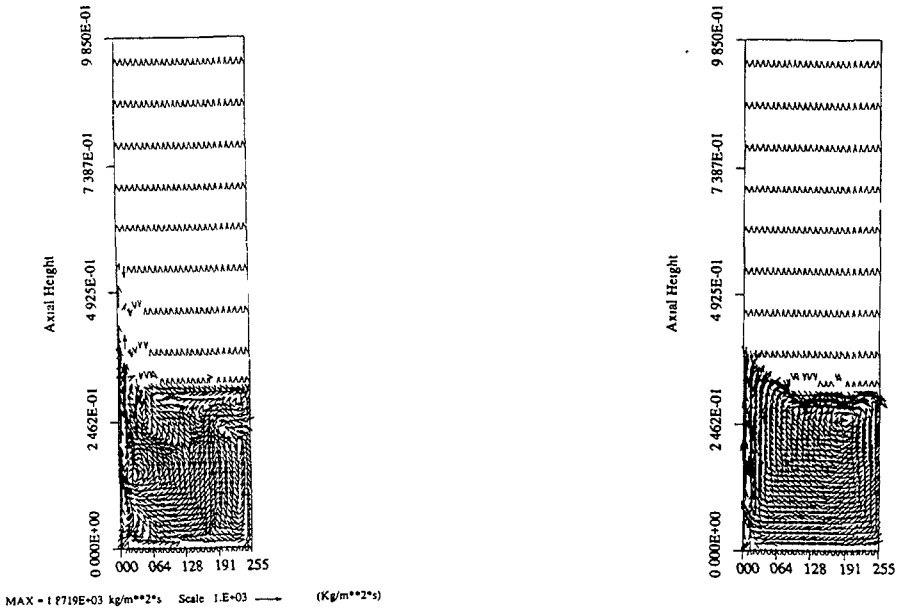

Fig.2: Velocity field in the water phase, in the absence of turbulent modelling (left), or in the presence of it (right), in an adiabatic experiment.The central axe of the cylindrical tank, where the air injection takes place, is left in the picture.

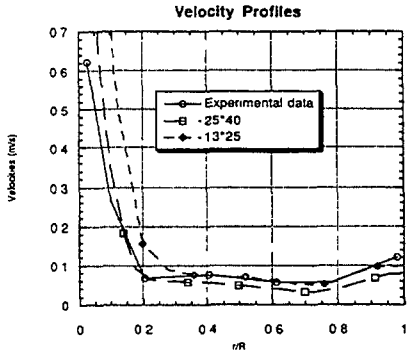

Fig.3: Radial profiles of modulus of velocities in the liquid continuous phase, at half the height of the pool, in the presence of turbulent modelling. Results are compared with experimental data, for two mesh sizes. The central axe of the cylindrical tank, where the air injection takes place, is left in the picture.

3.8. Application of turbulent model to boiling pools experiments

Let us now focus on the Sebulon experiment [32], in which a slice of water is volume heated, till its boiling, and laterally cooled. The experiment is dedicated to investigate flow phenomena in the boiling pools that can take place in LMFBR severe accidents transition phase. Let us consider a case where a large volume of water and a low heating power is considered, that is to say an electric power of 5500 W, whereas the water pool in the tank is 5 cm in depth, 20 cm in width, 80 cm in height. The velocity field in each phase is numerically calculated, with the help of the SIMMER-III code, taking into account the previously defined turbulence model. The velocity field in the liquid continuous phase is represented in Fig.4. The flow is a downward one, close to the cooled solid walls, and an upward one, in the center of the pool. More over, due to turbulent effects, the geometrical features of the flow, over the domain, are not symmetrical ones, at a given time. In fact, in a given point, the direction of the flow is a perpetually changing one. In that case, numerical results look realistic, concerning the visual aspect of the flow. We now investigate the lateral wall heat flux, as soon as the global thermal balance, over the domain, is reached. Results look correct ones, at least for the great tendencies of phenomena. Nevertheless, one can see in figure Fig.4 that the experimental flux reaches its maximum value in the upper part of the liquid pool. It is due to the presence, in the upper part of the tank, of a downward flow in a liquid film, close to the cooled walls. The corresponding effect deals with condensation of vapour, not single phase natural convection. It cannot be investigated by the mean of such tool as the present turbulent model. It requires a specific approach. More over, one should notice that the physical properties of materials are different in qualification experiments, as the Sebulon one [32], and in the reactor case, where metals are expected to boil. Above all density and surface tension are different. One can expect the physics of condensation in the reactor case to have different features.

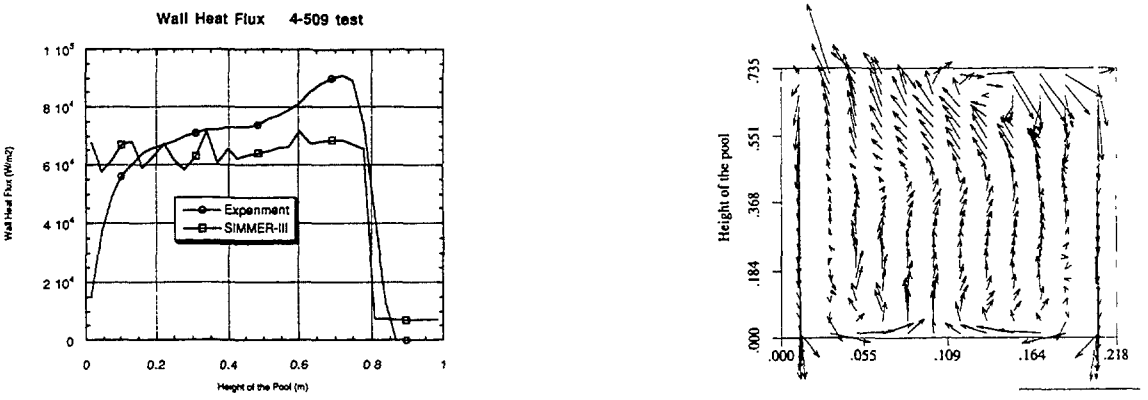

Fig.4: Heat flux distribution at the lateral vertical wall, in a rectangular boiling pool experiment (left), and velocity field in the liquid continuous phase (right). The previously defined turbulence model is taken into account.

4. SUBASSEMBLY MELTING AND PROPAGATION: CALCULATIONS OF SCARABEE EXPERIMENTS

In the present section, more attention will be paid on the calculations of reactor-like accident situations, through the calculations of some SCARABEE experiments. These tests were summarized recently [33]. They investigate: the degradation of a subassembly consecutively to a loss-of-flow situation (slow and partial to total instantaneous blockage) with the APL and BE series; the radial propagation of melt to neighbouring subassemblies with the PIA and PV tests; the boiling pool mechanisms in a subassembly geometry with the BF tests.

In the first part, we will investigate a slow pump run down situation through the APL3 experiment and a total instantaneous inlet blockage situation through the BE+3 experiment, and through pre-calculations of the TP-1 (also called BE+I) experiment. The second part of this section will deal with boiling pool calculations through the calculation of the BF2 experiment.

4.1. SCARABEE loss-of-flow APL3, BE+3 and TP1 calculations

The objective of these calculations is to investigate the ability of SIII to describe such extremely complex situations as the degradation of an assembly. A characteristic transient includes the following phenomena: sodium heat up and boiling; clad, fuel pellets and canwall (CW) melting; axial and radial melt propagation and relocation; lower and upper plug formations due to the freezing of the molten materials; pressurization (or not) of the subassembly consecutively to the fission product release.

The three tests under consideration involve a 37-pin bundle submitted to a nuclear power (at nominal level). TP-1 is in fact an experimental project with irradiated fuel. Therefore calculations concerning TP-1 cannot be confronted to an experimental support. BE+3 was an experiment rather similar to TP-1 (instantaneous blockage) except that in BE+3 the fuel was unirradiated, and a small argon gap was embedded between two canwalls. This particular geometry does not allow calculations after the first CW melting. Then the calculations consider the first stages of the transient only. Finally, only APL3 gives an experimental support for the calculations of the complete transient and will then receive more attention.

4.2. APL3 calculations

a- Boiling and melting events.

In 1-D APL3 calculations, we consider only one radial mesh inside the wrapper. The events before the sodium boiling are rather well represented. The boiling chart is represented in Fig.5 (left figure). The lines represent the experimental boiling and drying front in the first, third and fourth channel at the top of the fissile zone level. The empty and filled squares represent the level in the calculation were the boiling and the drying occurs. The boiling occurs with a good timing, with regards to the strong temperature radial profile in the experiment. However the incipient of boiling and the drying occur at nearly the same time in the calculation, whereas about 15 seconds separate these two phenomena in the experiment. Another problem lies in the overestimation of instabilities at the upper boiling level, leading at 57 s to a large rewetting. It has a noticeable influence on the following part of the transient. It seems to come from the modelling of the liquid-structure contact near the onset of dryout: it is no more predicted with a rough model which reduces the liquid-structure interfacial area over a given wall temperature, as shown on the right figure of Fig.5. When the sodium level oscillations are avoided, the timing for structure (clad + wall) melting is a correct one. The influence of the different criterion for breakup is rather small (~ 10 %) for the time of beginning of material melting. As an example, the calculations give a first CW breakup at 75 s, whereas it occurs at 72 s in the experiment.

In 2-D calculations (4 radial meshes, i.e. 1 mesh per sodium channel), the boiling is a bit better reproduced, as is seen on Fig.6, where the boiling fronts are represented on the left in different channels, and on the right the dryout fronts. The same conclusion holds for the structure breakup progression.

We conclude that the first events of the transient: boiling and melting of structures, are satisfactorily reproduced by SIII. However the SIII modelling of the boiling along heated walls seems to be a bit rough. The downward and radial progression is too rapid and the dryout is almost instantaneous. Future work is planned at CEA Grenoble to work on this point, in order to check if improvements of the boiling model are needed.

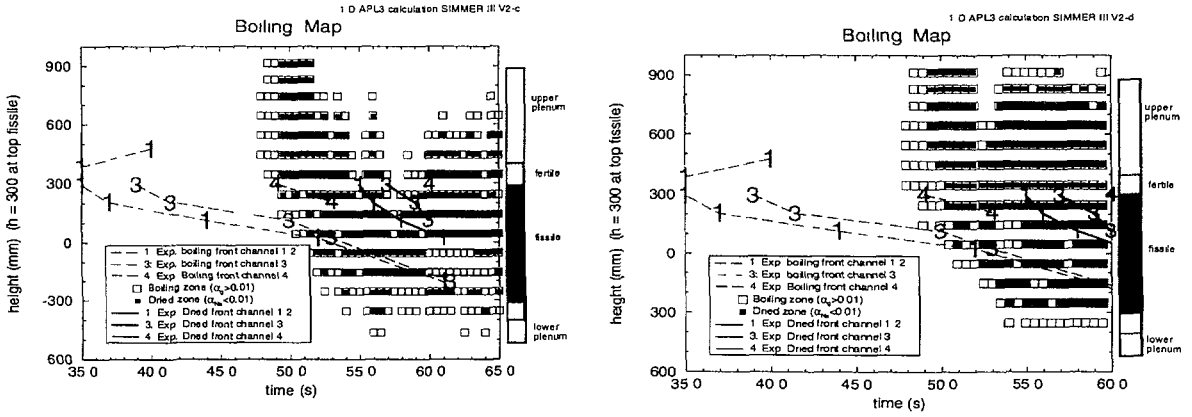

Fig.5: Calculated and experimental boiling map (boiling and drying) in 1-D APL3 calculation. Left: standard boiling model, right: with inclusion of a maximum wall temperature for the presence of liquid-structure contacts

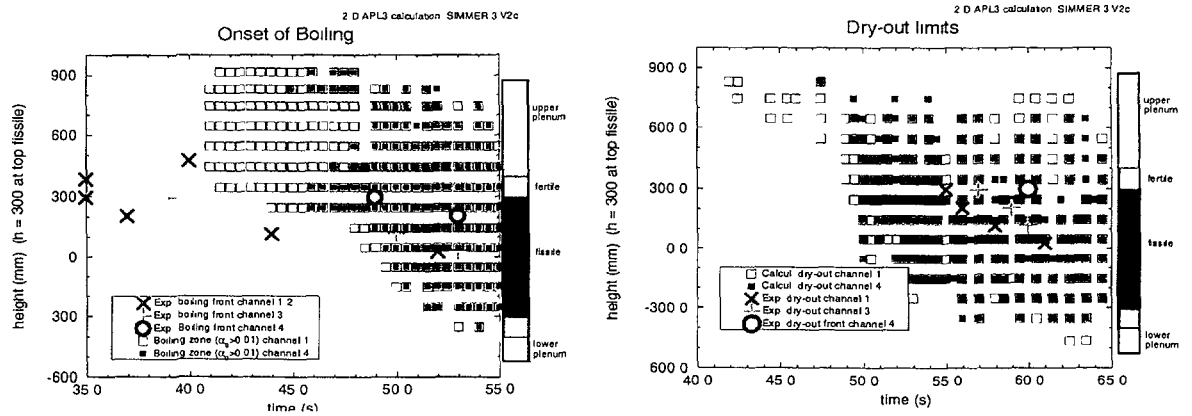

Fig.6: Confrontation of experimental and calculated boiling fronts (left figure) and dryout fronts (right) in 2-D APL3 calculation.

b- Molten material relocation

The prediction of the following part of the transient is less satisfying. The material relocation is very sensitive to a large number of parameters.

A first problem comes from the flowing of broken fuel pellets which are, for an important part, ejected out of the bundle (whereas their diameter is larger than the length scale between the pins in the non molten zones). This problem is very difficult to overcome due to the small number of velocity fields (2) allowed to reproduce the flow of 5 phases (fuel and steel particles, fuel, steel and sodium liquids), the third one being for the gas. Several parameters and small coding modifications have been tested but no tight blockage (i.e. not porous) with frozen steel was predicted. It is rather clear that in such extreme conditions, with all the materials included in a small volume, the number of velocity fields is a too small one.

A second limitation comes from the too rough flow configurations (Fig.1) for such cases. For example, in some calculations, a lower plug may be formed when the steel is forced to contact the structures, prior to other liquids. The third limitation is the lack of fuel crust formation over the pins. 2-D calculations did not lead to a more satisfying behaviour relatively to the material relocation problem.

We conclude that further studies are required to better simulate the tight blockages occurring during a complete loss-of-flow in a subassembly transient. The limitations of SIII in this kind of application can be historically explained by the fact that it was initially designed to describe the whole core transition phase of the accident, and that it is here attempted to use it for the initiating phase within one subassembly only.

4.3. TP-1 pre-calculations

In the previous calculations, a particular attention was paid on the plug formation because in the irradiated case, the eventual lower and upper plug might lead to an important pressurization through the fission product release (~ 100 bar expected). The objective of the TP-1 project was to give some answers to the questions relative to the pressurization of the bundle. As seen before, the SIII prediction of the molten material relocation and blockage is subject to uncertainties. We will see however that, regarding to this point, the situation is less critical in such cases with an instantaneous blockage. A supplementary important difficulty in the simulation of TP-1 comes from the simulation of the foam that is expected to take place after the fission product release. This point will not be discussed here and we will focus on events occurring prior to the eventual pressurization.

In order to check the code versus an experiment with an instantaneous inlet blockage, calculations with BE+3 were previously performed. The first events from boiling to structure melting were well reproduced in 1-D and 2-D calculations. Unfortunately, the calculations could not be run further, due to the difficulty in representing the following part of the transient with the BE+3 special geometry in which the pins were separated from the CW by a small argon gap (to ensure flatness of the temperature radial profile). For the TP-1 test, this argon gap was avoided because it might lead to unexpected effects. The cross section of TP-1 is given in Fig.7. On the contrary to APL tests, the assembly is cooled by a sodium flow, simulating the interassembly (IA) flow. This leads to a strong temperature radial profile.

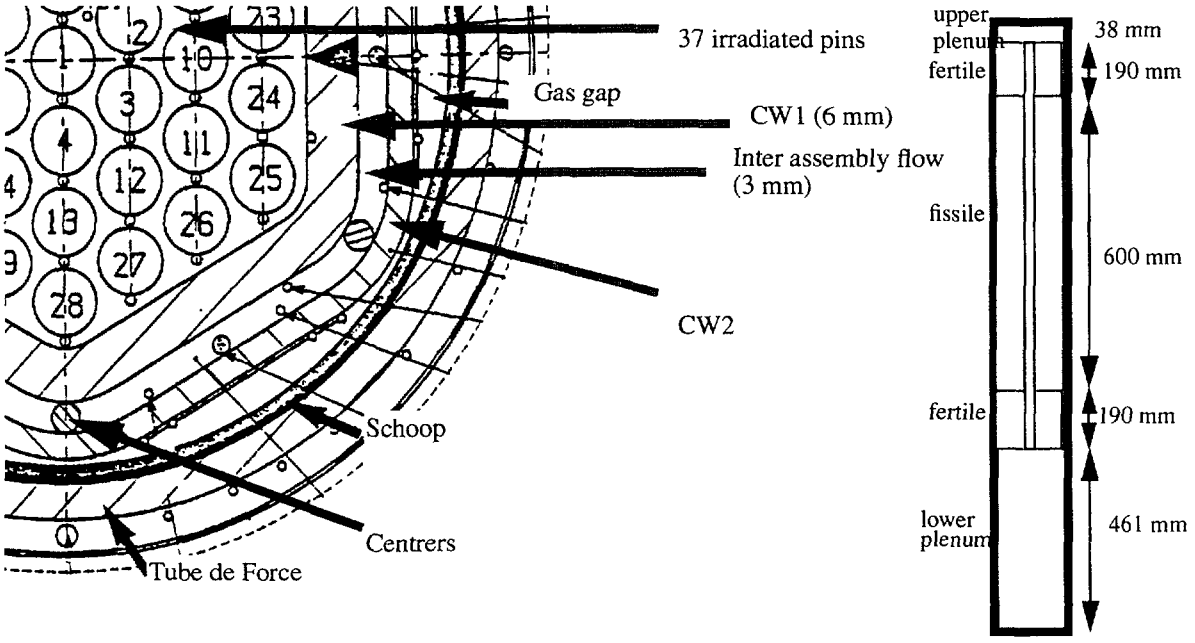

Fig.7: TP-1 cross section and pin geometry.

a- 1-D calculations

1-D pre-calculations were not satisfying regarding to the timing of the events. Due to the radially high temperature gradient, the boiling, drying and melting events occur very late regarding to the BE+3 experiment. Nevertheless, probably due to the total inlet blockage, the molten material progression and relocation seems to give better results than in APL3 calculations. A sketch of these events is given in Fig.8. A lower tight plug is obtained very soon, but no upper plug is even initiated. The canwall is slightly molten only, protected by a fuel crust. However, the delays calculated for these events are unacceptable since in BE+3 the fuel melting occurred at about 12 s. 1-D calculations are then not appropriate for these situations.

b- 2-D calculations

2-D calculations showed good results for the boiling, drying and melting events, regarding to the comparison with BE+3, as shown in Fig.9. One should notice that the boiling and drying occur firstly in the fertile zone, which indicates that the cooling along the pins in unheated sections might be inefficient. Nevertheless his has no effect on further events since the cladding breakup is evaluated in a very similar manner as reported for BE+3. A representation of the transient is given in Fig.10. It is seen that steel plugs are almost obtained at the bottom of the fissile zone. No tight upper plug is calculated. The external fuel pellet row is seen to remain intact. The canwall remains very thick and no wrapper failure by thermal attack is then predicted. In such a situation, since no upper plug exists, no pressurization is obtained.

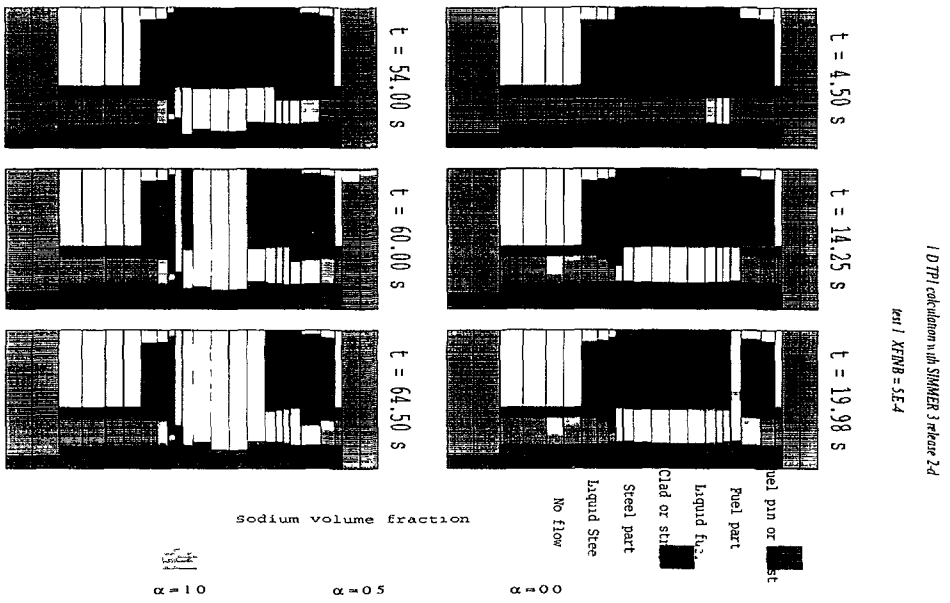

Fig.8: main event sequence in 1-D TP-1 pre-calculation. (green: Na flow, deep blue: clad or CW, light blue: molten steel, red: fuel pellets or fuel crust, orange: fuel particles, yellow: liquid fuel).

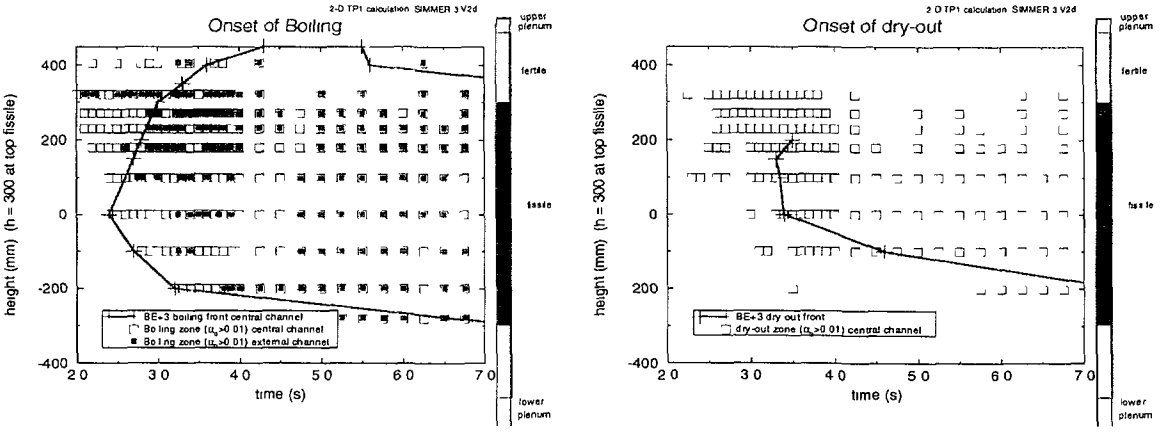

Fig.9: Confrontation of experimental BE+3 results and TP1 calculated boiling fronts (left figure) and dryout fronts (right) in 2-D TP-1 precalculation.

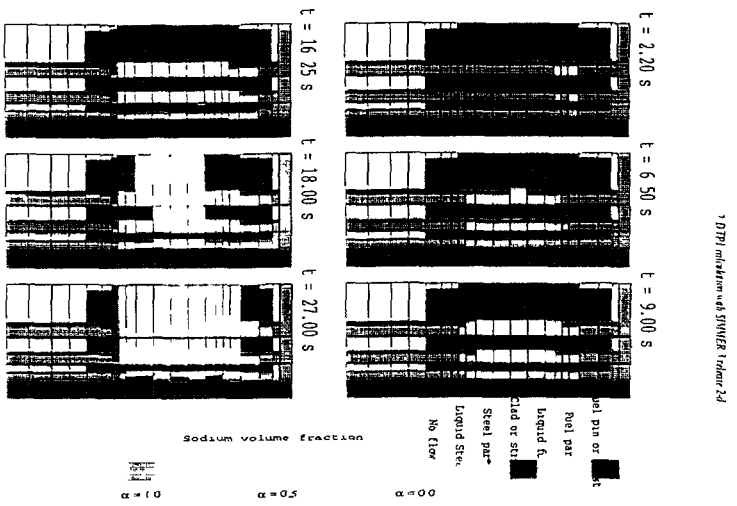

Fig.10: Representation of the transient in 2-D TP-1 pre-calculation.

4.4. Conclusions on APL3 and TP-1 calculations.

Regarding to SIMMER-II calculations [34], important improvements are reported with the SIII code. But there are some more or less important difficulties left. The boiling and drying occur with a good timing but for long transients (e.g. partial blockage), the incipient of boiling and the dryout might be too roughly estimated. These points are not important for total instantaneous blockage situations. The structure breakup events are generally well represented. On the other hand, the relocation of molten materials and subsequent refreezing within a subassembly needs further investigation. Concerning the plug formation, a crucial lack lies in the absence of fuel crust formation along the pins. Specific models for these events are clearly required (with for example the possibility of formation of non homogeneous plugs or crusts).

4.5. BF2 - Calculations.

The BF2 test is an experiment intended to study the boiling mechanisms of a liquid pool of fuel [33][36]. The geometry is similar to the preceding SCARABEE experiment, except that the subassembly is replaced by a closed crucible filled with 6 kg of UO_2. The ambient gas is mainly helium at the 0.035 bar (at 20 °C). The fuel is heated at 93 W/g during 60 s. The crucible is cooled by a lateral flow of sodium. The average pressure is about 0.5 bar. The pressure and temperature measurements showed large oscillations indicating a cyclic boiling mechanism with average frequency of 0.8 Hz. Simulating such transient is a very difficult task, because it deals simultaneously with: boiling / condensation and melting / freezing phenomena; important oscillations and cyclic liquid motion (no steady-state reached); complex liquid/structure contacts; presence of non condensable gases. At the present time, no code fully succeeded in this task, even if their use helped to understand the physics [35][36][37].

The present calculations show a moderate general agreement with the experiment. The good aspect concerns the average pressure which is well calculated. The flow is quite turbulent and no steady state is reached. Important pressure oscillations are reported, corresponding to a violent cyclic phenomena of boiling / condensation phases. However, the cycles are not as regular ones as in the experiment. Averaging the flow over ten seconds leads to the configuration depicted in Fig.11. From an averaged point of view, a convection roll takes place in the liquid part of the pool. The bottom of the pool is almost liquid over 100 mm. Over this single-phase layer lies a two-phase region where most of boiling / condensation phenomena occur. A type of liquid film takes place along the cooled wall. The crucible is seen to be protected by an important fuel crust which lies up to nearly 1 m. The average thickness of the film is of the same order of magnitude but the thickness profile is not very representative of the experimental one.

We also see in Fig.11 that the removed heat flux profile is moderately satisfying. This point represents in general (for other codes) the main discrepancy with the experiment. The maximum is rather well located, but the profile is clearly too flat, and does not reproduce the sharp decrease obtained at approximately 300 mm. It is expectable that most of the discrepancy concerning the heat flux profile comes from a too rough modelling of the crust. In the present calculation, the heat removed over the liquid pool corresponds almost to the injected energy in the crust. The profile of the heat transferred from the pool to the crust is rather good. Then a special attention should be paid to the crust modelling. Given the supposed flow configuration which is characterised by an increasing void fraction with the height, with a sloshing two-phase region at the pool surface, the porosity of the crust may increase with the height and the contact between the crust and structure may decrease with the height. Then this should reduce strongly the heat removed above the pool. The crust model available in SIII has to be further validated in situations where the crust is partly formed by sloshing.

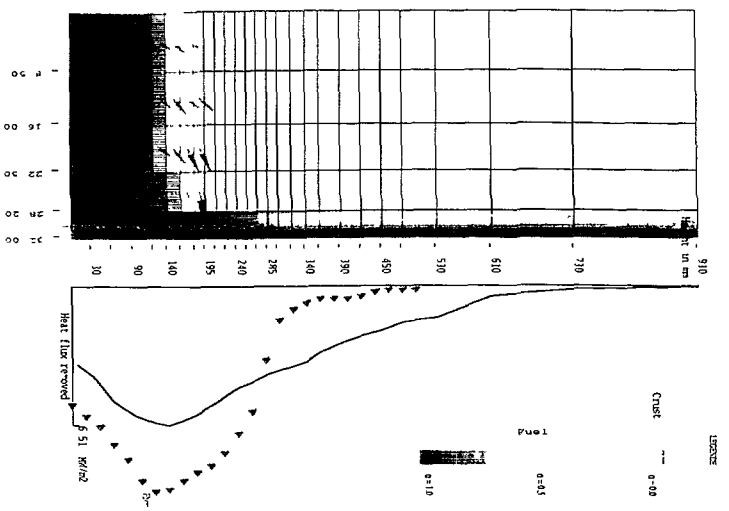

Fig.11: Average typical configuration of the flow and heat flux profile on sodium side.

5. INTEGRAL TESTS CALCULATIONS

5.1. Material expansion into pool

During the expansion phase of core disruptive accidents in LMFR, a large vapour bubble expands from the core inside the sodium pool and may threaten containment limits. The prediction by SIII of the dynamics of a large bubble expansion into a stagnant pool is assessed against the SGI experiments performed at FZK [38]. The experiments consist in injecting high pressure gas at the bottom of a low pressure water pool. It is a small scale, reactor like geometry. The SIII code proves to be able to calculate very well these experiments, without any adjustment [3]. The need for proper initial conditions and for a droplet entrainment model from large bubble/pool interface is outlined. An expansion phase test calculation at the reactor scale was also successfully conducted. In terms of the timing of events and of the calculated energy distributions, the general trends of the SIII results were found reasonable compared to the state of the art.

5.2. Fuel/Coolant interactions

Recently SIII was used by PNC and FZK to describe fuel/water or fuel/sodium interactions, with the calculations of the following experiments: THINA 564 and 562, FARO L06, KROTOS 28 [4]; QUEOS 08 and 12, PREMIX 01, 02 and 03 [5]. Among the experiments, the only ones with sodium are THINA, for which good results were obtained. None of them implied large amounts of fuel masses as it is the case in the TERMOS experiments where 110 kg of molten UO2 were poured into 130 kg of liquid sodium, via the gravity driven fall of a UO2 jet through the cover gas which is over the pool [39]. The interpretation of the results by people who carried out the experiment was: first the melt heated the sodium up to the saturation, the kinetics of which is controlled by by hydrodynamic fragmentation of the jet, followed by freezing driven fragmentation of the UO2 droplets; second, as sodium reached the saturation, the conditions for the pre-mixing phase (by film boiling) were realized, and they lead to the observed fuel/coolant interactions [40]. Three interactions occurred. The interpretation concerns the first and the second one. The understanding of the third one is poor. Given the extreme conditions of the experiment, few measurements are available. On the top of that the boundary conditions are unclear. On the other hand such a complex problem would require many data to check isolated results. Therefore our work is only a first step in the study with SIII of large scale fuel/sodium interactions.

SIII was found to be sufficiently robust to investigate such situations. A first calculation took into account the modelling of the jet fall through the gas. In this case, with the default parameters of the code, an increase of the interfacial area, and then a probably non-physical jet breakup (we can not check with data but only with orders of magnitude given by correlations) lead us to give up this modelling to focus on the phenomena within the sodium pool. Thus the jet was defined at the initial calculated time, just before its contact with the sodium pool, by a dispersed flow in which the UO2 droplets radius was set to the radius of the release tube. The result of this calculation is that the liquid UO2 penetration length in the pool and the kinetics of solidification are predicted within a reasonable order of magnitude. On the other hand, the total amount of UO2 that penetrates the pool is underestimated. Only one interaction is predicted, which is larger than the experimental first pressure peak. Despite the fact that this result is sensitive to the unclear boundary conditions, further investigations should consider the possibility of an overestimation of the heat transfers, itself maybe due to an overestimation of the fragmentation. Indeed the freezing-inhibited droplets fragmentation is not taken into account in SIII. The freezing-provoked droplets fragmentation is somehow calculated with the solid particles formation when freezing of the droplets occurs.

Anyway these calculations confirmed the interest of SIII to study fuel/coolant interactions, consistently with [4][5].

6. CONCLUSION

The SIMMER-III (SIII) code is dedicated to the analysis of core disruptive accidents of liquid metal fast reactors, which involves extremely complex multiphase multicomponent flows with heat and mass transfers. The CEA contribution to this code developed by PNC assessment is included in an international joint program in collaboration with PNC and FZK. The phase 1 of the assessment reached a milestone in 1996, showing that the multiphase fluid-dynamics model was basically valid and identifying limitations which have been studied ever since. In the present paper, a synthesis of the work performed at CEA/DRN/DTP in Grenoble since 1996 is presented. It deals only with multiphase flows, from basic models such as turbulence in boiling pools, to more integral tests such as SCARABEE. The reactor applications with neutronics are carried out at CEA/DRN/DER in Cadarache as far as CEA is concerned.

The two-phase flow modelling assessment is intimately linked with the advanced feature of SIII which is the interfacial area convection equation. The source terms of this equation due to bubble and droplets coalescence and breakup were judged satisfactory in a first step, considering the unknowns and limitations remaining in the state of the art. Anyway further data are required. Then it is shown that the code reasonably calculates the flow regimes, the pressure drop, and the entrainment rate in a 1-D fully developed air/water two-phase flow.

The classical transition phase problem of an internally heated boiling pool with laterally cooled walls is investigated. The boiling pool modelling is improved by the implementation of a turbulence model, which is possible because the Navier Stokes equation are solved by the code, and which is relevant because these equations are solved by a second order spatial discretization: with a first order discretization of the Euler equations, it was shown that the numerical diffusion effect overexceeds the real turbulence one. The model is based on a local approach which leads to an expression which gives an order of magnitude of the turbulent viscosity specific in each of the three parts of the two-phase re-circulating domain: a quasi single-phase one in the center of the bulk, the boundary layers in the vicinity of the walls, the bubbly region.

Three SCARABEE experiments involving a 37-pin bundle submitted to a nuclear power at nominal level, degraded consecutively to a loss of coolant, with the real reactor materials, were calculated. Large improvements since the previous SIMMER-II calculations were noticed. The structure breakup events are generally well predicted by SIII. The boiling and drying are predicted with a good timing, albeit for long transients with partial blockage the prediction of these events may require further studies. Further investigation may also concern the relocation of molten materials and subsequent refreezing within a subassembly. Besides these three tests, material expansion into pool with the SGI experiment and fuel/coolant interactions with the TERMOS experiment have shown the SIII applicability to more integral calculations, and reliable robustness.

ACKNOWLEDGEMENTS

The authors would like to thank many people in PNC. Valuable discussions with Satoru Kondo, Koji Morita, Yoshiharu Tobita, and David Brear were essential in performing these studies.

REFERENCES

[1] S. Kondo et al., "Status and Achievement of Assessment Program for SIMMER-III, a Multiphase Multicomponent Code for LMFR Safety Analysis", NURETH8, Kyoto, Japan, Sept.30- Oct.3, 1997.

[2] K. Morita et al., "SIMMER-III Applications to Key Phenomena of CDA in LMFR", NURETH8, Kyoto, Japan, Sept.30- Oct.3, 1997.

[3] F. Boulanger, P. Coste, "LMFR Accidents: Verification of the SIMMER-III Code for the Expansion Phase", NURETH8, Kyoto, Japan, Sept.30- Oct.3, 1997.

[4] K. Morita et al., "SIMMER-III Applications to Fuel-Coolant Interactions", OECD/CSNI Meeting on Fuel/Coolant Interactions, Tokaï, Japan, May 19-21 1997.

[5] P. Teyssier et al., "Assessment of the SIMMER-III code with experiments QUEOS and PREMIX", ICONE5, May 26-30, Nice, France, 1997.

[6] W. R. Bohl, "AFDM: An Advanced Fluid Dynamics Model, Volume V: The Convective Transport Algorithm", LA-11692-MS, Vol. V, Los Alamos National Laboratory Report (1990).

[7] M. Ishii, "Thermo-Fluid Dynamics Theory of Two-Phase Flow", Eyrolles, Paris (1975).

[8] Y. Tobita et al., "Interfacial Area Modeling for a Multiphase, Multicomponent Code for LMFR Safety Analysis", Proc. ICMF'91, Tsukuba, 2-365, 1991.

[9] M. Ishii, K. Mishima, "Liquid Transfer and Entrainment Correlation for Droplet-Annular Flow", Proc. of 7th Int. Heat Trans. Conf., Munchen, 1982.

[10] R. Clift et al., "Bubbles, Drops, and Particles", Academic Press, 1978

[11] M. Ishii, "Drag Coefficient and Relative Velocity in Bubbly, droplet or Particulate Flows", AIChe Journal, Vol.25 no5, pp.843-855, 1979.

[12] G. Kocamustafaogullari, M. Ishii, "Maximum Fluid Particle Size for Bubbles and Drops", ASME winter annual meeting, Miami, USA, Nov 17-21, 1985.

[13] C. Grossetête, 1994, "Experimental Investigation and Preliminary Numerical Simulations of Void Profile Development in a Vertical Cylindrical Pipe", EDF- Direction des Etudes et Recherches, PHD.

[14] M. Lance, J. Bataille, "Turbulence in the Liquid Phase of a Uniform Bubbly Air-Water Flow", J. Fluid Mech., Vol. 222, pp. 95-118, 1991.

[15] T.G. Theofanous, J. Sullivan, "Turbulence in Two-Phase Dispersed Flows", J. Fluid Mech., Vol. 116, pp. 343-362, 1982.

[16] D. Wilhelm, "AFDM: An Advanced Fluid Dynamics Model", Volume II, Los Alamos National Laboratory, 1990.

[17] A. Serizawa et al., "Turbulence Structure of Air-Water Bubbly Flow: III-Local Properties", Int. J. Multiphase Flow, Vol. 12, pp. 235-246, 1975.

[18] Y. Taitel et al., "Modelling Flow Pattern Transitions for Steady Upward Gas-Liquid Flow in Vertical Tubes", AIChe Journal, Vol. 26, n°3, pp.345-354, 1980.

[19] G. Kocamustafaogullari et al., "Measurement and Modelling of Average Void Fraction, Bubble Size and Interfacial Area", Nuclear Engineering and Design, Vol. 148, pp. 437-453, 1994.

[20] A. Blahak, H. Stadkte, "Modelling of Transport of Interfacial Area Concentration in Two-Phase Flow Systems", European Two-Phase Flow Group, Grenoble, June 3-5, 1996.

[21] M. J. Prince, H. W. Blanch, "Bubble Coalescence and Break-up in Air-Sparged Bubble Columns", AIChe Journal, Vol.36, no10, pp.1485-1499, 1990.

[22] G. Guido-Lavalle et al., "A Bubble Number Density Constitutive Equation", Nuclear Engineering and Design, Vol. 152, pp. 213-224, 1994.

[23] D.G. Owen, G.F. Hewitt, "Data and Analysis of Pressure Gradient and Liquid Entrainment in Vertical Annular Gas-Liquid Flow", European Two-Phase Flow Group Meeting, Marchwood, G.B., June 1985.

[24] D.G. Owen, et al., "Equilibrium Annular Flows at High Mass Fluxes: Data and Interpretation", Physico Chemical Hydrodynamics, vol.6, pp 115-131, 1985.

[25] P. Coste, Y. Tobita, "Two-Phase Channel Flow Modelling of SIMMER-III, a Multiphase, Multicomponent Code for LMFR Safety Analysis", ICMF'98, Lyon, France, June 8-12, 1998.

[26] D. Bestion, "The Physical Closure Laws in the CATHARE Code", Nucl. Eng. Des. 124 pp. 229-245, 1990.

[27] N. Zuber, J. A. Findlay, "Average Volumetric Concentration in Two-phase Flow Systems", J. of Heat Transfer, Trans. ASME, Series C, Vol. 87, pp. 453-468, 1965.

[28] M. Ishii, "One Dimensional Drift-Flux Model and Constitutive Equations for Relative Motion Between Phases in Various Two-Phase Flow Regimes", ANL-77-47, 1977.

[29] T. Ueda, "On the upward flow of gas-liquid mixture in a pipe", Nihon-kikai-gakkai ronbunsyu (in Japanese), Vol.33, No 248, pp. 601-625, 1967.

[30] W. R. Bohl, "Some Preliminary Thoughts on Turbulence Modeling in AFDM". AFDM documentation, 1988, and private communication with PNC, 1988.

[31] M. Burty, "Contribution à l'étude du brassage pneumatique de métaux liquides en poches de traitement et des transferts métal-laitier". PhD thesis of the "Institut National Polytechnique de Grenoble", October 23rd, 1989.

[32] J.M. Seiler et al., "One component, volume heating, boiling pool thermohydraulics". AIChE Symposium series number 288, Heat Transfer, part 2, vol. 88, pp. 54-63, San Diego, 1992.

[33] G. Kayser et al., "Summary of the SCARABEE-N Subassembly Melting and Propagation Tests with an Application to a Hypothetical Total Instantaneous Blockage in a Reactor", Nucl. Sc. and Eng., 128, pp.144-185, 1998.

[34] T.G. Williams et al., "SIMMER-II applications to tests in the SCARABEE-N program", Proceedings of the 13th LMBWG à Winfrith, 1988.

[35] Y. Tobita, "An Analysis of Boiling Pool Experiment by SIMMER-III", NURETH8, Kyoto, Japan, Sept.30- Oct.3, 1997.

[36] J.P. Breton et al., "The SCARABEE molten and boiling pool test series BF experimental results, modeling and interpretation", Proc. of the Int. Fast Reactor Safety Meeting, Snowbird, August 1990, vol.I, 357-365.

[37] D. Wilhem, G. Kaiser , "Analyzing the SCARABEE BF2 and BF3 Experiments", Proc. ARS'94 Int. Topl. Mtg. Advanced Reactor Safety, Pittsburgh, Pennsylvania, April 17-21, 1994, Vol.2, p.776, American Nuclear Society.

[38] D. Wilhelm et al, "Two simulant material experiments studying the fluid dynamics in core disruptive accidents", Mtg Science & technology of fast reactor safety, Guernsey, May 1986.

[39] D. Magallon et al., "Pouring of 100-kg-Scale Molten UO_2 into Sodium", vol. 98, pp79-98, Nuclear Technology , 1992.

[40] D. Magallon, "An Analysis of the melt penetration into Sodium in the FARO-TERMOS Experiments", Proc. 14th Mtg. Liquid Metal Boiling Working Group, Brasimone, Italy, April 16-18, 1991.

3-D THERMAL HYDRAULIC ANALYSIS OF TRANSIENT HEAT REMOVAL FROM FAST REACTOR CORE USING IMMERSION COOLERS

I. CHVETSOV, A. VOLKOV
State Scientific Center of Russian Federation,
Institute of Physics and Power Engineering,
Obninsk, Kaluga Region, Russian Federation

XA0055044

Abstract

For advanced fast reactors (EFR, BN-600M, BN-1600, CEFR) the special complementary loop is envisaged in order to ensure the decay heat removal from the core in the case of LOF accidents. This complementary loop includes immersion coolers that are located in the hot reactor plenum. To analyze the transient process in the reactor when immersion coolers come into operation one needs to involve 3-D thermal hydraulics code. Furthermore sometimes the problem becomes more complicated due to necessity of simulation of the thermal hydraulics processes into the core inter-wrapper space. For example on BN-600M and CEFR reactors it is supposed to ensure the effective removal of decay heat from core subassemblies by specially arranged internal circulation circuit: "inter-wrapper space".

For thermal hydraulics analysis of the transients in the core and in the whole reactor including hot plenum with immersion coolers and considering heat and mass exchange between the main sodium flow and sodium that moves in the inter-wrapper space the code GRIFIC (the version of GRIF code family) was developed in IPPE.

GRIFIC code was tested on experimental data obtained on RAMONA rig under conditions simulating decay heat removal of a reactor with the use of immersion coolers. Comparison has been made of calculated and experimental result, such as integral characteristics (flow rate through the core and water temperature at the core inlet and outlet) and the local temperatures (at thermocouple location) as well.

In order to show the capabilities of the code some results of the transient analysis of heat removal from the core of BN-600M - type reactor under loss-of-flow accident are presented.

1. INTRODUTION.

It is proposed that additionally to the normal heat removal route via the steam plant, the advanced fast reactors will be equipped with the Direct Heat Removal System (DRS). This system is intended for removal of decay heat from the core in the case of loss of station service power. Each DRS circuit includes an immersion cooler (IC)), installed in the reactor hot plenum and an air cooler. These two coolers are connected via intermediate sodium loop. The transportation of the heat from the core to immersion cooler occurs both by free convection of the sodium in the hot plenum of reactor and by circulation via primary loop. The energy that can be transported this way per time unit depends on reactor design and sometimes can be essentially limited due to stratification of the sodium in the hot plenum. In order to intensify the heat removal from the core subassemblies for advanced Russian fast reactor BN-600M and Chinese experimental fast reactor CEFR the innovative core design was proposed. In these projects the "cold" sodium from IC outlet is partly directed into subassembly inter-space via specially arranged gaps and holes in the reactor internal structures forming additional heat removal circuit.

For thermal hydraulic analysis of the transients in the core and in the whole reactor including immersion coolers and considering heat and mass exchange between the main sodium flow and sodium flowing in the inter-wrapper space GRIFIC code was developed.

2. GRIFIC CODE DISCRIPTION

The code contains the following modules:

- 3D thermal hydraulic model for calculation of sodium velocity, pressure and temperature in the primary circuit;
- 3D model for simulation of inter-wrapper sodium thermal hydraulics;
- set of 1D, 2D and 3D models for calculations of temperature distributions in "impermable" elements (pins, wrappers, etc.);
- 1D thermal hydraulic model of intermediate heat exchanger and immersion cooler; primary pump model.

For simulation of the main sodium flow in the reactor the GRIFIC code is solving a system of heat-and-mass exchange equations in an approximation of a model of viscous incompressible flow in a porous body, taking into account the buoyancy effect in Boussinesq approximation in the cylindrical coordinate system. This system of equations (1-5) in the divergent form is presented bellow:

$$\frac{\partial(\varepsilon U)}{\partial z}+\frac{1}{r}\cdot\frac{\partial(r\varepsilon V)}{\partial r}+\frac{1}{r}\cdot\frac{\partial(\varepsilon W)}{\partial\varphi}=J \tag{1}$$

$$\frac{\partial U}{\partial\tau}+\frac{1}{\varepsilon}\cdot\frac{\partial(U\varepsilon U)}{\partial z}+\frac{1}{\varepsilon r}\cdot\frac{\partial(rV\varepsilon U)}{\partial r}+\frac{1}{\varepsilon r}\cdot\frac{\partial(W\varepsilon U)}{\partial\varphi}= \tag{2}$$
$$=-\frac{1}{\rho}\cdot\frac{\partial P}{\partial z}+\nu\Delta U-\Lambda_z|\vec{\omega}|U-\frac{\rho(T)}{\rho_T}g+\frac{\Delta P_N}{L_N}+J\left\{\frac{U_J}{U}\right\}$$

$$\frac{\partial V}{\partial\tau}+\frac{1}{\varepsilon}\cdot\frac{\partial(U\varepsilon V)}{\partial z}+\frac{1}{\varepsilon r}\cdot\frac{\partial(rV\varepsilon V)}{\partial r}+\frac{1}{\varepsilon r}\cdot\frac{\partial(W\varepsilon V)}{\partial\varphi}-\frac{W^2}{r}= \tag{3}$$
$$=-\frac{1}{\rho}\cdot\frac{\partial P}{\partial r}+\nu\Delta V-\Lambda_r|\vec{\omega}|V+J\left\{\frac{V_J}{V}\right\}$$

$$\frac{\partial W}{\partial\tau}+\frac{1}{\varepsilon}\cdot\frac{\partial(U\varepsilon W)}{\partial z}+\frac{1}{\varepsilon r}\cdot\frac{\partial(rV\varepsilon W)}{\partial r}+\frac{1}{\varepsilon r}\cdot\frac{\partial(W\varepsilon W)}{\partial\varphi}+\frac{VW}{r}= \tag{4}$$
$$=-\frac{1}{\rho r}\cdot\frac{\partial P}{\partial\varphi}+\nu\Delta W-\Lambda_\varphi|\vec{\omega}|W+J\left\{\frac{W_J}{W}\right\}$$

$$C_p\rho\cdot\frac{\partial T}{\partial\tau}+\left(C_p\rho\right)\cdot\left[\frac{\partial(\varepsilon UT)}{\partial z}+\frac{1}{r}\cdot\frac{\partial(r\varepsilon VT)}{\partial r}+\frac{1}{r}\cdot\frac{\partial(\varepsilon WT)}{\partial\varphi}\right]= \tag{5}$$
$$=\frac{\partial}{\partial z}\lambda_z\frac{\partial T}{\partial z}+\frac{1}{r}\frac{\partial}{\partial r}\left[r\lambda_r\frac{\partial T}{\partial r}\right]+\frac{1}{r^2}\frac{\partial}{\partial\varphi}\left[\lambda_\varphi\frac{\partial T}{\partial\varphi}\right]+$$
$$+\sum_n\alpha_n\frac{\Pi_n}{S_n}\left(\Theta_n+T\right)_V+J\left(C_p\rho\right)\cdot\left\{\frac{T_J}{T}\right\},$$

where $|\vec{\omega}| = \sqrt{V^2 + U^2 + W^2}$

U, V, W - velocity components in axial (*z*), radial (*r*) and azimuth (φ) directions; *P* - pressure; *T* - temperature of sodium.

Porosity of medium for coolant ε is a function of coordinates and porous medium resistance coefficients Λ_z, , Λ_r and Λ_φ may depend on flow parameters. The thermal hydraulic properties - effective kinematic viscosity ν, coolant density ρ and specific heat capacity C_P are the functions of sodium temperature T. Effective conductivity coefficients of porous medium can be different for different directions. The sum $\sum_n \alpha_n \cdot \frac{\Pi_n}{S_n} \cdot (\Theta_n + T)$, takes into account heat exchange with the structures coming in contact with the primary coolant and Θ_n are the surface temperatures of these structures.

The system of governing equations for inter-wrapper sodium is the same as (1)-(5), but it is solved only for subdomain where the inter-wrapper sodium presents. The mass source J is not equal to zero only on the boundaries of this subdomain where mass exchange between the main sodium flow and inter-wrapper space takes place. The source term J is expressed as a function of pressure difference:

$$J = A + B \cdot \left[P_J(r, z, \varphi) - P(r, z, \varphi)\right] \quad (6)$$

where $P_J(r,z,\varphi)$ and $P(r,z,\varphi)$ - pressure distributions respectively in the inter-wrapper space and in the main sodium flow.

The system of equations (1-5) is solved numerically by the iterative finite-difference method [1].

3. CODE VALIDATION

The capability of the code to simulate correctly natural convection phenomena in the complicated design similar to pool-type reactor with immersion coolers were tested on the RAMONA rig.

RAMONA (reactor model designed for natural convection studies) - is a thermal hydraulic rig geometry similar to that of the pool- type fast reactor, intended for studying transient processes taking place in the reactor on transition phase from nominal steady state operating conditions to decay heat removal conditions with the use of IC [2].

Main characteristics of the RAMONA rig (Fig. 1):

The core is simulated by 8 circular channels formed by 9 heater rings;

IHXs - 8 straight tube counter flow type heat exchangers;

ICs - 4 straight tube counter flow type heat exchanges;

PPs - 4 centrifugal pumps;

ACS - a hollow cylinder with permeable walls;

Coolant - water.

The rig height is 0.58m. The rig radius - 0.5m.

In the region of pump positioning a constant head is assumed ensuring a coolant flow rate through the core of G=0.84kg/s under nominal conditions.

The core power under rated conditions is N=30kW. Heat removal is carried out only through IHXs.

The experiment scenario implies the following sequence of events [3]:

At the initial time (0s) a reduction of heaters capacity to 1 kW takes place. Simultaneously, reduction of coolant flow rate through the core is started. On the 120ths pumps are shutdown and water flow rate through the core is fully determined by natural convection. Secondary coolant flow rate through IHXs is reduced to 0 by 18s. On the 240ths

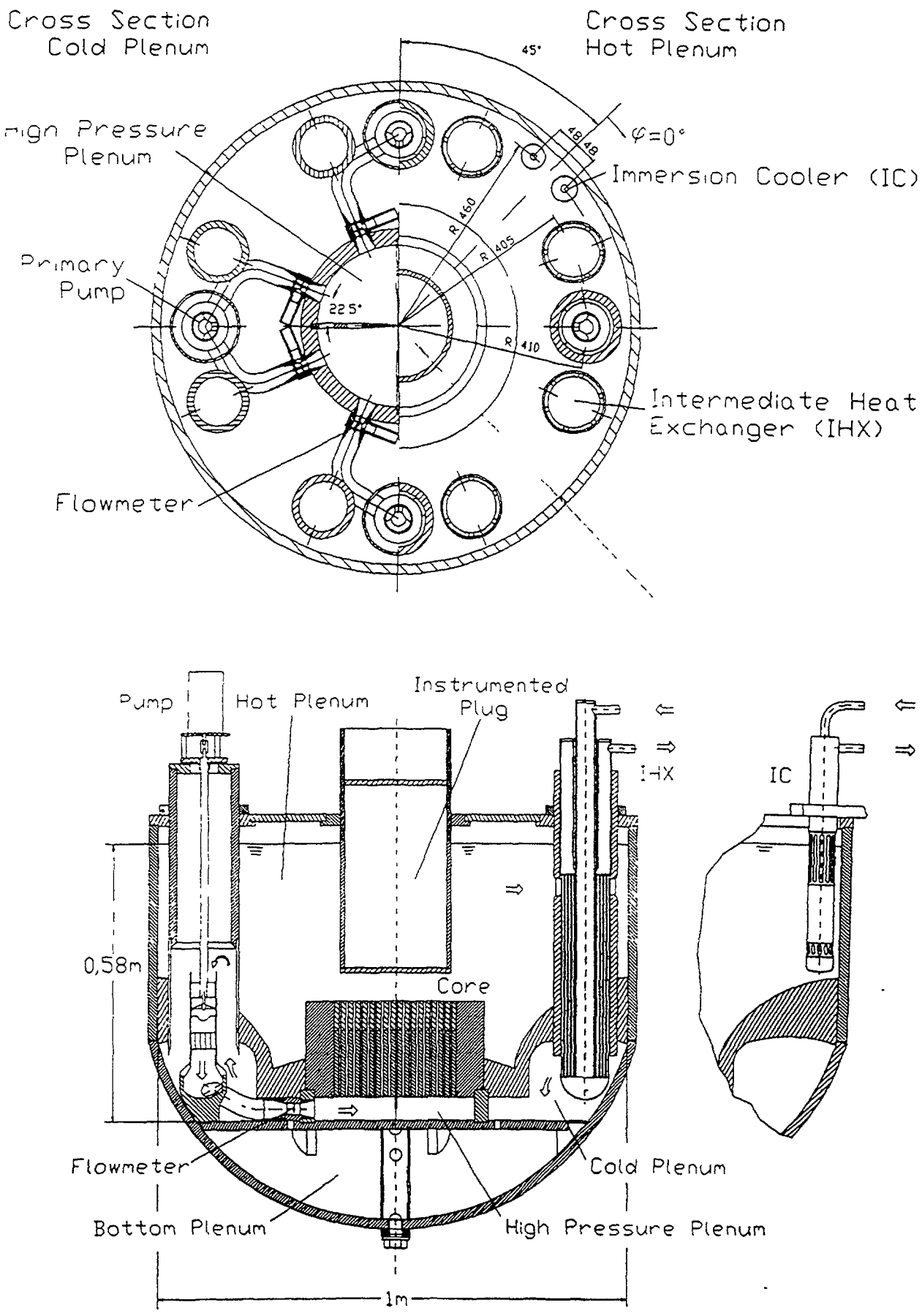

Fig. 1 **RAMONA Transient Model**

ICs are switched on. In so doing changing of water flow rate and inlet temperature through the secondary loop of IC simulates air heat exchanger operation.

The calculation was performed for the 4 initial hours of transient. Three-dimensional calculations model represents a cylindrical sector with an angle of 90° and comprises all the main components of the facility:
one forth of the core and of ACS, two IHXs, one IC and one pump.

Fig.2 illustrates the calculated region. The numerals denote:
3 ⇒ the core;
4, 5 ⇒ above core structure;
2, 6 ⇒ support structure;
7, 8, 9 ⇒ IC;
13 ⇒ pump;
14 ⇒ pump piping;
10 ⇒ dummy region simulating the vessel shape.

Dash-dot lines show thermocouple trees arrangement, a reading of the height of thermocouples positioning (Fig.9-12) is taken from the bottom of the cold plenum.

The calculations of one steady state and one transient (BENCHMARK-CASE 1, [3]) conditions was carried out. Calculated velocity and temperature fields for vertical section passing through the IC are shown in Fig.3,4. In Fig.5-8 the comparison of the obtained data with the experimental result is made with regard to integral characteristics : water flow rate through the core, average temperatures at its inlet and outlet. The calculation represents correctly all peculiarities of flow rate dynamics under these conditions during the whole 4 hour period. The calculated flow rate deviation from the experimental data is mainly within +10÷-20%. An agreement for "average temperatures at the core inlet and outlet" is even better (Figs.7-8) and the difference from the experiment does not exceed 1°C for the most part of the transient process.

In Figs.9-12 the dynamics of local temperature values in different rig components at points where thermocouples are positioned is shown. In Fig.9 temperatures in the hot plenum (HT1.*) are presented. The calculations give an overestimated temperature value - by about 1°C in the upper part and by 2°C in the lower one..

The most significant difference between calculation and experimental result for the hot plenum consists in different intensity of heat exchange rates for the coolant in the annular cavity formed by the support ring "2" and item "6" and the rest of the hot plenum volume located above. As it can be seen from Fig.10, in the experiment coolant contained within the cavity is heated slower resulting in the more abrupt temperature rise on the upper boundary of the cavity. Similar picture is also observed in the cold plenum (Fig.11) where temperature drop along the height is higher than that obtained by calculation. However, dynamics of the average flow temperature on the cold section of the stream is simulated by the calculation to a much better accuracy (Fig.12).

Scheme diffusion may be one of the causes of that more intensive heat exchange is calculated in free volumes.

4. HEAT REMOVAL PROBLEM CALCULATION FOR BN-600M – TYPE REACTOR

The vertical section of *BN-600M – type* reactor passing through IC is schematically represented on Fig. 13. The arrows show the expected pattern of sodium flow in the reactor after primary pump shutdown and immersion coolers coming into operation. Sodium from hot plenum passes through IC tube bundle, discharges through outlet windows and goes downwards. Then it enters rod shielding, steel annular shielding and annular gap forming

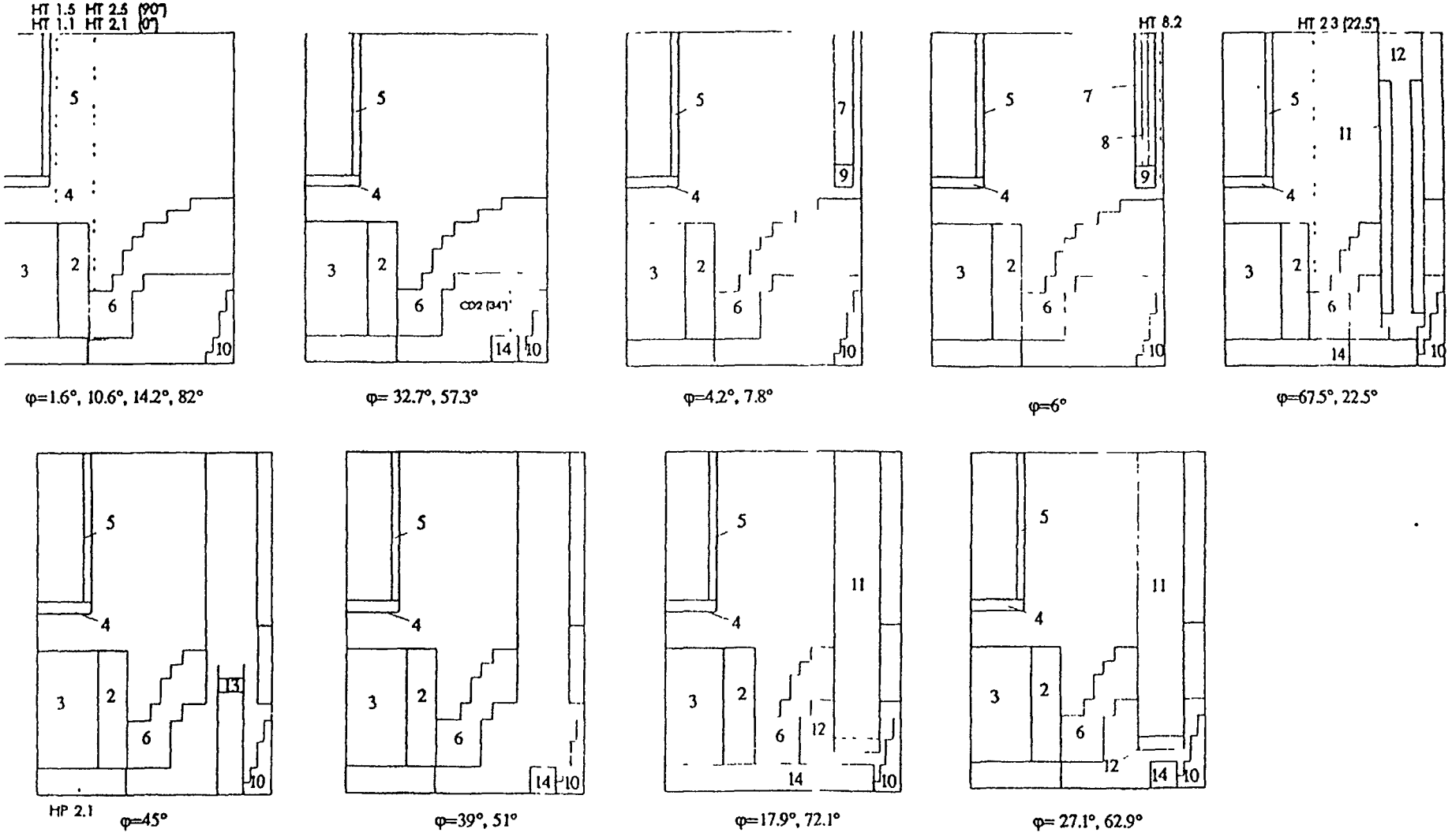

Fig.2 Calculational region.

three parallel regressive flows. And then through the holes in the shielding and structures "cold" sodium is directed into inter-subassembly space where it cools core during its upward movement. The GRIFIC calculations showed that the flow distribution described above is established in the reactor in a few ten seconds after beginning of the accident. Sodium temperature in the "hottest" point reaches its maximum value and then gradually decreases (Fig. 14).

To estimate the efficiency of the core cooling by organised sodium flow in the inter-wrapper space the same accident - (LOF) - was analysed using GRIFIC code, for the case.

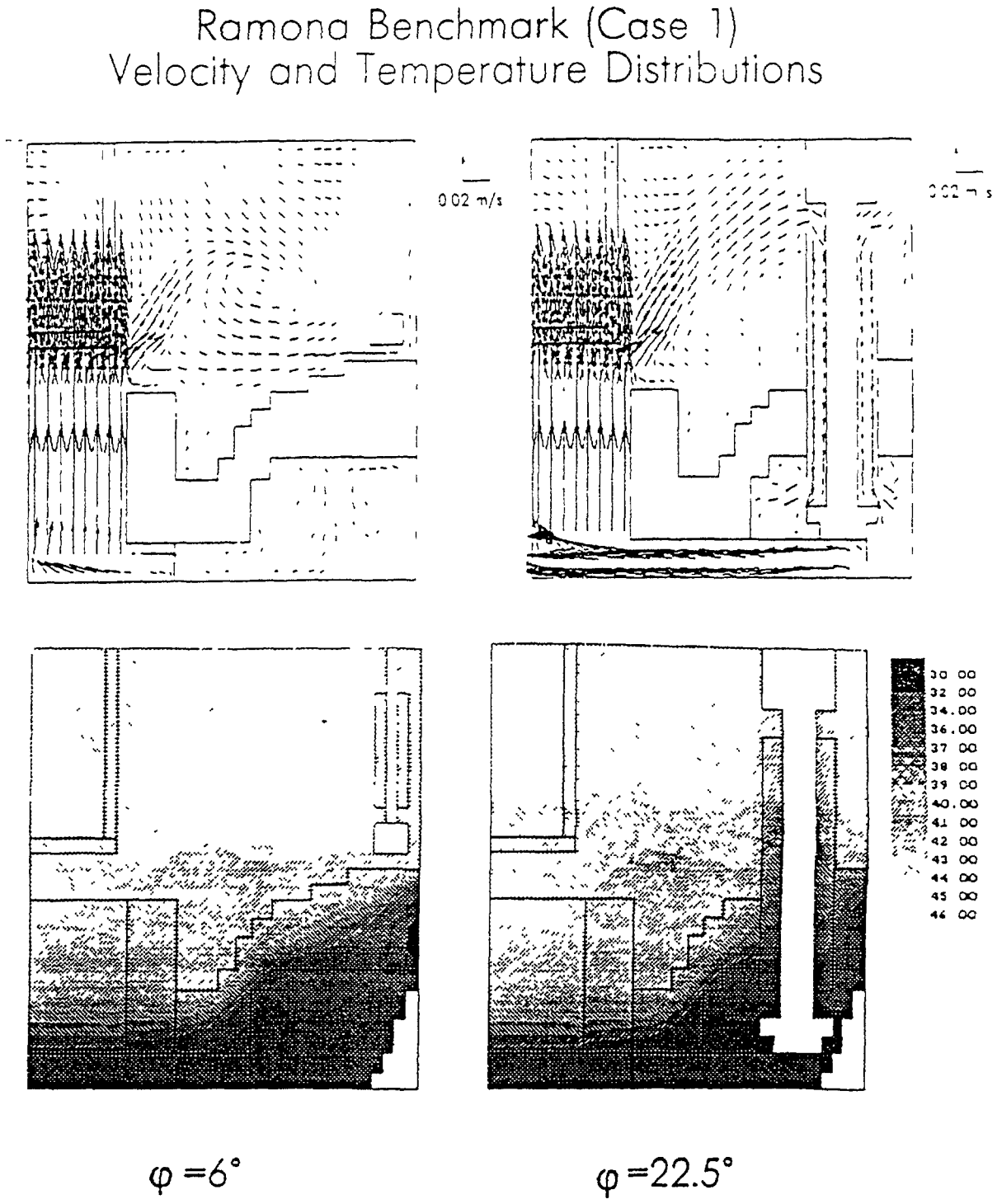

Fig.3

When the sodium velocity in the inter-wrapper space is supposed to be equal zero. The maximum sodium temperature histories for these both cases are presented on (Fig 14). One can conclude from the figure, that sodium circulation in the inter-wrapper space effects essentially heat removal from the core.

Ramona Benchmark (Case 1)
Velocity and Temperature Distributions

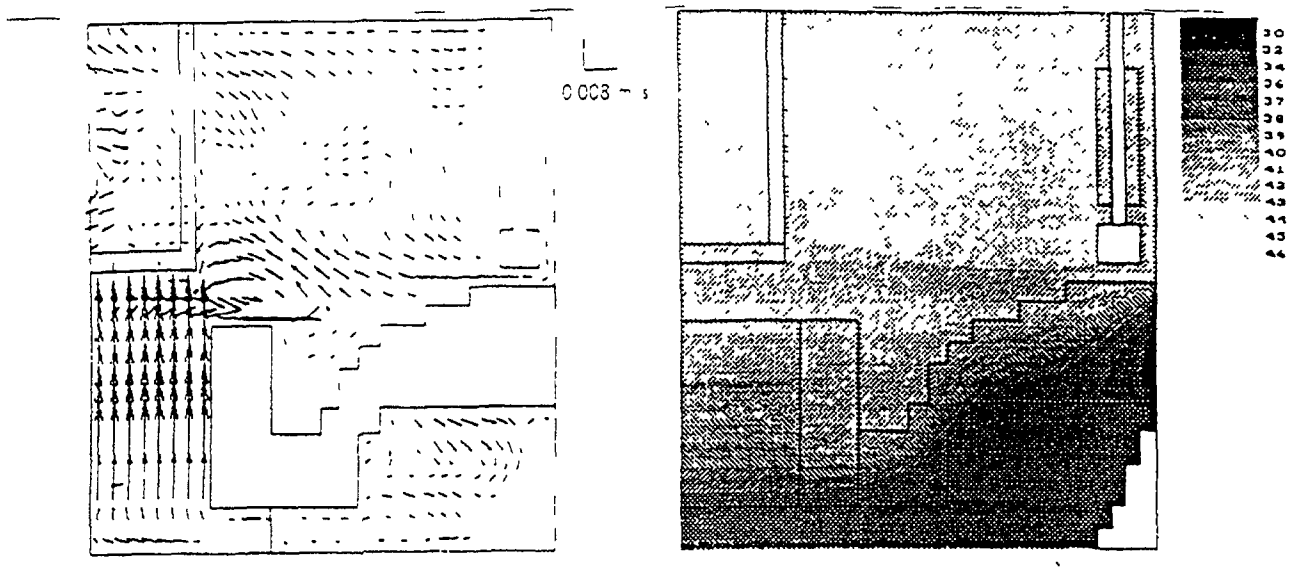

t=50s

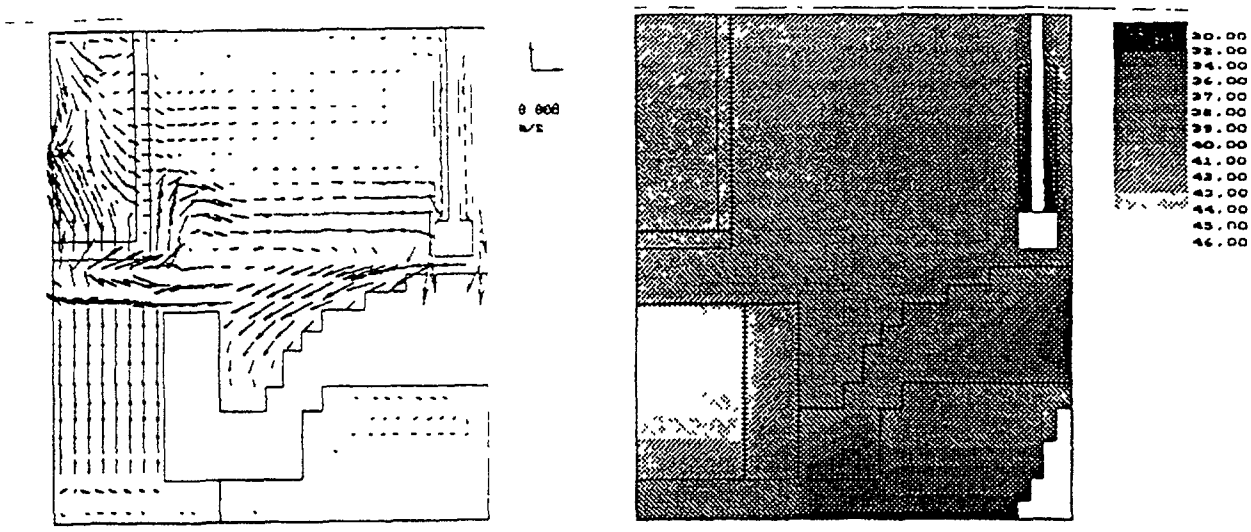

Time=3500s

Fig.4

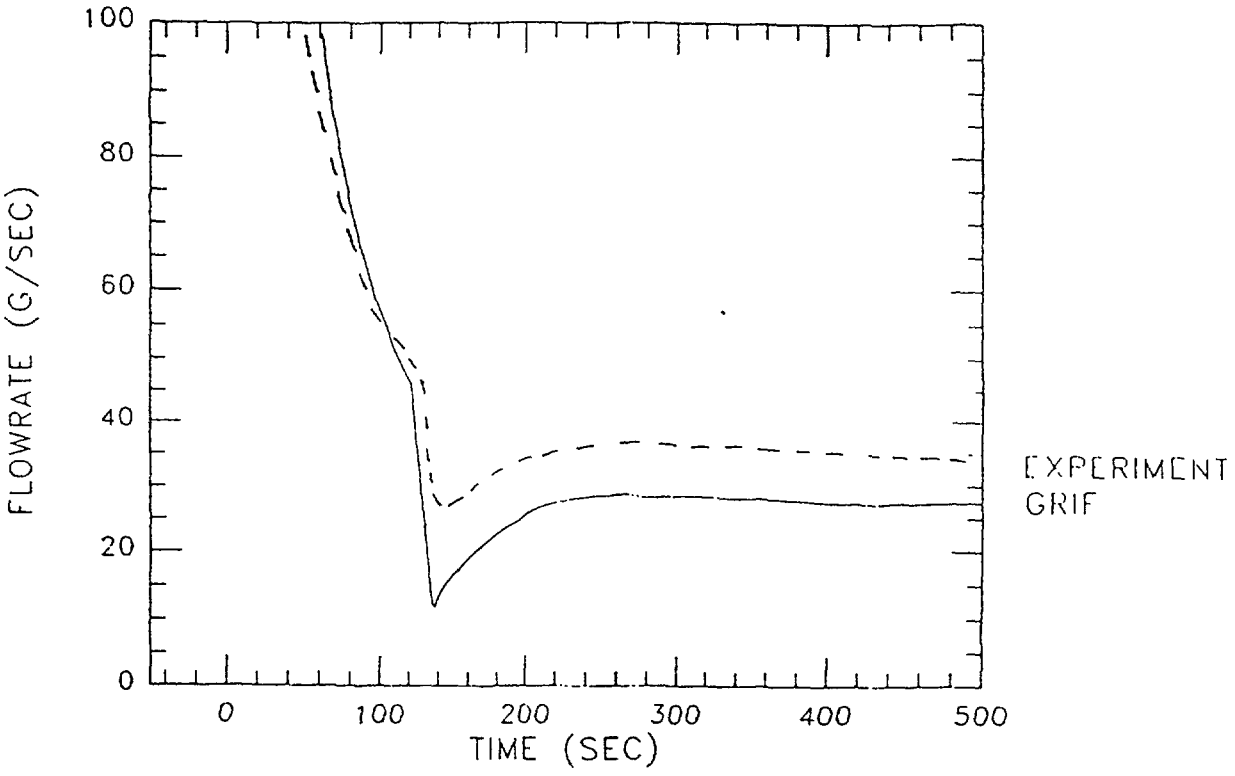

Fig.5 CORE FLOW RATE (0-500SEC)
(BENCHMARK-CASE1)

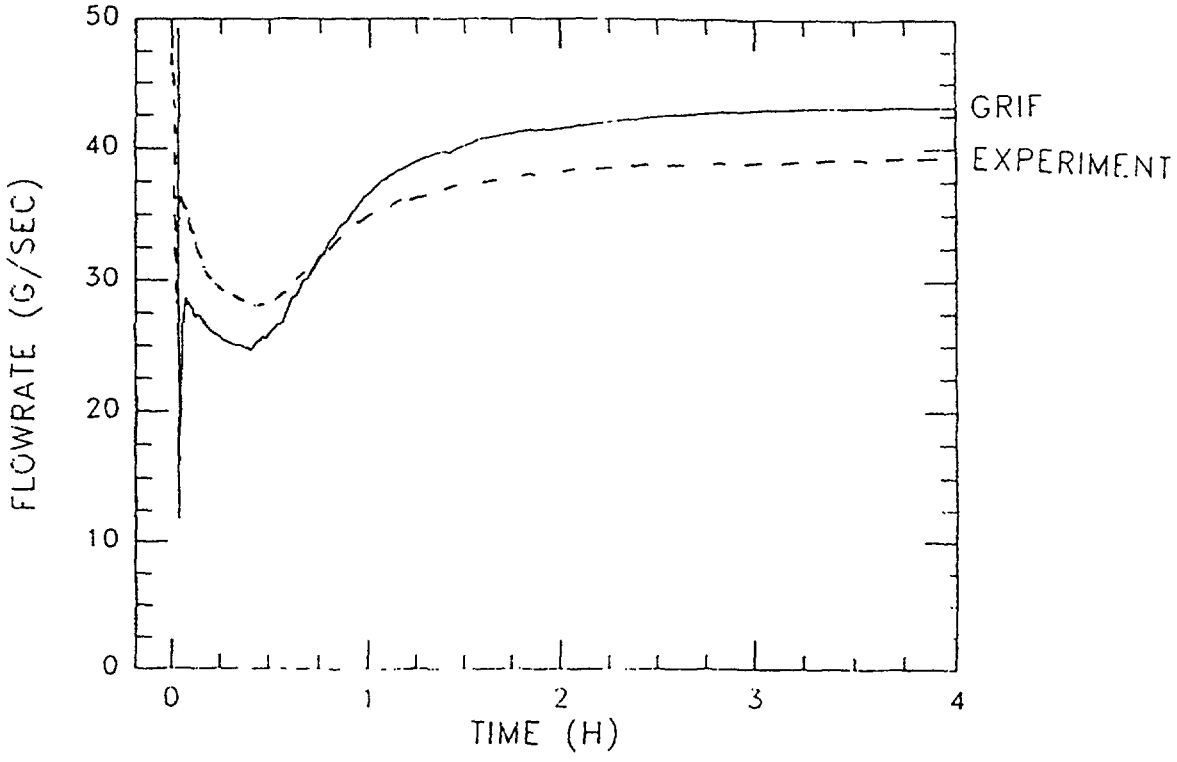

Fig.6 CORE FLOW RATE (0-4H)
(BENCHMARK-CASE1)

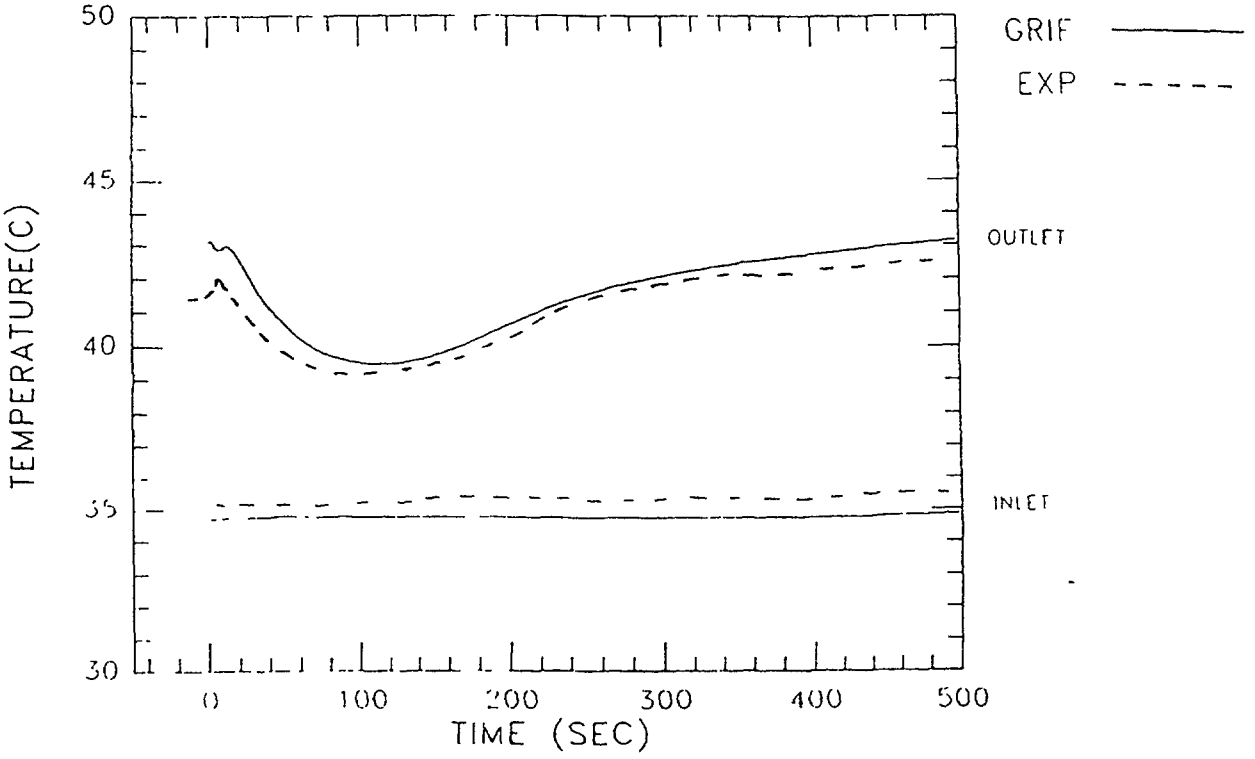

Fig.7 CORE INLET AND OUTLET TEMPERATURES (0-500S) (BENCHMARK-CASE1)

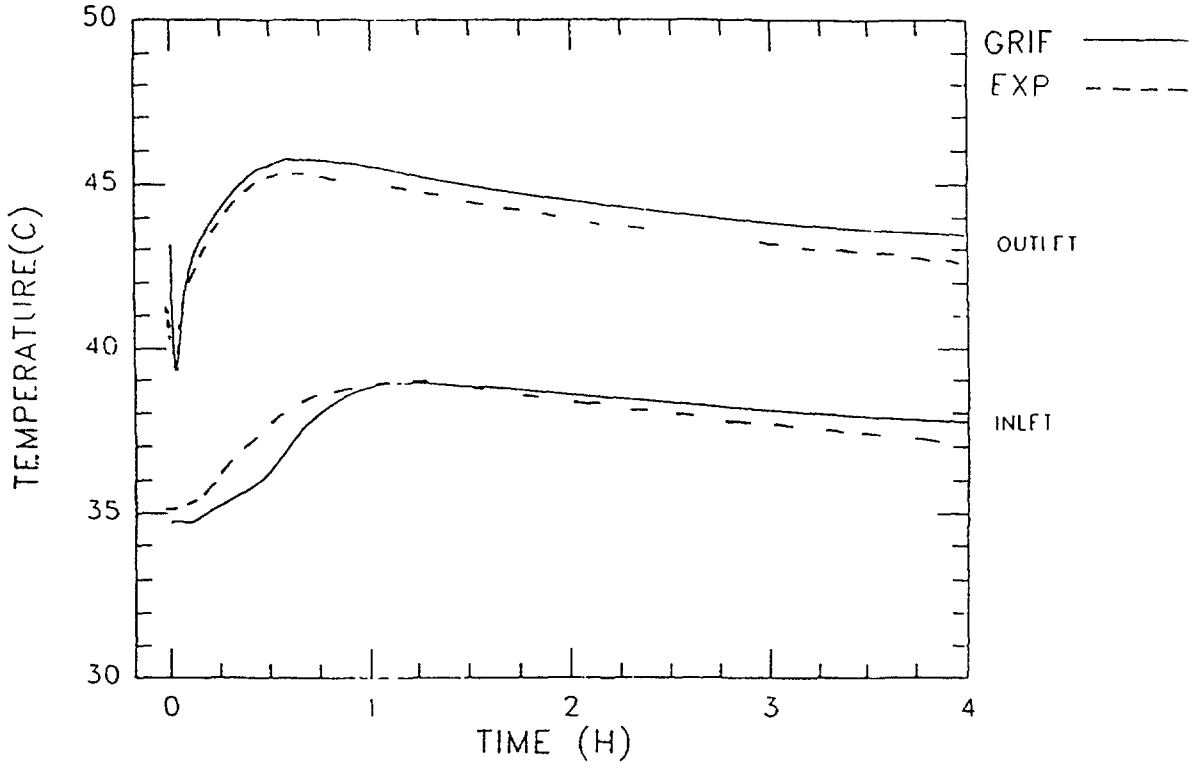

Fig.8 CORE INLET AND OUTLET TEMPERATURES (0-4H) (BENCHMARK-CASE1)

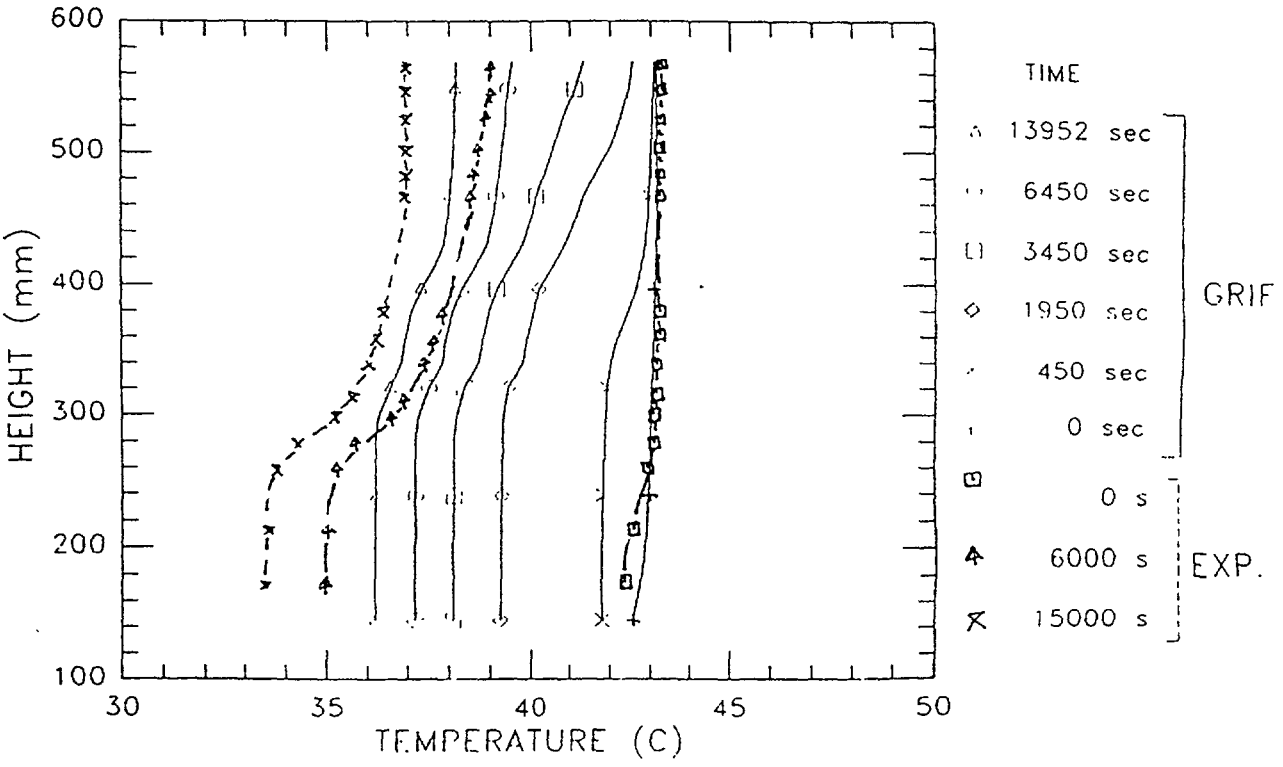

Fig.9 HOT PLENUM AXIAL DIRECTION TEMP. DISTRIBUTION (CASE1,HT23)

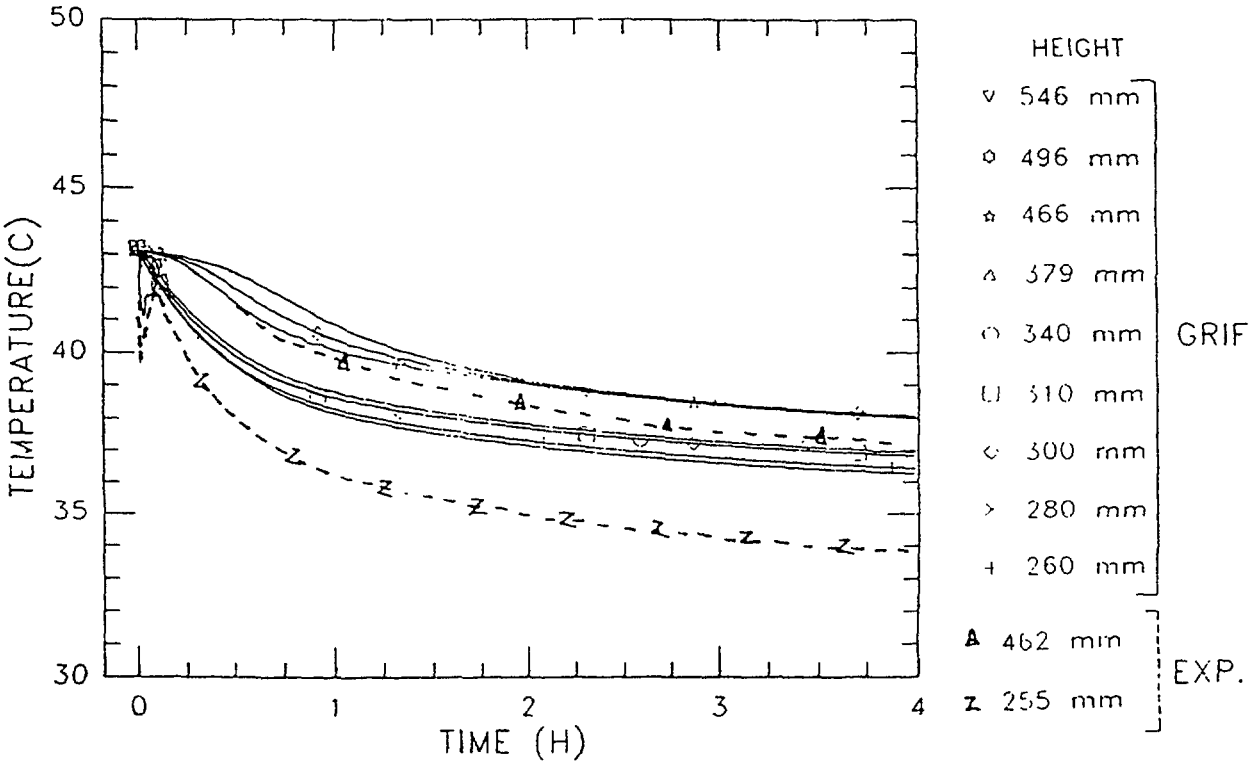

Fig.10 TEMPERATURE COURCES OF HOT PLENUM HT1-1 TREE (CASE1, 0-4H)

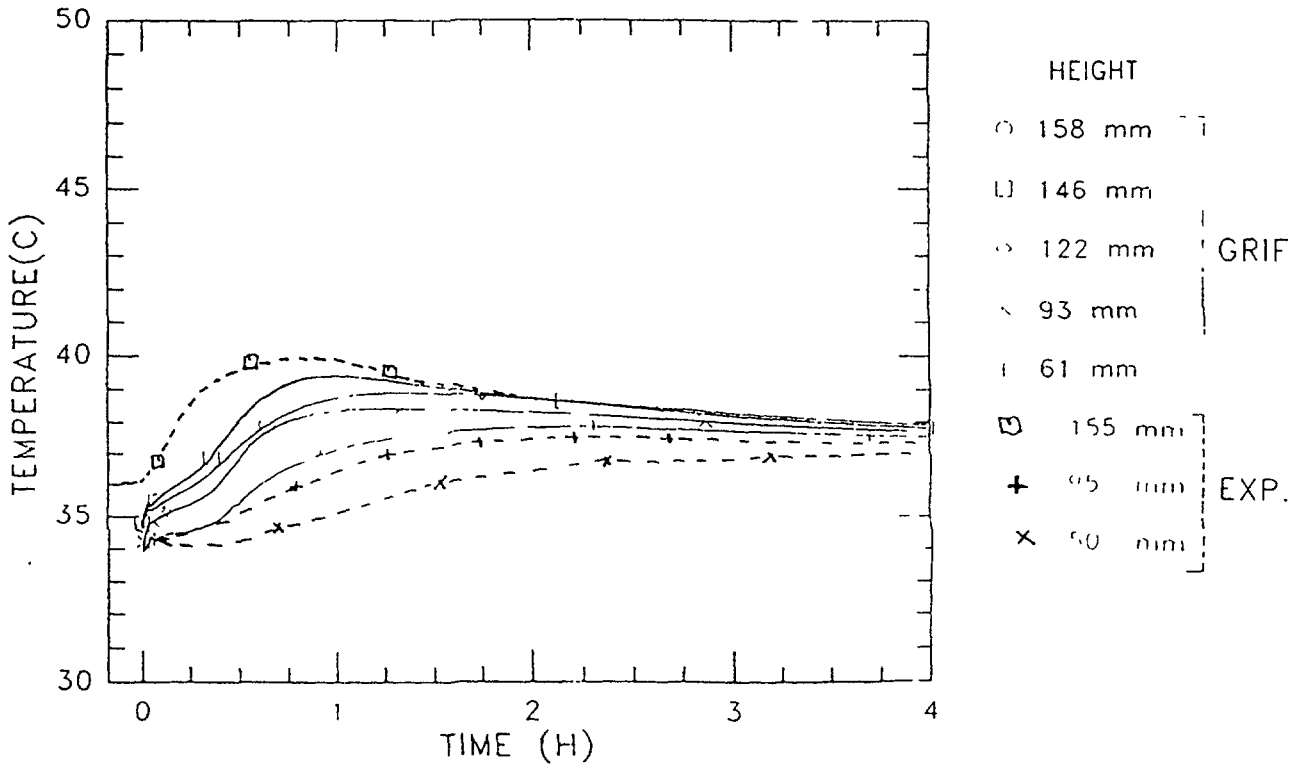

Fig.11. TEMPERATURE COURCES OF COLD PLENUM CD2 TREE (CASE1, 0-4H)

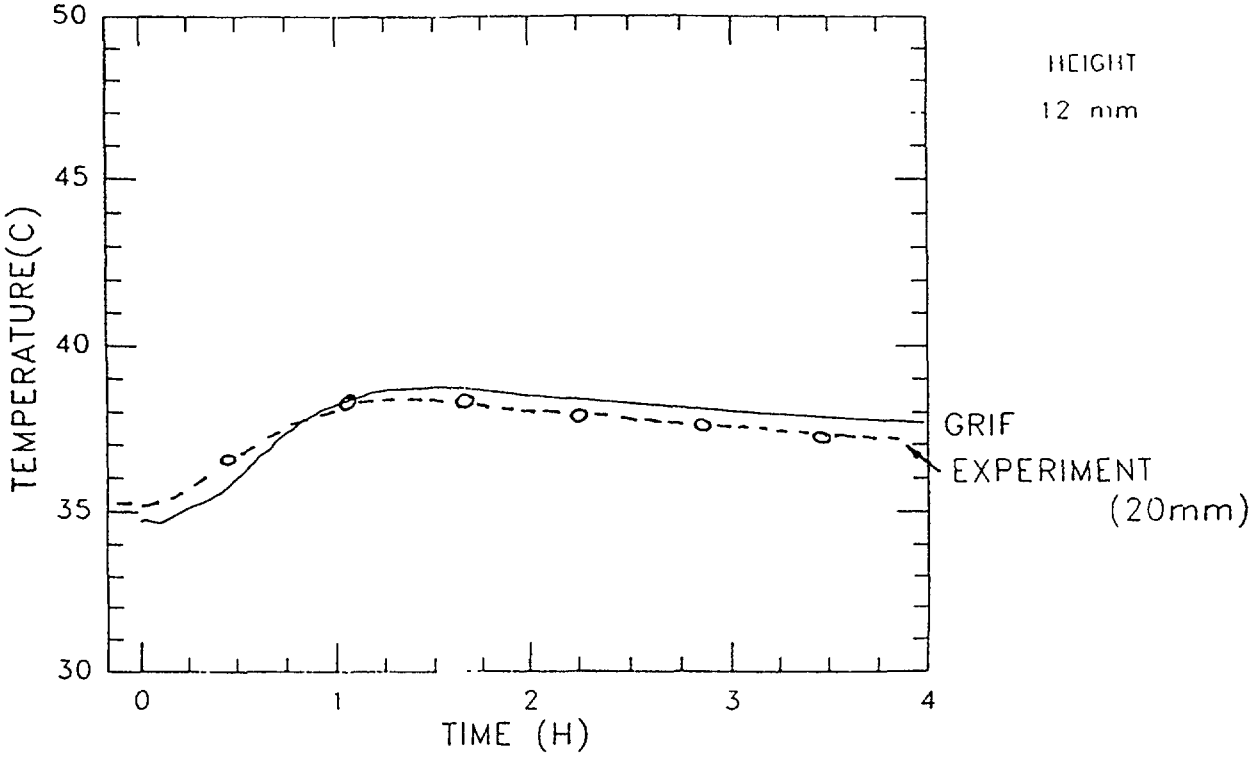

Fig.12 TEMPERATURE COURCES OF HIGH PRESSURE PLENUM HP2-1 TREE (CASE1, 0-4H)

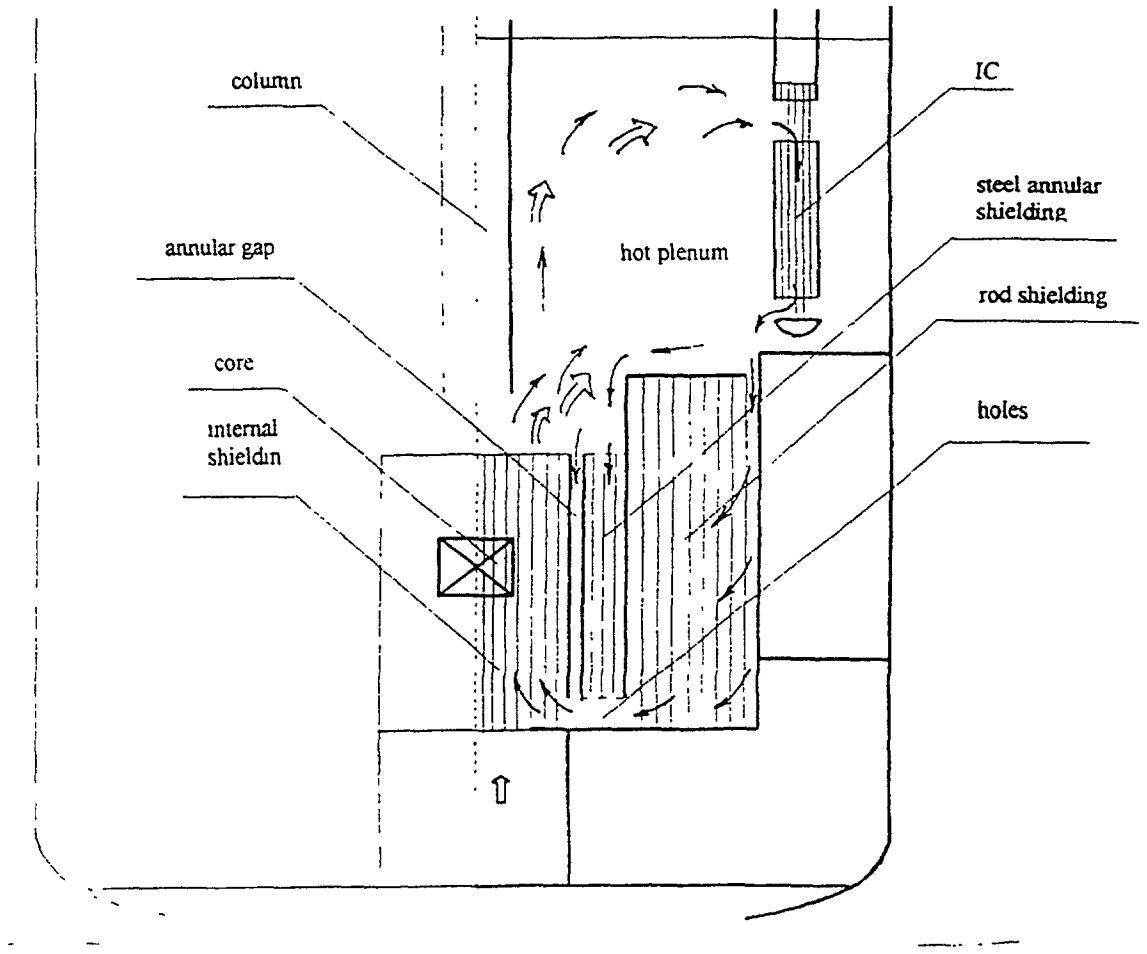

Fig.13. Schematic flow scheme of decay heat removal for BN-600M – type reactor.

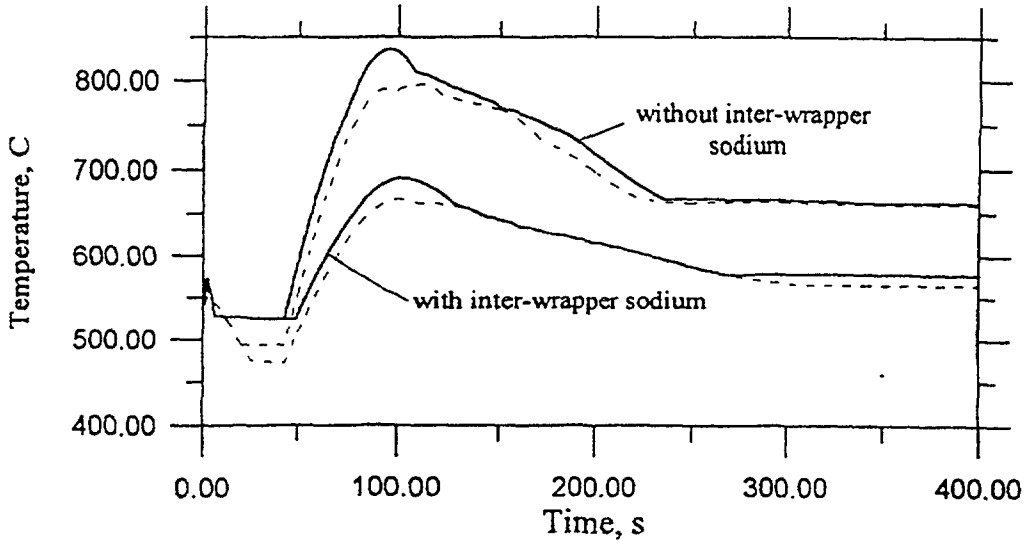

Fig. 14. Maximum sodium temperature history during LOF-accident.
— main sodium
- - inter-wrapper sodium

5.CONCLUSION

On the basis of the GRIFIC code testing it can be stated that for the pool-type plants :

- the GRIFIC code assures an adequate accuracy of integral characteristics (such as flow rate through the core, its inlet and outlet temperatures);
- it allows to calculate correctly local temperature values for the most components of the flow section;
- to improve the accuracy of the modelling one can recommend to enhance the order of finite difference scheme for approximation of convective terms.

NOMENCLATURE

U, V, W - velocity components in axial (z), radial (r) and azimuth (φ) directions;
ε - porosity of medium for coolant;
ν - effective kinematic viscosity;
ρ_T - coolant density;
Λ_z - porous medium resistance coefficient in axial,
Λ_r - radial,
Λ_φ - azimuth directions;
P - pressure;
T - temperature;
C_P - specific heat capacity of coolant;
λ_z - effective conductivity coefficient of porous medium in axial,
λ_r - radial,
λ_φ - azimuth directions;
Π - perimeter;
S - longitudinal section area;
α - heat transfer coefficient;
ΔP_N – primary pump head;
ΔL - primary pump dimension.

REFERENCES

[1] LEONCHUK Ì., CHVETSOV I., CHVETSOVA L. Calculation of Space-dependent Heat and Mass Exchange in (R,Φ,Z) – geometry. Preprint IPPE-1977., Obninsk 1989.(in Russian).

[2] WEINBERG D., KAMIDE H., MARTEN K., HOFFMAN H. Thermohydraulic Investigations on the Transition from Forced Nominal to Natural Circulation DHR Operation Conditions in the Reactor Model Ramona. Description of a Benchmark Problem. Karlsruhe, 1990.

[3] WEINBERG D., OSHIMA H., MARTEN K., HOFFMAN H. Thermohydraulic Investigations on the Transition from Forced Nominal to Natural Circulation DHR Operation Conditions in the Reactor Model Ramona. Experimental results of Case 1 and Case 2. Karlsruhe, 1991.

LOW-REYNOLDS NUMBER k-ε TURBULENCE MODEL FOR CALCULATION OF FAST-REACTOR-CHANNEL FLOWS

V.I. MIKHIN
State Scientific Center of Russian Federation,
Institute of Physics and Power Engineering,
Obninsk, Kaluga Region, Russian Federation

Abstract

For calculating the turbulent flows in the complex geometry channels typical for the nuclear reactor installation elements the low-Reynolds-number k-ε turbulence model with the model functions not containing the spatial coordinate like y^+ is proposed. Such spatial coordinate is usually used for modeling the turbulence near the wall correctly. The model completed on the developed flow of the non-viscous incompressible liquid in the plane channel correctly describes the transition from the laminar regime to the turbulent one. The calculated skin friction coefficients obey the well-known Dean and Zarbi - Reynolds laws. The mean velocity distributions are close to that obtained from the empirical three-layer Karman model.

1.INTRODUCTION

The existing k-ε turbulence models are far from being complete [1]. The assertion is based on the following facts. The high-Reynolds-number k-ε turbulence models first developed permit simulating the turbulence only in the flow core. For determining the turbulence quantities at the turbulent core boundary they use the empirical relationships which are different for different flow classes. In this case the results obtained with using such models must always be verified by comparison with known empirical results.

As an alternative to the high-Reynolds number variants the low-Reynolds number turbulence models are worked out. Such models permit simulating the turbulence in the overall flow region including the near-wall one. In such models they use the most common and universal boundary conditions for the turbulent energy and it's dissipation rate [2,3,4]. The possibility of modeling the turbulence in the overall flow region including the near-wall is achieved by introducing in the equation system the model functions of two arguments : the turbulent Reynolds number R_t and the non-dimensional spatial coordinate determining the position of an arbitrary flow point relatively to the solid surface. Often they make use of y^+ as such coordinate. But at moderate turbulent numbers ($Re \leq 10^4$) the influence of that coordinate on turbulent quantities can be significant in the overall flow region [1]. It should lead to the modeling results non-single-valued in the complex geometry channels in which that coordinate can be determined by different way. Such models are not suitable for calculating the flows in the channels with rough walls. The presence of such coordinate in the equation system significantly complicates the numerical algorithm of solving such system. It is also clear from physical view point, the models containing in the differential equations y^+ as a parameter can not be considered as correct models.

But still worse matter is about the four-parameter turbulence model containing in addition to the transport equations for k and ε yet two equations for the squared temperature fluctuations and the dissipation rate of this value [3]. Even the simple comparison of the y^+ values with scale constants entering in the model functions in combination with y^+ shows the significant influence of the coordinate y^+ on the turbulent quantities in the overall flow region at any Reynolds numbers for liquids with small Prandtl numbers. This circumstance one alone makes this model to be not suitable for modeling the turbulent heat transfer in liquid sodium.

Thus the problem of creating a complete turbulence model is that of working-out the low-Reynolds number model not containing the model functions of the spatial coordinate like y^+. The model presented below meets this condition. The model functions and constants have been worked out at the stable developed turbulent flow in the plane channel.

2.GAVERNING EQUATIONS

The k-ε turbulence model includes [2] the continuity equation

$$\frac{\partial U_i}{\partial x_i} = 0 \tag{1}$$

and the Reynolds equation

$$\frac{\partial U_i}{\partial \tau} + U_j \frac{\partial U_i}{\partial x_j} = -\frac{1}{\rho}\frac{\partial P}{\partial x_i} + \frac{\partial}{\partial x_j}\left[\nu\left(\frac{\partial U_i}{\partial x_j} + \frac{\partial U_j}{\partial x_i}\right) - \overline{u_i u_j}\right]. \tag{2}$$

The Bussinesk hypothesis

$$-\overline{u_i u_j} = \nu_t\left(\frac{\partial U_i}{\partial x_j} + \frac{\partial U_j}{\partial x_i}\right) - \frac{2}{3}k\delta_{ij} \tag{3}$$

expresses the turbulent stress tensor $\overline{u_i u_j}$ in the Reynolds equation via the mean velocity deformations $\partial U_I / \partial x_J$ by means of the eddy viscosity ν_t. The eddy viscosity is determined through the turbulent energy k and it's dissipation rate ε by the Kolmogorov relationship

$$\nu_t = c_\mu f_\mu \frac{k^2}{\varepsilon} \tag{4}$$

where f_μ is a model function, c_μ is a constant. The values of k and ε are obtained from solving the kinetic energy equation

$$\frac{\partial k}{\partial \tau} + U_j \frac{\partial k}{\partial x_j} = \frac{\partial}{\partial x_j}\left[(\nu + \frac{\nu_t}{\sigma_k})\frac{\partial k}{\partial x_j}\right] - \overline{u_i u_j}\frac{\partial U_i}{\partial x_j} - \varepsilon \tag{5}$$

and the dissipation rate one

$$\frac{\partial \varepsilon}{\partial \tau} + U_j \frac{\partial \varepsilon}{\partial x_j} = \frac{\partial}{\partial x_j}\left[(\nu + \frac{\nu_t}{\sigma_\varepsilon})\frac{\partial \varepsilon}{\partial x_j}\right] - c_{\varepsilon 1}\frac{\varepsilon}{k}\overline{u_i u_j}\frac{\partial U_i}{\partial x_j} - c_{\varepsilon 2} f_\varepsilon \frac{\varepsilon^2}{k}. \tag{6}$$

In low-Reynolds-number k-ε turbulence models [2,3] the functions f_μ and f_ε in the equations (4) and (6) depend on the turbulent Reynolds number and non-dimensional spatial coordinate (usually they make use of y^+).

At the solid surfaces the following boundary conditions are assumed.

The kinetic energy is assumed to be zero:

$$k_w = 0. \tag{7}$$

For the dissipation rate the second kind boundary condition

$$\left(\frac{\partial \varepsilon}{\partial n}\right)_w = 0 \tag{8}$$

had been proposed and proved [4]. This boundary condition combined with (7) allows modeling the turbulence in the overall flow region including the laminar sublayer[4]. The calculations of the developed turbulent flow in the plane channel with using the equations (1)-(6), the boundary conditions (7),(8) and the model functions of the work [2] give the relationship for the skin friction coefficient coinciding with the well-known Dean and Zarbi-Reynolds laws [4]. The mean velocity distributions coincide with that calculated from the three-layer Karman model:

$$U^+ = \begin{cases} y^+, & y^+ \le 5 \\ 5.0 \ln y^+ - 3.05, & 5 < y^+ \le 30 \\ 2.5 \ln y^+ + 5.50, & y^+ > 30 \end{cases}$$

But [1] the spatial coordinate y^+ can substantially influence on the turbulent quantities in the overall flow region including the points at the most removed from the solid surface. On that the relationship of the eddy viscosity via the turbulent Reynolds number at $Re \le 10^4$ shows: the relationship has the hysteresis character in the flow region with maximum velocity values, fig.1.

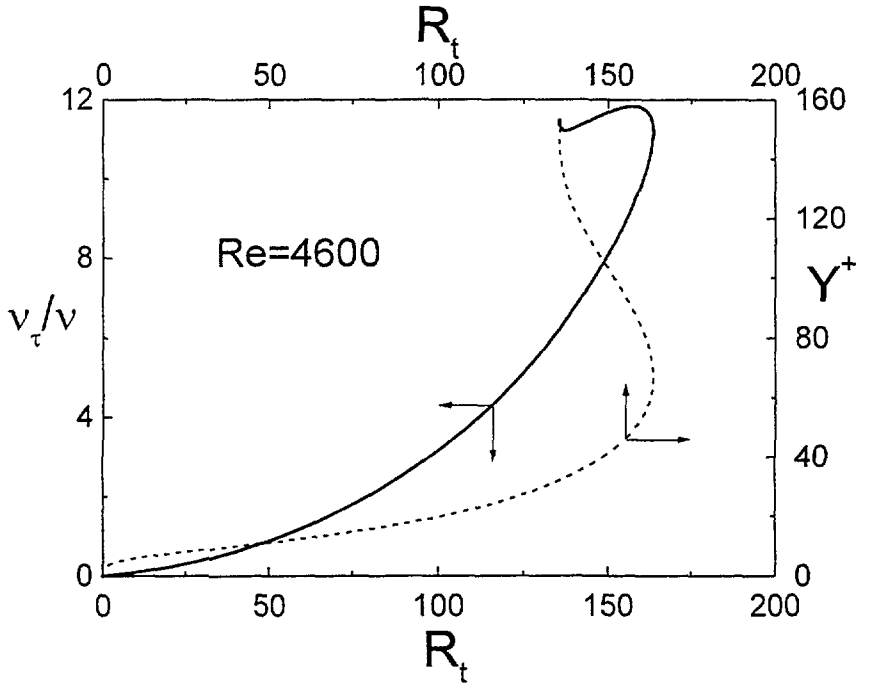

Fig.1. Eddy viscosity dependence via turbulent Reynolds number

That must lead to the non-single-valued results of modeling the turbulent flows in the complex geometry channels (in which the parameter y^+ can be determined by different way).

3. MODEL FUNCTIONS NOT CONTAINING SPATIAL COORDINATE AS ARGUMENT

To take into account the turbulence behavior near the solid surface the parameter z_t has been introduced instead of the spatial coordinate. The fourth power of the parameter,

$$z_t^4 = \frac{k^2}{\nu\left[\nu\left(\frac{\partial U_i}{\partial x_j}\right)^2 + \varepsilon\right]},$$

can be considered as the modified turbulent Reynolds number, which coincides with the ordinary turbulent Reynolds number R_t in the flow region with the small averaged-velocity deformations $\partial U_I / \partial x_j$, but essentially defers near the wall where averaged flow energy dissipation rate exceeds ε. The model functions proposed are the functions of two arguments: the turbulent Reynolds number and the parameter z_t.

Model functions and constants:

$$f_\mu = \left(1-\exp\left(-\frac{z_t}{0.85}\right)\right)^2\left[1+\left(\frac{2.6}{R_t^{0.75}}-1\right)\exp\left(-\left(\frac{R_t}{200}\right)^2\right)\right], \tag{9}$$

$$f_\varepsilon = \left(1-\exp\left(-\frac{z_t}{0.3}\right)\right)^2\left[1-0.5\exp\left(-\frac{z_t^4}{0.62}\right)\right], \tag{10}$$

$$\sigma_k = \frac{1.3}{1+15\exp\left(-\frac{z_t^4}{20}\right)} \tag{11}$$

$$c_\mu = 0.09, \quad c_{\varepsilon 1} = 1.5, \quad c_{\varepsilon 2} = 1.9, \quad \sigma_\varepsilon = 1.3.$$

4. COMPUTAITIONAL RESULTS

The results of modeling the developed turbulent non-compressible viscous liquid flow in the plane channel with using the equations (1)-(6), boundary conditions (7),(8) and the model functions (9)-(11) are in the following.

The proposed turbulence model correctly describes the transition from the laminar to the turbulent regime: at $Re < 1.3\cdot 10^3$ the numerical modeling gives only the laminar flow, at $Re \geq 1.6\cdot 10^3$ the turbulent flows are obtained only. The calculated skin friction coefficients obey the Dean law at $1.6\cdot 10^3 \leq Re \leq 5\cdot 10^4$ and the Zarbi - Reynolds law at $Re \geq 5\cdot 10^4$,fig.2. The mean velocity distributions are close to that obtained from the empirical three-layer Karman model, figs. 3. (The plots on the figure 3 for the Dean and Zarbi - Reynolds lows have been taken from the work [2].)

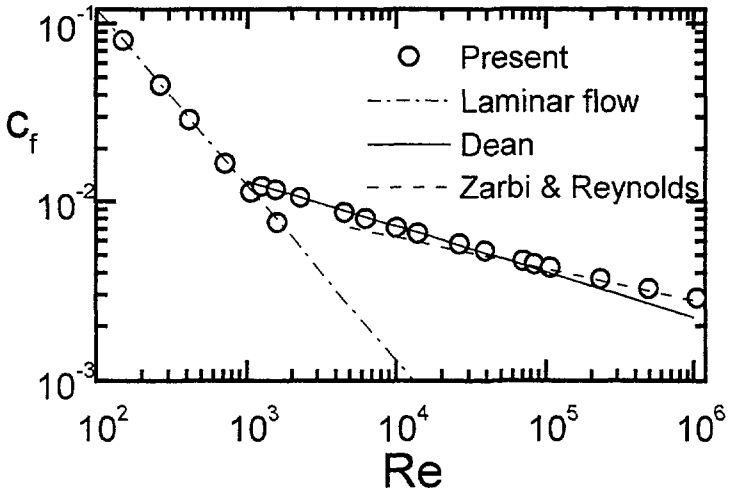

Fig.2. Skin friction coefficient as function of Reynolds number

The turbulent energy and dissipation rate distributions at $y^+ \geq 8$ are similar to those obtained from the calculations with using the same equation system and the same boundary conditions but with model functions of the work [2], fig.4. But at $y^+ < 5$ the turbulent energy

values compared with the values at the channel axis are much greater than that calculated with using the model [2].

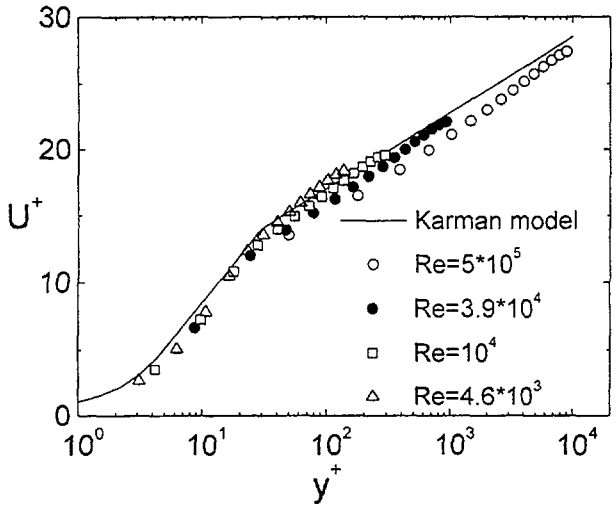

Fig.3. Mean velocity distributions

In spite of that the eddy viscosity within the layer $y^+ < 5$ is small with respect to kinematic one, fig.5. That agrees with the Karman model according to which the dependence of the mean velocity vie y^+ is linear at $y^+ < 5$. Thus the calculations with using the model [2] shows on the existence of the laminar sublayer as the flow domain ($y^+ < 5$) with the turbulent energy and respectively eddy viscosity vanished. According to the results obtained with

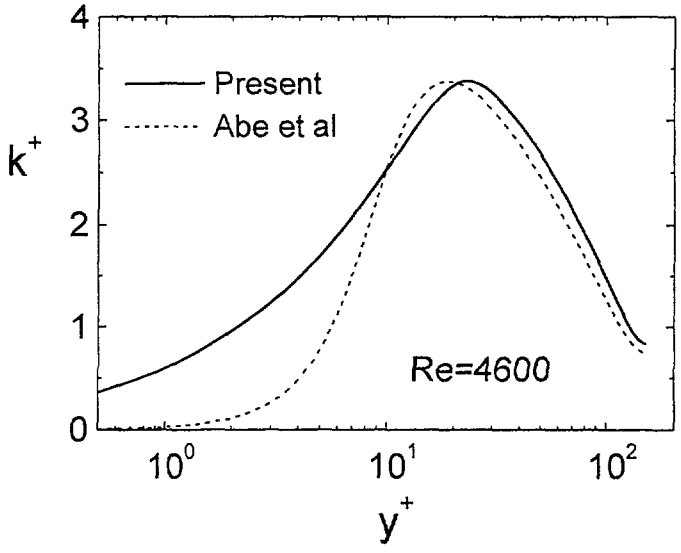

Fig.4. Turbulent energy distributions

using the model proposed one can tell about the viscous sublayer as the flow domain within which the eddy viscosity is small over the kinematic one but the turbulent energy can be compared with that in

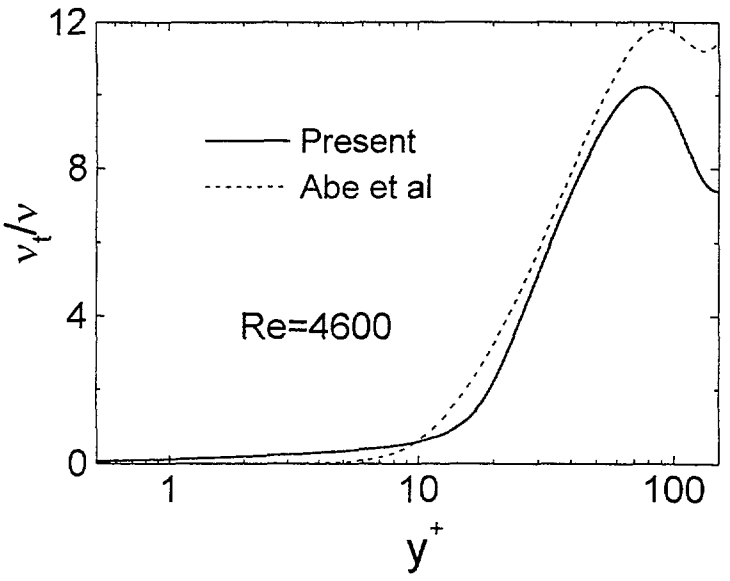

Fig.5. The eddy viscosity distributions

the turbulent core. From physical view point this result can be interpreted in the way that at the sufficient small distance from the wall the correlation between the longitudinal and transversal velocity fluctuations is vanished with the turbulent energy being substantially different from zero. From mathematical view point this result is explained by the character of the model function f_μ dependence from the parameter z_t.

CONCLUSIONS

The low Reynolds number turbulence model with the model functions not containing a spatial coordinate as an argument and allowing the turbulence modeling in the overall flow region including the viscous sublayer is proposed. The model is intended for the calculations of the turbulent flows in the complex geometry channels typical for the nuclear power installation elements and in the channels with rough walls.

NOMENCLATURE

c_f – mean skin friction coefficient, $\tau_w / 0.5\rho U_m^2$

k – turbulent energy, $\overline{u_i u_i} / 2$;

k^+ – non-dimensional value of k, k / u_τ^2;

P – ensemble-averaged static pressure;

Re – Reynolds number, $U_m \delta / \nu$;

R_t – turbulent Reynolds number, $k^2 / \nu\varepsilon$;

U_i, u_i – ensemble-averaged velocity and turbulent fluctuations in i-direction;

U – ensemble-averaged velocity in longi-tudinal direction;

U_m – channel bulk velocity;

U^+ – non-dimensional value of U, U/u_τ;

u_τ – velocity scale, $\sqrt{\tau_w / \rho}$;

x_i – Cartesian coordinate in i-direction;

y – length from wall surface,

y^+ – non-dimensional length from wall, $u_\tau y / \nu$;

δ – width of plane channel;

δ_{ij} – unit tensor;

ε – dissipation rate of turbulence energy, $\nu\overline{\left(\partial u_i / \partial x_j\right)^2}$;

ε^+ – non-dimensional value of ε, $\varepsilon\nu / u_\tau^4$;

ν, ν_t – kinematic and eddy viscosity;

ρ – density;

τ – time;

τ_w – wall shear stress; $\rho\nu\left(\partial U / \partial y\right)_w$.

REFERENCES

[1] MIKHIN V.I., FETISOVA L.N. About Incompleteness of k-ε Tourbulence Model. - IPPE Preprint -2556, Obninsk, 1996.

[2] ABE K., KONDOH T., NAGANO Y. A new turbulence model for predicting fluid flow and heat transfer in separating and reattaching flows -1. Flow field calculations // Int. J. Heat Mass Transfer. v.37. ¹ 1, pp. 139-151, 1994.

[3] SATO H., SHIMADA M., NAGANO Y. A two-equation turbulence model for predicting heat transfer in various Prandtl number fluids // Proceedings of the Tenth International Heat Transfer Conference, 1994, Brighton, UK, v.2, p.443-448.

[4] MIKHIN V.I., FETISOVA L.N. To Definition of a Boundary Condition for Energy Dissipation Speed in k-ε Tourbulence Model. - IPPE Preprint -2451, Obninsk, 1995.

[5] MIKHIN V.I. Low-Reynolds k-ε Tourbulence Model with Model Functions not Included the Spatial Coordinate as Argument. - IPPE Preprint - 2654, Obninsk, 1997.

DEVELOPMENT OF THERMOHYDRAULIC CODES FOR MODELING LIQUID METAL BOILING IN LMR FUEL SUBASSEMBLIES

G.A. SOROKIN, E.F. AVDEEV
Institute of Nuclear and Power Engineering,
Obninsk, Kaluga Region

A.V. ZHUKOV, G.P. BOGOSLOVSKAYA, A.P. SOROKIN
State Scientific Center of Russian Federation,
Institute of Physics and Power Engineering,
Obninsk, Kaluga Region

Russian Federation

Abstract

An investigation into the reactor core accident cooling, which are associated with the power grow up or switch off circulation pumps in the event of the protective equipment comes into action, results in the problem of liquid metal boiling heat transfer. Considerable study has been given over the last 30 years to alkaline metal boiling including researches of heat transfer, boiling patterns, hydraulic resistance, crisis of heat transfer, initial heating up, boiling onset and instability of boiling. The results of these investigations have shown that the process of liquid metal boiling has substantial features in comparison with water boiling. Mathematical modeling of two phase flows in fast reactor fuel subassemblies have been developed intensively. Significant success has been achieved in formulation of two phase flow through the pin bundle and in their numerical realization. Currently a set of codes for thermohydraulic analysis of two phase flows in fast reactor subassembly have been developed with 3D macrotransfer governing equations. These codes are used for analysis of boiling onset and liquid metals boiling in fuel subassemblies during loss-of-coolant accidents, of warming up of reactor core, of blockage of some part of flow cross section in fuel subassembly.

1. INTRODUCTION

Regarding to physical and thermal dynamic properties of liquid metal coolants, choosing the sodium as a coolant in fast breeder reactors was to be an ideal decision. The nominal performance outlet sodium temperature is much less than its boiling temperature. However, boiling is possible in improbable severe accident. Among the consequences of such a process may be the pin superheating, loss of pressure. Furthermore, it can cause the reactivity to enhance due to positive void reactivity factor of sodium.

Specific problems arise in studying coolant boiling. Vapor generation in any part of subassembly, taking into account the great difference between specific volumes of vapor and liquid, is a strong disturbing factor responsible for a realignment of hydrodynamics, causing the flow to become insatiable. Study of possible failures calls for the problems concerned with fuel pin cooling under conditions of low flow rate or natural circulation.

In this connection to the liquid metal boiling was given much attention over the last three decades. Heat transfer, flow patterns, hydraulic resistance, crisis, mechanism of boiling, problems of stability were being discussed. Results of studies presented, for example in [1-10] have shown that boiling in liquid metal has specific features in comparison with water boiling, among these are:

- the growth of liquid metal vapor bubble is of explosion character, with the rate of bubble growth being in order of 10 m/s and the process of growth defined by iterative forces;
- the main two-phase flows in liquid metal are the same as those in common liquids, with the disperse-annular flow dominating at the pressure close to atmospheric;

- two-phase friction with the energy supplied is lesser than those in adiabatic flows, that is connected with the vapor pushes the interface out of the main flow;
- phase transition in disperse-annular liquid metal flow is, as a rule, performed by evaporation of near wall film provided bubbles do not generated at the wall (boiling is absent), heat transfer coefficient is as great as hundreds of kW/m^2, an influence of mass velocity and quality appears to be moderate.

Attention in studying bundle liquid metal boiling focuses on the analysis of transient and emergency performance caused by the drastic changes in power and by the various blockages, by pump shut-down.

Most general approach for solving these problems, which was realized in many scientific works, is two-liquid model of two phase flow within pin bundle. This model represents two system of governing conservation equations for mass, momentum and energy written for each phase. As far as averaged fields of parameters for phases are interdependent, it is necessary to account an interaction effects.

Two-fluid model is a power apparatus for study two phase phenomena, especially in flow areas, where phases are "weakly" bounded: stratification including different direction of phase flows, sudden mixing, sudden acceleration of the flow etc.

In practical applications because of high level of commonness of two-fluid model, especially due to large numbers of closing parameters, one can assume some simplifications: lowering of equation step and/or partial or full refusal from two liquid description.

The important aspect of subchannel model is description of mechanisms and parameters of mass, momentum and energy exchange (mixing) between two adjacent channels: microtransport (turbulent exchange), caused by the gradient of phase concentration, momentum or energy gradient; macrotransport (convection exchange), caused by pressure disbalance, drift (or diffusion) of steam phase, which are proportional to gradient of mass velocity in adjacent channels.

2. MODELING OF TWO PHASE LIQUID METAL FLOW.

2.1 Dynamic approaches in two phase liquid metal coolant.

The analysis of transient coolant flows in pin bundle has become especially urgent in connection with investigating transient operating conditions of reactor and the analysis of various emergency situations as well. The first models for calculating sodium boiling in the reactor channel were based on consideration of a single bubble expansion [11]. It was due to sodium tendency to superheating which was initially estimated as very high and, also, due to very fast transition to slug, annular flow pattern. Further development of calculation models were carried out towards increasing the number of bubbles generated in the channel. In this case, in modern model sodium superheating above the saturation temperature is, as a rule, taken to be no more than 20°C.

It should be noted that these models are in good agreement with experimental data. Up-to date codes for calculating the ULOF and UTOP type accidents- SAS 4A, SAS 3D, EAC-1, FRAX. CAPR-1, CARMEN - most often represent boiling with the use of version of well known multi-bubble models as SAS-2A (USA) and BLOW-3 (Germany). Later the models were made more complicated due to improvement in an account of friction, liquid film motion and its separation, and due to an added criterion of pin dryout. In the framework of such a model the initial thickness of liquid film is taken on the base of the liquid fraction over the channel cross section, as equal. Crisis occurs when 1/3 of its initial thickness remains. The first code developed in Russia for fast reactor channel dynamic calculations taking into account sodium boiling was also based on a single-bubble model.

The main content of up-to-date models is conservation equations for mass, energy and momentum for the two-phase non-equilibrium flow, closing relations and inherent boundary conditions. A delay in the development of such models for sodium is concerned with large great non-linearity and a discontinuity of derivative at the liquid-steam interface, as for sodium the ratio between liquid density to steam density is larger than for water. Of importance is also the relationship between the absolute pressure of the medium and pressure drop over the channel.

A 3D two-liquid model has been obtained by using temporal or statistical averaging. The model is expressed in terms of two sets of conservation equation governing the mass, energy and momentum balance in each phases. However, since the average fields of one phase are not independent on the other phase, the interaction term appear in the field equations as source term. For the most general dynamic problems such models were developed previously [12].

A similar system of governing equations can be used also in subchannel analysis of nuclear reactor core. In this case, a surface of the control volume is determined by the subdivision of reactor core into elementary channels. For doing so, as a rube, additional equation of momentum balance in transverse direction, as well as respective modeling notions on substance transport between the channels. Ignoring these effects and also analyzing the process going on in simply connected domain a system assume the terms mentioned to be left out.

Interphase exchange terms are derived from the balance conditions at the interface. It requires the local phase parameters on each side of the interface to be averaged with the mixture satisfying the mutual exchange conditions. Initial and boundary conditions, relations of turbulence transport of heat and momentum should be amplified by governing relations for each of interaction terms in two-fluid model. At present, technical difficulties restrict obtaining experimental information, as the established relations under development are defined by the significant uncertainties.

It should be marked that the system of equations is either only possible nor totally validated. The local transient equations are being derived and studying in a number of R&D centers.

Two-liquid model is a very powerful procedure and is best capable of describing the two-phase phenomena where the flow areas are available with the loosely held phases. Flow stratification (in particular, in horizontal channels) including those under counter-current motion of the phases as well as sudden mixing (one phase injects into another) and two phase flow under acceleration are an examples. Let us notify that these phenomena are far of the whole list of events attended on loss of coolant accidents. That is why the two-fluid model is a basis of the majority of developments in this direction. In practice, because of a high level of generality of the equations and a large amount of closing relations a simplification are needed to define numerical results. The first way to simplify equations is connected with the reduction of dimension (number of space coordinates), the second assumes the abandonment of the two-liquid description (reduction of phase number).

2.2. Two-phase non-equilibrium flows.

In order to have analyzed transient and accident flow in 1D approximation a large amounts of codes were developed, basically, concerned with steam generators design [13-15].

Quality and efficiency analysis of codes developed are of prime interest for practice. Reference [16] can be presented as an example, although it is based on the traditional, simple homogeneous slip model but containing detailed analysis of numerical efficiency of the models. The algorithm TRANS [17] uses a "hybrid" approach introduce the combining a finite difference implicit process (for mass and momentum balances) and the method of characteristics (for energy balance).

The use of the formal average conservation equations is a reasonable expedient to the transition to the 1D description. This results in the appearance of averaged factors (C=0,1, ...) referred to as distribution parameters. Representation of 1D equation containing distribution parameters which are equal to 1 is appropriate to the assumption on the plane profiles of phase parameters to be accepted. Forms and number of distribution parameters depend on the kind of two-fluid model. Analytical relationships for averaged factors were gained in [18].

2.3. Subchannel two-phase codes.

A great variety of subchannel codes is conditioned by, on the one hand requirements on researches for the specific reactor cores, and on the other hand, attempts to develop specific codes capable of processing as various structures, and different performances. Accepted description of two-phase flows can be classified by types of the model, namely: homogeneous, of separate flow and drift flow.

A very important feature of two-phase models is the description of the following exchange mechanisms between the adjacent channels:

(1) Microtransport referees to as turbulent mixing which arises from the random turbulence in the clearance between channels. Energy transport direction in this event is set so that the enthalpy gradient between channels is reduce. Analysis of the data available is presented in [19].

(2) Macrotransport referees to as transverse (or convective) flow which is governed by the difference in axial pressure gradients in the channels under consideration (change in the channels geometry, dissimilar heat fluxes and other irregularities). Physical prerequisites accepted in deriving mathematical models, empirical relationships as well as native and abroad codes are discussed in [19].

(3) Drift (or diffusion) of steam phase is taken as proportional to gradient of mass velocity in adjacent channels. Using this opperach it has become possible to explain the observed during experiments tendency to the steam runs into the high-velocity channels of subassembly.

2.4. Two-phase codes taking into account axial diffusion.

Recently, a number of codes has been developed on the basis of 3D macrotransport equations in terms of axial diffusion (momentum and energy) partially, in the framework subchannel analysis and, basically in the frame of a porous body model [20-22]. The main group of the codes was developed to analyze two-phase thermohydraulics but some of them have a single-phase versions including those applied to reactor fuel subassemblies cooled by liquid metal, as a rule. Two-phase flow is simulated, by homogeneous model, basically. To solve liquid dynamic equations the methods ICE [23], SIMPL [24] and their modifications are used. The codes applied to fast breeder reactors have been developed to analyse loss of flow accidents, blockades of subassembly cross section, subassembly warming up (Table 1).

2.5. Three-liquid models (heat transfer crisis).

To analyze heat transfer crisis in disperse-annular flow the three-liquid models are currently used [21], in which three interacting phases are under consideration, namely: liquid film, vapor core and disperse (drop) flow. In this case, as a rule, the following assumptions are allowed: the phase temperatures is equal to saturation temperature, velocities of vapor and drops are equal.

A considerable gain in physics and mathematics of three-liquid models turns into a serious problems associated with a rich variety (in comparison with two-liquid models) of closing relations and difficulties in their numerical realisation.

TABLE I. THE SYSTEMATISATION OF COMPUTER CODES FOR REACTORS SUBASSEMBLIES WHICH WORK IN NON-STATIONARY MODES WITH SINGLE- AND TWO-PHASE COOLANT FLOWS

References	Code	Approximation	Single-phase flow	Two-phase flow		Non-stationary flow	Numerical method	Country
				Homogenius	Non-homogenius			
	SABRE-1	Porous body model	+	–	–	+	ICE	Great Britain
	SABRE-2	Porous body model	+					
[38]	SABRE-3	Porous body model	–	+	–	+	IMPL based	
	SABRE-3B	Porous body model; subchannel		+			on SIMPLE	
[39]	BACCHUS	2-D Porous body model	–	+	–	+	Implicit scheme on biased mesh, interative Newton method (ICE type)	France
[40], [41]	TOPFRES	Subchannel	+	–	+	+	ICE	Japan
[42]	UZU	Porous body model	+	–	–	+	ICE	Japan
[36]	COBRA-IV	Subchannel	–	+	–	+	ICE	USA
	COMMIX-1	Porous body model	+	–	–	+	ICE	USA
[43], [44]	COMMIX-1a	Porous body model	+			+		
	COMMIX-2	Porous body model	–	+	+	+	IMF	
[45]	PORTER	Porous body model	+	–	–	+	Semi–implicit scheme, interative method	Russia
[46]	BACCHUS -3D/TP	2-D Porous body model	–	–	+	+	ICE	Germany
[47]	COMMIX-2/KFK	Subchannel	–	–	+	+	Interative method using upper relaxation	Germany
[48]	SABENA	Subchannel	–	–	+	+	Semi–implicit scheme, interative Newton method	Japan
[49]	TEMP-MF	Subchannel	+	–	+	+	Semi–implicit scheme, interative method	Russia

3. SOME RESULTS OF EXPERIMENTAL INVESTIGATIONS.

Experimental investigations of liquid metal boiling in fuel bundles were carried out in Germany, Japan, USA, France and Russia. The large serious of experiments were carried out by Japanese scientists. Typical results show that in transient states with sodium boiling in a 37-fuel element assembly with coolant flow rate drop we observed [25] (fig. 1):

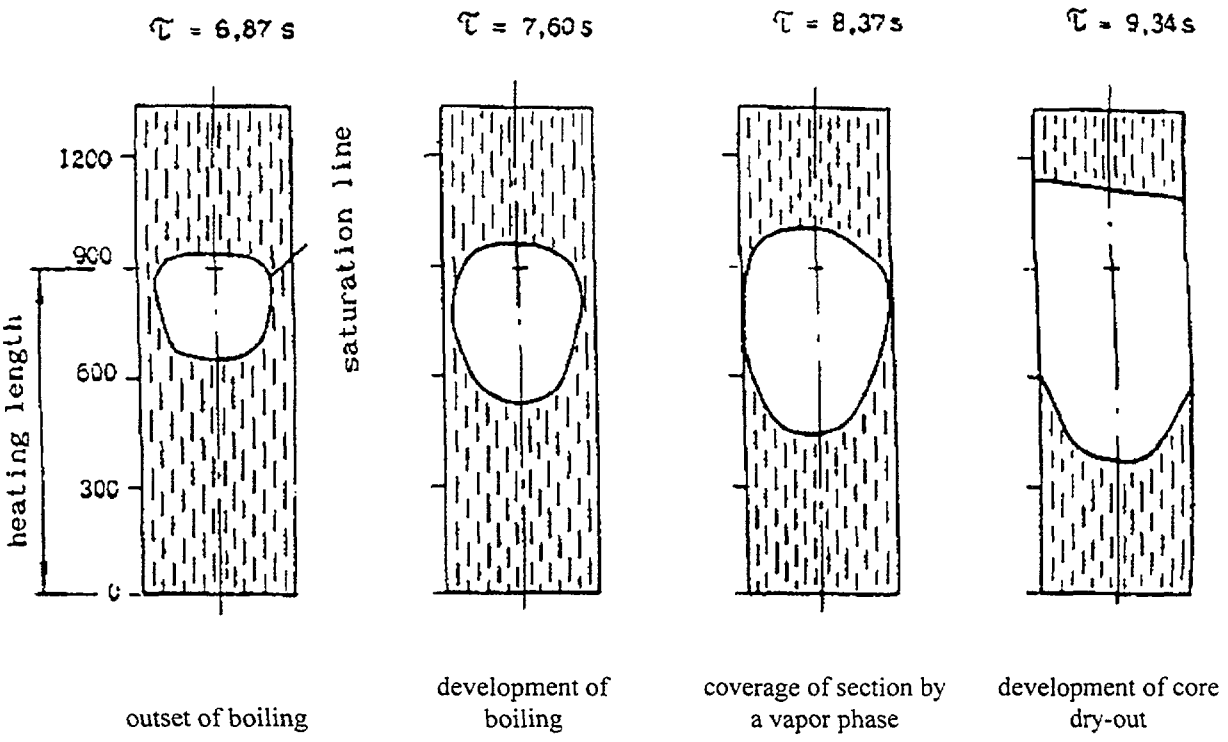

Fig. 1. Development of boiling area in fuel assembly with fuel assembly coolant flow rate reduction

- The maximum value of near-wall superheating 36 C independent on heat flow density, system temperature and pressure enhancement rate.
- First the bubble was farmed at the end of the heated area, then it expanded basically in an up flow direction in the central cells and down flow in the non heated area according to saturation temperature area propagation.
- When the bubble covered all the flow cross-section, the inlet flow rate fell drastically.
- The inlet flow velocity was pronouncedly oscillated as a shell-shaped blister grew and collapsed and inlet flow rate variation (reversing) was observed.
- Liquid film dry-out crisis the fuel element surface occurred after the flow rate reversing outset.
- Recurrent wetting terminated the film dry-out, but dry-out occurred again at a subsequent flow rate reverse. This recurred a few times. Step-by-step the film region expanded resulting in fuel element surface temperature elevation.

Last time experiments on liquid metal boiling continues in IPPE (Russia) for the regime of natural convection.

3.1. Experimental contour and test section.

Fig. 2 presents a schematic diagram of experimental contour to study eutectic Na-K alloy (22% Na; 78% K) boiling in the 7-pin bundle when coolant moves under the action of

natural circulation. The contour represents two vertical channels of 3m length connected in top and bottom parts. The left (downwards) channel is made of the pipe ∅ 30×2 mm, and the right (upwards) – of the pipe ∅ 50×1,5 mm. In the bottom part of the upwards channel the test section itself is positioned, which is the bundle of the 7 pin-simulators.

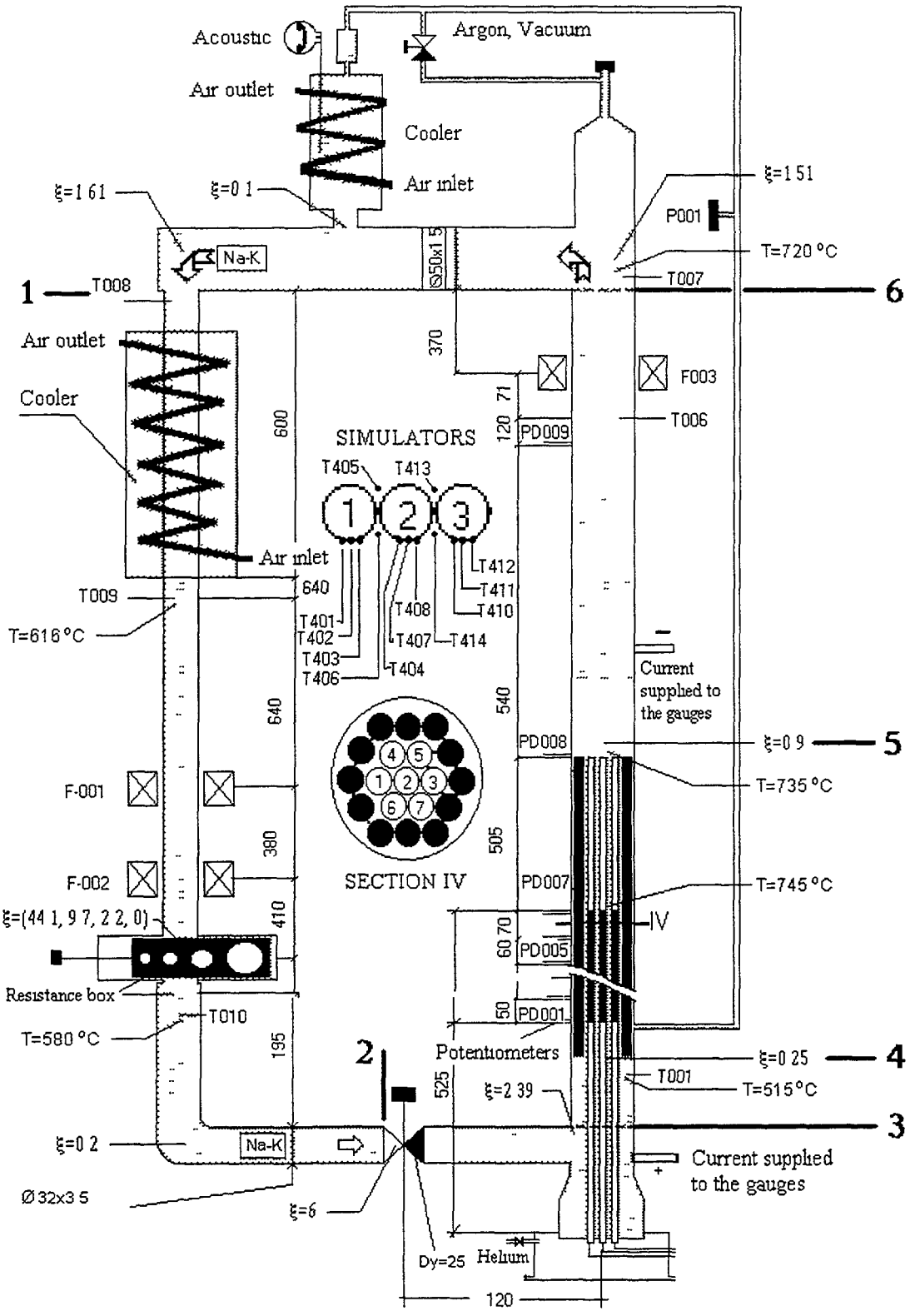

Fig. 2. Schematic diagram of 7-pin test section.

The bundle consists of 7 simulators and 12 pin-displacers, arranged in triangular manner with relative pitch s/d=1.185 and being jacketed for stainless steel tube of 50x1.5 mm in diameter and 3 m in length. The pin-simulators represent standard made pipes of stainless steel X18H10 of 8x1 mm in diameter, inside of which the helical heaters of molybdenum wire of 1 mm in diameter are inserted. Helix diameter is 4 mm, length is 420 mm. The clearance between heater and pin cladding is filled with the powder of magnum oxide.

The fact that the model bundle is equipped by a lot of measurement channels, containing various primary converters (gauges), transition apparatus (shielded or not shielded wires, current feeds, cable joints and so on), normalising converters which serves to receive, amplify, filtrate and compensate readings, measurement apparatus allows obtaining voluminous experimental data on liquid metal boiling in the bundle.

3.2. Experimental results.

A series of experiments to study process of liquid metal boiling (eutectic alloy of sodium and potassium) in fast reactor out-of-pile subassembly under conditions of natural convection at various mass velocity due to variation in hydraulic resistance of the contour have been carried out. Experimental technique is that the power supplied to the bundle increases while coolant does not move, that is natural convective motion of coolant occurs. As power increases, coolant temperature increases up to saturation temperature and onset of boiling is observed (Fig. 3). Three modes of boiling have been observed:

- Nucleate mode, which initiates at the beginning of the process. Its feature is a stable values of all parameters (coolant temperature, pin wall temperature, pressure drop over the bundle, inlet and outlet coolant flows). Enhancement of power causes the nucleated mode to transfer to slug one.
- Slug mode arises at heat flux from 125 to 170 kW/m^2. Specific feature of this mode is its pulsating character. Large-scale bubbles (slugs) are generated at 40 seconds and more intervals, which at the instance of coming to the surface result in drastically increase of inlet flow and significant pulsations in all measured parameters. Thus, pulsations of parameters are of hydrodynamic nature and are defined by not only boiling in the bundle, but processes in circulation contour as a whole. It is significant that pin wall temperature does not exceed saturation temperature, that indicates the liquid film is placed at the pin surface. As the bundle power increases, frequency of the slug generation increases and temperature pulsation amplitude reduces. At heat flux from 210 to 230 kW/m^2 the transition to disperse-annular flow is observed.
- Disperse-annular flow incorporates a stable behaviour of parameter to be measured. Evaporation of liquid and drop entertainment from the pin surface causes dryout heat transfer crisis being attended with melting of pin cladding and onset of severe accident.

Disperse-annular mode is limiting boiling mode, which provides reasonable heat removal.

Experiments have shown that in transition from nucleate to disperse-annular flow, coolant flow through the contour increases by a factor of three. At heat flux above 250 kW/m^2 coolant flow reduces and disperse-annular pattern transfers into disperse one (post dryout mode).

Results of the experimental data processing as a relationship between mass velocity and void fraction are presented in Fig. 4. Average values processed in co-ordinates mass velocity–void fraction indicate areas of stable (nucleate) flow – A, unstable (slug) flow – B, and stable (disperse-annular) flow – C. Approximate borders can be drawn between these areas (Fig. 3). In order to refine inter-flow boundaries the further experiments are required.

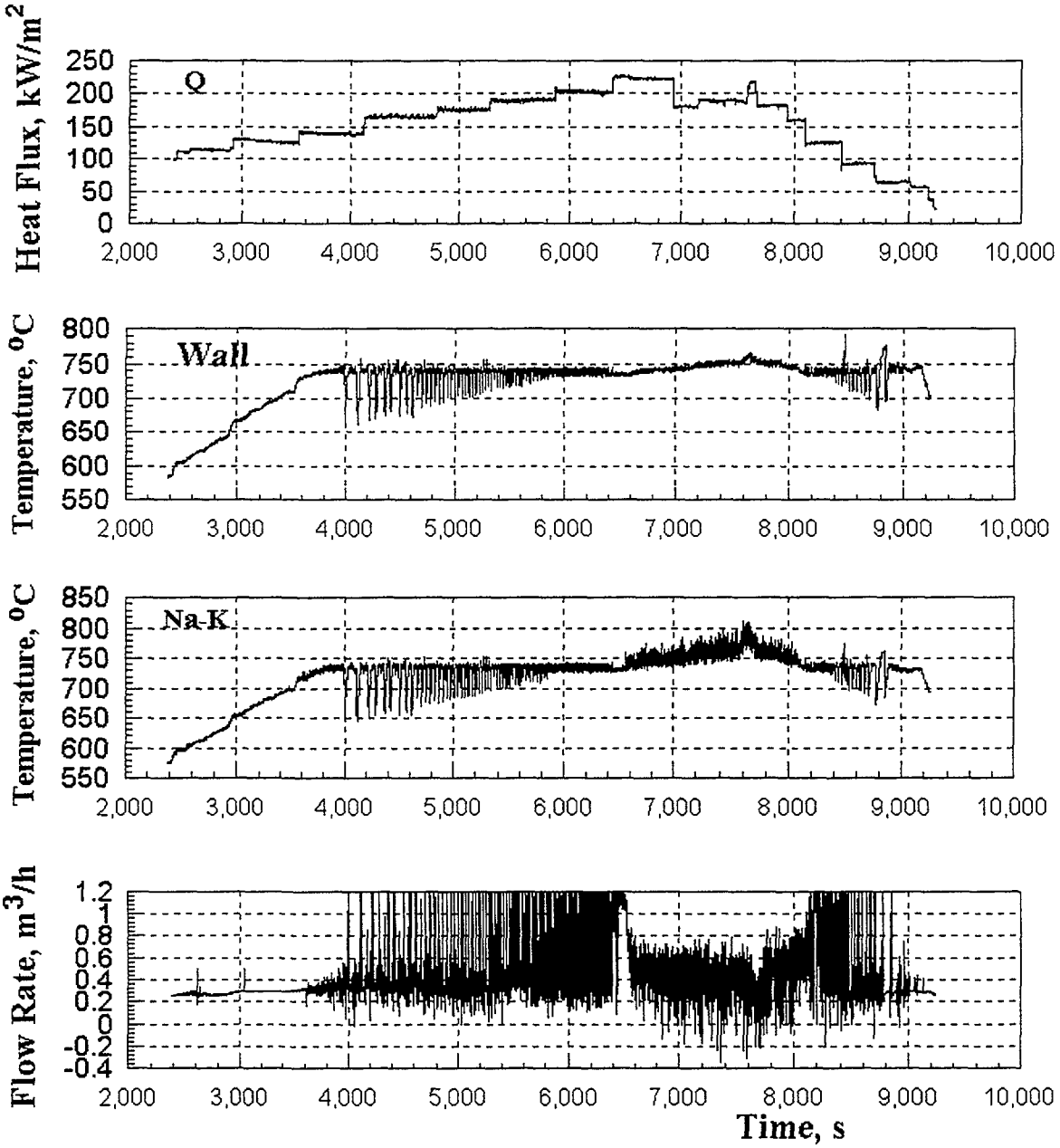

Fig. 3. Heat flux, wall temperature, coolant temperature in section IV, coolant flow rate in the experiment with the spacer d=20 mm.

3.3. Pool boiling.

In boiling of mixture representing an ideal solution (as it has been shown above, eutectic Na-K alloy is just such a solution) dependence of heat transfer coefficient α on concentration of low boiling component c' (in our case it is potassium, T_{boil} = 1033 K) has one extremum (minimum). In this event, heat transfer coefficient of mixture may be lesser than its additive value:

$$\alpha_{NaK} < \alpha_K \cdot c'_K + \alpha_{Na}\left(1 - c'_K\right) \quad (1)$$

where α_{Na}, α_K - boiling heat transfer coefficients for pure Na and pure K at the same pressure.

Experimental data on potassium pool boiling and boiling in pipes [26] and on sodium-potassium boiling in pin bundles presented in form of the heat transfer coefficient as follows:

$$\alpha = A \cdot q^m \cdot P^n \quad (2)$$

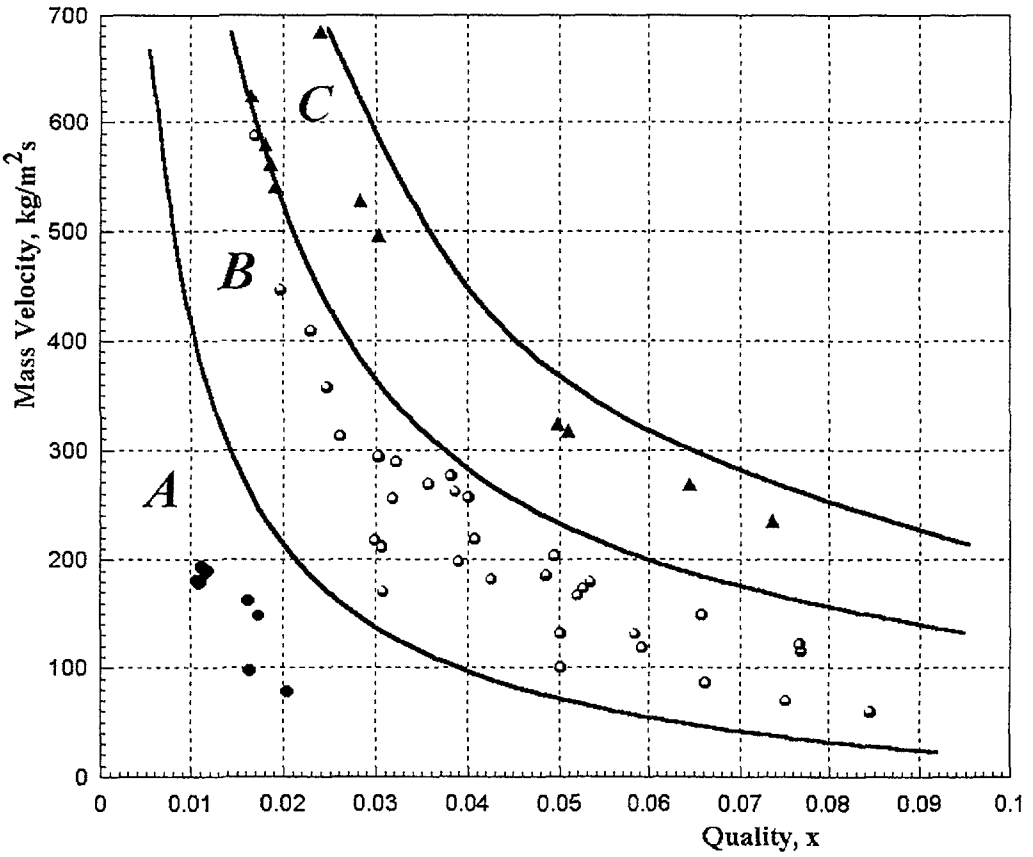

Fig. 4. Experimental pattern map.

are in a good agreement (Fig. 5). Factors A, m, n are of the same values as Na and in Na-K alloy: $A = 4.5 \div 7.5$, $m = 0.7$, $n = 0.1 \div 0.15$.

In criterion form the heat transfer coefficient is generalised by the following equation [26], [27]:

$$Nu = 8.7 \cdot 10^4 \, Pe^{0.7} Kp^{0.7} \tag{3}$$

where:

$$\mathrm{Nu} = \frac{\alpha}{\lambda'} \sqrt{\frac{\sigma}{\rho' - \rho''}} \quad \text{– Nusselt Number;}$$

$$\mathrm{Pe} = \frac{qc\rho'}{r\rho''\lambda'} \sqrt{\frac{\sigma}{\rho' - \rho''}} \quad \text{– Peclet Number;}$$

$$Kp = \frac{p}{\sqrt{\sigma g(\rho' - \rho'')}}.$$

Fig. 6 presents data on liquid metal boiling heat transfer generalised in accordance with (3). It is apparent that experimental data gained by the authors on Na-K alloy are consistent with the relation, that indicates that there is possibility to convert NaK data to sodium.

Thus, eutectic Na-K alloy and Na are similar substances and data on boiling of one coolant can be transferred to other one.

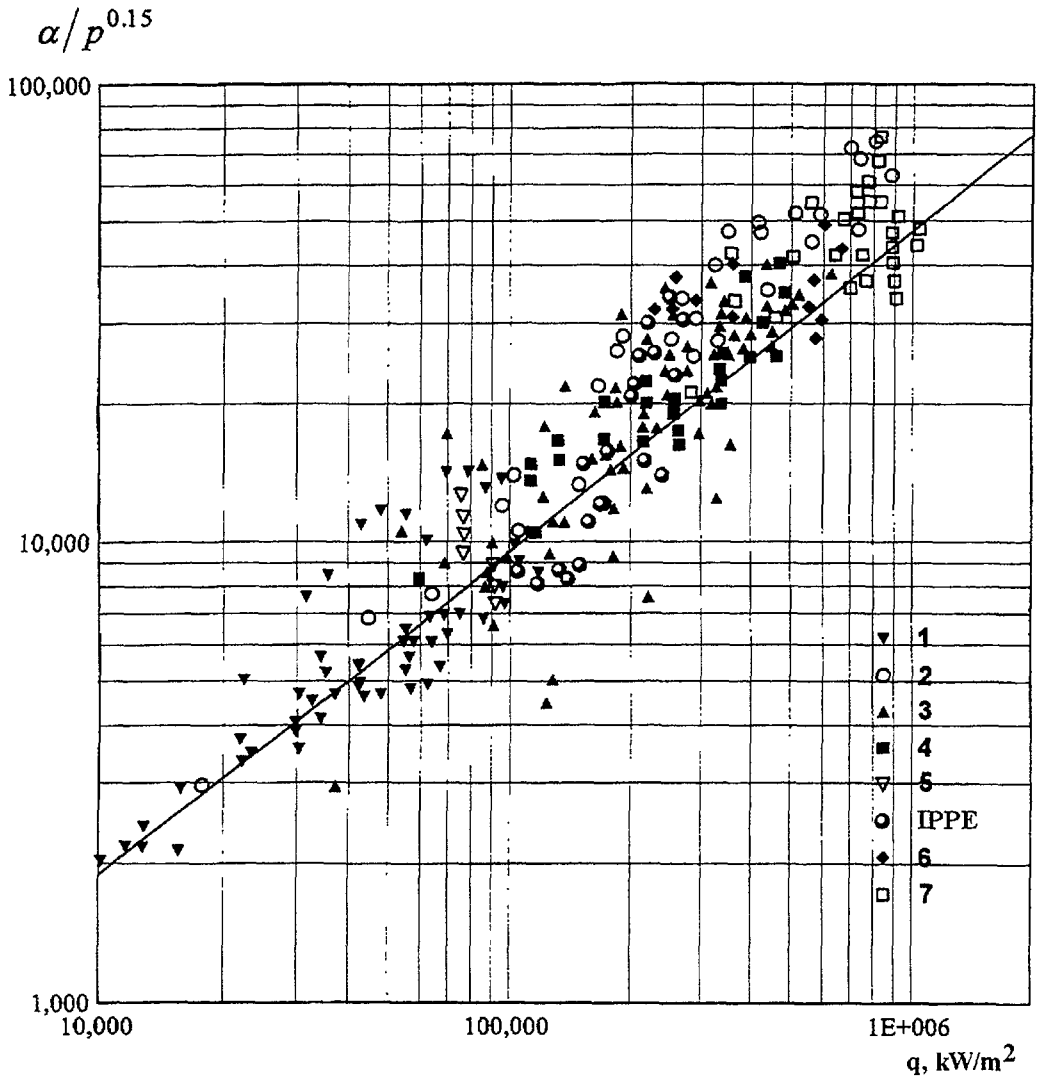

Fig. 5. Comparison of experimental data on liquid metal boiling heat transfer.

Potassium:

1 – pool boiling
2 – tube D= 10 mm (heat exchanger)
3 – tube D= 6 mm (electrical heating)
4 – tube D= 10 mm (electrical heating)
5 – tube D= 22 mm (electrical heating)
6 – tube D=8.3 mm (electrical heating)
7 – tube D= 4 mm (electrical heating)

Eutectic alloy Na-K:

IPPE – 7-pin bundle D=35.2 mm (electrical heating)

3.4. Crisis of heat transfer in liquid metal.

The experimental data on critical heat flux [9], [28-30], received at round tube Na and K boiling, as well those at pin bundle boiling were analysed in the following range of parameters: mass flow rate 1.69 – 402 kg/m^{2}s; pressure 0.01 – 3.0 bars; hydraulic diameter of the channel 4.0 – 9.0 mm; length of a heated section 200 – 1000 mm. For this area of parameters the value of critical heat flux (CHF) varied within 32.3 - 7370 kW/m^2.

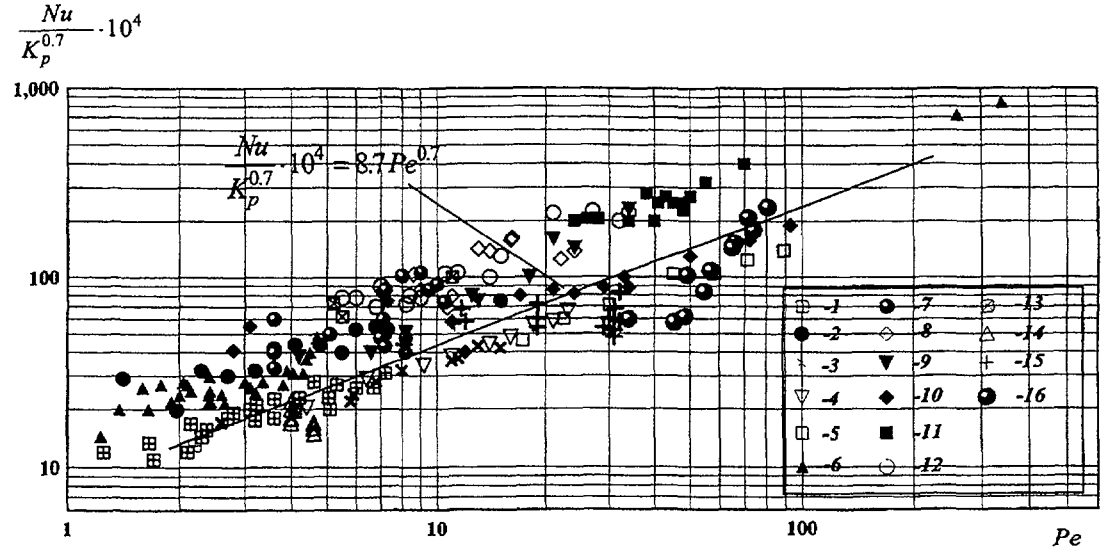

Fig. 6. Experimental data on liquid metal boiling heat transfer.

1, 2, 3, 4, 5 –	potassium pool boiling at p= 1.2; 1.1; 0.7; 0.4; 0.04 × 10^5 Pa.
6, 7 –	sodium pool boiling at p= 1.0; 0.472 × 10^5 Pa.
8, 9 –	sodium pool boiling at p= 0.26; 1.0 × 10^5 Pa.
10 –	sodium pool boiling.
11 –	sodium, slot d=2 mm.
12 –	sodium, slot d=4 mm.
13 –	sodium, slot d=1 mm.
14, 15 –	potassium, tube d=22 mm; 8.3 mm.
16 –	7-pin bundle IPPE (authors data).

$$q_{кр} = 0312 \frac{G^{0.95}}{L/D_r} r$$

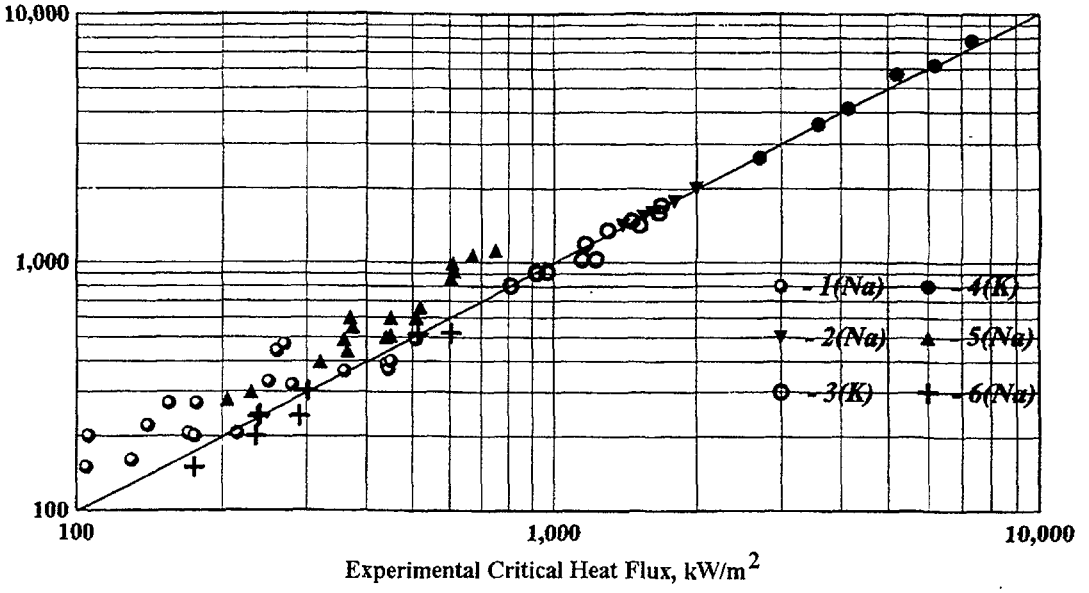

Fig. 7. Comparison of experimental and predicted data on sodium and potassium critical heat flux:

1 – Yamaguchi K.; 2, 3 – Chang S.H., Lee Y.-B.; 4, 5 – Kottowski H.M., Savatteri C.; 6 – Kaiser A.

As a result of generalisation of the available data the relationship is received:

$$q_{cr} = 0{,}312 \cdot \frac{G^{0,95}}{L/D} \cdot r, \tag{4}$$

where G – mass velocity, kg/s; r – specific heat of vaporisation, kJ/kg; L – length of heated section, m; D – hydraulic diameter of the channel, m.

From a fig. 13 it is observed, that the relationship obtained describes rather well all the data, without regard to the experimental operating conditions.

3.5. Some numerical analysis.

With the use of the code THB an experiments to be performed have been predicted, with the contour geometry, inherent hydraulic resistance, value and distribution of the power supplied to the bundle being input. Predicted distributions of pin wall temperature, coolant temperature, coolant flow are close to those observed in experiments (Fig. 8). Code THB allows a dynamics of the process of natural circulation boiling to be calculated.

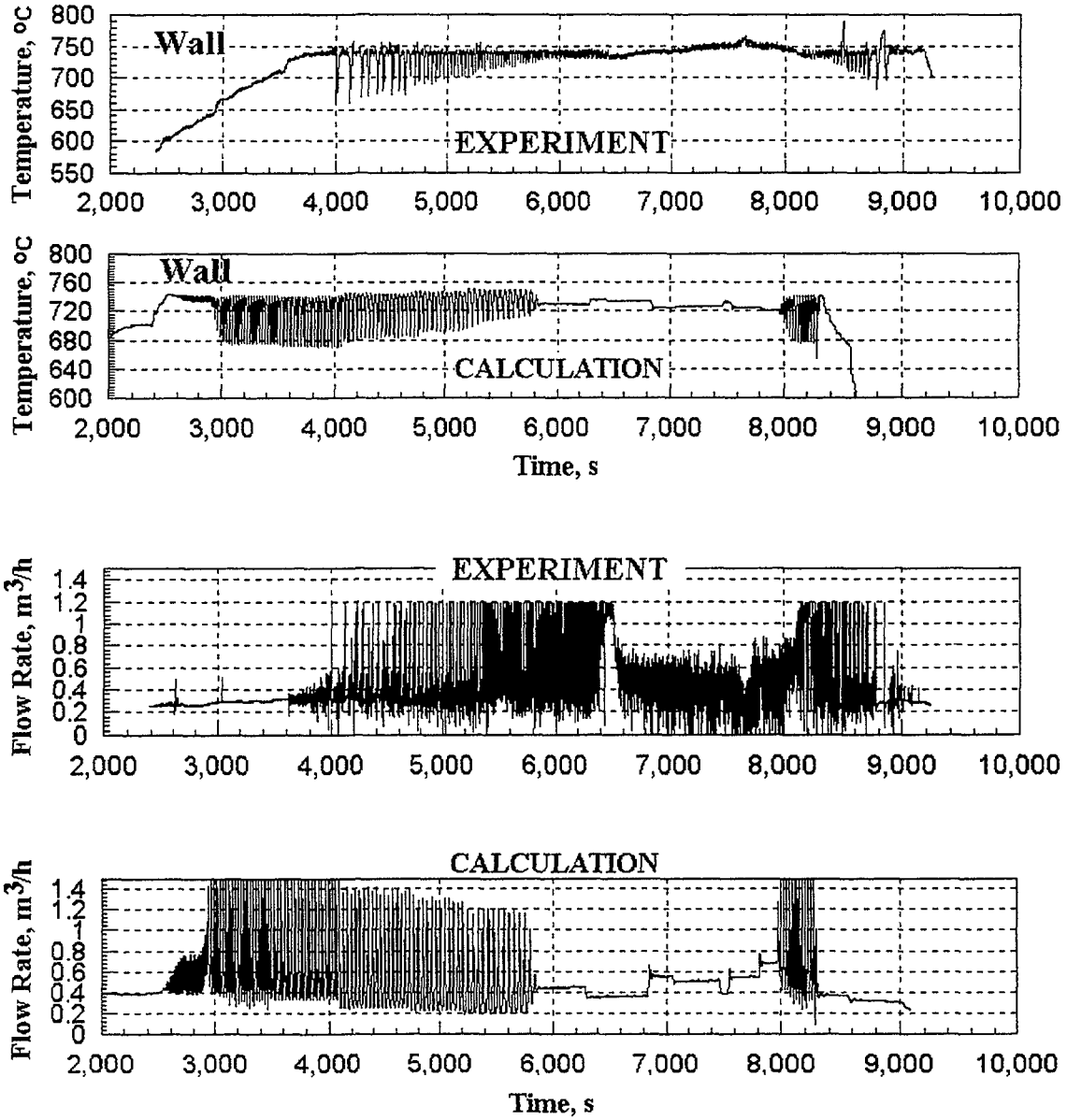

Fig. 8. Comparison between experimental and calculated data on wall and coolant temperature (for experiment with spacer d=20 mm).

4. NUMERICAL MODELING

Numerous investigations in different countries (FRG, USA, Japan, Belgium, Netherlands, USSR) were carried out for the case when a section of flow area in a fuel assembly is plugged [31]. The onset of plugging is related to the availability of oxides in the flow, coolant contamination, fuel element failure.

Plugging involves essential variation in velocity, pressure and temperature of coolant. Even insignificant plugging is a potential source of local coolant boiling, fuel element failure and accident propagation. The basic issue is elucidation of fuel element cool-down limits in the post-blockage boiling area, the nature of two-phase flow development. However, in addition to thermohydraulic factors This process is affected by the geometry of the total assembly and circuit, which makes the insight into the experimental results considerably difficult. The work by Votani, Haga [32] appears representative: 29% flow area blockade in the center of a 37-rod assembly with a relative spacing pitch ~ 1.2, the thermal flow density at an initial period of time was 127 W/sm. At the initial instant of time boiling was not observed. In 16 seconds with the thermal flow density on the elements increased to 135 W/sm, a local coolant boiling emerged directly outside the blockade. As power augmented by the instant of time 70 s, its size enlarged and continued growing subsequently (fig. 9). However, the dry-out area was restricted locally, the flow reduction was barely perceptible. Temperature and pressure fluctuations were detected since the instant of boiling onset.

With a section of flow area plugged in the peripheral fuel assembly region, coolant boiling was observed in the recirculation area center and when propagating it did not cover the area in the direct vicinity of blockage surface for a long time. The superheating value required for coolant boiling-up is as low as 30 C and it drops as the flow velocity in fuel assemblies increases.

Three types of non-stationary conditions were identified from the initiation of boiling to the crisis (dry-out) onset:

(1) - dry-out takes place in boiling variations,

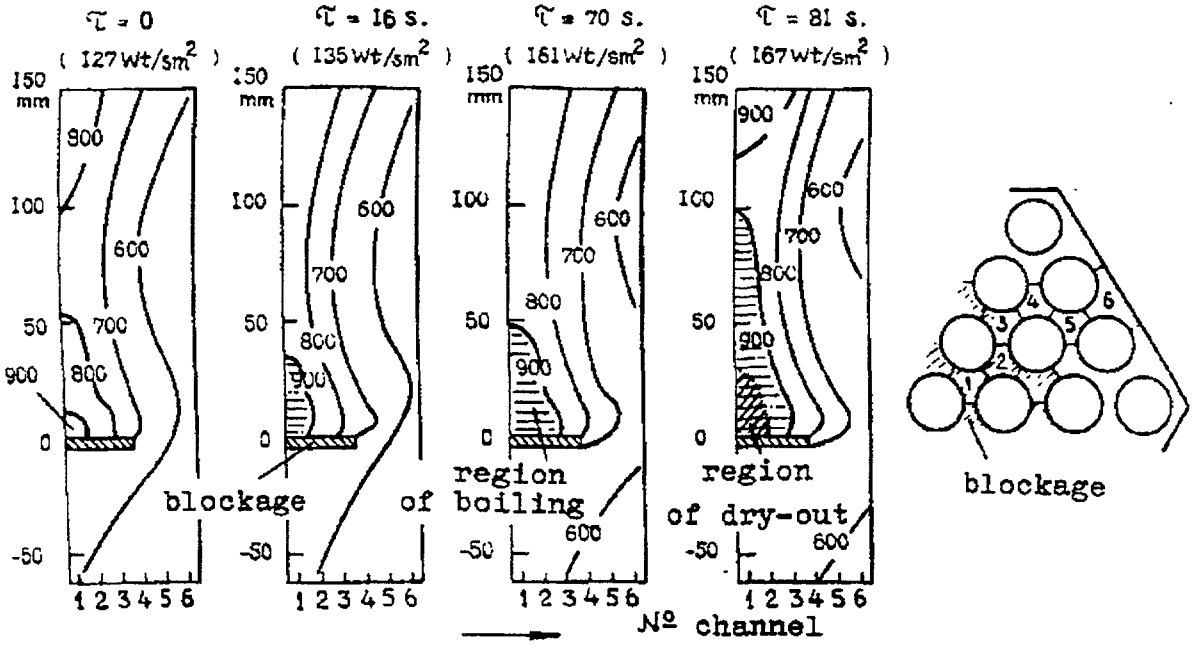

Fig 9 Evolution of boiling with fuel assembly power augmentation accompanied by flow area section plugging in the fuel assembly center.

(2) - dry-out follows the transition from the oscillatory to steady-state conditions,

(3) - dry-out is encountered during steady-state boiling irrespective of fluctuational boiling occurrence. For heat transfer mechanism explorations between the two-phase flow and the fluid region the experiments were made on a water test rig with visualization of gas injection flow directly to the post-blockage area [33]. A liquid film was observed, which wraps around the rods (fig. 10).

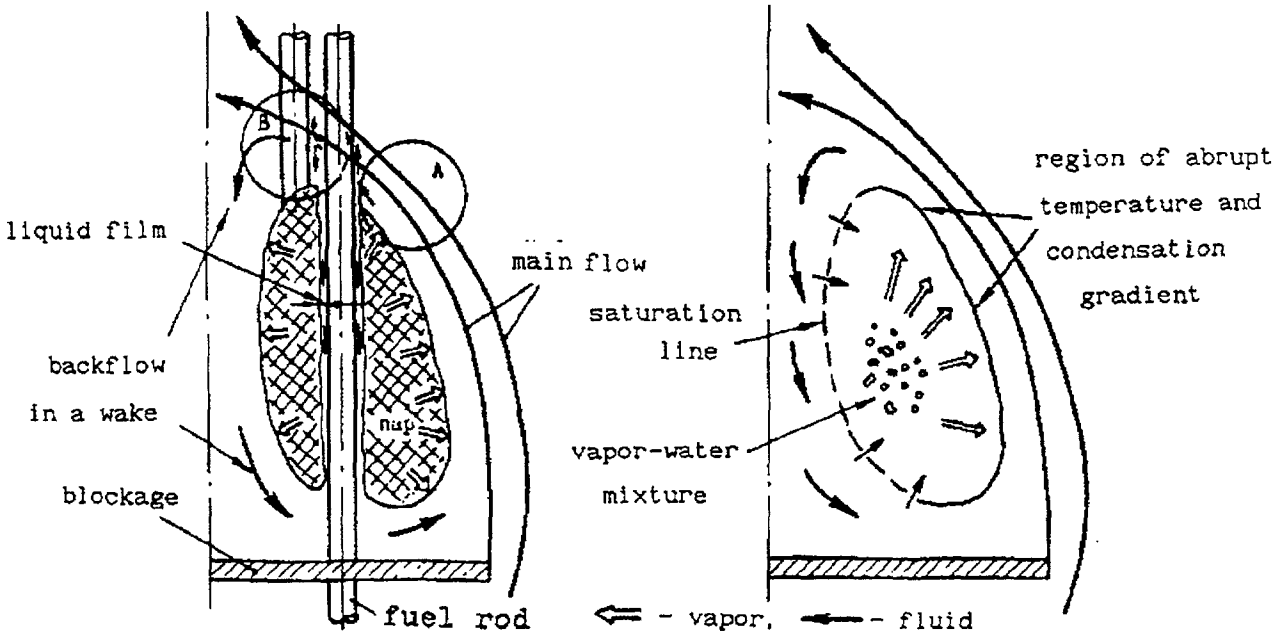

Fig.10 Illustration to heat mass transfer in coolant boiling in the region onside the blockage of fuel assembly flow area section.

The two-phase flow occurs solely in the region around a gas cavity. The fluid/gas interface is not fixed, is subjected to occasional variations, particularly in the region "A". Observation is made of the waves moving down flow in the liquid film. A detailed consideration is also given to the mechanisms of film dry-out on the rods, entrainment of drops and their precipitation in the two-phase flow, liquid film recovery due to boiling region fluctuation. The results obtained show, that the local blockage does not result in rapid propagation of failure in fuel element bundles.

In fission gas escape accidents an occurrence of any (or all within the fuel assembly) of the two-phase flow forms ranging from the bubble to dispersion-annular conditions [34] is feasible. With the gas released in the region out side the blockage with a flow velocity below the lower critical value (~ 2 m/s). The gas readily escapes from the wake region. As the velocity grows, a gas cavity is formed which is capable of filling the total recirculation region. The flow velocity exceeding the upper critical value (~ 5 m/s), the gas cavity is subdivided to small bubbles circulating in the wake region (fig. 11).

As the external flow velocity rises fuel assembly cool-down deteriorates. Post-blockage superheating essentially rises as the evolving gas flow rate increases. With the maximum attained, a certain reduction in superheating is observed (fig. 12).

Post-blockage gas release as a result of fuel element failure may be responsible for the further failure of fuel elements in fuel assemblies. For the failure of elements adjacent to the failed fuel element the perturbations should be prolonged for the fuel element to get heated up to the damage threshold temperature. It depends on the fuel element time constants, local thermal and hydraulic characteristics of coolant.

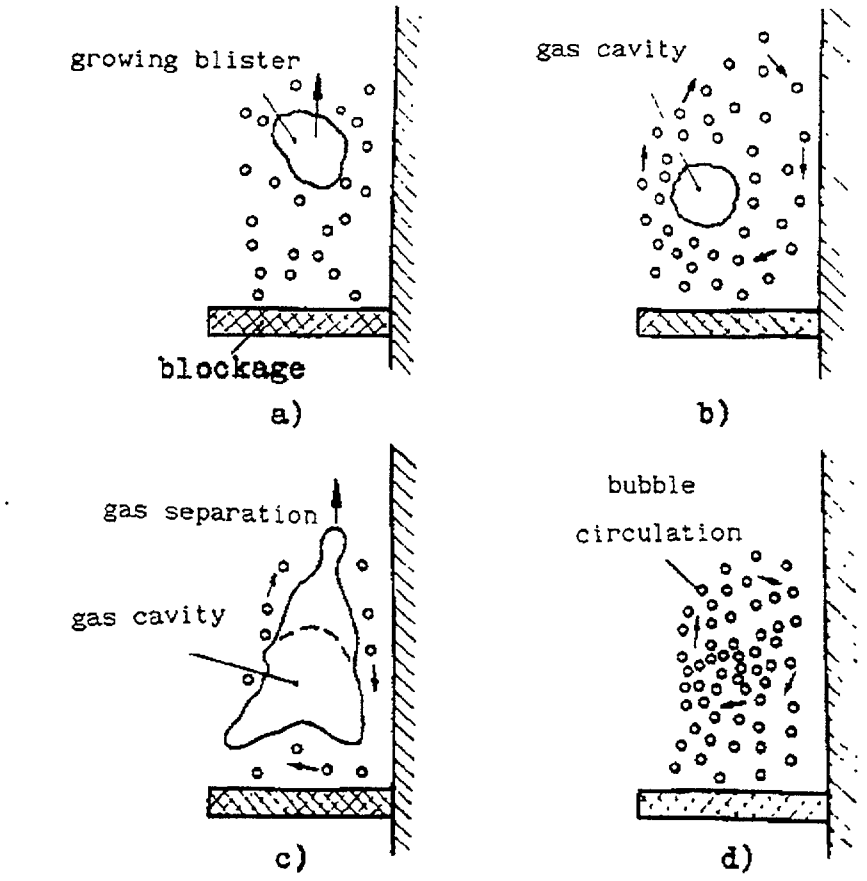

Fig.[11] schematic diagram of two-phase flow pattern with post-blockage gas injection.

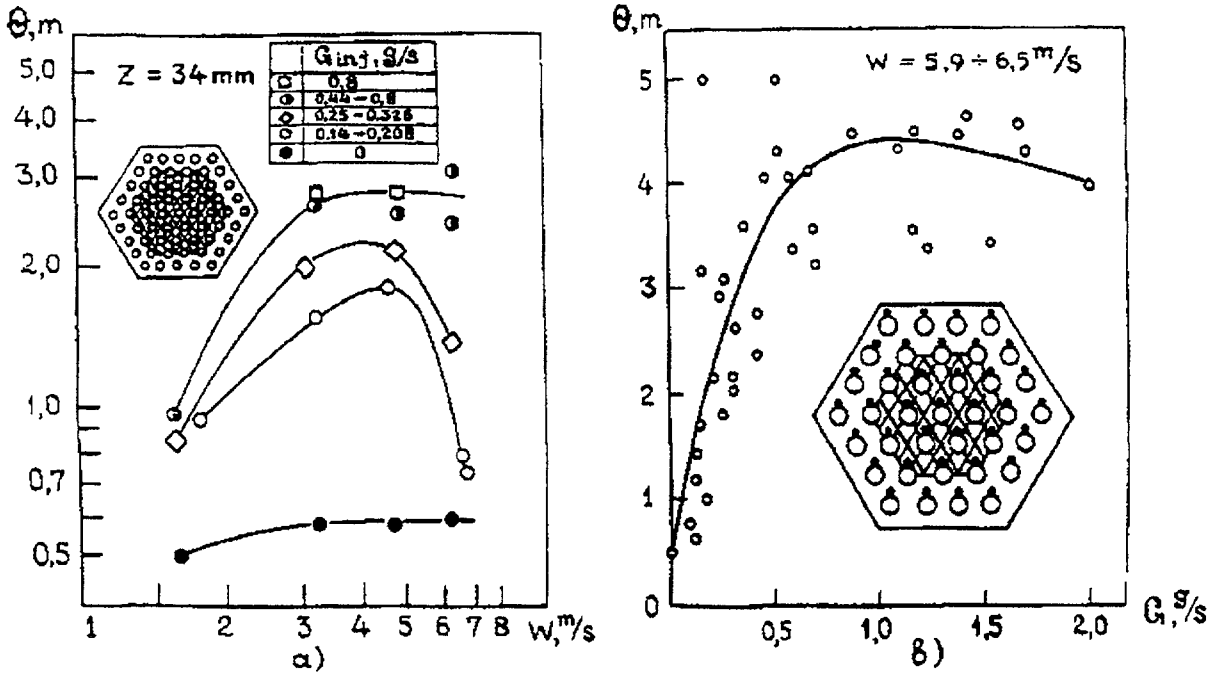

Fig[12] Dependence of parameter $\Theta = \Delta T/(dT/dz)$ on coolant flow rate in fuel assemblies with different flow rates of injected gas (a) and on injected gas flow rate (b) (z is the distance from the blockage).

CONCLUSION

Thus the following items should be noted:

(1) Nowadays the complete correct statement of a set of macrotransport equations have been developed describing hydrodynamics and heat transfer in two-phase flows of reactor fuel assemblies. The experimental results available can be a basis for design code development for liquid-metal coolant boiling fuel assemblies.

Currently a set of codes for thermohydraulic analysis of two phase flows in fast reactor subassembly have been developed with 3D macrotransfer governing equations taking into account axial diffusion: TOPFRES, BACCHUS-3D/TP, COMMIX-2/KFK, SABENA with phase separation, SABRE-3(3B), COBRA-4, COMMIX-1(1A), BACCHUS in the framework of homogeneous model. Method ICE and its modifications are used for solving two phase flow dinamics in the codes mentioned above.

These codes are used for analysis of boiling onset and liquid metals boiling in fuel subassemblies during loss-of-coolant accidents, of warming up of reactor core, of blockage of some part of flow cross section in fuel subassembly. The use of separated phase flows and account of inter-channel exchange lead to significanty better coincidence of calculation results with experimental data than in case of homogeneous flow model. This results are confirmed for coolant flow rate through the subassembly, for void fraction distribution and finally for critical heat flux.

(2) The information acquired as a result of experimental and calculated activities demonstrates a physical pattern of temperature fields formation, onset and evolution of boiling in fuel assemblies and dry-out under such circumstances as dramatic coolant flow rate drop in fuel assemblies, augmentation of fuel element power rating in fuel assemblies, plugging in a section of fuel assembly flow area.

The results obtained show the post-local blockage boiling not to result in fast propagation of fuel rot bundle failure. Post-blockage gas release due to fuel element failure can be the cause of the further fuel element failure in fuel assemblies. Investigation of regularities in the effect of diverse factors of temperature fields formation (flow or power variation rate, values of Reynolds and Peklet numbers, fractions of plugged flow are of fuel assemblies requires additional systematic experimental and calculated studies.

(3) Comparing the results of calculation with experimental data under fuel assembly coolant boiling indicates their difference in individual situations. Experimental and calculated fundamental investigations of flow pattern and liquid-metal coolant fuel assemblies under coolant boiling, derivation of complete relations, further development of numerical models and non-stationary heat transfer problem solution techniques with coolant boiling in a three-dimensional approach are a requirement.

(4) There are only limited experimental data available on liquid metal natural circulation boiling at low heat fluxes. An influence of many factors is in essence not studied, such as pressure, densities ratio, geometry, length of heated section, relation between hydraulic resistances over parts of contour and others. Stability of liquid metal boiling in the system of parallel bundles is not understood. Further investigations will allow obtaining a required validation of stable heat removal in fast reactor core.

REFERENCES

[1] ZEIGARNICK YU., LITVINOV V.D. Heat Transfer and Pressure Drop in Sodium Boiling in Tubes // Nuclear Science and Design, v.72, № 1.

[2] DWYER O., HSU C. Evaporation of the Microlayer in Hemispherical Bubble Growth in Nucleate Boiling of Liquid Metals // Intern. Journal of Heat and mass Transfer, 1976, v. 19, № 2, p. 185.

[3] SUBBOTIN V.I., SOROKIN D.N., et al. Heat Transfer in Liquid Metal Natural Convection Boiling, M., Nauka, 1969.
[4] BORISHANSKI V.M., KUTATELADZE S.S., et al. Liquid Metal Coolants, M., Atomizdat, 1976.
[5] KIRILLOV P.L. Heat Transfer in Liquid Metal Flows in Round Tube (Single- and Two-Phase Flows // Doctor of Science Thesisis, IVTAN, Moscow, 1968.
[6] SHAH M.M. A Survey of Experimental Heat Transfer Data for Nucleate and Poll Boiling of Liquid Metals and New Correlations // International Journal of Heat and Fluid Flow, 1992, v. 13, № 4, p. 370-379.
[7] CHANG S.H., Lee Y.B. A New Critical Heat Flux Model for Liquid Metals under Low Heat Flux-Low Flow Conditions // Nuclear Engineering and Design, 1994, v. 148, № 3, p. 487-498.
[8] KAIZER A., HUBER F. Sodium Boiling Experimental A Low Power under Natural Convection // Nuclear Engineering an Design. 1987, v.100, №3, p. 367-376.
[9] YAMAGUCHI K. Flow Pattern and Dryout under Sodium Boiling Conditions // Nuclear Engineering and Design, 1987, v. 99, p. 247-263.
[10] KOTTOWSKI H.M., SAVATERI C. Evaluation of Sodium Incident Overheat Measurements with Regard to the Importance of Experimental and Physical Parameters // International Journal of Heat and Mass Transfer, 1977, v. 20, № 42, p. 1281-1300.
[11] CRONENBERG A.W. et. al. A Single-Bubble Model for Sodium Expulsion from Heat Channel // Nuclear Engineering and Design, 1971, v. 16, ? 3.
[12] ISHII M. Two-Fluid Model Hydrodynamic Constitutive Relations // Nuclear Engineering and Design, 1984, v. 82, ? 2-3, p. 107-126.
[13] SPASSKOV V.P. et al. Complex of Programs to Predict Transient Thermal and Hydraulic Processes in Designing WWER // Problems of Nuclear Science and Engineering. Physics and Engineering, 1981, Issue 7(20), p.72.
[14] KOLEV N.I. Comparision of the RALIZA-2/02 Two-Phase Flow Model with Experimental Data // Nuclear Engineering and Design, 1985, v. 85, p. 217-237.
[15] BOGOSLOVSKAYA G.P., BOGATYREV I.L., ZHUKOV A.V. et al. Two-Liquid Model of Two-Phase Flow Prediction // Preprint IPPE-1991, Obninsk, 1991.
[16] GERLIGA V.A., KIRILLOV V.V. Conservative Difference Scheme for Steam Generating Channel Dynamic Equations // Problems of Nuclear Science and Engineering. Physics and Engineering, 1982, Issue 6(19), p.43.
[17] MIRONOV YU.V., RAZINA N.S., FOMICHEVA T.I. et al. Analysis of Transients in Nuclear Reactor Contours // Atomic Energy, 1986, v.60, ¹4, p.255-260.
[18] KORNIENKO Y.N., KUZEVANOV V.S., SOROKIN A.P. The Technique of Calculation of Non-equilibrium Two-Phase Flows in Pin Bundles Using Quasi-Two-Dimensional Approaches and Subchannel Approximation // Advanced in Gas-Liquid Flows, Winter Annular Meeting of ASME, Dassal, Texas. Nov. 25-30. 1990, FED, v. 99, p. 321-330.
[19] ZHUKOV A.V., SOROKIN A.P., MATJUKHIN N.M. Inter-channel Exchange in Fast Reactors. M., Energoatomizdat, 1989.
[20] MACDOUGALL J.D., LILLINGTON J.N. The SABRE Code for Fuel Rod Cluster Thermohydraulics // Nuclear Engineering and Design. 1984, v. 82, ? 2-3, p. 171-190.
[21] NINOKATA H., OKANO T. SABENA: Subassemby Boiling Evolution Numerical Analysis // Nuclear Engineering and Design. 1990, v. 120, ? 3, p. 349-367.
[22] KUMAEV V.Y., LEONCHUK M.P., DVORTSOVA L.I. Numerical Procedure for Calculating 3-D Coolant Flow in Pin Bundles // Preprint IPPE-1733, Obninsk, 1985.
[23] KARLOW F.H., AMSDEN F.F. A Numerical Fluid Dynamics Method for All Flow Speeds // Journal of Computational Phisics. 1974, v. 8, ? 2, p. 197-213.

[24] PATANKAR S. Numerical Solution of Liquid Heat Transfer and Hydrodynamics. M., Energoatomizdat, 1984.
[25] HAGA K. Loss-of flow Experiment in a 37-Pin Bundle LMFBR Fuel Assembly Simulation // Nuclear Engineering and Design, 1984. v. 83, ¹ 2-3, p. 305-318.
[26] KIRILLOV P.L., YURIEV YU.S., BOBKOV V.P. The hand book on thermohydraulic calculations (nuclear reactors, heat exchanges, steam generators). Moskow, Energoatomizdat, 1990.
[27] GALIN N.M., KIRILLOV P.L. Heat- and Mass Transfer (In Nuclear Power Engineering). Moskow, Energoatomizdat, 1987.
[28] CHANG S.H., LEE Y.-B. A new critical heat flux model for liquid metals under low heat flux-low flow conditions // Nuclear Engineering and Design, 1994, v.118, ¹ 3, p. 487-498.
[29] KOTTOWSKI H.M., SAVATTERI C. Fundamentals of liquid metal boiling thermohydraulics // Nuclear Engineering and Design, 1984, v.82, ¹ 3, p.281-304.
[30] KAISER A., PEPPLER W. Type of flow, pressure drop, and critical heat flux of a two-phase sodium flow // Nuclear Engineering and Desing, 1974, v.30, ¹ 3, p.305 – 315.
[31] MANTLIK F.,ZHUKOV A.V., SOROKIN A.P., et al. Survey of Thermophysical Investigations of Fuel Element Assemblies with Partially Plugged Flow Area // Report LJJV 6057-T. Prague: DSTI INR (REZ), 1982.
[32] VOTANI M., HAGA K. Experimental Investigation of Sodium Boiling in Partially Blocked Fuel Subassemblies // Nuclear Engineering and Design , 1984, v.82, ¹ 2-3, p. 319-328.
[33] HUBER F., PEPPIER W., Boiling and Dryout behind Local Blockages in Sodium Cooled Rod Bundles // Nuclear Engineering and Design, 1984, v.82, ¹ 2-3, p. 341-363.
[34] HAGA K., YAMAGUCHI K. Investigation of Effect of Gas Release on Coolability of Locally Blocked LMFBR Fuel Subassemblies // Journal of Nuclear Science and Technology, 1985, v.28, ¹ 8, p. 619-636.

DEVELOPMENT OF GRIF-SM — THE CODE FOR ANALYSIS OF BEYOND DESIGN BASIS ACCIDENTS IN SODIUM COOLED REACTORS

I. CHVETSOV, I. KOUZNETSOV, A. VOLKOV
State Scientific Center of Russian Federation,
Institute of Physics and Power Engineering,
Obninsk, Kaluga Region, Russian Federation

XA0055047

Abstract.

GRIF-SM code was developed at the IPPE fast reactor department in 1992 for the analysis of transients in sodium cooled fast reactors under severe accident conditions. This code provides solution of transient hydrodynamics and heat transfer equations taking into account possibility of coolant boiling, fuel and steel melting, reactor kinetics and reactivity feedback due to variations of the core components temperature, density and dimensions. As a result of calculation, transient distribution of the coolant velocity and density was determined as well as temperatures of the fuel pins, reactor core and primary circuit as a whole.

Development of the code during further 6 years period was aimed at the modification of the models describing thermal hydraulic characteristics of the reactor, and in particular in detailed description of the sodium boiling process. The GRIF-SM code was carefully validated against FZK experimental data on steady state sodium boiling in the electrically heated tube; transient sodium boiling in the 7-pin bundle; transient sodium boiling in the 37-pin bundle under flow redaction simulating ULOF accident. To show the code capabilities some results of code application for beyond design basis accident analysis on BN-800- type reactor are presented.

1. INTRODUCTION.

In order to evaluate consequences of severe beyond design accidents resulting in the sodium boiling in the core, several codes, such as SAS-4A, FRAX-5 and PHYSYRAC were developed in the late 70-ies - early 80-ies. These codes were mainly applied for the analysis of two beyond design accidents, namely ULOF and UTOP accidents. Inevitable core disrupture in these accidents was assumed for these codes development, and the main task was to analyze dynamics of the core heating, sodium boiling onset, fuel elements melting and molten mass relocation processes in order to predict possible core damage. Indeed, for the designs well-known at that time it was impossible to avoid fuel element melting in severe beyond design accidents, in particular, in the ULOF accident, since considerable positive component of the sodium void reactivity effect was caused by the core designs applied.

GRIF-SM code was developed in Russia approximately ten years later for the similar application [1]. By this time certain changes occurred in the understanding of the reactor safety problem. Self-protection concept was pushed into the foreground, according to which reactor design should provide decay heat removal by the passive means and assure core integrity even in severe accidents. Within the framework of this concept new BN-800 reactor core design was proposed with the sodium plenum replacing upper radial blanket. Owing to this measure it became possible to achieve near zero integral value of the sodium void reactivity effect. Moreover, since the sodium boiling onset in case of accident would occur on the upper core boundary, where the sodium void reactivity effect value is negative, this gave grounds for the hope for appropriate heat removal from the core under sodium boiling conditions avoiding fast fuel elements melting.

Taking into account the above considerations, during the development of GRIF-SM code attention was paid rather to the detailed description of the reactor thermal hydraulics on the stage of sodium boiling in order to prove the possibility to prevent fuel elements melting, than to the analysis of consequences of the core disrupture and molten fuel and steel

relocation. This change of priorities was the main point determining initial structure of GRIF-SM code and the trends of its further modification.

Therefore the key features of GRIF-SM code caused by the specified task are as follows:

- trend towards maximum possible degree of detail in the modeling of space characteristics of sodium boiling in the core in order to improve accuracy of sodium void reactivity effect evaluation;
- modeling of space distribution of thermal hydraulics parameters not only in the core but also in the reactor as a whole. This is required, first, in order to take into account core channels coupling and, second, for more correct evaluation of the coolant flow rate in the primary circuit in case of vapor release into the upper reactor plenum.

2. GRIF-SM CODE DISCRIPTION

Code consists of several modules. The block diagram of the program is shown on fig.1. In a block "primary sodium thermal hydraulics" space distributions of the following characteristics of sodium vapour flow are calculated: a velocity, pressure, enthalpy,

GRIF-SM code structure

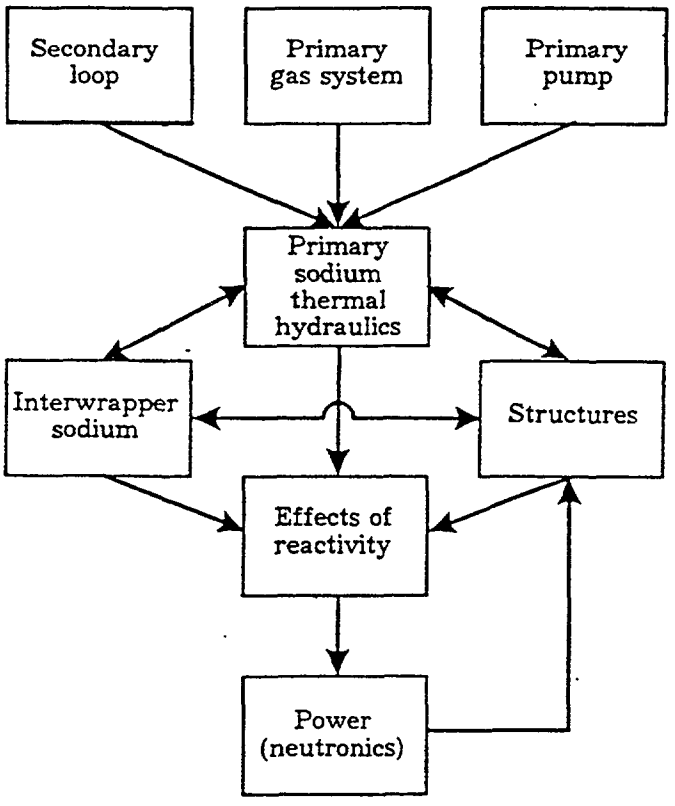

Fig.1

temperature, density and vapour quality for each step on a time. The system of equations of coolant thermal hydraulics includes:

continuity equation

$$\frac{\partial \rho}{\partial \tau} + \left(\vec{\nabla}\varepsilon\bar{u}\right) = G$$

equation of motion

$$\frac{\partial \bar{u}}{\partial \tau} + \frac{1}{\varepsilon}\left(\vec{\nabla}\varepsilon\frac{\hat{\psi}}{\rho}\bar{u}\right)\bar{u} = -\vec{\nabla}P - \hat{\Lambda}\bar{u} + \left(\vec{\nabla}\nu\vec{\nabla}\right)\bar{u} + \vec{F}$$

enthalpy equation

$$\varepsilon\frac{\partial \rho E}{\partial \tau} + \left(\vec{\nabla}\varepsilon\bar{u}\right)\frac{\psi}{\rho}E = \left(\vec{\nabla}\hat{\lambda}\vec{\nabla}\right)T + \varepsilon\left(\frac{\partial \rho}{\partial \tau} + \tilde{\psi}\left(\frac{\bar{u}}{\rho}\vec{\nabla}\right)P\right) + q_v$$

equations of state

$$\rho = \rho(P, E) \quad ; \quad T = T(P, E)$$

where main required variables are: u-mass velocity; P-pressure; ρ-density; E-enthalpy and coefficients: ψ,ψ,ψ- function of the slip ratio and sodium thermal hydraulic properties; ε-porosity; Λ-friction coefficient; λ-thermal conductivity; ν-viscosity.

The sodium boiling is described by slip-model of a two phase flow. The factors of friction and slip ratio for two phase flow are defined on Loccart-Martinelly correlation. There are taken into account in GRIF-SM code then main kinds of heat transfer in one and two phase flow: forced liquid and vapour sodium flow; boiling of under heated sodium; bubble boiling; film boiling; dryout (in case, when the size of a heat flux exceeds critical significance) and film condensation.

Dynamics of distribution of temperature in pins, control rods, subassembly wrappers, grids and other primary circuit elements, essentially influencing on a course of development of accident, is calculated in a block a "Structure".

The core is submitted by set of parallel channels. For each channel is calculated 2D distribution of temperature in a fuel and cladding for one pin in the channel. After the beginnings of fuel or clad melting the transient position of molten cavity is calculated in view of latent heat of melting. Model of thermal destruction of fuel pin is realized.

Two-dimensional temperature distribution is also calculated for SA wrapper as the distribution of temperature on thickness of a wrapper is important for the correct simulation of sodium vapour condensation in the top part of core subassemblies where heat release is small. Inter-wrapper sodium thermal hydraulics is simulated on base 1D model in a separate module.

The intermediate heat exchanger model is a part of the "Secondary loop" module. It includes equation of thermal conductivity for IXH tubes and 1D energy equation for the secondary sodium. The temperature and flow rate of secondary sodium on the IXH entrance versus time are specified.

The model of a primary gas system is intended for determination of changes in time of pressure in the reactor gas cavity, which is necessary for a module "Primary sodium thermal hydraulics" as a boundary condition. The primary gas system consists of several cavities, connected with one another, which can be partially filled in liquid and vapour sodium and inert gas. At severe accident sodium vapour can get in a gas system. The opportunity of its condensation at contact to "cold" designs is also considered.

The reactor power time dependence is calculated within the frame of "point kinetics" model with 6 groups of delayed neutrons.

During the reactivity calculations the following thermal effects are taken into account: sodium density reduction due to thermal expansion and boiling; axial and radial expansion of a core as a whole; fuel and clad material density changing; expansion of control rods and its drives; Doppler effect.

3. TESTING OF GRIF-SM CODE USING EXPERIMENTAL DATA

Results of testing of the code on KfK experimental data on sodium boiling in pipes, 7-pin and 37- pin bundles will be below also indicated.

3.1. Steady state sodium boiling in electrically heated pipe.

In this case in each of experiments the position of boiling point on height and pressure drop in the tubular test section were measured for different sodium velocity values varied in the range 0.5-5 m/s. The test tube had inner diameter 0.0066 m and with direct electrical heating, thermal power up to 300 W/cm^2 was available. As it follows from Fig.3 and Fig.4, in the total investigated range of coolant velocities on both parameters good agreement with experiment is observed.

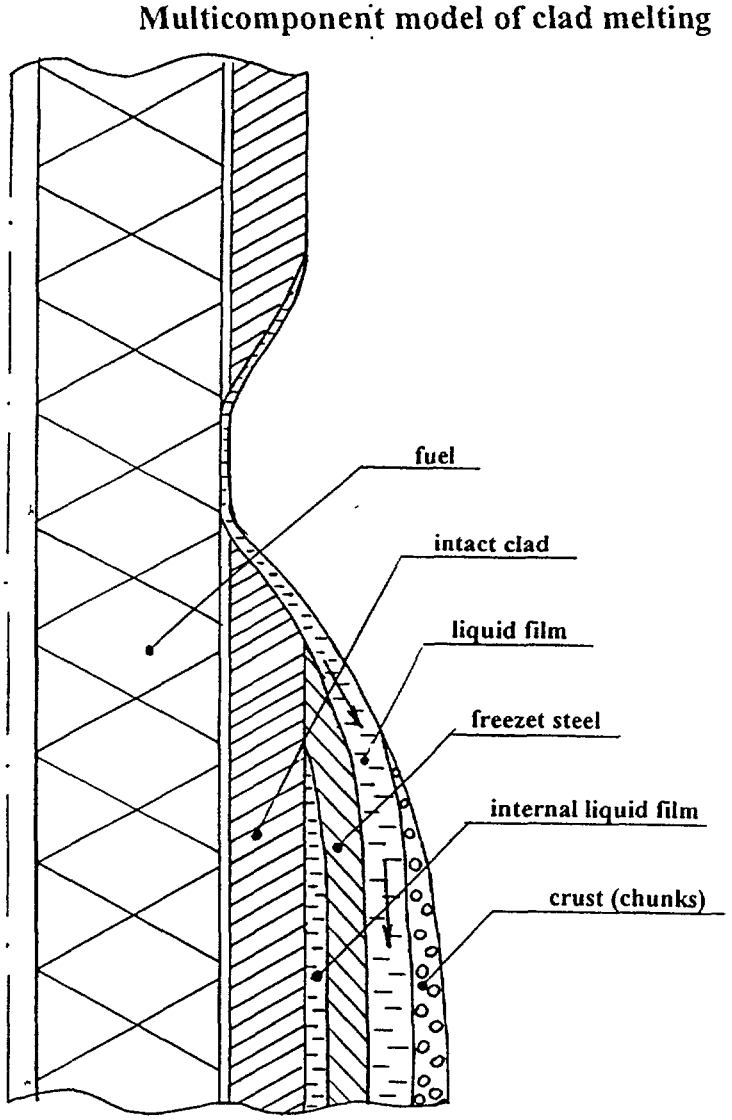

Fig 2

Boiling point position as a function of sodium velocity at the experimental channel inlet.

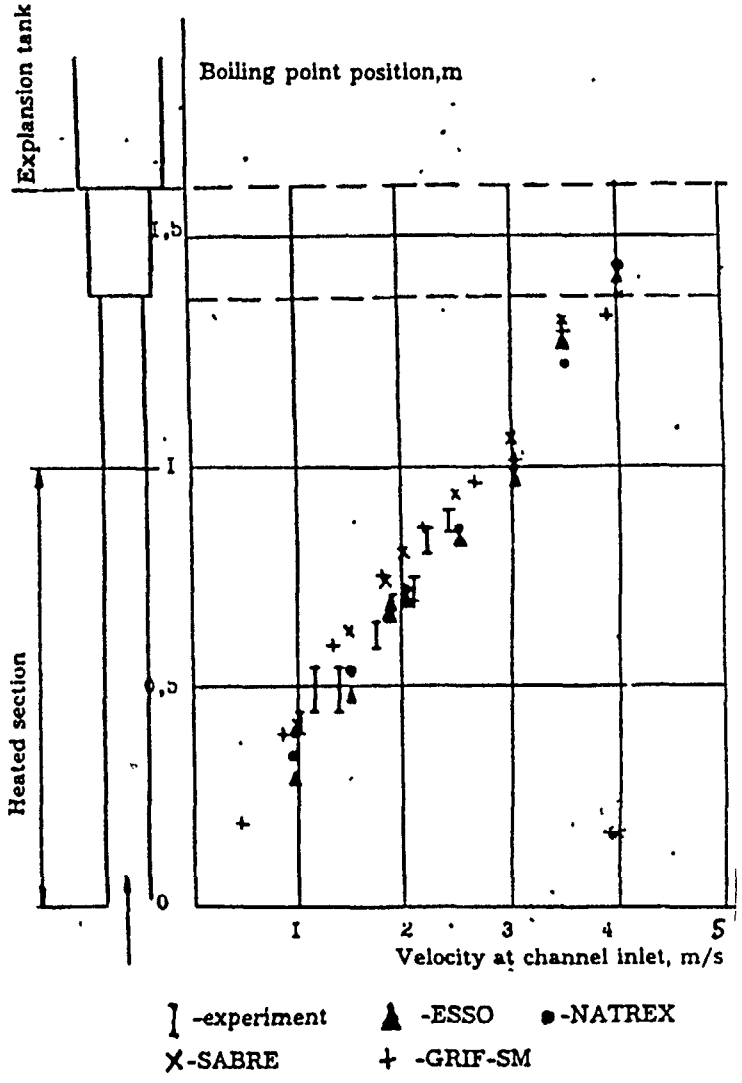

Fig.3.

Pressure drop between the points P11 and P14 as a function of sodium velocity at the channel inlet.

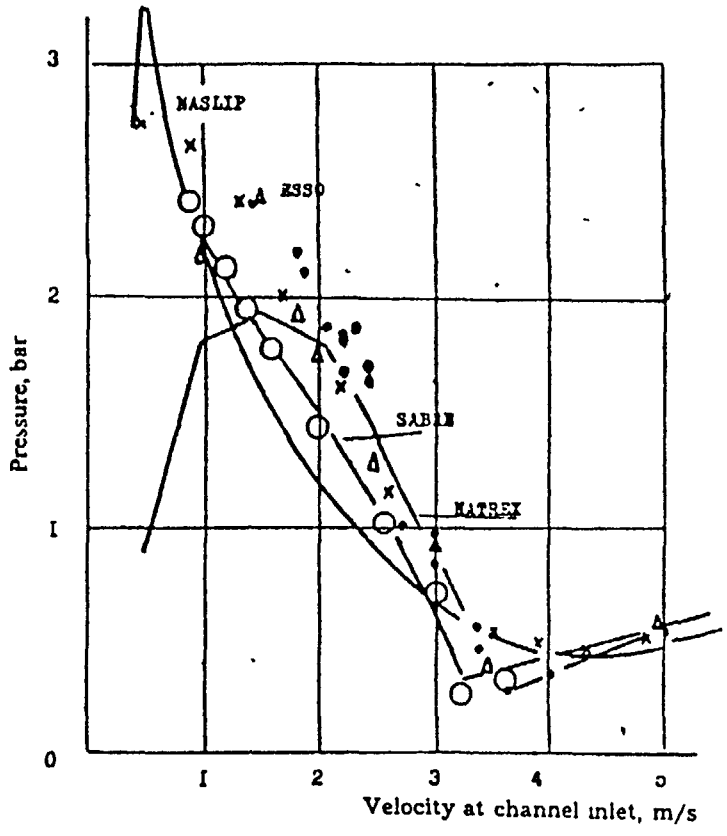

Fig.4.

3.2. Dynamics of sodium boiling in 7-rod bundle.

The testing section was 7-pin assembly, put in a hexagonal wrapper (Fig. 5). Heated part of the bundle had a length of 0.6 m. Heaters power is constant and equal to 114 kW. During experiment the sodium flow rate was linearly reduced from 100 % to 30 % for 10 seconds and then remained constant (Fig. 6). Sodium temperature and volumetric vapour quality in various cross-sections on height were measured. In accordance with flow rate reduction sodium temperature at the outlet a heated part of the bundle increases (Fig.7). The boiling in experiment begins in 9 seconds after beginning of transient in the unheated part of bundle. In accordance with GRIF-SM calculations the boiling begins in the same point, but with small delay near 0.15s. The process of moving of the lower boundary of vapour bubble is equally well calculated by both codes, as to the upper boundary, as it is visible from Fig.8. GRIF-SM gives a little overestimated velocity of its movement in comparison with experiment, while COMMIX-2 underestimates it.

3.3. Modelling of ULOF accident on 37-rod assembly.

Main geometrical characteristics of test assembly were close to those of the SNR-300 reactor core subassembly (Fig.9). The pin simulators of 0.006 m diameter were located in hexagonal wrapper with a pitch of 0.0079 m. The real distribution of power rating over height

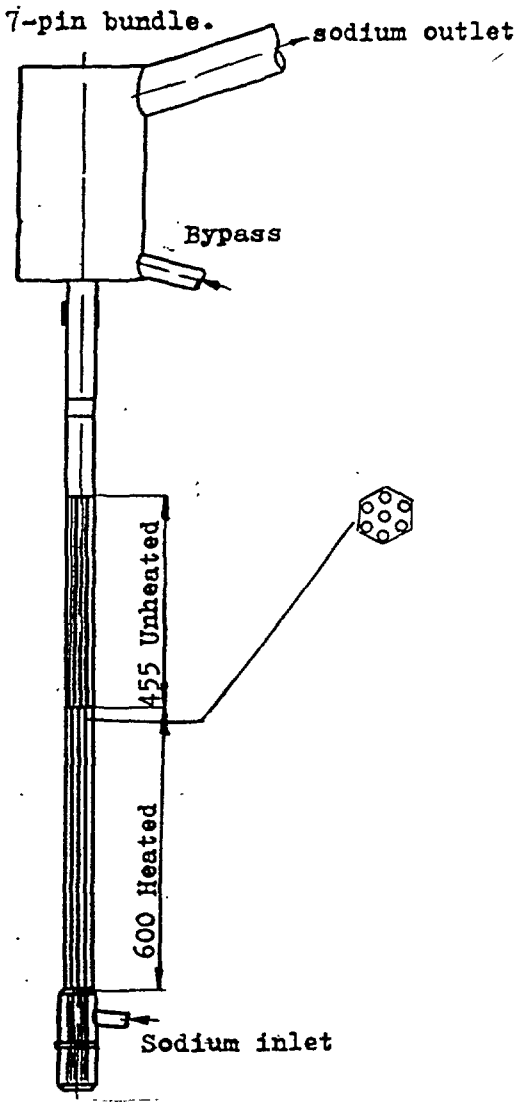

Fig.5.

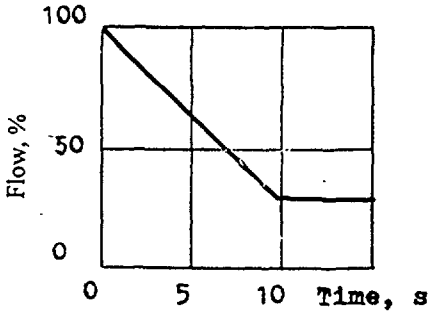

Fig.6.

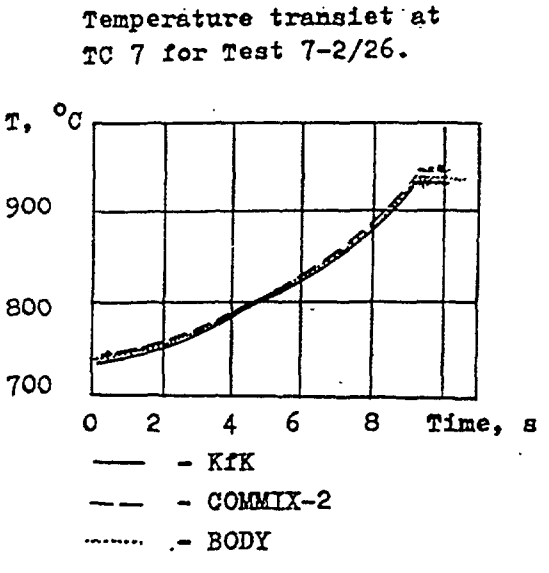

Fig.7.

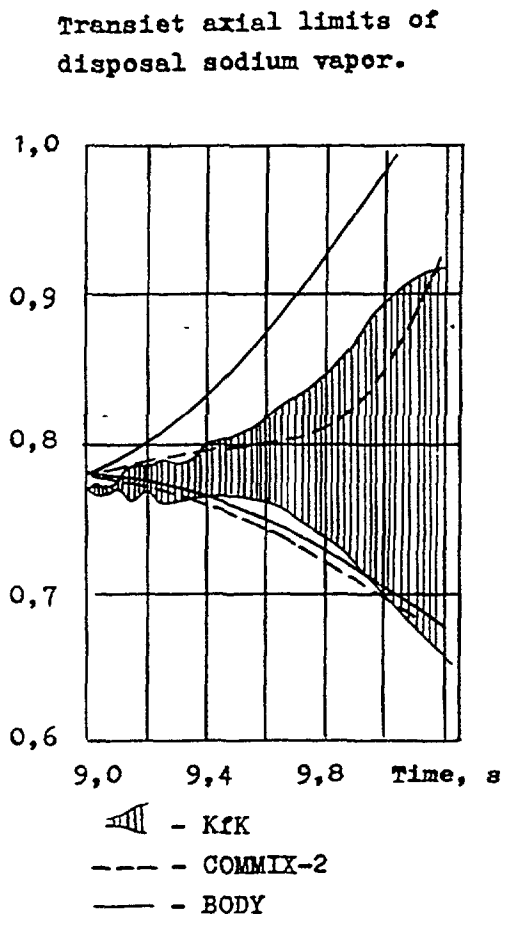

Fig.8.

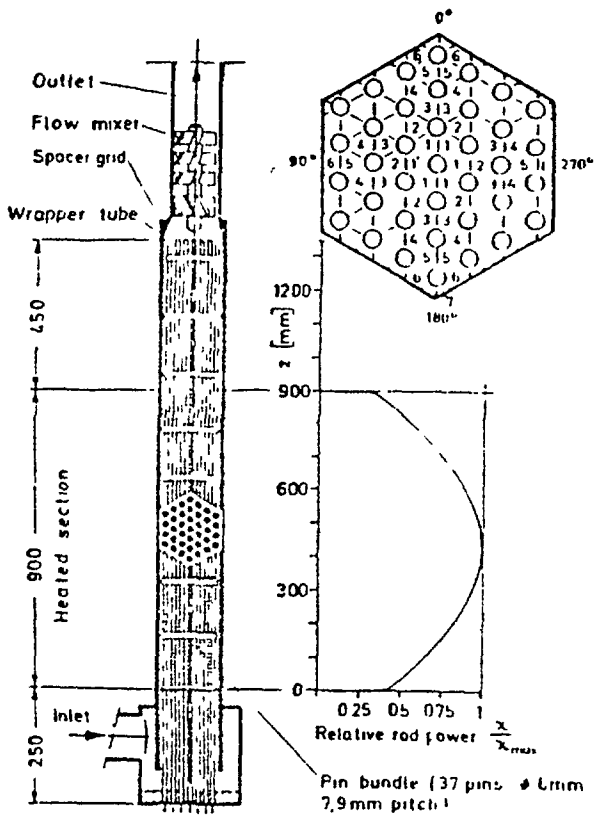

Schematic diagram of the KNS 37 pin bundle

Fig.9.

was taken into account. Maximum linear power of one element was 320 W/cm. The experiment consisted of decrease of the coolant flow rate through assembly according to the law, close to hyperbolic. The power remained constant up to the moment, when there was threat of thermal destruction of simulators. During experiment, pressure and sodium flow rate in various elements of a rig (Fig.10), as well as temperature and vapour quality in various points of assembly were measured. The obtained data permit to look after the movement of fronts of boiling either at the height of assembly, or at its cross section.

Experimental results were calculated using 2D version of the GRIF-SM code. The whole assembly was simulated in calculations, including inlet device, rod bundle and outlet flow mixer. The results of comparison of GRIF-SM calculations with experimental data are given in Fig.11-13.

There is a good agreement between calculated inlet flow rate and experimental results (Fig.11), but the flow reverse occurs approximately tenth of second later in calculations. Another difference is that GRIF-SM calculation gives the oscillations of flow rate after the boiling onset. As it follows from Fig.12 and Fig13, GRIF-SM simulates in appropriate way the vapour generation and boiling fronts spreading till the moment of power termination. The behaviour after power termination is similar to that of the peripheral channels but cooling of sodium vapour in the top part of central channels seems to be underestimated in the calculations.

3.4. ULOF accident simulation on BN-800 type reactor.

It ought to consider as a verification activity the participation of GRIF-SM code in comparative calculations of ULOF-accident on BN-800-type reactor in which also the codes

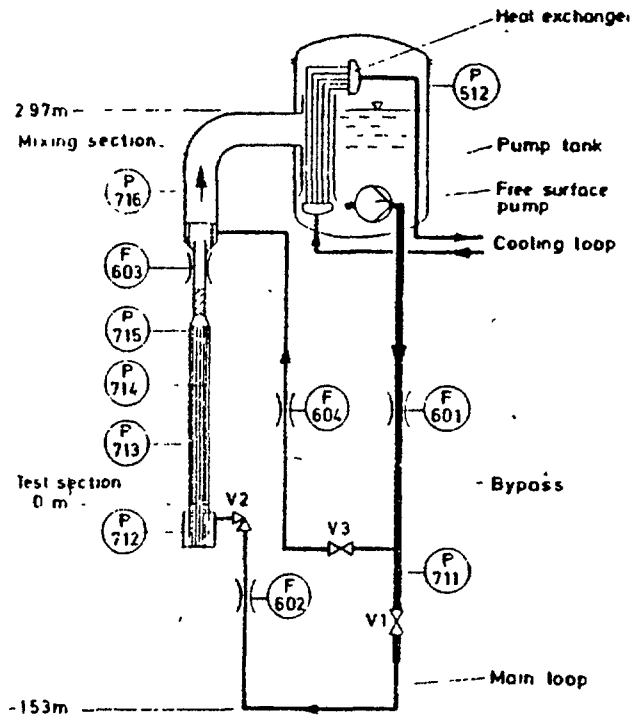

Simplified flow sheet of the KNS sodium boiling loop

Fig.10.

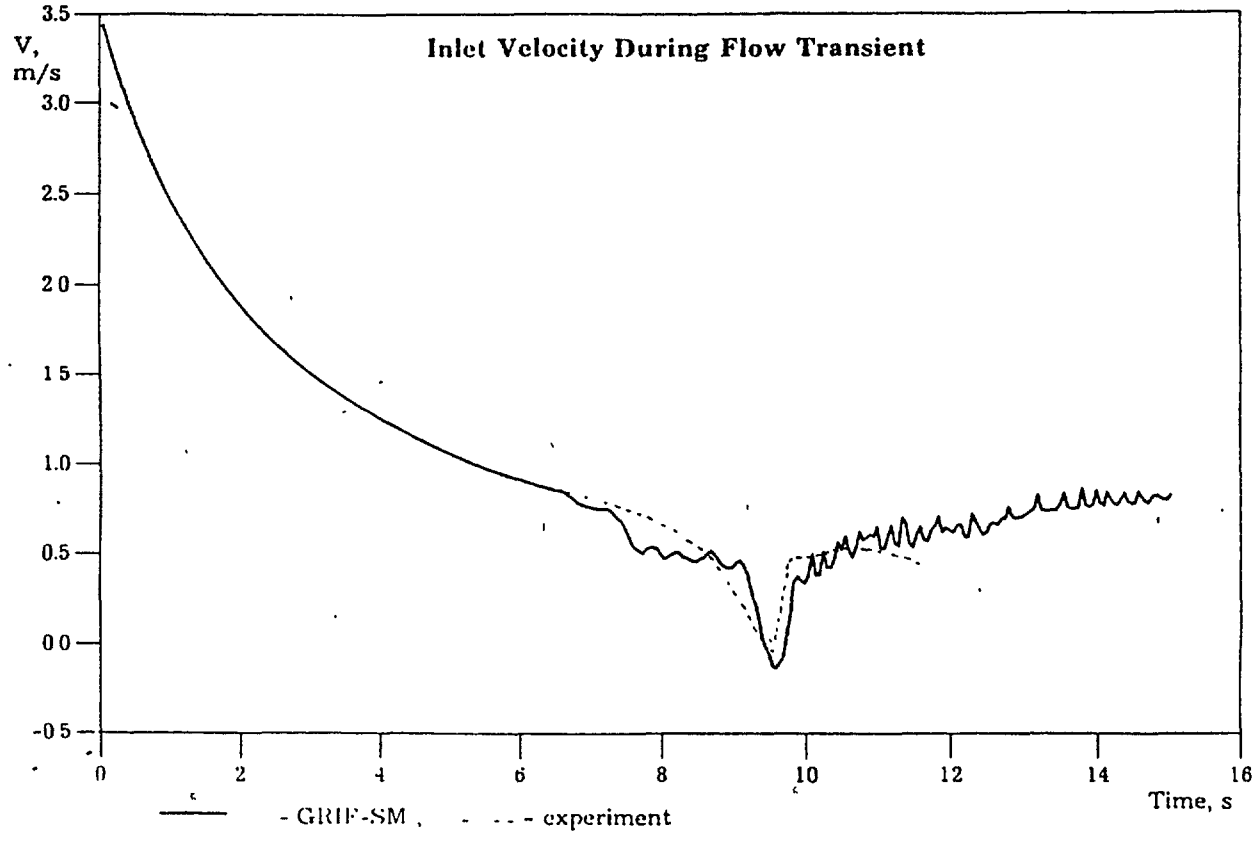

Fig.11.

Vapor volumes as a function of time

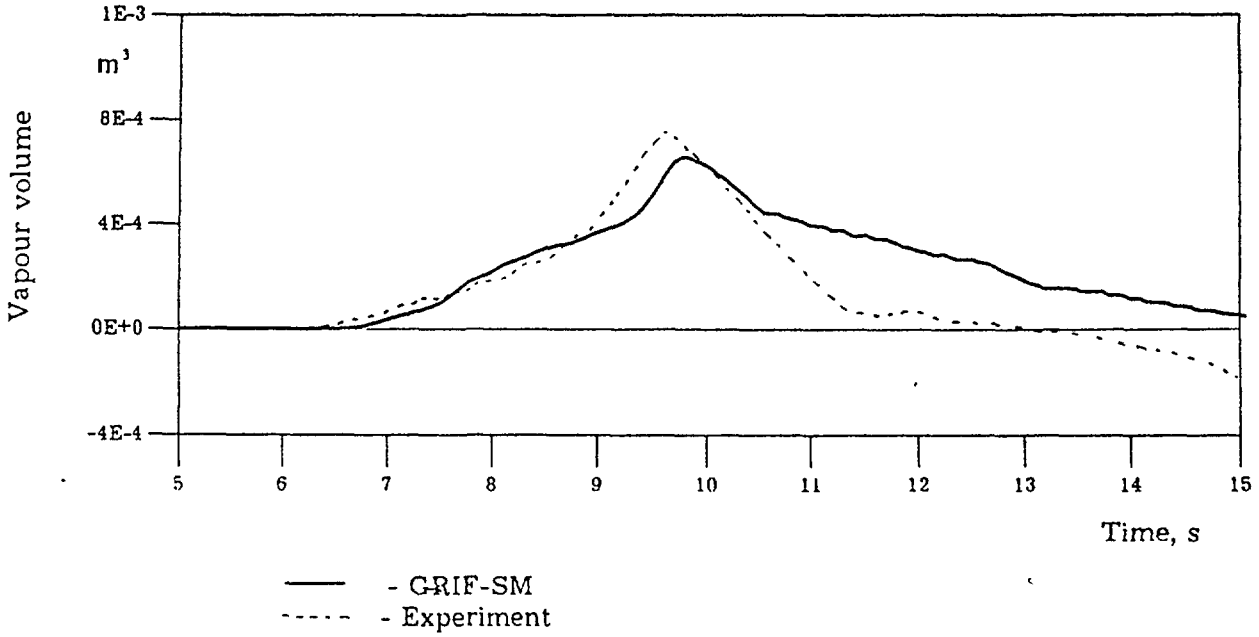

Fig.12.

Axial development of the boiling boundary

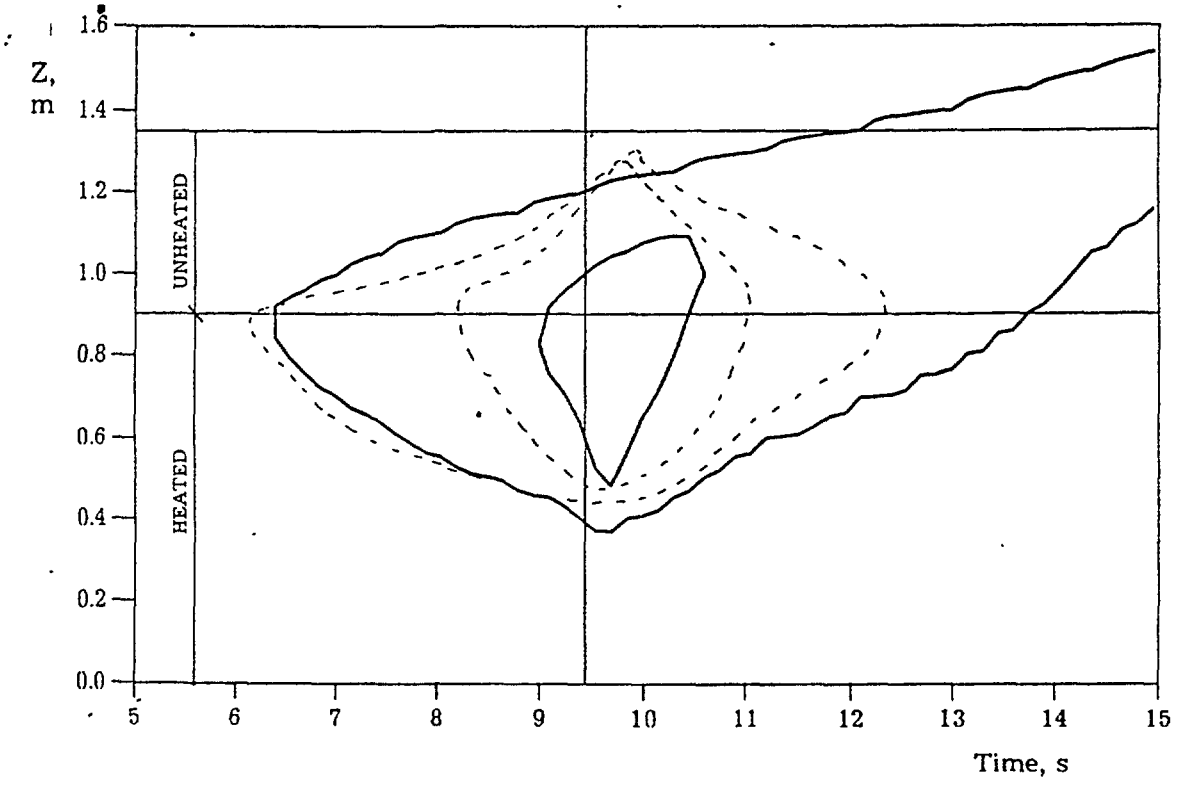

Fig.18 ——— - GRIF-SM
------ - Experiment

Fig.13.

SAS-4 A (Germany, FZK), FRAX-5 (Great Britain, AEA) and PHYSIRAC (France, CEA) participated. Comparison has shown, that all of them have given rather similar results.

4. TRENDS OF THE CODE MODIFICATION

Sodium worth in fast reactors strongly depends on space coordinates, and zone of positive sodium void reactivity effect values is kept in the central part of the core. Therefore it is rather important to provide as high as possible accuracy in description of sodium density distribution over the core radius. For this purpose, the number of channels consisting the core has been increased to 30. This makes significant improvement of the calculation accuracy.

The experiments have shown, that in fast reactors considerable heterogeneity of the SA radial temperature profile can occur. Usually, owing to the heat transfer to the sodium flowing outside SA, the coolant temperature in the peripheral channels of the SA is lower than that in the central channels. As a result of this, sodium boiling would not start at once over the whole SA cross section area, but first in the SA centre with its further gradual propagation to the periphery. In order to simulate both general (over the reactor core) and local (over SA) distribution of thermal hydraulic parameters a new version of GRIF-SM code was developed which was called BOS (Boiling Subassembly) [2].

In the typical fast reactor ~ 10% of the core flow cross section relates to the inter-wrapper sodium. Its temperature and hence its density during the transient may be significantly different from those of sodium flowing inside fuel subassemblies.

In order to make proper evaluation of distribution of the inter-wrapper sodium temperatures the following points should be taken into account:

(1) possibility of lateral flow of inter-wrapper sodium in addition to the axial flow;
(2) possibility of its boiling onset in sufficiently long duration processes.

This was made for the modified version of the code, i.e. when the inter-wrapper sodium thermal hydraulics is described within the framework of two-dimensional two-phase model.

TABLE I. DEVELOPMENT HISTORY OF GRIF-SM CODE

Module	Initial version	Updated versions
1. Primary sodium thermal hydraulics.	4 channel presentation of the core.	30 channel presentation of the core. 2D-simulation of velocity and temperature distribution inside subassembly (BOS code).
2. Inter-wrapper sodium	1D and 1 phase thermal hydraulic model.	2D and 2 phase thermal hydraulic model.
3. Structures.	The set of 1D-3D models for temperature calculations in fuel pins, SA wrappers. Simplified 'thermal' model of pin melting.	Multicomponent model of pin melting and molten steel relocation (CANDLE module).
4. Neutronics.	"Point kinetics" with 6 group of delayed neutrons.	3D space time kinetics (GVA-code-{GRIF-SM+VOLNA}).

If the assumptions concerning accident scenario are too conservative, conditions for the sodium burn-out appear resulting in the fuel element melting which occurs very soon. In order to make analysis of such accidents within the framework of the modified code version, CANDLE code module has been developed [3], which is capable of evaluating molten steel relocation within the core.

The main characteristics of the model used as a basis for CANDLE module are as follows:

(1) 5-component simulation of pin clad melting:
   - intact clad,
   - liquid steel film,
   - frozen steel,
   - crust,
   - internal liquid film.
(2) 1-D thermal hydraulics models for every component.
(3) Components a), c), e), are fixed, components b) and d) are moving together.
(4) Molten fuel is fixed.
(5) Intact fuel stubs are fixed.

Relative location of the model components is shown in Fig.2.

Another trend of the code modification concerns development of algorithms of joint solution of thermal hydraulics and space neutronic kinetics equations. Within the framework of point kinetics, components of the core reactivity are usually represented as algebraic functions (which are often linear) of material concentration values, coefficients in these relationships being considered constant during accident. Actually, if significant disturbance of the initial configuration takes place, i.e. vapor bubbles are formed and steel and fuel melt is relocated within the core, then material worth become strongly dependent on changing configuration. This effect is necessary to take into account when determining either amplitude or form factors of the power density values. Code package called GVA implements joint space and time analysis of neutronic and thermal hydraulic reactor characteristics. This package is actually a combination of two codes, namely GRIF-SM and VOLNA, the latter being neutronic code capable of solving equations of space and time neutron transfer using quasi-stationary method [4].

5. APPLICATIONS

Below results of analysis of some beyond design accidents are given with reference to the BN-800 reactor having near zero value of integral sodium void reactivity effect. There are three radial enrichment zones in the reactor core, and the upper axial blanket is replaced by the sodium plenum.

Calculation area simulating the reactor is shown in Fig.14. The core is represented by 10 parallel annular channels, each of them being divided into three subchannels having different fuel burnup values.

5.1. ULOF accident.

After the main pumps are shut down, sodium flow in the primary and secondary circuits decreases according to the near hyperbolic law. Core sodium and fuel element cladding temperatures increase, whereas the fuel temperature decreases because of the reactor power reduction. As a result of this, negative contribution is given to the reactivity value by the sodium density effect, radial core expansion and control rod drive bars thermal expansion (Fig. 15). Doppler effect and axial core expansion give positive components of the reactivity. The total temperature reactivity effect remains negative, and the reactor power is decreased.

However, on the 38th second sodium boiling starts in the 5/1-st channel of the medium enrichment zone.

Calculational region simulating BN-800 type reactor geometry

k															
29	25	25	25	25	25	25	25	25	25	25	25	25	28	25	25
28	25	25	25	25	25	25	25	25	25	25	25	25	28	28	37
27	25	25	25	25	51	51	51	51	51	51	51	51	28	28	37
26	25	25	25	25	51	51	51	51	51	51	51	51	28	28	30
25	25	25	25	25	51	51	51	51	51	51	51	51	27	27	30
24	51	51	51	51	51	51	51	51	51	51	51	51	27	27	30
23	51	51	51	51	51	51	51	51	51	51	51	51	27	27	30
22	33	34	35	36	24	24	24	24	24	24	24	24	27	27	30
21	45	46	47	48	49	49	49	49	49	49	52	69	27	27	30
20	40	41	42	43	44	44	44	44	44	44	52	68	27	27	30
19	40	41	42	43	44	44	44	44	44	44	52	68	27	27	30
18	40	41	42	43	44	44	44	44	44	44	52	68	27	27	30
17	18	19	20	21	22	22	22	22	22	22	52	32	27	27	30
16	13	14	15	16	17	17	17	23	23	23	52	39	27	27	30
15	13	14	15	16	17	17	17	23	23	23	52	39	27	27	30
14	13	14	15	16	17	17	17	23	23	23	52	39	27	27	30
13	13	14	15	16	17	17	17	23	23	23	52	39	27	27	30
12	13	14	15	16	17	17	17	23	23	23	52	39	27	27	30
11	13	14	15	16	17	17	17	23	23	23	52	39	27	27	30
10	13	14	15	16	17	17	17	23	23	23	52	39	27	27	30
9	13	14	15	16	17	17	17	23	23	23	52	39	27	27	30
8	13	14	15	16	17	17	17	23	23	23	52	39	27	27	30
7	13	14	15	16	17	17	17	23	23	23	52	39	27	27	30
6	13	14	15	16	17	17	17	23	23	23	52	39	27	27	30
5	13	14	15	16	17	17	17	23	23	23	52	39	27	27	30
4	53	54	55	56	57	57	57	57	57	57	52	57	27	27	30
3	63	64	65	66	67	67	67	67	67	67	67	67	27	27	30
2	2	3	4	5	6	7	8	9	10	11	12	31	27	27	29
1	1	1	1	1	1	1	1	1	1	1	1	1	26	26	29
	1	2	3	4	5	6	7	8	9	10	11	12	13	14	15 i

1 -lower inlet header;
2,3,4,5,6,7,8,9,10,11,12,31 -subassembly inlets
13,14,15,16 -low enrichment zone;
17 -middle enrichment zone;
23 -high enrichment zone;
18,19,20,21,22,32 -pin tail zone;
24,33,34,35,36 -subassembly heads and outlet windows;
45,46,47,48,49 -upper axial shield;
40,41,42,43,44 -sodium layer;
53,54,55,56,57 -bottom axial blanket;
63,64,65,66,67 -pin gas volumes;
52 -radial blanket;
39,68,69 -inner radial shield and storage;
51 -upper outlet plenum;
26 -entrance region
29 -pump and downcomer;
27 -intermediate radial shield;
28 -rod shield;
30, 37 -intermediate heat exchanger;
25 -upper column and other impermeable elements;

Thick solid lines - impermeable boundaries
Double think solid lines - the boundaries between zones with different enrichment

i-radial number of unit
k-axial number of unit

Fig.14.

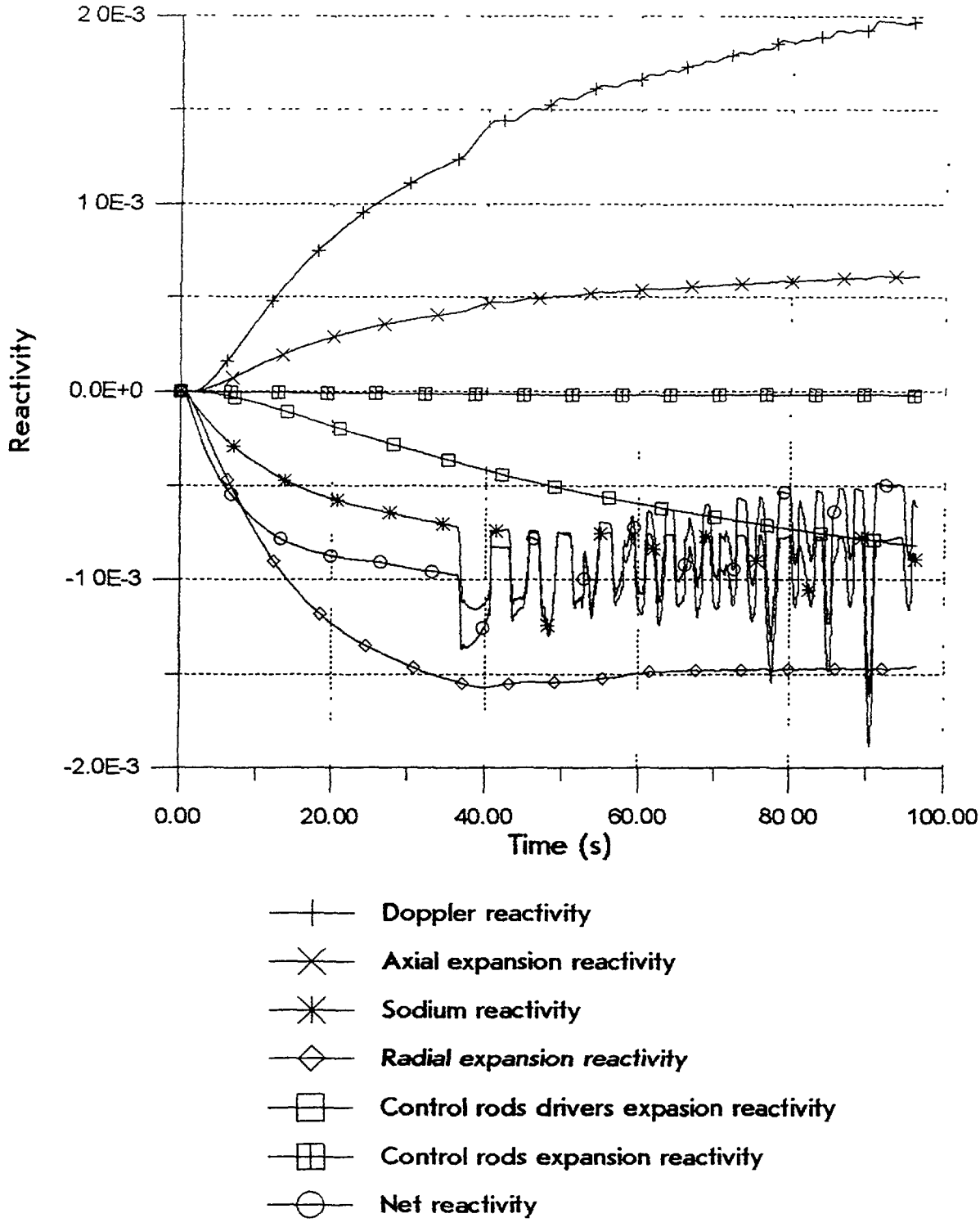

Fig.15. **Reactivity versus time.**

The sodium-vapour mixture is spreading into the sodium volume and the upper axial blanket causing negative effects of reactivity, power decrease and cessation of boiling. In the process an increase of power and sodium boiling take place again. And again sodium vapour movement into the sodium volume and the upper axial blanket results in the negative effects of reactivity, power decrease and cessation of boiling (Fig. 18). In the reactor, self-sustained oscillations of power set up with periodic coolant boiling. Reactor power in this case is oscillating and gradually decreases (Fig. 16).

There are oscillations of the outlet sodium temperature, which does not exceed saturation temperature. Slight oscillations of maximum fuel temperature also occur (Fig. 17), this temperature approaching sodium boiling point. Thus, neither fuel nor cladding melting takes place.

5.2. ULOF accident analysis taking into account parameters distribution over the subassembly cross section.

ULOF accident version with the deliberately increased severity has been considered with reference to the BN-800 reactor. In this analysis, two negative components of temperature reactivity effect were neglected, namely core radial expansion and control rod drive bar expansion components. The calculation was made using GRIF-SM code initial version and BOS code version.

The difference between these methods is more significant after the boiling start (Fig.19). Owing to the non-uniformity of SA temperature profile boiling starts earlier, namely: 13.18 s (BOS) and 17.66 s (GRIF-SM). As it was observed before, sodium boiling is initiated at the core outlet in the SA central area of the "hottest" channel 5/1. Then the boiling starts successively in 1/1, 2/1, 3/1, 4/1, 7/1 and 5/2 channels. Along with the increase of the number of boiling channels vapour bubble growth in the SA is observed. Fig.20 shows spatial distribution of mass velocity for all channels where the boiling has started by this time. It is obvious that on this stage the boiling occurs only in the upper part of the most subassemblies (where the sodium void reactivity effect is negative), However the height of the boiling area in 5/1 channel is 42% of the core height, and hence the boiling front has penetrated into the area of positive sodium void reactivity effect.

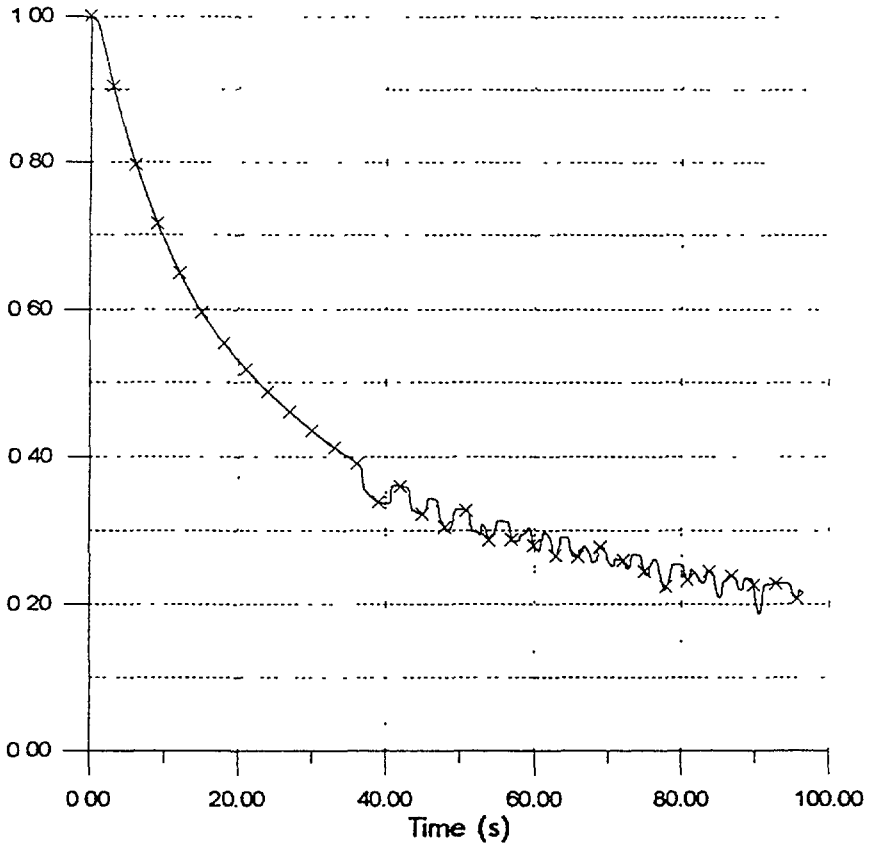

Fig.16. **Relative reactor power.**

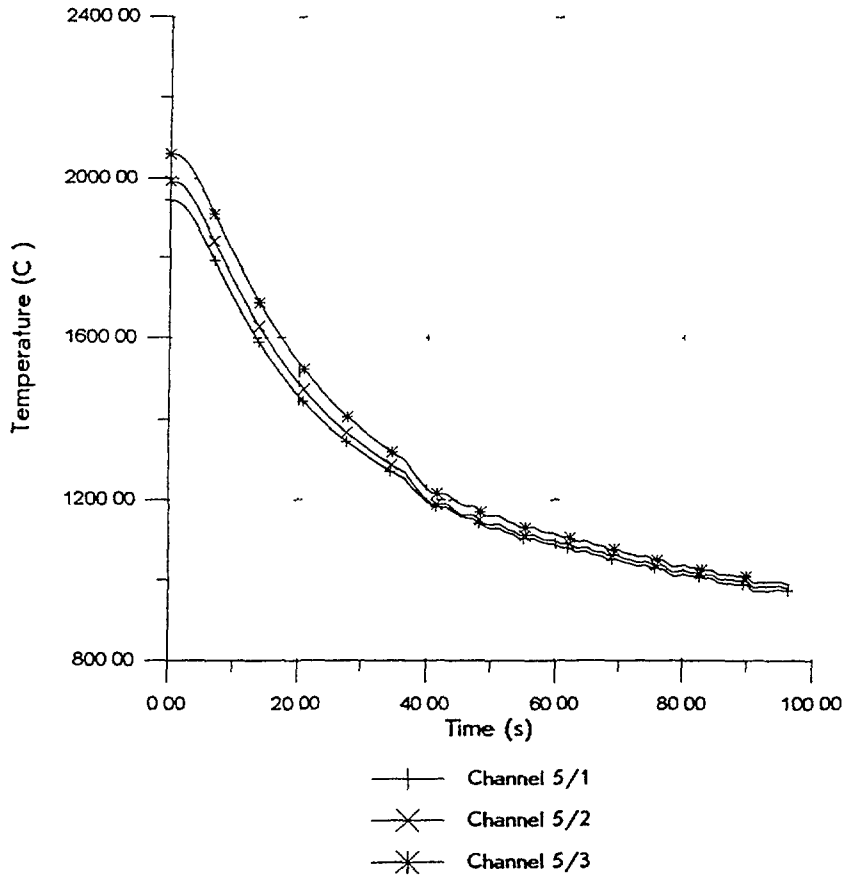

Fig 17 Fuel inner surface temperature in the central cross section of the core.

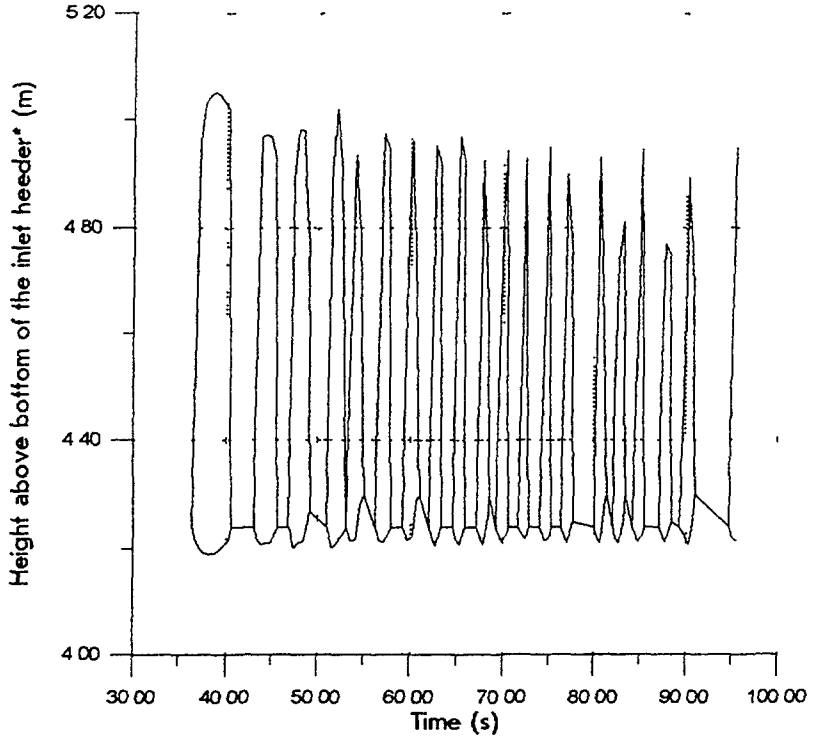

Fig 18 . Channel 5: Boiling front.

*) The height of the fissile zone is 4.24 m.

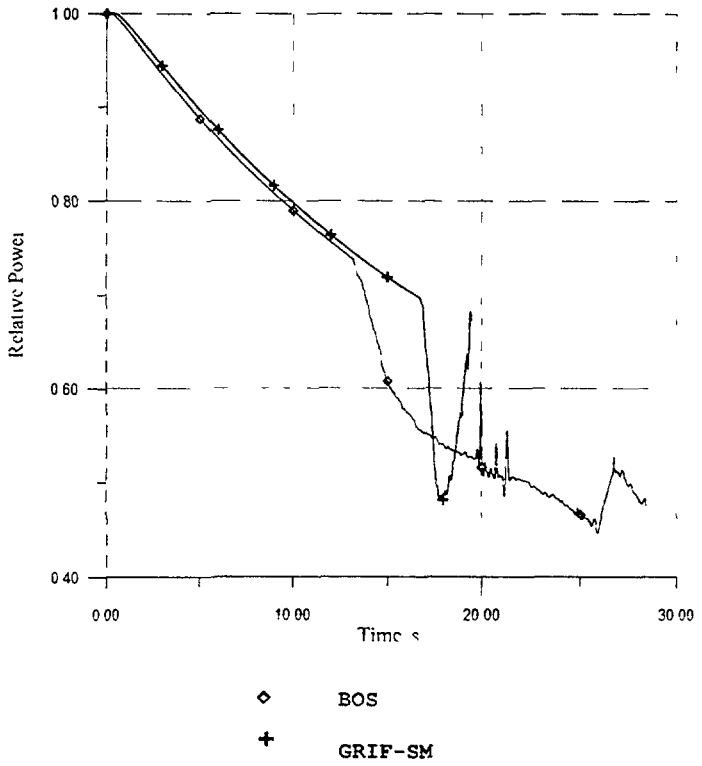

Fig.19. ULOF accident on BN-800 like reactor
Radial effect is neglected

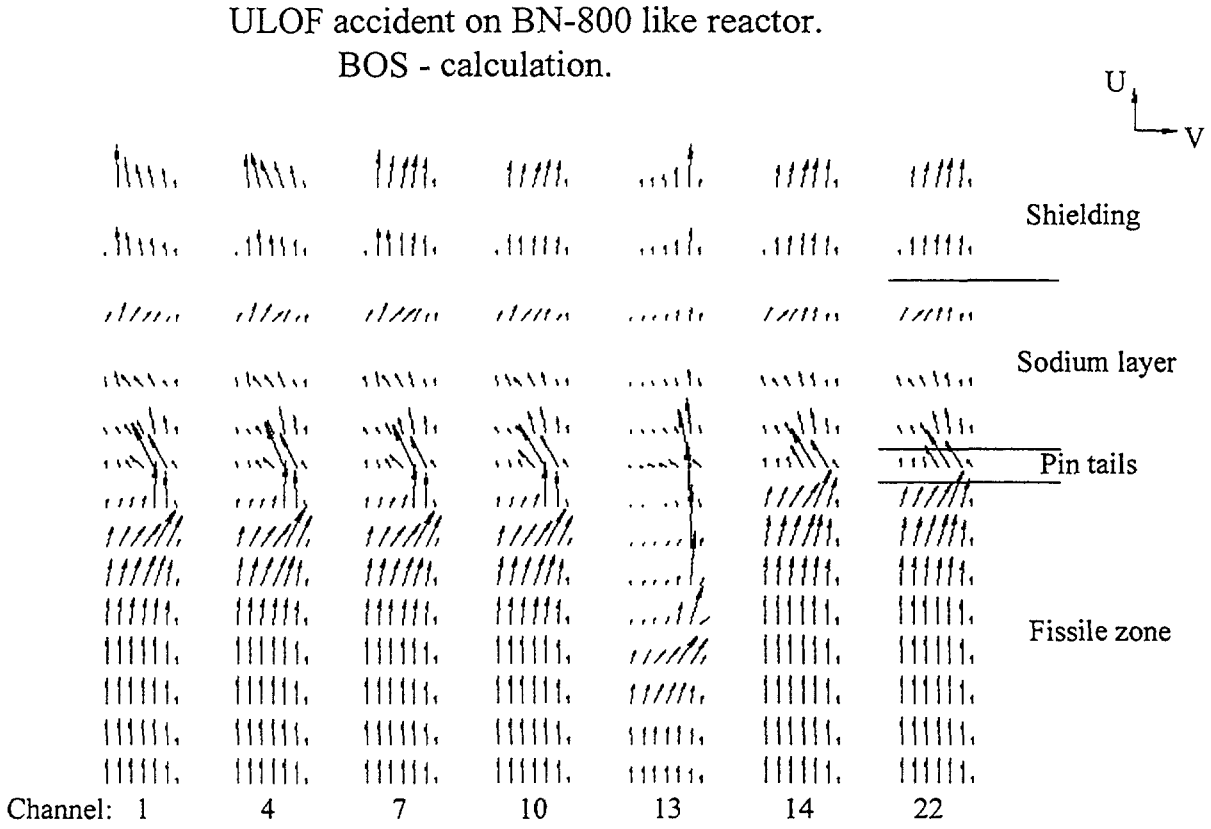

Fig.20. Mass flow rate distribution on subassembies (U=U, V=V*10) , [kg/(s•m•m)].
Time = 22 s.

It would be interesting to compare the results on reactor power for the boiling stage obtained using GRIF-SM code (i.e. taking into account parameters distribution within the subassembly) and BOS code. In the GRIF-SM evaluations, the following scenario was realized: sodium boiling was initiated on the upper boundary of the core, and therefore additional negative reactivity was first inserted causing power decrease. However, according to the essence of one-dimensional model of SA sodium boiling, taken for GRIF-SM code, onset of boiling means blockage of the total SA cross section area by the sodium vapour bubble. SA pressure drop decreases too fast, and sodium flow decreases causing in its turn increase of the vapour generation rate. Intensive expansion of the vapour bubble results in the vapour penetration into the area of positive sodium void reactivity effect and power increase.

Entirely different picture is obtained when using BOS code. Vapour bubble is formed first in the central part of SA cross section, where it is passed over by the single-phase coolant flow (Fig.20). As a result, SA pressure drop increases more slow, the boiling process is more stable, and the rate of the reactor power decrease is lower.

Thus, the conclusion can be made on that from the standpoint of boiling stability one-dimensional boiling model gives deliberately conservative results.

However, in spite of more favorable course of the accident dry-out conditions are achieved in 5/1 channel by 20^{th} second, followed by fast increase of cladding temperature.

5.3. Accident with closing of three check valves of the primary pump.

It has been assumed that in the initial state the reactor is operated at the rated power. By the beyond design basis accident scenario, closing of thee check valves takes place despite inhibitory interlocking in their control schemes preventing closing of more than one check valve. When reactor operates on three heat removal loops all the check valves are in the open state. In case of a valve stem break the valve is kept in the open state by the flow. Closing of the check valve is made only automatically by the "loop disconnection" signal under plant operation conditions on three loops. According to calculation, the probability of closing of three check valves of the primary pumps during time interval between the two nearest planned maintenance (3000 hours) is $2.3*10^{-7}$. The main contribution to this probability is made by a general-cause failure of control system elements. After closing of check valves and a decrease of sodium flow rate through the reactor the safety system operates. The reactor is brought to a subcritical state. However, sodium circulation though the primary pipe line – "the core - the upper mixing plenum - intermediate heat exchangers - primary pump - check valves -feeding header - core diagrid" - fully ceases.

In the reactor, complicated circulation sodium currents arise including the core, the mixing plenum and the upper part of intermediate heat exchangers. In some fuel subassemblies of the core downward motion of sodium takes place, in other ones-upward motion. In the process the upward and downward motion zones in the core are moving, sodium motion in subassemblies changing its direction. Sodium in the core boils up, boiling zones periodically displacing in accordance with the movement of downward and upward motion zones. The temperature of sodium reaches the saturation temperature from time to time (Fig.21). Due to decrease of decay heat release sodium boiling fully ceases in 400 second from the beginning of the accident.

In the course of this accident analysis, advantages of the approach taken as the basis for GRIF-SM code were demonstrated, i.e. that all the main components of the reactor, such as core, inlet and outlet plenums and intermediate heat exchanger are simulated within the framework of one calculation area. In this case the core decay heat is removed by the internal flow circuit formed to incorporate all the above mentioned components.

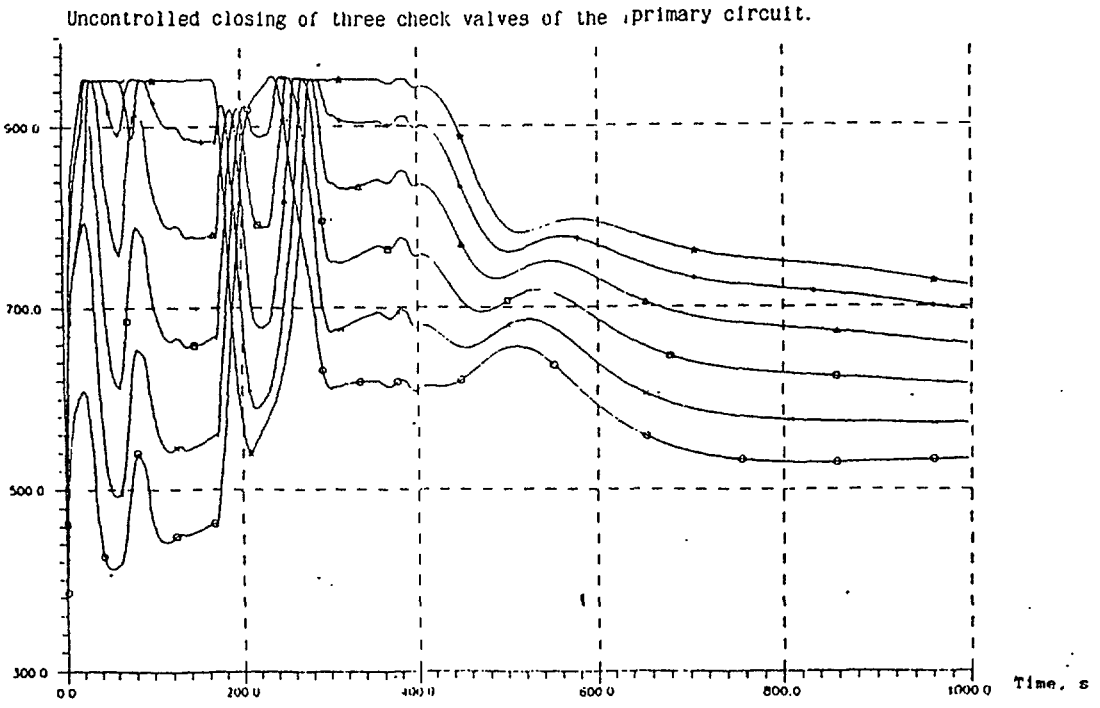

Fig.21. -sodium temperature in LEZ1 in various sections of the core height with a pitch of 0.2 H_{core}

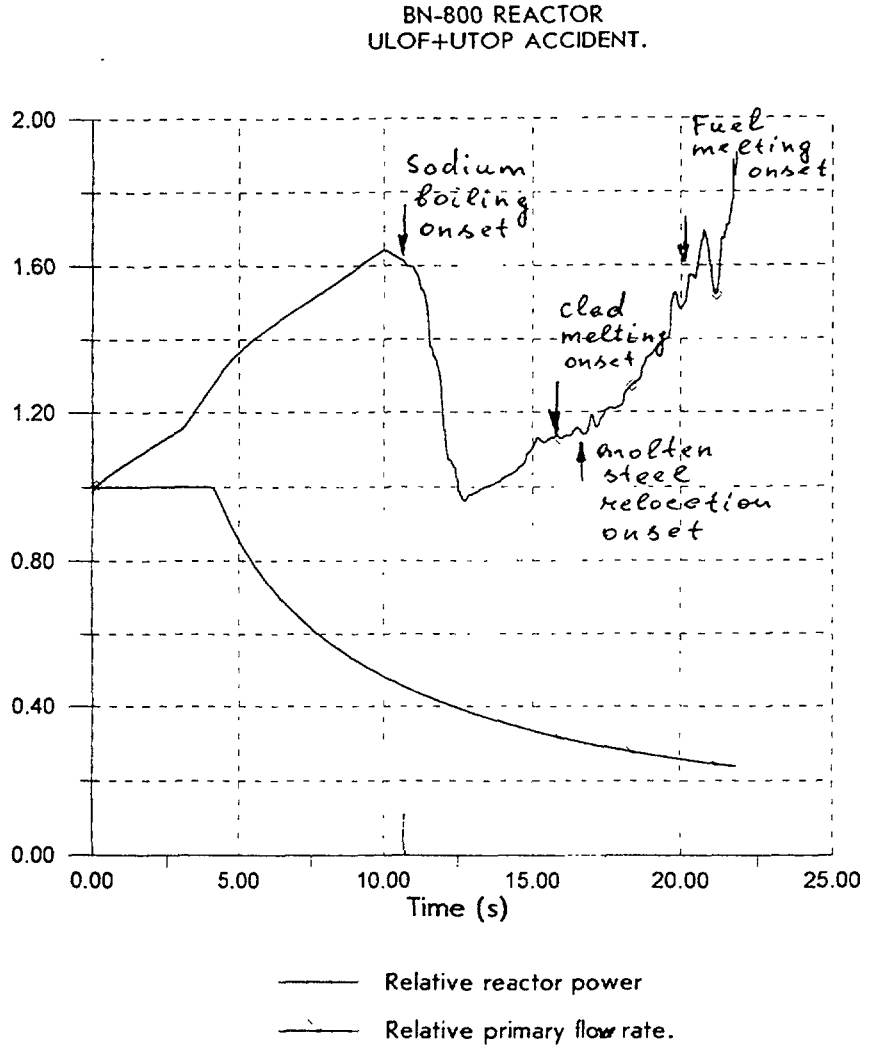

Fig.22.

5.4. UTOP + ULOF combined accident.

Incredible version of the UTOP accident with the primary pump speed decrease was considered. The accident starts with the unauthorized withdrawal from the core of one control rod followed by the withdrawal of 6 shim rods, all this being caused by several postulated failures. The analysis of the accident has been made using modified version of GRIF-SM code together with CANDLE module.

Sequential withdrawal of control rod and shim rods results in the power increase (Fig. 22). Decrease of the primary pump speed begins 4 seconds after the accident start. Sodium boiling onset on 11th second leads to the abrupt insert of negative reactivity (Fig. 23), however power level although decreased still remains sufficiently high, so 5 more seconds later melting of the fuel element cladding and molten steel relocation start. Melting takes

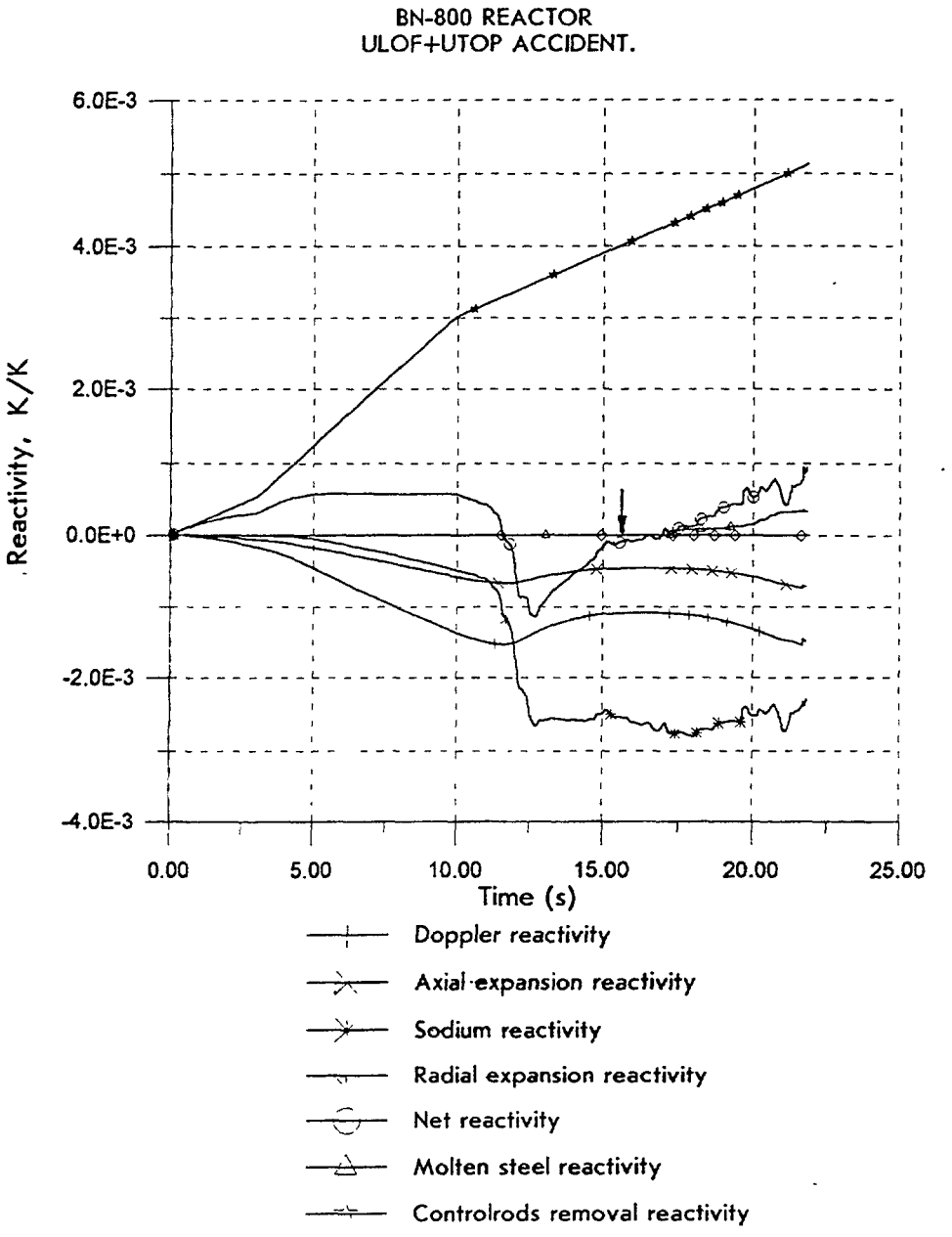

Fig.23. Reactivity versus time.

place under conditions when considerable sodium flow in the core is still maintained. This results in that sodium vapor flowing at high speed entrains the molten steel, which moves upwards as liquid film along the fuel elements, its solidification causing gradual plugging of the flow cross section area (Fig. 24). Steel relocation from the core central area to its upper boundary causes positive reactivity insertion and reactor power increase, thus resulting in the fuel melting.

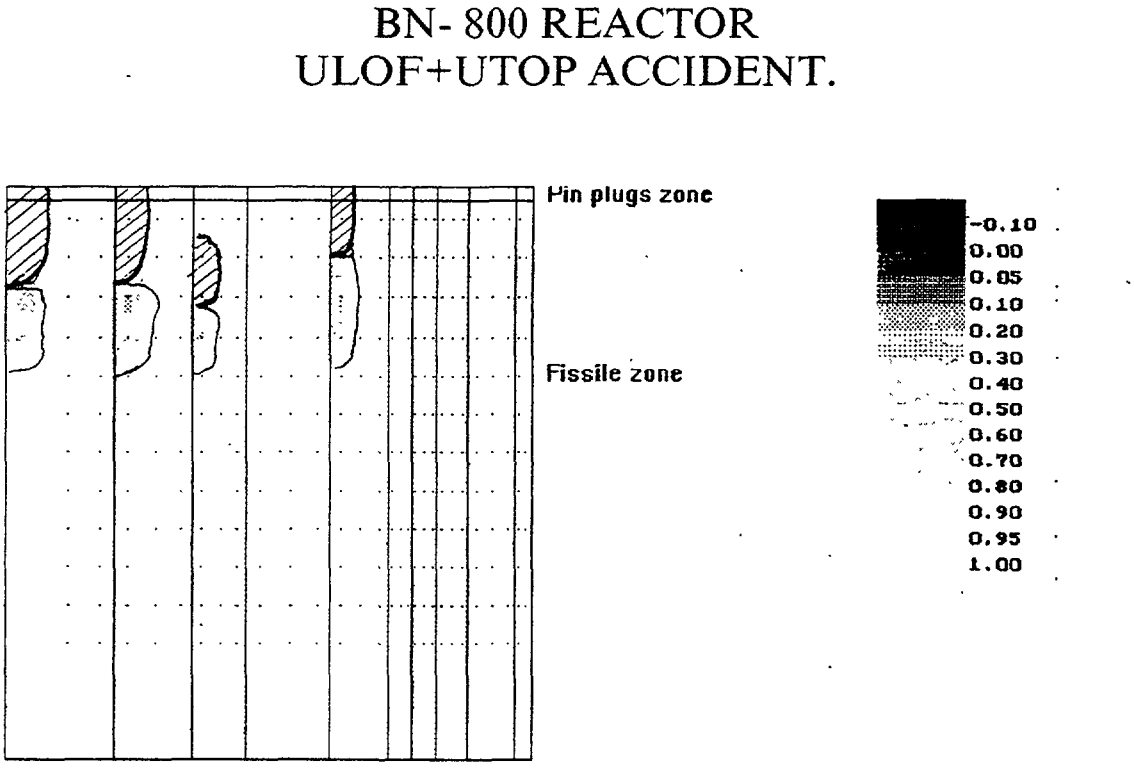

Fig. 24 Positions of "melted zones" and "removed steel zones in the core. Time=21s.

6. CONCLUDING REMARKS.

During the last eight years the program GRIF-SM is heavily used for the substantiation of nuclear safety of Russian fast reactors. For reactor BN-800 following accidents were studied: uncontrolled compensating rods removal; unprotected loss of flow; uncontrolled closing of primary reverse valves. Code was validated against experimental data on sodium boiling in electrically heated tubes and bundles. So it was shown, that GRIF-SM code is a universal computing tool capable to simulate emergency processes in fast reactor at the various initial conditions, when the sodium boiling is possible.

REFERENCES

[1] CHVETSOV I., KOUZNETSOV I., VOLKOV A. GRIF-SM – the Computer Code for Analysis of the Severe Beyond Design Basis Accidents in Sodium Cooled Reactors, International Topical Meeting "Sodium Cooled Fast Reactor Safety", vol.2, p.p. 2-83-2-101, October 3-7, 1994, Obninsk, Russia.

[2] CHVETSOV I., KOUZNETSOV I., VOLKOV A. ULOF Analysis Taking into Account Parameters Distribution within SA. 8-th Consultancy Meeting "IAEA/EC Comparative Analysis of Severe Accident in the BN-800-type Reactor". June 2^{nd}-5^{th}, 1998, Obninsk, Russia.

[3] CHVETSOV I., KOUZNETSOV I., VOLKOV A. Results of ULOF+UTOP Accidents Study for BN-800-like Reactor with a Near Zero Void Core. 7-th Consultancy Meeting "IAEA/EC Comparative Analysis of Severe Accident in the BN-800-type Reactor". 11-12 of December, 1997, Vienna, Austria.

[4] GINKIN V., KOUZNETSOV I., etc. The Code for Joint Solution of Space Time Kinetics and Thermal Hydraulics Equations Intended for Accident Analysis on LMFR, Preprint IPPE-2637.

A SIMPLE ANALYTICAL METHOD TO EVALUATE TRANSIENT BEHAVIOURS OF METAL FUELED FAST REACTORS

H. NINOKATA, Y. HIZUME, T. SAWADA, H. ENDO*
Research Laboratory for Nuclear Reactors,
Tokyo Institute of Technology,
Tokyo, Japan

Abstract

Through our experiences in transient calculations using a general purpose transient system analysis code, the thermal hydraulic and nuclear responses of a typical metal fueled fast reactor core against UTOP and ULOF are found to be approximated by quasi-steady state representation. With these observations transient fuel and coolant temperature distributions in the core are given by simple algebraic expressions. The influences of temperature dependence of material properties are discussed. With these temperature predictions under typical ATWS conditions, effective reactivity changes due to sodium coolant and fuel temperature changes are found to have a unique linear relationship under the extreme conditions of sodium boiling as well as fuel failures. On the basis of these limiting relations, passive shutdown or power stabilization capabilities of metal fueled large fast reactors in case of accidents are discussed.

1. INTRODUCTION

Future fast reactors would be required to have inherent and passive safety characteristics against anticipated transients without scram (ATWS) and to render no fear against core disruptive accidents, even if they are extremely unlikely with the present knowledge. For instance, in case of *unprotected transient overpower* (TOP) and *unprotected loss of flow* (ULOF) accidents, the reactor power during the transients should stay well below the levels corresponding to the temperatures in the core at which sodium boiling and fuel failures are assumed to take place. We call this specific safety characteristics as "*self-controllability.*" [1] These enhanced passive safety features could be achieved, in principle, by carefully selecting such design parameters as the core volume fractions of fuel (Pu), sodium coolant and steel structure and the materials arrangement, and also by specifying proper core geometry, linear heat rate and pump coast-down half time. The objective of the study is, focusing on a metal fueled fast reactor core cooled by sodium, to clarify and sort out the reactivity feedback mechanisms that are of complex nature due to thermal hydraulics and nuclear kinetics coupling.

In this paper a simple analytical model is described for the transient core temperature distributions and passive safety evaluation during UTOP and ULOF of metal fueled fast reactors. Comparisons are made between results from the simple analytical model with transient calculations using a transient system analysis code ARGO [2], which is well qualified for fast reactor safety analysis. An outline of the ARGO code is given in the Appendix. Major heat transfer models in the code are listed in Table I. Based on the simple analytical model to predict temperatures under typical ATWS conditions, effective reactivities due to sodium coolant and fuel temperature changes are defined. Then we derive unique linear relationships between the reactivities under the extreme conditions of sodium boiling as well as fuel failures. Using the relationships, passive shutdown or power stabilization capabilities of metal fueled fast reactors with are discussed.

TABLE I. MAJOR HEAT TRANSFER MODELS USED IN THE ARGO CODE

Heat transfer coefficients	-	$Nu = 7.0 + 0.025\,[(\varepsilon_H / \varepsilon_M)\,Pe]^{0.8}$
Heat conduction coefficients [W/cm/°C]	Cladding	$0.132 + 1.3 \times 10^{-4} T$
	Fuel pellet	$9.33\times10^{-2} + 1.54\times10^{-4} T + 7.50\times10^{-8} T^2$ (without porosity)
Gap conductance [W/cm²/°C]	-	100 (with sodium bond)

2. STEADY-STATE TEMPERATURE DISTRIBUTIONS

We consider the one-dimensional forced convection flow heat removal first. The simple energy balance equation yields the following:

$$\Delta T_C(z) \equiv T_C(z) - T_{C,in} \propto \frac{1}{F}\int_0^z q'''(\xi)\,d\xi \qquad (1)$$

* Present address: FBR Engineering Co., Ltd., Sea Fort Square Center Bldg 13F, 2-3-12 Higashishinagawa, Shinagawa-Ku, Tokyo 140 Japan

where T_C is the coolant temperature, $T_{C,in}$ is the inlet coolant temperature, F is the mass flow (Kg/s), and q'''(z) is the power density. It is easily found that, at any axial location z, temperature rises at the coolant-cladding interface, across the cladding, across the cladding-pellet gap and across the fuel pellet to the centerline are in proportion to the power density at the location q'''(z), if the material properties are assumed constant. For instance, in the fuel pellet,

$$q'''(z)\pi(R^2 - r^2) = 4\pi \int_{T_{F0}(z)}^{T_F(r,z)} k(T)dT \tag{2}$$

where r and R are the radial position in the pellet and the pellet outer radius, respectively. T_F and T_{F0} are the fuel pellet and pellet outer surface temperatures. If the heat conductivity $k(T)$ is assumed to be constant,

$$T_F(r,z) - T_{F0}(z) \propto q'''(z). \tag{3}$$

The pellet-cladding gap is filled with sodium. We assume, therefore, T_{F0} is equal to the cladding inner temperature. We denote the averages of radial temperature distribution in the cladding, gap and fuel pellet as $T_{CL}(z)$ and $T_F(z)$. Then the average fuel pellet temperature $T_F(z)$ can be expressed as

$$T_F(z) = \Delta T_F(z) + \Delta T_{CL}(z) + \Delta T_C(z) + T_{C,in} \tag{4}$$

with the definition of

$$\Delta T_F(z) \equiv T_F(z) - T_{CL}(z) \qquad \propto q'''(z) \tag{5a}$$

$$\Delta T_{CL}(z) \equiv T_{CL}(z) - T_C(z) \qquad \propto q'''(z). \tag{5b}$$

Equations (5a) and (5b) imply that the temperature rises are in proportion to q'''(z). It is noted that, where the point kinetics model is used for reactor kinetics, implying that the neutron flux shape remains constant, the power shape q'''(z) is invariant at any time.

3. TRANSIENT TEMPERATURE DISTRIBUTIONS

3.1. Major assumptions

We decompose the fuel average temperature into the following at the location **r** in the core and at time t:

$$T_F(\mathbf{r},t) = \Delta T_F(\mathbf{r},t) + \Delta T_{CL}(\mathbf{r},t) + \Delta T_C(\mathbf{r},t) + T_{C,in} \tag{6}$$

where $\Delta T_C(\mathbf{r},t)$ is the coolant temperature rise from the core inlet as given by Eq. (1). In the same way, the cladding and coolant bulk temperatures can be defined as:

$$T_{CL}(\mathbf{r},t) = \Delta T_{CL}(\mathbf{r},t) + \Delta T_C(\mathbf{r},t) + T_{C,in} \tag{7}$$

$$T_C(\mathbf{r},t) = \Delta T_C(\mathbf{r},t) + T_{C,in} \tag{8}$$

Under the conditions that the transients are slow and mild against UTOP and ULOF, the system response can be described by quasi-steady sate calculation. This is the case for the metallic fueled fast reactor cores that consist of high conductivity materials and are designed to have strong negative feed back features.

In the context that follows, therefore, we could assume that the shapes of transient temperature distributions in the axial direction are close enough to those of steady state approximation. This assumption will be justified in comparison of transient calculations by the ARGO code and those by simple analytical calculations. Further, since the neutron flux, hence q'''(z,t), does not change its shape very much during the transients, Eqs. (5) and (1) suggest that both $\Delta T_F(z,t)$ and $\Delta T_{CL}(z,t)$ would retain the constant shape q'''(z,0) and $\Delta T_C(z,t)$ the shape of $\int_0^z q'''(\xi,0)d\xi$.

3.2. Case of constant material properties

The simplest case is for the constant material properties. This implies that $\Delta T_F(\mathbf{r},t)$, $\Delta T_{CL}(\mathbf{r}, t)$ and $\Delta T_C(\mathbf{r}, t)$ could be factorized by "shape functions," that are given by $\Delta T_F(\mathbf{r},0)$, $\Delta T_{CL}(\mathbf{r},0)$ and $\Delta T_C(\mathbf{r},0)$, and "amplitude functions" of $g_F(t)$, $g_{CL}(t)$ and $g_C(t)$: i.e.,

$$\Delta T_F(\mathbf{r}, t) = g_F(t) \times \Delta T_F(\mathbf{r},0) \tag{9}$$

$$\Delta T_{CL}(r, t) = g_{CL}(t) \times \Delta T_{CL}(r, 0) \quad (10)$$

$$\Delta T_{C}(r, t) = g_{C}(t) \times \Delta T_{C}(r, 0) \quad (11)$$

3.3. Case of temperature dependent material properties: *Code Predictions*

If we take into account the temperature dependency of material properties, g's in Eqs (9)-(11) are dependent on the location r in the core In order to illustrate the transient temperature behaviors, a metal fueled FBR core is studied as an example A major specification of the reactor plant is shown in Table II

TABLE II MAJOR RECTOR CORE AND PLANT SPECIFICATIONS

Thermal power	MWth	2600
Average linear heat rate	W/cm	270
Total mass flow	Kg/sec	13200
Average core inlet/outlet temperature	°C	355/510
Height of active core H	cm	100
Height of axial blanket region(lower/upper)	cm	35/35
Diameter of active core	cm	390
# of driver core fuel subassemblies	-	354
# of radial blanket subassemblies	-	150
# of fuel pins/driver core subassembly	-	271
Total length of fuel pin	cm	170
Fuel pin diameter	mm	7 5
fuel pitch	mm	8 84
cladding thickness	mm	0 42
cladding material		HF9 (Ferrite)
Wrapping wire diameter	mm	1 3
Wrapping wire pitch	cm	20
Pump coast-down half time $\tau_{1/2}$	sec	10 0

For this core we have performed system transient calculations under Unprotected Loss of Flow (ULOF) and Unprotected Transient Over-power (UTOP) conditions using a system transient analysis code ARGO

Computational results from the ARGO code are shown in Figs 1-9 Figure 1 displays the steady-state axial distributions of coolant, cladding and fuel pellet average temperatures along the hottest fuel subassembly Figures 2-5 are the results for the UTOP and Figs 6-9 for the ULOF

3 3 1 UTOP results

Starting from the steady state at t=0 s, UTOP calculation was performed with the external reactivity insertion rate of 5 ¢/s for 10 s We are interested in the peak coolant and fuel temperatures Let us denote t_{max} as the timing when the peak coolant or fuel temperature is attained Figure 2 shows the power history, Figure 3 the temperature distributions at t_{max} (≈ 150 s), Figure 4 the temperature rise from cladding to fuel ΔT_F at t=0 and t=t_{max}, Figure 5 the ratios of $\Delta T_F(z,t_{max})/\Delta T_F(z,0)$, $\Delta T_{CL}(z,t_{max})/\Delta T_{CL}(z,0)$, and $\Delta T_C(z,t_{max})/\Delta T_C(z,0)$ As shown in Fig 5, the ratios for cladding and coolant are almost constant and Eqs (10) and (11) are a good approximation to the transient distribution However it is not so for the fuel with g_F in Eq (9) varies from 1 6 to 1 9 From these figures the influence of temperature dependency of the fuel conductivity should not be neglected while that of cladding and coolant is not of great significance over the range of interest

3 3 2 ULOF results

A ULOF transient is triggered by a pump trip with the coast-down half time 10 s Figure 6 displays the course of power and flow transients with power to flow ratio (P/F) indicating t_{max} is about 80 s It is noted that the power decrease due to negative feedback is slower than flow reduction and as a result temperatures increase up to 80 s and stay constant afterwards in this event Figure 7 shows the temperature distributions at t_{max} , Figure 8 the temperature rise from cladding to fuel ΔT_F at t=0 and t=t_{max} , and Figure 9 shows again the ratios of $\Delta T_F(z,t_{max})/\Delta T_F(z,0)$, $\Delta T_{CL}(z,t_{max})/\Delta T_{CL}(z,0)$, and $\Delta T_C(z,t_{max})/\Delta T_C(z,0)$ In contrast to the UTOP case, these ratios are nearly constant and Eqs (9)-(11) are a satisfactory approximation to the transient distributions in the ULOF case This is due to the fact that the power is already low enough at t_{max} and the temperature dependency of the fuel conductivity does not prevail

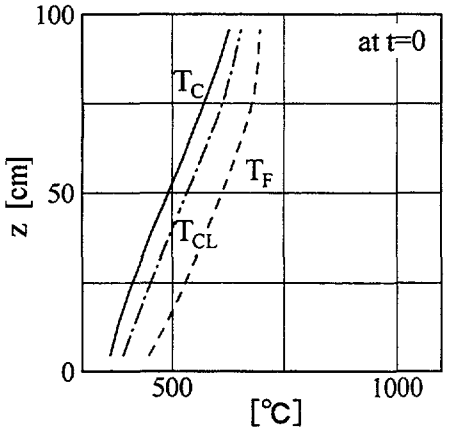

Fig.1 Steady-state axial temperature distributions

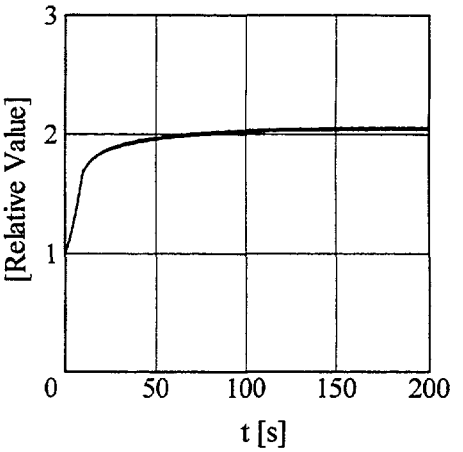

Fig.2 Power history (UTOP)

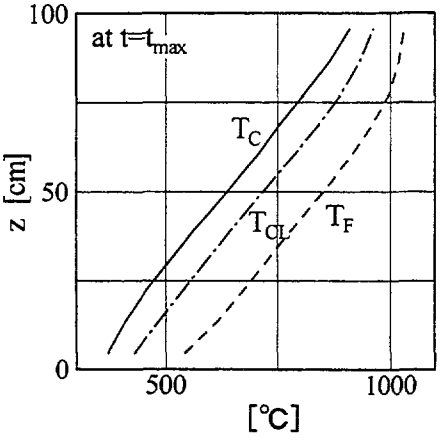

Fig.3 Temperature axial distributions at t=t_{max} (UTOP)

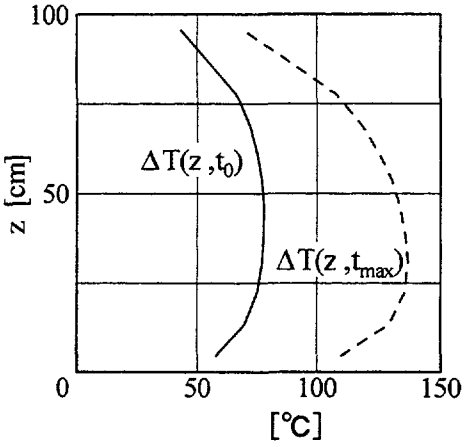

Fig.4 Fuel temperature increase axial distributions (UTOP)

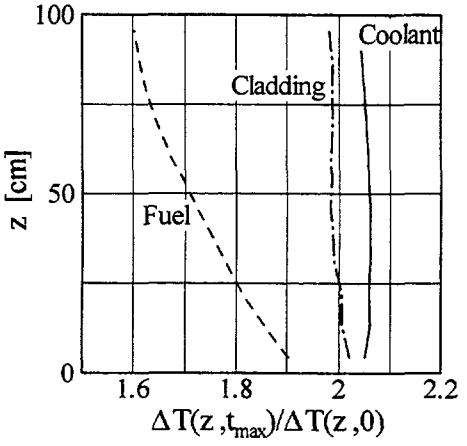

Fig.5 Axial distribution of temperature change ratio between t=0 and t=t_{max}(UTOP)

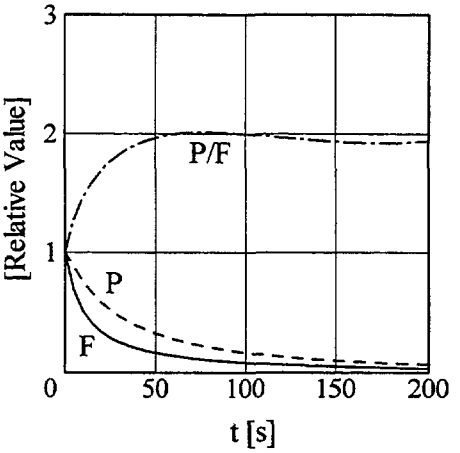

Fig.6 Course of power and flow transients with power to flow raito P/F (ULOF)

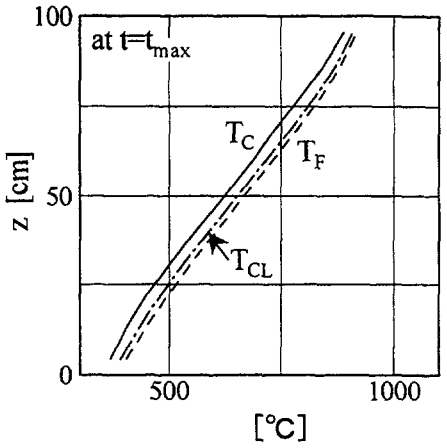

Fig.7 Temperature axial distributions at $t=t_{max}$(ULOF)

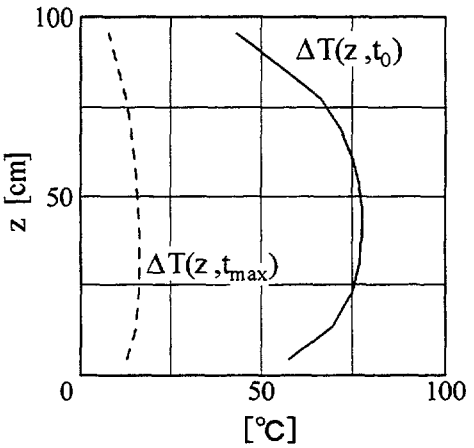

Fig.8 Temperature increase axial distributions (ULOF)

4. SIMPLE ANALYTICAL METHOD

In this section we try to derive simple analytical method to describe the transient temperature distributions in the metallic fueled fast reactor core under the condition that the power and flow histories q'''(z,t) or P(t) and F(t) are known in advance.

4.1. Coolant temperature profile

For the axial temperature distribution of the coolant in a fuel subassembly in the core, the energy balance with the quasi-steady state assumption and *constant* heat capacity of the coolant leads to:

$$T_C(z,t) = \frac{P(t)/F(t)}{P(0)/F(0)} T_C(z,0) + \left(1 - \frac{P(t)/F(t)}{P(0)/F(0)}\right) T_{C,in} \tag{12a}$$

or

$$\Delta T_C(z,t) = \frac{P(t)/F(t)}{P(0)/F(0)} \Delta T_C(z,0) \tag{12b}$$

where $P(t) = \int q'''(\vec{r},t)d\vec{r}$, $\vec{r} \in$ *fuel subassembly*

is the total power and $F(t)$ is the total mass flow in the fuel subassembly. From Eq. (12b), we have

$$g_C(t) = \frac{P(t)/F(t)}{P(0)/F(0)}. \tag{13}$$

4.2. Fuel temperature distribution

For the fuel temperature distribution in the pellet, we approximate the heat conductivity $k_F(T)$ in the form of aT_F+b. Note that this is an approximation to the pellet before irradiation and nor pores are present. Figure 10 compares the linear approximation with the actual $k_F(T)$ model used in the ARGO code. Then the integral equation (2) is solved and yields the fuel pellet temperature distribution:

$$T_F(r,z,t) = -\frac{b}{a} + \sqrt{\left\{T_{F0}(z,t) + \frac{b}{a}\right\}^2 + \frac{q'''(z,t)(R^2 - r^2)}{2a}} \tag{14a}$$

where the pellet outer surface temperature $T_{F0}(z,t)$ is given by $T_C(z,t)+\Delta T_{CL}(z,t)$. It is noted here that $T_F(r,z,t)$ signifies the radial temperature distribution in a pellet at the axial location z and at time t, while $T_F(z,t)$ in Eq. (4) or Eq. (5a) denotes the radially averaged fuel temperature at z. The average fuel pellet temperature $T_F(z,t)$ would be close enough to that given by Eq. (14a) with $r = R/\sqrt{2}$:

$$T_F(z,t) = -\frac{b}{a} + \sqrt{\left\{T_{F0}(z,t) + \frac{b}{a}\right\}^2 + \frac{q'''(z,t)R^2}{4a}}. \tag{14b}$$

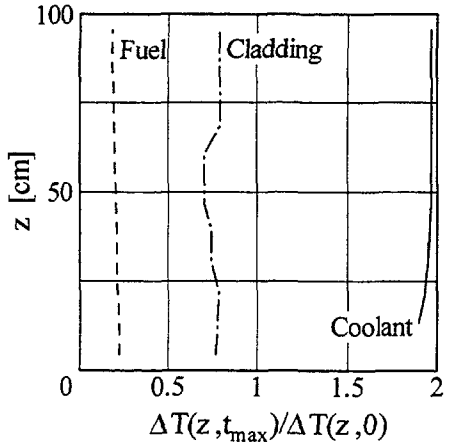

Fig.9 Axial distribution of temperature change ratio between t=0 and t=t_{max}(ULOF)

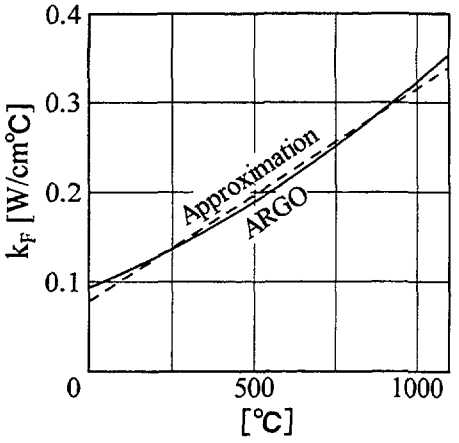

Fig.10 Fuel conductivity as a function of temperature

$\Delta T_{CL}(z,t)$ is given by

$$\Delta T_{CL}(z,t) = q'''(z,t)\frac{R^2}{2k_{CL}}\ln\left(\frac{R_0}{R}\right). \tag{14c}$$

In Equation (14c), R is the cladding inner diameter, which is approximated by pellet outer diameter, and R_0 is the cladding outer diameter; k_{CL} is the heat conductivity of the cladding (assumed to be constant). From Eq. (6),

$$\begin{aligned}\Delta T_F(z,t) &= T_F(z,t) - T_{F0}(z,t)\\ &\cong T_F(z,t) - \Delta T_{CL}(z,t) - T_C(z,t)\end{aligned}$$

or with a help of Eqs. (14b), (14c) and (12a), we have:

$$\begin{aligned}\Delta T_F(z,t) \cong &\left[-\frac{b}{a}+\sqrt{\left\{T_{F0}(z,t)+\frac{b}{a}\right\}^2+\frac{q'''(z,t)R^2}{4a}}\right]\\ &-\left[q'''(z,t)\frac{R^2}{2k_{CL}}\ln\left(\frac{R_0}{R}\right)\right]-\left[\frac{P(t)/F(t)}{P(0)/F(0)}\Delta T_C(z,0)+T_{C,in}\right].\end{aligned} \tag{15}$$

Based on the Eq. (15), we derive the amplitude function similar to $g_F(t)$ to be re-defined in terms of power P(t) and flow F(t) in the next Section 5.

For a special case of the constant fuel heat conductivity, Eq. (5) readily gives the following:

$$g_F(t) = g_{CL}(t) = \frac{P(t)}{P(0)}. \tag{16}$$

Figure 11 shows a comparison of $\Delta T_F(z,t_{max})$ predicted by the ARGO code in the UTOP calculation and by Eq. (9) with g_F defined by Eq. (16). The discrepancy is attributed to the neglect of temperature dependency of the fuel conductivity. Using Eq. (15), this discrepancy is reduced as will be shown in 5.3.

5. REACTIVITY AND TEMPERATURE DISTRIBUTIONS

5.1. Total reactivity and reactivity coefficients

The total reactivity $\rho_{tot}(t)$ added up to time t since the onset of any transient at t=0 will be expressed as:

$$\begin{aligned}\rho_{tot}(t) = &\int d\mathbf{r}\left[K_{Dop}(\mathbf{r})+K_{F,\exp}(\mathbf{r})\right]\cdot\left[T_F(\mathbf{r},t)-T_F(\mathbf{r},0)\right]+\int d\mathbf{r}K_{Clad}(\mathbf{r})\cdot\left[T_{CL}(\mathbf{r},t)-T_{CL}(\mathbf{r},0)\right]\\ &+\int d\mathbf{r}\left[K_{Na}(\mathbf{r})+K_{SA,\exp}(\mathbf{r})\right]\cdot\left[T_C(\mathbf{r},t)-T_C(\mathbf{r},0)\right]+\rho_{ext}(t)\end{aligned} \tag{17}$$

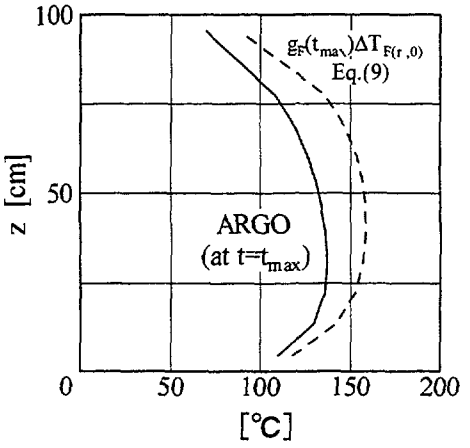

Fig.11 Comparison of $\Delta T_F(z,t_{max})$
predicted by ARGO and Eq.(9) (UTOP)

where K_{Dop}, $K_{F,exp}$, K_{Clad}, K_{Na} and $K_{SA,exp}$ are the reactivity coefficients due to the fuel Doppler effect, fuel axial expansion, cladding axial expansion, coolant density change and subassembly radial expansion, respectively; ρ_{ext} is the external reactivity inserted:

$$\rho_{ext}(t) = \int_0^t \dot{\rho}_{ext}(\tau)d\tau \,. \tag{18}$$

Equation (17) can be re-written as:

$$\rho_{tot}(t) = \int d\mathbf{r}K_F(\mathbf{r})\left[\Delta T_F(\mathbf{r},t) - \Delta T_F(\mathbf{r},0)\right] + \int d\mathbf{r}K_{CL}(\mathbf{r})\left[\Delta T_{CL}(\mathbf{r},t) - \Delta T_{CL}(\mathbf{r},0)\right] + \int d\mathbf{r}K_C(\mathbf{r})\left[\Delta T_C(\mathbf{r},t) - \Delta T_C(\mathbf{r},0)\right] + \rho_{ext}(t)$$

and simplified as:

$$\rho_{tot}(t) \cong \int d\mathbf{r}K_F(\mathbf{r})\left[\Delta T_F(\mathbf{r},t) - \Delta T_F(\mathbf{r},0)\right] + \int d\mathbf{r}K_C(\mathbf{r})\left[\Delta T_C(\mathbf{r},t) - \Delta T_C(\mathbf{r},0)\right] + \rho_{ext}(t) \tag{19}$$

where the following new definition of reactivity coefficients have been introduced.

$$\begin{aligned} K_F(\mathbf{r}) &= K_{Dop}(\mathbf{r}) + K_{F,exp}(\mathbf{r}) \\ K_{CL}(\mathbf{r}) &= K_{Dop}(\mathbf{r}) + K_{F,exp}(\mathbf{r}) + K_{Clad}(\mathbf{r}) \\ K_C(\mathbf{r}) &= K_{Dop}(\mathbf{r}) + K_{F,exp}(\mathbf{r}) + K_{Clad}(\mathbf{r}) + K_{Na}(\mathbf{r}) + K_{SA,exp}(\mathbf{r}) \end{aligned} \tag{20}$$

In Eq. (19) a contribution of cladding temperature rise is neglected in comparison with the others.

5.2. Effective reactivities and a linear relationship

Here we further define the effective reactivity $\rho_{eff,fuel}$ and $\rho_{eff,cool}$ due to fuel and coolant temperature increments,

$$\rho_{eff,fuel} \equiv \int d\mathbf{r}K_F(\mathbf{r})\Delta T_F(\mathbf{r},0) \tag{21a}$$

$$\rho_{eff,cool} \equiv \int d\mathbf{r}K_C(\mathbf{r})\Delta T_C(\mathbf{r},0) \tag{21b}$$

and the amplitude functions G_F and G_C:

$$G_F(t) \equiv \frac{\int d\mathbf{r}K_F(\mathbf{r})\Delta T_F(\mathbf{r},t)}{\int d\mathbf{r}K_F(\mathbf{r})\Delta T_F(\mathbf{r},0)} \tag{22a}$$

and

$$G_C(t) \equiv \frac{\int d\mathbf{r}K_C(\mathbf{r})\Delta T_C(\mathbf{r},t)}{\int d\mathbf{r}K_C(\mathbf{r})\Delta T_C(\mathbf{r},0)} \,. \tag{22b}$$

G_F and G_C would be equal to g_F and g_C (Eqs. (9) and (11)) if the material properties as well as the reactivity coefficients are constant.

By substituting Eqs. (21) and (22) into Eq. (19), we finally obtain the relationship among the effective reactivities $\rho_{eff,fuel}$ and $\rho_{eff,cool}$:

$$\rho_{eff,cool} = -\frac{G_F(t)-1}{G_C(t)-1}\rho_{eff,fuel} + \frac{\rho_{tot}(t)-\rho_{ext}(t)}{G_C(t)-1}. \tag{23}$$

It is worth while to note here that $\rho_{eff,fuel}$ and $\rho_{eff,cool}$ are the effective reactivities that depend only on the steady-state nuclear and thermohydraulic information.

A special case is with constant material properties. Because $G_C(t)=g_C(t)$, $G_F(t)=g_F(t)$ in this case, Eq. (23) becomes

$$\rho_{eff,cool} = -\frac{g_F(t)-1}{g_C(t)-1}\rho_{eff,fuel} + \frac{\rho_{tot}(t)-\rho_{ext}(t)}{g_C(t)-1} \tag{24a}$$

$$= -\frac{\frac{P(t)}{P(0)}-1}{\frac{P(t)/F(t)}{P(0)/F(0)}-1}\rho_{eff,fuel} + \frac{\rho_{tot}(t)-\rho_{ext}(t)}{\frac{P(t)/F(t)}{P(0)/F(0)}-1}. \tag{24b}$$

Equation (24b) is obtained with the use of Eqs. (13) and (16).

5.3. Amplitude functions for the fuel and coolant temperature rises

In order to facilitate the integration in Eqs. (22a) and (22b) analytically, we assume the reactivity coefficients K(**r**)'s are uniform although this is not correct physically. Then Eqs. (22a) and (22b) become:

$$G_F(t) \approx \frac{\int d\mathbf{r}\Delta T_F(\mathbf{r},t)}{\int d\mathbf{r}\Delta T_F(\mathbf{r},0)} \text{ and } G_C(t) \approx \frac{\int d\mathbf{r}\Delta T_C(\mathbf{r},t)}{\int d\mathbf{r}\Delta T_C(\mathbf{r},0)}. \tag{25}$$

$\Delta T_F(\mathbf{r},t)$ in Eq. (25) contains the fuel pellet surface temperature T_{F0} ($\cong T_C(r,t)+\Delta T_{CL}(r,t)$) as shown in Eq. (15). In an attempt to make the integration tractable, we introduce additional simplification, i.e., $T_{F0} \cong T_C(r,t)$ yielding

$$\Delta T_F(z,t) \cong \left[-\frac{b}{a}+\sqrt{\left\{T_C(z,t)+\frac{b}{a}\right\}^2+\frac{q'''(z,t)R^2}{4a}}\right]-T_C(z,t), \tag{26}$$

and for the axial coolant temperature profile we introduce the following approximation:

$$T_C(z,t) = \frac{P(t)/F(t)}{P(0)/F(0)}\cdot\frac{T_C(H,0)-T_{C,in}}{H}z+T_{C,in}. \tag{27}$$

Here H is the active core height; $T_C(z,0)$ is given by the steady-state heat balance; and $T_C(z,t)$ is now a function of P(t)/F(t) and linear in z. Figure 12 shows good agreement of $\Delta T_F(z,t_{max})/\Delta T_F(z,0)$ predicted by the proposed model based on Eqs. (26) and (27) with that given by the ARGO code in the UTOP case. This figure demonstrates an improvement over the constant materials property model which yields a constant $\Delta T_F(z,t_{max})/\Delta T_F(z,0) = P(t_{max})/P(0) = 2.0$.

Substituting Eq. (26) with (27) into $G_F(t)$ defined by Eq. (25), we obtain:

$$G_F(t) = \frac{\int_0^H dz\sqrt{\left\{T_C(z,t)+\frac{b}{a}\right\}^2+\frac{q'''(z,t)R^2}{4a}}-\int_0^H T_C(z,t)dz-\frac{b}{a}H}{\int_0^H dz\sqrt{\left\{T_C(z,0)+\frac{b}{a}\right\}^2+\frac{q'''(z,0)R^2}{4a}}-\int_0^H T_C(z,0)dz-\frac{b}{a}H}. \tag{28}$$

Because T_C(z,t) is linear in z, all integration in Eq. (28) is analytically possible and in consideration of q'''(z,t) $\propto$ $P(t)$, the amplitude function $G_F(t)$ is expressed in a complicated algebraic form as a function of $P(t)$ and $F(t)$.

The amplitude function $G_C(t)$ of Eq. (25) is readily obtained by substituting Eq. (27) and given as:

$$G_C(t) = \frac{P(t)/F(t)}{P(0)/(F(0)} . \tag{29}$$

6. PASSIVE SAFETY EVALUATION METHOD

In this section, we derive the amplitude functions $G_F(t)$ and $G_C(t)$ at t_{max} where t_{max} is the timing at which the onset of either fuel melting or sodium boiling takes place. Then the effective reactivity relationship, Eq. (23), and its variant, Eq. (24) are applied in evaluating the "self-controllability" of Fast Reactors defined in the INTRODUCTION.

6.1. Highest temperatures under limiting conditions

6.1.1. UTOP

In the event of UTOP, the flow F(t) is constant. Therefore we concentrate on obtaining the power at t_{max} which corresponds to either fuel melting or sodium boiling.

6.1.1.1 Fuel melting case

The highest temperature in the fuel is attained at the center of the fuel pellet and at the elevation z_{max} which we obtain by solving the following:

$$\left.\frac{\partial T_F(r,z,t_{\max})}{\partial z}\right|_{r=0} = 0 \tag{30}$$

with $T_F(r,z,t_{max})$ at r=0 being given by:

$$T_F(0,z,t_{\max}) = -\frac{b}{a} + \sqrt{\left\{\frac{P(t_{\max})}{P(0)}\cdot\frac{T_C(H,0)-T_{C,in}}{H}z + T_{C,in} + \frac{b}{a}\right\}^2 + \frac{q'''(z,t_{\max})R^2}{2a}} . \tag{31}$$

This is a variant of Eq. (14a) with the assumption $T_{F0} \cong T_C(z,t)$ in Eq. (14a) and Eq. (27) for $T_C(z,t)$ in the same manner as we derived Eq. (26). The algebraic equation derived from Eq. (30) becomes tractable thanks to the linear profile of the coolant temperature and solved for z_{max} in terms of $P(t_{max})$. z_{max} is substituted into Eq. (30) to obtain the highest fuel centerline temperature $T_{F,max}$. Equating $T_{F,max}$ to the fuel melting temperature, we obtain a cubic equation with respect to $P(t_{max})$ which finally can be solved for $P(t_{max})$. In case the obtained z_{max} is out of range, i.e., $z_{max} > H$, the peak temperature is to be calculated from Eq. (31) with z=H. In this case $P(t_{max})$ is obtained by solving a quadratic equation.

6.1.1.2 Sodium boiling case

The highest temperature of the sodium is at the top of the active core. We can solve the following equation from Eq. (29) for $P(t_{max})$:

$$\frac{P(t_{\max})}{P(0)} = \frac{T_{Na,B} - T_{C,in}}{T_C(H,0) - T_{C,in}} , \tag{32}$$

where $T_{Na,B}$ is the sodium boiling temperature.

6.1.2 ULOF

In the event of ULOF, in particular for metallic fueled fast reactor cores, it has been pointed out that the temperatures prediction with the constant material properties is reasonably good as shown in Section 3. Also it is

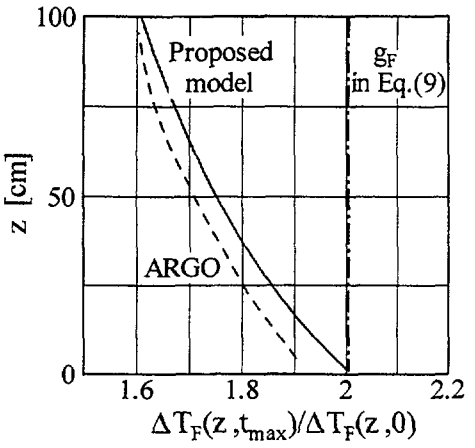

Fig.12 Axial distribution of fuel average temperature change raitos compared between ARGO and proposed model (UTOP)

unlikely that the fuel melting takes place prior to the onset of sodium boiling. This implies that we could use Eq. (29) to obtain $P(t_{max})/F(t_{max})$. The equation to be solved is:

$$\frac{P(t_{\max})/F(t_{\max})}{P(0)/F(0)} = \frac{T_{Na,B} - T_{C,in}}{T_C(H,0) - T_{C,in}}. \tag{33}$$

Different from the UTOP case where we have $P(t_{max})$ by Eq. (32), we need to have $P(t_{max})$ by solving the one-point kinetics equation with reactivity feedback from temperature changes. In this paper, however, we used the calculated result for $P(t_{max})$ by the ARGO code.

6.2. Self-controllability limit lines: *Present Model*

For both UTOP and ULOF events, we have analytical expressions for $P(t_{max})$ and $P(t_{max})/F(t_{max})$ that are to be substituted into Eq. (27) to give $T_C(z, t_{max})$. This temperature is now substituted into G_F (Eq. 28)and G_C (Eq. 29), which are used in Eq. (23) to obtain:

$$\rho_{eff,cool} = -\frac{G_F(t_{\max})-1}{G_C(t_{\max})-1}\rho_{eff,fuel} + \frac{\rho_{tot}(t_{\max})-\rho_{ext}(t_{\max})}{G_C(t_{\max})-1}. \tag{34}$$

We call the line depicted by this linear relationship as "*self-controllability limit line*" because the line consists of any combination of ($\rho_{eff,cool}$, $\rho_{eff,fuel}$) that correspond to the limiting condition, i.e., either fuel failure or sodium boiling that should be avoided during ATWS. For the UTOP case, it is considered that the reactivity change around t_{max} is very small and we can assume $\rho_{tot}(t_{max}) \approx 0$. For the ULOF case, $\rho_{ext}(t)=0$ and from Eq. (24b) with $\rho_{eff,fuel}=0$, we get:

$$\rho_{tot}(t_{\max}) = \frac{P(t_{\max})/F(t_{\max})}{P(0)/F(0)}\rho_{eff,cool} \tag{35}$$

implying $\rho_{tot}(t_{max})$ to be constant. In the following example, we use -1.7×10^{-3} $\Delta k/k$ for $\rho_{tot}(t_{max})$ which was obtained from ARGO parametric survey calculations.

Once the steady state temperature distributions are known for any metallic fueled fast reactor core and the distributions of all reactivity coefficients in the reactor core are provided by a multi-dimensional neutron transport or diffusion code, e.g., CITATION [3], two effective reactivities can be calculated through Eqs. (21a) and (21b). The steady state temperature distributions may be obtained through calculations by such a system transient analysis code as the ARGO code. If a combination ($\rho_{eff,cool}$, $\rho_{eff,fuel}$) is located above the line, the fast reactor core is judged to suffer sodium boiling or fuel melting under the ULOF or UTOP condition. If below the line, then the fast reactor core is considered to have the self-controllability and does not suffer significant fuel failure even under the ULOF/UTOP conditions.

Figure 13 illustrates the self-controllability lines for UTOP and ULOF in which comparisons are made among the lines generated based on:

i) the predicted fuel and sodium temperature distributions by the ARGO code in Eq. (23)
ii) the constant material property model, i.e., Eq. (24b)
iii) the present model, i.e., Eq. (34)

together with the plots as the reference case from a set of transient calculations using the ARGO code with a variation of reactivity coefficients as parameters. These reference plots have been picked up from a body of combinations ($\rho_{eff,cool}$, $\rho_{eff,fuel}$) only when the peak fuel temperature reached the melting temperature or when the peak sodium temperature reached the boiling temperature. It is noted that, in the event of UTOP, Eq. (24b) becomes $\rho_{eff,cool} = -\rho_{eff,fuel} + \text{const}$ because F(t) = F(0), which does not explain well the trend given by the ARGO. In contrast, the present model gives much better agreement due to a reasonable consideration of the temperature dependency of the fuel heat conductivity.

In the event of ULOF, the peak temperature is attained when power to flow ratio is maximum while the power is much lower than that at steady state (about 10 % of nominal power). This means $G_F(t_{max})$ hence $\Delta T_F(t_{max})$ is much smaller than that of UTOP. Therefore the influence of temperature dependency of the fuel conductivity is not conspicuous. As a result Eq. (24b) is a good approximation to the ULOF transient as shown in Fig. 13..

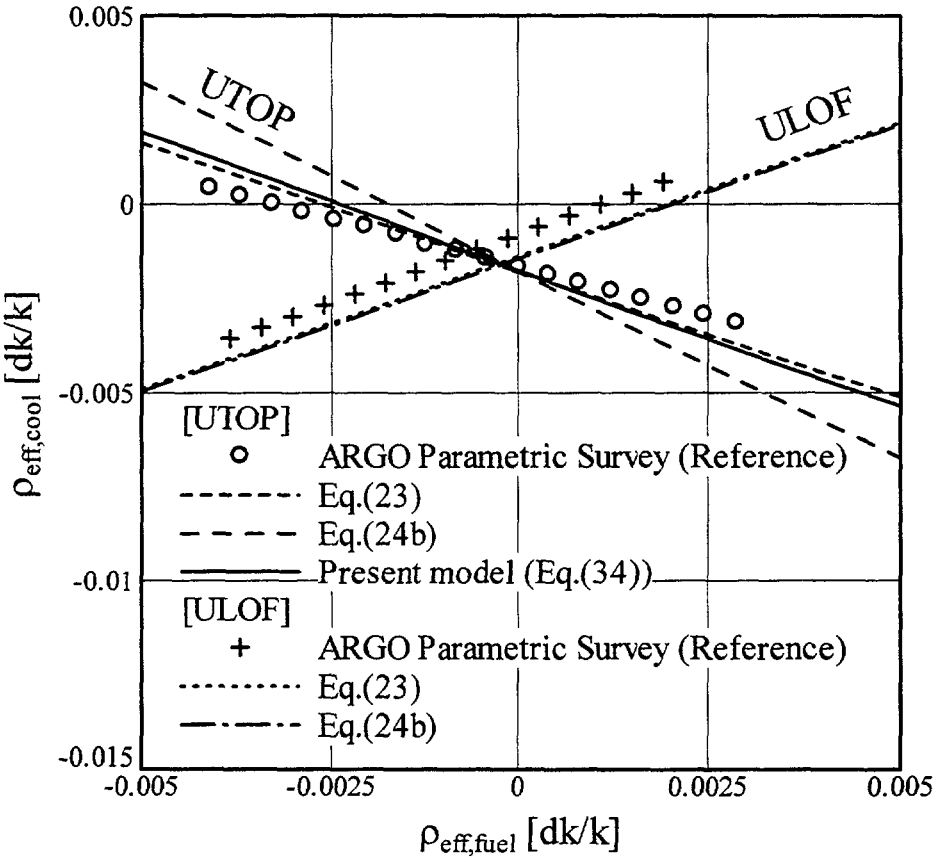

Fig.13 Self-controllability limit lines for UTOP and ULOF

6.3. Example: assessment of the self-controllability of an ma burner core

In the remaining of this section, we evaluate the self-controllability of an MA burner core with metallic fuels as an example. In designing a fast reactor core, one could select the design parameters including a set of core material volume fractions, geometry, core arrangement and configurations. These parameters in turn determine the reactivity coefficient through diffusion or transport calculations, that should fall into the region where the self-controllability conditions are satisfied.

In general, it was shown that, in order to meet the self-controllability requirement for the ULOF, it was essential to have a flat core at a cost of higher burn-up swing. This approach, however, resulted in a higher burden onto the control rod strategy leading to a core design vulnerable against UTOP events. For example, keeping the volume fractions of fuel, coolant and structure in the metal fuel core constant, i.e., 41%, 37% and 22%, respectively, and the active core volume and power density constant (=4.52 m^3 and 575 Mw/m^3), it was found that the core height and radius are around 68 cm and 146 cm that minimized the burnup swing. For the core of this aspect ratio, we investigated the influences of loading both Minor Actinides (MAs) and Fission Products (FPs) onto the self-controllability performances. The FPs (^{129}I, ^{107}Pd, ^{99}Tc) were packed in the region around the active core so that the FPs do not give direct effects on the nuclear characteristics of the core. In order to maintain the breeding ratio higher than or equal to unity, we installed a blanket region in the center of the core (see Fig. 14).

In Fig. 15, the effective fuel and coolant reactivity changes of two cores of different heights, i.e., h = 40 cm and 68 cm are plotted with MA concentration as a parameter. In case of UTOP, a total amount of reactivity insertion due to hypothetical one rod withdrawal would be small enough and was set 30 ç conservatively for the h = 68 cm core while 50ç for the h = 40 cm core. With these reactivity insertions, the self-controllability limit lines for ULOF and UTOP were drawn as shown in Fig. 15. The higher MA concentration resulted in less fulfillment of the self-controllability as well as less breeding ratio for a flatter metal core (h = 40 cm) while the h = 68 cm core gave a sufficient margin to the limit lines keeping the breeding ratio nearly unity. To enhance negative feedback effects further a moderator (BeO) was introduced into the fuel. A slight spectral shift resulted

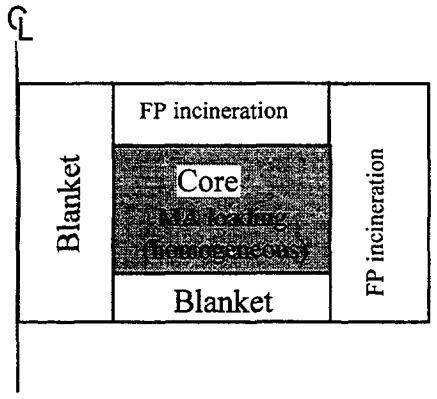

Fig.14 Metal Fuel Core Configuration for MA and FP incineration

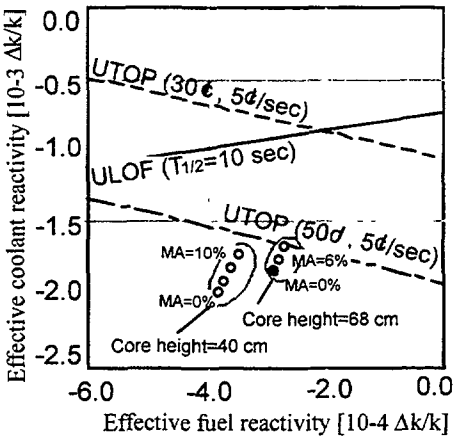

Fig.15 Estimation of self-controllability by reactivity correlation model for reactor cores loaded with MA's

in a more favorable result due to the coolant reactivity and Doppler coefficients that make the effective reactivities satisfy the "self-controllability condition" with more margin to the limit as shown in Fig. 15. As a conclusion, it was shown that a metallic fueled FBR core could be designed that has capabilities of breeding fuel and incinerating FPs (although the MA nuclides are limited to only three) and that has the self controllability characteristics, simultaneously.

7. CONCLUSIONS

We took advantage of the fact that the thermal hydraulic and nuclear responses of metal fueled fast reactor cores to UTOP and ULOF can be described by quasi-steady state representation.

It is shown that the assumption of constant material properties gives a good approximation to the temperatures of coolant and fuel predicted by a system transient analysis code in the ULOF transient. However this assumption collapses for the UTOP transient because the temperature dependency of the fuel conductivity gives not negligible influences on the fuel temperature profile.

A simple analytical method to describe the transient fuel temperature that includes the temperature dependency of the fuel conductivity has been proposed. The influences of temperature dependence of fuel

conductivity are reasonably predicted under the UTOP condition. This model yields fuel and coolant temperatures as functions of power and flow which are required to be provided in advance. However, when focusing on the extreme condition of sodium boiling or fuel melting, we can prescribe the power to flow ratio or power by the heat balance.

The effective coolant reactivity $\rho_{eff,cool}$ and effective fuel reactivity $\rho_{eff,fuel}$ have been defined as those due to sodium coolant and fuel steady-state temperature distributions. Based on proposed model for the transient temperature predictions under typical ATWS conditions, the effective reactivities have been correlated into a unique linear relationship under the limiting conditions of sodium boiling as well as fuel failures. These lines have been found to give better agreement with the ARGO code prediction under the limiting conditions than the constant material property model.

The above linear relationship holds in particular when the system behaviors can be approximated by quasi-steady state transient, which is true for slow transient of UTOP and ULOF of metal fueled fast reactors with relatively quick nuclear feedback mechanisms. Using these limiting relations, we have evaluated the passive shutdown or power stabilization capabilities of a metal fueled fast breeder reactor with MA and FP burning capabilities in case of accidents.

The proposed general and simple method allows us to evaluate the transient behaviors of any given fast reactor cores subject to accidents, typically ULOF and UTOP, without carrying out a number of time-consuming system transient calculations to find the reactor system to have sufficient passive safety features. Also the model provides us with clear physical insights into the complicated feedback mechanisms related to the nuclear and thermohydraulics coupling phenomena.

REFERENCES

[1] SHIMIZU, A. et al., "Self-consistent nuclear energy systems," Proc. Global Environment and Nuclear Energy Systems, pp. 25-32, Susono, Japan, October (1995).
[2] ENDO, H., KUMAOKA, Y., GOLAN, S. and NAKAGAWA, H. "Passive safety features of a bottom-supported fast breeder reactor vessel", Nuclear Technology, Vol.99, p.318, (1992).
[3] FOWLER, T.B. et al., "Nuclear reactor core analysis code: CITATION," ORNL-TM-2496, Rev. 2, Oak Ridge National Laboratory (1971).

APPENDIX

Outline of the ARGO code [2]

The primary and secondary coolant system, the decay heat removal system, and the core are modeled by a flow network model that includes the models for flow mixing in the plenum, and heat transfer between sodium and the in-vessel structure. The multi-channel and single pin model is used for core neutronics and thermal calculations. A core is normally represented by six channels: inner core, outer core, control rods, radial blanket, radial shield and the hottest channel characterized by the maximum power-to-flow ratio in the steady state. The reactor power transient is calculated by the point kinetics model with six delayed neutron precursor groups. The reactivity feedback effects are calculated by taking into account the spatial distribution of the reactivity coefficients of core materials including those for coolant, steel Doppler and fuel volumetric expansion. The thermal expansion of the structure is also considered for the reactor vessel, control rod drive lines, fuel subassembly elements, and core support structure. The radial displacement is also modeled for the core and core support structure.

CODES FOR 3-DIMENSIONAL THERMOHYDRAULIC CALCULATION OF FAST REACTOR CORE IN STEADY STATE, TRANSIENT AND ACCIDENT CONDITIONS

Yu.K. BUKSHA, E.E. MARINENKO, A.A. TOUZOV
State Scientific Center of Russian Federation,
Institute of Physics and Power Engineering,
Obninsk, Kaluga Region, Russian Federation

Abstract

For the analysis of transient and emergency processes during reactor operation it is necessary to have a set of codes, which calculate physical processes with a various degree of accuracy. Codes CORT and BUMT for three-dimensional thermohydraulic calculation of fast reactor core in steady stae, transient and accident conditions are described in this paper.

The code CORT calculates thermohydraulics of the whole fast reactor core or group of subassemblies in simplified approximation. The core is described as a set of coupled one-dimensional channels or is divided into a set of ring zones, each of those is also represented by one subassembly (S/A).

The detailed three-dimensional calculation of particular S/A is carried out by code BUMT.

For description of S/A thermohydraulics the authors have chosen so called "subchannel model". In this model the S/A is split into number of channels exchanging one by one with mass, momentum and energy. The coefficients of inter channel exchange are calculated on the basis of empirical correlations. The subchannel model is supplemented by detailed (two-dimensional in each axial cross-section) calculation of fuel pin and S/A wrapper temperatures.

For solution of hydrodynamic equations the full-implicit scheme is used.

Code BUMT was verified [10] using experimental data for S/A-simulators and results of calculations obtained by other codes [11], [12].

These codes when used in complex with neutronic code and first circuit thermohydraulic code could describe in detail the thermal state of coolant and performance of fuel pins and construction elements of reactor during steady and transient states of its operation.

1. INTRODUCTION

To ensure efficient and safe operation of fast reactor it is necessary to solve a wide spectrum of problems, connected with performance substantiation of the reactor core in nominal and emergency operation conditions.

The basis of this substantiation is the ability of designers to predict rather accurately the S/A temperature state. Thus, the development of mathematical models and codes for thermohydraulic calculation of S/As is an important task. The thermohydraulic calculation consists of obtaining coolant temperature fields and velocity and temperature fields in fuel pins and S/A wrapper, taking into account non-uniform distribution of parameters in fuel pins bundle (cross-sections, coolant flow rates, power generation, etc.).

One of the most important factors which defines temperature and velocity fields in S/A, is transverse exchange by mass, momentum and energy (so called inter-channel exchange). The calculation of inter channel exchange coefficients are based mainly on empirical correlations.

One of the possible approaches to description of thermohydraulic state of S/A, which takes into account the interactions between channels, complex geometry of S/A and its deformations, is a so-called subchannel method of S/A calculation [4], [5], [11], [12]. In this method the S/A is described as a set of interacting channels. The method is also supplemented by detailed calculation of temperature distribution in fuel, fuel pins cladding and S/A wrapper. This approach is implemented into code BUMT.

However, the detailed calculation of each S/A of the core could require a lot of time and powerful computers. Therefore, it seems reasonable to calculate the core using simplified models. The reactor core is represented as a set of coupled one-dimensional channels or split into a set of ring zones, each of those is also represented by one subassembly (S/A). This approach was used in code CORT. The calculational results of code CORT could be used as thermal boundary conditions for detailed three-dimensional calculations of the particular S/A.

The integration of these codes with neutronic code and first circuit thermohydraulic code into one calculational unit will allow to describe in detail the state of coolant, fuel and construction elements of the reactor either in steady-state or transient modes of its operation.

2. THREE-D TRANSIENT CALCULATION OF S/A THERMOHYDRAULICS.

2.1. Mathematical model.

The aim of thermohydraulic calculation of reactor core S/A is to obtain the distributions of coolant pressure and velocity fields, distributions of temperature fields in coolant, fuel, fuel pins cladding and S/A wrapper in steady state and during transient processes.

The fast reactor S/A consists of fuel pin bundle, enclosed into hexagonal wrapper. The fuel pins are located in triangle geometry. Fuel pins are hold on by two grids and are spaced by one-way coiled wires. The side fuel pins is spaced by elliptic wire. In the peripheral cells the outers for regulating coolant heating could be placed.

The subchannel approach is based on the consideration of velocity, pressure and enthalpy values averaged over the channel. For each elementary channel the system of equations of mass, momentum and energy macro-transfer is written. There are three types of channels in S/A: central, side and corner (Fig. 1).

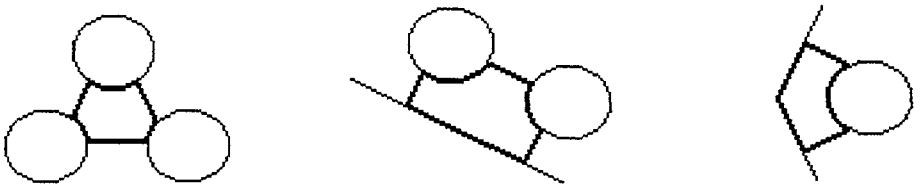

Fig. 1. S/A channels: 1 - central channel; 2 - side channel; 3 - corner channel.

In subchannel model the equations of macro-transfer are obtained on the basis of integration of initial differential equations written in Reynolds form for turbulent flow on the elemental channel cross-section. The detailed derivation of the equations of subchannel model is given in papers [4, 5]. The final equations for calculation of averaged flow parameters in channel *i* have the following form:

Mass conservation equation:

$$\frac{\partial}{\partial t}\rho_i S_i + \frac{\partial}{\partial z}\rho_i V_i S_i + \sum_j \rho_{ij} W_{ij} \Delta x_{ij} = \sum_j \mu_{ij}^{\rho} V_{ij}^{*} (\rho_j - \rho_i)\overline{S}_i \qquad (1.1.1)$$

Axial component of momentum conservation equation:

$$\frac{\partial}{\partial t}\rho_i V_i S_i + \frac{\partial}{\partial z}\rho_i V_i V_i S_i + \sum_j \rho_{ij} V_{ij}^{**} W_{ij} \Delta x_{ij} = -S_i \frac{\partial P}{\partial z} + \rho_i g_z S_i +$$

$$\sum_j \mu_{ij}^{V} \rho_{ij} V_{ij}^{*} (V_j - V_i)\overline{S}_i - \frac{\xi_i}{2 d_g} \rho_i V_i |V_i| S_i + \frac{\partial}{\partial z}\rho_i (\nu + \nu_T) S_i \frac{\partial}{\partial z} V_i + \rho_i f_i \qquad (1.1.2)$$

Transverse component of momentum conservation equation:

$$\frac{\partial}{\partial t}\rho_{ij}W_{ij} + \frac{\partial}{\partial z}\rho_{ij}W_{ij}V^{*}_{ij} = \frac{P_i - P_j}{\Delta\tilde{y}_{ij}} - \frac{\xi_{ij}}{2\Delta x_{ij}}\rho_{ij}W_{ij}|W_{ij}| + \rho_{ij}f_{ij} \qquad (1.1.3)$$

Enegry conservation equation:

$$\frac{\partial}{\partial t}\rho_i h_i S_i + \frac{\partial}{\partial z}\rho_i h_i V_i S_i + \sum_j \rho_{ij}h_{ij}W_{ij}\Delta x_{ij} = q_V S_i + \sum_k q_{ki}\Pi_{ki} + \sum_j \mu^{h}_{ij}\rho_{ij}V^{*}_{ij}(h_j - h_i)\bar{S}_i + \frac{\partial}{\partial z}\frac{\lambda+\lambda_T}{C_p}S_i\frac{\partial h_i}{\partial z} \qquad (1.1.4)$$

where: ρ_i и ρ_j - coolant density in channels i and j;

ρ_{ij} - coolant density on the boundary of channels i and j;

h_i и h_j - coolant enthalpy in channels i and j;

h_{ij} - coolant enthalpy on the boundary of channels i and j;

Θ_i - coolant temperature in channel i;

P_i - pressure in channel i;

S_i и $\bar{S}_i$ - local and average cross-section area of channel i;

Δx_{ij} - width of the gap between channels i and j;

Δy_{ij} - effective distance of interaction between cells;

V_i, V_j - axial component of coolant velocity in channels i, j;

V^{*}_{ij} $= 0.5*(V_i+V_j)$;

V^{**}_{ij} - axial velocity in donor cell;

W_{ij} - transverse component of velocity in the gap between channels i and j;

μ^{ρ}_{ij}, μ^{v}_{ij}, μ^{h}_{ij} - coefficients of inter-channel exchange by mass, momentum and energy;

ξ_i - coefficient of axial hydraulic resistance;

d_g - hydraulic diameter of channel i;

f_i, f_{ij} - mass forces in axail and transverse directions;

ν и ν_T - molecular and turbulent kinematic viscosity coefficients;

λ и λ_T molecular and turbulent heat conductivity coefficients;

q_V - internal power generation in fluid;

q_{ki} - heat flux from fuel pin *k* to coolant in channel *i*, or heat flux from point *k* of the wrapper to coolant in channel *i* for peripheral channel;

Π_{ki} - perimeter of contact of fuel pin *k* and coolant in channel *i*.

The energy conservation equation (1.1.4) can be converted into equation for calculation of coolant temperature:

$$C_{pi}\left(\rho_i\frac{\partial}{\partial t}\Theta_i S_i + \rho_i\frac{\partial}{\partial z}\Theta_i V_i S_i + \sum_j \rho_{ij}\Theta_{ij}W_{ij}\Delta x_{ij}\right) = q_V S_i + \sum_k q_{ki}\Pi_{ki} + \sum_j \mu^{h}_{ij}\rho_{ij}C_{pij}V^{*}_{ij}(\Theta_j - \Theta_i)\bar{S}_i + \frac{\partial}{\partial z}(\lambda+\lambda_T)S_i\frac{\partial\Theta_i}{\partial z} \qquad (1.1.5)$$

The system of equations (1.1.1)-(1.1.5) is supplemented by the following boundary conditions: the walls of the wrapper are impermeable (normal component of coolant velocity is equal to zero), the coolant pressure and temperature at inlet of S/A are given, the coolant pressure at outlet of S/A is given.

It should be noted that system of equations (1.1.1)-(1.1.5) describes in common way thermohydraulics of coolant in the free-shaped channel with different cross-sections in axial direction. This allows to take into account during calculation of S/A the deformation (such as wrapper shape changing, bending and displacing of fuel pins, etc.) which appears either during operation or as a sequence of technological deviations in process of S/A fabrication.

The presented subchannel model is supplemented by detailed (two-dimensional in each axial cross-section) calculation of temperature distributions in fuel, fuel pin cladding and S/A wrapper.

To close the system of equations for subchannel model, the empirical correlations for coefficients of heat transfer, coefficients of hydraulic resistance for axial and transverse coolant flow and coefficients of inter-channel exchange by mass, momentum and energy are used.

2.2. Algorithm for solution of finite-difference equations system.

When choosing the scheme of finite-difference approximation of equations that describe the thermohydraulics of coolant and temperature fields of fuel pins and S/A wrapper, the authors tried to use economical schemes without restrictions (or with such restrictions but physically validated) on the time step of calculation. The reason was that the code, in which the chosen scheme should be used, must calculate the processes with different duration.

For the solution of equations system the full-implicit scheme IMPL, based on the idea of method SIMPLE, was used [7, 8]. The appliance of fully implicit scheme that has no restriction on time step can essentially decrease the duration of calculation of slow processes. In the fully implicit scheme the following difference time approximation is used:

$$\frac{(\rho S)_i^n - (\rho S)_i^{n-1}}{\delta t} + \frac{\partial}{\partial z}(\rho V S)_i^n + \sum_j (\rho W \Delta x)_{ij}^n = \sum_j (\mu_{ij}^{\rho} V_{ij}^* (\rho_j - \rho_i)\bar{S}_i)^n \quad (1.2.1.)$$

$$\frac{(\rho VS)_i^n - (\rho VS)_i^{n-1}}{\delta t} + \frac{\partial}{\partial z}(\rho VVS)_i^n + \sum_j (\rho V^{**} W \Delta x)_{ij}^n =$$

$$= -S_i\left(\frac{\partial P_i}{\partial z}\right)^n + \frac{\partial}{\partial z}(\rho_i \nu S_i)^n \frac{\partial}{\partial z}(V_i)^n + \sum_j (\mu_{ij}^{V} \rho_{ij} V_{ij}^* (V_j - V_i)\bar{S}_i)^n - \quad (1.2.2.)$$

$$- \left(\frac{\xi_i}{2 d_g} \rho_i V_i |V_i| S_i\right)^n + (\rho_i f_i S_i)^n$$

$$\frac{(\rho W)_{ij}^n - (\rho W)_{ij}^{n-1}}{\delta t} + \frac{\partial}{\partial z}(\rho_{ij} W_{ij} V_{ij}^*)^n = \left(\frac{P_i - P_j}{\Delta \tilde{y}_{ij}}\right)^n -$$

$$- \left(\frac{\xi_{ij}}{2\Delta x_{ij}} \rho_{ij} W_{ij} |W_{ij}|\right)^n + (\rho_{ij} f_{ij})^n \quad (1.2.3)$$

$$(\rho_i C_{pi})^n \left(\frac{(\Theta_i S_i)^n - (\Theta_i S_i)^{n-1}}{\delta t} + \frac{\partial}{\partial z}(\Theta_i V_i S_i)^n + \sum_j (\rho_{ij} \Theta_{ij} W_{ij} \Delta x_{ij})^n\right) =$$

$$= (q_V S_i)^n + \sum_k (\alpha_{ki}(T_k - \Theta_i)\Pi_{ki})^n + \sum_j (\mu_{ij}^h \rho_{ij} C_{pij} V_{ij}^*(\Theta_j - \Theta_i)\bar{S}_i)^n + \quad (1.2.4)$$

$$+ \frac{\partial}{\partial z}(\lambda S_i)^n \frac{\partial(\Theta_i)^n}{\partial z}$$

$$(\rho C_p)^n \frac{T^n - T^{n-1}}{\delta t} = (\nabla \lambda \nabla T)^n + (q_v)^n \quad (1.2.5)$$

where: dt - time step, indexes *n* and *n-1* are related to values on current and previous time step.

The system of equations (1.2.1) - (1.2.5) is solved by iteration method. On each iteration step the following procedures are carried out:

(1) Calculation of axial and transverse components of velocity respectively:

$$\rho_i^{n,m-1} S_i^n \frac{V_i^{n,m^*} - V_i^{n,m-1}}{\delta t'} + \frac{(\rho_i V_i)^{n,m-1} S_i^n - (\rho V_i)^{n-1} S_i^{n-1}}{\delta t} + \frac{\partial}{\partial z}(\rho_i V_i)^{n,m-1} V_i^{n,m} S_i^n +$$

$$+ \sum_j (\rho_{ij} W_{ij})^{n,m-1} \Delta x_{ij}^n V_{ij}^{**n,m} = -(S_i)^n \frac{\partial P_i^{n,m-1}}{\partial z} + \frac{\partial}{\partial z}(\rho_i \nu)^{n,m-1} S_i^n \frac{\partial}{\partial z}(V_i)^{n,m} +$$

$$+ \rho_i^{n,m-1} f_i^n S_i^n + \sum_j (\mu_{ij}^V \rho_{ij} V_{ij}^*)^{n,m-1} (V_j^{n,m} - V_i^{n,m}) \bar{S}_i^n - \quad (1.2.6)$$

$$- \left(\frac{\xi_i}{2 d_g} \rho_i |V_i| \right)^{n,m-1} (2 * V_i^{n,m} - V_i^{n,m-1})$$

$$\rho_{ij}^{n,m-1} \frac{W_{ij}^{n,m} - W_{ij}^{n,m-1}}{\delta t'} + \frac{(\rho W)_{ij}^{n,m-1} - (\rho W)_{ij}^{n-1}}{\delta t} + \frac{\partial}{\partial z}(\rho_{ij} V_{ij}^*)^{n,m-1} W_{ij}^{n,m} =$$

$$= \left(\frac{P_i - P_j}{\Delta \tilde{y}_{ij}} \right)^{n,m-1} - \left(\frac{\xi_{ij}}{2\Delta x_{ij}} \rho_{ij} |W_{ij}| \right)^{n,m-1} (2W_{ij}^{n,m} - W_{ij}^{n,m-1}) + \rho_{ij}^{n,m-1} f_{ij}^n \quad (1.2.7)$$

In the equations above the linearization of square-low terms describing the hydraulic resistance was made.

(2) Calculation of temperature of coolant, fuel pin and S/A wrapper:

$$(\rho_i C_{pi})^{n,m-1} (S_i^n \frac{\Theta_i^{n,m} - \Theta_i^{n,m-1}}{\delta t'} + \frac{\Theta_i^{n,m-1} S_i^n - \Theta_i^{n-1} S_i^{n-1}}{\delta t} +$$

$$+ \frac{\partial}{\partial z}(\Theta_i^{n,m} V_i^{n,m^*} S_i^n) + \sum_j (\rho_{ij}^{n,m-1} \Theta_{ij}^{n,m} W_{ij}^{*n,m^*} \Delta x_{ij}^n)) =$$

$$= (q_{Vi} S_i)^n + \sum_k (\alpha_{ki}^{n,m-1} (T_k^{n,m-1} - \Theta_i^{n,m}) \Pi_{ki}^n + \quad (1.2.8)$$

$$+ \sum_j (\mu_{ij} \rho_{ij} C_{pij})^{n,m-1} V_{ij}^{*n,m^*} \bar{S}_i^n (\Theta_j^{n,m} - \Theta_i^{n,m}) + \frac{\partial}{\partial z} \lambda^{n,m-1} S_i^n \frac{\partial \Theta_i^{n,m}}{\partial z}$$

$$\rho C_p^{n,m-1} \frac{T^{n,m} - T^{n-1}}{\delta t} = \nabla \lambda^{n,m-1} \nabla T^{n,m} + q_v^n \quad (1.2.9)$$

First, the coolant temperature field is calculated, using the values of cladding and wrapper temperatures from the previous iteration. Then the temperature fields in the fuel pins and subassembly wrapper are calculated on the basis of "new" coolant temperature field.

(3) The calculation of intermediate values of coolant density is carried out on the basis of "new" temperature and "old" pressure values:

$$\rho^{n,m*} = \rho(\Theta^{n,m}, P^{n,m-1}) \tag{1.2.10}$$

(4) The equation for pressure calculation is obtained on the basis of continuity equation. Continuity equation (1.1.1) is approximated as follows:

$$\frac{\rho_i^{n,m*} S_i^{\,n} - (\rho S)_i^{\,n-1}}{\delta t} + \frac{\partial}{\partial z}\rho_i^{\,n,m*} V_i^{\,n,m} S_i^{\,n} + \sum_j \rho_{ij}^{\,n,m*} W_{ij}^{\,n,m} \Delta x_{ij}^{\,n} = \\ = \sum_j (\mu_{ij}^{\rho} V_{ij}^{*} (\rho_j - \rho_i) \bar{S}_i)^{n,m*} \tag{1.2.11}$$

To eliminate the velocity components from the equation (1.2.11), the expressions for calculation of the velocity correctors are substituted into this equation.

$$\rho_i^{n,m-1} \frac{V_i^{\,n,m} - V_i^{\,n,m*}}{\delta t'} = -\frac{\partial \delta P_i^{\,n,m}}{\partial z} \tag{1.2.12}$$

$$\rho^{n,m-1} \frac{W_{ij}^{\,n,m} - W_{ij}^{\,n,m*}}{\delta t'} = -\left(\frac{\delta P_j - \delta P_i}{\Delta \tilde{y}_{ij}}\right)^{n,m} \tag{1.2.13}$$

A Poisson-type equation for the calculation of pressure variation $dP^{n,m}$ is obtained as a result of this operation.

Finally the pressure is calculated using the following expression:

$$P^{n,m} = P^{n,m-1} + \delta P^{n\,m} \tag{1.2.14}$$

(5) Corrected values of axial and transverse components of the velocity are directly calculated on the basis of equations (1.2.11) and (1.2.12).

In equations (1.2.6) - (1.2.14) subscript m designates the iteration number, symbol * corresponds to the values of velocities, calculated at step 1.

The iterations are terminated when the given pressure accuracy is reached. In the aforesaid equations it is assumed that dt' < dt in order to improve the convergence of the iteration method. This full-implicit finite-difference scheme does not have any limitation of Courant-type on time step value, but the number of iterations can significantly increase, when the larger time step is used. The calculation experience proved that it is possible to use much longer time step (than time step from Courant condition) for the calculation of slow processes.

Detailed description of the finite-difference schemes is given in references [1], [2] and [3].

3. THERMOHYDRAULIC CALCULATION OF THE CORE ON THE BASIS ON SIMPLIFIED MODELS

The thermohydraulic calculation of the whole core can be carried out using the simplified models. Two approaches are applied. In the first, more detailed approach, the reactor core is described as a set of one-dimensional heat-exchanging flow channels, each of those represents one subassembly of the reactor. In the second approach the core is divided into a set of ring zones; each zone is also represented by one-dimensional flow channel. The mathematical model of one-dimensional flow channel is given below.

The differential equations of one-dimensional model of the subassembly are the equation of mass, momentum and energy conservation.

Mass conservation equation:

$$\frac{\partial \rho S}{\partial t} + \frac{\partial G}{\partial z} = 0 \tag{2.1}$$

Momentum conservation equation:

$$\frac{\partial G}{\partial t} + \frac{\partial}{\partial z}\frac{G^2}{\rho S} + \frac{S\,\partial P}{\partial z} + \rho g S + \frac{k|G|\,G}{2d_g \rho S} = 0 \tag{2.2}$$

Energy conservation equation:

$$\rho C_p S\frac{\partial T}{\partial t} + C_p G\frac{\partial T}{\partial z} = q_{V_*} S + \alpha_T \Pi_T (T_T - T) + \sum_{i=1}^{N} \alpha_C \Pi_C (T_C - T) \tag{2.3}$$

where:
ρ - coolant density,
S - cross-section area,
G - mass flow rate,
z - axial coordinate,
g - gravity acceleration,
k - hydraulic resistance coefficient,
d_g - hydraulic diameter,
T_T - temperature at the external surface of the fuel pin,
T_C - temperature in neighboring subassembly (or outside the core),
Π_C - perimeter of heat exchange with neighboring subassembly,
Π_T - perimeter of heat exchange with fuel pin,
α_T - coefficient of heat exchange with fuel pin,
α_C - coefficient of heat exchange with neighboring subassembly.

The fuel pins are also described by the one-dimensional model (heat conduction equation). The calculation of the whole core is performed consequently, one subassembly after another.

4. TEST CALCULATIONS AND VERIFICATION OF CODE BUMT

Several thermohydraulic calculations of BN-800-type subassembly have been performed with code BUMT to demonstrate the code capabilities [1].

An unheated subassembly, fuel pins of which are spaced by wire, is considered in order to study influence of inter-channel exchange on the temperature fields in the subassembly. The transient process is initiated by increasing of power up to its nominal value in one side fuel pin. Account of interchannel exchange decreases the coolant heating in comparison with insulated channel and leads to heat redistribution into the neighboring channels. The area of temperature "smoothing" for the subassembly with wire spacing (convective and molecular-turbulent interchannel exchange) is significantly larger, that results in decreasing of maximum coolant heating to ~15 ^{0}C (~150 ^{0}C for the subassembly without wire spacing). One-way coiled coolant flow in side channels due to wire spacing leads to an asymmetry of temperature field. The steady-state temperature field is shown in Fig. 2. The distribution of coolant temperature at the subassembly outlet during the transient process is given in Fig. 3. Generally, the results obtained during test calculations comply with the physical understanding of the transient processes in the subassemblies and the calculations, performed with one-dimensional codes.

4.1. Verification of code BUMT

The verification of code BUMT ([1], [10]) has been performed using the results of experiments, carried out with subassembly-simulator at liquid metal experimental facilities in IPPE, and the results of calculations of thermohydraulic code MIF-2 [11], [12].

The subassembly, simulating the fast reactor subassembly, consists of 37 electrically heated pins, situated in triangular bundle and enclosed in hexagonal wrapper. The fuel pin simulator is a steel tube. There is an Ni-Cr alloy heating element in the tube which provides uniform heat supply to the inner surface of simulator. The geometrical parameters of subassembly-simulators were chosen on the basis of geometrical similarity to real subassemblies of fast reactors.

4.1.1. Simulating subassembly with wire spacing and outers, uniform power distribution in subassembly cross-section

In this calculation the 37-fuel pin simulating subassembly with wire spacing and outers in side channels is considered at uniform power distribution in the subassembly cross-section.

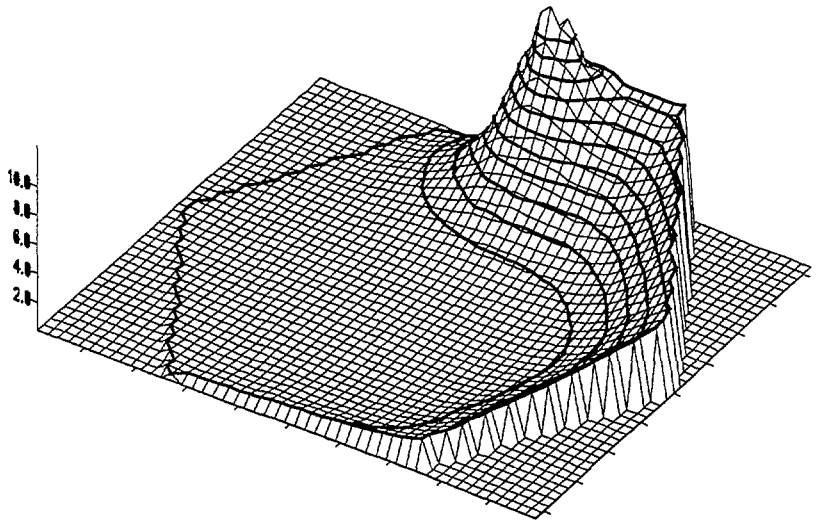

Fig. 2. Distribution of coolant heating on channels at core outlet at different moments (S/A with wire, steady state after increasing of side pin power up to nominal value, T= 10 seconds).

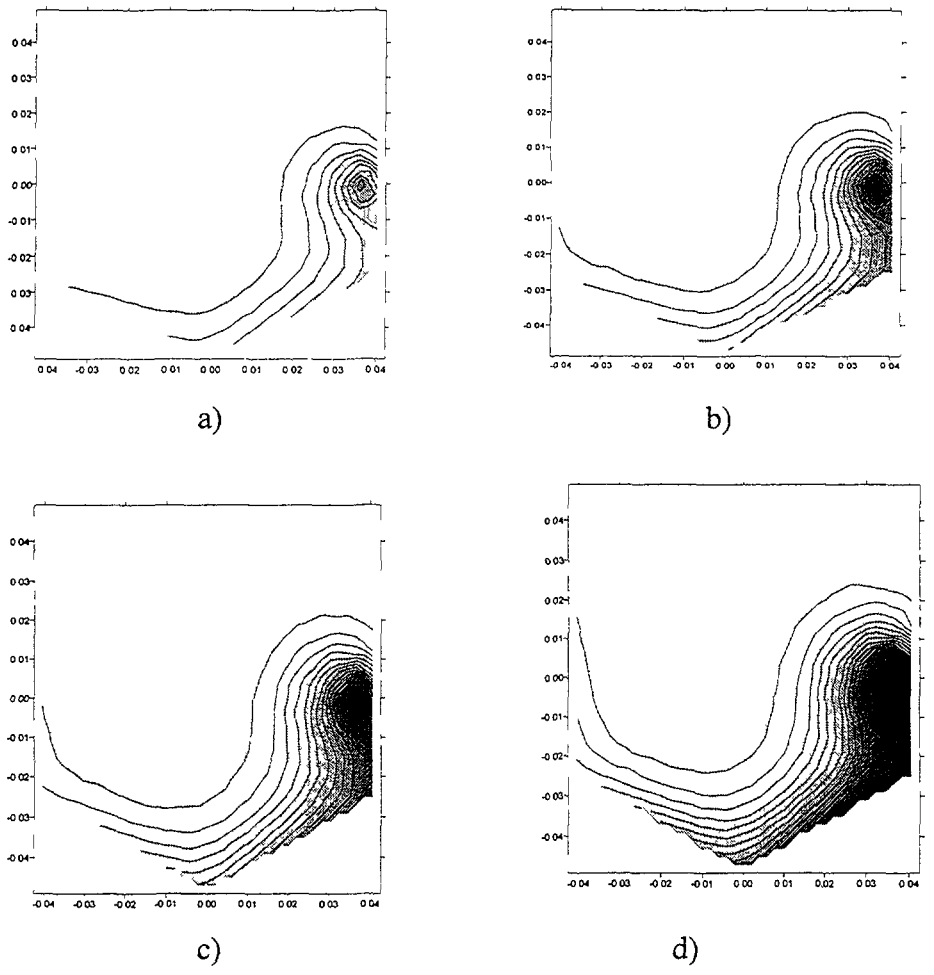

Fig 3. Distribution of coolant heating at core outlet at different moments (S/A with wire, after increasing of side pin power up to nominal value)
a) T= 1 sec; b) T= 2 sec; c) T= 3 sec; d) T = 10 sec

The experimental temperature distribution along the subassembly radius shows that there is an underheating of the coolant in the periphery channels in comparison with central channels. It can be explained by the fact that the flow area of periphery channels is greater than the one of central channels and, therefore, the flow rates in periphery channels are greater. The calculational results (temperature distribution along the radius), shown in Fig. 4 are well agreed (within the limits of experiment accuracy) with experimental data.

4.1.2. Simulating subassembly with wire spacing, without outers, non-uniform power distribution in subassembly cross-section

In the subassemblies of the reactor core periphery area, having non-uniform power distribution in the cross-section, the "smoothing out" of temperature field occurred not only near periphery of the subassembly, but on the whole subassembly cross-section.

In this calculation the 37-fuel pins simulating subassembly with wire spacing and without outers in side channels is considered at non-uniform power distribution in the subassembly cross-section.

The experimental data (Fig. 5) show that the coolant heating at the subassembly outlet follows the power distribution. The underheating of coolant is observed at the periphery of the

subassembly. The temperature field is more uniform than the power field. The transverse interchannel exchange leads to significant "smoothing" of temperature.

It can be seen from Fig. 5 that the calculation results correspond to the experimental ones.

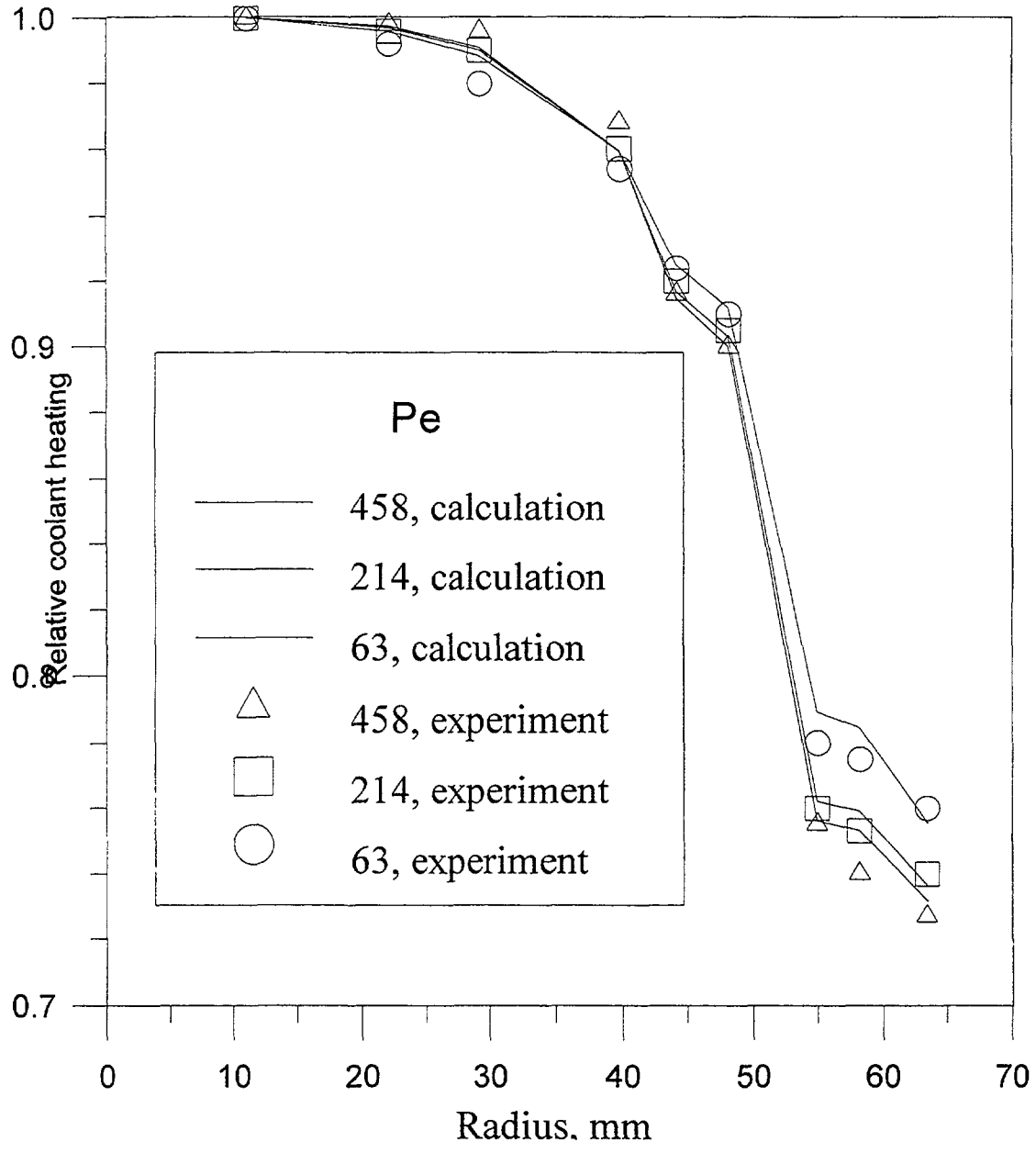

Fig. 4. Relative coolant heating depending on radius at different flow rates through S/A. S/A-simulator, 37 fuel pins, without outers in side cells, uniform power on cross-section of S/A.

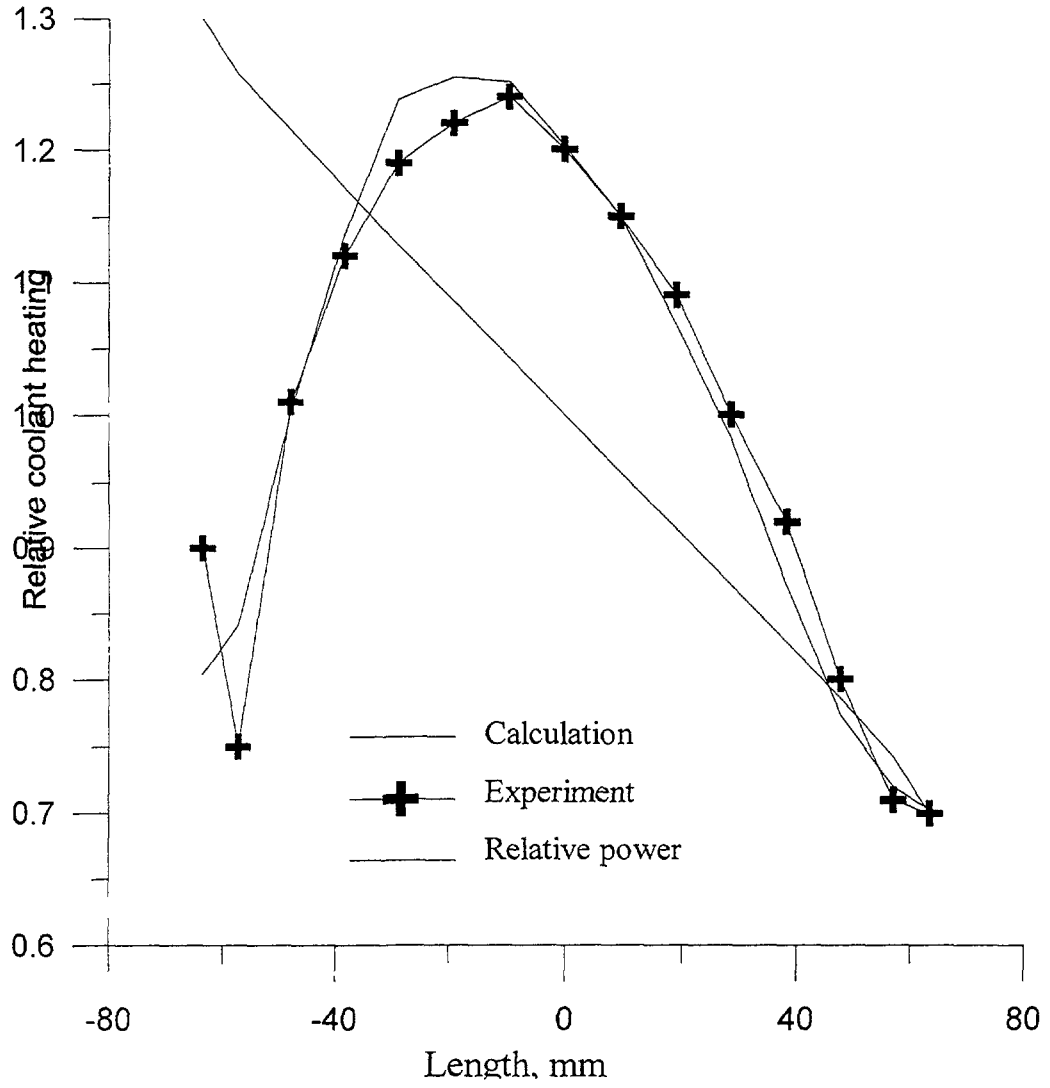

Fig. 5. Relative coolant heating depending of length. S/A-simulator, 37 fuel pins, without outers in side cells, gradient power on cross-section of S/A

$q = q_{max}(1-0.375\ l/l_0)$.

CONCLUSIONS

The codes for thermohydraulic calculation of the fast reactor core have been developed.

Code CORT calculates the thermohydraulics of the whole core of fast reactor on the basis of simplified models.

Code BUMT calculates steady-state and transient three-dimensional coolant velocity and temperature fields, fuel pin temperatures, subassembly wrapper temperatures.

Code BUMT uses the subchannel model which takes into account inter-channel exchange by mass, momentum and energy.

Code BUMT allows to carry out thermohydraulic calculation of subassemblies, having significant non-uniformity of geometrical parameters and power distribution.

The calculations, performed with code BUMT, show good compliance with experimental data and the calculations, carried out with other thermohydraulic codes.

REFERENCES

[1] BUKSHA YU.K., MARINENKO E.E., TOUZOV A.A. "Code BUMT for 3-dimensional calculation of transient thermohydraulic processes in S/A of liquid metal fast reactor core", Obninsk, IPPE report N 9346, 1996.

[2] BUKSHA YU.K., VORONKOV A.V., IONKIN A.A., MARINENKO E.E., TOUZOV A.A. "The development of code for calculation of thermohydraulic parameters of fast reactor subassembly: Mathematical model", preprint №12, 1996, KIAM, Moscow.

[3] BUKSHA YU.K., VORONKOV A.V., IONKIN A.A., MARINENKO E.E., TOUZOV A.A. "The development of code for calculation of thermohydraulic parameters of fast reactor subassembly: Finite-difference schemes", preprint №11, 1996, KIAM, Moscow.

[4] ZHUKOV A.V. et al. "Interchannel exchange in subassemblies of fast reactors: theory and physics of the process", Moscow, Energoatomizdat, 1989.

[5] ZHUKOV A.V. et al. "Interchannel exchange in subassemblies of fast reactors: calculational codes and applications", Moscow, Energoatomizdat, 1991.

[6] KIRILLOV P.L. et al. "Reference book on thermohydraulic calculations", Moscow, Energoatomizdat, 1990.

[7] MACDOUGALL J.D., LILLINGTON J.N. "The SABRE code for fuel rod clusters thermohydraulics". Nucl. Eng. and Des., 1984, Vol. 82, N 2-3.

[8] PATANKAR S.V. "Numerical methods for solution of heat exchange and fluid dynamic problems", Moscow, Energoatomizdat, 1984.

[9] GONCHAROV A.L. Preprint N130, Keldysh Institute of Applied Mathematics, 1987, Moscow

[10] KAMAEV A.A., TOUZOV A.A. "Verification of the code for 3-D thermohydraulic calculations of fast reactor subassembly", report of "Technoliga", 1997.

[11] ZHUKOV A.V., SOROKIN A.P. et al. "Verification of the code MIF-2 for subchannel hydraulic calculations of fast reactor subassembly", report of IPPE, N8182, 1992.

[12] ZHUKOV A.V., SOROKIN A.P. et al. "Influence of ununiform power generation on the temperature fields in fast reactor subassembly", report of IPPE, N7377, 1987.

CALCULATION OF FLUID FLOW AND HEAT TRANSFER INA ROD BUNDLE WITH GEOMETRICAL DISTURBANCE BASED ON THE "LOCALLY EXACT" FINITE-DIFFERENCE SCHEME

V. KRIVENTSEV, H. NINOKATA
Research Laboratory for Nuclear Reactors,
Tokyo Institute of Technology,
Tokyo, Japan

Abstract

The results of numerical simulation of fluid flow and heat transfer in the rod bundle with geometrical disturbance are presented. The geometry of the rod bundle was chosen according to the benchmark problem for 9th IAHR Working Group Meeting (April 7-9, 1998, Grenoble, France). For such a case, experimental data for local velocity and wall shear stress distributions were obtained by group of F. Mantlic at NRI (Czech Republic). Another series of the experiments which provide a data on the wall temperature profiles had been done at the IPPE (Russia). Both experiments provide complete set of data for comparison with the results of numerical simulation.

Reynolds equation for axial velocity component has been simulated in two dimensions. Turbulent shear stresses have been simulated by turbulent eddy viscosity with anisotropy defined for radial and azimuth components. Secondary flows have not been taken into consideration. The averaged energy conservation equation closed with anisotropic turbulent conductivity coefficients was simulated.

Reynolds and energy conservation equations have been discretizated by the Efficient Finite-Difference (EFD) scheme based on the "locally exact" analytical solution. The comparison of the accuracy of the EFD method and traditional central-difference scheme has been performed.

The benchmark problem has been simulated using components of the Computational Object-Oriented Library for Fluid Dynamics (COOLFD) which is a new-generation programming tool aimed to improve the development of the CFD application for complex calculation areas such as rod bundle of nuclear reactor.

Comparison of calculated results and experimental data is presented for the local shear stress, axial velocity and the wall temperature distributions in the "geometrically disturbed" region around dislocated rod.

1. GOVERNING EQUATIONS

Reynolds equation for steady-state fully developed turbulent incompressible flow in two-dimensional orthogonal coordinate system may be written for axial velocity component as following:

$$\frac{\partial}{\partial x_1}\left(\left(\nu+\nu_1^T\right)\frac{\partial W}{\partial x_1}\right)+\frac{\partial}{\partial x_2}\left(\left(\nu+\nu_2^T\right)\frac{\partial W}{\partial x_2}\right)=-\frac{1}{\rho}\frac{\partial P}{\partial z}, \qquad (1)$$

where W is an axial velocity component; ν is kinematic viscosity; ν_1^T and ν_2^T are components of anisotropic turbulent eddy diffusivity; ρ is density; P is the pressure and x_1 and x_2 are the dimensions of the orthogonal coordinate system. Here, W is unknown dependent variable. Boundary conditions were applied as zero velocities on the walls, zero stresses on the outer symmetry lines and as a constant mean velocity given by conditions of the experiment. Pressure drop $\frac{\partial P}{\partial z}$ in axial direction (which is supposed to be a constant in case of fully-developed flow) depends on wall shear stress distribution and, therefore, should satisfy a flow distribution with mean velocity above.

Also, an equation of energy conservation for steady-state fully developed turbulent incompressible flow in two-dimension was written as following:

$$\rho c_p W \frac{\partial T}{\partial z} = \frac{\partial}{\partial x_1}\left(\left(\lambda + \varepsilon_1^T\right)\frac{\partial T}{\partial x_1}\right) + \frac{\partial}{\partial x_2}\left(\left(\lambda + \varepsilon_2^T\right)\frac{\partial T}{\partial x_2}\right), \tag{2}$$

where T is temperature of the fluid; λ is thermal conductivity; ε_1^T and ε_2^T are components of anisotropic turbulent eddy thermal conductivity which were defined using turbulent Peclet number $Pe_T = \nu^T / \varepsilon^T$ as

$$\varepsilon_i^T = \frac{\nu_i^T}{Pe_T}, \tag{3}$$

As it was mentioned, secondary flows are not considered in this analysis. The reason is not only additional complexity of numerical simulation of full-components Navie-Stoks equations but also uncertainty with definition of turbulent eddy diffusivity. These coefficients are derived to fit experimental velocity distributions and for most data available it is not clear whether turbulent eddy diffusivity includes the effect of secondary flows or not. It should be noted here, that for those rod bundle flow experiments where the only axial velocity component is measured it is impossible in principal to calculate true turbulent viscosity components.

2. FINITE-DIFFERENCE DISCRETIZATION

Finite-difference method based on the "locally exact" control volume scheme was applied in this work. Detailed description of the Efficient Finite-Differencing scheme was given at [[5]]. In this section, let us consider an application of the EFD discretization to the governing equations (1) and (2). The main idea of the EFD scheme is based on the idea to use the exact analytical solution of the simplified one dimensional equation convection-diffusion in the finite-difference estimation of the interface flux of the transported quantity (shear stress in case of the Eq. (1) and heat flux in Eq. (2). This simplified equation can be written for each control volume for each direction and all other terms of the original equation including transport terms from other directions and transient term are collected in the extra-source term. In doing so, with EFD, we assume that both that extra source term and the diffusion coefficient (turbulent diffusivity in our case) are distributed linearly within the neighboring nodes. For example, for first direction, this simplified equation can be written as follows:

$$\frac{\partial}{\partial x_1}\left(\left(\nu_1\left(x_1^{i-1}, x_2^j\right) + \frac{\nu_1\left(x_1^i, x_2^j\right) - \nu_1\left(x_1^{i-1}, x_2^j\right)}{x_1^i - x_1^{i-1}}\left(x - x_1^{i-1}\right)\right)\frac{\partial W}{\partial x_1}\right) = S_1\left(x_1^i, x_2^j\right) - S_1\left(x_1^{i-1}, x_2^j\right), \tag{4}$$

where

$$\nu_1(x_1, x_2) = \nu + \nu_1^T(x_1, x_2) \text{ and } S_1(x_1, x_2) = -\frac{\partial}{\partial x_2}\left(\left(\nu + \nu_2^T(x_1, x_2)\right)\frac{\partial W}{\partial x_2}\right) - \frac{1}{\rho}\frac{\partial P}{\partial z}.$$

Taking into account the values of transported quantity at i and $i+1$ points as a boundary conditions we can solve Eq. (4) analytically and derive the expression for the shear stress value at the interface between i and $i+1$ control volumes (the following is for simplified case when the source term is assumed to be a constant):
while the regular central-difference scheme gives it as follows:

$$\rho\tau = \left(\nu + \nu_1^T\right)\frac{\partial W}{\partial x_1} = \left(\frac{v_1^l - v_1^{l-1}}{\log\frac{v_1^l}{v_1^{l-1}}}\right)\frac{W_l - W_{l-1}}{x_1^l - x_1^{l-1}} + \left(x_1 - x_1^{l-1}\right)S_1\left(\frac{v_1\left(x_1, x_2\right)}{v_1^l - v_1^{l-1}} - \frac{1}{\log\frac{v_1^l}{v_1^{l-1}}}\right), \quad (5)$$

$$\rho\tau = v_1\left(x_1, x_2\right)\frac{W_l - W_{l-1}}{x_1^l - x_1^{l-1}}, \quad (6)$$

Expression (5) was used in this work for finite-difference discretization, as well as for estimation of shear stresses at the rod walls. Similar ones were written for energy conservation equation (2) and numerical estimation of heat fluxes on the wall of the rod bundle.

3. MESHING SYSTEM

In calculation of this problem we used an orthogonal coordinate transformation. This transformation was performed using the grid generation components of the COOLFD library. First, meshing systems were generated for each typical rod as shown at the Fig. 1. The all these mesh systems were assembled together to represent the whole rod bundle. In doing so, the visual components of the COOLFD library where used as shown at the Fig. 2.

4. EDDY DIFFUSIVITY COEFFICIENTS

The coefficient of turbulent viscosity in radial direction was applied from data of Nijsing and Eifler [[2]] as follows:

$$\frac{\nu_r}{u^* \hat{y}} = \left[1 - \exp\left(-0.407\frac{y}{\hat{y}}\right)\right]\exp\left(-e\frac{y}{\hat{y}}\right), \quad (7)$$

where $e = \log\left[\frac{1-\exp(-0.407)}{0.07}\right]$.

The expression of Neelen [[3]] was used for eddy diffusivity in azimuth direction:

$$\frac{\nu_r}{u^* y} = \exp\left(u_1 \exp\left[u_2\frac{\hat{y}}{R} + u_3\right] + u_4\right) \times \left[1 + A_r\left(B_r^2 - B_r + \frac{1}{3}\right) - A_r\left(B_r - \frac{y}{\hat{y}}\right)^2\right] \quad (8)$$

where

$$u_1 = 0.118; \quad u_2 = -13.8;$$

$$u_3 = \left(\frac{2d_h}{d}\right)^{0\,238} + 3.52;$$

$$u_4 = 0.215\left(\frac{2d_h}{d}\right) + 5.1\left(\frac{S}{d}\right)^{0\,149} - 6.94;$$

$$A_r = 3.0; \qquad B_r = 0.6$$

In spite of the fact that relations above were obtained for radial and azimuth directions relatively to the rod wall, we used them directly in our case of the orthogonal for v_1 and v_2 correspondingly. The grid lines of the orthogonal meshing system are practically coincide with polar coordinate system near the wall and for the region in the center of subchannel the radial and azimuth direction cannot be defined clear.

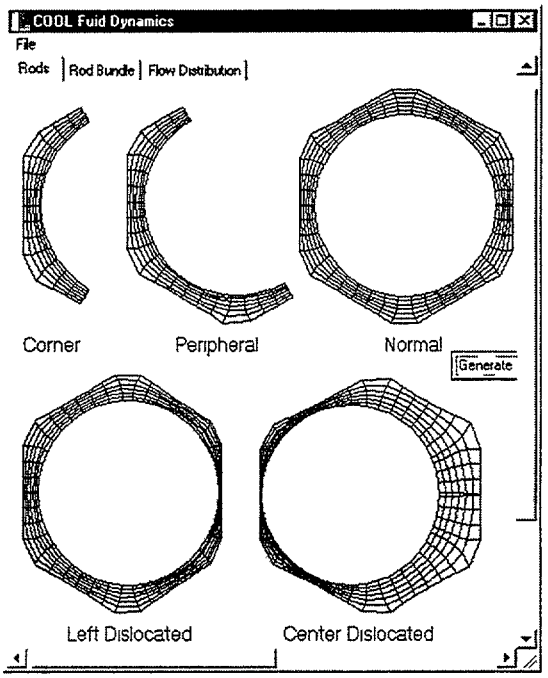

Fig. 1 Elementary grid components calculated for corner, peripheral, and central rods: regular, left-side neighbor of dislocated rod and central dislocated rod

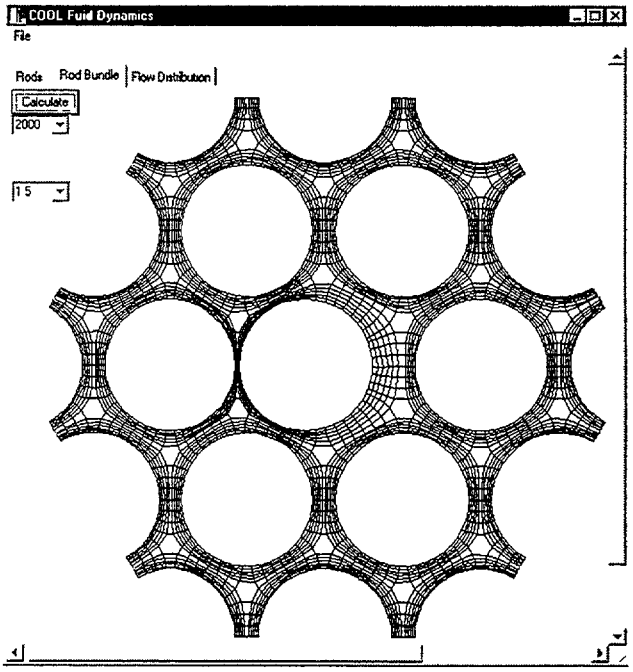

Fig. 2 Elementary grid components assembled in the rod bundle

5. NUMERICAL PROCEDURE

The computational part of the COOLFD library was used to calculate numerical solution. At this stage, the simple Gauss-Zeidel method was used to produce solution at each inner iteration. Dynamic velocities u^* were recalculated for all wall points and then, all the values of turbulent eddy diffusion and thermal conductivity would been recalculated for the entire region. An outer iteration loop was used to adjust the pressure gradient which should produce the flow distribution with mean velocity as given by experimental conditions (<W> = 48.34m/s).

The calculation of the flow distribution in the 17-pin rod bundle divided into the 8808 control volumes took about 3min in total of CPU time on Personal computer with Intel Pentium-II 400Mhz processor. In addition, the calculation of temperature distribution with energy conservation equation demands about one minute more. Some samples of the visual object which serves to calculate region are shown at the Fig. 3 and Fig. 4.

6. RESULTS OF CALCULATION

The results of numerical simulation of fluid flow were compared with experimental data presented by group of F. Mantlic at 9th IAHR Working Group Meeting (April 7-9, 1998, Grenoble, France). Calculated wall temperature distribution was compared with the liquid metal experiment performed in IPPE ([4]).

The local shear stress distributions at the wall of rods No 6, 1, and 7 are shown at the Fig. 5, Fig. 6 and Fig. 7. Here, one can see that traditional central-difference scheme underestimates the shear stresses significantly while EFD scheme generate quite satisfactory results (taking into account the complexcity of the problem itself as well as insufficient data on eddy diffusivity for rod bundle with geometrical disturbance). The samples of the velocities profiles for rods 6 and 7 are given at the plots in Fig. 8 and Fig. 9.

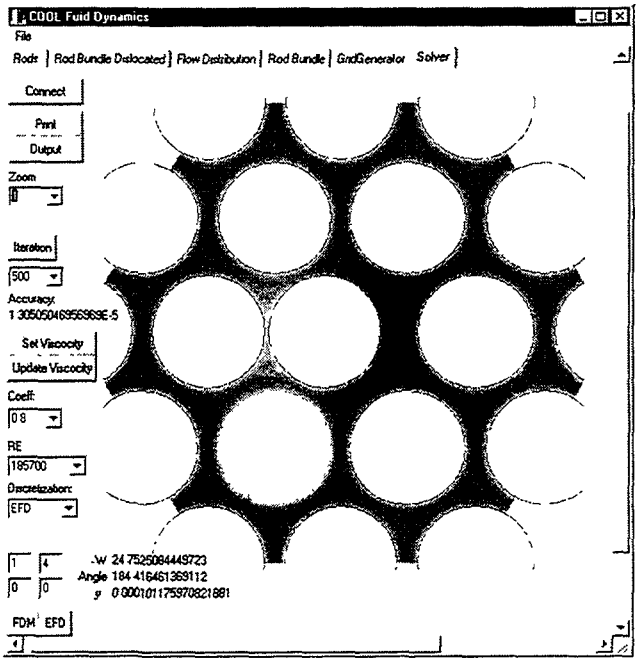

Fig. 3 Sample of flow distribution at the experimental 17-pin rod bundle with disclocated central rod

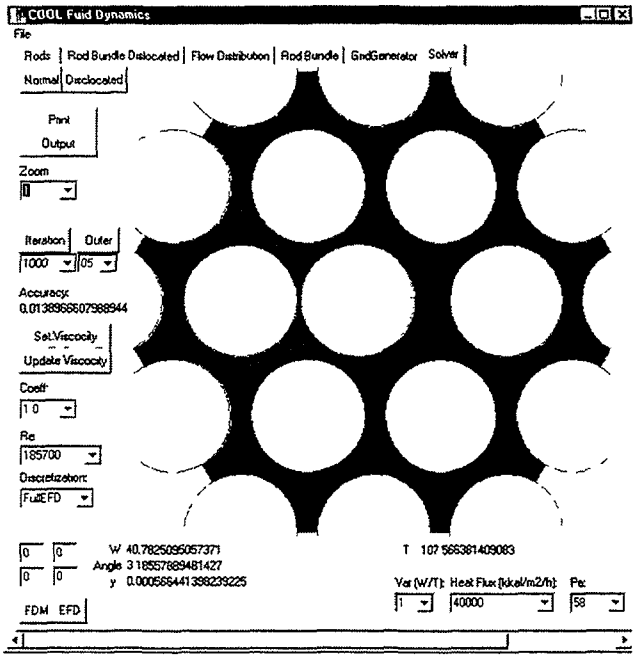

Fig. 4 Sample of temperature distribution at the 17-pin rod bundle with dislocated central rod

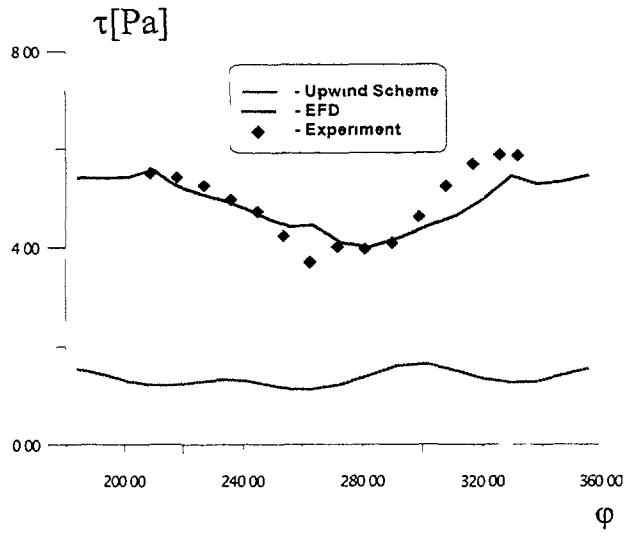

Fig. 5 Wall shear stress distribution; Rod No 6

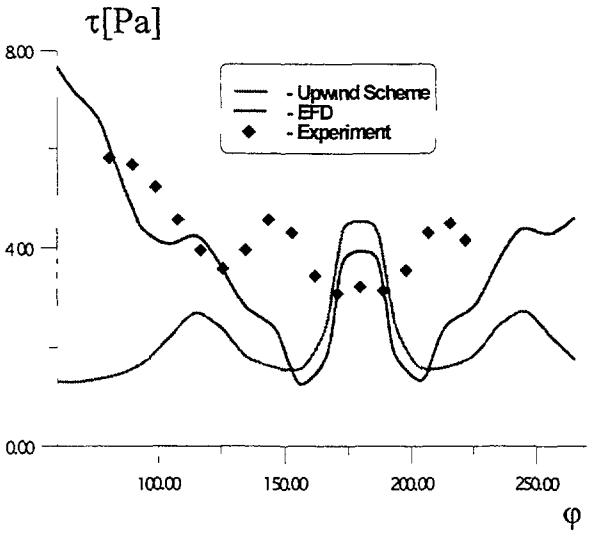

Fig. 6 Wall shear stress distribution; Rod No 1

The comparison of calculated temperature distribution around the central dislocated rod with experimental data are shown at Fig. 10 and Fig. 11 for Peclet numbers 218 and 58 correspondingly.

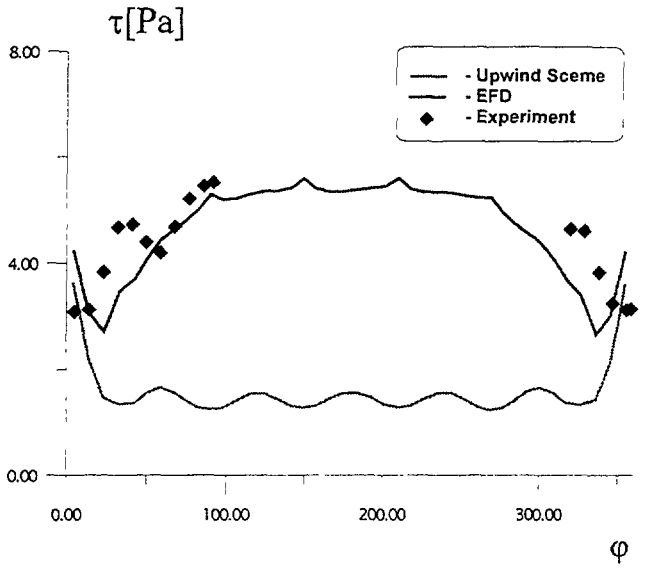

Fig. 7 Wall shear stress distribution; Rod No 7

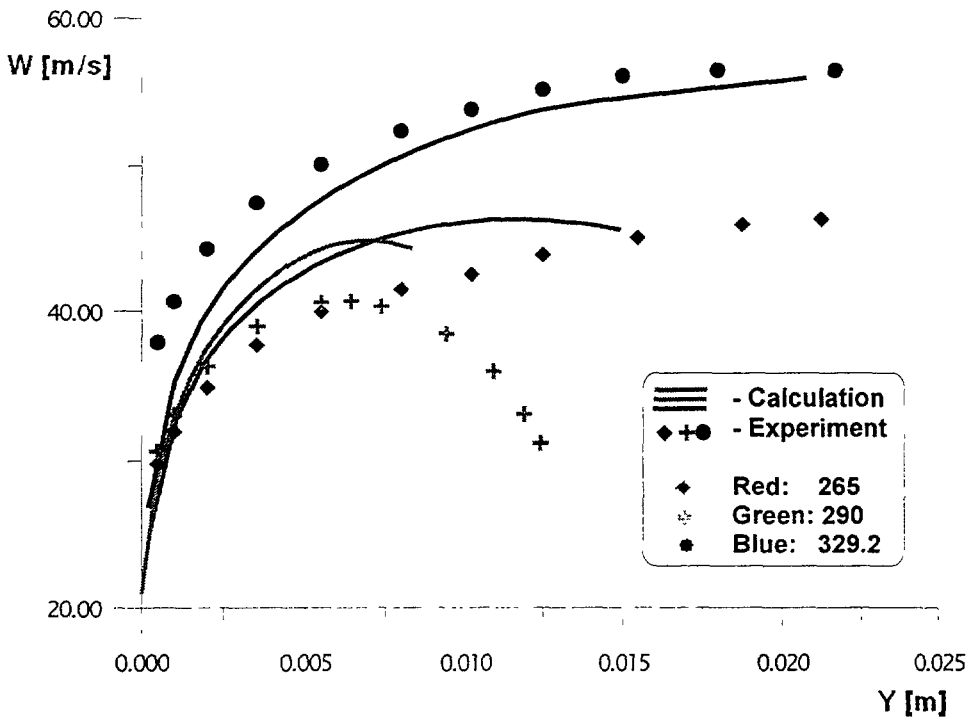

Fig. 8 Axial Velocity Distribution; Rod No 6

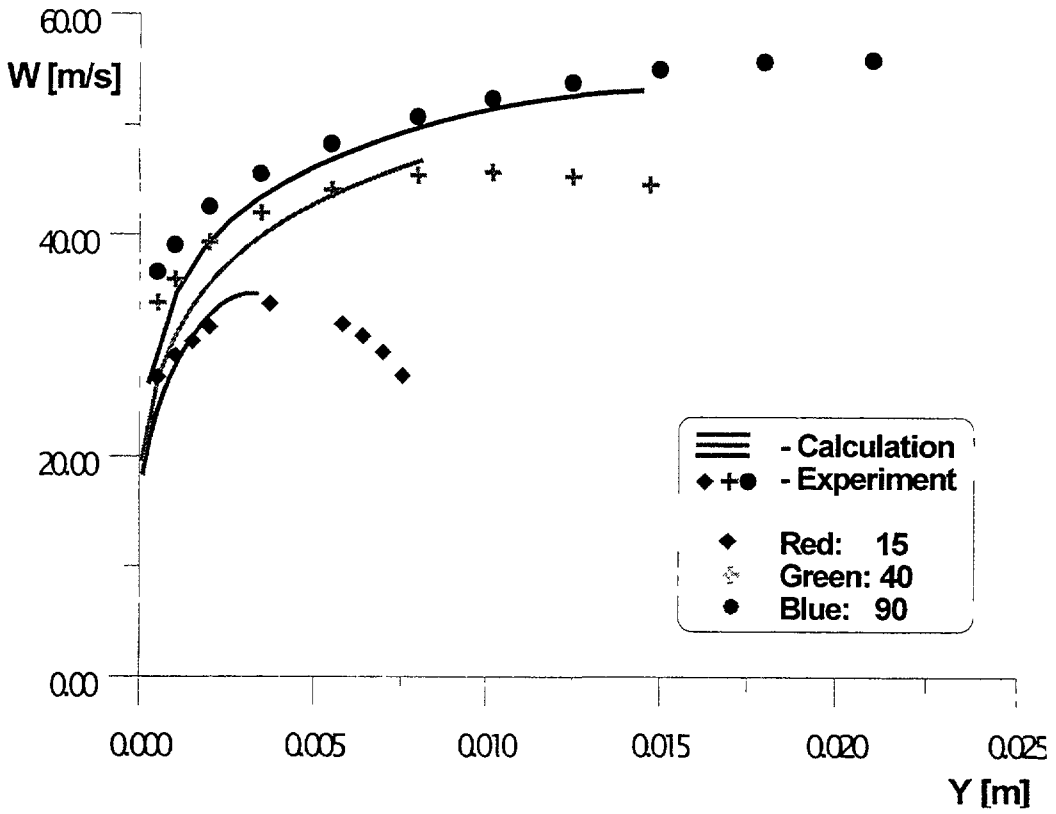

Fig. 9 Axial Velocity Distribution; Rod No 7

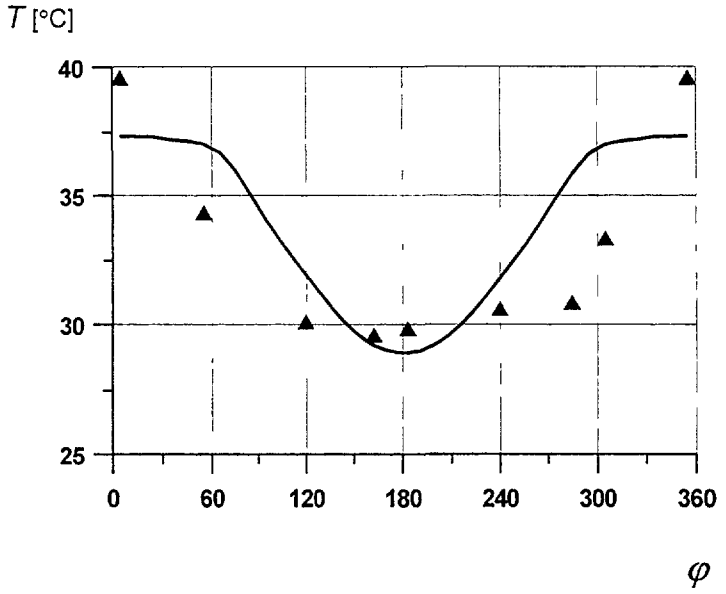

Fig. 10 Wall Temperature Distribution Around the Central Rod; Pe = 218

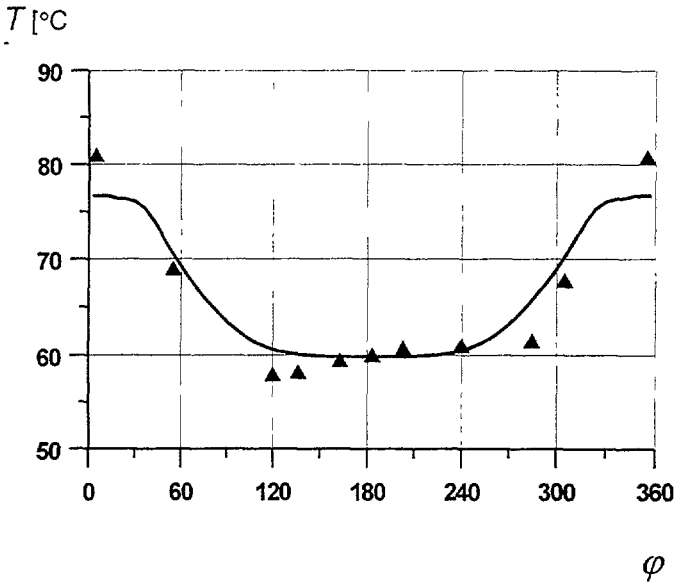

Fig. 11 Wall Temperature Distribution Around the Central Rod; Pe = 58

7. CONCLUDING REMARKS

The results of numerical calculation show a satisfactory agreement with experimental data both for flow and temperature distribution. It proves the applicability of the COOLFD software and EFD scheme for numerical simulation of fluid flow and heat transfer in complex regions, such as a rod bundle of nuclear reactor. Some additional work should be done to improve the calculation procedure. First of all, more accurate model of the turbulence should be implemented. Also, authors believe that three-dimensional simulation, taking into account secondary flows, could improve the numerical accuracy significantly.

REFERENCES

[1] PATANKAR S.V., Numerical Heat Transfer and Fluid Flow, Hemisphere, Washington, D.C., 1980.

[2] NIJSING R., EIFLER W., "Temperature Fields in Liquid-Metal-Cooled Rod Assemblies", Progress in Heat and Mass Transfer, 1971, v.7, p. 115-149

[3] NEELEN N., "Modeling of Transport of Momentum in Parallel Turbulent Flow Through a Rod Bundle", Dr. Eng. Thesis, TU Braunschweig, Germany, 1986.

[4] ZHUKOV A.V., KIRILLOV P.L., MATUHIN N.M., SOROKIN A.P. et al, "Thermal Hydraulics Analysis of Fuel Assemblies of Fast Reactor cooled by liquid metal", Moscow, Energoatomizdat, 1985 (in Russian)

[5] KRIVENTSEV V., NINOKATA H., "An Effective Finite-Difference Scheme For Transient Problems of Heat and Mass Transfer", Proceeding of 8th International Topical Meeting on Nuclear Reactor Thermal-Hydraulics (Nureth8), Kyoto, 1997, Vol.1, pp.572-580

[6] KRIVENTSEV V., NINOKATA H., "An Application of Object-Oriented Programming in Numerical Simulation of Fluid Dynamics in Complex Geometry", Proceeding of Spring Meeting of the JSME, Tokyo, March-April 1998

FLOW RESISTANCE IN ROD ASSEMBLIES

A.S. KORSUN, M.S. SOKOLOVA
Moscow Engineering Physics Institute,
Institute of Physics and Power Engineering,
Moscow, Russian Federation

Abstract

The general form of relation between the resistance force and the velocity vector, resistance tensor structure and possible types of anisotropy in the flow thorough such structures as rod or tube assemblies are under discussion. Some questions of experimental determination of volumetric resistance force tensor are also under consideration.

There is a resistance force that acts from the solid component of the porous body on the fluid flow in it. The specific value of this force, i.e. divided to the unit volume of liquid phase, can be performed as:

$$\vec{f} = -\rho K \vec{u}. \tag{1}$$

The porous body model approximation in application to the fluid flow in such structures as pin or tube assemblies was developed in works [1, 2] in IPPE. In order to determine resistance force components in the flow thorough the tube assembly with the arbitrary angle between flow and assembly axis following correlations were recommended:

$$\vec{f}_z = -\rho \frac{\lambda_{fz}}{2d_h} u u_z, \quad \vec{f}_r = -\rho \frac{\lambda_{fr}}{2d_h} u u_r \tag{2}$$

Comparison of (1) and (2) shows, that the friction factor K has been a tensor with the components along the main axes:

$$k_{\eta\eta} = \frac{\lambda_{fz}}{2d_h} u, \qquad k_{\xi\xi} = \frac{\lambda_{fr}}{2d_h} u. \tag{3}$$

The correlations (2) practically have no direct experimental confirmation and as it has been shown in [3] where are reasons to doubt in their adequacy, especially in determination of the resistance force component normal to the velocity vector, i.e. the buoyancy force.

The analysis fulfilled in [3] by means of the matrix polynomial theory, showed that the resistance force can be presented as vector correlation:

$$\vec{f} = -\rho\, a(u, \mathrm{Cos}^2\varphi)\vec{u} - \rho\, b(u, \mathrm{Cos}^2\varphi)(\vec{u}\vec{n})\vec{n} \tag{4}$$

or in the equivalent tensor form:

$$f_i = -\rho K_{ij} u_j, \tag{5}$$

where K_{ij} – the resistance tensor with the components:

$$\left\{k_{ij}\right\} = \begin{pmatrix} a + bn_x n_x & bn_x n_y & bn_x n_z \\ bn_x n_y & a + bn_y n_y & bn_y n_z \\ bn_x n_z & bn_y n_z & a + bn_z n_z \end{pmatrix} \tag{6}$$

and where: $\vec{u}$, u – velocity vector and its modulus,
$\vec{n}$ – unit vector along the assembly axis,
n_x, n_y, n_z – its projections on the co-ordinate axes,
φ – the angle between the velocity vector and the assembly axis.
Matching the z- axis with the direction along the pins ($n_x = n_y = 0$, $n_z = 1$) we get:

$$\left\{k_{ij}\right\} = \begin{pmatrix} a & 0 & 0 \\ 0 & a & 0 \\ 0 & 0 & a+b \end{pmatrix}, \tag{7}$$

i.e. the main resistance tensor components are equal to

$$k_{xx} = a(u,\cos^2\varphi);\ k_{hh} = a(u,\cos^2\varphi) + b(u,\cos^2\varphi), \tag{8}$$

and they are even cosines functions of the angle between the velocity vector and the assembly axis.

Taking into account the relation (8) the resistance tensor can be written in the following form:

$$k_{ij} = k_{\xi\xi}\delta_{ij} + (k_{\eta\eta} - k_{\xi\xi})n_i n_j, \tag{9}$$

where δ_{ij} is the unit vector.

Analysing the correlations (4) and (5) some possible types of resistance anisotropy can be marked out:

1 type : $b = 0$, $a = a(u, \cos^2\varphi)$.

The resistance depends on the direction, but for any velocity vector the resistance force is opposite to it (4). The resistance tensor becomes the scalar value. The $a(u, \cos^2\varphi)$ correlation is defined from the experimental measurement results for flow resistance over inclined assembly

$$a(u, \cos^2\varphi) = \frac{\lambda_f(\varphi)}{2d_h}u. \tag{10}$$

2 type : $a = a(u)$, $b = b(u)$.

Factors a and b in (4) do not depends on the angle between the velocity vector and assembly axis and are determined by the friction factor for longitudinal and transversal flow over the tube assembly. This case agrees with the hypothesis (2). According to the correlation (4) the buoyancy force is equal to

$$f_b = \rho b u \cos\varphi \sin\varphi = \rho(k_{\eta\eta} - k_{\xi\xi})u \cos\varphi \sin\varphi.$$

3 type · The general case when $b \neq 0$ and one or both factors depends on the angle.

Experiment has to show what type of anisotropy takes place in fact.

The rough experimental scheme is shown on Fig. 1. The porous structure (tube or pin assembly) with the length l is inserted into the flat channel with the height h. The angle between the channel and assembly axes is a. The flow in the channel is longitudinal.

The steady-state flow velocity distribution in the porous media is described by the equations:

$$\frac{\partial}{\partial y}u_y u_z + \frac{\partial}{\partial z}u_z^2 = -\frac{1}{\rho}\frac{\partial P}{\partial z} + \nu_{y\delta}\left(\frac{\partial^2 u_z}{\partial y^2} + \frac{\partial^2 u_z}{\partial z^2}\right) - k_{zy}u_y - k_{zz}u_z, \tag{11}$$

$$\frac{\partial}{\partial y}u_y^2 + \frac{\partial}{\partial z}u_y u_z = -\frac{1}{\rho}\frac{\partial P}{\partial y} + \nu_{y\delta}\left(\frac{\partial^2 u_y}{\partial y^2} + \frac{\partial^2 u_y}{\partial z^2}\right) - k_{yy}u_y - k_{yz}u_z, \tag{12}$$

$$\frac{\partial u_z}{\partial z} + \frac{\partial u_y}{\partial y} = 0, \tag{13}$$

$$\left.\frac{\partial u_z}{\partial y}\right|_{y=0} = 0, \quad \left.\frac{\partial u_z}{\partial y}\right|_{y=h} = 0. \tag{14}$$

According to (9) the tensor components are equal to: $(n_x = 0, n_y = \sin\alpha, n_z = \cos\alpha)$:

$$k_{yy} = k_{\eta\eta}\sin^2\alpha + k_{\xi\xi}\cos^2\alpha,$$
$$k_{zz} = k_{\eta\eta}\cos^2\alpha + k_{\xi\xi}\sin^2\alpha, \tag{15}$$

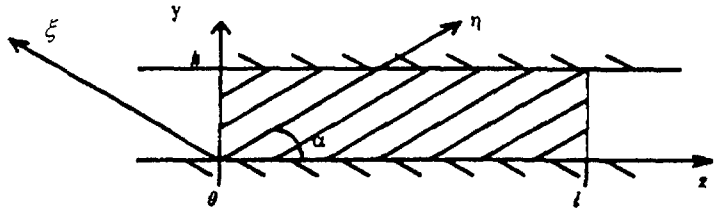

Fig. 1.

$k_{yz} = k_{zy} = (k_{\eta\eta} - k_{\xi\xi})\sin\alpha \cos\alpha$.

The effective viscosity can be approximated as:

$$v_{ef} = C_V u d_h, \tag{16}$$

where C_V is constant value.

Far away from the entrance of the porous body the velocity distribution becomes equable over the cross section:

$$u_z = u_0 = \text{const}, \quad u_y = 0. \tag{17}$$

According to (11) and (12) the pressure drop distribution is:

$$-\frac{1}{\rho}\frac{\partial P}{\partial z} = k_{zz} u_0, \quad -\frac{1}{\rho}\frac{\partial P}{\partial y} = k_{yz} u_0, \tag{18}$$

i.e. for such flow, when the angle between the velocity vector and assembly axis exists, not only longitudinal but also transversal pressure gradient occurs. The k_{zz} and k_{yz} factors can be calculated by means of the measured pressure gradients and in accordance with the correlation (15) the main tensor components for the angle set can be defined:

$$k_{\eta\eta} = k_{zz} + k_{zy}\,\mathrm{tg}\alpha, \quad k_{\xi\xi} = k_{zz} - k_{zy}\,\mathrm{ctg}\alpha. \tag{19}$$

The experimental measurement of the transversal pressure gradient as well as the longitudinal one is essential and important because it is impossible to define two unknown values ($k_{\eta\eta}$, $k_{\xi\xi}$) only by measuring one parameter - the resistance of the longitudinal flow.

Fig. 2 shows some results of numerical calculations of the problem (11 – 14) from the article [3]. The calculations result show that in a case of liquid flow in the channel with the anisotropic porous insert the non-uniformity of the longitudinal velocity through the channel height occurs while the pressure is approximately constant. Alignment of the non-uniformity of the velocity distribution (Fig. 2a) and increasement of the transversal pressure drop (Fig. 2b) take place on the "inlet" section of the porous insert. Near the porous insert exit the "outlet" section exists, where the inverted changes take place. The transversal pressure drop decreases and the uniform velocity distribution becomes non-uniform. The velocity distribution non-uniformity in the "outlet" section id opposite to those in the "inlet" section. In the central part of the insert the velocity and pressure drop distributions conform to the solution (17), (18).

The numerical calculation results and approximate analytical solution [4] show that the "inlet" and "outlet" sections of the flow lightly influence to the longitudinal pressure drop, and the longitudinal pressure gradient can be defined be measuring total pressure drop for the rod assembly. The transversal pressure drop ought to be measured outside of the "inlet" or "outlet" sections of the porous insert, as it springs out the Fig. 2b.

In order to estimate the "inlet" and "outlet" section length dependence on the angle and the regime parameters the approximate analytical solution of the problem (11 – 14) has been done. It has been based on the one-parameter lineal approximation for the longitudinal velocity and has used the integral form for the momentum equations (11, 12).

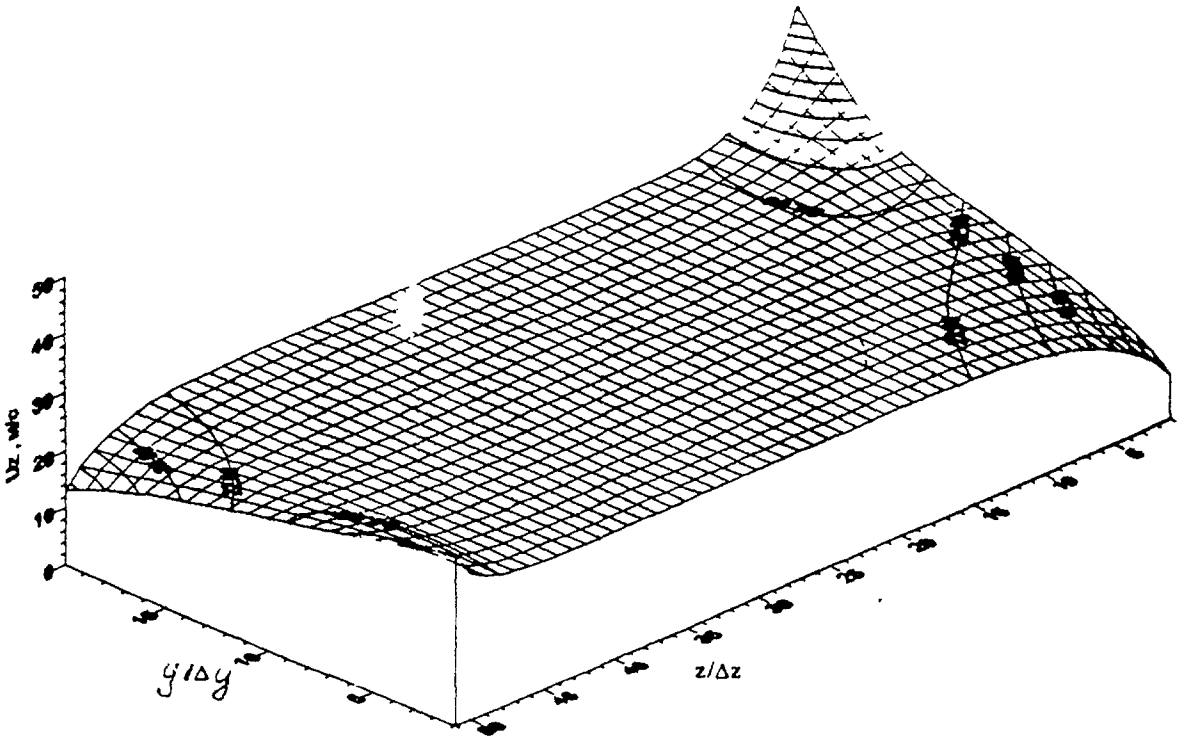

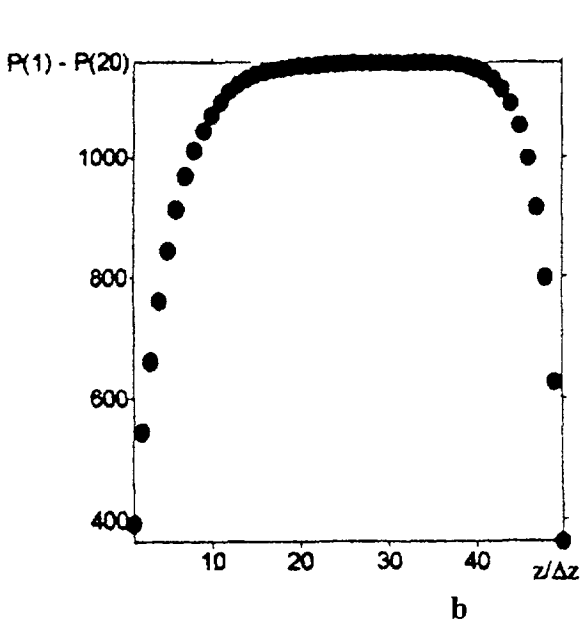

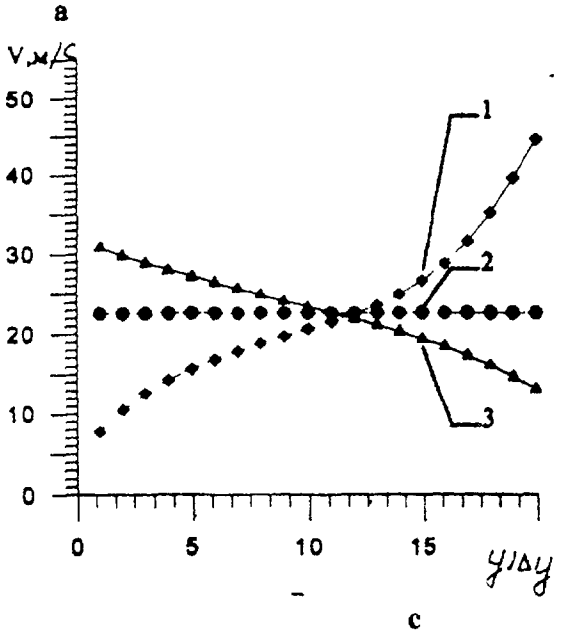

Fig. 2. The flow through the porous structure ($\alpha=10°$, $h=3$ *m*, $k_{\eta\eta}=3.8$, $k_{\xi\xi}=62$, $u_0=22.6$ *m/c/c*): a) longitudinal velocity component distribution in the channel; b) transversal pressure drop distribution along the channel: c) longitudinal velocity distribution through the height of the channel in the entrance (1), the exit (3) and in the centre (2) of the poorhouse insert.

According to the solution above the velocity irregularity decreases in accordance with the exponential law with the exponent equal to l_1 and l_2, accordingly (length of "inlet" and "outlet" sections are equal to 2-3 $l_{1,2}$):

$$l_1 / h = \left(1 + \sqrt{1 + \tilde{k}_{zz}\left(8\tilde{v} + \tilde{k}_{yy} / 3\right)}\right) \Big/ 2\tilde{k}_{zz}, \tag{20}$$

$$l_2 / h = \left(4\tilde{v} + \tilde{k}_{yy} / 6\right)\left(1 + \sqrt{1 + \tilde{k}_{zz}\left(8\tilde{v} + \tilde{k}_{yy} / 3\right)}\right)^{-1} \tag{21}$$

where $\tilde{k}_{ij} = k_{ij} h / u_0$, $\tilde{v} = v_{ef} / u_0 h$.

Fig. 3 shows the l_1 and l_2 dependence on the angle. The approximation (3) has been used for the main tensor components calculations.

The general form of the resistance force dependence on the velocity vector is defined. The main tensor resistance components are established to be the functions of the angle between the assembly axis and velocity vector. Different types of the flow resistance are possible in dependence if the different types of the functions, including the case when the resistance force vector is strictly opposite to the velocity vector for any angle , i.e. the buoyancy is absent.

The measurements of the assembly resistance for various angles of the flow only are not adequate for experimental determination of the resistance tensor. It is necessary also to measure the transversal pressure gradient in the flow. This measurement ought to be fulfilled on the stabilised part of the flow, outside of the "inlet" or "outlet" sections of the porous insert.

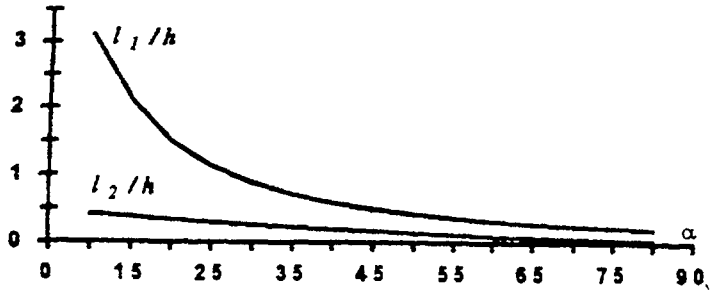

Fig. 3. Dependence of l_1 /h and l_2 /h on the angle of the flow *(d = 5 mm ,s/t = 1.25 , h = 60 mm, Re = 3e+4)*.

NOMENCLATURE

a, b – factors for $\vec{f}$ in (4);
d_h – hydraulic diameter, mm;
K, k_{ij} – resistance tensor and its components;
$\vec{n}$, n_i – unit vector and its components ($n_i = \cos(\vec{n}\vec{x}_i)$);
$\vec{f}$ – volumetric resistance force;
u, $\vec{u}$ – mean fluid velocity modulus, vector;
x, y, z, r, x_i – co-ordinates;
α – angle between assembly and channel axis (Fig. 1);
φ – angle between assembly axis and velocity vector;
λ_{fz}, λ_{fr} – friction factors for longitudinal and transversal flow through the assembly;
ρ – liquid density, kg/m;
ξ, η – main anisotropy axes directions.

REFERENCES

[1] SUBBOTIN V.I. et al., Reactor thermophysics problem solutions by means of the computers. M.: Atomizdat, 1979.

[2] MITENKOV P.M., GOLOVKO V.F., USHAKOV P.A., JURJEV JU.S. Design of Heat exchanging apparatus for APP. M.: Energoatomizdat, 1998.

[3] KORSUN A.S., VIKULOVA S.V. To the definition of the resistance of the anisotropic porous body. "Proc. of the Second Russian National Conference on Heattransfer", M.: 26-30 Oct. 1998, (in print.)

[4] KORSUN A.S., KOROTKOVA I.S. Flow velocity distribution in the channel with anisotropic porous insert. "Proc. of the Second Russian National Conference on Heattransfer", M.: 26-30 Oct. 1998, (in print.)

MODELS AND CHARACTERISTICS OF INTERCHANNEL EXCHANGE IN PIN BUNDLES COOLED BY LIQUID METAL

G.P. BOGOSLOVSKAYA, A.V. ZHUKOV, A.P. SOROKIN
State Scientific Center of Russian Federation,
Obninsk, Kaluga Region, Russian Federation

Abstract

Experimental results on convective and turbulence mass, momentum and energy exchange in pin bundle cooled by liquid metal obtained by electromagnetic and thermal track techniques are generalized. The basis for analytical models of convective, turbulence exchange by momentum and energy, as well as heat transport due to fuel pin heat conduction are presented. Correlations derived are analyzed in comparison with the other authors' data. An influence of interchannel exchange on coolant and pin temperature distributions is illustrated by some examples.

1. INTRODUCTION

The need to improve fast breeder reactor performance calls for the solution of the problems concerning thermal physical validation of fuel subassembly operation under nominal and non-nominal conditions.

Researches relating thermal hydraulics in complex geometry, as well as the data available, point once again to the computer codes for thermal hydraulic predictions based on subchannel approach [1] need an experimental consideration of coolant mixing in fuel subassemblies. Classic studies presented for examples by N.Todreas [2] and A.Zhukov [3] have revealed the individual regularities of the processes, the later investigations have enabled the relationships for mixing factors to be obtained within wide ranges of geometrical and flow parameters. According to the classification of thermal mixing processes, three main components can be selected: molecular and turbulence diffusion, convective, thermal exchange due to pin heat conduction.

Analysis of convective and turbulence exchange in fuel subassemblies cooled by liquid metal are given in [4-7]. The principle feature of mixing in fast reactor subassembly is a powerful transverse convective exchange associated with the wire wraps on fuel pins.

Diffusive inter-channel heat transfer in liquid metal as compared with water or gas coolants contains significant component due to fuel pin heat conduction. An influence of pin bundle deformation on the exchange intensity is also essential.

Systematic experimental and analytical researches performed in the Institute of Physics and Power Engineering (Obninsk) allowed these questions to be answered, the set of closing correlation needed to solve system of macro-transport equations in the framework of subchannel approximation [8] to be obtained.

The paper presents generalized data, as well as campared with the data of other authors [2, 4, 6, 11-52]. Works [7-9] have demonstrated that transverse inter-channel exchange by mass, momentum and energy is one of the most essential factor in velocity and temperature behavior in fast reactor fuel subassembly.

2. INTERCHANNEL CONVECTIVE EXCHANGE

Internal area of subassembly. Local measurements performed with the use of electromagnetic technique in liquid metal pin bundles [5] have shown that transverse mass transfer over inter-pin gap is governed by periodic (sinusoidal) law (Fig.1), that defines the

periodic (sinusoidal) variation in local mixing factors. The local mass mixing factor, representing the ratio between mass flow passing from *i*-th to *j*-th channel through the unit gap height and axial component of coolant flow rate throughout the channel, is described with a sufficient accuracy by single harmonics:

$$\mu_{ij}^{m}\left(\varphi_{ij}\right)=\left(G_{ij}/G\right)\cdot\mu_{ij,max}^{m}\cdot\sin\varphi_{ij} \tag{1}$$

where $\varphi_{ij}=(2\pi z/h)-\alpha_{ij}$ (α_{ij} is the wire wrap phase entering the j-th channel from the i-th channel).

Amplitude $\mu_{ij,max}^{m}$ (m^{-1}) in (1) follows to the formula [7,8]:

$$\mu_{ij,max}^{m}=\left(1.047/h\right)\cdot\Phi\left(s/d\right)\cdot\Psi(Re) \tag{2}$$

where functions inserted are as follow:

$$\Phi\left(s/d\right)=2.57\ \left(s/d\right)-3.57\ \exp\left(-119(s/d-1)^{2\,12}+1\right) \tag{3}$$

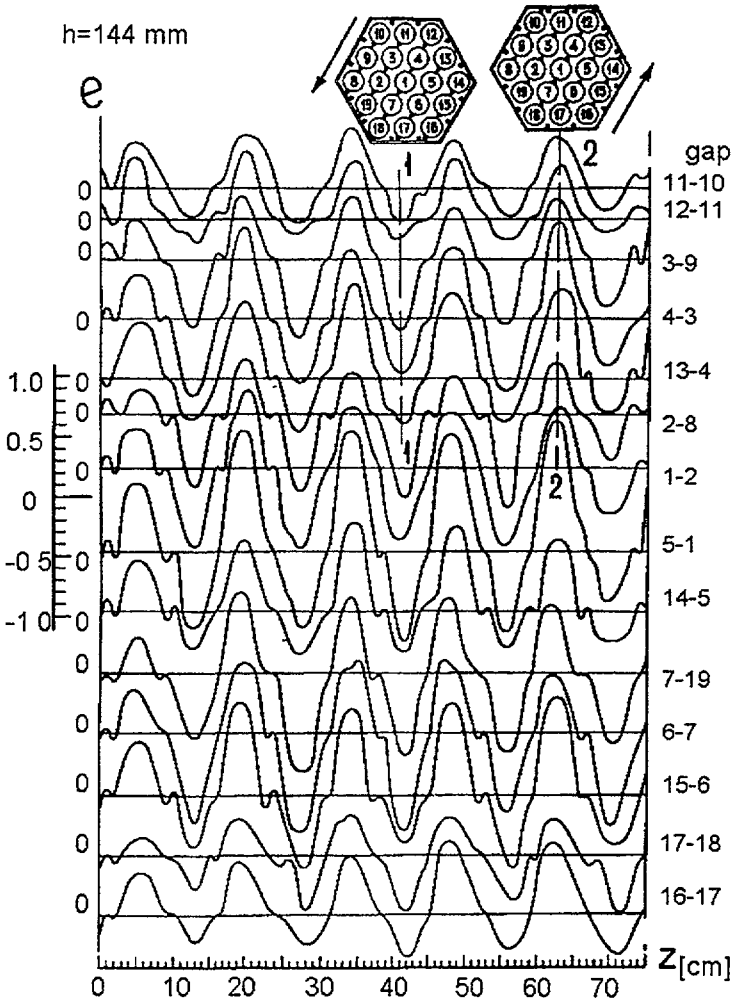

Fig. 1. Variation in transverse flow-over the height of gaps in diverse cells of fast reactor fuel assembly mock-up (the arrows indicate directions of transverse flow in cross-sections 1-1, 2-2)

$$\Psi(\mathrm{Re}) = 1.087 - 0.754\exp\left(-0.132\cdot 10^{-3}\cdot \mathrm{Re}\right) \qquad (4)$$

$1.01 \le s/d \le 1.4;\ 2 \le h/d \le 50;$

$2\cdot 10^3 \le \mathrm{Re} \le 2\cdot 10^5.$

The mixing factor averaged over the gap height, calculated with (1)-(4) at $z \ge h$ is:

$$\mu_c^m = (1.047/\pi h)\cdot \Phi(s/d)\cdot \Psi(\mathrm{Re}) \qquad (5)$$

The formula's accuracy is ±10%.

Function $\Phi(s/d) = 3\mu_c^m \cdot h$ represents the length averaged mixing factor (calculated to three gaps) multiplied by wrapping pitch. This function establishes the relationship between mixing factor and pitch-to-diameter ratio. The function $\Psi(\mathrm{Re})$ has been determined from the analysis of experimental data (Fig.2). The strongest dependence of mixing factor on Reynolds number is observed provided that $\mathrm{Re} < (20\div25)\cdot 10^3$. As the subassembly wrapper is approached, μ_c^m reduces (Fig.3), in this case it should be noted the necessity exists to define correctly the flow rate in the given channel, where mixing factor is calculated.

Experimental data show [6] that due to deceleration of flow and wave effect the reduction of pressure takes place downstream behind the wire wrap. Convective mass transfer intensity calculated with the use of pressure difference in lateral direction agrees with the experimental data for s/d<1.25.

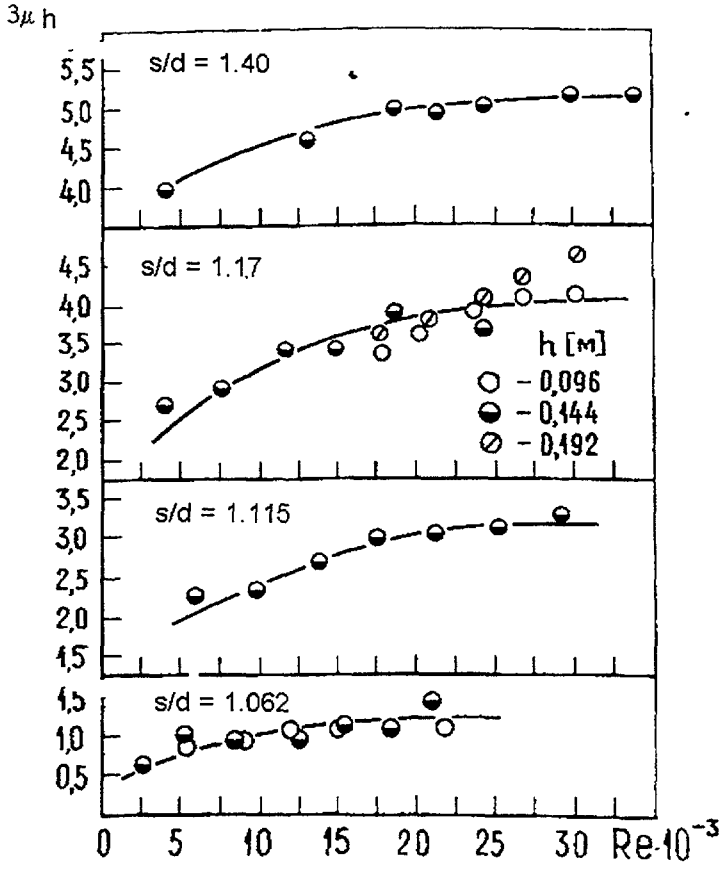

Fig. 2. Dependence of mass-mixing factor on Reynolds number: O – h=96 mm; ● – h=144 mm; ∅ – h=192 mm.

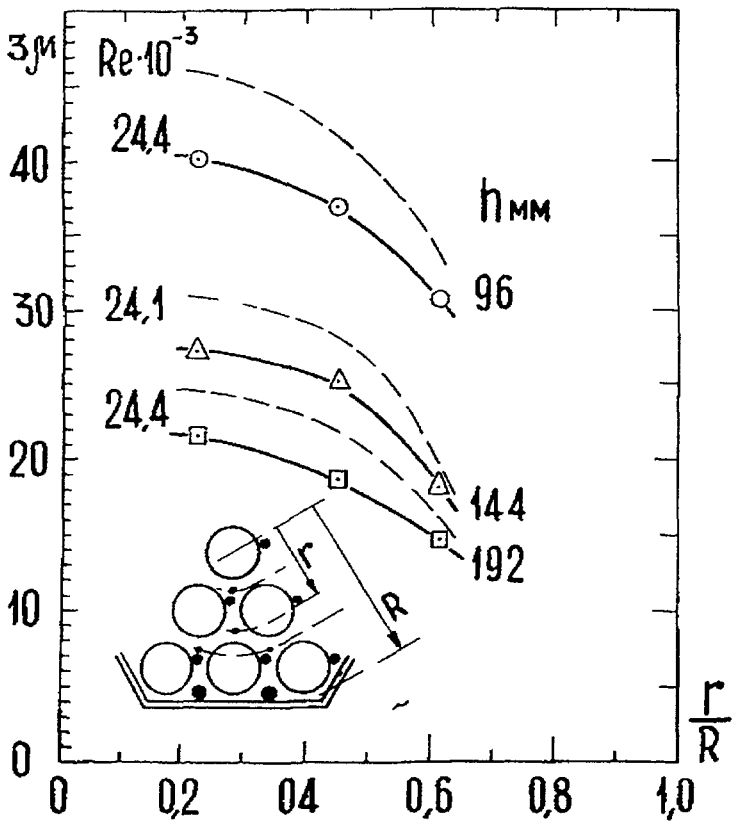

Fig. 3. Variation in the mixing factor over the radius of fast reactor fuel element assembly mock-up (s/d=1.17):

— - on an assumption of uniform velocity distribution over the model cross-section,

O, Δ, □ – taking into account the velocity profile over the model cross-section.

Experiments [10] performed with the thermal track technique have demonstrated that the local thermal mixing factor is defined by the relationship (Fig.4):

$$\mu^t_{c,ij} = \frac{Q_{ij}}{\rho\frac{W_i + W_j}{2} H^* \bar{\omega}} \cong \beta^t \cdot \mu^m_{c,ij}\left(\varphi_{ij} - \pi/3\right) \tag{6}$$

where β^t - non-equivalence factor between transport of mass and energy ≈ 0.7; H^* - enthalpy in the donor channel.

Having averaged the transverse heat flux in the inter-channel gap over the initial angle of wire wrap orientation, the integral values of thermal mixing factors can be obtained as:

$$\mu^t_c = \frac{\int_0^{2\pi} Q_{ij}\, d\alpha_{ij}}{\rho\left[\left(W_i + W_j\right)/2\right]\left(H_i - H_j\right)\bar{\omega}} \tag{7}$$

where:

$$\mu^t_c = \left(\mu^t_{c,ij}\right)^{max}/\pi = \beta^t \cdot \mu^m_c = \left(\beta^t/3h\right)\cdot \phi^m(s/d)\cdot \psi(Re) \tag{8}$$

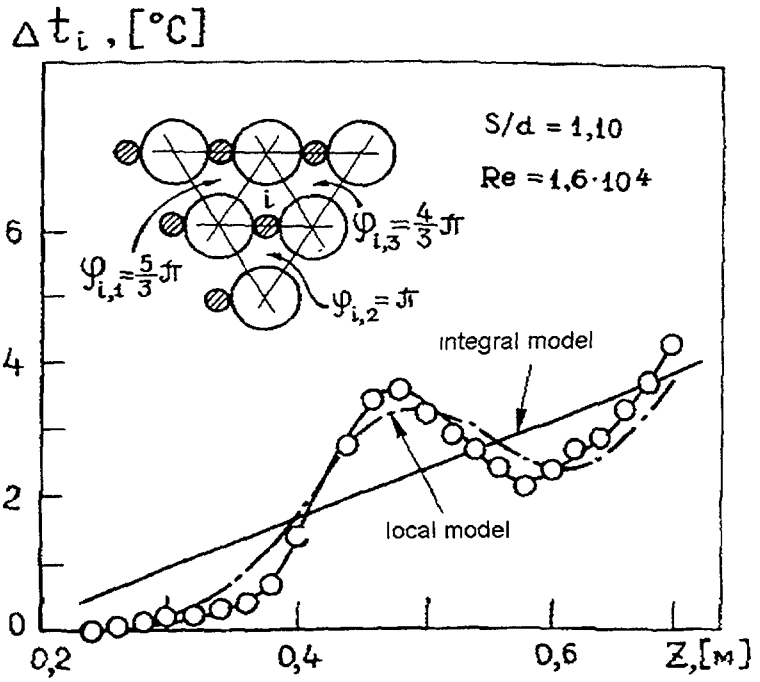

Fig. 4. Variation in coolant overheating over cell length in the event of only with central rod produces energy in mock-up fast-reactor assembly: –o– - experimental data, – ◦– ◦– - local model of exchange, —— - integral model.

Relationship (8) is in a fair agreement with the experimental data on convective interchannel heat transfer (effective value disregarding an influence of heat conduction and turbulence diffusion) gained by authors from different countries, Table 1) - Fig.5a [5,6,10-31].

Note, that formulas in references [32-34] yield the essentially different results.

The factor of non-equivalence between heat and mass transfer (β^t) was predicted on the basic of the model of mole convective exchange around the fuel element spaced by wire wrap (as well as between momentum and mass exchange). Assuming that inter-channel exchange by substance (either mass or heat) is due to moles (vortices), whose interaction with environment is defined as [28]:

$$\psi(M_0) = \psi(M) + [\psi(M) - \psi(M_0)]\frac{1-\exp(-\alpha_\psi)}{\alpha_\psi} \tag{9}$$

$$\alpha_\psi = (10.5 + \frac{2.7}{Pr_\psi})\frac{\nu}{R^2}\frac{r}{W}$$

(where R - mole radius; r - free length of the mole; W - transverse velocity of the mole) and the mole, being responsible for convective exchange in the section z and formed in the section $(z - h/6)$, follows a wire wrap trajectory and has a radius equal to the gap width between pins, we obtain in common case:

$$\beta^\psi = 1 - 0.4\frac{1-\exp(-\alpha_\psi)}{\alpha_\psi} \tag{10}$$

TABLE I. PARAMETERS OF TEST BUNDLES, EXPERIMENTAL TECHNIQUES AND SOME RESULTS OF EXPERIMENTS ON INTERCHANNEL EXCHANGE IN THE INTERNAL AREA OF SA.

1	2	3	4	5	6	7	8	9	10	11	12	13
№	Autor	Number of pins	d[mm]	s/d	h[mm]	h/d	L[mm]	L/h	$Re*10^4$	$St\frac{\Delta S}{\varpi}$ [1/m]	Coolant	Experimental technique
1	Okamoto [11]	91	6,3	1,22	255	40,5	1800	7,6	0,4-1,5	3,5-4,0	Water	Injection of $NaCO_3$
2	Cushann [12]	19	9,07	1,115	152	16,8	343	2,25		8,1	Na	16 heated pins
3	Millholen [13]	37	5,85	1,23	304	52	343	1,2	4,1	1,8		
4	Marian [14]	127	6,35	1,2	304	48	1830	6	3,9	4,0		heating of the central pin
5	Hines			1,28		24		12	5,5	3,2	Water	injection of ink
6	Bump [15]	91	4,42	1,28	152	34,2	443	2,9	7,2	2,7		
			17	1,33	450	26,5		1,8	4,2	1,8		
					300	14,2		2,6	2,5-5,5	2,0-3,5		injection of hot water
7	Skok [16]	7	21	1,14	450	21,5	800	1,8		2,0	Water	
					600	28,5		1,3	4,2	1,2-1,6		
			23	1,065	450	19,5		1,8		0,6-0,9		
	[17]	61	6,0	1,167	100	16,7	660	6,6	2-15	5,7-7,7	Air	heating of the central pin
								10		10-11,3		
8	Baumann	61	6,0	1,32	200	33,3	1000	5	0,8-7,0	4,6-6,0	Na	
	[18]				300	50		3,3		2,5-3,3		
9	Collingham [19]	217	5,84	1,24	300	51,3	1445	4,8	1-3	2,7-3,3	Water	injection of $NaNO_3$
	[10]	37	16,5	1,185	375	22,8		1,87	0,2-0,6	2,4	Na	heating of the central pin
10	Zhukov A.V., et al				96	5,05	755	7,9	2,8-4,0	19		electro-magnetic transducer
		19	19	1,17	144	7,6		5,2	0,4-3,5	11,4	NaK	
					192	10,1		3,9		10		
	[5]	169	6,1	1,15	100	16,4	775	7,55		10,7		

TABLE I (CONTINUE).

1	2		3	4	5	6	7	8	9	10	11	12	13
		[20]			1,062	96	5,05		7,9		3,4		
			19	19		144	7,6	755	5,2	0,2-10	2,35		electro
10	Zhukov A.V.,				1,115						6,1	NaK	magnetic
	et al		19	19	1,23	144	7,6	755	5,2	0,4-3,6	1,02		transducer
		[21]			1,40						10,75		
11	Bolle	[22]	6	200	1,10	2960	14,8	5920	2	2-5	0,43	Air	Pitot tube
12	Fontana	[23]	19	5,75	1,24	300	52			0,1-7	2,9-4,8	Water	heating of the central pin
13	Griazev V., et al	[24]	37	6,0	1,10	100	16,7	400	4	0,8-2,4	3,6-5,6	Na	free-of-uel pin within SA
14	Chiu	[25]	61	12,73	1,065	50,8	4	1524	30	0,17-1,7	2,16	Water	injection
						101,6	8		15		10,8		of salt
15	Hanson	[26]	61		1,25		2,4					Water	injection
							4,8						of salt
			19	15,0	1,09	300	20	600	2,0	0,3-2,3	1,8		6 heated pins
16	Mijaguchi	[27]	91	6,3	1,21	262	41,7	524	2,0	0,5-6,5	2,75	Na	7 heated pins
			169	6,5	1,21	306	47,1	930	3,0	0,5-5,5	2,0		12 heated pins
17	Patch	[6]	48	12,8	1,07	100	7,9	5000	50	0,4-2,2	6,58	Air	Pitot tube
						100	5,6		17,8	6,4	1,26		injection of salt
18	Waters	[28]	7	17,8	1,20	250	14	1780	7,1	6,2	0,83		injection of
						450	25		4,0	6,2	0,4		Na^+
19	Shimazaki	[29]	7	20,1	1,11	250	12,5	1830	7,3	2,4	0,91	Water	injection of $MnCl_2$
20	Bishop	[30]	19	12,7	1,20	380	30	1220	3,2	5,4	3,74		injection
21	Lane	[31]	19	1,52	1,08	230	15	500	2,2	5,4	2,74		of $LiNO_3$

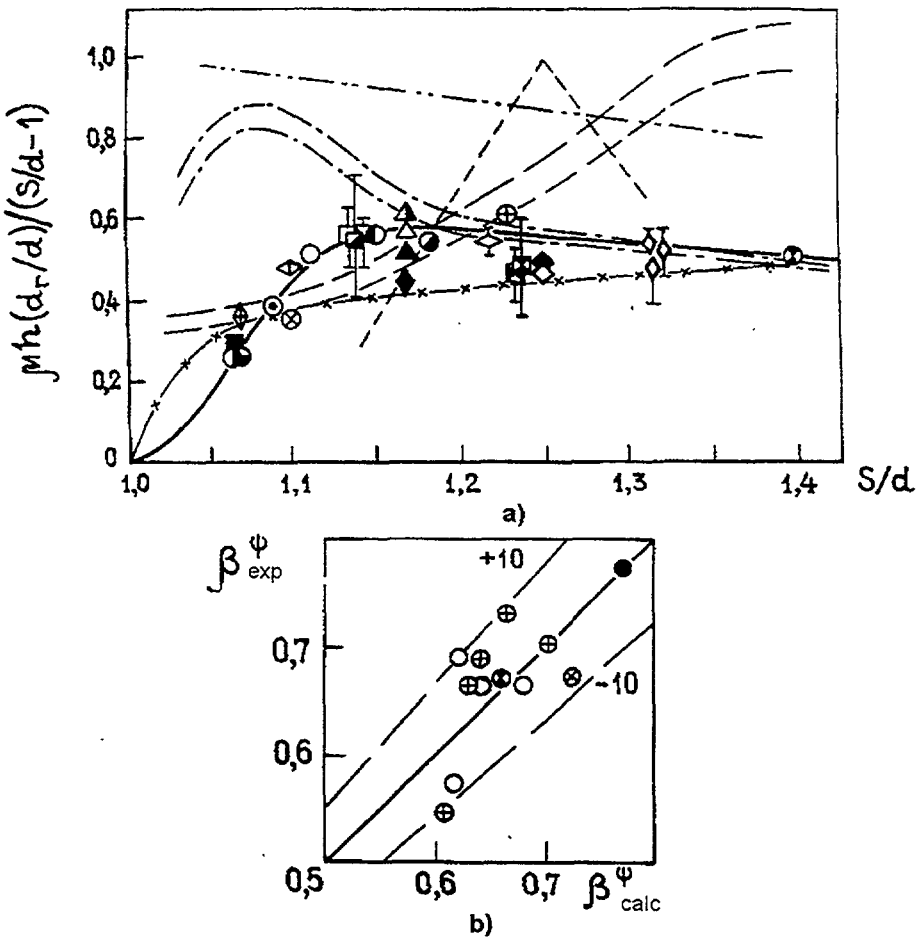

Fig. 5. Variation in thermal convective mixing factor (a) against a relative pin bundle pitch, comparison of calculated and experimental values non-equivalence factor between mass and heat transport (b) on the data of the different authors.

and for mass and thermal exchange, respectively:

$$\alpha^m = \frac{4.4}{2\pi\,\mathrm{Re}}\gamma(h/d, s/d), \qquad \alpha^t = \frac{1}{2\pi\,\mathrm{Re}}\left(\frac{0.9}{\mathrm{Pr}} + 3.5\right)\cdot\gamma(h/d, s/d)$$

where

$$\gamma(h/d, s/d) = \frac{(h/d)^2\left[2\sqrt{3}/\pi(s/d)^2 - 1\right]}{(s/d-1)^2 s/d}$$

Calculations by the formula (10) give results being in agreement with experimental data (Fig. 3).

Edge area of subassembly. The same orientation of wire wrap in the space between subassembly wrapper and the close to wrapper row of pins produces oneward-directed transverse flow of mass through the gaps.

Mass convective mixing in edge area is a result of integration of hydrodynamic data [6, 20, 21, 32, 36-39], Fig.6:

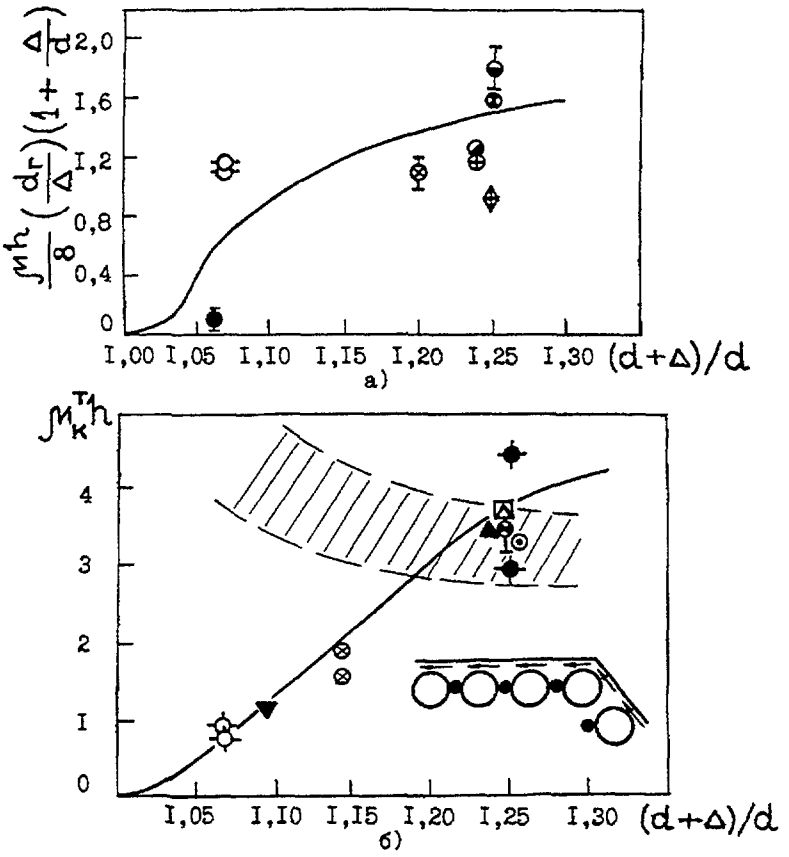

Fig. 6. Comparison of experimental data on convective interchannel mass (a) and velocity (b) transport in the gaps between fuel assembly wrapper tube and peripheral area of fuel assembly with a calculating by formulas (11) and (12) on the data of the different authors.

$$\mu^{m}_{c,p} = \frac{\overline{G_{ij}}}{G_{in}} = \frac{1}{h}\left[17.34\,\Delta/d + 144(\Delta/d)^2 - 373.4(\Delta/d)^3\right]\cdot\psi'(\mathrm{Re}) \qquad (11)$$

where

$$\psi'(\mathrm{Re}) = 1 - 0.694\exp\left(-0.132\cdot10^{-3}\,\mathrm{Re}\right)$$

$$0 \le \Delta/d \le 0.25; \quad 7.6 \le h/d \le 52 \qquad 0.6\cdot10^{3} \le \mathrm{Re} \le 2.9\cdot10^{4},$$

here Reynolds number is defined through the velocity in the edge channel and hydraulic diameter of the edge channel.

The ratio between transverse flow (G_{ij}) and axial flow in internal channels (G_{in}) in (11) is somewhat conventional, but a handy way of solving conservation equations in the framework of subchannel approach.

Results of thermal experiments on convective interchannel exchange by energy in the edge area are described by the relationship:

$$\mu^{t}_{c,p} = \frac{Q_{ij}}{\left[\rho\left(W_i + W_j\right)/2\right]h_j\bar{\omega}\Delta z} = 0.5\ \mu^{m}_{c,p} \qquad (12)$$

$$0 \le \Delta/d \le 0.25; \quad 7.6 \le h/d \le 52; \qquad 0.6\cdot10^{3} \le \mathrm{Re} \le 7\cdot10^{4}.$$

Value of $\mu^{m}_{c,p}$ is defined by (11).

3. MOLECULAR AND TURBULENT EXCHANGE

Experimental data on molecular-turbulent mixing in a bundle of smooth pins, gained using tracer or thermal trail techniques, have an essential variability that owes to the occurrence of macro-flows due to geometrical distortions, redistribution of flow through the subassembly length contributing to the exchange up to 50%, to the flow disturbances in the injection point, etc. Direct data on interchannel momentum exchange, as well as heat exchange in the event of liquid metal flow, are lacking in the literature.

According to the findings of Czechoslovakian specialists on pin bundle hydrodynamics, the area of velocity field deformation was expected to be localized in small number of channels (Fig. 6). In this event, momentum mixing factor can be attained as a result of data processing on shear stresses and coolant velocity [51]:

$$\mu_{turb}^{m} = \frac{\lambda}{\pi} \frac{\sum_{k} \tau_{ke}^{*} \Pi_{ke}^{*} - \sum_{k} \tau_{k1}^{*} \Pi_{k1}^{*}}{\frac{\left(W_e^2 - W_1^2\right)}{2}\left[\frac{2\sqrt{3}}{\pi}(s/d)^2 - 1\right]d} \tag{13}$$

where $\tau_{ke}^{*} = \overline{\tau_{ke}}/\overline{\tau_k}$; $\bar{\tau} = \lambda/8 \cdot \rho \overline{W}^2$; $\Pi_{ke}^{*} = \Pi_{ke}/d$.

Processing the data [41], performed by the authors, has allowed the data μ_{turb}^{m} to be obtained in the range s/d= 1.03÷1.25 (fig.6).

Findings of liquid metal experiments are described by the relation [42]:

$$\mu_{turb}^{t} = \frac{1}{Pe^{0.7}} \cdot \frac{\sqrt{s/d - 1}}{s/d} \cdot \frac{1}{d} \tag{14}$$

$1.1 \le s/d \le 1.35$; $70 \le Pe \le 1600$.

Analysis performed by the authors on the basic of the notions that molecular-turbulent exchange presents a composition of the gradient transfer, caused by molecular diffusion and small scale turbulent eddies, and convective transfer, caused by large scale eddies (so called secondary flows) has allowed the relationships for the factors of molecular-turbulent momentum and energy exchange to be obtained:

$$\mu_{turb}^{m} = \frac{0.0293 - 0.051(s/d - 1)}{\left[\frac{2\sqrt{3}}{\pi}(s/d)^2 - 1\right] Re^{0.1} d}\left\{1 - \exp\left[-40(s/d - 1)\right]\right\} \tag{15}$$

$1.0 \le s/d \le 1.6$; $10^4 \le Re \le 2 \cdot 10^5$.

$$\mu_{turb}^{t} = \left\{\frac{350}{Pe}\frac{s/d - 1}{s/d} + \frac{0.318}{s/d\sqrt{s/d - 1}}\right\}\left[1 - \exp\left[-0.62 \cdot 10^{-4}\, Re \cdot Pr^{0.33}\right]\right] +$$

$$+ \frac{0.038}{\left[\frac{2\sqrt{3}}{\pi}(s/d)^2 - 1\right] Re^{0.1}} \cdot \frac{10^{-2}}{d}\left\{1 - \exp\left[-40(s/d - 1)\right]\right\} \tag{16}$$

$1.0 \le s/d \le 1.32$; $70 \le Pe \le 1500$.

TABLE II. EXPERIMENTAL PARAMETERS AND MEASUREMENT TECHNIQUE FOR RESEARCH INTERCHANNEL EXCHANGE IN THE EGDE AREA OF SUBASSEMBLY

№	Author	Number of pins	d [mm]	$\frac{d+\Delta}{d}$	h [mm]	h/d	L [mm]	L/h	Re*10^4	Coolant	Experimental technique
1	Zhukov A.V. et al. [20]	19	19	1,20	144	7,6	745	5,2	2,9	Na	Electro-magnetic measurements of
	[21]			1,062					1,68		transverse component of velocity
2	Patch L., et al [6]	48	63,5	1,07	500	7,9	5000	10	2,2	Air	Measurement of transverse component
3	Sha W.T.et al [36]			1,24	304						of velocity by Pitot tube
4	Lafay J., et al [37]			1,25	152						
5	Lorenz J., et al [38]	91		1,24		48				Water	Injection of salt
6	Chin C.,	61	12,73	1,063	50,8	48	1524	30	0,2	Water	Injection of salt
	et al [25]				101,6	24		15	0,7		
7	Collingham R. [19]	217	5,84	1,24	300	51,3	1445	4,8	1,0-3,0	Water	Injection of salt
8	Hanson A.S. [26]	61		1,25		24				Water	Injection of salt
						48					
9	Chen Y.	61	6,125	1,25		48			0,064	Water	LDA measurements of transverse comonent of velocity
	et al [39]					24			0,45		
10	Wheeler C. [32]	7		1,25		48				Air	
11	Skok J. [16]	7	21	1,14	300	14	800	2,6	4,2	Water	Injection of hot water
					600	28		1,3			
12	Peederson D., et al [40]	91		1,2		48				Water	
13	Fontana M., et al [23]	19	5,75	1,24	300	52			0,1-7,0	Water	Pin heating
14	Inhibashi E.	19		1,09		21					
	[32]	61		1,20		43					

TABLE III. EXPERIMENTAL PARAMETERS AND MEASUREMENT TECHNIQUE FOR INVESTIGATIONS OF MOLECULAR-TURBULENT EXCHANGE ON SMOOTH PIN BUNDLES

№	Author	Country	S/d	Re*10^4	Coolant	Measurement technique
1	Rowe, Angle	USA [41]	1,03÷1,15	0,7÷32	Water	Heating of central pin
2	Polianin	Russia [42]	1,20÷1,22	2,2÷5,4	Water	Tracer
3	Voj	USA [43]	1,27	1,0÷2,0	Air	Tracer
4	Piatrella	USA [43]	1,20	1,5÷5,0	Air	Tracer
5	Roidt	USA [44]	1,25	7,0	Air	Tracer
6	Markoczy	USA [45]	1,15÷1,28	5,0÷50	Air	Heating of central pin
7	Gabrianovich	Russia [46]	1,3÷1,5 1,15	1,0÷5,0	Air	Tracer
8	Ingesson	Sweden [4]	1,10÷1,62			Empirical relationship
9	Rogers	USA [2]	1,05÷1,40			Empirical relationship
10	Rudzinski, Singh	Canada [47]	1,05		Water and air	KNO_3CH_4
11	Scale	Canada [48]	1,10÷1,375	9,0		Empirical relationship
12	Mantlic	Czech Republic [49]	1,07; 1,12; 1,14; 1,14	4,8; 18,6; 18,2; 17,2	Air	Velocity measurement
13	Zhukov	Russia [50]	1,13÷1,32	0,4÷5,0	Liquid metal	Heating of central pin

4. MIXING DUE TO PIN'S HEAT CONDUCTION

In the event of different coolant temperatures in the channels surrounding the pin, the non-uniform distribution of heat flux around the pin is observed, that causes heat transfer between channels due to heat conduction of the pin.

Using correlation between temperature distribution local heat flux, founded by P.A. Ushakov , we can write:

$$\mu_\lambda^t = \frac{5.33}{Pe \cdot d} \cdot \frac{\varepsilon_1}{1 + (2d_e/d)(\varepsilon_1/Nu)} \tag{17}$$

This formula shows that heat exchange factor due to pin heat conduction reduces with Peclet number and pin diameter, increases with parameter of equivalent heat conduction, predicted on the basic of first harmonics in temperature distribution and weakly depends on the pitch-to-diameter ratio.

5. INFLUENCE OF MIXING ON VELOCITY AND TEMPERATURE FIELDS FORMATION

An effective values of integral hydrodynamic and thermal mixing factors in FBR subassembly can be expressed as:

$$\mu_{ef}^m = \mu_c^m + \alpha \cdot \mu_{turb}^m \tag{18}$$

$$\mu_{ef}^t = \mu_c^t + \alpha \cdot \mu_{turb}^t + \mu_\lambda^t \tag{19}$$

where α can be predicted according to [43].

At the same time it should be noted that precise predictions are defined by the reasonable inclusion of exchange phenomena. In the event of considerable deformation of subassembly associated with radiative effects, convective and turbulent exchange in compact arrangement, as well as exchange due to heat conduction are of a great importance (Fig.7). Neglect of these factors is responsible for the significant error in predicted temperatures.

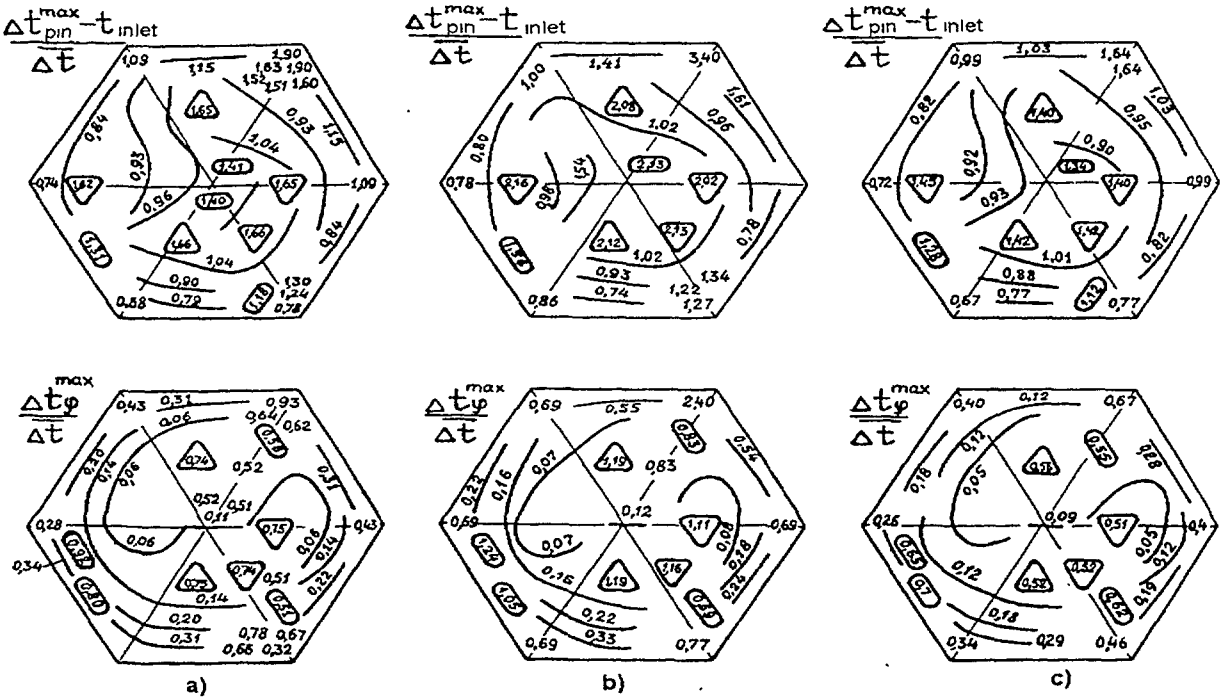

Fig. 7. Comparison of calculated results for <<Phenix>> reactor deformed assembly; a) having regard to centrifugal effect and heat transfer due to fuel elements'heat conduction; b) without consideration of these two effects; c) having regard to the effects mentined when metallic fuel is used λ_{fuel}=30 W/m K.

CONCLUSION

Generalization of the data on liquid metal mixing in pin bundle has allowed the relationships for integral mixing factors of convective transport, molecular and turbulence diffusion of mass, momentum and energy, as well as heat transfer due to heat conductivity of pin to be derived.

NOMENCLATURE

d	fuel pin diameter
d_e	equivalent diameter
G	coolant flow rate
H	enthalpy
h	wire wrap pitch
Q	heat flux
s	bundle pitch
W	coolant velocity
z	axial coordinate

α_{ij} initial phase of wire wrap
α_{ψ} coefficient
β non-equivalence transport factor
Δ clearance between near-wall pins and subassembly cover
ε equivalent heat conduction
ξ hydraulic resistance
λ thermal conductivity
μ mixing factor
ρ density
τ shear stress
φ wire wrap phase
ω surface
ψ, γ, ϕ functions
Π perimeter of the channel

SUBSCRIPTS

c convective
ef effective
i, j number of channels
ij number of inter-channel gap
k pin number
λ exchange due to heat conduction
$turb$ turbulent
p peripheral

SUPERSCRIPTS

m exchange by mass
t exchange by heat

REFERENCES

[1] ZHUKOV A.V., et al. Subchannel Thermohydraulic Prediction of Nuclear Reactor Fuel Subassembly Behaviour. Atomic Energy, 1981, v.51, N°5, p.307-311.

[2] ROGERS J.TY., TODREAS N.E. Coolant Interchannel Mixing in Reactor Fuel Rod Bundles Single Phase Coolant. Heat Transfer in Rod Byndle. ASME, 1968.

[3] ZHUKOV A.V., et al. Interchannel Interaction of Coolant in Cylindrical Rod Lattices. Preprint IPPE-417, Obninsk, 1973.

[4] INGESSON L., et. al. Heat Transfer between Subchannels in a Rod Bundles. Heat Transfer, Amsterdam, 1970, v.3, p.FC7.11, 1-11.

[5] ZHUKOV A.V., et.al. Measurement of Local Hydrodynammic Characteristics of Interchannel Interaction in Fast Reactor Fuel Elements. Preprint IPPE-665, Obninsk, 1976.

[6] PATCH L., et al. Experimental Studies of Flow Distribution in a Wire Wrapped LMFBR Blanket Assembly . Report on the International Meeting on Reactor Heat TYRansfer, Karlsruhe, 1979.

[7] ZHUKOV A.V., et al. Thermohydraulic Calculation of Fuel Subassemblies Cooled by Liquid Metal. M., Energoatomizdat, 1985.

[8] ZHUKOV A.V., et al. Interchannel Exchange in Fast Reactor Fuel Assemblies. M., Energoatomizdat, 1989.
[9] KAZACHKOVSKI O.D., et al. Temperature Fields in Deformed Fuel Assemblies of Fast Reactor. Atomic Energy, 1988, v.65, N° 2, p.89-97.
[10] ZHUKOV A.V., et al. Experimental Investigations of Intechannel Interactions in Wrapped Rod Bundles. Preprint IPPE-556. Obninsk, 1975.
[11] OKAMOTO Y., et al. Symposium "Progress in Sodium Cooled Fast Reactor Engineering", Monako. IAEA/SM-130/5. 1970.
[12] CUSHMAN R.A. Trans. ANS, 1971, v.14, N°1, p.250.
[13] MILLHOLEN M.K., et al. Trans. ANS, 1970, v.13, N°2, p.307.
[14] MARIAN V.R., et al. Trans. ANS, 1970, v.13, N°2, p.806.
[15] BUMP T.R., et al. Trans. ANS, 1966, v.9, p.285.
[16] SKOK J. Mixing of the Fluid due to Helicoidal Wire on Fuel Pins ina Triangular Arrays. Progress in Heat And Mass Transfer. New York, 1973, v.7, p.251-262.
[17] BAUMANN W., et al. Atomkernenergie, 1969, v.14, p.298-304.
[18] BAUMANN W., et al. Coolant Cross-Mixing of Sodium Flowing in Line through Multirod Bundles with Different Spacers Arangements. Report on International Heat Transfer Seminar, Trogir, Yugoslavia, 1971.
[19] COLLINGHAM R.E., et al. Nucl. Engnrg and Des. 1973, v.23, N°3, p.393-400.
[20] ZHUKOV A.V., et al. Preprint IPPE-799, Obninsk, 1977.
[21] ZHUKOV A.V., et al. Preprint IPPE-867, Obninsk, 1978.
[22] BOLLE L., et al. International Meeting on Reactor Heat Transfer, Karlsruhe, 1973.
[23] FONTANA M.H., et al. Trans. ANS, 1972, v.15, N°2, p.855.
[24] GRYAZEV V.M., et al. Thermophysics and Hydrodynamics of Core and steam Generators for Fast Reactors, Prague, Edit. ChSKAE, 1978, v.1, p.182-209.
[25] CHIU, et al. International Meeting on Reactor Heat Transfer, Karlsruhe, 1979.
[26] HANSON A.S., e tal. CO-2245-51TR, 1977.
[27] MIJAGUCHI K., et al. IWGFR/29, 1979, p.58-75.
[28] WATERS E.D. HW-70178, Hanford Laboratories, 1963.
[29] SHIMAZAKI T.T., et al. Heat Transfer Conference, TID-7529, Part 1, Book 1, 1957, p.273.
[30] BISHOP A.A., et al. Trans. ANS, 1961, v.4, N°1, p.102.
[31] LANE A.D., et al. Can. J.Chem. Eng, 1963, v.41, N°5, p.97-112.
[32] KHAN E.U., et al. Nucl. Eng. and Des., 1975, v.35, N°1, p.1-12.
[33] CHIU C., et al. Trans. ANS, 1978, v.30, p.547-548.
[34] DZYUBENKO B.V., IFZh, 1979, N°5, p.777-783.
[35] BULEYEV N.I. Theoretical Model of Turbulent Exchange in Turbulent Fluuid Flow. Proceeding of Theird International Conference on Peaceful Use of Atomic Energy, New York, 1965.
[36] SHA W.T., et al. Trans. ANS, 1976, v.24, p.344-346.
[37] LAHEY, et al. CEA-CONF-3491. 1975.
[38] LORENZ J.J., et.al. Nucl. Eng. and Design, 1977, v.40, N°2, p.315.
[39] CHEN Y.B., et al. Trans. ANS, 1974, v.19, N°1, p.323-324.
[40] PEDERSEN D.R., et al. Trans. ANS, 1974, v.19, N°1, p.306-307.
[41] ROWE D.S., et al. Trans. ANS, 1967, v.10, N°2, p.655.
[42] POLYANIN L.N. Atomic Energy, 1969, v.26, N°3, p.279-285.

[43] NIJSING R., et al. .Nucl. Eng. Des., 1974, v.30, N°2, p.145-185.
[44] ROIT R., et al. Heat Transfer, 1972, v.96, N°2, p.61-68.
[45] MARCKOZY G., et al. Trans. ANS, 1975, v.20, N°1, p.758-761.
[46] GABRIANOVICH B.N., et al. Thermophysical Investigations, M., VIMI, 1977, p.23-33.
[47] RUDZINSKI K.F., et al. Can. J. Chem. Eng., 1972, v.50, N°2, p.297-309.
[48] SEALE W.J. Int. J. Heat and Mass Trans., 1981, v.24, N°4, p.768-70.
[49] ZHUKOV A.V., et al. Preprint IPPE-1816, Obninsk, 1986.
[50] ZHUKOV A.V., et al. Preprint IPPE-757, Obninsk, 1977.
[51] ZHUKOV A.V., et al. Turbulent Interchannel Impulse Exchange in Reactor Fuel Assemblies. Preprint IPPE-2015, Obninsk, 1989.
[52] BOWRING R.W. AEEW-R582, London, 1968.

DEVELOPMENT OF SUBCHANNEL ANALYSIS CODE MATRA-LMR FOR KALIMER SUBASSEMBLY THERMAL-HYDRAULICS

WON-SEOK KIM, YOUNG-GYUN KIM
Korea Atomic Energy Research Institute,
Taejon, Republic of Korea

Abstract

In the sodium cooled liquid metal reactors, the design limit are imposed on the maximum temperatures of claddings and fuel pins. Thus an accurate prediction of core coolant/fuel temperature distribution is essential to the LMR core thermal-hydraulic design. The detailed subchannel thermal-hydraulic analysis code MATRA-LMR (Multichannel Analyzer for Steady States and Transients in Rod Arrays for Liquid Metal Reactors) is being developed for KALIMER core design and analysis, based on COBRA-IV-i and MATRA. The major modifications and improvements implemented into MATRA-LMR are as follows: a) nonuniform axial noding capability, b) sodium properties calculation subprogram, c) sodium coolant heat transfer correlations, and d) most recent pressure drop correlations, such as Novendstern, Chiu-Rohsenow-Todreas and Cheng-Todreas. To assess the development status of this code, the benchmark calculations were performed with the ORNL 19 pin tests and EBR-II seven-assembly SLTHEN calculation results. The calculation results of MATRA-LMR for ORNL 19-pin assembly tests and EBR-II 91-pin experiments were compared to the measurements, and to SABRE4 and SLTHEN code calculation results, respectively. In this comparison, the differences are found among the three codes because of the pressure drop and the thermal mixing modellings. Finally, the major technical results of the conceptual design for the KALIMER 98.03 core have been compared with the calculations of MATRA-LMR, SABRE4 and SLTHEN codes.

1. INTRODUCTION

Subassemblies in most liquid metal cooled reactors (LMRs) are surrounded and cooled by sodium. Sodium thermophysical properties differ from those of ordinary fluids. Compared to water, the thermal conductivity is 100 times higher, and the boiling point is much higher, about 900 ℃ at atmospheric pressure. Present core designs of the sodium cooled reactors have many common points such as the short heated length and the triangular rod arrangement in a hexagonal duct which forms a closed channel by itself. The main differences from the thermal-hydraulic point of view are the types of rod spacers: grids or helical wires.

The design of liquid metal reactor cores requires the accurate prediction of the peak temperatures of the rod and the coolant to ensure that certain economic and safety considerations will be met. Thus, to achieve a safe and economical design, it is necessary to use reasonably, rather than extremely, conservative design limits. Many of these relate to fuel, cladding, and coolant outlet temperatures for steady-state and transient conditions. For instance, no significant fuel melting is allowed in the fuel, the cladding temperature must also be consistent with corrosion considerations, the core assembly mixed mean outlet coolant temperature and the difference in the mixed mean coolant temperature at the exit of adjacent assemblies must be within allowable limits to ensure structural integrity of the upper internal structures during the prescribed lifetime, and the sodium temperature must not exceed its boiling point [1].

Since a typical liquid metal reactor core comprises several thousands of fuel pins clustered in groups of several hundreds of pins per assembly, a complete thermal-hydraulic analysis requires the knowledge of coolant distributions and pressure losses throughout the core. In order to ensure that these design bases are satisfied, in the past years many efforts have been made to in locally important regions as flow blockages.

Whereas MATRA is designed to handle a wide variety of single and two phase flow problems for PWR, MATRA-LMR is intended for LMR applications. In this respect, MATRA-LMR is a modified version of MATRA with three major features. First, sodium properties correlations are built in the code as a subprogram. Second, correlations of heat transfer coefficients are changed for sodium coolant. Third, MATRA-LMR has an additional model for pressure drop correlations such as Novendstern, Chiu-Rohsenow-Todreas and Cheng-Todreas which are developed for the flow field induced by wire wraps. Figure 1 shows the MATRA-LMR code development procedure. The following describe the modified features of the MATRA-LMR code in detail.

2.1. Sodium properties and heat transfer coefficient

In recent years, COBRA-IV-I code, with its various versions, has been widely used in analyzing the thermal-hydraulic performance of nuclear reactor cores. However, COBRA-IV-I can not be directly used for LMR cores, because it does not model the sodium coolant. MATRA-LMR has been developed for the analysis of sodium cooled LMRs. MATRA-LMR has sodium properties tables in the code as a default subprogram, while it can be still used as in tabular form.

An LMR needs a high heat transfer coolant in order to exploit the advantage of a tight arrangement of thin fuel pins. Heat transfer coefficients are higher for liquid metals than for other fluids because of their high thermal conductivities compared to other fluids. High thermal conductivity allows heat to be transported far out into the fluid with relatively little resistance. The consequences of these differences are in the heat transfer correlation for the Nusselt number. The behavior of Nusselt number (Nu) for liquid metals follows the relation:

$$Nu = A + B\ (Pe)^C \qquad (1)$$

where Pe = the Peclet number, i.e., Pe = Re Pr.

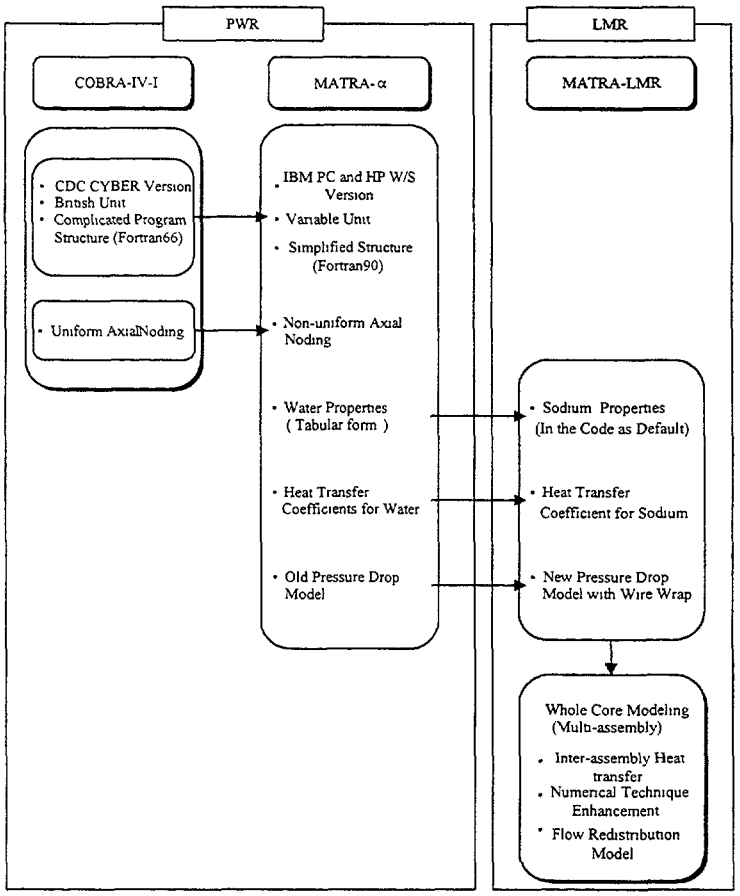

Fig. 1 MATRA-LMR code development procedure

In the MATRA-LMR code, the switch for selecting the heat transfer coefficient which is sensitive to boundary conditions and channel shapes, such as Lyon-Martinelli [8], Westinghouse, and Schad-Modified [9] correlations, has been implemented.

2.2. Pressure drop

The design and safety analysis of LMR requires the accurate predictions of the coolant velocity and temperature distributions in the core. Numerical approximations of the governing equations such as energy, momentum, and continuity equations are normally employed to obtain this information in subchannel analysis code as COBRA-IV-I code.

In MATRA-LMR, basic equations, which describe the properly averaged values of pressure, enthalpy, and velocity fields for each computational cell, can be derived from the governing equations just like in COBRA-IV-i. The subchannel codes require some input parameters that must eventually be supplied through physically based empirical correlations. This is especially true when attempting to model a complex geometry LMR subassemblies which have helically wrapped fuel pins.

Most LMR designs utilize wire wraps to space the fuel pins in the hexagonal assembly channel. The wire wrap spacer system utilizes small wires spiraling around each fuel pin to position the pins within their hexagonal duct. Because of the complex geometry caused by the wire wrap, simple equivalent diameter techniques are not sufficient to predict accurately the pressure drop in the fuel pin region of the reactor. An accurate prediction of the pressure drop is needed in order that plant parameters may be optimized. Because testing of all possible configurations is not practical, and the pressure drop in the pin bundle is a substantial portion of the total plant pressure loss, a method to predict the pressure drop more accurately in fuel assemblies utilizing wire wrap spacing is required.

COBRA-IV-I has the pressure drop model for smooth pipes with equivalent diameter techniques. This model is very simple but, however, out of date. In the case of wire wrap spacing rods, the flow area in central subchannels is the area surrounded by three rods excluding the area taken up by the wires. Only 50% of the wire area is on the average in that subchannel. Similarly, the wetted perimeter is the sum of the perimeters of the three rods in the subchannel plus 50% of the wire perimeters. This is the basic idea proposed by Novendstern. Based on this idea, new techniques have been developed to improve the accuracy from the experimental work. The following three pressure drop models have been implemented in MATRA-LMR, such as Novendstern, Chiu-Rohsenow-Todreas and Cheng-Todreas models.

Novendstern model

Novendstern's analysis [10] took advantage of all the previous methods, together with experimental data. In this model the wire wrap is accounted for by means of an effective friction factor. Using the flow conditions for the central subchannel, the pressure drop is determined by,

$$\triangle P = M\ f_{smooth}\ (L/D_{e1})\ (\rho V_1^2/2) \tag{2}$$

The multiplication factor, M, is used to get the effective value from the pressure drop calculated with the smooth tube friction factor. It primarily accounts for the wire lead and fuel pin pitch-to-diameter ratio,

$$M = \left[\frac{1.034}{(P/D)^{0.124}} + \frac{29.7(P/D)^{6.94}(Re)^{0.086}}{(H/D)^{2.239}} \right]^{0.885} \tag{3}$$

The Blasius relation for the friction factor, f_{smooth}, is applicable for the flow conditions in LMR, hence,

$$f_{smooth} = 0.316/Re_1^{0.25} \tag{4}$$

Chiu-Rohsenow-Todreas (CRT) model

The average subchannel flow rates for the interior and edge subchannels of wire-wrapped LMR assemblies are important parameters in the core thermal-hydraulic analysis. The analytic method evolved by Novendstern cannot predict these parameters accurately enough to yield reliable assembly coolant predictions. The major drawback of the above method is that they do not take into account the following two effects in the determination of the subchannel friction factor and of the subchannel flow split. One of these two effects is the form pressure drop induced by the wires and the other is the effect of the transverse momentum, which can affect the determination of the friction factor.

The CRT model [11] represents an improvement over the simpler Novendstern model. The principal difference is that the CRT model divides the pressure drop across the channel into two components, one due to friction losses, and one due to form losses from flow perpendicular to the wire wrap. The CRT model treats the mechanisms responsible for the pressure drop in greater detail. In the CRT model, pressure drop parameters are derived for channels 1 (interior) and 2 (edge) only. The values for the corner channels (channel 3) are assumed to be the same as for the edge channels since the corner channels have so little influence on the flow. The resulting pressure drops for channel 1 and 2 are shown below,

$$\triangle P_1 = f_{s1} \frac{L}{D_{e1}} \frac{\rho V_1^2}{2} \left[1 + C_1 \frac{A_{r1}}{A_1'} \frac{D_{e1}}{H} \frac{P^2}{(\pi P)^2 + H^2} \right] \tag{5}$$

$$\triangle P_2 = f_{s2} \frac{L}{D_{e2}} \frac{\rho V_2^2}{2} C_3 \left\{ 1 + \left[C_2 n \left(\frac{V_T}{V_2} \right)_{gap} \right]^2 \right\}^{1.375} \tag{6}$$

Cheng-Todreas (CT) model

This correlation by proposed by Cheng-Todreas [12] based on the model for the subchannel friction factor and mixing parameters are calibrated by the available data.

$$\triangle P_i = f_i \, (L/D_{ei}) \, (\rho V_i^2/2) \tag{7}$$

- Interior

$$f_1 = \frac{1}{Re_1^m} \left[C_{f1}' \left(\frac{P_{w1}'}{P_{w1}} \right) + W_d \left(\frac{3A_{r1}}{A_1'} \right) \left(\frac{D_{e1}}{H} \right) \left(\frac{D_{e1}}{D_w} \right)^m \right] \tag{8}$$

- Edge

$$f_2 = \frac{C_{f2}'}{Re_2^m} \left[1 + W_s \left(\frac{A_{r2}}{A_2'} \right) \tan^2 \theta \right]^{\frac{(3-m)}{2}} \tag{9}$$

- Corner

$$f_3 = \frac{C_{f3}'}{Re_3^m} \left[1 + W_s \left(\frac{A_{r3}}{A_3'} \right) \tan^2 \theta \right]^{\frac{(3-m)}{2}} \tag{10}$$

3. BENCHMARK CALCULATIONS

3.1. Brief Descriptions of the Benchmark Codes

3.1.1. SABRE4 Code

SABRE4 (Subchannel Analysis of Blockage in Reactor Elements) is a 3-D subchannel code designed to calculate the thermal-hydraulics of a fast reactor subassembly. The SABRE4 code was originally developed as a single phase steady state code with the object of calculating flow and temperature distributions behind blockages in fast reactor fuel elements. It has now been developed into a general purpose rod bundle code.

The SABRE4 code permits calculation of steady-state or transient, single or two phase flows and the geometrical options include general representation of grids, wire wraps, multiple blockages and bowed pins, etc. Transient flows may be calculated using either semi-implicit or fully implicit time solution methods and the temperature distributions within the fuel pins are determined as well as the velocity and temperature of the coolant. General inlet boundary conditions are available, including pressure, velocity and total mass flow, and the outlet boundary condition is taken as a constant pressure. The wire wrap model introduces a grid resistance tensor with its principal axes along and perpendicular to the wire, resulting in a very satisfactory modelling of inducement of swirl [13]. The more detailed description for the wire wrap model is given below.

Wire wrap model

Experimental observations of the flow in wire wrapped bundles indicate that the wire wraps have two main effects. Firstly, they increase the overall pressure drop in the bundle and, secondly they divert the flow locally in the direction of the wraps. The model used in SABRE4 is based on the assumption that the effects of a wire wrap can be represented solely by its direction and resistance characteristics. Thus the model does not take any direct account of the geometrical differences in cross-sectional area due to the presence of the wire wrap. The differences in area and perimeter are however included in the derivation of the wrap resistance coefficients, which are referred to velocities in the superficial areas in the bundle. The effects of the wire wraps on the flow in a wire wrapped bundle are represented by resistance terms in the axial and lateral momentum equations for the subchannels. However, actual subchannel flow areas are not modified as they are in MATRA-LMR.

The flow components parallel and perpendicular to a wire wrap are analyzed independently. Parallel flow depends on the pressure gradient in this direction, and perpendicular flow depends on the pressure difference across the wrap.

- Tangential pressure gradient

$$-\frac{\partial p}{\partial s} = K_s \rho v_s^2 \tag{11}$$

- Normal pressure gradient

$$-\frac{\partial p}{\partial n} = K_n \rho v_n |v_n| \tag{12}$$

where s and n are distances measured in the tangential and normal directions, K_s and K_n are resistance coefficients in these directions, v_s and v_n are the components of the flow velocity v in these directions. These equations yield the axial and lateral pressure gradients due to the wire wraps. The pressure drop characteristics are added to the subchannels where the wire wraps pass.

3.1.2. SLTHEN Code

The above two codes use the sophisticated physical modeling processes to simulate the crossflows between subchannels. They couple the momentum equations with energy equations by solving the velocity distributions from the momentum equations and then by using these velocities in the energy equations. They also use iterative procedures for the finite difference equations to obtain convergent solutions. Because of these characteristics, it requires a large amount of computer time to solve the flow equations for every channel in a bundle using the conventional subchannel analysis model. In order to enhance the computational efficiency, the simplified energy equation mixing model called ENERGY was developed in the mid 1970s specifically for LMRs. To model the crossflow caused by the wire wrap of the fuel pin, an effective eddy diffusivity is employed. The velocities in the internal and the wall region of an assembly can be obtained from the theoretical flow split method. These approximations enable the momentum equations to be decoupled from the energy equations. Once the flow is split, the temperatures and the pressure drops are calculated along the axial noding with the finite difference equations. These simplifications enable a significant reduction of the storage space and the running time required for computation [14].

The wire-wrapped rods are packed in an array which is enclosed by a duct. As a result there is a region of flow next to the duct wall which is quite different in character from the flow in the central region. Figure 2 shows the geometry of subchannels and wire wraps. In the central region the mean flow oscillates around each rod as it progresses in an axial direction. This oscillation of flow may be imagined to form an effective eddy diffusivity superimposed on the normal eddy diffusivity associated with turbulence. In the outer region near the wall the flow field is quite different. The difference in the flow pattern in the outer and inner regions of the assembly suggests that the bundle flow be divided into two regions. As shown in figure 3, region I is the inner region where the wire wrap mixing effect can be modeled by an effective eddy diffusivity ε. Region II is the outer region which can be modeled additionally by an average circumferential swirl flow due to the unidirectional wire wrap in that area.

The SLTHEN (Steady-state LMR core Thermal-Hydraulics analysis code based on ENERGY model) code is a modified version of the SUPERENERGY2 code, which is a multi-assembly, steady-state subchannel analysis code based on the above simplified energy equation mixing model. This code improves the numerical schemes of SUPERENERGY2 to

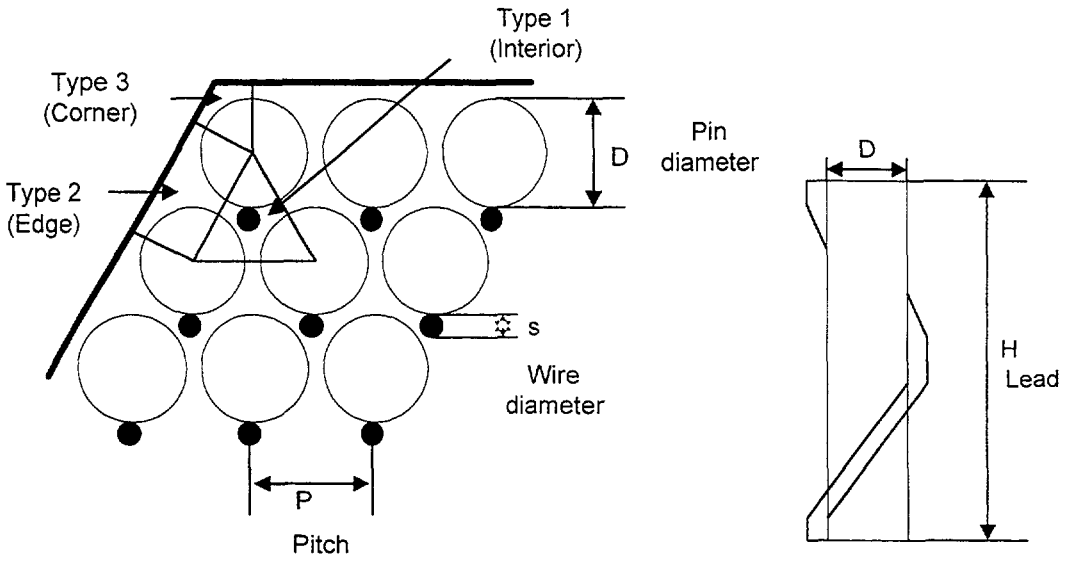

Fig. 2 Geometry of subchannels and wire wrap

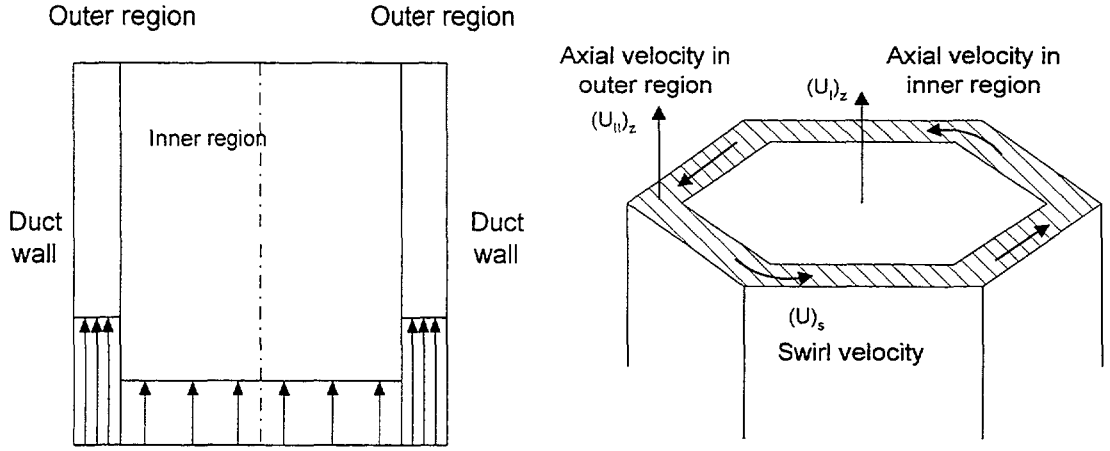

Fig. 3 Flow field in the two regions of ENERGY model

accommodate the axial convection due to the interassembly gap flow and to enhance the computational efficiency by adopting θ method. Fuel and cladding temperature calculation models are also developed, and the recent correlations for the flow split and mixing parameters are incorporated [15].

3.2. ORNL 19 pin test

ORNL 19 pin tests were performed in the fuel failure mockup (FFM), a large high temperature sodium facility built specifically for testing simulated LMR fuel rod bundles at design power, flow and temperature. The fuel was simulated by electric cartridge heaters fabricated to duplicate reactor fuel rod configuration and heat flux. Rod bundle 2A, which had 19 simulated fuel rods in a hexagonal duct, was the second bundle operated in the FFM. The rods were 5.84 mm in diameter, and the wire wrap spacers were 1.42 mm in diameter and were wrapped around the fuel rod on a 30 48 cm pitch. The FFM bundle 2A fuel rod had a 53.34 cm heated length which started 40.64 cm from the bottom, i.e. axial power profile consisted of three parts, zero power from the bottom to 40.64 cm high and from 93.94 cm to the top, and only the center part between 40.64 cm and 93.94 cm was a heated zone. The total length of the fuel rod was 101.6 cm. Both the axial and the radial power profile were uniform, and liquid sodium was used as coolant. The primary purpose of the tests were to measure temperature distributions within the rod bundle, at the duct wall and at the exit [16].

Several runs were performed during the course of experimentation with the bundle 2A with varying flow and power. Simulations in this paper, however, were done for two cases: one is the high power/flow case which has 3.0378 kg/s and 16975 W/rod and the other is the low power/flow case which has 4.087E-2 kg/s and 263 W/rod. The inlet temperature is 315 ℃ and the outlet pressure is 1.013E5 Pa. The detailed input data for 19 pin tests are shown in table 1. Figure 4 shows the subchannel numbering scheme for MATRA-LMR and SABRE4 code respectively.

Firstly, to see the effect of the number of axial nodes on the calculated temperatures, calculations were repeated for the high power/flow case with an increasing number of nodes

Table 1 Input parameters for ORNL FFM-2A 19 pin test

	Input parameter	Value
Rod information	Rod diameter (m)	5 84E-3
	Rod pitch (m)	7 26E-3
	Wire wrap diameter (m)	1 42E-3
	Wire wrap pitch (m)	0 3048
	Rod pitch/rod diameter	1 243
	Duct inside flat-to-flat distance (m)	3 41E-2
	Heated length (m)	0 5334
	Total length (m)	1 016
Initial conditions	System pressure (Pa)	1 0132E5
	Inlet temperature (℃)	315
	Inlet mass flow (kg/s) (high / low)	3 0378 / 4 087E-2
	Average rod power (W) (high / low)	16975 / 263
	Axial power distribution	uniform
	Radial power distribution	uniform
Calculation parameters	Wire pitch fraction (δ)	0 0833
	Turbulent mixing factor (β)	0 01
	Conduction shape factor (G_k)	0 5
	Number of axial nodes	80 (MATRA-LMR)
		20 (SABRE4)
Correlations	Pressure drop model	
	- Novendstern, CRT	$0.316 Re^{-0.25}$
	- CT	$Re^{-0.18}$
	Heat transfer model	Lyon-Martinelli

Figure 5 shows the peak temperature of subchannel 1 according to the number of axial nodes such as 40, 80, and 120. The 40 node case showed a little lower temperature than the others which have almost the same temperatures. Considering the computing time and computer core storage, however, 80 node case is supposed to be and adopted as a reasonable case for MATRA-LMR code calculations of ORNL 19 pin tests.

Figure 6 shows the comparisons for the pressure drop models used in MATRA-LMR code with ORNL 19 pin tests. The accuracy of the pressure drop data was the important parameter for predicting the temperatures in the fuel bundle. The three models used have similar trends to the experimental results as shown in figure 6. But the Novendstern model generally predicted high and inaccurate temperatures, especially for the internal regions. One possible reason is that

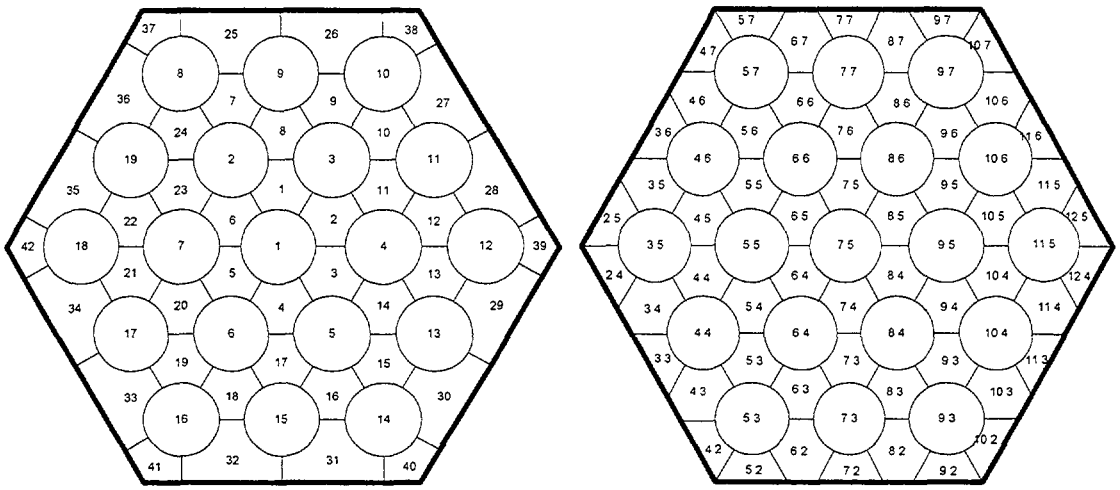

Fig. 4 Subchannel numbering schemes

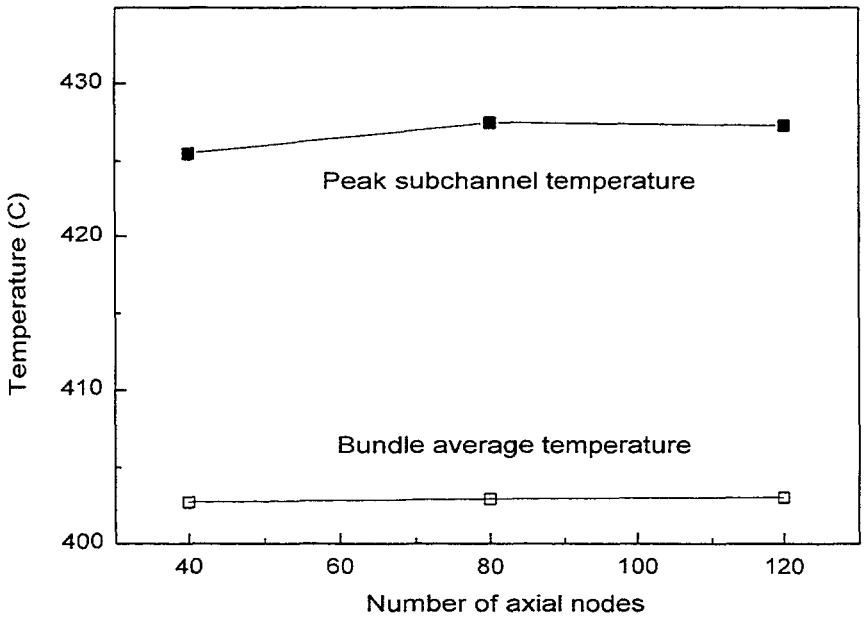

Fig. 5 Temperatures according to the number of axial nodes (MATRA-LMR)

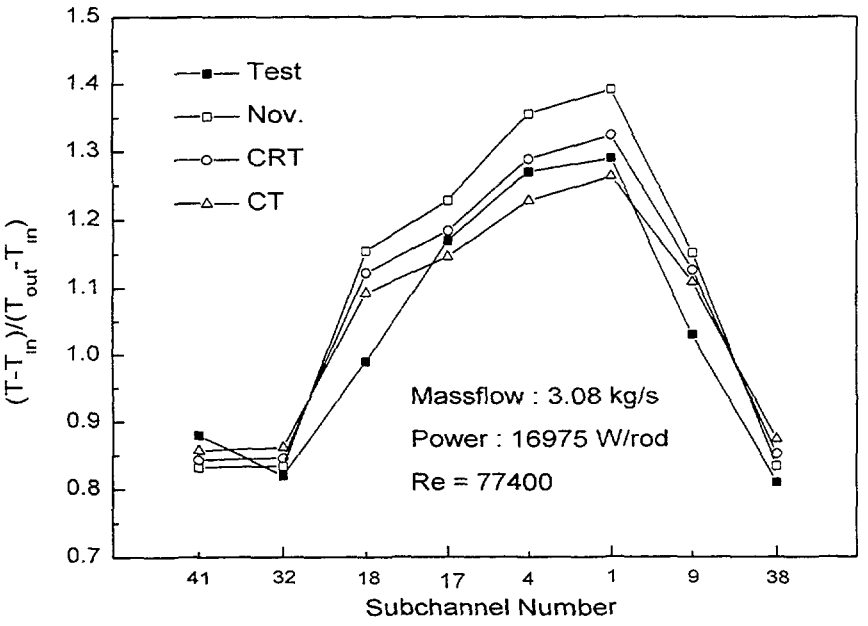

Fig. 6 Normalized temperatures at the end of the heated length (high power/flow)

the Novendstern model does not take into account the form loss induced by the wires. And it uses the same pressure drop for the internal and the edge regions which have differences in geometry and flow behavior. The CRT model was more accurate, though it predicted a little higher temperatures than the experimental results. On the contrary, the model proposed by Cheng and Todreas predicted a little lower temperatures than the experimental results. Based on the above comparisons, the CRT model was adopted to use as reasonable results.

Figure 7 shows the normalized temperatures at the end of the heated length for high power/flow case of 3.08 kg/s and 16975 W per rod. Temperature profiles are plotted in figure 7 for the calculations with MATRA-LMR, SABRE4 and SLTHEN codes, and compared with the

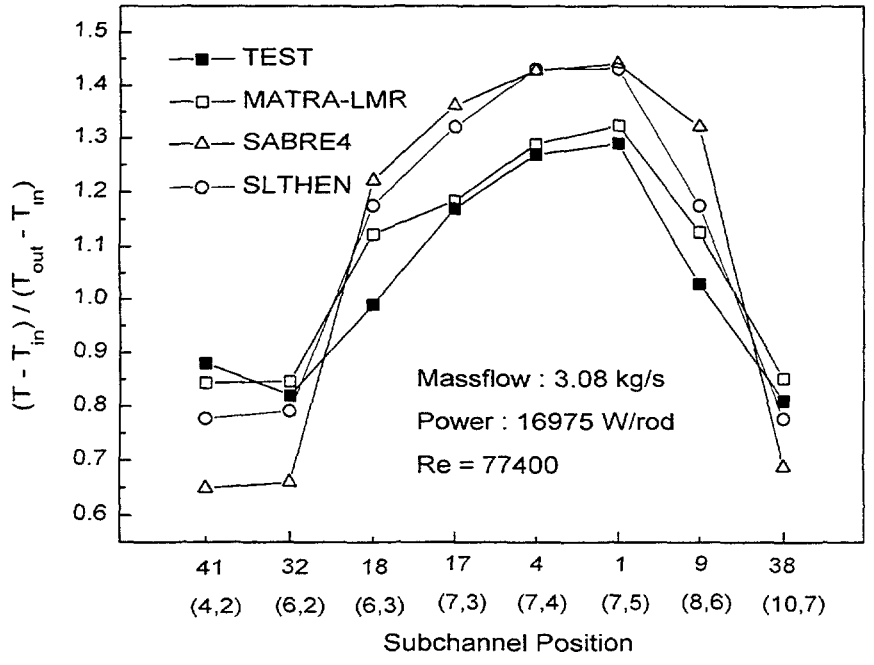

Fig. 7 Normalized temperatures at the end of the heated length (high power/flow)

experimental results at the same axial location MATRA-LMR predicted the experiment within 15% maximum, but the other two codes showed much different behaviors from the experiment SABRE4 underpredicted so much at the outer region, i e edge and corner sides Although it predicted well the temperatures of the interior channels, it failed to predict the temperatures of the peripheral subchannels The difference between MATRA-LMR and SABRE4 calculations comes partly from the modeling of pressure drop induced wire wraps For instance, the wire wrap model in SABRE4 assumes that the effects of the wraps can be represented as specified resistance coefficients tangential and perpendicular to the wraps Geometrical differences in area and wetted perimeter are included in the derivation of these coefficients, while actual subchannel flow areas are modified in MATRA-LMR On the other hand, SLTHEN overmedicated the temperatures in the interior side Unlike the above two codes, SLTHEN uses a relatively simple model to reduce the computational time For instance, an effective eddy diffusivity is employed for the physical model of the crossflow caused by the wire wrap The velocities in the internal and the wall regions of an assembly can be obtained from the theoretical flow split method These approximations enable the momentum equations to be decoupled from the energy equations Once the flow is split, the temperatures and the pressure drops are calculated along the axial noding with the finite difference equations According to the simple model, there are only two velocity fields for the inner and the outer regions respectively, and the same subchannel velocity is maintained in each region while the other two codes have different velocities corresponding to the heat source in each subchannel

Figure 8 shows the axial temperature profiles in the interior and the edge subchannels for high power/flow case with MATRA-LMR and SABRE4 codes As discussed above, both codes show excellent agreement with the experimental results in the interior subchannel 1 But in the edge subchannel 32, SABRE4 underpredicted temperatures more than MATRA-LMR The following figures show more detailed reason on it

Figures 9, 10 and 11 show the subchannel crossflow velocities in the interior, at the interface between the interior and the edge, and between the edge gaps for high power/flow case, respectively Subchannel crossflow velocities in the interior gap between the channels 1 and 6 show that the two codes predicted almost the same temperatures, i e 0 25 m/s, as shown in figure 9 Figure 10 shows the crossflow velocities as a function of axial position for interface gap between the interior and the edge channels 9 and 26 Compared to the case of interior channels as shown figure 9, the magnitudes of the crossflow velocities were larger, but still the two predictions were in good agreement On the contrary, for the crossflow velocities in the

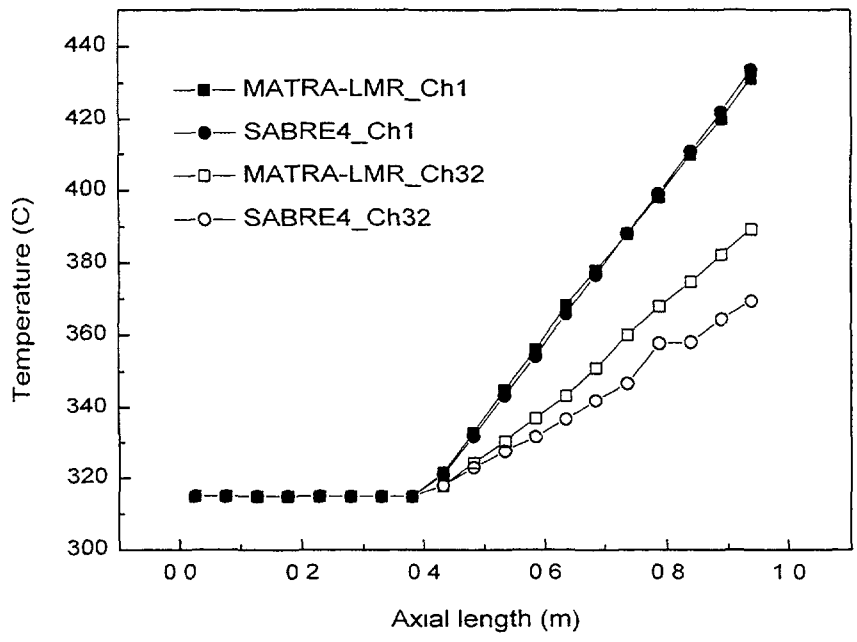

Fig 8 Axial temperature profiles in the interior and the edge subchannels (high power/flow)

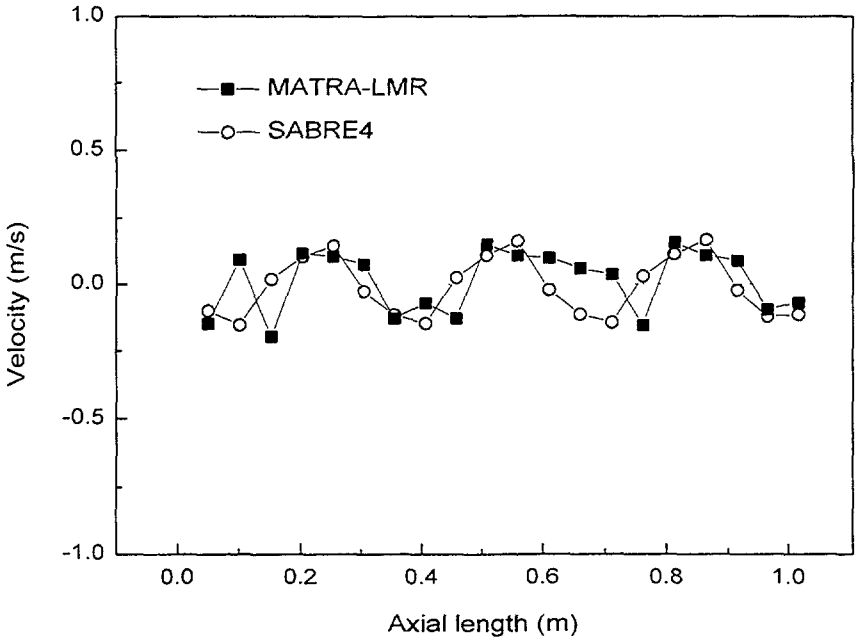

Fig. 9 Subchannel crossflow velocities in the internal gap (Channel 1 to 6)

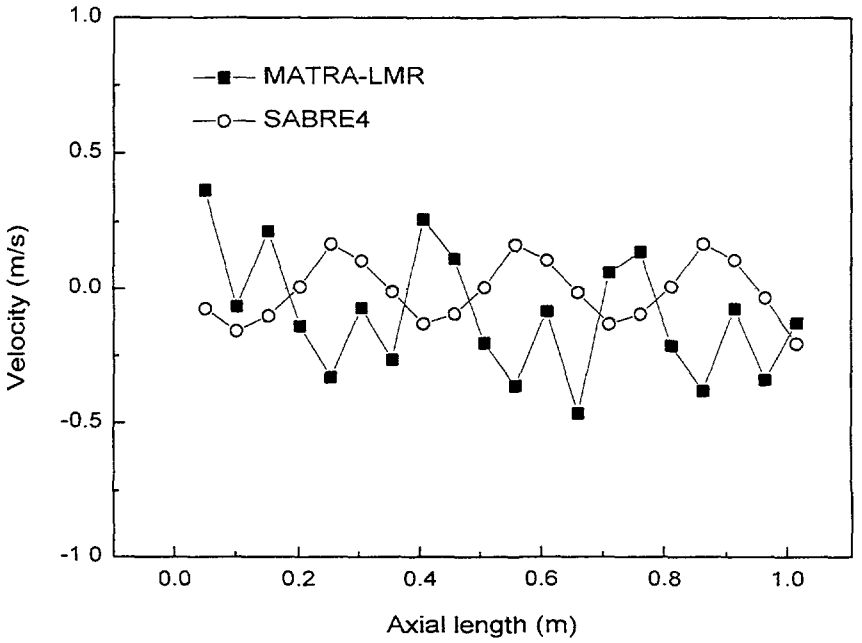

Fig. 10 Subchannel crossflow velocities in outer gap (Channel 9 to 26)

edge gaps the two predictions show different behaviors as shown in figure 11. There is one circumferential swirl flow due to the unidirectional wire wrap in the edge subchannels. That is the summation effect of swirl forces by wire wraps passing through adjacent edge gaps near the duct wall. MATRA-LMR predicted larger crossflow velocities than SABRE4. In this calculation, the axial average velocity was predicted about 7.5 m/s by MATRA-LMR and the crossflow velocity about 1.5 m/s. The above behavior in the edge side make a significant effect for temperature predictions. This difference might cause the temperature underpredictions with SABRE4 at the outer regions.

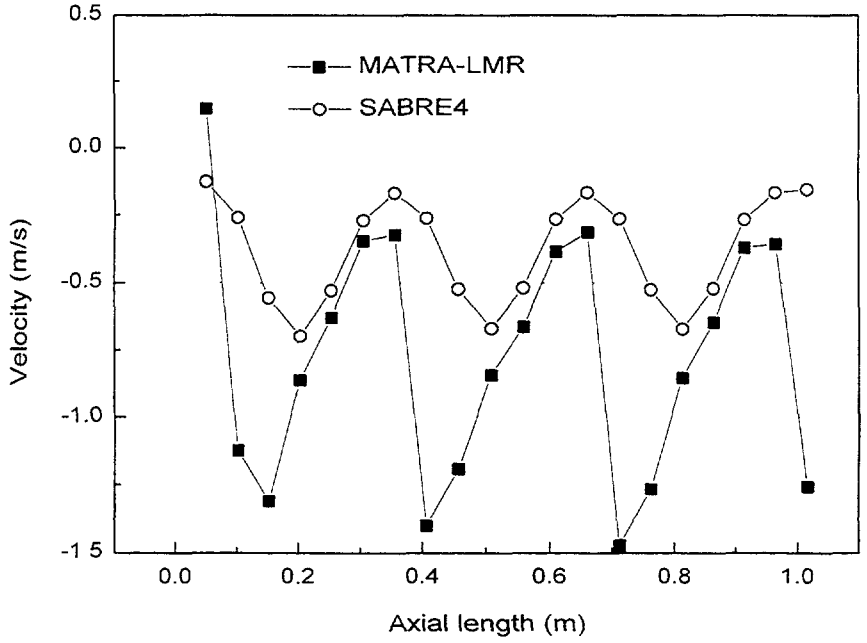

Fig. 11 Subchannel crossflow velocities in the edge gap (Channel 25 to 26)

Figure 12 shows the normalized temperatures at the end of the heated length for the low power/flow case of 4.09E-2 kg/s and 263 W/rod. In this case, SABRE4 calculations are in reasonably good agreement with the experiment. MATRA-LMR calculations are higher in the internal region and slightly lower in the outer region than the experimental results. While the temperature profiles remain relatively stable at the higher power/flow case, the conductive heat transfer has more important influences on the temperature distributions throughout the bundle at the lower power/flow case. In this low power/flow case, Reynolds number is 1000, while 77400 for high power/flow case. So the calculation conditions was out of application of SLTHEN because of its basic models. Further studies are needed for the low power/flow cases.

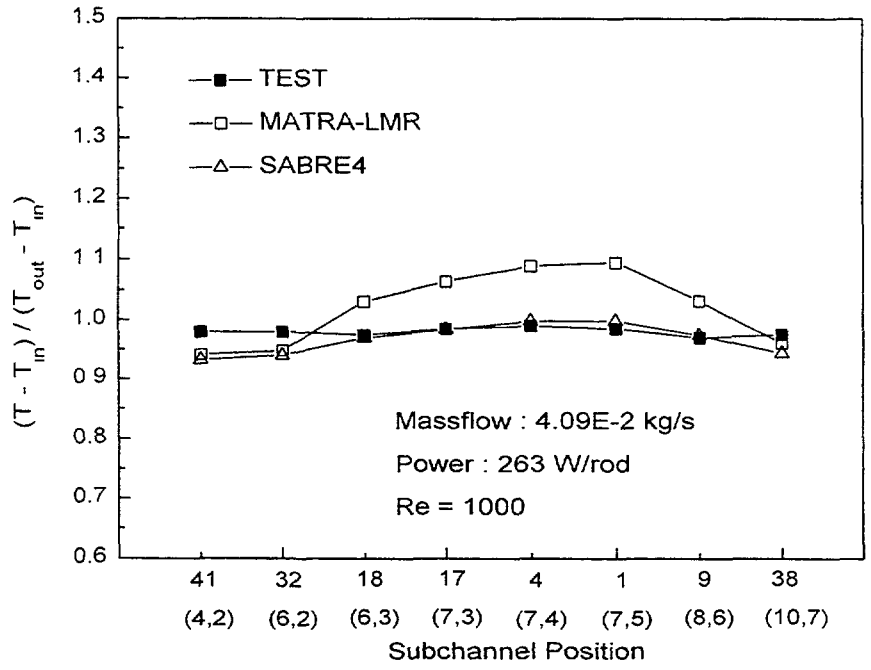

Fig. 12 Normalized temperatures at the end of the heated length (low power/flow)

3.3. EBR-II 91 pin test

EBR-II experiment which is used in this paper is a seven assembly problem This seven assembly problem is composed of one 7 pin assembly, two 61 pin assemblies, and four 91 pin assemblies as shown in figure 13 The power and flow rate of each assembly are also shown in the figure Two 91 pin assemblies are calculated for the comparisons high power assembly of 0 63 MW and 3 889 kg/s and low power assembly of 0 37 MW and 3 076 kg/s

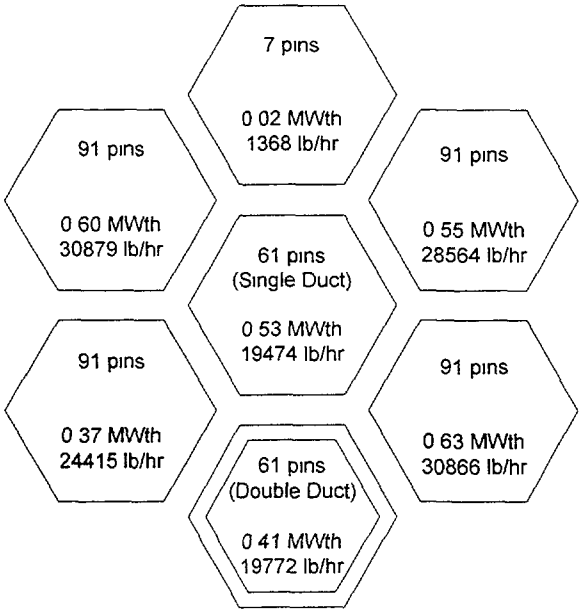

Fig 13 Layout of EBR-II seven-assembly problem

Table 2 gives the comparisons of the above three codes on the average exit and peak subchannel temperatures It was observed that MATRA-LMR predicted slightly different temperatures from the other two codes by as much as 3% higher in the average exit and lower in the peak subchannel temperatures Whereas the computational time of MATRA-LMR is 75% less than SABRE4 but is considerably larger than SLTHEN Based on the results, MATRA-LMR which is being developed for predicting temperature distributions in wire wrapped LMR fuel rod bundles matches the available data with the same precision as complicated or simplified subchannel analysis codes which are used now

3.4. Application to the KALIMER Core Design

Korea Advanced Liquid Metal Reactor (KALIMER), a 150 MWe pool-type sodium cooled prototype reactor, is currently under conceptual design study with the target schedule to complete its construction by the mid-2010s An initial design concept also was proposed through the feasibility study of various innovative design features Based on the insight and results from the previous work, the KALIMER program plan was updated to call for the completion of the basic design and supporting R&D work by 2006

The KALIMER core system is designed to generate 392 MWth of power The reference core utilizes a homogeneous core configuration in radial direction with two driver fuel enrichment zones, surrounded by a layer of blanket assemblies The reference core has an active core height of 100 cm and a radial equivalent diameter of 172 cm, and the height-to-diameter ratio for the active core becomes 0 581 The physically outermost core diameter of all assemblies is 344 7 cm Major design parameters and geometric characteristics of the assembly are given in table 3

A KALIMER radial blanket assembly was chosen to calculate the temperature distributions with MATRA-LMR code, and to compare the results with SABRE4 and SLTHEN codes Figure 14 shows the subchannel numbers where the temperatures are compared across the assembly As

Table 2 Calculation results for EBR-II 91 pin test

High power/flow case

Parameters	MATRA-LMR	SABRE4	SLTHEN
1 Average exit temperature (℃)	512 9	498 0	495 1
2 Peak subchannel temperature (℃)	560 6	574 6	571 0
3 Bundle average pressure drop (MPa)	0 057	0 042	0 051
4 Computing time (sec) (HP J200 Workstation)	330	1440	0 78

Low power/flow case

Parameters	MATRA-LMR	SABRE4	SLTHEN
1 Average exit temperature (℃)	475 2	465 0	462 0
2 Peak subchannel temperature (℃)	510 4	520 1	512 3
3 Bundle average pressure drop (MPa)	0 042	0 032	0 034
4 Computing time (sec) (HP J200 Workstation)	378	1440	0 78

Table 3 Input parameters for KALIMER 98.03 design

Core	Core thermal output (MWth)	392 2
	Core electric power (MWe)	150 0
	Core inlet / outlet temperature (℃)	386 2 / 530 0
	Total flow rate (kg/s)	2143
	Active core height (mm)	1000
	Core diameter (mm)	3447 3
	Core configuration	radial homogeneous
	Pins per fuel assembly (driver/radial blanket)	271 / 127
127 pin assembly	Total axial height (mm)	3163 0
	Rod outer diameter (mm)	12
	Rod pitch (mm)	13
	Wire wrap diameter (mm)	0.95
	Wire wrap lead (mm)	300
	Cladding thickness (mm)	0 54
	Duct wall thickness (mm)	3 7
	Duct inside flat-to-flat distance (mm)	149 8
	Nominal linear pin power (W/cm)	34 91
	Assembly nominal flowrate (kg/s)	4 59
	Assembly coolant inlet temperature (℃)	386 2
	Number of axial nodes	250 (MATRA-LMR 64 (SABRE4)
	Radial power distribution	uniform

shown in figure 15, three results are in good agreement in the inner region, though SABRE4 predicted a little higher temperatures. The flat temperature profiles were found in the inner region for this blanket calculation. In these calculations, they showed the similar mixing behavior induced by wire wraps in the inner region, because the radial power profile is assumed to be uniform. On the other hand, in the outer region where the peripheral swirl flow occurred, as illustrated in figure 15, MATRA-LMR predicted higher temperatures than the other two codes, because MATRA-LMR generated larger swirl flow. The Reynolds number was 11100 in this calculation. Based on the calculation results for high power/flow case of ORNL 19 pin test mentioned above, it may be concluded that the MATRA-LMR gives more precise predictions than the other two codes for both regions of the bundle. All the calculations were performed on the HP J200 workstation. The required computational times were 1758, 2400 and 1.38 sec for MATRA-LMR, SABRE4 and SLTHEN codes respectively.

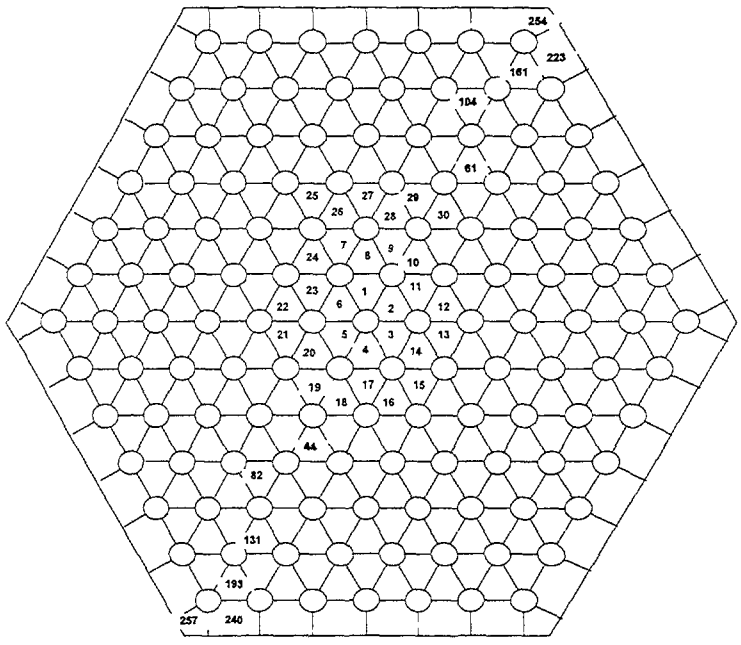

Fig 14 MATRA-LMR 127 pins subchannel numbering scheme

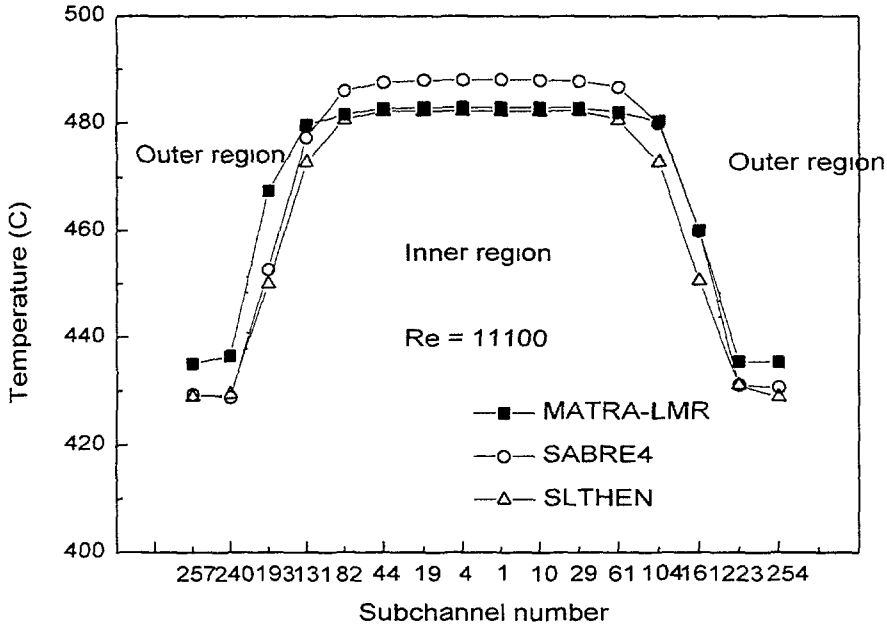

Fig. 15 Temperatures at the end of the heated length
(KALIMER127 pin radial blanket assembly)

4. CONCLUSIONS

The development status of the detailed subchannel analysis code MATRA-LMR was assessed from the benchmark calculations with SABRE4 and SLTHEN codes. The MATRA-LMR calculations for the ORNL 19-pin assembly tests and EBR-II 91-pin experiments were compared to the measurements, and to SABRE4 and SLTHEN code calculation results, respectively.

The comparison results for ORNL 19 pin tests showed that there was a good agreement between MATRA-LMR calculations and the experimental data as shown in the axial temperature profiles. Also the accuracy of the pressure drop models was compared for the ORNL 19-pin assembly tests. The results indicated that the CRT predictions were in good agreement with the experimental results better than the other methods. SABRE4 overmedicated the temperatures in edge side and SLTHEN results showed higher temperatures in the internal region. The differences are found among the three codes because of the pressure drop induced by wire wrap. In comparisons for EBR-II seven assembly problem calculations, it was observed that MATRA-LMR predicted slightly different temperatures from the other two codes by as much as 3% higher in the average exit and lower in the peak subchannel temperatures. Whereas the computational time of MATRA-LMR is 75% less than SABRE4 but is considerably larger than SLTHEN. In the application for KALIMER design, MATRA-LMR predicted quite as well as the other two codes.

From the all the benchmark calculations, it can be concluded that MATRA-LMR code is a reliable analysis tool for KALIMER subassembly design and performance analysis. The current version of MATRA-LMR is used only for a single subassembly analysis, but it is planned to extend for the multi-assembly whole core calculations.

REFERENCES

[1] WALTAR, A.E., REYNOLDS, A.B., "Fast Breeder Reactors", Pergamon Press (1981).

[2] TANG, Y.S., et al., "Thermal Analysis of Liquid-Metal Fast Breeder Reactors", ANS (1978).

[3] STEWART, C.W., et al., "COBRA-IV: The Model and The Method", PNL (1977).

[4] WHEELER, C.L., et al., "COBRA-IV-i : An Interim Version of COBRA for Thermal-Hydraulic Analysis of Rod Bundle Nuclear Fuel Elements and Cores", BNWL-1662 (1976).

[5] BASEHORE, K.L., TODREAS, N.E., "SUPERENERGY-2: A Multiassembly Steady-State Computer Code for LMFBR Core Thermal-Hydraulic Analysis", PNL (1980).

[6] DOBSON, G.P., O'NEILL, J.M., "A User's Guide to the Sabre Code", *RSSD 261*, AEAT (1992).

[7] YOO, Y.J., HWANG, D.H., "Development of Subchannel Analysis Code MATRA α -version," *Proc. of KNS Autumn Meeting.*, Taegu, Korea, October 24-25 (1997).

[8] LYON, R.N., "Liquid Metal Heat Transfer Coefficients," *Chem. Eng. Prog*, pp. 47-75 (1951).

[9] CARELLI, M.D., KAZIMI, M.S., "Heat Transfer Correlation for Analysis of CRBRP Assemblies", Westinghouse Report, CRBRP-ARD-0034 (1976).

[10] NOVENDSTERN, E., "Turbulent Flow Pressure Drop Model for Fuel Rod Assemblies Utilizing A Helical Wire-wrap Spacer System", *Nuclear Engineering and Design*, 22, pp. 19-27 (1972).

[11] CHIU, C., ROHSENOW, W.M., TODREAS, N.E., "Turbulent Flow Split Model and Supporting Experiments for Wire-wrap Core Assemblies", COO-2245-56TR, MIT (1978).

[12] CHENG, S.K., TODREAS, N.E., "Hydrodynamic Models and Correlations for Bare and Wire-wrapped Hexagonal Rod Bundles - Bundle Friction Factors, Subchannel Friction Factors and Mixing Parameters", *Nuclear Engineering and Design*, 92, pp. 227-251 (1986).

[13] MacDOUGALL, J.D., LILLINGTON, J.N., "The Sabre Code for Fuel Rod Cluster Thermohydraulics", *Nuclear Engineering and Design*, 82, pp. 171-190 (1984).

[14] KHAN, E.U., et al., "A Porous Body Model Predicting Temperature Distribution in Wire-Wrapped Fuel Rod assemblies", Nuclear Engineering and Design 35 1-12 (1975).

[15] YANG, W.S. (1997), "An LMR Core Thermal-Hydraulics Code Based on the ENERGY Model", *Journal of Korean Nuclear Society*, 29, No. 5, pp. 406-416 (1997).

[16] FONTANA, R.E., et al., "Temperature Distribution in the Duct Wall and at the Exit of a 19-Rod Simulated LMFBR Fuel Assembly (FFM Bundle 2A)", *Nuclear Technology*, 24, pp. 176-200 (1974).

HYDRODYNAMIC MODULE VALIDATION OF THE HYCO-3DT CODE

A.S. KORSUN, S.G. VITRUK
Moscow Engineering Physics Institute,
Moscow

P.A. USHAKOV, B.N. GABRIANOVICH
State Scientific Center of Russian Federation,
Institute of Physics and Power Engineering,
Obninsk, Kaluga Region

Russian Federation

XA0055054

Abstract

Verificated hydrodynamical module of a program complex "THEHYCO-3DT", created in frame neutronic termalgidrodinanical of a program complex "SKETCH" in MEPI on faculties "Therophysics " and "Physics NPP" for modeling three-dimensional non-stationary neutrons - and is termal- of physical processes in an active zone perspective NPP fuel subassemblies without wrapper tube. The data of experiment and results of account are submitted.

1. INTRODUCTION.

The efficient algorithms for mathematical modelling of transient events ranging from normal operational slates to catastrophic accident excursions have been created in Moscow Engineering Physics Institute [1,2,3]. In particular computer code named **SKETCH** (Space **K**inetic and **T**hermal **HY**drodynamic) with thermal hydrodynamic module **THEHYCO-3DT** (**THE**rmal **HY**drodynamic **CO**de - **3 D**imensional **T**ransient) has been developed for analysing of transient events processes in passive safety core without assemblies duct walls. This report is mainly concerned with the hydrodynamic module validation of THEHYCO-3DT code.

2. MATHEMATICAL MODEL.

The multilevel mathematical model of core thermohydrodynamics is used in computer code THEHYCO-3DT for complex calculation (Fig. 1)

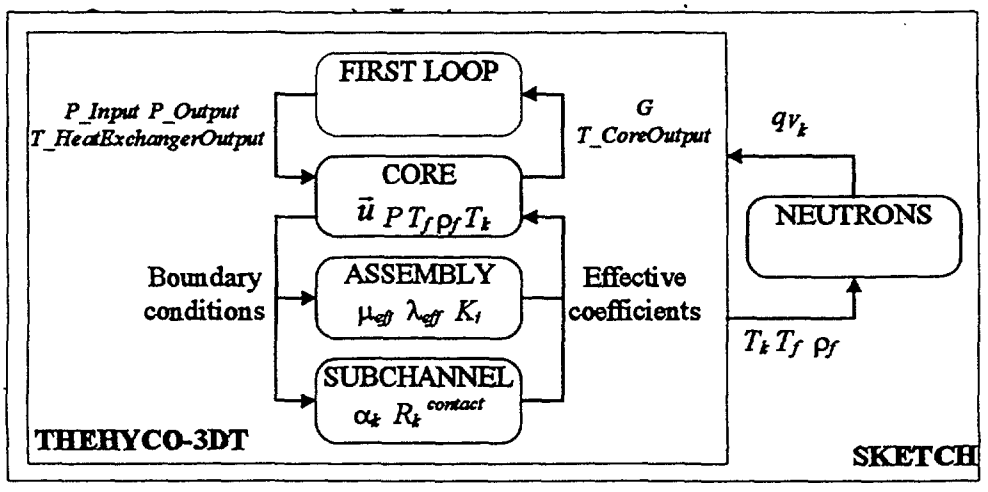

Fig. 1. The core multilevel model, realised in computer code SKETCH.

3. MODEL ADEQUASY.

Each module of thermal hudrodynamic code THEHYCO-3DT has been tested separately, but complex experiment is still required. The hudrodynamicmodule is the most significant one. For this module P.A. Ushakov, B.N. Gabrionovich have carried out the experiment on assembly, flowed by air.

The assembly consised of 563 wire wrap rods ([11÷12] rows × 49 colums). In the Fig. 2, the experimental assembly is shown (d - rod diameter, L - assembly length, T - period of wire wrap, s - distans between centres of adjacent chennels). The velocity field has been measured inside the assembly under the conditions of 37% input or/and output blockages.

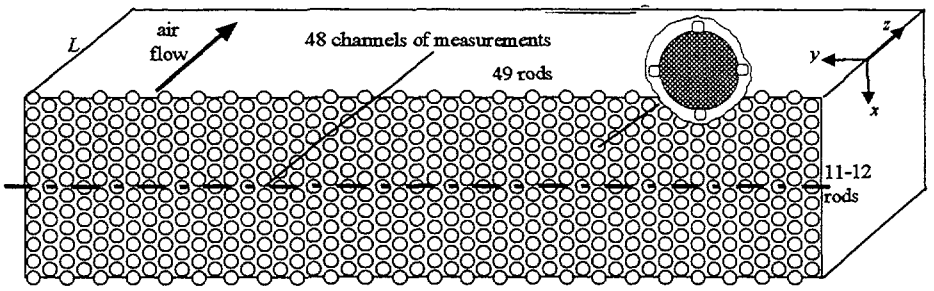

Fig. 2. Experimental assembly (d=15 mm, L/d=84, T/d=62, s/d=1.13, Re=7900)

- **the central blockage of input or output**

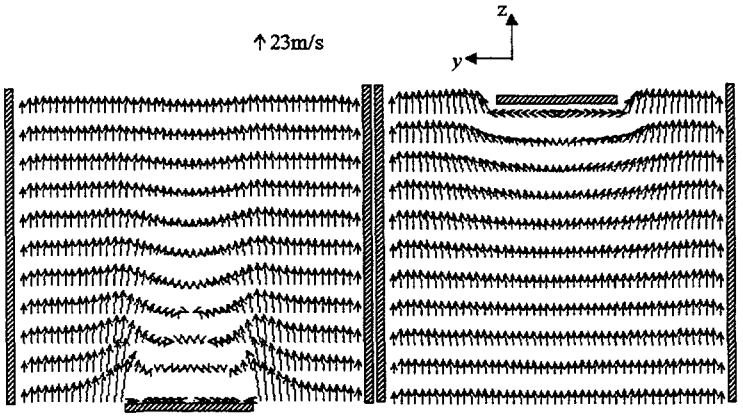

Figure 3. Velocity field.

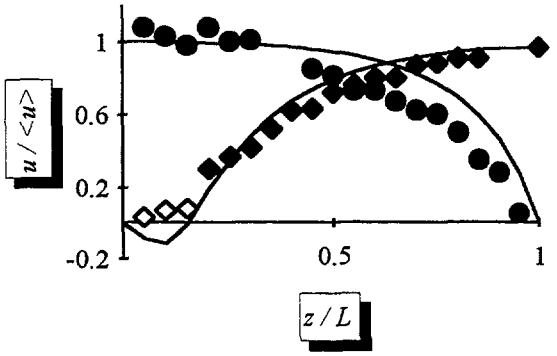

(- calculation, ♦ ● experiment, ◊ accuracy loss)

Figure 4. Axial velocity in central channel.

- the wall-adjacent blockage of input or output

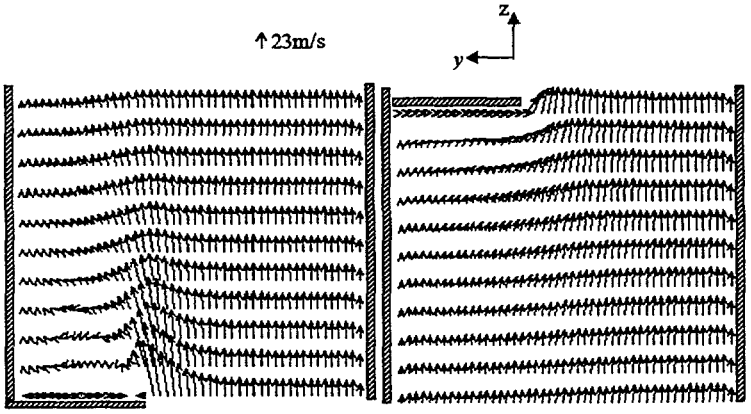

Figure 5. Velocity field.

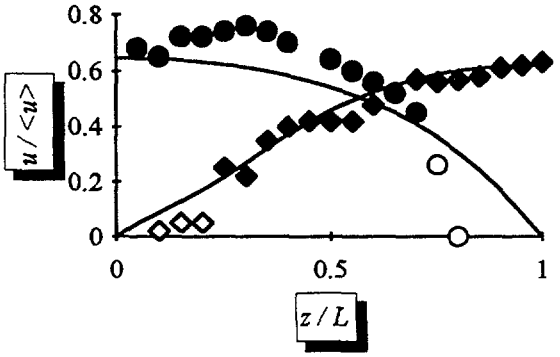

(- calculation, ♦ ● experiment, ◊ O accuracy loss)
Figure 6. Axial velocity in wall-adjacent channel.

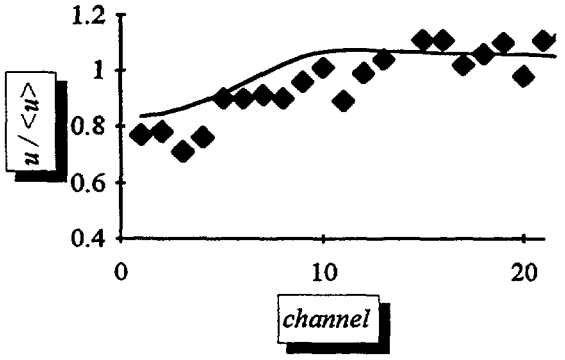

Figure 7. Axial velocity in cross section (z=L/2) under the central blockage of input.

- **the wall-adjacent blockage of input and output**

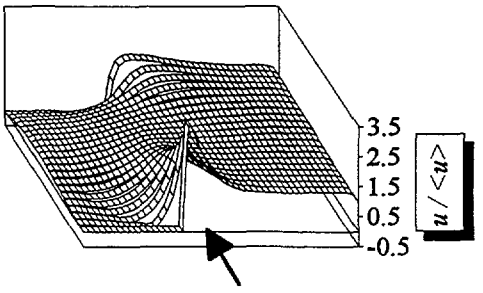

Fig. 8. Velocity field.

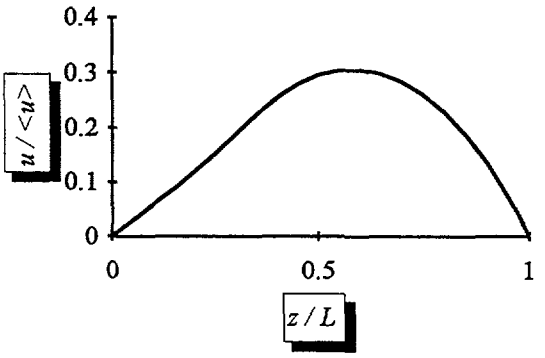

Fig.9. Axial velocity in well-adjacent chennel (down) (experimental data are impossible)

CONCLUIONS

The experimental results good agree with calculations ones. It should be pointed out that the porous media model, used in THEHYCO-3DT, is universal approach. That is why code works in core as well as in assembly and with air as well as with liquid metal. But for any intended code application effective dynamic viscosity μ_{eff} (kg/ms), effective thermal conductivity λ_{eff} (W/m K), coefficients of resistance-form force coefficients K_i (l/m) for fluid and heat transfer coefficient α_k (W/m^2 K),contact termal resistance $R_k^{contract}$ (m^{2}K/W) for k-type fuel rod must be correctly defined and further liquid metal experimental data are required for LMFBR code validation.

The code requires 486DX or higher processor and about 4 Mb of memory, only.

REFERENCES

[1] SCHUKIN N. V., KORSUN A.S., VITRUK S.G., ZIMIN V.G., ROMANIN S.D. Mathematical Model and Computer Code for the Analysis of Advanced Fast Reactor Dynamics // Proceedings of the Joint International Conference on Mathematical Methods and Supercomputing in Nuclear Application, M&C+SNA'93: Congress and Exhibition Centre Karlsruhe, Germany, v.1, (April 19-23, 1993).

[2] SCHUKIN N. V., ZIMIN V.G., ROMANIN S.D., VITRUK S.G., KORSUN A.S., BATURIN D.M. Validation and Verification of Computer Code SKETCH for the Analysis of Advanced Fast Reactor Dynamics // Proc. of 1994 Topical Meeting on Advances in Reactor Physics, Knoxville, USA, v. 2, pp. 313-323, (April 11-15, 1994)

[3] SCHUKIN N. V., ZIMIN V.G., ROMANIN S.D., VITRUK S.G., KORSUN A.S., BATURIN D.M. The Code SKETCH for Space Dynamic Modelling of Enhanced Fast Reactor // Issues of Nuclear Science and Design, Moscow, Russian.

SPECIAL FEATURE OF TEMPERATURE FIELD FORMATION IN THE SYSTEM OF INTERACTING FUEL SUBASSEMBLIES IN FAST REACTOR CORE

I.L. BOGATIRJEV, A.V. ZHUKOV, N.M. MATJUKHIN,
A.P. SOROKIN, P.A. USHAKOV
State Scientific Center of Russian Federation,
Institute of Physics and Power Engineering,
Obninsk, Kaluga Region, Russian Federation

Abstract

Model experiments simulating interacting of fuel subassemblies in fast reactor being under operational reactor conditions have been analyzed to define the influence of geometrical and flow parameters on temperature distribution. In a new version of subchannel code MIF-AZ relationships developed on the basis of experimental results were taken into account. The predictions let us assess an influence of inter-subassembly heat transfer as well as deformation of pin bundles and duct observed in reactor campaign on temperature distribution.

1. INTRODUCTION

The effect of inter-subassembly heat transfer can be a significant influence on the system behavior. The magnitude of this effect depends on several factors including the extent of radial power variation within subassembly, the flow characterization as well as geometric one.

There are a lot of papers, for example [1-4], concerning the influence of inter-subassembly heat transfer on temperature distribution within fuel subassembly placed in the reactor core periphery, that is where the maximum radial power gradient across the subassembly is provided. It should be noted that for the most part these studies have been carried out under idealized conditions.

In any case, the inter-subassembly heat transfer tends to reduce the radial temperature non-uniformity across the core thereby providing an extra safety margin.

In the reactor campaign the pin bundle, as such, and subassembly duct are subjected to deformation of different origin. Study of the interaction between subassemblies being under deformation is obviously complex problem. It calls for detailed rod bundle thermal-hydraulic experiments and predictions based on relations derived from the tests.

This paper is concerned with the effect of factors mentioned above on temperature field in the system of interacting fuel subassemblies of fast breeder reactor.

2. EXPERIMENTS

Test bundle that has been mounted on the 6B facility consists of 37 electrically heated fuel pin simulators arranged in triangular manner with relative pitch s/d=1.17 and enclosed into hexahedral duct. Some simulators have been made as turning ones that allow measurings to be carried out of the azimuthal temperature distribution at simulator wall by thermocouples embedded at different length distances. Coolant temperature within bundle cells is measured by thermocouples, too. As to velocity profiles that are defined with the use of electromagnet transducers.

Test bundle with hexagon has been enclosed into additional hexahedral cover and rate of coolant flowing throughout the gap between the main duct and additional conditions on subassembly duct. Detaled description of the 6B test facility is given, for example, in [6].

Experiments performed as the Peclet number varies from 60 to 400 have shown that temperature distribution on edge pin simulation depends to a large degree on the length distance from the beginning of the heating (Fig.1).

It is clear that variation of temperature nonuniformity is of instabilized character. The enhancement of the flow moving throughout the gap between subassembly duct and cover from 0 to 20% causes the value of maximal nonuniformity of simulator temperature to increase by a factor of 1.25÷1.5.

3. DESCRIPTION OF THE MODEL

Termahydraulics calculation of subassembly in the special case that it's duct is under non-adiabatic conditions has been developed on the basis of subchannel approach [5-7]. Steady-state conservation equations of mass, momentum and energy written for each individual channel by which the subassembly is divided are supplemented with conservation equations for cells placed in inter-subassembly gap. A complete temperature distribution around the pin simulator Is determined by the interpolating procedure starting from the calculated temperatures in characteristic points of perimeter (narrow or wide parts of the channels) as the base. In its turn temperature in these points is defined as superposition of mean over channel coolant temperature calculated by the set of conservation equations solving in the framework of subchannel approach and local superheating (underheating) of pin simulator wall.

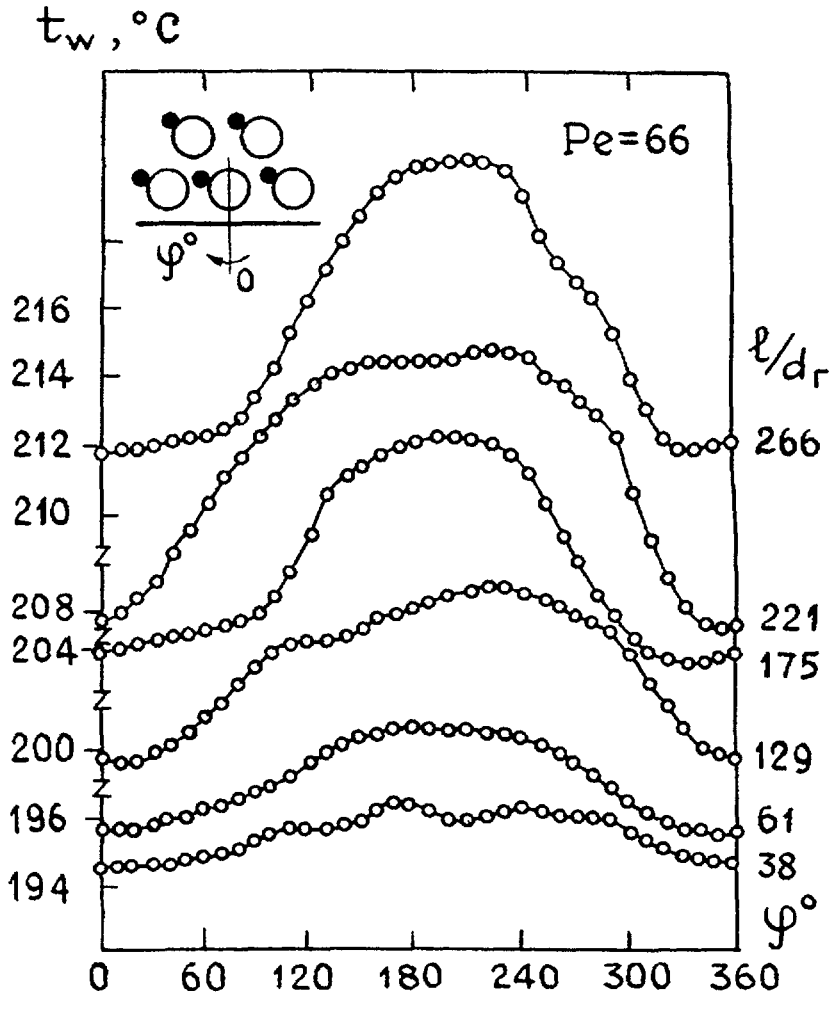

Fig.1 Azimuthal temperature distributions of edge pin simulator

In a handling a problem the system of seven interacting subassemblies with adiabatic conditions at external boundary of the system has been examined. Mathematical model prescribes the arbitrary profile of heat release throughout the length of pin as well as pin and subassembly duct deformation of different kind. throughout the gap can be changed arbitrarily, too.

Mathematical model has been realized in the code MIF-AZ [9] which were verified on a considerable body of experimental results.

4. SUBASSEMBLIES ARRANGED AT THE CORE CENTRE

The relationships for subassembly radial distribution of velocity and coolant temperature in the case that non-adiabatic conditions are imposed on subassembly duct as well as for maximal azimuthal nonuniformity of edge pin temperature have been obtained from the calculations.

Velocity profile in stabilized case can be expressed as:

$$\frac{W_i}{\overline{W}} = \frac{W_0}{\overline{W}}\left[1-\left(1-\frac{W_E^{\mu}}{W_0}\right)e^{-\frac{R_E-R_i}{d\Gamma_M}}\right] \tag{1}$$

where

$$\frac{W_E^{\mu}}{W_0} = \frac{W_E^0}{W_0}+\left(1-\frac{W_E^0}{W_0}\right)\left[1-\frac{1-e^{-\Gamma_M}}{\Gamma_M}\right] \tag{2}$$

$$\Gamma_M = 0{,}57\frac{\mu_{\Sigma}^{W} d_{r_0}}{\lambda}\left(1+\frac{\omega_0}{\omega_E}\right)$$

Temperature profile in subassembly cross section is:

$$\frac{\Delta t_i}{\overline{\Delta t}} = \frac{\sum_{j=1}^{N}\left(\frac{d_{r_j}}{d_{r_0}}\right)^{\frac{5}{7}}\omega_i \Big/ \left(\frac{\lambda_j}{\lambda_0}\right)^{\frac{4}{7}}}{\sum_{j=1}^{N}\omega_j} \times \left[1-\left(1-\frac{\Delta t_E}{\Delta t_0}\right)e^{-\frac{R_E-R_i}{d\sqrt{T_M}}}\right] \tag{3}$$

where

$$\frac{\Delta t_E}{\Delta t_0} = \frac{1}{g_{eff}}\left\{1+\left[\frac{g_{eff}}{1+\frac{\mu_{i\xi}^T}{\mu_{eff}^T}e^{-T_П}}\right]f(T_M)\right\} \tag{4}$$

$$f(T_M) = 1-\frac{1-e^{-T_M}}{T_M}\left[1+0{,}16T_M+0{,}008(T_M)^2\right]$$

$$g_{eff} = g_E + g_{leak}e^{-\frac{1}{T_П}}$$

$$T_M = \frac{\mu_{eff}^T L}{g_{eff}}\left[1+\frac{\mu_{i\xi}^T}{\mu_{eff}^T}e^{-T_П}\right]$$

$$T_П = \frac{\mu_{i\xi}^T L}{g_{leak}}, \qquad g_E = \frac{W_E^\mu \omega_E}{W_0\omega_0}, \qquad \Delta t_0 = \frac{4qL}{Pe_0\lambda}$$

Relative maximal azimuthal non-uniformity of edge pin temperature is described as:

$$\frac{t_w^{max}-t_w^{min}}{\Delta t_0} = \left(1-\frac{1}{g_{eff}}\right)\frac{1-e^{-T_M}}{T_M}+\frac{Pe}{8}\frac{d}{L}\left[\frac{z}{z+1}\Delta T_{tri}^{max}+\frac{1}{z+1}\Delta T_{squ}^{max}\right] \tag{5}$$

Relations (l),(3),(5) have indicated that in the case of uniform heat release distribution over subassembly cross section velocity temperature and azimuthal temperature non-uniformity of edge fuel pin depend on initial geometrical parameters and dimensionless complexes Γ_M, T_u, $T_П$.

If the momentum exchange is only slightly being presented ($\tilde{A}_M<1$) what is typical for the bundle involving only smooth pins the velocity distribution depends to a large extent on ratio between hydraulical diameters and friction coefficients in edge and central channels. Intensive interchannel exchange involved within wire wrapped pin bundle ($\Gamma_M>3$) can significantly level off velocity distribution.

In a similar manner the radial nonuniformity of temperature is reduced by intensification of interchannel heat transfer. It is followed from formula (3) that as heat transfer throughout subassembly duct is only moderate $\left(\mu_{i\xi}^T, м^{-1}\right)$ or inter-subassembly coolant flow is small $\left(g_{leak} << 1\%\right)$, inter-subassembly heat transfer has in a very small extent influence on temperature field formation. Once inter-subassembly heat transfer is significant $\left(\mu_{i\xi}^T > 2, м^{-1}\right)$ or coolant flow through out the gap is great $\left(g_{leak} > 2\%\right)$ the coolant temperature in edge region of subassembly is diminished on some tenths of value of mean coolant heating along subassembly. Also it increases significantly the edge pin

azimuthal temperature non-uniformity. At the same time heat transfer throughout the duct exerts influence on temperature of, at a maximal, three – four rows of pins adjusting to duct.

5. TEMPERATURE FIELD IN PERIPHERAL REGION THE OF CORE

Prediction of temperature distribution in the group of interacting subassemblies which are in peripheral region of fast reactor core when non-uniform heat in subassembly cross section takes place has shown that as flow throughout the gap being small $(g_{leak} > 2\%)$ there is some drop of maximal coolant temperature in that region of subassembly where heat release is higher, at the same time there is rise of coolant temperature in adjacent subassembly with the lower heat release. The flow throughout the inter-subassembly gap Is higher, the coolant temperature In peripheral region of subassembly is lower (Fig.2)

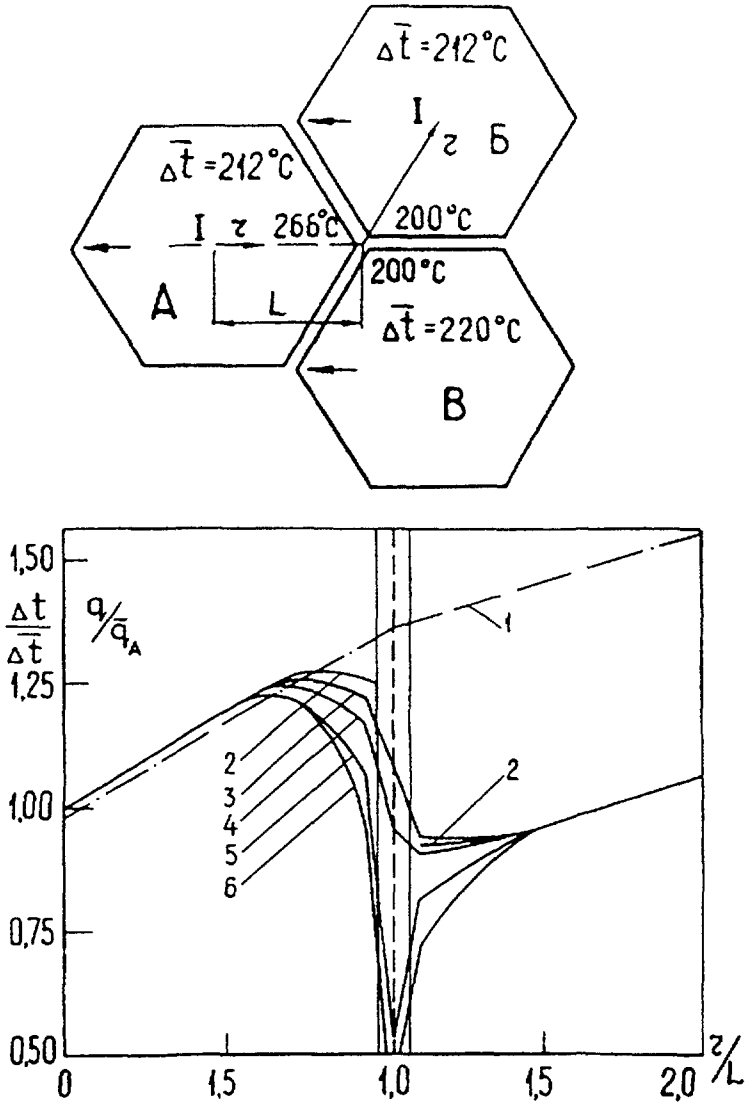

Fig. 2 Prediction of temperature distribution in the system of interacting subassemblies that is situated at the core periphery:

1 — energy generation profile,
2 — temperature distribution achieved without inter-subassembly exchange,
3 — coolant does not flow throughout inter-subassembly gap,
4, 5, 6 — relative coolant flowing throughout inter-subassembly gap is of value 2%, 4%, 100% respectively.

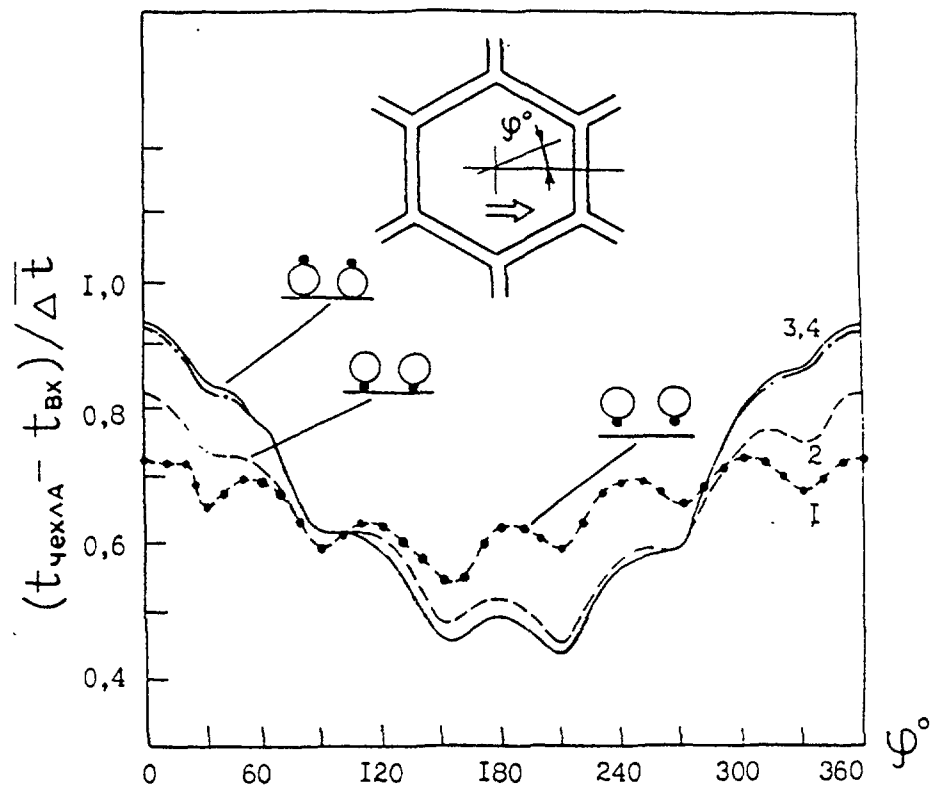

Fig.3 Azimuthal temperature distributions of the subassembly duct

6. TEMPERATURE FIELD IN THE SYSTEM OF DEFORMED SUBASSEMBLIES

Non-uniform heat release provokes transient course of radiation deformation of the duct and pin bundle, the deformation character exchanging in campaign.

When pin bundle bows to the side of center of reactor core and edge pins touch by a wire wrap (or in the deadline case with a pin wall), the contact takes place in the middle core cross section that there is significant rise of maximal pin temperature as well as maximal azimuthal temperature non-uniformity.

At the same time near opposite sides of subassembly duct the decrease of pin temperature that is connected with the rise of the width of gap between edge pins and duct. However azimutnal temperature nor-uniformity increases in this case. Pin bundle deformation leads to increase of azimuthal temperature non-uniformity of subassembly wrapper more twice as large as edge pins touching with wire wrap by duct (at the middle cross section) and is approximately greater by 4 as edge pins touching with pin wall by duct in comparison with nondeformed pin bundle (Fig. 3).

When pin bundle deformation occurs in direction to core periphery the lesser effects of temperature field deformation take place.

Presence of reflectors or control protection system leads to some deformation of temperature field in peripheral region of adjacent subassemblies.

CONCLUSIONS

Experiment and predictions have shown the inter-subassembly heat transfer exert local influence on temperature behavior of edge pins. There ara reduction of edge pin temperature (except separate situation), increase of azimuthal temperature non-uniformity on edge pins. Deformation of pin bundle as well as subassembly duct in campaign leads to significant additional non-uniformities of temperature.

NOMENCLATURE

d	- pin diameter, m
h	- wire wrap pitch, m
L	- length of heat release part, m
N	- number of subchannel which subassembly cross section is divided on
Pe	- Peclet number
Re	- Reynolds number
q	- heat release rate , w/m^2
s	- pitch of pin array, m
t	- temperature, ^0K
$T_м, T_п, \Gamma_м$	- dimensionless parameters
ΔT^{max}	- maximal azimuthal non-uniformity of pin temperature, ^0K
W	- coolant velocity, m/s
Z	- coefficient showing how temperature profile deviates from cosin law
Δ	- width of gap between edge pin and subassembly duct, m
Δt	- coolant heating, ^0K
Σ	- thermal similarity parameter of pin
λ	- friction loss
λ	- heat conductivity, $w/(m\ ^0K)$
μ	- interchannel exchange coefficient, 1/m
ω	- flow section area, m^2

SUBSCRIPTS

E	- edge
D	- displacer
r	- hydrodynamics
squ	- square
leak	- coolant flowing throughout inter-subassembly gap
п	- gapbetween inner and edge subchannels
tri	- triangular
T	- heat
eff	- effective
f	- liquid
i, j	- subchannel number
iξ	- heat transfer through subassembly duct
k	- number of harmonic in expansion into a
0	- inner region of subassembly
μ	- taking into account interchannel heat transfer
–	- average value

REFERENCES

[1] CHANG L.K. Nuclear Engineering and Design, 1977, n.42, n.2, p.223-236.

[2] CHEN B.C., et al. Nuclear Engineering and Design, 1975, v.35, n.3, p.423-443.

[3] CARELLI M.D., et al. Transactions of the American Nuclear Society, 1975, v.21, n.l, p.393-395.

[4] SNA W.T., et al. Transactions of the American Nuclear Society, 1975, v.22. n.l, p.575-576.

[5] ZHUKOV A.V., et al. Atomic energy, 1981, v.51, n.5, p.307-311.
[6] ZHUKOV A.V., et al. Interchannel exchange in fast reactor fuel subassemblies (theoretical principles and physics). M., Energoatomizdat, 1989 (in Russian).
[7] ZHUKOV A.V., et al. Interchannel exchange in fast reactor fuel subassemblies: codes and applications. M., Energoatomizdat, 1991, (in Russian).
[8] ZHUKOV A.V., et al. Thermal physics investigations. 1977, p.17-22 (in Russian)
[9] ZHUKOV A.V., et al. Preprint IPPE-1062, Obninsk, 1980 (in Russian).
[10] SUBBOTIN V.I., et al. Hydrodynamics and heat transfer in atomic power plants (basis of design). M..Atomizdat, 1975 (in Russian)

METHODS OF STATISTICAL CALCULATION OF FAST REACTOR CORE WITH ACCOUNT OF INFLUENCE OF FUEL ASSEMBLY FORM CHANGE IN PROCESS OF CAMPAIGN AND OTHER FACTORS

G.A. SOROKIN, A.V. ZHUKOV, G.P. BOGOSLOVSKAYA, A.P. SOROKIN
State Scientific Center of Russian Federation,
Institute of Physics and Power Engineering,
Obninsk, Kaluga Region, Russian Federation

XA0055056

Abstract

The method of calculation of a temperature field in fast reactor core using criterion equal thermotechnical reliability of subassembles in various zones throttling taking into account change thermohydraulic characteristics of subassembles during campaign under influence change form of core, redistribution heat generation, casual any deviation of various parameters is stated. The distribution of the statistical characteristics of a temperature field in subassembles is calculated on subchannel method with account of an interchannel exchange and feature of influence of deformation on a temperature field in subassembles using Monte-Carlo method. The results of the calculations show that deformation can have significant influence on a temperature mode of core. It is necessary to make thermohydraulic analysis of core during campaign at a stage of preliminary study of the projects fast reactors.

1. INTRODUCTION

Thermohydraulic analysis of reactor core is performed in three steps (Fig. 1) [1]:

- coolant flow distribution over the core;
- flow rate and coolant temperature over subassembly cross section and with the length;
- temperature behavior in separate pins.

The input data are geometry, variation in power production with the core length and across the core, flow rate through the core, coolant and structure properties (Fig. 2).

The main factors controlling temperature behavior (deformation of pins and subassembly cover, power production in reactor core) in their turn depend on temperature behavior in the reactor core (Fig. 3).

Thus, the problem on reactor core temperature behavior is conjugate to the problem of deformation of the core units and power distribution (neutron physical calculation). Predicting reactor core deformation is a very combined problem that, as a rule, also is divided into the stages determining deformation of the cover, pin bundle and separate pins. The ensuing iterative procedure is possible to predict temperature behavior in fast reactor elements taking into account their deformation (Fig. 4).

The first approximation of the input data may be taken as that of nominal geometry. The main block involves neutron-physical part, prediction of coolant flow distribution over the core, thermohydraulic analysis of separate subassembly, estimation of pin and wrapper deformation. The thermal stress in the wrapper and pins are determined, using the data found. The procedure is repeated until the convergence conditions are met i.e., for criterion of normal performance.

Predictions based on the pattern outlined allow the changes in subassembly geometry, in temperature behavior and in performance of the core units to be followed in campaign.

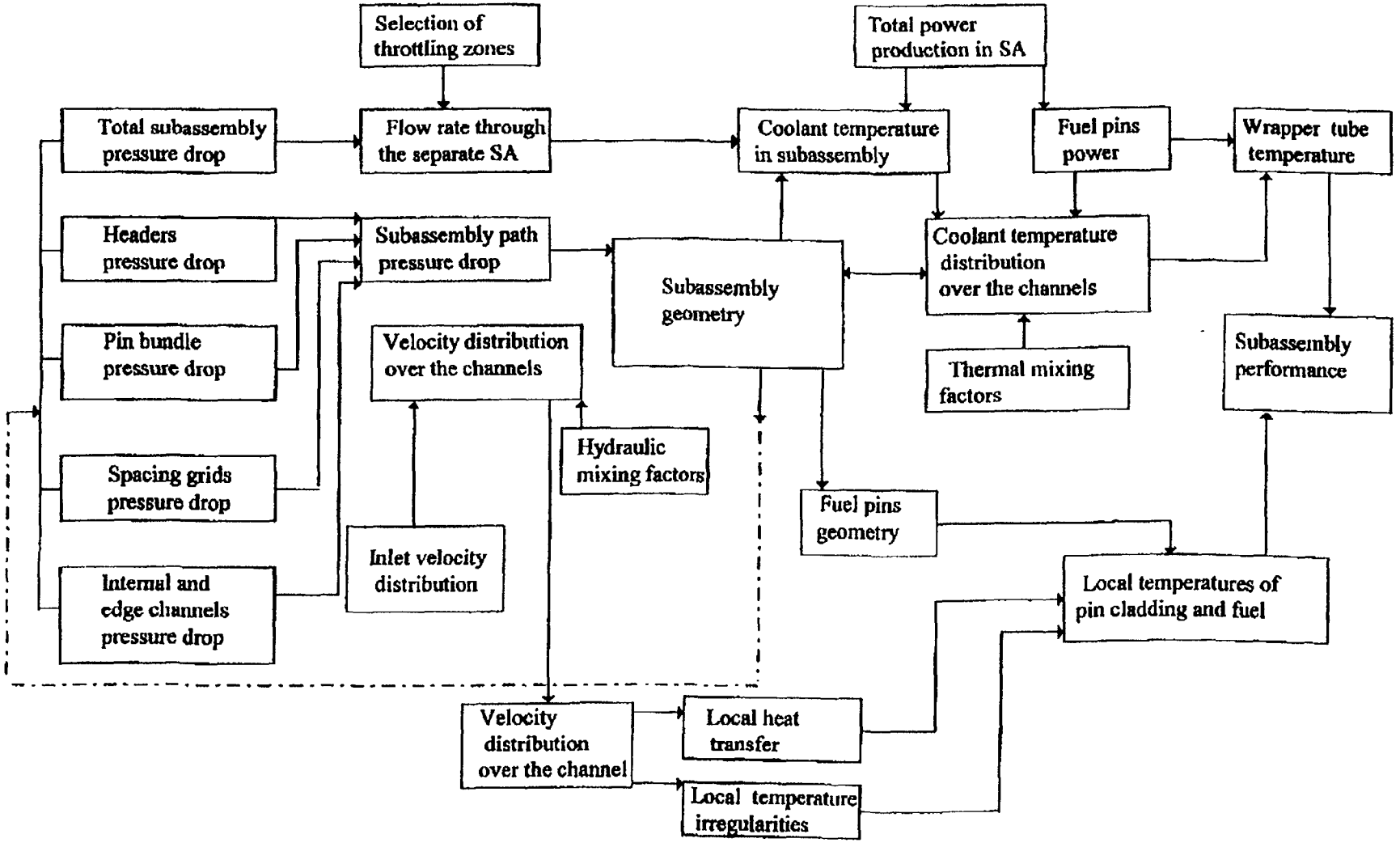

Fig. 1. Thermalhydraulic analysis of reactor core of an assembly type

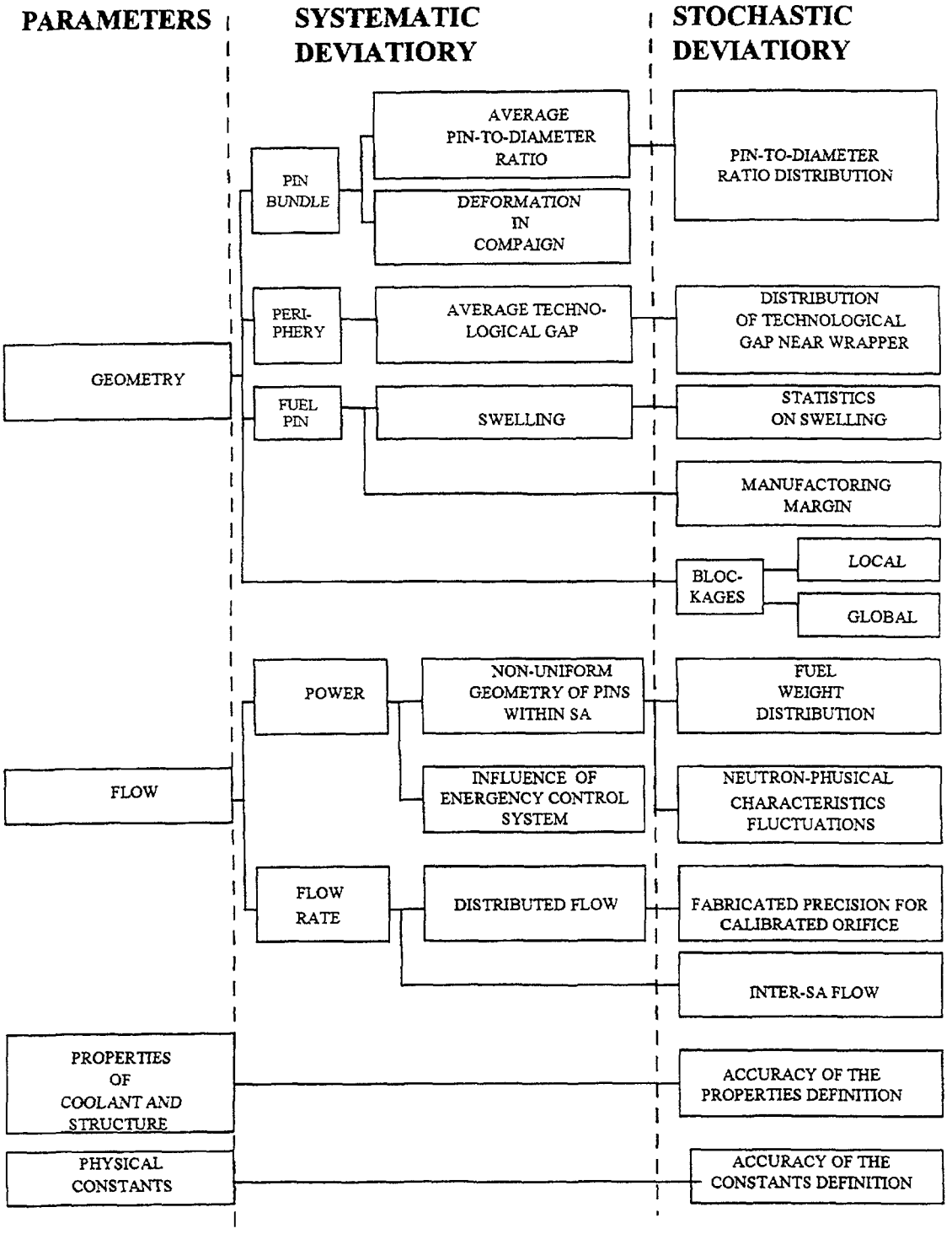

Fig. 2 Classification of deviations of parameters from nominal values

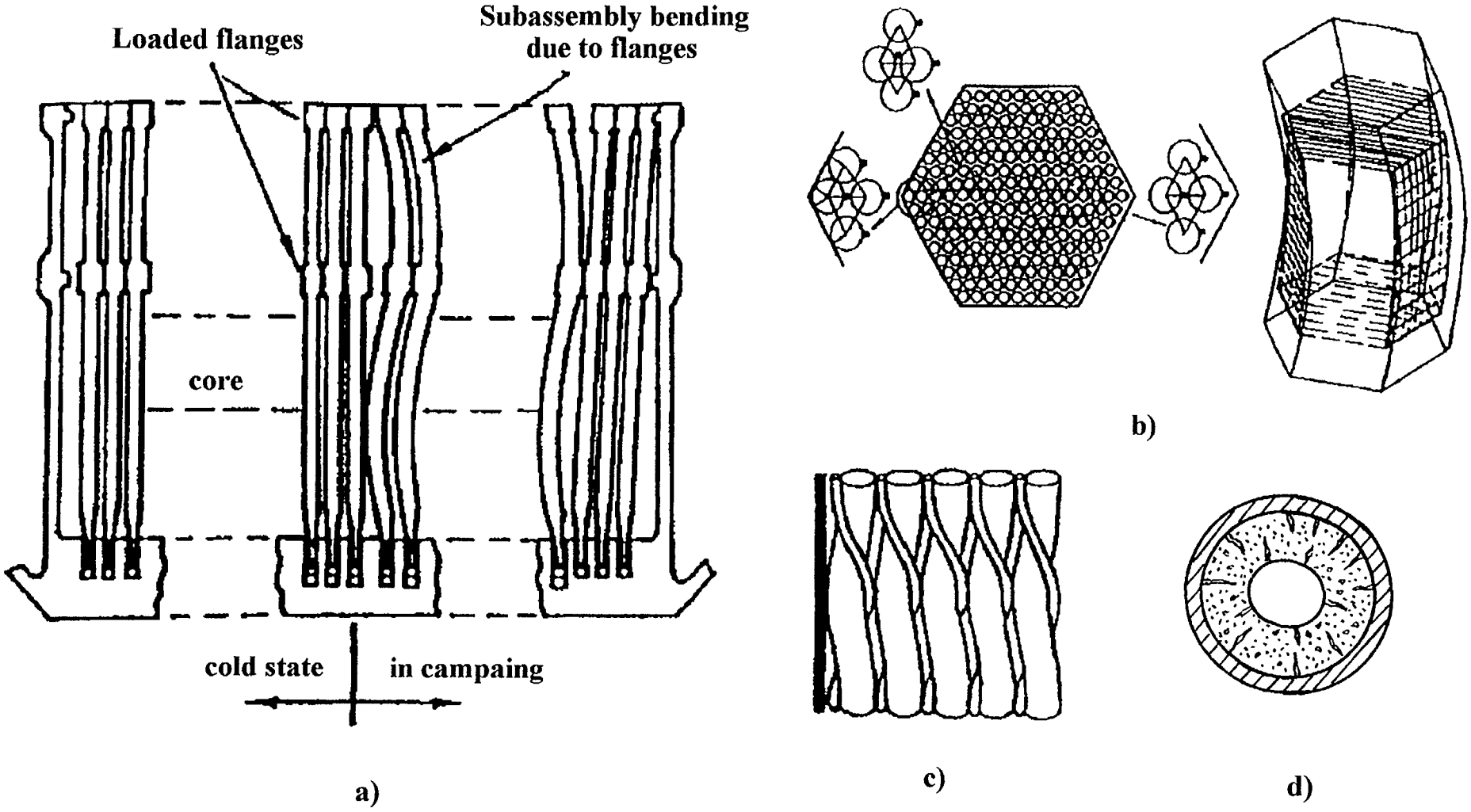

Fig. 3. Subassembly core deformation (a), bundle and wrapper tube (b), twisting pins (c), swelling (d)

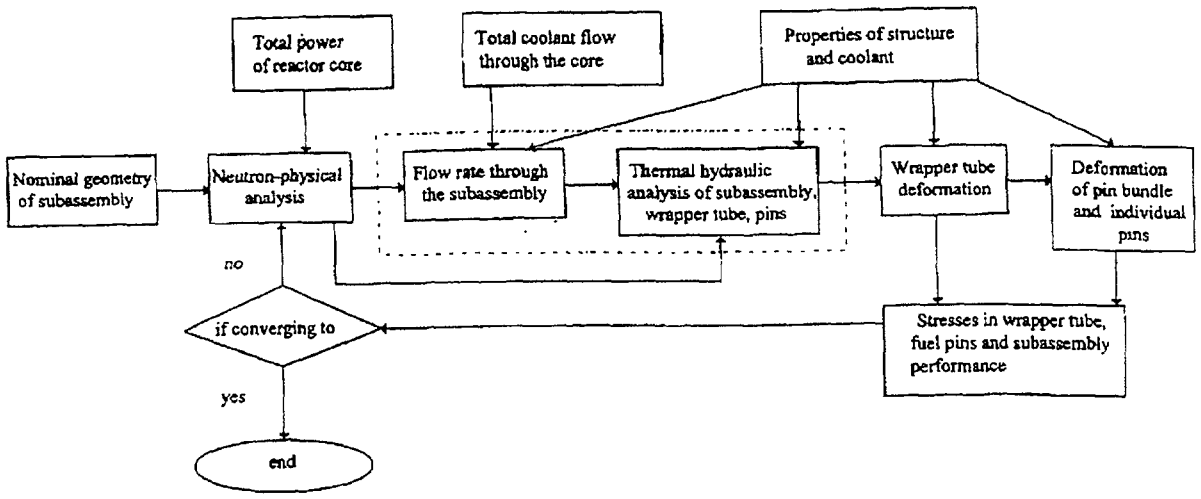

Fig. 4. Scheme of combined analysis of reactor core taking into account fuel pins deformation in compaign

2. FLOW DISTRIBUTION OVER REACTOR CORE BASED ON THE STATISTIC ESTIMATION OF TEMPERATURE BEHAVIOR TAKING INTO ACCOUNT MIXING AND DEFORMATION.

The main input parameters in predicting flow distribution over reactor core are the power and geometrical characteristics of subassembly and their changes in campaign.

In the fast reactor design, as a rule, the problem on maximum coolant temperature is solved with the nominal performance of reactor core in mind. The most simple approach is the flow distribution based on the uniform temperature distribution through the subassembly [2]. The drawback to the approach is an incomplete use of thermal possibilities of subassembly of a lesser power. Another procedure starts from the same margin till allow value to determine parameter, i.e., till maximum pin wall temperature [3-5]. If the power production varies in campaign, so called, distribution with envelope is used. This procedure assumes that coolant flow through the subassembly does not change in campaign. The common limitation of the procedures indicated is an incomplete consideration of change in engineering and operating parameters.

Prediction of flow distribution based on the estimation of maximum pin temperature with the, so called, hot spot factors ignores inter-channel and inter-subassembly exchange, as well as parameters' mutual correlation with the random deviations being small as compared with the nominal ones [6-8]. So, temperature is estimated in one point, in fact, where the maximum temperature occurs. But to provide a reliable design of reactor core all areas with high temperature have to be considered at least. In this event, inter-channel and inter-subassembly heat transfer in reactor core has to be, taken into account.

Subassembly performance is limited by that the maximum pin temperature (having regard to hot spot factors) should not exceed value prescribed for various steels. It is well to bear in mind that this criterion do not completely reflect conditions of nominal performance of the pins. It is evident that maximum azimuthal non-uniformity of pin temperature should be taken into account as well as pressure of fission gas, level of pin wall swelling, deformation of the subassembly wrapper and pins etc.

In general case, the criterion has to be combined.

Thus, an allowable temperature of the pin is expressed as a function of other limiting parameters:

$$t_{limit}=f(\text{steel properties}, \Delta t_{\varphi},, p...) \quad (1)$$

where Δt_{φ} - maximum azimuthal non-uniformity of pin temperature, p - fission gas pressure.

Thermal reliability is governed by the number of allowable failures (pin's destructions) occurring in a separate subassembly. If the possibility of pin failure does not exceed p_o that the possibility, the pin temperature, in separate subassembly that not exceed P_o is:

$$P(t_w^{max} > t_{limit}) \le P_o \quad (2)$$

Statistic evaluation of temperature in the i-th subassembly allows the values t_i not to exceeding allowable value to be calculated and the factor k_i is found:

$$k_i = \frac{t_i - t_{BX}}{\overline{\Delta t_i}} = f\left(\Gamma, q^{max}/\bar{q}, Pe, \bar{t}\right), \quad (3)$$

where t_{inlet} -core inlet temperature, Δt_i - mean coolant heating in the i-th subassembly, Γ- geometry, Pe - Peclet number based on the mean velocity, $\bar{t}$ - mean coolant temperature, $\left(q^{max}/\bar{q}\right)$ - non-uniformity in power production over the subassembly cross section.

It should be noted that statistic analysis allows an inter-channel heat and mass transfer being responsible for the temperature behavior in the subassembly, to be taken into account. It also allows for various deviation of parameter from nominal distribution [70].

Coolant flow rate through the subassembly at the given inlet temperature is limited by relationship:

$$G_{\Sigma} \ge \frac{\max\left[\sum_i \frac{\beta_i}{\alpha_i}\frac{K_i^0 K_{Q_i}}{K_{G_i}} Q_i N_i\right]}{\Delta t_{limit}^{id}}, \quad (4)$$

where N_i -number of subassemblies in the i-zone ; Q_i -maximum power production in the i- th zone; $K_{Q_i} = (Q_i^{max} / Q_i^o)$ - factor describing the rise in power production in campaign (index "o" means the beginning of operation); $K_{G_i} = (G_i^{min} / G_i^O)$ - factor describing the reduction of coolant flow through the subassembly in the i-th zone; $\alpha_i=(t - t_{inlet}) / (t^{id} - t_{inlet})$ - factor which accounts the change in allowable pin temperature as compared to the temperature under ideal conditions; $\beta_i=K_i / K_i^o$ -factor which shows how K_i varies in campaign.

Maximum temperature of the coolant can be found as follows:

$$\Delta t_{core}^{max} = \frac{\sum_i \sum_j \left(Q_j\right)_i}{\max\left\{\sum_i \left[\frac{\beta_i}{\alpha_i}\frac{K_i^0 K_{Q_i}}{K_{G_i}} Q_i N_i\right]\right\}} \Delta t_{limit}^{id}, \quad (5)$$

where j -subassembly number in the i -th zone.

Relationships (4) and (5) indicate that changes in power production and coolant flow thought the subassembly cause an increase in the temperature non-uniformity that results in the lesser possible coolant temperature in the zone under consideration.

If an allowable value of pin temperature t_{allow} is give less than limit temperature t_{limit} the optimal reactor flow distribution is calculated on the basic of the maximum thermal reliability of the more loaded subassembly as follows:

$$G_i = \frac{\beta_i \frac{K_i^0 K_{Q_i}}{K_{G_i}} Q_i}{\sum_i \left[\beta_i \frac{K_i^0 K_{Q_i}}{K_{G_i}} Q_i N_i \right]} G_\Sigma, \qquad (6)$$

where

$$G_\Sigma = \frac{\max\left[\sum_i \beta_i \frac{K_i^0 K_{Q_i}}{K_{G_i}} Q_i N_i \right]}{\Delta t_{allow}}, \qquad (7)$$

$\Delta t_{allow} = t_{limit} - t_{inlet}$.

Average coolant heating in various zones is calculated as:

$$\Delta t_i = \frac{\sum_i \beta_i \frac{K_i^0 K_{Q_i}}{K_{G_i}} Q_i N_i}{\beta_i \frac{K_i^0 K_{Q_i}}{K_{G_i}} G_\Sigma}. \qquad (8)$$

At given total flow rate the optimization of flow distribution (6) allows the thermal reliability of the reactor zone to be enhanced. In this event, pin temperature compatible with the condition $P(t_w^{max} > t_{limit}) \le P$ can be found as:

$$t_{limit} = t_{inlet} + \frac{\max\left[\sum_i \beta_i \frac{K_i^0 K_{Q_i}}{K_{G_i}} Q_i N_i \right]}{G_\Sigma}. \qquad (9)$$

3. STATISTIC ESTIMATION OF TEMPERATURE FIELD

Statistic estimation of temperature field implies that a series of the temperature field elements is defined using stochastic distribution of input parameters followed by statistic processing (to find mathematical expectation, variance and distribution function).

The stochastic distribution of parameters in the specific case can be found from the distribution functions deduced from experiments or analytical studies (i.e., [7, 10]). Calculating the global parameters, such as flow rate throughout the subassembly, total power production, sizes and local parameters, such as the pitch-to-diameter ratio, the pin diameter, the pin wall thickness, power production of the pin are distributed in random manner. It should be noted that in the event of subassembly deformation in campaign the distributions of input geometrical parameters have a significantly greater variance than those in nominal bundle [11].

Thermohydraulic analysis involves the subchannel procedure by code MIF. The end of calculation means the convergence of mathematical expectations of coolant temperature, maximum pin temperature and non-uniformity of pin temperature. As a result of, the analysis, distributions of temperature characteristics are determined, too.

4. THERMOHYDRAULICS CALCULATIONS OF DEFORMED SUBASSEMBLIES

In the special case that subassembly is subjected to deformation in campaign a coolant flow is of irregular character, with the bundle flow being practically longitudinal (quasi-stable). Predictions have shown that even in case of large deformation (when pins bending is

so great that compact channels are formed) the transverse component of velocity does not exceed about 30% of axial component and pressure out-of-balances for a length not more than (0.1÷0.2) d_h. Thus, macro-transport equation of momentum in transverse direction can be approximately written as $p_i - p_j = c_{ij} * w_{ij}$ or substituted by the relationship p=idem (hypothesis of isobaric flow), with the value w_{ij} being determined from the mass equation.

The feature of thermohydraulic analysis in deformed subassemblies is also that the transverse mass transfer due to centrifugal effect is taken into account in the channel when bending.

By assuming that transverse flows due to centrifugal effect are in balance with central channels, it is easy to verify that specific momentum and energy fluxes (Fig. 5) are in proportion with the transverse flow:

$$\left.\begin{aligned} P_{ij} &= \rho_{ij} w_{ij}^{C} w^{**} \Delta s_{ij} \\ Q_{ij} &= \rho_{ij} w_{ij}^{C} h^{**} \Delta s_{ij} \end{aligned}\right\} \tag{10}$$

where: ** - index of the donor-channel .

$$w^{**} = \begin{cases} w_i, & \text{if } w_{ij}^{C} > 0 \\ w_j, & \text{if } w_{ij}^{C} < 0 \end{cases} \qquad h^{**} = \begin{cases} h_i, & \text{if } w_{ij}^{C} > 0 \\ h_j, & \text{if } w_{ij}^{C} < 0 \end{cases}$$

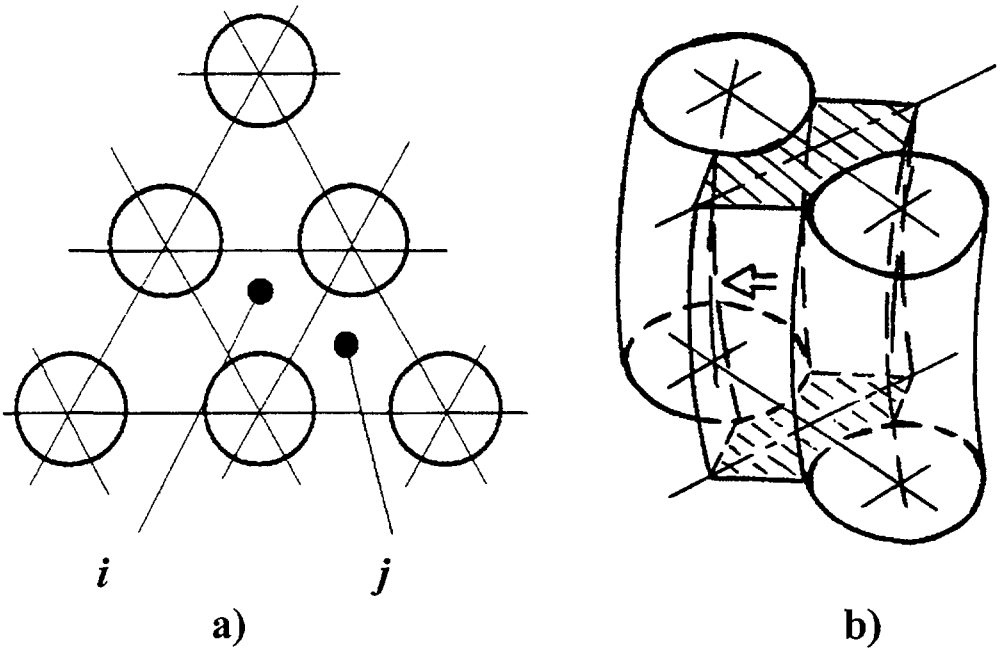

Fig. 5 The scheme of group interacting triangular cells (a) and elementary cell in a gap between elements (b).

Having performed the needed transformations for the purpose to exclude pressure and assuming p=const in subassembly cross section [12], we find the macro-transport equations in isobaric approximation:

$$\frac{d(w_i\omega_i)}{dz} = \frac{1}{2w_i - w_i^*}\left\{ w_i^2 \frac{d\omega_i}{dz} - \xi_i \frac{w_i^2}{8}\Pi_i + \sum_{j=1}^{3} \mu_{ij}^{M} \frac{w_i + w_j}{2}\left(w_j - w_i\right)\overline{\omega} + \right.$$

$$\left. + \mu_c^{M} \frac{w_i + w^{**}}{2}\left(w^{**} - w_i\right)\overline{\omega} - \frac{\omega_i}{\sum_{i=1}^{N} \frac{\omega_i}{2w_i - w_i^*}} \sum_{i=1}^{N} \frac{1}{2w_i - w_i^*}\left[w_i^2 \frac{d\omega_i}{dz} - \right. \right. \tag{11}$$

$$-\xi_i \frac{w_i^2}{8}\Pi_i + \sum_{j=1}^{3}\mu_{ij}^{M}\frac{w_i + w_j}{2}\left(w_j - w_i\right)\overline{\omega} + \mu_c^{M}\frac{w_i + w^{**}}{2}w^{**}\overline{\omega}\Bigg]\Bigg\};$$

$$\frac{d}{dz}\left(w_i\omega_i t_i\right) = \frac{1}{\rho c_p}\sum_{k=1}^{3}q_{ki}\Pi_{ki} + q_{vi}\omega_i + t_i^{*}\frac{d\left(w_i\omega_i\right)}{dz} +$$

$$+\sum_{j=1}^{3}\left(\mu_{ij}^{T}\frac{w_i + w_j}{2} + \mu_{\lambda}^{T}\overline{w}\right)\left(t_j - t_i\right)\overline{\omega} + \mu_{Ц}^{T}\frac{w_i + w^{**}}{2}t^{**}\overline{\omega}; \tag{12}$$

$$w_i^{*} = \frac{1}{2}\sum_{j=1}^{3}\left[\left(w_i + w_j\right)\left|w_{ij}\right| + \left(w_i - w_j\right)w_{ij}\right]\Delta s_{ij}\Big/\sum_{i=1}^{3}w_{ij}\Delta s_{ij};$$

$$t_i^{*} = \frac{1}{2}\sum_{j=1}^{3}\left[\left(t_i + t_j\right)\left|w_{ij}\right| + \left(t_i - t_j\right)w_{ij}\right]\Delta s_{ij}\Big/\sum_{j=1}^{3}w_{ij}\Delta s_{ij}. \tag{13}$$

In (11) and (12) the hydraulic and thermal mixing factors due to centrifugal effects can be expressed as:

$$\left.\begin{aligned}\mu_C^{M} &= \frac{P_{ij}}{\frac{\rho\left(w_i + w_j\right)}{2}w^{**}\overline{\omega}} = \frac{w_{ij}^{Ц}}{\frac{w_i + w_j}{2}}\frac{\Delta s_{ij}}{\overline{\omega}},\\ \mu_C^{T} &= \frac{Q_{ij}}{\frac{\rho\left(w_i + w_j\right)}{2}h^{**}\overline{\omega}} = \mu_C^{M}\cdot\beta\end{aligned}\right\} \tag{14}$$

Local mixing factors due to convective exchange and molecular - turbulent diffusion are in the forms, respectively:

$$\left.\begin{aligned}\mu_{ij}^{M} &= \mu_{C_{ij}}^{M} + \alpha\cdot\mu_{MT_{ij}}^{M};\\ \mu_{ij}^{T} &= \mu_{C_{ij}}^{T} + \mu_{MT_{ij}}^{T},\end{aligned}\right\} \tag{15}$$

where α - coefficient considering mutual relation between convective exchange and molecular - turbulent diffusion.

Three parameters $\mu_{ij}{}^{M}$, $\mu_{ij}{}^{T}$, α are defined on the basic of [13-15].

From momentum balance for the clearance between channels we can write the following relationship for the mixing factor due to centrifugal effect 1/m:

$$\mu_{ij}^{M} = 1.58\,\mathrm{Re}^{0.143}\left[\frac{s/d - 1}{\frac{2\sqrt{3}}{\pi}\left(s/d\right)^2 - 1}\right]^{1.143}\left(\frac{s}{R_{ij}}\right)^{0.57}\frac{1}{d}, \tag{16}$$

where: R_{ij} - curvature radius.

Coefficient of non-equivalence between heat transfer and momentum transport β may be thought of as being about 0.7 in deformed geometry. Then, on the basic of (14) we have:

$$\mu^{T} = 0.7\mu^{M} \tag{17}$$

As it was evaluated, the thermal and hydraulic mixing factors due to centrifugal effect can achieve some unites.

In the event of pin out-of-roundness, that may be responsible for the significant decrease in the width of inter-pin clearance, the transverse convective flows is more intensive than those evaluated with the averaged parameters of pin bundle. For example, the limiting

degree of the out-of-roundness attended with the pins touch each other results in the value of 40% of that defined using averaged parameters:

$$\overline{w_{ij}\Delta s_{ij}} = 0.4\overline{w_{ij}}\,\overline{\Delta s_{ij}}. \tag{18}$$

Once you have decided upon the averaged parameters of subassembly as the reference one, it should be introduce correction on the out-of-roundness:

$$\mu_{ij} = \mu(s/d)\beta' \tag{19}$$

where correction factor β is determined as follows:

$$\beta' = \overline{w_{ij}\Delta s_{ij}} \Big/ \left(\overline{w_{ij}}\,\overline{\Delta s_{ij}}\right). \tag{19a}$$

Macro-transport equations are also supplemented by the equations for the cells chosen in the clearance between subassemblies. Velocity and temperature boundary conditions are given at the bundle inlet. System (11) and (12) is resolved by the explicit finite difference approach by layers beginning from the inlet.

Code MIF was verified on experimental data on temperature behavior in the model bundle being exposed to deformation in the edge area under conditions of uniform power distribution over the cross section as well as under conditions of strong coolant flow through the clearance between subassemblies. There is a good agreement of coolant temperature distribution over the outlet cross section.

5. RESULTS OF CALCULATION

As statistic estimations of pin temperature behavior in reactor, taking into account inter-channel and inter-subassembly heat and mass transfer, has shown the optimization of flow distribution over reactor carried out in the procedure mentioned above that could result in the more flat temperature profile than those based on the condition when maximum temperatures of the most loaded pins are the same in various zones of reactor (Fig. 6).

Calculations of temperature fields BN-600 in the case of nonuniformed show (Fig. 7, 8) that dispersion of temperature field calculated with the influence of mixing on ten times less then calculated without the influence of mixing. It give an influence on the temperature level with hot spot factors.

Let us demonstrate the possibilities of the code on the example of PHENIX subassembly deformation (Fig. 9, a), when pin bundle and subassembly wrapper are banded. First of all the rearrangements of collant flow and temperature are observed. Coolant passing close to the sides with the lesser distance from the edge pins becomes more heated and significantly subheated near the opposite sides. Predictions show the large temperatures of pin wall and enhanced azimuthal pin temperature non-uniformity in the event of the channels are formed close to compact ones (Fig. 9-b).

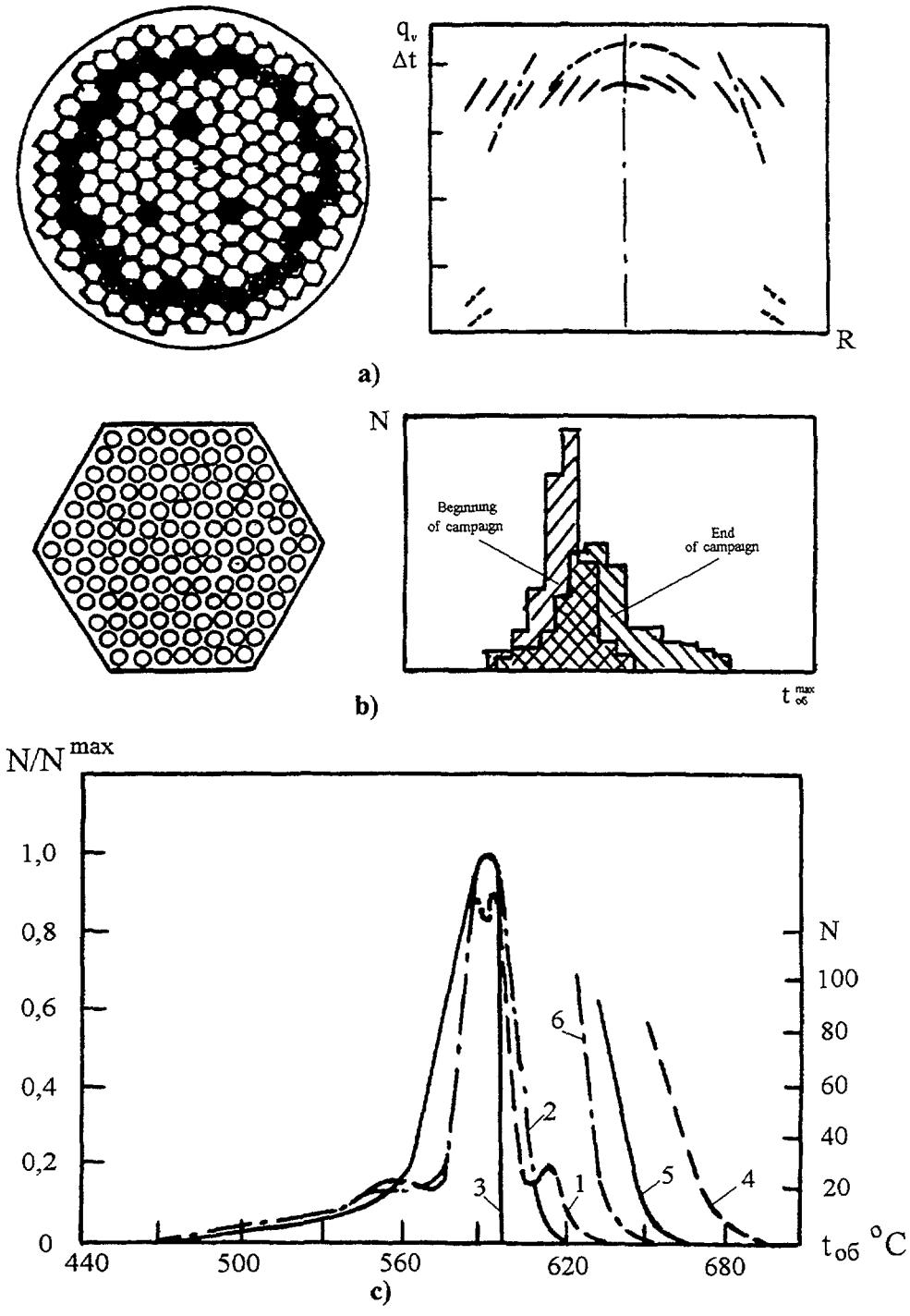

Fig. 6. The calculation of heat generation and cooling temperature on radius of core (a), fuel distribution in subassembly (b) and in core (c):

Calculation without the factor overheating:

1 – without interchannel exchange, 2 – with interchannel exchange, 3 – calculation of optimize throtting;

Calculation with the factor overheating:

4÷6 – similarly curve 1÷3

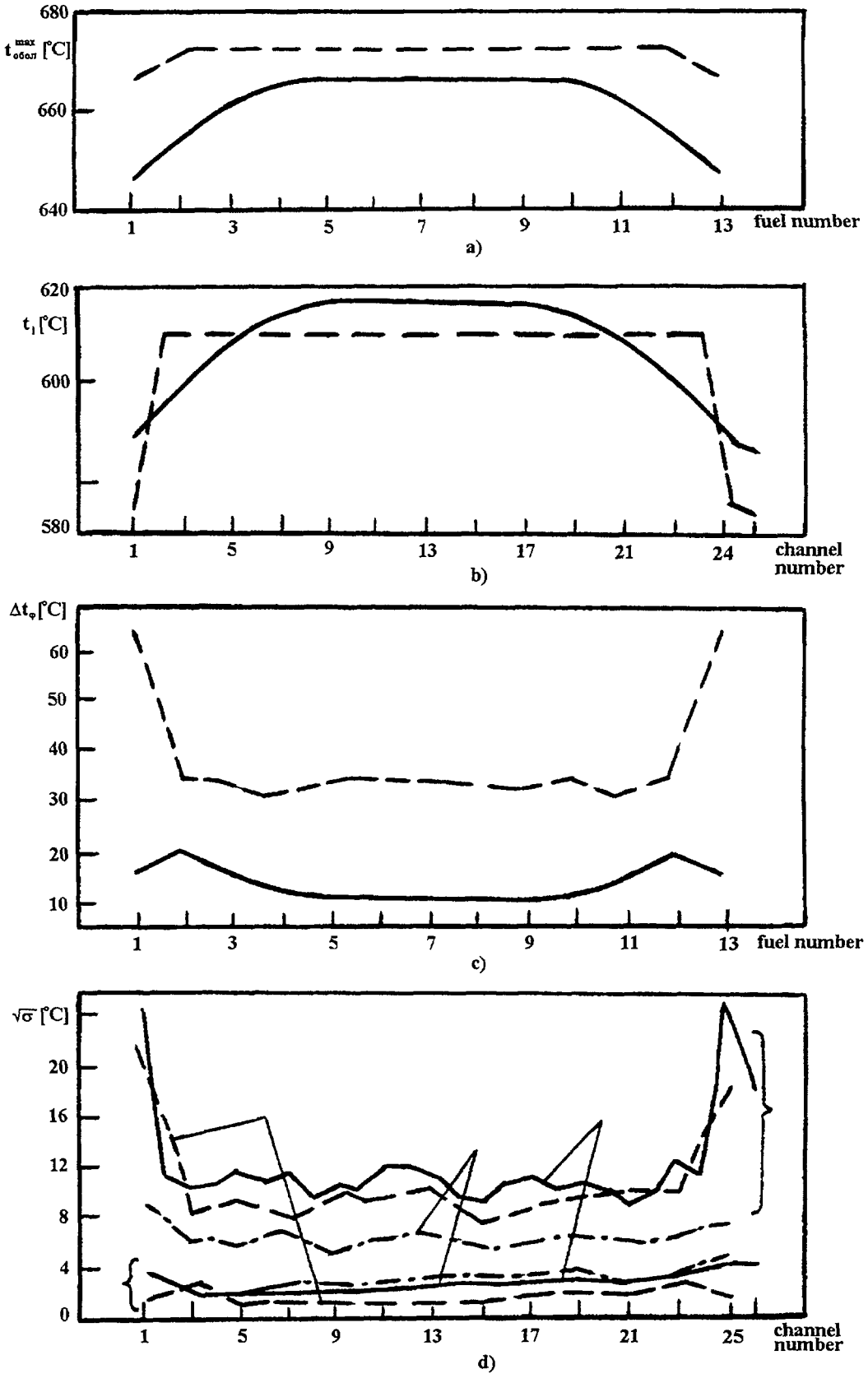

Fig. 7. Distributions of maximal temperature of fuel cladding (a), heating of the coolant (b), non-uniformity of temperature around fuel (c) and their root-mean-square deviations (d)

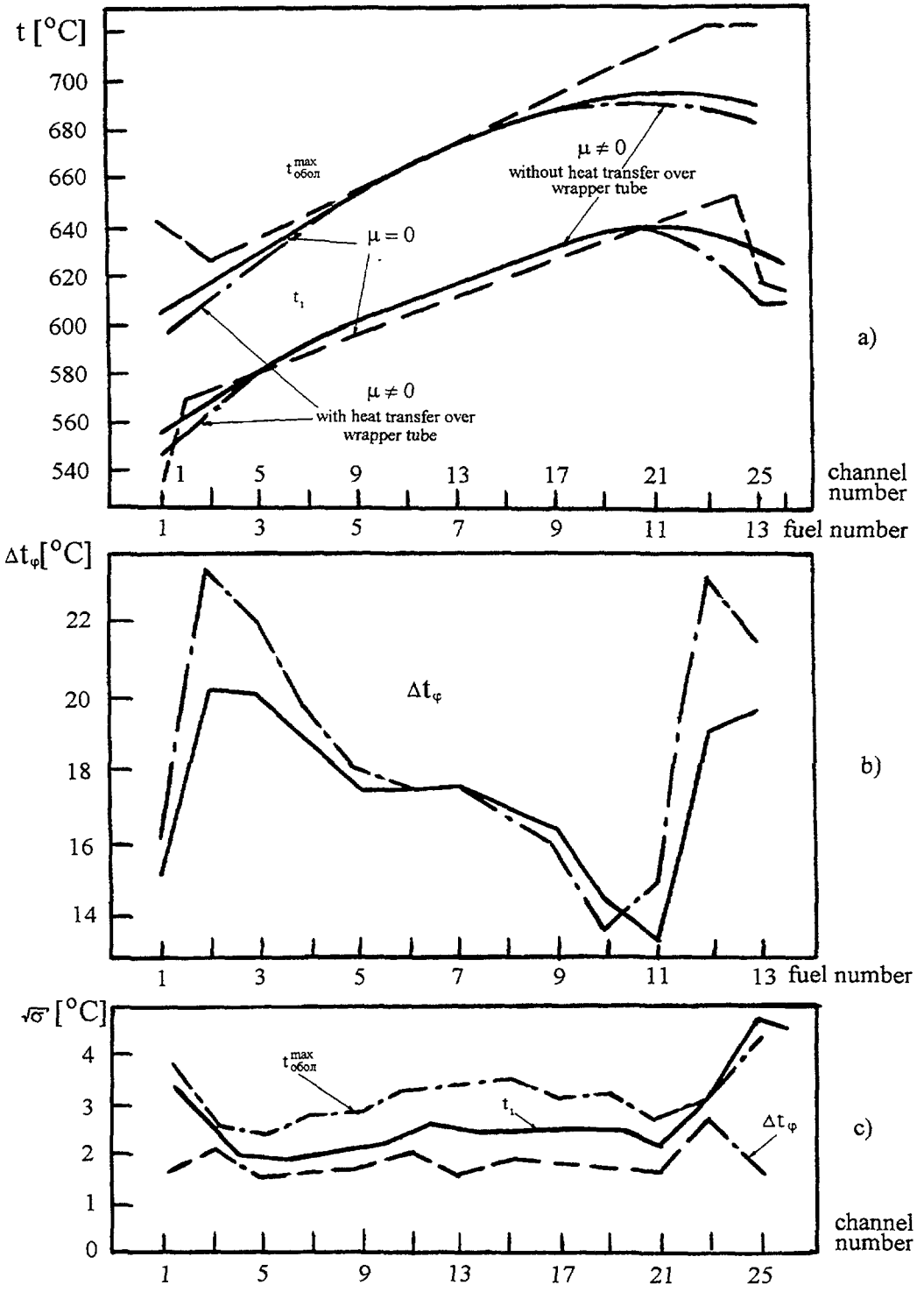

Fig. 8. Distributions of maximal temperature of fuel cladding and heating of the coolant (a), non-uniformity of temperature around fuel (b), their root-mean-square deviations (c) in the case of non-uniform heat generation fuel in the cross section of subassembly $q^{max}/\overline{q} = 1,2$

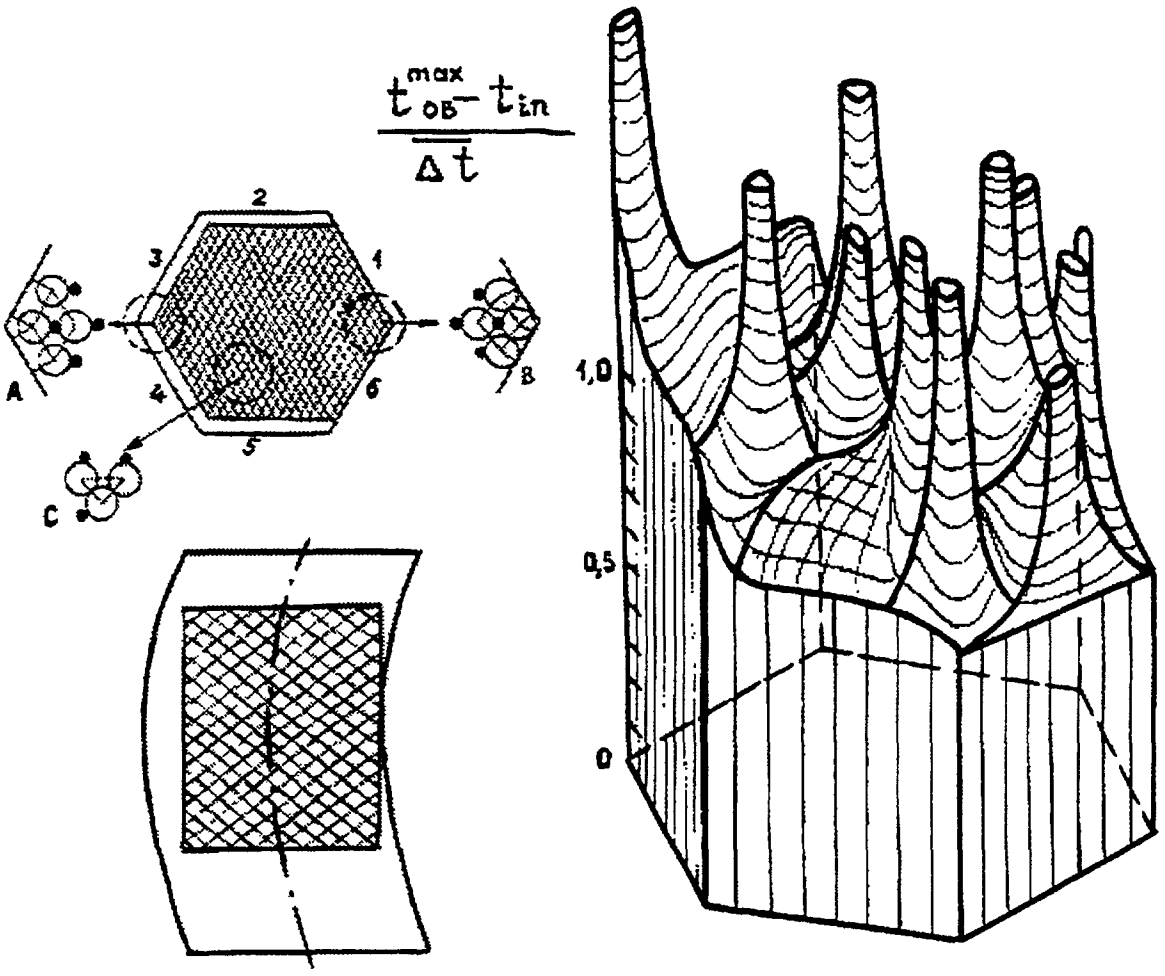

Fig. 9. The scheme of cross and longitudinal sections deformed subassembly (a), distribution of maximum temperature of fuel cladding in subassembly cross section on the core center of reactor "Phenix" (b)

REFERENCES

[1] ZHUKOV A.V., SOROKIN A.P., USHAKOV P.A. Thermal Physic Validation of Fast Reactor Subassembly Temperature Fields Having Regard to Hot Spot Factors //Preprint IPPE-1778, Obninsk, 1986.

[2] KRAMEROV A.J., SHEVELEV A.V. Nuclear Reactor Engineering, M., Energoatomizdat, 1984.

[3] MIKHAN I.J., SOLONIN B.I. et al. Nuclear Reactor Designing, M., Energoizdat, 1982.

[4] USYNIN G.B., KUSMARTSEV E.V. Fast Breeder Reactors, M., Energoatonizdat, 1985.

[5] WATERS A., REYNOLDS A. Fast Breeder Reactors, M., Energoatomizdat, 1986.

[6] KLEOMIN A.N., POLIANIN L.N., STRIGULIN M.M. Thermal Hydraulic Calculation and Technological Realibility of Nuclear Reactors, M., Atomizdat, 1980.

[7] KURBATOV I.M., TIKHOMIROV B.B. Estimation of Random Temperature Deviations in Reactor Core // Preprint IPPE-1090, Obninsk, 1980.

[8] CARELLI M.D. Hot Channel Factor for Rod Temperature Calculations in LMFBR Assemblies // Nuclear Engineering and Design. 1980, v. 62, N° 2.

[9] ZHUKOV A.V., SOROKIN A.P., USHAKOV P.A. et al. Statistic Estimation of Fast Reactor Core Having Regard to Deformation in Campaign // Preprint IPPE-1845, Obninsk, 1987.
[10] BOGOSLOVSKAYA G.P., ZHUKOV A.V., SOROKIN A.P. et al. Calculation of Statistic Temperature Characteristics in BN-600 Subassembly Using Monte-Carlo Procedure // Preprint IPPE-1376, Obninsk, 1985.
[11] TIKHOMIROV B.B., SAVITSKAYA L.V. et al. Models of Statistic Estimetion of Radiative Deformations // Paper on French-Soviet Seminar «Problems of Reactor Core Thermal Hydraulics», Cadarache, 1986.
[12] KAZACHKOVSKI O.D., SOROKIN A.P., ZHUKOV A.V. et al. Lumped parameters in the problem on temperature behavior in deformed fast reactor subassemblies under diabatic boundary conditions // Preprint IPPE-1672, Obninsk, 1985.
[13] ZHUKOV A.V., SOROKIN A.P., MATJUKHIN N.M. Interchannel Exchange in Fast Reactor Subassemblies: Theoretical Foundations and Physics of the Process, M., Energoatomizdat, 1989.
[14] RECOMMENDATIONS ON THERMAL HYDRAULIC CALCULATION OF FAST REACTOR CORE // PTM 1604. 008-88. State Committee on Nuclear Energy. M., ONTI IPPE, 1988
[15] KIRILLOV P.L., ZHUKOV A.V. Modern Methods of Thermal Hydraulic Analysis of Reactor Subassemblies // Text-Book, Obninsk, OINPE, 1988.

THE APPROXIMATE THERMAL-MODEL-TESTING METHOD FOR NON-STATIONARY TEMPERATURE FIELDS IN CENTRAL ZONES OF FAST REACTOR ASSEMBLIES

V.I. MIKHIN, N.M. MATUKHIN
State Scientific Center of Russian Federation,
Institute of Physics and Power Engineering,
Obninsk, Kaluga Region, Russian Federation

Abstract

The approach to generalization of the non-stationary heat exchange data for the central zones of the nuclear reactor fuel assemblies and the approximate thermal-model-testing criteria are proposed. The fuel assemblies of fast and water-cooled reactors with different fuel compositions have been investigated. The reason of the non-stationary heat exchange is the fuel-energy-release time dependence.

For studying the non-stationary heat exchange processes in the nuclear reactor assemblies the approaches to the approximate modeling of such processes and the way of the experimental and calculated data generalization are necessary. Below the approach to the approximate modeling of the non-stationary nuclear-reactor-assembly heat exchange caused by the time change of the fuel energy release is stated. The approximate thermal-model testing is realized on the models which represent themselves as the assemblies of the fuel element imitators.

The imitator construction consisting of a tube heated outwards by an electric spiral [1,2] is considered. The electric spiral is isolated from the tube wall by the silicon-organic layer. The imitator tube may be one- or two-layer tube consisting of two subshells.

With purpose to obtain the approximate thermal-model-testing criteria the numerical investigations of the non-stationary assembly-central-zone temperature fields for the water-cooled and fast reactors have been carried out. The experimental an numerical investigations of the non-stationary temperature fields in the assembly models have been carried out also. The reason of the non-stationary behavior is the time energy-release variation in the fuel or in the imitators.

The maximum temperatures and maximum temperature irregularities take place at the assembly periphery. Determining these values by means of numerical solution of the detailed heat transport equations for the concrete fuel elements systems with the distant ridges seems to be not possible. That is why the research range is restricted to the central assembly zones, where the azimuth temperature irregularities are small and the distant ridge influence is not essential. The numerical results have been obtained from the joint solution of the non-stationary heat transport equations for the fuel elements and the heat-transfer agent (the method have been stated in detail in the work[3]). Such approach has permitted to avoid using the empirical quantities like the heat-transfer coefficient. Therefore the results obtained can be regarded as sufficiently reliable and adequate to the research aim.

The calculations have been carried out for the turbulent coolant flow regime for the wide Reynolds number range. The fuel assemblies with different coolants (water, sodium, lead) with uranium and uranium dioxide fuel have been investigated. The thermal resistance value of the contact sublayer between the fuel element core and shell has been varied in wide range.

The experimental and calculated results have been obtained for the energy-release jump. The generalization on the arbitrary energy-release lows is assumed to be achieved by

using the Duhamel integral. The numerical calculation results for the nuclear reactor fuel assemblies and the typical distributions of the non-stationary temperature fields in fuel and coolant have been stated in detail in the work[3]. The basic result of the research is in the following. At the energy-release jump the fuel-element shell temperature θ (or the relative coolant temperature) on the energy-release-zone exit is approximately described by the exponential relationship

$$\theta = \theta_\infty \left[1 - \exp\left(-t / t_p\right)\right], \tag{1}$$

where θ_∞ – is the established temperature value, t - is the time, t_p – is the temperature relaxation parameter for the fuel assemble. This relationship is universal for all fuel assembly variants if the relaxation parameter is determined by the formulae:

$$t_p = \frac{2}{\pi}\left(t_{TB} + t_q + h_q / w\right), \tag{2}$$

$$t_{TB} = \frac{d^2}{4a_0}\left[0.1729 + 0.9452\left(\frac{\Delta_1}{\lambda_1} + \frac{\Delta_K}{\lambda_K}\right)\frac{\lambda_0}{d_0}\right], \tag{3}$$

$$t_q = \frac{\pi d_0^2}{4\omega}\frac{\left(\rho c_p\right)_0}{\left(\rho c_p\right)_f}\frac{h_q}{w}, \tag{4}$$

where d – is the fuel element diameter; d_0 – the core diameter; Δ_1 – the shell thickness; Δ_K – the thickness of the contact sublayer between the core and the shell; $\lambda_0, \lambda_1, \lambda_k$ – the heat conductivity coefficients of the fuel, the shell and the contact sublayer; a_0 – the fuel temperature conductivity; $\left(\rho c_p\right)_0$ and $\left(\rho c_p\right)_f$ – the density and heat-capacity products for the fuel and the coolant respectively; h_q – the energy-release-zone length; w – the average coolant velocity; ω – the coolant passage cross-section.

In the formula (2) t_{TB} – is the temperature relaxation parameter for the fuel assembly element under the isothermal condition on it's surface. The expression (3) for the parameter t_{TB} has been found from the analytical solution of the non-stationary heat conductivity task for the fuel assembly element under the zero boundary condition on it's surface.

The parameter t_q in the formula (2) is the time $t_q \equiv \left(\rho c_p\right)_0 \Delta T / q_v$ for the fuel temperature to rise on the relative coolant temperature value ΔT under the volume fuel-energy-release density q_v. Determining the relative coolant temperature from the energy balance we obtain for t_q the expression (4). The parameter t_q role is important at the Reynolds numbers about and less then 10^4. At such relatively small Reynolds numbers the coolant temperature variation in the flow direction leads to the essential axial irregularity of the fuel-assembly-element-core temperature [3].

The investigation of the non-stationary thermal conductivity task for the fuel element flowed around by the coolant flat flow shows on the necessity to consider the coolant transport time through the energy-release zone h_q / w. The influence of h_q / w on the temperature relaxation in the assembly becomes essential at the small Reynolds numbers and relatively low fuel heat capacity.

It is to be emphasized although the individual components of the parameter t_p have been found from analytical solutions of the heat conductivity task for the fuel element the final formula (2) has been obtained as the generalization result of much calculation data. The constant $2 / \pi$ in the formula (2) has been obtained as the result of such generalization.

The formulae (2)- (4) do not contain empirical values like the heat transfer coefficient. It indicates on the unessential influence of the coolant boundary layer thermal resistance on the assembly temperature relaxation.

In fig.1 in coordinates $\left(t / t_p, \theta / \theta_\infty\right)$ the exponential relationship (1) is presented by the solid line, by the dots the fuel-element-shell-temperature dynamics at the energy-release-zone exit is presented. The data for the annular channels formed by placing the fuel element in the circular pipe with the adiabatic condition on it's outside wall are presented also. The assembly and annular channel parameters are brought together in table 1.

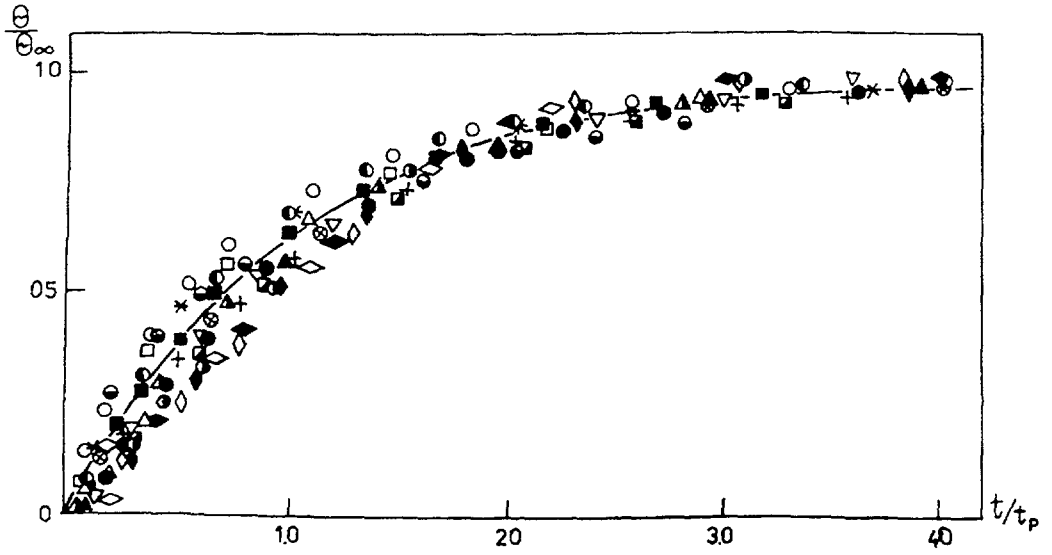

Fig. 1

In the table 1 the following notations are used:

$$R_0 = d_0 / d, \qquad R_1 = \left(d - 2\Delta_1\right) / d, \qquad H = 2h_q / d,$$
$$\Lambda_0 = \lambda_0 / \lambda_f, \quad \Lambda_1 = \lambda_1 / \lambda_f, \quad A_0 = a_0 / a_f,$$
$$A_1 = a_1 / a_f, \quad R_T = \left(\Delta_k / \lambda_k\right) / \left(2\lambda_f / d\right),$$

Re– Reynolds number; Pr– Prandtl number; õ - the relative assembly space; R_a – the ratio of the external to internal radiuses for the annular channel; λ_f and a_f – the coolant heart and temperature conductivity coefficients; a_1 – the fuel-element-shell temperature conductivity.

The insignificant data dispersion, fig.1, for the fuel-element-shell-temperature dynamics shows that t_p is the generalized dynamic characteristic of the fuel assembly.

The reactor constant t_{PE}, representing itself as the sum of two components (the fuel element constant t_0 and the constant depending on the coolant outlay through the assembly) has been proposed in the work [4] as an assembly dynamic characteristic. We make here use of the terms of the work [4] for t_{PE} and t_0. The significant data dispersion for the fuel-element-shell-temperature dynamics is observed if data are presented in coordinates $\left(t / t_0, \theta / \theta_\infty\right)$, fig.2, or in coordinates $\left(t / t_{PE}, \theta / \theta_\infty\right)$, fig.3.

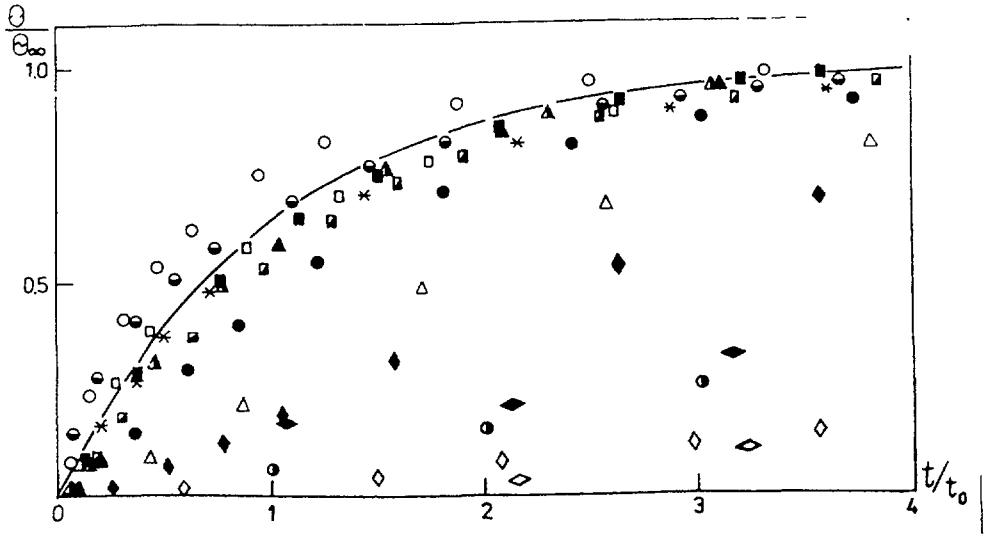

Fig. 2

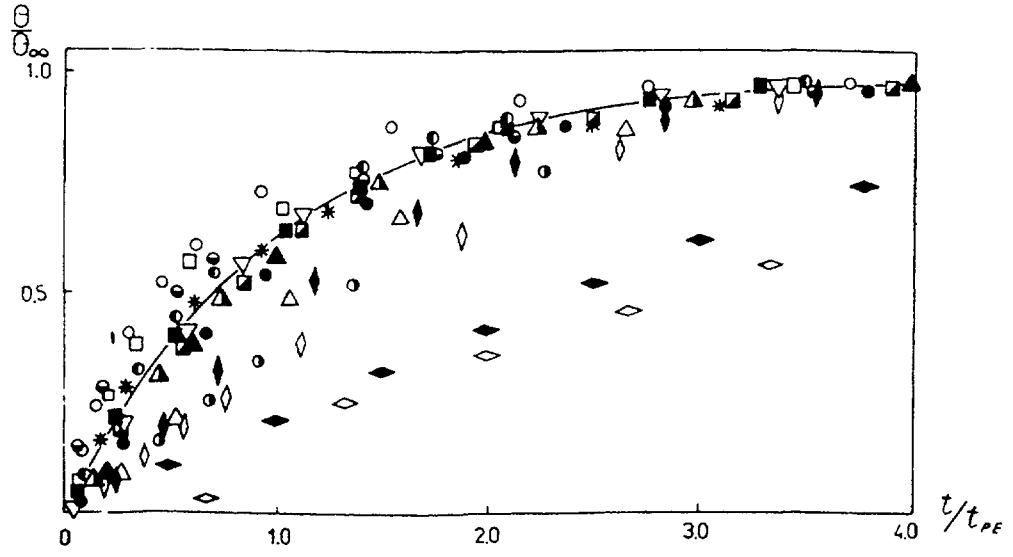

Fig. 3

Thus neither the fuel element constant nor the reactor constant can be regarded as the generalized dynamic characteristic of the assembly.

It is to be noted that the fuel element constant t_0 includes the heat transfer coefficient representing itself as the empirical value called to consider the influence of the thermal coolant resistance on the temperature relaxation time in the assembly [4].

The formulae for the fuel-element and reactor constants [4] have been obtained with the aid of the approaches stated in [5] and containing a number of assumptions. In particular they suppose the fuel-element-shell thickness to be small with respect to the fuel-element radius. Therefor it is possibly to neglect the curvature of the fuel-element-core surface. Such assumption is quite not suitable for the fuel-element imitators. The heat capacity of the imitator electric spiral effects on the imitator temperature relaxation time. At that time the internal and external radiuses of the electric spiral essentially differ from the imitator shell radius.

The numerical investigation results for the different assembly models including the models with the triangular and square imitator packing have shown the imitator temperature relaxation parameter t_p to be the sum of three items [6] by analogy with the expression (2):

$$t_p = \frac{2}{\pi}\left(t_{им} + t_q + h_q / w\right).$$

Here

$$t_q = \frac{\pi\left(d_0^2 - d_{in}^2\right)}{4\omega} \frac{\left(\rho c_p\right)_0}{\left(\rho c_p\right)_f} \frac{h_q}{w}$$

is the time for the heater electric spiral temperature to rise on the value being equal to the relative coolant temperature in the model; $\left(\rho c_p\right)_0$ – is the density and heat-capacity product for the electric spiral; d_0 and d_{in} are the external and internal diameters of the effective electric spiral layer. The value of d_{in} is determined from the condition the layer mass on the imitator length unit is equal to the actual mass of the electric spiral.

The imitator structure complexity has not allowed to obtain the explicit expression for the parameter $t_{им}$ representing itself as the imitator temperature relaxation parameter at the isothermal condition on the imitator surface. For determining $t_{им}$ the one-dimensional non-stationary heat-conductivity-task solution for the imitator with the zero boundary condition on it's surface and at the energy-release jump has been used. The value of t_p was found from the condition

$$\theta\left(2t_{им} / \pi\right) / \theta_\infty = 1 - e^{-1} \cong 0.632, \qquad (6)$$

where $\theta\left(2t_{им} / \pi\right)$ is the temperature at the internal surface of the electrical spiral layer at the time $t = 2t_{им} / \pi$, θ_∞ is the established value of that temperature. The coefficient $2 / \pi$ has been introduced in the definition of $t_{им}$ for obtaining the t_p formula like (2).

In reality the heat transfer from the electrical spiral to the silicon-organic layer is realized through the some air layer. For the values t_p determined by the way stated above to correspond the actual assembly models the effective thickness h_B of the air layer must be known. From comparing the calculated and experimental values of t_p it has been determined that the ratio of h_B to the electrical spiral wire radius r_n is the same for the different models:

$$h_B / r_n = 0.45.$$

In fig.4 in coordinates $\left(t / t_p, \theta / \theta_\infty\right)$ the exponential relationship (1) is presented by the solid line, by the dots the imitator shell temperature dynamics at the energy-release-zone exit is presented. The model parameter are brought together in table 2.

In the table 2 the following notations are used:

$$\tau_{им} = \frac{t_{им} \cdot w}{h_q}, \quad \tau_p = \frac{t_p \cdot w}{h_q}.$$

In fig.5 in coordinates $\left(t / t_p, \theta / \theta_\infty\right)$, where t_p is the experimental relaxation parameter value the data on the imitator shell temperature dynamics at the exit of the energy release zone are presented. The data have been obtained at the different models under the instantaneous cut-off of the electrical loading.

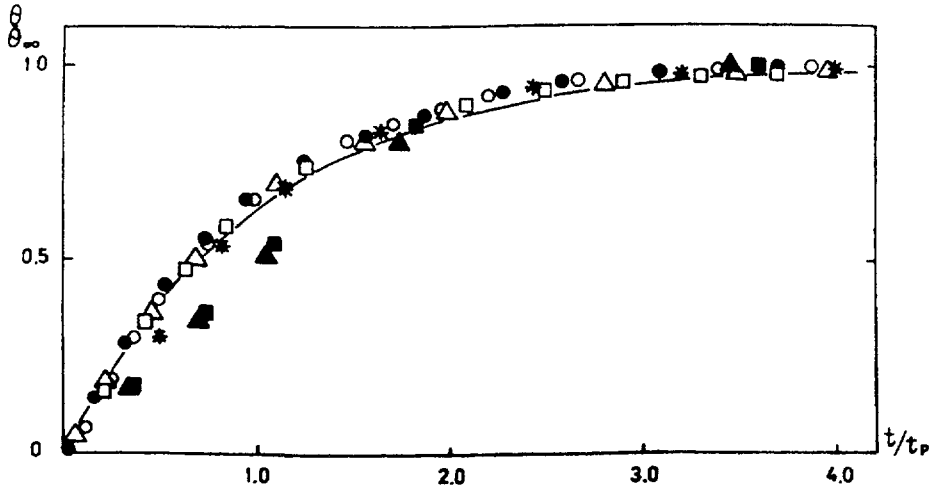

Fig. 4

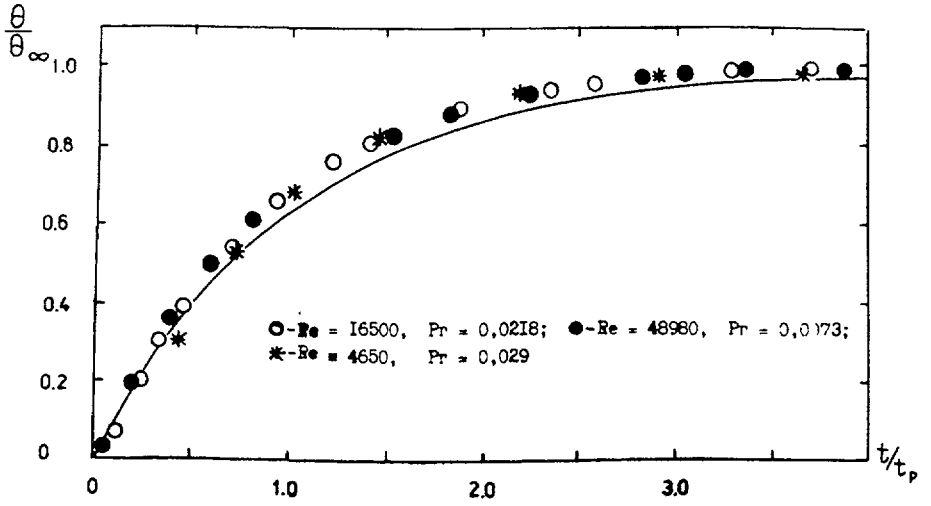

Fig. 5

Figures 4 and 5 show that the relaxation parameter t_p can be regarded as the generalized dynamic characteristic of the model. It allows to state the approximate modeling condition as the equality of the non-dimensional relaxation parameter values for the assembly and it's model. If the coolant transport time through the energy-release zone is taken as the time scale then the approximate modeling condition is

$$\left(\frac{wt_p}{h_q}\right)_{assembly} = \left(\frac{wt_p}{h_q}\right)_{model}$$

CONCLUSIONS

(1) The simple formula containing no empirical quantities and determining the assembly temperature relaxation parameter through the assembly parameters was obtained.

(2) The relaxation parameter is the generalized dynamic assembly characteristic allowing to present the fuel-element-shell-temperature dynamics or the relative coolant temperature as the universal time relationship.

(3) The method of determining the temperature relaxation parameter for the assembly model was worked out.

(4) The approximate modeling condition for the non-stationary heat exchange in the fuel assembly was stated as an equality of the non-dimensional parameter relaxation values in the assembly and it's modal.

REFERENCES

[1] USHAKOV P.A. The Aproximated Thermal Modeling of Cylindrical Elements.- Liquid Metals. M: Atomizdat, 1967, p.137-148.

[2] MIKHIN V.I. For the Aproximated Thermal Modeling of Fuel Pins with Non-uniform Heat Allocation.- IPPE Preprint-1497, Obninsk, 1983.

[3] MIKHIN V.I., FETISOVA L.N. The Numerical Investigation of Non-stational Themperature Fields in Central Zones of Nuclear Reactors Fuel Subassemblies – IPPE Preprint-2240, Obninsk, 1992.

[4] KOUZNETSOV I.A. Accident and Trasient Processes in Fast Reactors. M.: Energoatomizdat, 1987.

[5] KRAMEROV A.YA., SHEVELIOV YA.V. Engineering Calculations of Nuclear Reactors. M.: Energoatomizdat, 1984, 736 ps.

[6] MIKHIN V.I., MATJUKHIN N.M. The Questions of Transient Processes Numerical and Experimental Modeling in WWER Cores // Proceedings of the International Conference "Thermal-Physics–95", Obninsk, 1995, v. 1.

THE PROBLEMS OF THERMOHYDRAULICS OF PROSPECTIVE FAST REACTOR COMCEPTS

A.A. SEDOV
RRC Kurchatov Institute,
Moscow, Russian Federation

Abstract

In this report the main requirements to fast reactors in system of future multicomponent Nuclear Power with closed U-Pu fuel cycle are regarded. The peculiarities of different liquid-metal (sodium and lead-alloyed) coolants as well as the thermohydraulics problems of prospective FR concepts are discussed.

Presently the rate of development of the Nuclear Power is significantly lower comparatively with that one during 60 – 80th years of the century. Assured resources of cheap uranium, saturated market of the light-water reactors, fierce competition from the side of Gas-Oil Power in electricity production, "cold" attitude of public as the result of nuclear accidents are practically stipulated an absence of interest to construction of new nuclear power plants, despite of permanent advancement of the operated plant's safety, considerable improvement of analytical and numerical modelling and hardware support, appearance of great deal of the new concept projects of NPPs, being prospective from a view-point of safety and economy.

The fast sodium-cooled reactors LMFRs are in the most squeeze situation now. High specific construction costs of LMFR NPP. sodium chemical aggressive reactivity, expensiveness of the U-Pu closed fuel cycle, while plenty of cheap uranium is available, are the main reasons of closing the LMFR programs in USA, Great Britain, German and now in France. However, an interest to fast reactors (FR) does not fall down, because on the base of these very reactors it is possible to develop the future Nuclear Power, which is able to provide enhanced fuel breeding, usage of maximum fissile actinides. minimization of radioactive wastes and decrease of the scale of disturbance of current gas, thermal and radioactive planet balance in the next century.

The LMFR experience shows that they can be reliable and safety operated, provided high technical culture. However, the LMFBR ideology was formed in period of solving the task of minimization of the fuel doubling time. In the result the Fast Breeder Reactors (LMFBR) with tight - lattice ducted Fuel Assemblies have been created. This causes a number of LMFBR's lacks and disadvantages, which lower the operation reliability and reactor safety potential. Some of them are:

- High volumetric share of structure materials in core (~ 20%);
- Significant shift of radial power profile in course of fuel burning, because of MOX-fuel Core Breeding Ratio is below 1;
- Considerable excess of the core reactivity for burn-up (~ 5$);
- High value of the FA hydraulic resistance, and hence, low capability of the core to develop natural coolant circulation under accident condition;
- Insertion of the positive reactivity in the result of blockage of FA flow area and consequent boiling of sodium coolant;
- Significant temperature axial and azimuthal gradients in structural elements under condition of large fast-neutron fluence . resulting in considerable deformation of FE, fuel rods bending, local declination of the flow area and consequent overheating of the fuel rod claddings;
- Destructive impact of vibration and corrosion-erosion process onto core structural

elements under condition of high-speed coolant flow (7-10 m/s) and high temperatures of fuel rod claddings (up to 650 – 700 °C).

Without doubts, future FRs should base on the experience of the current LMFBR reactors. But, they will have to meet the requirements of the future Nuclear Power, in front of which there will be a number of its own problems as well as the troubles, derived from present Nuclear Power. So, conceptual projects of prospective FR should now oversee a few steps from the current situation on the "chess board" of Nuclear Power. These conceptual projects should answer the principle questions of work with equilibrium quantity of radionuclides, providing the safety, positive neutron balance of the Nuclear Power for enhanced fuel breeding, minimization of rate of radioactive waste accumulation and non-proliferation. The answering this questions requires carrying out experimental-theoretical works in justification of new kinds of fuel compositions, coolants and structure materials, development new approaches to physical and mathematical modelling.

In structure of future large-scale Nuclear Power should be multicomponent [1]. This NP should solve the task of minimization of all actinides in fuel cycle and minimization of their final disposal. In such NP the Power Fast Reactors (PFR) will carry out a function of enhanced breeding of fuel, for the Power Thermal Reactors (PTR) and enlarging of NP scale. Another important role of FR-closing the fuel cycle for all dangerous actinides.

For minimization of equilibrium quantity of Pu in NP closed fuel cycle this actinide should be effectively applied in PTR. These reactors should also widen a sphere of nuclear energy utilization.

For utilization (fission) of minor actinides (Cm, Am, Np) and burning dangerous long-lived fission products (^{129}I, ^{99}Tc, ^{90}Sr, ^{137}Cs, ^{135}Cs), some share of burner-reactors must be essential. In the concept of future NP [1] function of reactor-burner will carry out high-flux molten-salt reactor (MSR).

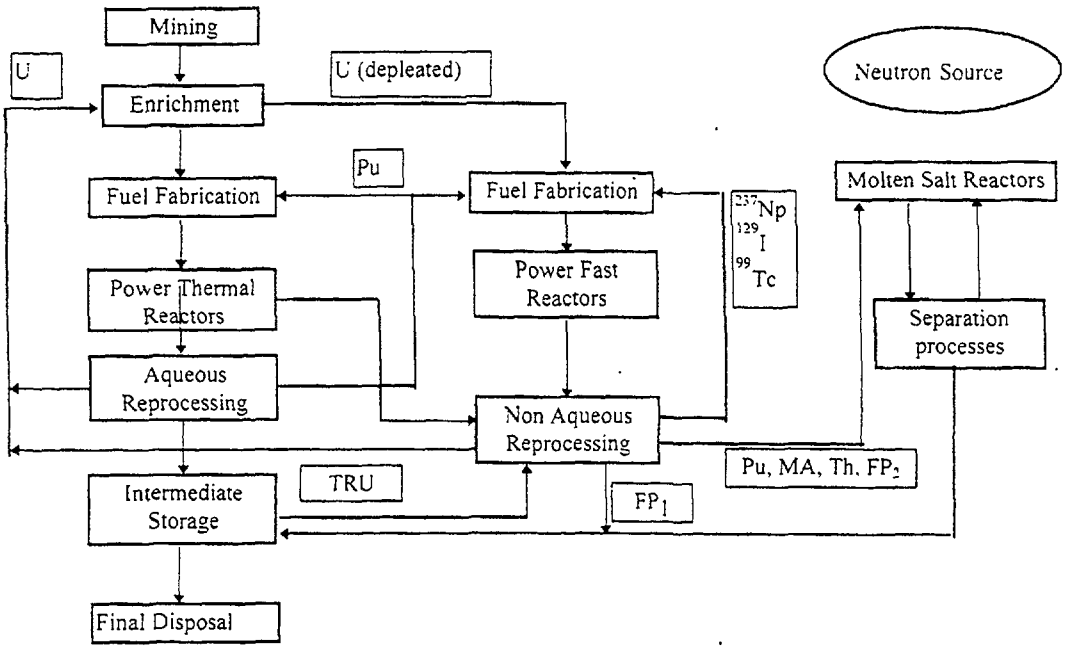

FIG. 1. Multi-component nuclear energy system with closed fuel cycle for all actinides and dangerous long lived fission products. FP_1, FP_2 — short lived and long lived FP respectively. Designations: FP — Fission Products; MA — minor actinides (Cm, Am, Np): TRU — transuranic actinides.

Anyway, whatever future NP to be, fast reactors will be one of more important its component. In carrying out above-mentioned functions in structure of Nuclear Power, fast reactors should meet a number of requirements, imposed by NP:

(1) Specific mass power rate (power rate per unit of mass) of fuel should be as great as possible. This requirement is derived from intention to minimize the equilibrium quantity of Pu and other actinides through minimization of lifetime of them in NP closed fuel cycle. In turn, this requires to decrease irradiation time of fuel in reactor while increasing its burn-up.

(2) Core design should guarantee, that excess of core reactivity for burnup is less than 1$. Such quality can principally enhance a safety potential of reactor.

(3) Power Coefficient of Reactivity (PCR) and Temperature Coefficient of Reactivity should be negative with a good margin to provide reliable feedback compensation of power and temperature rise in normal operation and accidents. Requirement of negative Void Effect of Reactivity (VER) should not prevail over other important reactor characteristics as breeding gain and minimum excess of reactivity for burnup. Instead, the general requirement to NPP with FR, limiting the risk of prompt and delayed fatalities in the result of accident on such NPP by the value 0.1% of the risk, which is characteristic for given place.

(4) Breeding ratio of FRs should amount 1.3-1.5 to supply thermal and burner reactors by Pu (Th). So, it causes a necessity to apply both axial and radial blankets in reactor. Another trouble, neutron fluence in reactor vessel and structures, require to make tight and thick blankets to mitigate problems with NPP decommissioning.

(5) Coolant of reactor contour should not accumulate a large quantity of dangerous long-life radioactive products.

(6) Core design should assure a 'good' thermohydraulics, providing reliable heat removal from core fuel elements in normal and accidental regimes, high margin to boiling, minimum non-uniformity of coolant heating and minimum temperature gradients in structures of Fuel Assemblies in core and blankets.

(7) Core design together with coolant chemical properties and technology should not allow appear dangerous sediments of impurities (corrosion and erosion products, debris etc.), which could negatively affect to capability of heat transfer in reactor core, heat exchangers etc., and lead to local concentration of high-radioactive products upon streamlined surfaces.

Let's do now a brief comparative analysis of compositions on the basis of lead and sodium as coolants for the fast reactors. The application of sodium engineering for NPP with fast reactors has solid experience, and in this sense sodium as the coolant for a today's day is rather competitive. However, such negative its features as fire-risk, not so large margin up to boiling (see. Tab. I[1]), yield of long-life radioactive ^{26}Al in it, rather high radio-activating of primary circuit structures result in necessity of searching for new compositions for use them as coolants in reactors, and first of all in fast reactors in order to increase their safety.

In Russia there is an experience of designing, creation, operation and maintenance of the ship nuclear installations with liquid-metal coolant. In the time, when a problem was decided on what material to use as the coolant, it was selected an eutectic alloy 44.5%Pb-55.5%Bi, mainly, on the reasons of its fire safety, while the melting temperature point of the given alloy not strongly exceeds that one for sodium (see Tab.I). The operated installation had low power and was enough compact. So, its mass-dimensional performance was rather acceptable.

---

[1] Data presented in Tab. I are taken from [2-5]

Quite another matter is a power reactor. Here, the high density of lead-alloyed coolants at, practically, identical volumetric thermal capacity results in essential increase of weight of reactor installation.

Let's compare coolants on the basis of lead and sodium in specific weight of the coolant in the primary (reactor) circuit per unit of the reactor power:

$$M_{coolant} = 1000\frac{\rho\tau}{c_V \Delta T} = 1000\frac{\tau}{c_p \Delta T}[\text{tons / MWt}], \quad (1)$$

Where

τ – time period of circulation of the coolant in the primary circuit; c_V - = ρ C_p – volumetric thermal capacity of the coolant; C_p – mass isobaric thermal capacity of the coolant, (see Tab.I); ρ – coolant density; ΔT – mean-mixed heating of coolant in reactor.

So, for the reactor with thermal power 1000 MWt and reactor temperature heating 100 K with the time of circulation in the primary circuit 30s, the weight of the sodium coolant will make 240 tons, while the weight of the lead coolant at the same parameters – 2040 tons. As one can see from (1), so essential difference in weight is caused by a difference only of one thermodynamic parameter – mass thermal capacity, which is a 7.5 – 8.5 times lower for lead-alloyed coolants, than for sodium (see Tab.I).

TABLE I. COMPARISON OF THERMAL-PHYSICAL PROPERTIES OF PB- AND NA-BASED COOLANTS

Properties(at atmospheric pressure)	**Coolant**			
	Pb	**44.5%Pb 55.5%Bi**	**97.7%Pb 2.3%Mg**	**Na**
Melting temperature, °C	327.4	123.4	248.7	98
Boiling temperature, °C	1745	1670	1610	881
Fusion heat, kJ/kg	23	25	26	112
Vaporization heat, kJ/kg	860	820	920	3890
Density at 500°C, kg/m^3	10470	10050	9560	833
Volumetric expansion coefficient, 1/K	$1.12*10^{-4}$	$1.34*10^{-4}$	$1.22*10^{-4}$	$2.93*10^{-4}$
Heat conduction at 500°C, W/m K	15.4	14.4	22	66
Specific heat at 500°C, kJ/kg K	0.147	0.146	0.168	1.254
Kinematic viscosity at 500°C, m^2/s	$17.6*10^{-8}$	$12.8*10^{-8}$	$15.3*10^{-8}$	$29.0*10^{-8}$
Prandtl number, Pr	0.0178	0.0131	0.011	0.0046
Saturated vapor pressure, bar	$5.1*10^{-6}$	$8.7*10^{-5}$	$2*10^{-5}$	0.009
Surface tension coefficient, N/m	0.44	0.42	0.35	0.155

The decrease of specific weight of the coolant in the primary circuit $M_{coolant}$ is possible, for instance, due to increase of volumetric fuel rating in reactor core and decrease of the time of circulation t. Both of them require reduction of flow cross-sections in the primary circuit. However, deterioration of the circuit hydraulic characteristics will simultaneously take place. So, the limitation on weight of the reactor installation with the lead-alloyed coolants could be also a reason of limitation of its power.

Let's consider now those characteristics of coolants, which influent hydraulics of reactor installation. From the thermal balance in reactor core it is easy to define the coolant velocity in it:

$$W_{coolant}^{core} = \frac{q_V H^{core}}{\varepsilon_{coolant} \rho c_p \Delta T}, \quad (2)$$

Where q_V – specific volumetric fuel rating in reactor core; $\varepsilon_{coolant}$ – volumetric fraction of the coolant in the core.

One can define a hydrodynamic pressure of the coolant P_{din} as a function of the coolant velocity:

$$P_{din} = \frac{\rho\left(W_{coolant}^{core}\right)^2}{2} = \frac{\left(q_V H^{core}\right)^2}{2\rho\left(c_P \Delta T \varepsilon_{coolant}\right)^2} \quad (3)$$

The value of hydrodynamic pressure is a parameter, determining the pressure loss due to friction and drag, and, besides, the dynamic vibrational loads on the fuel assembly in the core.

The value of volumetric fuel rating q_V, the height of the core H^{core} and volume fraction of the coolant $\varepsilon_{coolant}$ are determined mainly by desirable neutron-physical characteristics of reactor (reactor breeding ratio, core breeding ratio, void reactivity effect etc.), which, in turn, are caused by a functionality of the given reactor type in the Nuclear Power system. The upper limit of the core coolant heating ΔT is caused by required lifetime of structural materials under conditions of high-temperature cyclic loads, stresses from temperature non-uniformity, high-temperature corrosion; the lower limit of the core coolant heating ΔT is caused by some guaranteed temperature margin to the freezing point of the coolant, and also by parameters of steam-power heat cycle (e.g. in LMFBR the value of ΔT amounts 190-210°C, in the case of power reactor using the 44.5%Pb-55.5%Bi coolant that value should be decreased to 130-170°C; as for such lead-alloyed coolant as Pb and 97.3%Pb-2.7%Mg with high temperature point of freezing, the value of ΔT should not exceed 130°C).

As one can see from above adduced expression for P_{din} , value of hydrodynamic pressure is inversely proportional to density and squared thermal capacity. At the same geometric and power parameters of the core the value of the hydrodynamic pressure of the lead-alloyed flow is a 5-6 times higher than that one of the sodium flow.

In fast sodium breeder reactors with a rather tight fuel lattice (pitch-to-diameter ratio is 1.15 - 1.2) the value of dynamic pressure reaches 20 - 40 kPa. The arising vibrational loads, affecting the fuel rods in the assemblies are rather great. Under such conditions the fuel assemblies keep their workability due to dense packing of bundle of the rods, spaced by wrapped wires; the rod bundle, in turn, is kept by a thick duct.

In PWR fuel assemblies with looser fuel lattice (pitch-to-diameter ratio is 1.35-1.44) the value of the dynamic pressure amounts 10-12 kPa. The vibrational loads at such hydrodynamic pressure are not so high as in LMFBRs. PWR ductless fuel assemblies, spaced by thin-walled grids, keep rather well their workability under such vibrational loads.

The velocity of lead-alloyed coolants in the power reactors should be limited by the value of 1–1,5 m/s, and hydrodynamic pressure by 10-15 kPa. The reason of such limitation is an intensification of processes of core structure materials dissolving and erosive wear with increase of the coolant hydrodynamic pressure. Let's mark here, that the less is difference in densities of structural materials and coolant and the higher is the coolant temperature, the more intensive is the rate of structural material dissolving.

Limitation on velocity at use of lead-alloyed coolants results in necessity of decrease of volumetric fuel rating and increase of coolant fraction in the core, that, on one hand, is useful from a point of view of reduction of the core reactivity excess for burnup compensation and decrease of the void reactivity coefficient and effect, but, on the other hand, results, as it was said above, in increase of the reactor and whole primary circuit weight.

Fig. 1 demonstrates an influence of the fuel lattice pitch-to-diameter ratio, specific mass fuel rating in the core and the fuel rod diameter to the value of hydraulic resistance of the primary circuit in the fast liquid-metal reactors. On the Figure the points are marked, which respect to some operated reactors with the sodium coolant. Also a typical example of

hydraulic resistance of the primary circuit with the 44.5%Pb-55.5%Bi coolant and loose fuel lattice is adduced.

Let's compare now the fast reactors cooled by lead-alloyed and sodium coolants on ability of the primary circuit to develop the natural circulation in it in nominal operation and emergencies. Under a level of the natural circulation (n.c.) of the coolant let's imply a percentage of the coolant flowrate relatively to its nominal value due to developing of the natural circulation in the primary circuit at the nominal level of heating in reactor.

Ability of the primary circuit to develop n.c. determines, in main, a level of temperatures of the core structural and fuel components in emergency processes. In LMFBR reactors, for example, rather dangerous is the situation with de-energizing of electric drivers of the Main Circulation Pumps (MCP) at malfunctioning of emergency protection. At a low level of n.c. in such situation the temperature feed-backs have no time to stabilize reactor in acceptable asymptotic state. Heating of the sodium coolant, eventually, results in its boiling and, at presence of positive void reactivity coefficient, lead to a neutron runaway of reactor.

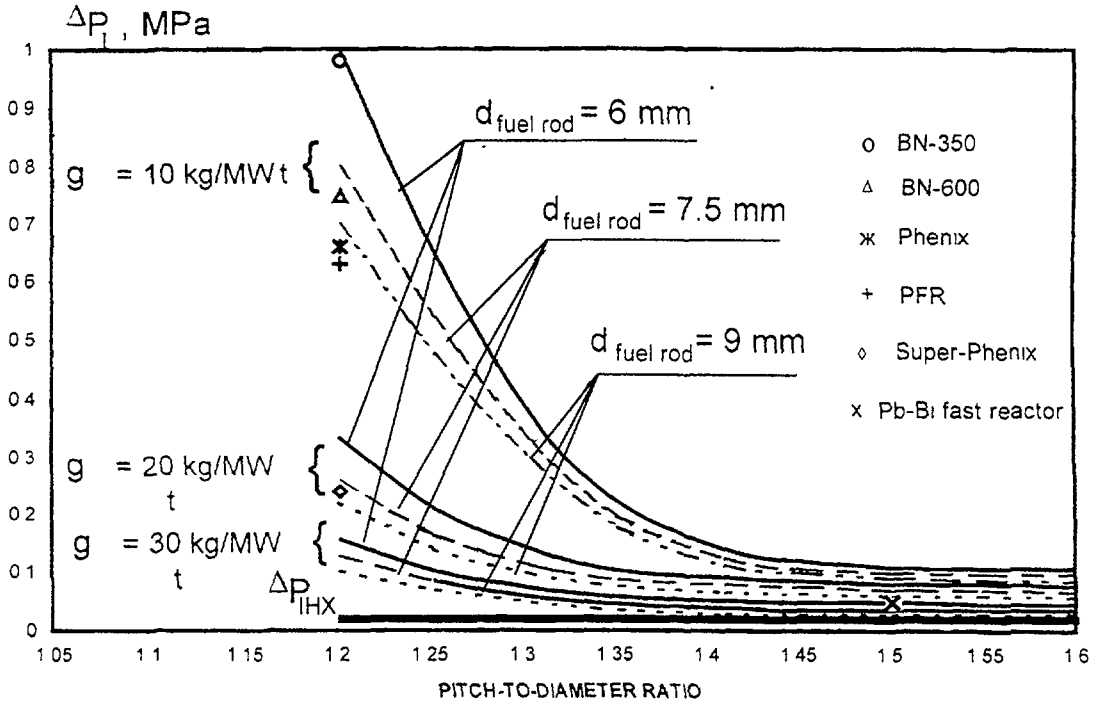

Fig. 1. Hydraulic resistance of the primary circuit of the fast reactors of integral layout with a free coolant surface in the reactor vessel versus a fuel lattice pitch-to-diameter ratio, specific mass fuel rating and fuel rod diameter at a nominal coolant heating in the reactor ΔT=160 °C; core height H_{core}=1m. Notation: ΔP_I - hydraulic resistance of the primary circuit; g - specific mass fuel rating in the core (kg-of-fuel/ MWt); $d_{fuel\ rod}$ – diameter of fuel rod; ΔP_{IHX} – hydraulic resistance of Intermediate Heat Exchanger on a side of the primary circuit

As an example let's consider a situation with a primary circuit blow-down more detail. Provided the asymptotic condition of the primary circuit is got, the pressure head of natural circulation

$$\Delta P_{nc} = \Delta T_0\, t\, \rho\, \beta\, g\, H_{pull}$$

counterbalances the hydraulic resistance of the primary circuit with the running-out pumps

$$\Delta P_I \approx \left(\Delta P_0^{core} + \Delta P_0^{INX} + \Delta P_0^{pump}\right)\omega^2 \qquad (4)$$

Here: ω – level of the natural circulation; ΔT_0 – nominal heating in reactor; $t=\Delta T/\Delta T_0$ - relative heating; ρ, β – density and volumetric extension coefficient of the coolant; g - gravity; H_{pull} – primary circuit «pulling» height (equals approximately a distance from the core middle up to middle of IHX); ΔP_0^{core}, $\Delta P\ P_0^{IHX}$, – hydraulic resistance of the core and IHX respectively in the nominal regime; ΔP_0^{pump} – hydraulic resistance of the stopped pump at the 100 % flow rate in the primary circuit.

By equating the expressions for ΔP_{nc} and ΔP_I, one can get a percentage of the flowrate through the reactor in a mode of natural circulation:

$$\omega(t) = K\sqrt{t}, \tag{5}$$

where

$$K = 100\%\sqrt{\frac{g\rho\beta\Delta T_0 H_{pull}}{\Delta P_0^{core} + \Delta P_0^{IHX} + \Delta P_0^{pump}}}. \tag{6}$$

Percentage of the reactor power (from nominal value), can be approximately defined as follows:

$$q(t) = Kt^{2/3} \tag{7}$$

From adduced expressions one can see, that both the percentages of the reactor flowrate and power are determined by the relative heating t and some parameter K, which reflects hydraulic quality of the primary circuit, its ability to develop the natural circulation. The value of K equals to percentage of the reactor flowrate and the power at the nominal heating (t=l):

$K=\omega(1)=q(1)$.

To make more clear: how the coolant thermodynamic properties influent ability of the primary circuit to develop n.c., let's transform the expression (6), factoring the term ΔP_0^{core} out off the brackets in denominator:

$$K = 100\%\sqrt{\frac{g\rho\beta\Delta T_0 H_{pull}}{\Delta P_0^{core}(1 + x^{IHX} + x^{pump})}}, \tag{8}$$

where $x^{IHX} = \Delta P_0^{IHX} / \Delta P_0^{core}$ and $x^{pump} = \Delta P_0^{pump} / \Delta P_0^{core}$.

Let's express now ΔP_0^{core} through hydrodynamic pressure P_{din} (formula 3) and core drag coefficient ζ_{core}. Now we can transform formula (8) as follows:

$$K = 100\%\sqrt{\frac{g\rho\beta\Delta T_0 H_{pull}}{\Delta P_0^{core}(1 + x^{IHX} + x^{pump})}} = 100\%\sqrt{\frac{g\rho\beta\Delta T_0 H_{pull}}{\zeta_{core}\Delta P_{din}(1 + x^{IHX} + x^{pump})}} =$$

$$= 100\%(\rho c_P\sqrt{\beta})\frac{\varepsilon_{coolant}(\Delta T_0)^{2/3}}{q_V H_{core}}\sqrt{\frac{2gH_{pull}}{\zeta_{core}(1 + x^{IHX} + x^{pump})}} \tag{9}$$

From (9) one can see, that the percentage of natural circulation K is determined by design features of the core (q_V, $\varepsilon_{coolant}$, H_{core}, ζ^{core}), hydraulic characteristics of the primary circuit (H_{pull}, x^{IHX}, x^{pump}). The influence of thermodynamic properties of the coolant is exhibited by a complex $(\rho c_P\sqrt{\beta})$. And taking into account that the core hydraulic resistance coefficient ζ^{core} is proportional to $Re^{-0.2}$ (Re – Reynolds number), and Re is inversely proportional to kinematic viscosity of the coolant, one can finally obtain, that the complex consisted of the coolant properties, influencing the percentage of the core flowrate in n.c. regime looks like the following: ($\beta^{0.5}\rho c_P \nu^{-0.1}$).

It is interesting to mark, that the value of this complex is about the same for all the coolants adduced in Tab.I, independently either a coolant is on the basis of lead or sodium.

So, the hypothetical replacement one liquid-metal coolant for another in the given reactor, practically, will not change anything from a point of view of ability of the primary circuit to develop the natural circulation.

Actually, the main parameter, influencing this ability, is the core fuel volumetric rating q_V. This is the parameter, which forms hydraulic performance not only reactor, but also whole primary circuit, since it influents determinantly a volumetric coolant fraction in the core, hence the values of the flow cross-sections in the core as well as the value of the core flowrate, coolant velocity and hydrodynamic pressure. The latter, as it was mentioned above, defines the pressure loss from friction and drag forces in reactor and entirely primary circuit. Hydraulic resistance of the reactor and required reactor flowrate, in turn, determine a performance of MCP, and, therefore, its design. The design of IHX in integral layout of the primary circuit with a free level of the coolant in the vessel is determined by the value of reactor flowrate and vessel sizes (diameter, height), since the hydraulic resistance of IHX in integral layout with free coolant level is limited by the value 0.2 – 0.25 bar, that is stipulated by the requirement of cavitation-free operation of the Main Circulation Pumps and inhibition for gas bubbles, captured by the coolant flow from the free surface, to get the core.

Another one important moment of the core thermohydraulics concerns a scale of non-uniformity of temperatures of Fuel Assembly structures. As rule, temperature distortion across FA, first of all, depend on a scale of temperature heating:

$$T_{max}(z) - T_{mean}(z) = \left(\left(1 + \frac{k_{power} \sqrt{\frac{\rho}{\rho_{max}}} - 1}{k_{mixing}} \right) - 1 \right) \Delta T_{mean}(z) .$$

Therefore, in decreasing temperature drop in reactor core one can decline temperature differences and hence, reduce both stresses and bending of Fuel Assembly.

Let's compare now the coolants, adduced in Tab.I on their properties, which influent heat-transfer capability of the coolant. The main thermodynamic characteristic, influencing heat removal efficiency of the coolant is its thermal conductivity. Obviously, the sodium coolant has not a competitor on this parameter. Its thermal conductivity is a ~ 4.4 times higher, than that one of lead or Pb-Bi alloy.

Besides, it is necessary to mark, that lead-alloyed coolants are more troubled, than the sodium one, by formation of additional thermal resistance at the fuel rod surfaces consequently of a separation of impurities from the coolant flow and their adhesion at the hot surfaces. Experiments [6-7] have shown, that the heavier impurities move, mainly, in to the flow core, whereas the light impurities and gases are separated at the walls of the channels. For example, lead oxides, transported by the flow of Pb - Bi alloy are accumulated on the walls of the channels, whereas iron particles are suspended in the flow core. Measures, preventing similar appearances can be a systematic monitoring and control of a liquid metal chemistry, mainly, on the contents of oxygen in it. It is important also to apply initially pure metals in processing the coolants, careful cleanup of the protective inert gases from oxygen and moisture.

In some cases the heavy metals Pb and alloy Pb-Bi can be protected by nitrogen. More preferable. however, to use reductant gas mixtures (argon - hydrogenous, nitrogen - hydrogenous and so on) with periodic change of a gas ullage under the free coolant level, where water vapor and other volatile oxidant products can be accumulated.

Rather perspective coolant among lead-based liquid metals is an eutectic alloy of lead and magnesium 97.3%Pb-2.7%Mg. Its thermal conductivity is a 1.5 time higher, than Pb and Pb-Bi one, the thermal capacity is higher by 15 %, that it is important for improving the mass-

dimensional characteristics of the reactor (see formula 1) and decrease of hydrodynamic pressure (see formula 3).

In the work [5] it was carried out the experimental study of thermodynamic properties of this alloy, regularities of its interaction with structural materials and ceramics, gaseous solubility and oxides behavior in the liquid metal. The work [5] and consecutive studies of alloy 97.3%Pb-2.7%Mg have shown, that the process engineering of this material in many respects is similar to a process engineering of more investigated lead-based coolants - Pb and Pb-Bi.

It is necessary also to mention a problem, related with a volatility of saturated vapors above a free coolant surface in reactor. In the result of condensation of these vapors on the more cold surfaces of the structures, located in upper plenum of the reactor, impurities can be concentrated due to adhesion at these surfaces from condensing vapors, and these concentrates can be high-radioactive ones.

In Tab.I the data on saturated pressure for the liquid-metal coolants at the temperature 500°C are adduced. One can see, that sodium is a leader there (p_s = 0.009 bar). Volatility of saturated vapors of Pb-Bi alloy results in carry-over of high-radioactive and high-toxic Polonium, being a yield of neutron capture by Bismuth in reactor core, and deposition of Po-containing concentrates on «cold» surfaces. Besides, the value of saturated pressure of Pb-Bi alloy ($p_s = 8.7 \cdot 10^{-5}$bar) is the highest among the lead-based coolants because of presence of a great quantity of Bismuth in this alloy. The liquid lead ($p_s = 5.1 \cdot 10^{-6}$ bar) and alloy 97,3%Pb-2.7%Mg ($p_s = 2 \cdot 10^{-5}$ bar) are in the better position.

CONCLUSION

In multicomponent Nuclear Power system the Power Fast Reactors (PFR) will carry out a function of enhanced breeding of fuel, for the Power Thermal Reactors (PTR) and enlarging of NP scale. Another important role of FR – closing the fuel cycle for all dangerous actinides, minimization their equilibrium quantity. This will require from future Power Fast Reactors to increase mass power rate of fuel, provide high level of breeding (BR ~ 1.3-1.5), minimize a loss of neutrons and fissile actinides together with providing high level of operation reliability and safety.

REFERENCES

[1] ALEKSEEV P.N., PRUSAKOV V.N., PONOMAREV-STEPNOI N.N., SUBBOTINE S.A. Harmonization of Fuel Cycles for Nuclear Energy System with the Use of Molten Salt Technology // NED, 173 (1997) 151-158.

[2] BORISHANSKY V.M. et al. The Liquid-Metal Coolants // Atomizdat, Moscow, 1976.

[3] KIRILLOV P.L. et al. Thermal - Hydraulic Calculations Handbook // Energo-atomizdat, Moscow, 1990.

[4] ANDREEV P.A. et al. The Liquid-Metal Coolants for Nuclear Reactors // Sudpromgiz, Leningrad, 1959.

[5] SOKOLOVSKY B.I. et al. The Physical-Technical Properties of Alloys, Based on Lead-Magnesium Eutectic // Levovsky University, USSR MinVUS, Levov, 1990.

[6] ANDREEV A.S. et al. The Liquid Metals // Gosatomizdat, Moscow, 1963.

[7] ANDREEV A.S. et al. The Problems of Magnetohydrodynamics and Plasma Dynamics // Izd. AN LatvSSR, Riga, 1962.

THE THERMALHYDRAULICS OF A PIN BUNDLE WITH A HELICAL WIRE WRAP SPACER. MODELING AND QUALIFICATION FOR A NEW SUB-ASSEMBLY CONCEPT

B. VALENTIN
CEA/CEN Cadarache,
DRN/DEC/SECA/LTEA,
St Paul-lez-Durances, France

Abstract For the sub-assembly composed by an hexcan and a pin bundle with an helical wire wrap spacer, the calculation of the maximum clad temperatures, with the design code CADET, imposed to correctly evaluate the heat and mass transfers due to the helical wire The models use theoretical and experimental arguments which are presented after a brief description of the hydraulic behavior of a such bundle The design of a new sub-assembly concept in the framework of high plutonium consumption in fast reactor projects needs to quality the models from RAPSODIE, PHENIX and SUPER-PHENIX programs The qualification program, which could be used, is described the approach is notably comparative for the hydraulic fields and the past experimental results will be useful Another approach is briefly presented It uses a multidimensionnal code (TRIO) which solves Navier-Stokes equations The utility and the limits of a such method are described

1. INTRODUCTION

For a fuel or breeder sub-assembly (S/A), the power is dissipated in a pin buddle The pin bundle itself consists of fuel or breeder pellets, a clad and an helical wire wrap spacer in a hexcan In the past, many hydraulic and thermalhydraulic studies were undertaken with two objectives first to achieve optimum performances for each S/A and the whole core, second to respect the safety criteria on the clad (and the hexcan) to avoid mechanical failure
The evaluation of clad temperatures is done by calculation The physical modeling used at present comes from studies performed in the framework of RAPSODIE, PHENIX and SUPER-PHENIX (SPX) programs It is based on theoretical and experimental experience
The high plutonium consumption in a LMFBR project introduced new concepts in the fuel sub-assembly (call heterogeneous S/A) characterized by a great number of pins, a large wire wrap spacer diameter in comparison with the clad diameter and a heterogeneous distribution of power with one third of empty pins These different points show that the present codes must be qualified
The selected method is based on the experience acquired (mentioned above) and will be analytical, experimental and comparative with the SPX standard fuel S/A Are the present codes adapted to the new concept ? If not, what models should be changed and qualified ?

A good prediction of the Maximum Clad Temperature (MCT) requireds a correct knowledge of the global and local thermalhydraulics of the pin bundle One of the main effects to take into account is the mixing of the coolant fluid due to the wire wrap spacer which imposes local thermalhydraulic couplings between two parts of the bundle

Two calculation method or geometrical modeling, are used The first is a refined mesh of the calculated domain on which Navier-Stokes equations, with turbulence models are solved (TRIO code, Menant & al, 1994) This approach requires a large computer memory and is limited to bundles with 7, 19 or 37 pins for one or two pitches of the helical wire, but it is an efficient method for a qualitative analysis The second method uses the sub-channel notion Three types are defined (triangular, rectangular and corner sub-channels) For each of them, pressure velocities and temperatures are averaged on space The distinction between two next sub-channels is made by the fictitious border which is common and where the thermalhydraulic couplings occur This approach

requires physical models from theoretical, analytical and experimental arguments. This approach is used in the design code CADET.

2. ON HYDRAULIC BEHAVIOR OF A PIN BUNDLE WITH A HELICAL WIRE WRAP SPACER.

2.1. The influence of a helical wire.

From the thermalhydraulic point of view, the presence of helical wires is very important because they are at the origin of the transversal flow which is a predominant mode of heat transfer. It is not the only effect because these wire wrap spacers create secondary local flows (wake behind the wire which obstructs the clad cooling), increase the level of turbulence (which ensures a good mixing of the coolant fluid which means more uniform temperatures) and the pressure drop.

2.2. Main hypothesis.

In this study, the calculation of the MCT is for the nominal operation of the reactor. The flow is a forced convection regime and the hydraulic fields are totaly imposed by the enclosed geometry. The hydraulic and the thermal fields are uncoupled. For theses reasons, only the hydraulic aspect is discussed.

2.3. Avalaible experiences.

Numerous hydraulic experiences are avalaible They concern The same kind of S/A (of pins distributed on a triangular pitch, helical wire wrap spacer , hexcan) with different numbers and pin diameters: 19 pins for Lafay & Menant (1975), 61 pins for Chen & al (1977), Cheng-Todreas (1986) and Fennech & al (1987), 91 pins for Lorenz & al (1973) and 217 pins for a PHENIX fuel S/A. The presentation below is a synthesis of such publications where one notes the coherence of the results.

2.4. Axial velocity.

In a triangular sub-channel the axial velocity (V_Δ) profile is greatly influenced by the presence of the helical wire.

The zone where V_Δ is maximum, is located before the wire and it passes through the neck (without wire) toward the adjacent sub-channel to always remain in front of the wire. The V_Δ velocity is greater than the mean bundle velocity V_b (up to 20 %) near the two necks which are at the opposite side of the one containing the spacer wire. The minimum of velocity appear in the wake of the wire and is lower than V_b. Generally speaking, the velocities in a triangular sub-channel are always greater than the mean velocity for each point outside the wake. The axial velocity behavior is cyclical, that's allow the flow to be predicted in the other sub-channels.

For the peripheral sub-channels, Chen & al, (1977) measured the axial peripheral velocities ($V_\square$) in a 61 pin bundle. They plotted the evolution of the $V_\square(z)/V_b$ ratio for laminar and turbulent flows. They showed that the extreme values of the $V_\square(z)/V_b$ ratio are independent from the hydraulic

regime The average value of this ratio approaches 1 in a turbulent flow the flow approaches, on average, an iso-velocity distribution These results are coherent whatever the pin number The maximum value of $V_{\square}(z)/V_b$ appears when the helical wire arrives near the neck between a rectangular sub-channel and a triangular sub-channel just before entering in the latter The minimum value of $V_{\square}(z)/V_b$ appears just after the neck between a triangular and rectangular sub-channels when the wire is already in the rectangular sub-channel These results are in agreement with those of Lorenz & al (1973) and Lafay & al (1975)

2.5. Transverse velocities in the bundle periphery.

The peripheral sub-channels are where a transversal and gyratory flow induced by the helical wire occurs This flow is periodic, when it is fully developed, and function of the wire position The transverse flow reaches a maximum value on one or two sixth wire pitches when the wire is on the opposite side of the peripheral pin - hexcan neck The axial velocity becomes more axial when the wire goes in and stays in the neighbouring triangular sub-channel Between these two positions, on one sixth pitch, there is a partial blocking when the wire arrives near the hexcan The passage of this neck induces a higher pressure in front of the wire and a lower pressure behind it Then the transverse velocity $U_{\square}$ becomes negative to statisfy the balance pressure arround the helical wire Roidt & al (1980) have shown a similar behavior for the triangular sub-channel with an inversion of the transverse flow on the whole neck width when the helical wire is nearly 60 degrees before the concerned neck

The experimental results of Lafay & al (1975) show, for a 19 pin bundle, that the angle formed by the transverse velocity vector and the axial velocity vector do not correspond to the wire rolling up angle whereas Fennech & al (1987) mention, for a 217 pin bundle, that the peripheral transverse flow follows the rolling up angle In general, the transverse velocity remains weak in the rectangular sub-channels (< 5 %) but for a 7 pin bundle, this velocity was significant Cheng & al (1986) think that this point is a characteristic of bundles with few pins (less that 19 pins)
For the mass transfers between triangular and rectangular sub-channels, the exchange is always due to a suction by the wire wrap spacer and not by a thrust The exchange periods are longer in the direction which is triangular to the rectangular sub-channel rather than in the opposite way But the transfers from rectangular to triangular sub-channels present higher values

3. A PIN BUNDLE MODELING.

3.1. Introduction

The heatings may be different between each sub channel because the power distribuution of a S/A depends on its own position in the core The section flow (i e the velocities and the flowrate) are not the same for a triangular, a rectangular and a corner sub channel However, phenomena tend to equalize the sub-channel temperatures movement of the wire wrap inside a sub-channel, heat and mass transfers from a sub-channel to an adjacent one due to the helical wire, high levels of thermal diffusivity (for a liquid metal) and turbulent diffusivity The modeling presented below, uses a geometrical approach to calculate the deflected flow by the helical wire and average values for the axial velocity the pressure and the temperature The temperature is evaluated with a classical thermal balance inside a sub-channel which takes into account the heat transfers with an adjacent sub-channel and the boundary conditions

3.2. The deflected flow by the helical wire.

3.2.1. The main hypothesis.

Triangular - triangular exchange:

- equality of inlet and outlet flow for each level,
- the mass transfer is done at the neck between two sub-channels, in function of the location and the rotation of the wire,
- the exchange flow is a sinusoidal function : $q_{\Delta\to\Delta} = \alpha_{\Delta}.\sin(2\pi z/h - \varphi)$ **(3.1)**, is evaluated with the equalization of the sweept area (S_{sweep}) by the helical wire and the surface of the sinus function $S_{sin} = \sqrt{3}/2$ (Fig. 1) **(3.2)**,
- the flowrate and the velocity are constant for each sub-channel of same type : $q_j = \rho S V_j$,
- the deflected flow is proportional to the triangular sub-channel flowrate, and is written : $q_{\Delta\to\Delta}$ (on $\pi/3$) $= (S_{sweep}/S_{\Delta}).q_{\Delta}$ **(3.3)**.

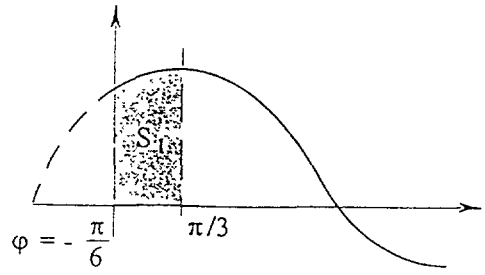

Fig. 1. Surface of the sinus function on one sixth of wire pitch.

Triangular -rectangular exchange:

- the hypothesis which supposes that the deflected flow is proportional to S_{sweep} remains applicable
- the exchange law will be identical to the triangular - triangular exchange law.

peripheral - peripheral sub-channel exchange:

- the helical wire imposes the direction of the deflected flowrate ($q_{\square\to\square}$),
- the mass transfer is determined by the location of the helical wire, the deflected flow is weak when the wire wrap is in the hexcan corner, and it is maximum at the opposite side of the hexcan corner.
- for the peripheral sub-channel located on the same face of the corner, the deflected flow is identical,
- the flowrate and the velocity is constant for each sub-channel of the same type : $q_j = \rho S U_j$,
- the deviated flowrate on a wire pitch is proportional to the axial flowrate ($q_{\square}$), and the sweept area (S_{sweep}) in the sub-channel.

3.2.2. Deviated flowrate for triangular sub-channels ($q_{\Delta\to\Delta}$).

From § 3.2.1. one writes : $q_{\Delta\to\Delta} = (a_{\Delta}.q_{\Delta}/S_{\Delta}).\sin(\theta + \pi/6)$ **(3.4)**

The deflected flowrate is evaluated for 60 degrees of wire movement. The integration of eq. (3.4) gives with eq. (3.2) and eq. (3.3) :

$$q_{\Delta\to\Delta}\ (\text{on } \pi/3) = (a_{\Delta}.q_{\Delta}/S_{\Delta}).\sqrt{3}/2 = (a_{\Delta}.q_{\Delta}/S_{\Delta}).S_{sin} = (S_{sweep}/S_{\Delta}).q_{\Delta} \quad \textbf{(3.5)}$$

S_{sweep} is calculated with : $S_{sweep} = (\pi/6).\{(D_{pin}/2 + D_{wire})^2 - (D_{pin}/2)^2\}$ **(3.6)**

D_{pin} and D_{wire} are respectively the pin and the wire diameters. a_Δ is deduced from eq. (3.5) and eq. (3.6). Experimental results show that one must remove the wire section to S_{sweep}. Then :

$$a_\Delta = (S_{sweep} - S_{wire}).q_\Delta / S_\Delta = 0.3023\ D_{wire}(2D_{pin} - D_{wire}) \quad \textbf{(3.7)}$$

The design code CADET uses an average deflected flow on a half pitch (h/2) of the helical wire. Then eq. (3.1) is integrated between $5\pi/6$ and $11\pi/6$, then :

$$q_{\Delta\to\Delta}\ (\text{on h/2}) = (a_\Delta.q_\Delta/S_\Delta).\int \sin(\theta + \pi/2)d\theta = 0.6046\ D_{wire}(2D_{pin} - D_{wire}).q_\Delta/S_\Delta \quad \textbf{(3.8)}$$

3.2.3. Deflected flow for peripheral sub-channels ($q_{\square\to\square}$).

From § 3.2.1. and the method used for the triangular sub-channels, one writes :

$$q_{\square\to\square} = K\,(S_{sweep}/S_\square).q_\square \quad \textbf{(3.9)}$$

S_{sweep} idem (3.6) is calculated for 120 degrees of wire movement with :

$$S_{sweep} = (3\pi/12).D_{wire}.\{D_{pin} + D_{wire}\} \quad \textbf{(3.10)}$$

The deviated flowrate is deduced from eq. (3.9) and eq. (3.10), then :

$$q_{\square\to\square} = K.(3\pi/12).D_{wire}.\{D_{pin} + D_{wire}\}q_\square/S_\square \quad \textbf{(3.11)}$$

3.3. Flow distribution in the bundle.

in a S/A with hexcan, the flowrate is : $Q_{S/A} = \sum_j Q_j$ **(3.12)**

The pressure loss is : $\Delta P_j = 0.5\ f\ (\Delta z/Dh_j)\ \rho\ U_j^2$ with $f = a\ R_e^{-b}$ **(3.13)**

where *j* index represents the current sub-channel. An isobaric hypothesis for each flow section of the S/A ($\Delta P_j = \Delta P$) allows us (with $U_j = Q_j / \rho S_j$) to calculate the flowrate in forced convection for a sub-channel *j* :

$$Q_j = (S_j\ Dh_j^\beta\ /\ \sum_j S_j\ Dh_j^\beta)\ Q_{S/A} \qquad \text{with } \beta = (1 + b)/(2 - b) \quad \textbf{(3.14)}$$

various experimental data show that the flow distribution in the S/A tends towards an iso-velocity distribution. This observation is introduced in the design code CADET with the following model :

$$Q_j = (\ S_j / \sum_j S_j\ )\ Q_{S/A} \quad \textbf{(3.15)}$$

3.4. The thermal balance.

3.4.1 Hypothesis.

- the thermal balance is made for each sub-channel j on a Δz axial mesh between z and Δz,
- for this Δz axial mesh, the flowrate is constant,
- the sinusoidal laws for the transverse exchanges between sub-channels are replaced by an average flowrate (q_j^{adj}) calculated with the above models,
- each sub-channel is coupled (transverse thermal coupling) with
  - one or several adjacent (*adj* index) sub-channels,
  - a thermal boundary condition (*out* index),
- the transverse thermal coupling between two sub-channels is modeled with an equivalent thermal diffusivity B_j^{adj},
- this thermal coupling is composed of three terms

B_j^{adj} thermal coupling due to the deflected flow (models in § 3.2),

$B_j^{adj} = q_j^{adj} C_p \Delta z$ ⇨ if *j* and *adj* are triangular sub-channels **(3.16.a)**

$B_j^{adj} = 0$ ⇨ if *j* and *adj* are peripheral sub-channels **(3.16.b)**
⇨ and *adj* precedes *j* in the direction of the wire rolling up

$B_j^{adj} = q_j^{adj} C_p \Delta z$ ⇨ if *j* and *adj* are peripheral sub-channels **(3.16.c)**
⇨ and *adj* follows *j* in the direction of the wire rolling up

This two last points allow us to simulate the global gyratory flow in the periphery of a bundle

B_j^{adj} thermal coupling by conduction in the coolant fluid (Fourier's law)

$$B_j^{adj} = \lambda / l_j^{adj} \; d_j^{adj} \; \Delta z \qquad (3.17)$$

B_j^{adj} thermal coupling due to the turbulent diffusion

$$B_j^{adj} = 9.0\,10^{-3} \rho C_p \nu R_e^{0.84} \; \Delta z \; l_j^{adj} / d_j^{adj} \qquad (3.18)$$

where d_j^{adj} is the neck width between the j and adj sub-channels and, l_j^{adj} the center of gravity distance

- the coolant fluid temperature is assumed as constant inside a sub-channel
- the temperature variation inside a mesh is linear. The mean temperature of this mesh will be

$$\theta_j = \{ T_j(z) + T_j(z + \Delta z) \} / 2 \qquad (3.19)$$

3.4.2. The thermal balance equation.

If P_j is the power dissipated in the sub-channel j inside a mesh of Δz height, the equation is written

$$q_j(z) C_p \{ T_j(z+\Delta z) + T_j(z) \} = P_j - \Sigma_{adj} B_j^{adj} \{ \theta_j - \theta_{adj} \} - B_j^{out} \{ \theta_j - \theta_{out} \} \qquad (3.20)$$

4. QUALIFICATION FOR STANDARD FUEL S/A SPX TYPE.

4.1. Introduction.

The equation of the thermal balance is programed in the design code CADET. The transversal exchanges needed by eq. (3.20) are those of § 3 and they have been adjusted on hydraulic water

experiments. In the same way, the friction coefficient laws coming from a bibliography have been compared for an SPX fuel S/A, to experimental data.

4.2. The deflected flow for the thermal couplings.

4.2.1. Triangular - triangular exchanges.

Experimental data show that D_{wire} must be replaced by d_j^{adj} in the analytical law (3.8) then

$$q_{\Delta\to\Delta} = q_{j\to adj} = C_1\ 0.6046.d_j^{adj}(2D_{pin} - d_j^{adj}).q_\Delta/S_\Delta \qquad \textbf{(4.1)}$$

(4.1) slightly modified, is also used for triangular ($\Delta = j$) - rectangular ($\square = adj$) sub-channel exchange

$$q_{\Delta\to\square} = q_{j\to adj} = C_2\ 0.6046.d_j^{adj}(2D_{pin} - d_j^{adj}).(q_j+q_{adj})/(S_j+q_{adj}) \qquad \textbf{(4.2)}$$

The adjustment of eq. (4.1) and (4.2) allow us to find the mean deviated flowrate measured on a half pitch of the helical wire. For fuel S/A SPX type, the retained mean value is 0.7 for C_1 and C_2.

4.2.2. Peripheral exchanges for the thermal couplings.

In (3.11), the ratio $q_\square/S_\square$ is replaced by a summ on all the sub-channels of the same bundle face. The new expression is also adjusted on experimental data to find the mean deflected flow measured on a half pitch of the helical wire. For a fuel of S/A SPX type, the best value is ~ 1 for C_3.

$$q_{\square\to\square} = q_{j\to adj} = C_3.\pi D_{wire}.\{D_{pin} + D_{wire}\}.(\Sigma_j\, q_{\square j} / \Sigma_j\, S_{\square j}) \qquad \textbf{(4.3)}$$

Nota bene : when the clad temperatures are computed, the variation of C_1, C_2 and C_3 around their mean values have a weak influence.

4.3. The friction coefficient laws.

Different experimental studies allowed us to calculate and qualify the pressure loss in the sub-channel (Cheng-Todreas, 1986 - Engel-Bishop, 1979 - Hoffmann & al, 1973 - Markley-Novendstern, 1980 - Pontier, 1968 - Rehme, 1973 - Zhukov-Ushakov, 1986).

4.3.1. Influence of the friction law for the flowrate distribution in the bundle.

For three different fuel S/A : SPX S/A (with 271 pins which dissipated power), first a heterogeneous S/A (with 397 pins) and a second heterogeneous S/A (with 469 pins), taken in the same constant temperature conditions (425 °C), with the same flowrate ($Q_{S/A}$ = 50 kg/s), the calculations were made with two friction laws (Pontier, 1968 and Cheng-Todreas, 1986 which differentiate each type of sub-channel).

The results show maximum differences on the axial velocity (V_l) of 1.3 % on V_Δ, 6.5 % on $V_\square$ and 17,8 % on V_{corner}. For the Cheng-Todreas law, the ratio : average velocity in peripheral sub-channels / average velocity in the bundle tends toward 1 as in the experimental data.

The consequences on the heating are directly inversely proportionnal to these velocities. The thermal couplings between the sub-channels, and the fact that the MCT is located in the triangular sub-channel zone greatly attenuate the impact of these differences.

The search of a differentiated pressure loss law by a sub-channel is not necessary.

4.3.2. Comparaison of the friction laws with the experiment.

Experimental measurements in water were made for an SPX fuel S/A. The results are presented below on Fig. 2.

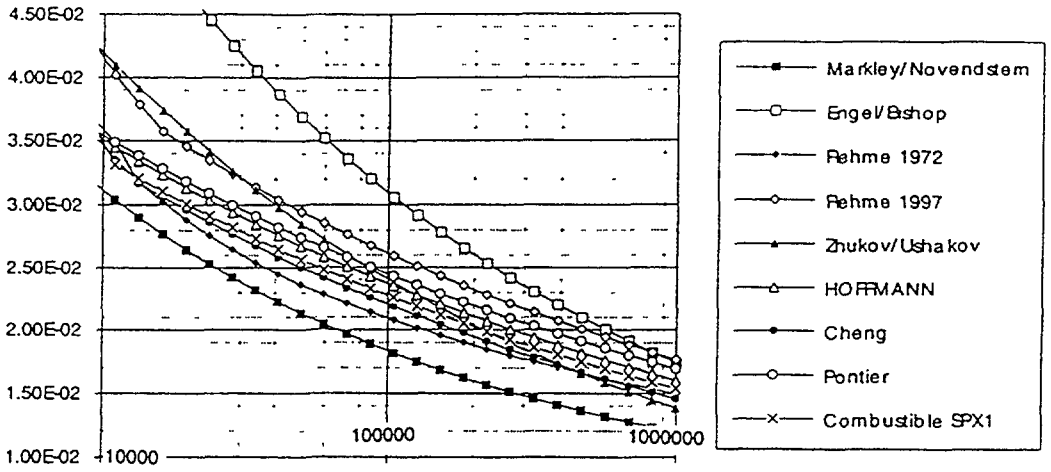

Fig 2 : Friction coefficients versus Reynolds number

The Rehme laws and the Cheng-Todreas law give the best results. But the latter has the advantage of being validated on a great number of experiments and on a greater scale.

5. QUALIFICATION FOR A NEW CONCEPT OF FUEL S/A.

5.1. Introduction.

A heterogeneous S/A (see § 4.3.1) will be taken as an example. The first concept which influences the hydraulic fields, is a ratio wire wrap spacer diameter / clad diameter greater than the SPX S/A one (see § 4.3.1). The second concept is the presence of one third of empty pins which could modify the thermal fields, but thermal and hydraulic fields are uncoupled (see § 1). The approach to this program, developed below, is comparative and will detail the differences between SPX and a heterogeneous fuel S/A which must be qualified. At that time, the experimental program will be defined.

5.2. Geometry and hydraulic fields.

Water tests are foreseen with the global and local hydraulic measurements detailed below.

• *Global measurements* : they will give the friction coefficient law, for various regimes, which will allow us to determine the bundle flow distribution in the design code CADET.

• *Local measurements* : of velocities, pressure in the inlet and oulet zones of the bundle will be completed with measurements in different peripheral sub-channels, at the same level on the six faces of the bundle and on a helical wire pitch of the same bundle face. These experimental data will be used to evaluate the mass transfers between the peripheral sub-channels and between the triangular and the peripheral sub-channels. These exchanges will be compared with the experiences performed for PHENIX and SPX S/A which were on few pin bundles (from 7 to 61 pins) experiments.

The FAIDE supporting experimental program conducted by CEA on a 7 to 37 pin bundle gives information on the velocities inside the triangular sub-channels. The experimental data will be compared with the results of the CADET code and a multidimensionnal analysis with the TRIO code (see § 1). The latter is qualitatively efficient for parametric studies. A heterogeneous fuel S/A will be computed with the TRIO code in order to ensure that no physical phenomena are forgetten and in particular, in the design code CADET.

5.3. Approach of a heterogeneous bundle.

Three effects are foreseeable in this bundle. The first is the presence of one third of empty pins. These could give high temperature heterogeneities in the sub-channel (for CADET, this tempetaure is constant). On the other hand, the helical wire increases the mixing of the coolant fluid but pertubs the clad/fluid heat transfer. These antagonistic effects will be evaluated by multidimensionnal computations. First, a triangular sub-channel without wire will be calculated alone and finely meshed. The computation will quantify the empty pin effect. Second, the helical wire wrap spacer will be introduced in the mesh, and the calculations will allow us to analyse the effects due to the increase of the wire diameter. The objective is to demonstrate the limited thermal effects for this new S/A concept.

6. CONCLUSION.

The introduction of a new concept of S/A, called heterogeneous S/A because they are composed of one third of empty pins, imposes the analysis of the modeling used in the design code CADET which computes the maximum clad temperatures (MCT). This MCT evaluation needs to take into account all the heat transfers in the bundle and in particular the transversal one due to the presence of an helical wire wrap spacer. The present models have been qualified on a typical fuel S/A and applied to RAPSODIE, PHENIX and SPX reactors. The new concept of S/A needs to be either completly validate or only verified . An approach, both experimental (dedicated past programs or future programs) and by computations is proposed. For the heterogeneous S/A presented above, the high level of turbulence, the high value of the thermal conductivity and the important mixing due to the helical spacer wire allow us to foresee possible limited consequences for the MCT.

GEOMETRICAL DATA

SPX fuel S/A:

D_{pin} = 8.5 mm.

D_{wire} : 1.2 mm.

P_{pin} : 9.8 mm.

h_{wire} : 180 mm.

First heterogeneous fuel S/A:

D_{pin} = 6.55 mm.
D_{wire} : 1.44 mm.
P_{pin} : 8.09 mm.
h_{wire} : 150 mm.

Second heterogeneous fuel S/A:

D_{pin} = 6.35 mm.
D_{wire} : 1.20 mm.
P_{pin} : 7.35 mm.
h_{wire} : 180 mm.

NOTATION

B_j^{adj} : Coupling coefficient between *j* and *adj* sub-channels.
B_j^{out} : Coupling coefficient between *j* sub-channels and the boundary condition.
d_j^{adj} : Neck width between *j* and *adj* sub-channels.
C_p : Specific heat of the coolant fluid.
D_{pin} : The pin diameter.
D_{wire} : The helical wire diameter.
D_{hj} : The hydraulic diameter of the current sub-channel.
h : The helical wire pitch.
l_j^{adj} : Centre of gravity distant between *j* and *adj* sub-channels.
MCT : Maximum Clad Temperature of the sub-assembly.
P_j : Dissipated power in a current sub-channel *j*.
P_{pin} : The net pin pitch.
$q_{S/A}$: S/A flowrate.
$q_{\Delta\rightarrow\Delta}$: Deflected flow between two triangular sub-channels.
$q_{\square\rightarrow\square}$: Deflected flow between two rectangular sub-channels.
S_{sweep} : sweeped area by the helical wire.
S_Δ : Section of a triangular sub-channel.
$S_\square$: Section of a rectangular sub-channel.
T_j : Temperature of a current sub-channel *j*.
U_Δ : Transverse velocity in a triangular sub-channel.
$U_\square$: Transverse velocity in a rectangular sub-channel.
V_Δ : Axial velocity in a triangular sub-channel.
$V_\square$: Axial velocity in a rectangular sub-channel.
V_b : Mean velocity in the bundle.
z : Level calculation.
ΔZ : A mesh height.
λ : Thermal conductivity of the coolant fluid.
θ : mean temperature of a ΔZ mesh height.
ρ : Density of the coolant fluid.

ACKNOWLEDGEMENTS

The author would like to thank the people who worked on the heterogeneous S/A program and notably Mr Collard and Mr L. Hoff.

REFERENCES

CHEN Y. B., TODREAS N.F., "velocity measurements in edge subchannel of uria wrapped LMFBR fuel sub-assemblies," US Atomic Energy Commision MIT 02 139 (1977)

CHENG S. K., TODREAS N.F., "hydrodynamic models and correlations for bare and wire-wrapped hexagonal rod bundles - bundle friction factors, sub-channel friction factors and mixing parameters," Nuclear engineering and design 92, 227-251 (1986)

ENGEL F. C., BISHOP A. A.,MARKLEY R.A.., "Laminar, transition and turbulent parallel flow pressure drop across wire-wrap-spacer rod bundle," Nuclear engineering and design 69, 290-296 (1979).

FENNECH H., BENNETT F.O., "axial static pressure variations in inner and side sub-channels of a 61-tube wire wrap bundle," Nuclear engineering and design 104, 83-92 (1987).

HOFFMANN M., BAUMGARTNER E., "communication to IAEA symposium in Bruxelle," IAEA SM 173/IV/-20 (1973).

LAFAY J., MENANT B., BARROIL J., "local pressure measurements and peripheral flow visualisation in water 19-rod bundle compared with FLICA II B calculations. Influence of helical wire-wrap spacer system," ASME publications - heat transfer conference San Francisco (1975).

LORENZ J. J., GINSBERG T., "experimental mixing studies in simulated wire-wrap fuel sub-assemblies," International reactor heat transfer conference Karlsruhe (1973).

MENANT B., VILLAND M., GRAND D., "detailed numerical studies of the thermohydraulics in the hot plenum of liquid metal fast breeder reactor," Proc. 6th NURETH", Grenoble (1994).

NOVENDSTERN E. H., "turbulent flow pressure drop model for fuel rod assemblies utilizing a helical wire-wrap spacer system," Nuclear engineering and design 22, 19-27 (1974).

PONTIER M., "pressure drop in a pin bundle," CEA report not published (1968).

REHME K., "pressure drop correlations for fuel element spacers," Nuclear technology 17, 15-23 (1973).

REHME K., "simple method of predicting friction factors of turbulent flow in non circular channel," Int. J. Heat Mass Transfer 16, 933-950 (1973).

ROIDT R. M., BARTHOLET T., HARPER L. J., "Experimental determination of interior subchannel crossflow and axial flow in a model of Clinch River breeder reactor fuel sub-assembly rod bundle with wire wrap spacer," Westhinghouse contract E(111) 2395 (1980).

ZHUKOV A. V., SOROKIN A.P., TITOV P.A. USHAKOV P.A., "analysis of a fast reactor's fuel-rod bundle flow resistances," Sov. At. Energy English transl. 60, 369-374 (1986).

THERMAL HYDRAULIC BEHAVIOR OF SUB-ASSEMBLY LOCAL BLOCKAGE IN CHINA EXPERIMENT FAST REACTOR

ZHIMIN YANG
China Institute of Atomic Energy,
Beijing, China

Abstract

The geometrical parameter ratio of pitch to diameter of China Experiment Fast Reactor (CEFR) subassembly is 1.167. To address the thermal hydraulic behavior of subassembly local blockage which may be caused by deformation of cladding due to severe swelling and thermal stresses and by space swirl loosening etc., the porous numerical model and SIMPLE-P code used to solve Navier-Stokes and energy equations in porous medium was developed, and the bundle experiment with 19 pins with 24 subchannels blocked in the sodium coolant was carried on in China Institute of Atomic Energy (CIAE). The comparison of code predictions against experiments (including non-blockage and ten blockage conditions) seems well. The thermal hydraulic behavior of fuel subassembly with 61 fuel pins blockage of CEFR is calculated with SIMPLE-P code. The results indicate that the maximum temperature is 815℃ when the blockage area is about 37% (54 central subchannels are blocked). In this case the cladding won't be damaged and no sodium coolant boiling takes place.

Keywords subassembly blockage thermal hydraulic behavior

1. Introduction

The local blockage of subassembly in a sodium cooling fast reactor can cause the temperature rise in the wake zone, thereby it may cause the sodium boiling and fuel rod burnout. It's necessary to study local blockage situation with experiments and theory to know of the effect of temperature behavior of local blockage, for safety analysis and subassembly design evaluation.

The following reasons may give rise to blockage: 1) deformation of cladding due to fuel swelling resulting in flow area reduction; 2) fragment of spacing grid or fragment of damaged fuel assemble in flow channel; 3) swirl spacing taking off or break; 4) corrosion product or impurity deposition in flow channel, etc..

The geometrical parameter pitch to diameter ratio P/D of CEFR lattice cell is 1.167 (the pitch P is 7mm and fuel rod diameter D is 6mm). This value is smaller, and it's needed to study this situation. So the experiment of 24 subchannels blockage in 19 pins were performed. The experiment aim is to estimate the phenomena of non-blockage and blockage and to serve for the development, improvement and assessment of computer codes. The qualified tool is necessary to make reliable predictions with respect to cooling conditions in local blockage. A two-dimensional code has been developed in CIAE (SIMPLE-P) which solves Navier-Stokes and energy equations in porous medium. The code is needed to compare with experiment for validity.

2. Description of test section

A scheme of test section is outlined in Fig.1. It consists of 19 parallel electrically heated pins (6mm outer diameter) which are arranged vertically in a triangular pitch (7mm) in hexagon and cooled by sodium flowing upwards. The geometrical parameter pitch to pin diameter ratio is equal to 1.167. A non heated pin zone (180mm), allowing hydraulic flow development, precedes the heated pin zone (400mm). At the beginning of the heated pin zone, there is a stainless steel plate (thickness 8mm) which forms 24 subchannels blockage (the ratio of blockage area to flow area is about 40.4%). The inlet temperature is from 250℃ to 400℃. The total electrical power is 500kW and the flow rate is from 4 m^3/h to 9 m^3/h.

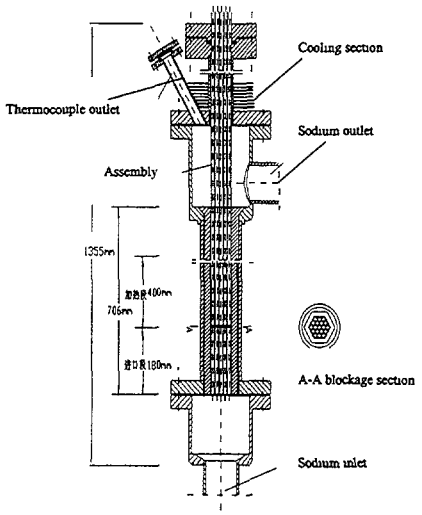

Fig.1 Experiment section of 19 pins with 24 blockage subchannels

The arrangement of thermocouples is in the wake zone (length 90mm behind blockage plate). Fig.2 is thermocouple arrangement. The bigger circle represents simulating assemble and the smaller circle represents swirl spacing thermocouples, the number beside the smaller circle is the axial measuring position from blockage plate. Measuring point is in the center of subchannels. The number in the center of subchannels is subchannels number. The subchannels No.1 to No.6 are regarded as the first ring subchannels (central subchannels), subchannels No.7, 10, 13, 16, 19 and 22 as the second ring, subchannels No.8, 9, 11, 12, 14, 15, 17, 18, 20, 21, 23, 24 as the third ring, the others as the fourth ring (circumference subchannels). The test conditions include of blockage and non-blockage.

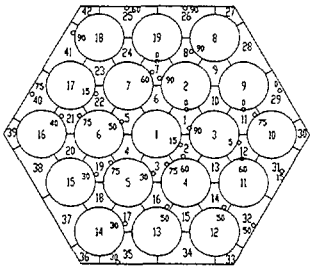

Fig 2 Thermocouple arrangement

3. Numerical model and SIMPLE-P code

The numerical calculation code SIMPLE-P was developed to analyze the flow pattern and temperature distribution in local blockage problem. SIMPLE-P code is a general thermal hydraulic code for 2-D, laminar and turbulent, steady state and transient problems. The selection of either rectangular Cartesian or cylindrical coordinates is provided. Conservation law of mass, momentum and energy in porous medium is solved in SIMPLE-P code.

Mass conservation equation

$$\frac{\partial \rho \varepsilon}{\partial t} + div(\Phi \rho \vec{U}) = 0$$

Momentum conservation equation

$$\frac{\partial(\varepsilon \rho U)}{\partial t} + div(\rho \Phi \vec{U} U) = div(\mu \Phi gradU) - \frac{\partial \Phi P}{\partial x} + \varepsilon R_x + \varepsilon F_x$$

Energy conservation equation

$$\frac{\partial(\varepsilon \rho T)}{\partial t} + div(\Phi \rho \vec{U} T) = div(\Phi \frac{k}{C_p} gradT) + \frac{G}{C_p}$$

where ε volume porosity

Φ surface permeability

G volumetric heat source W/m^3

R volumetric resistance N/m^3

For cladding temperature calculation, the following equation is used:

$$T^{o}_{clad} = T_c + \frac{q}{U_1 A_0}$$

$$T^{i}_{clad} = T_c + \frac{q}{U_2 A_0}$$

where Tc coolant temperature, ℃

q heat power, W

A_0 outer heat transfer area of cladding, m^2

$$U_1 = (\frac{1}{h_0})^{-1}$$

$$U_2 = (\frac{R_0 \ln(R_0/R_i)}{\hat{K}_c} + \frac{1}{h_0})^{-1}$$

$\hat{K}_c$ heat conductivity of cladding, $W/cm \cdot {}^{0}C$

R_i、Ro inner and outer radius of cladding, m

h_0 film coefficient of heat transfer, calculated by the following equation,

$$N_{N_u} = 4.0 + 0.33(P/D_F)^{3.8}(N_{P_e}/100)^{0.86} + 0.16(P/D_F)^{5.0}$$

The finite difference numerical technique and Patankar Simple method is used to solve the above equation.

4. Comparison of code prediction against experiment

From experiment the non-blockage and blockage data of temperature were obtained. The equivalent area method is used to change a hexagon to a circle. Then the cylindrical coordinate is used in SIMPLE-P code. The number of meshes is 99 in axial direction and 8 in radial direction.

4.1 Non-blockage comparison

For the following non-blockage experiment condition, the inlet temperature is 399.9℃, the flow rate is 8.15 m^3/h. The comparison of code prediction against experiment in central subchannels, second ring subchannels, third ring subchannels and circumference subchannels are shown in Fig.3 to Fig.6. Horizontal coordinate represents the axial position from blockage plate (m), vertical coordinate represent temperature value (℃).

From these figures it can be found that the maximum difference temperature between calculation value and experiment value is not more than 5.℃.

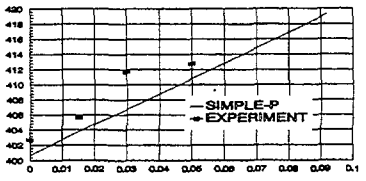

Fig.3 axial temperature distribution in the central subchannels

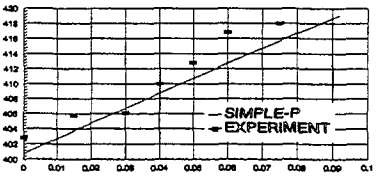

Fig.4 axial temperature distribution in the second ring subchannels

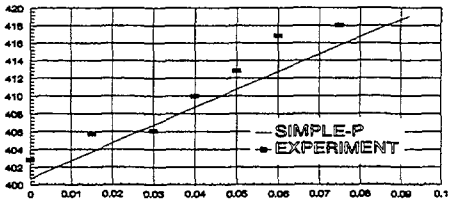

Fig.5 axial temperature distribution in the third ring subchannels

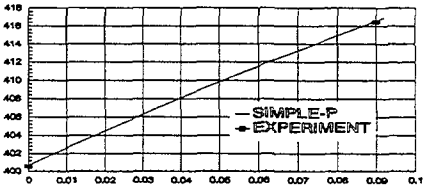

Fig.6 axial temperature distribution in the fourth ring subchannels

4.2 Blockage comparison

For the following blockage condition, inlet temperature 400.5℃, flow rate 8.06m³/h, heat power 171.91kW, the experiment results are showed in Fig.7. From the Fig.7 in non-blockage condition, we can see the temperature of every subchannel rises with the axial height increasing. The temperature of circumference subchannels rises little slowly than other subchannels, because volume porosity of the circumference subchannels is larger than the other subchannels and the volume heat power is less than the other subchannels. In the blockage condition, the highest sodium temperature is in the downstream zone of blockage plate. Temperature value drops with axial height increasing until x=75mm (from blockage plate), then the same as non-blockage value. This indicates there is a wake zone in the downstream of blockage plate. For the second ring subchannels, there is a highest temperature. It indicates that after this point the counter flow will mix with the cool sodium. For the other blockage condition,

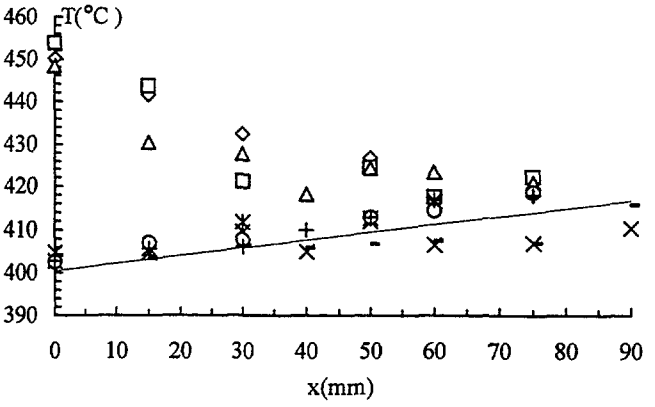

Fig.7 Experiment results (blockage and non-blockage condition)

◇Central (blockage) □ second ring (blockage) Δ third ring (blockage) × fourth ring (blockage)

✻ Central (non-blockage) O second ring (non-blockage) + third ring (non-blockage) – fourth ring (non-blockage)

the temperature distribution pattern is similar to above case since the blockage area is the same and the flow pattern is similar too.

Ten experiment blockage conditions have been calculated by SIMPLE-P code. Table 1 gives the maximum temperature comparison of experiment against calculation.

Table1 the maximum temperature comparison of experiment against calculation

No.	Inlet temperature ℃	Inlet flow rate (m^3/h)	Power (Kw)	Maximum temperature of experiment	Maximum temperature of calculation
1	400.5	8.12	151.22	442.92	443.99
2	400.5	8.06	171.91	453.67	450.32
3	400.5	8.11	132.21	437.62	438.70
4	399.9	8.07	115.37	432.36	433.20
5	400.5	8.12	77.88	423.60	422.33
6	249.8	9.03	153.71	285.71	286.27
7	250.4	6.98	155.64	297.66	296.75
8	249.8	5.98	156.1	306.14	304.08
9	249.8	5.05	155.81	319.07	312.7
10	250.7	3.98	156.58	344.53	326.78

For the condition No.1 and No.6, Fig.8 to Fig.15 is the temperature comparison between experiment and code predication.

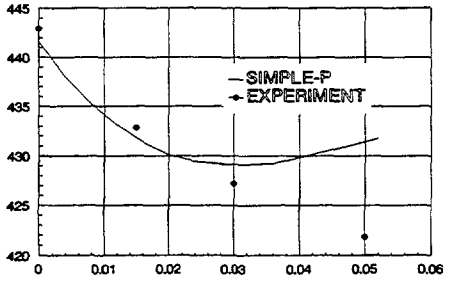

Fig.8 Condition No.1 central subchannels

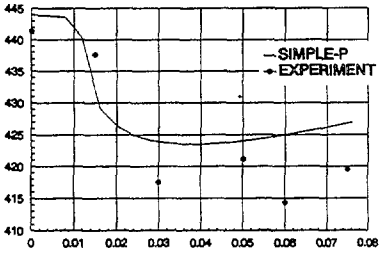

Fig.9 Condition No.1 second ring subchannels

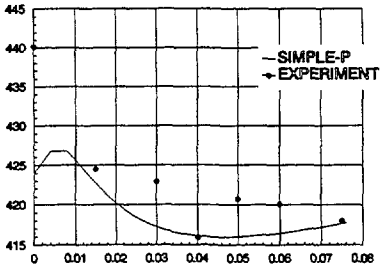

Fig.10 Condition No.1 third ring subchannels

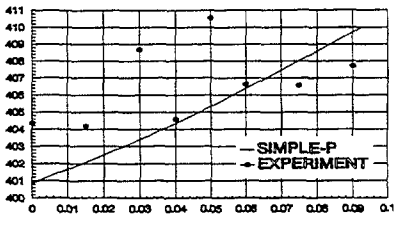

Fig.11 Condition No.1 fourth ring subchannels

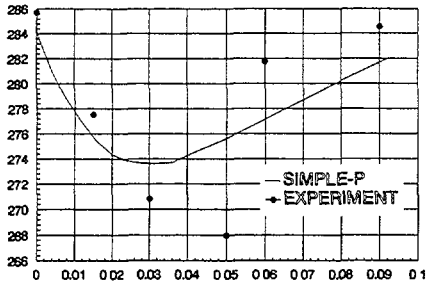

Fig 12 Condition No 6 central subchannels

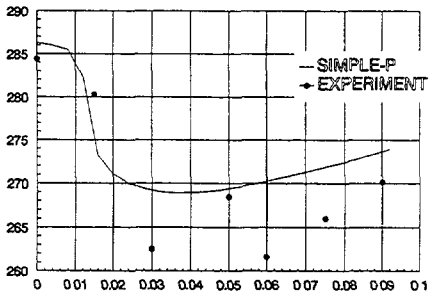

Fig 13 Condition No 6 second ring subchannels

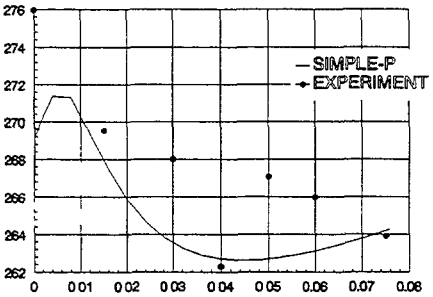

Fig 14 Condition No 6 third ring subchannels

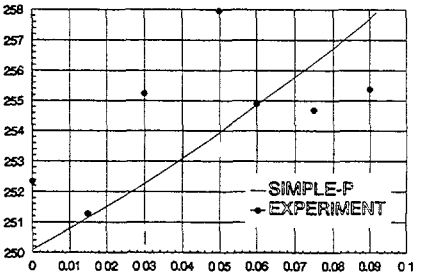

Fig 15 Condition No 6 fourth ring subchannels

Fig.16 is the sketch map of flow pattern from calculation in blockage condition. From this figure, we can see there is a wake zone in the downstream of blockage plate. This is agreeing with deduction from experiment.

The highest temperature maybe appears in point A or point B, or point C. Point A is a stagnate point where velocity is zero, the heat removing only depends on conduction. Point B is such a point where fluid continues being heated through counter flow and will mix with low temperature sodium, so point B is the highest temperature point. Point C is in the end of heating zone. In the downstream of blockage plate, the central fluid flow is less than normal situation because it is affected by blockage plate and can not recover to normal condition. For this reason the highest temperature may also appears at point C.

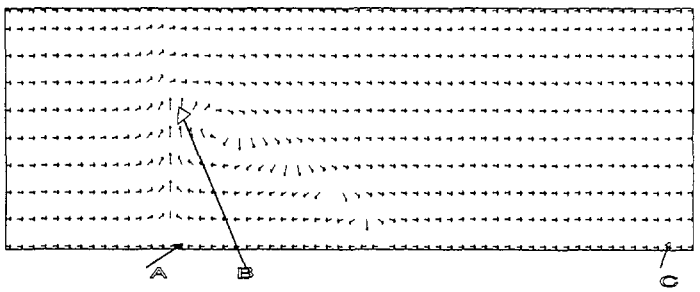

Fig 16 sketch map of flow pattern in blockage condition

From above comparison, the agreement between experiment and calculation seems well. Especially for the table 1, the calculation highest temperature is a little difference with experiment except condition No.10. The tendency of temperature distribution is agreeing in central

subchannels, second subchannels and circumference subchannels between code predication and experiment. There is a difference in third subchannels.

The cause of difference between computed and measured results is mainly attributed to following reasons: 1) very complex geometry, flow and heat transfer conditions; 2) two-dimensional model and cylindrical coordinate approximation; 3) not enough temperature measurement points; 4) measurement error in third ring subchannels caused by mixing of high and low temperature fluid; 5) resistance uncertainty in blockage; 6) non uniform power distribution in a subassembly; 7) porous model itself.

5. Thermal hydraulic behavior of CEFR blockage

The CEFR subassembly consists of 61 fuel rods in a hexagon. Inlet temperature is 360℃, inlet flow rate is 3.95kg/s and thermal power is 975 kW. The number of mesh is 78 in axial direction and 12 in radial direction for code prediction.

5.1 Flow rate reducing in blockage condition

When blockage takes place, it's assumed that the pressure difference between inlet and outlet does not change. The resistance increases because of the blockage. So the flow rate will reduce and flow rate reduction increases with blockage area increasing. Table 2 gives the calculation results.

Table 2 flow rate reducing with blockage area

Blockage area to total flow area	Flow rate reducing
3.85 % (6 central subchannels blockage)	0.2 %
15.4 % (24 central subchannels blockage)	1.4 %
34.71 % (54 central subchannels blockage)	6.6 %
47.6 %	15.1 %

5.2 The highest temperature results of calculation

The calculation results of 54 central subchannels blockage is given in this paper. Table 3 gives the highest temperature in difference height position. The calculation zone is in core (fuel section) from height position 250mm to height position 700mm (the core length is 450mm).

Table 3 highest temperature in difference height position

Height position	Highest temperature in blockage wake zone (temperature at same position in non-blockage condition)	The highest temperature in the full calculation zone in blockage condition
450 mm	719℃ (472℃)	815℃
500 mm	727℃ (500℃)	790℃
550 mm	726℃ (525℃)	760℃
600 mm	699℃ (547℃)	699℃
650 mm	642℃ (566℃)	642℃

The sketch map of flow pattern and temperature distribution is as Fig.17. From this figure, we can see the wake zone and highest temperature position.

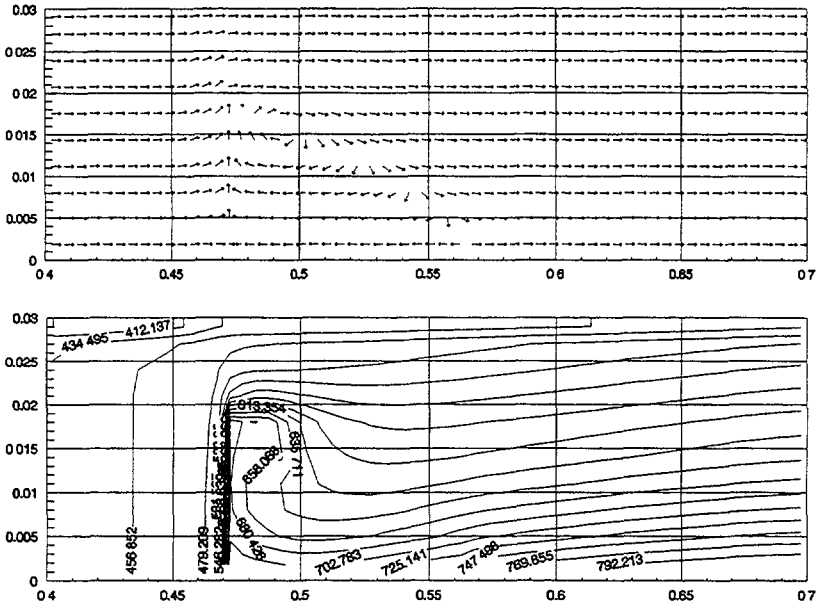

Fig.17 the sketch map of flow pattern and temperature distribution in blockage condition

6. Conclusion

The result agreement seems well through the comparison of SIMPLE-P code against experiment. The SIMPLE-P code which solve Navier-Stokes and energy equation in porous medium can be used for the calculation of blockage and other bundle pins condition.

Once a blockage of subassembly takes place in a sodium coolant fast reactor, the wake zone will be formed. In the downstream of blockage, the maximum temperature point maybe appears in three points. One is in the central subchannels behind the blockage, another is in the edge of blockage plate, and the third is in the end of heating zone. The maximum temperature's position depends on the value of blockage area.

The maximum temperature is 815℃ when the blockage area of CEFR is about 37% (54 central subchannels is blocked), the cladding cannot be damaged and no sodium coolant boiling occurs.

DESIGN APPROACH TO LOCAL BLOCKAGES

D.G. ROYCHOWDHURY, S. GOVINDARAJAN, S.C. CHETAL, S.B. BHOJE
Indira Ghandi Centre for Atomic Research,
Kalpakkam, India

Abstract

In LMFBR, whole core meltdown accident falls in residual risk category. Propagation of a local fault to whole core, however, needs attention.

Subassembly accidents are divided into two categories, Design Basis and Beyond Design Basis accidents. Design Basis is further classified into four categories. All events affecting fuel pin performance are identified and categorised. Total Instantaneous Blockage has been identified as the envelope of all local faults and categorised as BDB event and the safety objective is to demonstrate that no damage will propagate beyond six neighbouring SA. A core catcher has been provided for retention of core debris and cooling it by natural convection.

Local blockages may be active and passive. Active blockages can be detected by DND signal. For passive blockages, detection is difficult. Hence, development of a finite volume computer code based on the porous body formulation has been undertaken to define the maximum allowable defect. Experimental programmes have been undertaken to understand blockage mechanism, define maximum credible defect and the thermal-hydraulic behaviour of SA with local blockages. Also an experimental programme with a totally blocked SA with a bundle of heated pins has been undertaken to understand the behaviour of the SA.

1. INTRODUCTION

Fast reactor core is characterised by tight spacing of fuel pins, high power density and high burnup. This has led to a conceptual study on the blockage formation and its propagation. The whole core melt-down accident in fast reactor due to global causes have been made improbable due to high quality design, highly reliable and diversified safety systems, very good heat transport capability of liquid sodium under natural convection during Safety Grade Decay Heat Removal (SGDHR) and favourable inherent feed back mechanism. However, it is recognised that a local meltdown accident due to any fault in the subassembly (SA) level may propagate leading to whole core accident. Hence, understanding of local blockage phenomena is very much important for the operation of commercial fast reactors. Because of the presence of large number of pins, the probability of local blockage formation increases. Even if any local blockage is detected, it is preferable to operate the reactor until a scheduled shutdown to obtain high availability factor. Such operation with a local blockage is possible only if the consequences are small and known.

If a local fault reaches a critical size at a given coolant flow rate, it may cause local sodium boiling, dry-out and melting of pin cladding and fuel. The consequences could be either a non-energetic dispersion of the fault or accumulation of larger amount of molten material with the possibility of a fast coolant vaporisation, pressure generation and fast damage propagation to the whole fuel SA. The effect of the local faults on the reactor safety depends on several factors: size and thermo-physical properties of blockages, its location in the SA, fuel pin power and coolant velocity in the SA.

This paper discusses about the design approach to the local blockages for PFBR, 500 MWe, which is under design and focuses attention on the area for future studies.

2. SAFETY CLASSIFICATION

The main emphasis is here on the **accident prevention** rather than **accident containment**. Hence, it is prudent to optimise the safety provisions with regard to probable events rather than being concerned with hypothetical events. The SA accidents are divided into two major categories as follows:

- Design Basis (DB) accidents (frequency $>10^{-6}$ per year)
- Beyond Design Basis (BDB) accidents (frequency $< 10^{-6}$ per year).

The DB events are further classified into four categories.

A typical list of events considered to affect the fuel SA and classified into four categories is shown in fig. 1.

Design Basis Events

Category I	Power operation Shut down Start up Power changes
Category II	Reactor scram LOR Clad failure Inadvertent control rod withdrawal Argon bubbles Secondary circuit voiding Loss of off-site power
Category III	Seizure of primary sodium pump Fuel Sa drop during handling Station blackout
Category IV	Maximum credible blockage Rupture of the primary inlet pipe

Beyond Design Basis Accident

- Total instantaneous blockage of single SA at inlet
- Core voiding.

Main DBE for fuel design.

Fig. 1

From designer's point of view, it is necessary to define admissible damage levels in the fuel pin under different categories of event. These are

- No fuel pin failure up to design life time under category I and II;
- No loss of cladding integrity under category III for a single event;
- Clad failure is admissible under category IV events, however, coolable geometry of the SA should be retained.

While detailed structural analysis is required to check the cladding integrity under various categories of events, usually temperature limits are defined from thermo-hydraulics considerations. These design limits are shown below.

Table I – Design limits for Fuel Pin.

Event	Coolant	Clad midwall Temperature (K)	Fuel
Category I	No boiling	973	No melting
Category II	No boiling	1073	No melting
Category III	No boiling	1173	10% radial volume melting in maximum rated pin at active core mid-plane.
Category IV	No boiling	1473	50% radial volume melting in maximum rated pin at active core mid-plane.

Though it would be possible to show that coolant temperatures beyond boiling point may be admissible, it is prudent to keep the limit as the boiling point. This philosophy is strongly supported by the well-known DFR experiments in which even severe boiling conditions for extended periods did not induce fuel pin failure or caused only limited damage to the fuel pins[1].

3. DESIGN APPROACH

In the design approach, the availability of fault detection system and preventive action are assumed in limiting the consequences to the desired level. For the first two categories of events (I and II), it is necessary to consider all types of events including number of occurrences in the design lifetime and to show that the structural damage is within limits to ensure the integrity of fuel pins. For the latter two categories (III and IV), since design lifetime is not guaranteed, it is usually sufficient to consider the severest accident that is credible to demonstrate the design adequacy.

The strategy towards the local blockage is to divide the fault into two categories of accidents:

- Design Basis (DB) and
- Beyond Design Basis (BDB)

The DB strategy comprises of the following

a) Identification of initiating faults, their frequency and all their potential consequences;

b) Definition of Maximum Allowable Defect (MAD) limits taking into account protection systems;

c) Specification of Lines of Defence (LOD) to detect, mitigate and safely terminate the event;

d) Determination that the Maximum Credible Damage (MCD) that may occur;

e) Demonstration of MCD ≤ MAD, taking the LOD's and uncertainties into account.

If this goal (i.e. MCD ≤ MAD) is not achieved, design and/or protection system is to be improved.

Since, clad melting may lead to material relocation, the design MAD is chosen to be no clad melting. Wherever small margin exists between boiling and dry-out, this limits means no sodium boiling. This is required to maintain coolable geometry.

In principle, BDB strategy is similar to that of DB strategy. The safety objective is to demonstrate that with a MAD, no damage will propagate beyond six neighbouring subassemblies. This limit is drawn based on SCRABEE series of experiment [2].

4. MECHANISMS OF LOCAL BLOCKAGE

Any single SA incident that leads to the disturbance of the design power-to-flow rate ratio requires serious attention. Particular attention has been given for LMFBR safety analysis to cooling disturbances caused by local blockages within a fuel SA. The general aim of these studies is to

- Define the temperature profile behind the blockages as a function of flow, power, leakage flow through the blockage and inlet temperature,
- Establish the margin between the onset of boiling and onset of dry-out behind the blockages and characterise the types of boiling events,
- Collect the data for validating codes
- Pinpoint the limitation of the detection limits of blockages in relation to the measuring devices,
- Demonstrate whether the blocked SA can be cooled during power operation and by natural convection.

Local blockages may be initiated due to the following reasons:

a) Fuel loading error,

b) Failure of spacers,

c) Pin thermal deformation, pin swelling, bundle deformation,

d) Foreign materials left during construction, loose parts from structures, chemical products during operation,

e) Fragments from failed fuel.

Protection against SA plugging is provided at two levels, in design and safety action. The scenario with respect to protection against SA plugging is illustrated in fig. 2.

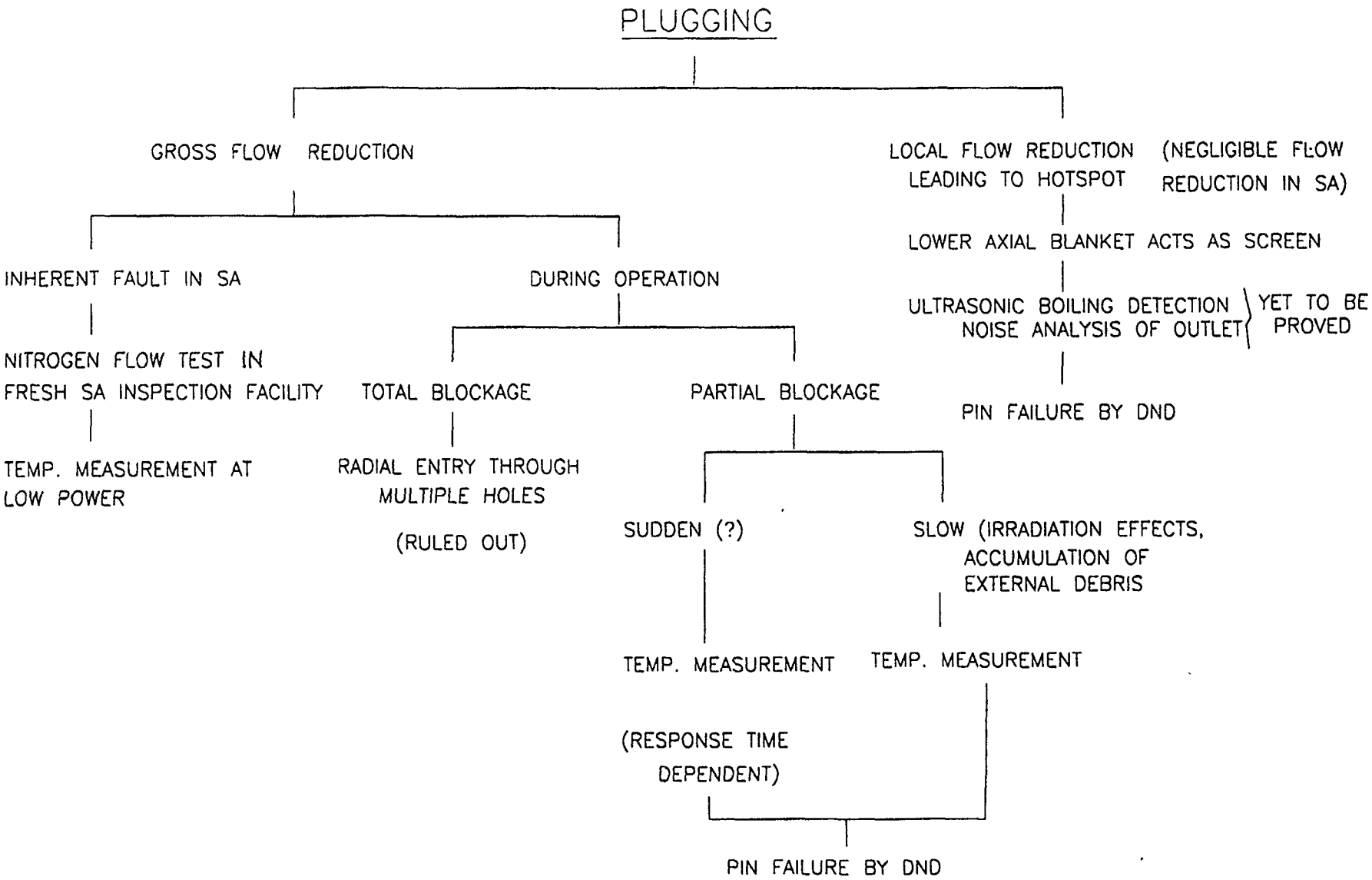

PROTECTION AGAINST SA PLUGGING

Fig-2

The mechanisms and history of blockage formation in a SA are only phenomenologically known. Pin deformation, transport of debris to the pin-bundle from the coolant circuit and getting lodged forming local blockage represent different mechanisms. This leads to different size, shape and physical property of the blockage. Even the geometry of the pin-bundle affects the nature of blockage formation. Experiments with pin-bundle having grid spacer indicate that the extension of blockages generated by trapped debris are generally small in axial direction, but can be spread over a large radial area. The critical size of particle for blockage formation is reported to be 0.9-1 mm, below which no blockage is expected. However, for wire-wrapped pin-bundle, such type of blockage is unlikely. A failed wire wrap or debris accumulation in a wire wrapped SA would lead to a long thin blockage. French study with ABACUS [3] programme reveals that the debris is essentially trapped at the bottom of the bundle. The debris concentration decreases from the bottom of the bundle due to the screening effect of the wire wrap. In no case more than one or two adjacent subchannels are expected to be blocked. Further growth is expected in the axial direction. Japanese [4] study in the formation of local blockage due to foreign materials revealed that the formation and growth of blockage strongly depends of particle diameter. The propagation of a subchannel blockage to the adjoining subchannels is practically impossible. Most of the blockages were observed at the inlet length, thereby indicating that blockage formation at the active core portion is unrealistic. The resulting blockage would be highly porous. For PFBR, the length of bottom plenum together with the bottom axial blanket is about 1 m. Hence, most of the external debris is expected to be deposited in this length. Since, there is no heat generation, the effect of the blockage formation in this portion will have little effect.

An analysis of available data reveals that in the case of cladding failure of one pin, the amount of material available is insufficient for global blockage formation. At the same time, a large blockage in the fast reactor can occur only as a result of fuel release from the pin failure. An oil ingress incident in the primary circuit has been reported in PFR and BN-600. The debris generated due to oil ingress then can be transported by sodium and gets lodged in SA causing partial blockage. Such an event has been reported in PFR [5].

A temperature drifting phenomena was observed in KNK-II[6]. The investigations had indicated large areas of depositions structured like rough plasters on the fuel rods. These deposits changed the resistance, which explains the temperature changes at the outlet of the fuel element.

As a whole, blockages can be classified as local covering a few channels or gross covering multi-channel region. Blockages can be active consisting of fuel debris, and non-active formed by foreign particles and will be highly porous resulting in high leakage flow. The inlet of the pin-bundle acts as the screen and most of the blockages due to external debris are formed at the inlet only. Blockage formation due to external debris in the active core region is unlikely and the same assumption is highly conservative. The rate of blockage growth would be very slow.

5. THERMO-HYDRAULIC BEHAVIOUR OF LOCAL BLOCKAGES

Both experimental, in-pile and out-of-pile and theoretical investigations has been carried out to understand the thermo-hydraulic behaviour of a SA with local blockages. Most of the earlier out-of-pile experiments were carried out with planar blockages covering several subchannels both central and edge. Because of the design of SA, such type of blockage formation is unrealistic. However, these experiments throw insight on the inadequacy of the measurement systems for the inactive blockages and thermo-hydraulic behaviour behind the

blockages. For a blockage covering 30% of the flow area, the flow reduction in the SA is ~1%, while the temperature rise across the blockage is ~310 K leading to sodium boiling[7]. Also, the smallest detectable blockage by temperature monitoring is 49% for edge blockage and 60% for the internal blockage.

The blockage mechanism experiments for external debris reveals that the blockage formation by particles always starts at high porosity corresponding to a high leakage flow. This leakage flow greatly influences the length of the reverse flow and hence, the temperature fields. Even a small leakage flow reduces a temperature rise of the coolant and that of fuel element behind the blockage. For example, for a leakage flow > 4%, the peak temperature decreases sharply reaching about half of its maximum value as the reverse flow disappears.

In-pile local blockage experiments, MOL 7C series, have been performed in BR2 reactor at SCK/Belgium[8]. The particular objective of these experiments was to investigate the consequences of local faults and the response of Delayed Neutron Detector (DND) to such fault. The burn up of fuel pins was one of the parameter of the test. The conclusions drawn from these experimental results are

In spite of the severe local damages the reminder of the bundle was still in a coolable state,

No energetic Molten Fuel Coolant Interaction (MFCI),

Clad failure before clad melting,

High earlier DND signals, far exceeding the usually trip level,

If a similar situation occurred in a reactor, automatic shutdown would have been initiated after a time delay of ~15 s due to transportation time of sodium from the core to DND.

Although the analysis of available experimental results has allowed to evaluate rough thermo-hydraulic characteristics of the blockages, additional systematic studies are required with porous and heat generating blockages. Also, there is little data available related to smaller blockages. Most of the data were obtained for blocked SA of smooth pins. However, the hydrodynamic characteristics of the blockage in the wake region will appreciably differ in the case of SA with wire-wrap due to higher lateral heat and momentum exchange.

6. TOTAL ONSTANTANEOUS BLOCKAGE (TIB)

TIB is defined as an instantaneous blockage at the inlet of fuel SA at nominal operating condition. TIB is considered as an envelope of all small blockages, which could evolve. The primary objective is to demonstrate that consequences of TIB does not cause melting to propagate beyond six immediate neighbouring SA. The SCRABEE[2,8] tests for fresh fuel indicate that

No significant fuel injection from the fissile zone and, consequently, automatic end of the accident by fuel dispersion is ruled out,
High heat transfer from boiling pool,
Rapid melt-through of the hexcan and symmetrical propagation,
No energetic MFCI, and
No systematic DND signal from blocked SA.

In any case, a delayed neutron signal can be assumed as soon as there is a penetration into the inter-assembly. This signal triggers the scram after a time delay of ~10-30 s. The main question is to know how far the melt propagates in this time and whether the resulting debris

can be successfully cooled at decay heat levels. With irradiated fuel, the important phenomena might be different.

A core catcher, an in-vessel core debris retention device, has been provided in PFBR for Post-Accident-Heat-Removal (PHAR) of the core debris resulting from BDB event of TIB of a single fuel SA by natural convection. It is designed to cover any fuel SA loaded up to in-vessel spent fuel storage location.

7. R&D ACTIVITIES IN IGCAR

7.1 Analytical

A 3-D computer code development for studying the thermo-hydraulic behaviour of fuel SA is under progress. A porous body formulation has been adopted in which rod bundles are represented by defining volume porosity, surface permeability, distributed resistance and heat source. A cell centred collocated finite volume method is formulated for non-orthogonal meshes. Equations are written in Cartesian co-ordinates and are discretised in physical plane. First order upwind and Quick scheme as a deferred correction to the first order upwind are used for the treatment of convective fluxes, while second order central differencing is employed for diffusive fluxes. In order to avoid decoupling between pressure and velocity a special interpolation technique is used when computing the mass fluxes at cell faces. The pressure correction equation is obtained by the SIMPLE algorithm. In order to accelerate the convergence rate, the preconditioned conjugate gradient square method is used in the solution of the algebraic equations. At present 2-D version of the code has been validated against benchmark problems and experimental results for laminar flows and natural convection studies. It, also, has been applied to complex geometries like flow over a single cylinder, across banks of staggered cylinders, eccentric cylinder placed in a cavity, natural convection studies in a porous medium. Once developed, the code will be used to define MAD in addition to find out thermo-hydraulic behaviour of fuel SA with non-nominal geometry.

For predicting the thermo-hydraulic behaviour of totally blocked SA at the inlet, another computer code is under development. This code takes into account the presence of neighbouring SA receiving full flow by the way of prescribing suitable convective boundary conditions. The code is based on porous medium approach. This finite volume code is formulated for orthogonal meshes. Staggered grid arrangement is employed to avoid decoupling between pressure and velocity. SIMPLE algorithm is used for obtaining pressure correction equation. The code will be validated against the experimental results.

7.2 Experimental

There is a need for obtaining a good insight into the SA behaviour under possible abnormal conditions. Towards this end following experimental programmes have been undertaken.

7.2.1 *Blockage mechanism studies,*

The objectives of these studies are

- general characterisation of the flow blockages in SA with helical spacer wire as a function of location, and properties of material of blockage;
- to study the size distribution of particles that induce blockage;
- to study the effect of the ratio of wire-wrap pitch to the wire diameter on the blockages;
- to study propagation/progression of blockages as a function of time; and
- to define MCD for PFBR SA.

Fig. 3 shows the experimental set up. The test will be conducted with i) 61 pin bundle with 5.1 mm pin diameter and 0.76 mm wire diameter and ii) 37 pin bundle with 6.6 mm pin diameter and 1.65 mm wire diameter. The pin bundle length is fixed at 600 mm. Demineralised water at 60°C will be circulated in the test loop form storage tank T1. The pump is rated at 7 kg/cm^2 discharge pressure with a maximum flow of 25 m^3/h. The test SA is supported in a sleeve mounted in tank T2 which also houses the debris injection system (fig. 4) to introduce particles of required size and material. The hexcan of the test section is made of transparent material for video-graphing the blockage formation and observing the flow distribution behind the blockage. A filter at the downstream of the test section is provided to prevent carry over of the injected debris to the other parts of the loop. Measurement would include pressure drop across the test section, flow rate, flow noise etc.

It is also planned to simulate the flow/freezing behaviour of molten fuel within SA with tin melted in situ and study relocation behaviour.

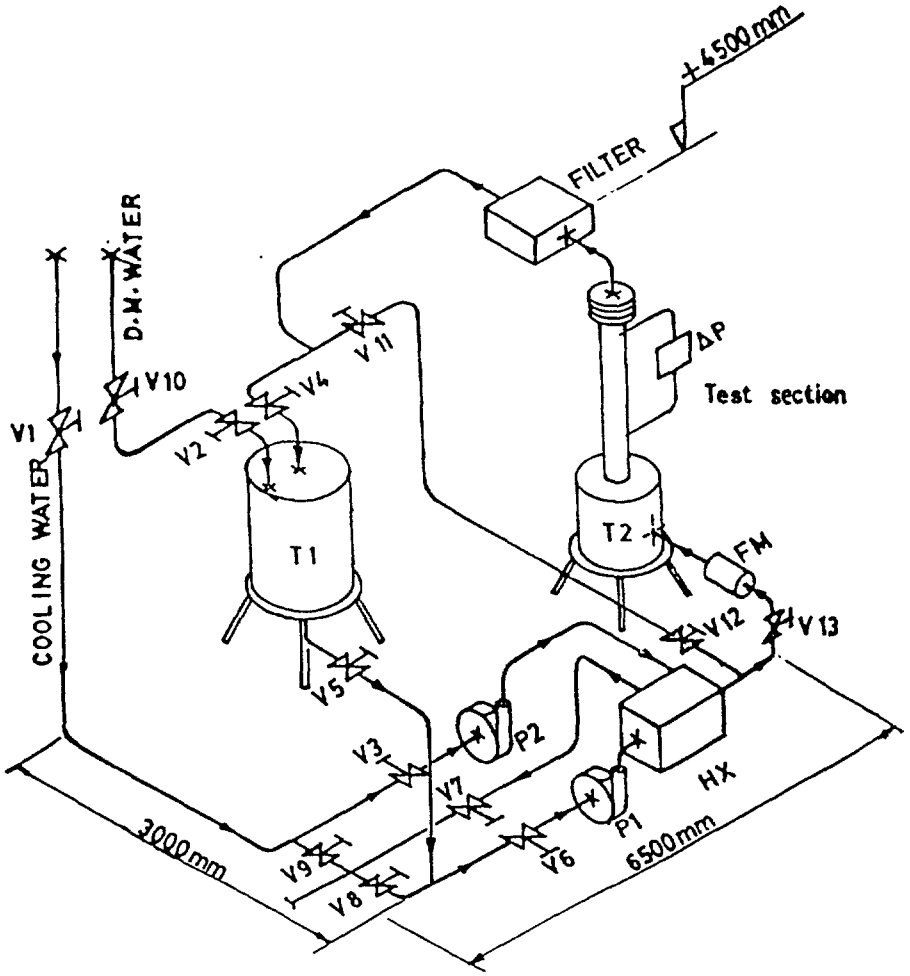

EXPERIMENTAL SETUP FOR FLOW BLOCKAGE STUDIES

Fig-3

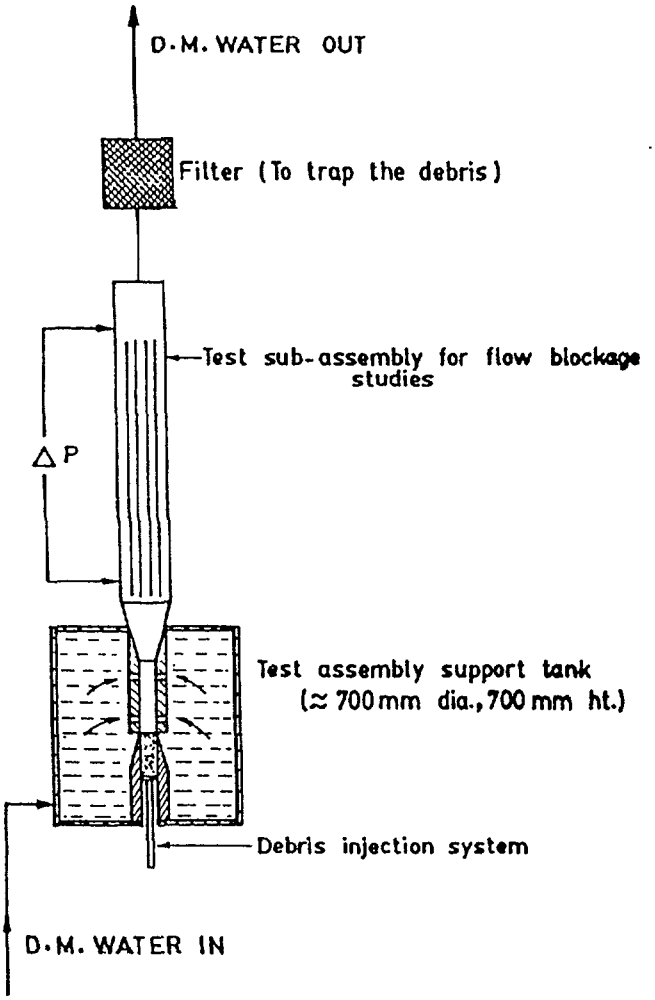

TEST SECTION FOR FLOW BLOCKAGE

Fig-4

7.2.2 Flow blockage studies.

Although the SA are checked for blockages in the Fresh SA Inspection Facility before loading into reactor, there is a finite chance that a blocked SA is loaded into the reactor. During low power operation, this can be detected by temperature monitoring. However, during start up of the reactor, the core temperature monitoring is initiated only above a certain power level to avoid spurious scram. It is necessary to ensure that the total blockage in a fresh SA, which is loaded in the refuelling campaign preceding start up, does not lead to melt down below the detection threshold. This requires data on the heat transfer from the blocked SA to its neighbouring SA.

Hence, an experimental programme with a totally blocked SA has been undertaken with the following objectives

- Assessment of steady state heat transfer from a blocked SA to the neighbouring SA taking into account natural convection inside the blocked SA;
- Establishment of the reactor power level beyond which the SA temperature monitoring is necessary;
- Evolution of transient temperature in the blocked SA in all details and the transient temperature distribution in the adjacent SA; and
- Validation of the computer codes.

Experiments will be conducted with both water and liquid sodium. In water experiment, detailed temperature v/s time history will be made under the following conditions:

- Water flow is blocked initially;
- The steady water flow in the SA stopped suddenly.

Water experiments will be carried out with local blockages also. In sodium experiment, sodium will be filled in the SA and sealed. Only the behaviour of the totally blocked SA will be studied.

Fig. 5 shows the experimental set-up proposed for the above experiments. The test section has a length of about 950 mm. The hexagonal tube with width-across-flats(inside) of 47.8 mm will contain either 19 heater pins of 8 mm diameter or 37 heater pins of 6 mm diameter.

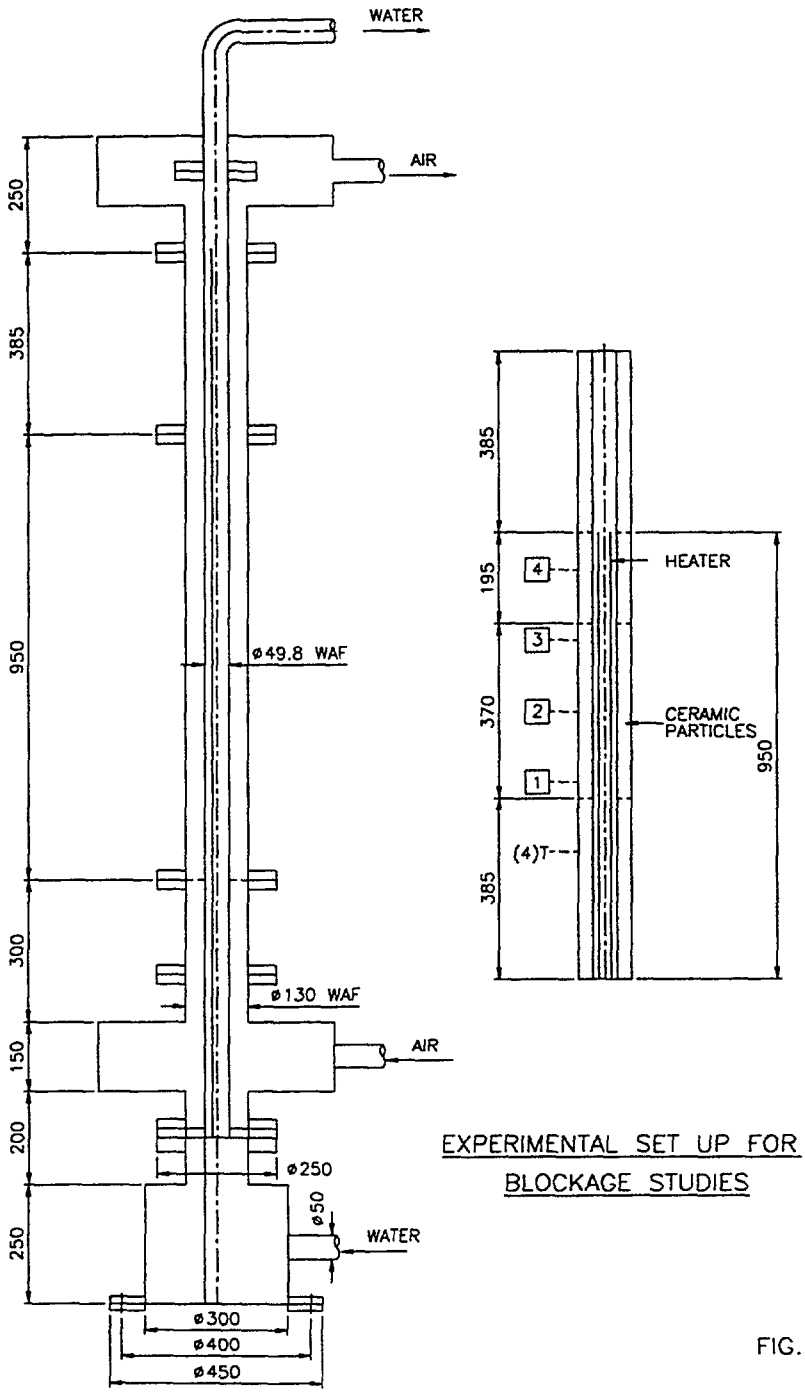

EXPERIMENTAL SET UP FOR BLOCKAGE STUDIES

FIG. 5

Thermocouples of 1.5 mm will be used as spacer wires. Heat removal by the liquid sodium flowing through the neighbouring SA will be simulated by blowing compressed air through packed bed with a maximum flow rate of 0.1 kg/s. For water experiment, the water flow rate through the test section will be 40 litres/min.

Measurement of temperature will be done at three levels in the test section. Other measurements would include upstream water and air flow, temperatures at both upstream and downstream and the pressure drop across packed bed.

8. CONCLUSION

A comprehensive design approach is followed in PFBR to mitigate the effects of local blockages.

Both analytical and experimental programmes has been under taken to address the problems concerning the blockages in the fuel SA and to understand and analyse the thermo-hydraulic behaviour of the SA under these condition.

REFERENCES

1. Smith D. C. G. et al, "DFR special experiments", IAEA-SM-225/49, Design, Constraction and Operating experience of Demonstration LMFBR's, Proc. of symposium, Bologna, 1978.
2. Moxon D. et al, SCARABEE An interpretation of pump trip and inlet blockage series, Int. Conf. Science & Technology of Fast Reactor Safety, Guernsey, 1986.
3. Fiorini G. L. et al, R & D supporting the IV category subassembly accident analysis in RNR 1500, Ibid.
4. Koyama K. et al, Study of local blockage in FBR fuel subassembly, Int. Conf. On Fast Reactor and Related Fuel Cycle, Kyoto, 1991.
5. Brear D. J. et al, An Analysis of the Events lead up to and during the oil ingress into primary circuit on 24-29 July 1991, AEA RS 5230.
6. Brockmann K. et al, Temperature drift at outlet temperature of the KNK II subassemblies, Int. Fast Reactor Safety Meeting, Snowbard, Utah, 1990.
7. Basmer P. et al, Experiments on local blockages, Mtg. Of Liquid Metal Boiling Working Group, Risley, 1975.
8. Morcan J. et al, Assessment of local melting in a typical Fast Breeder Reactor. Lessons from MOL 7C and SCARABEE experiments, Int. Conf. On Fast Reactor and Related Fuel Cycle, Kyoto, 1991.

NUMERICAL SIMULATION OF FUEL ASSEMBLY THERMOHYDRAULICS OF FAST REACTORS WITH THE PARTIAL BLOCKAGE OF CROSS SECTION UNDER THE COOLANT

A.V. ZHUKOV, A.P. SOROKIN
State Scientific Center of Russian Federation,
Institute of Physics and Power Engineering,
Obninsk, Kaluga Region, Russian Federation

Abstract

The problems of numerical modeling of thermohydraulics in assembly of fuel elements of fast reactors with the partial blockage of cross-section under the coolant are considered. The information about existing codes constructed on use of subchannel technique and model of porous body are presented. The results of calculation obtained by these codes are presented.

1. INTRODUCTION

The calculated researches of thermohydraulics of locked assemblies of rods, as three-dimensional flows with large perturbation of velocity fields, are based on two approaches: subchannel technique and model of a porous body. First from them is founded on a solution of the equations of impulse, mass and energy conservation in channels (cells) formed by adjacent fuel elements [1 - 5], second - on representation of a bundle of rods by an anisotropic porous medium with distributed on volume heat release (a quasi-homogeneous model) [6 - 10].

On the subchannel approach the following programs are based: COBRA-IIIC [11], THJ-3D [12], DECOS [13], UZU [14,15], ASFRE [16], SABRE [17], SABRENA-3D [26] etc.

The programs based on a model of a porous body are: THJNC-IV [18], COMMJX-1, COMMJX-2 [19], BACCHUS [20], TOODEE [21], UGRA, PROTVA [7,22], PORTER, TEMPER [23], THEHYCO-3DT [24], PHOENJCS [25] etc.

It is necessary to noted, that in most cases calculations of velocity and temperature fields in assembly with blockages, executed by these programs, had the purpose to debug a technique of calculation on an experimental material; however there are papers, for example [14, 15, 27 - 30], in which were investigated a structure and characteristics of velocity and temperature fields. In a number of works a quantitative agreement of results of calculation and experiment has a place , in other - only the qualitative agreement is observed.

A problem is set up below to analyze being available computational researches on thermohydraulics of locked assemblies of fuel elements to receive whenever possible integral picture in a problem of the computational approaches to study of thermohydraulics of fuel assembly with partial blockage of cross-section.

2. CALCULATIONS OF VELOCITY AND TEMPERATURE FIELDS IN LOCKED ASSEMBLY OF FUEL ELEMENTS, BASED ON THE SUBCHANNEL TECHNIQUE

The subchannel approach to calculation of velocity and temperature fields in locked assemblies of fuel elements is based on the solution of a set of equations of mass, momentum and energy balance, that allows to receive distribution of the flow rates and heating of the coolant on channels of considered assembly.

The existing programs of subchannel calculation differ by a degree of registration of various ways of interchannel exchange, various terms in equations of balances, formulation of boundary conditions, system of initial constants, and accordingly, by accuracy of the description of thermohydraulic characteristics of assemblies of fuel elements.

A special problem is the problem to formulate boundary conditions. With a set of balance equations usually set:

- Distribution of an enthalpy, longitudinal and transversal components of velocity, and also upstream pressure in assembly; or
- Distribution of transversal components of velocity at assembly inlet and pressure profile at assembly inlet and outlet.

The second version of boundary conditions formulation allows to take into account distribution of disturbances against a flow, that essentially increases accuracy of calculation in case of strong disturbances which have a place at assembly blockage. The type of boundary conditions determines the numerical scheme used for the solution of balance equations. The analysis conducted in [31, 32] testifies to necessity of further researches connected with boundary conditions.

The more in-depth and steep familiarity with a problem of the subchannel approach of calculation of fuel assembly thermohydraulics of reactors can be received from the paper [2].

Let's consider results of calculation of locked assemblies of rods obtained by the various authors at use of those or other programs of subchannel calculation, making some comments to the programs and analyzing results of calculation.

2.1. Program COBRA-IIIC

Results of calculation of velocity and pressure fields of the program COBRA-IIIC in assembly of smooth rods with local blockage [33] satisfactorily agree with experiment (fig. 1). As the authors [33] mark, the degree of agreement is largely determined by a correctness of values of resistance coefficients.

In the work [34] the good agreement of calculation results obtained by the same program and experimental data for assemblies with a degree of blockage 70 % and 90 % is reached at arrangement of blockade between stringers (fig.2). At the same time, as the authors [34] mark, the program COBRA-IIIC could not calculate velocities of the coolant in assembly at arrangement of blockade near the lattice, as unexpectedly there was a computational instability.

The initial constants for the program COBRA-IIIC are given in a table I.

2.2. About influence of selection of determining constants in the computational programs

Many authors (for example [35]) mark, that at calculation of locked assemblies of fuel elements not approximate but correct (in the full formulation) record of a balance equation for process of cross-sectional exchange by substation at approprINPE selection of determining constants is necessary. In particular, it is asserted by the authors of the paper [16], as the results, obtained by them, by the program ASFRE testify to strong relation of maximum temperature in assembly from selection of initial constants - resistance coefficients and characteristics of cross-sectional exchange. Last (especially resistance coefficients to a cross-sectional flow), under the judgment of the authors [16], to be determined with the special correctness.

The comparison of calculation results of Lin etc. [36, 37] with experimental data of Wantland [38] has revealed necessity of the correct taking into account the interchannel exchange stipulated wire wrapper on fuel elements. It is necessary to note, that the most full system of initial constants is the system offered in IPPE and published in papers [39 - 41] (generalizations of a system of constants see in [42, 43]). This system of constants with success is used in the programs of subchannel calculation of fuel elements assemblies.

The conducted in IPPE analysis [4] has shown equivalence of a system of balance equations recorded in subchannel representation, to a set of boundary layer equations. Non-

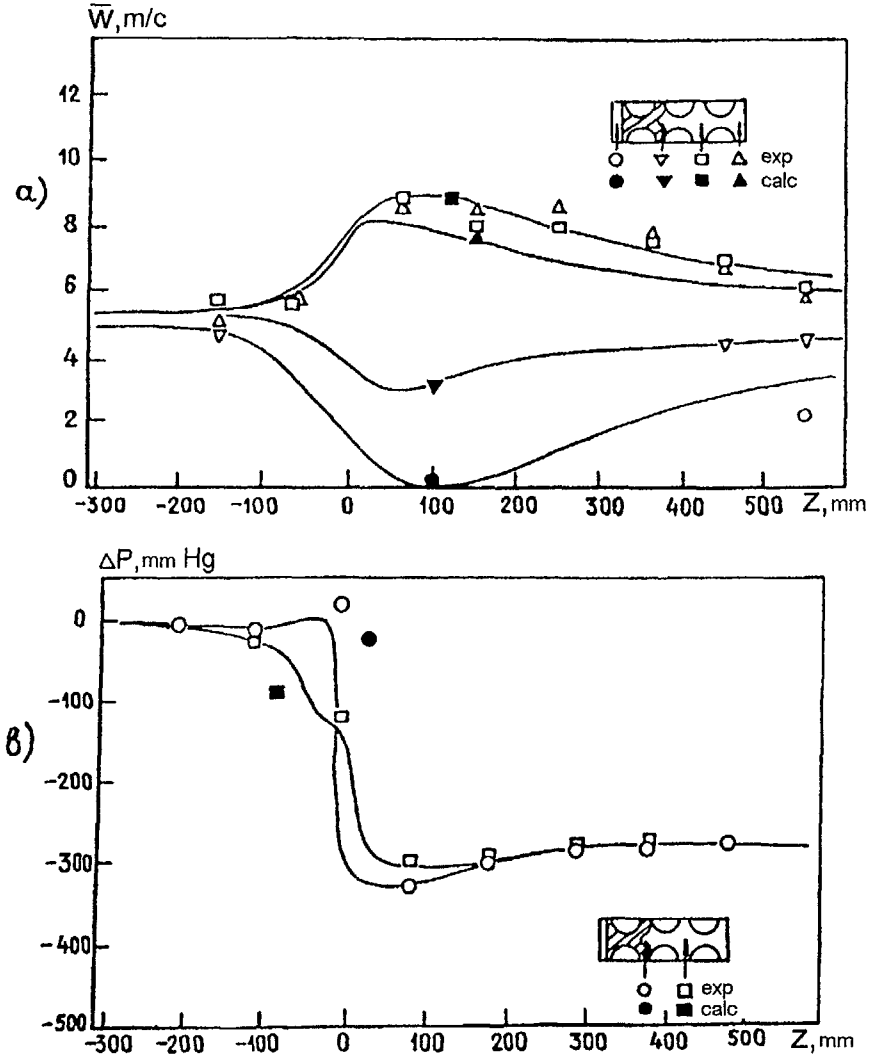

Fig. 1. Distribution of mean velocity of the coolant (a) and pressure drop (б) on length of channels in model assembly [33] (calculations by the COBRA-IIIC program).

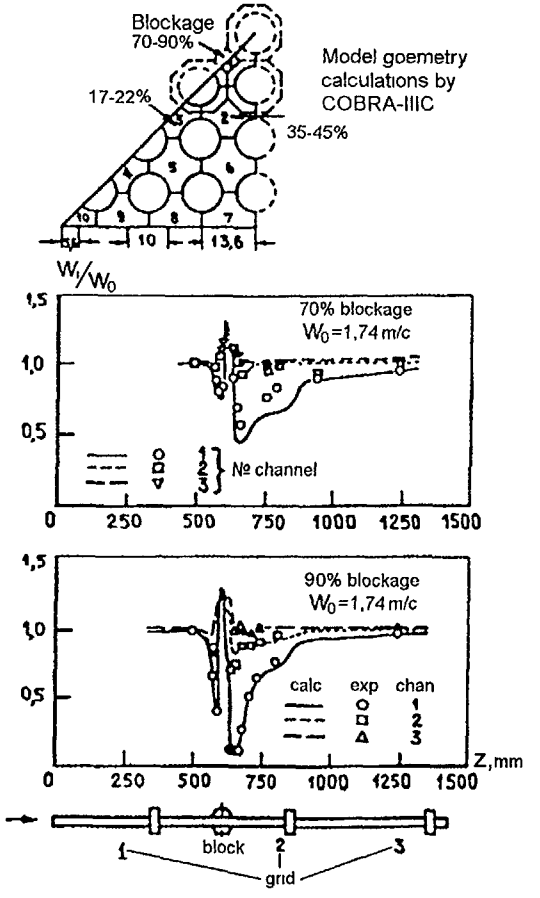

Fig. 2. Distribution of longitudinal component of velocity on length of channels № 1, 2, 3: ○, □, ▽, △ - experimental data; ——, ------, ····· -- calculation by the COBRA-IIIC program [34].

TABLE I. INPUT DATA FOR THE PROGRAM COBRA-IIIC USED IN THE PAPER [34]

№	Parameter	Labels in the program COBRA	Blockage degree 70%	Blockage degree 90%
1.	Resistance to a transversal flow	K_{ij}	0,02	0,02
2.	Momentum transfer	s/l	0,25	0,25
3.	Coefficient of turbulent momentum transfer	f_t	1,0	1,0
4.	Coefficient of friction for smooth rods	f	$0{,}34\,Pe^{-0,25}$	$0{,}34\,Pe^{-0,2}$
5.	Coefficient of loss on friction in an interchannel lattice	K_{S1}	1,14	1,14
6.	Coefficient of loss on friction in an interchannel blockage for channel 1	K_{S2}	0,5	0,5
	for channel 2		0,0	0,05
	for other channels		0,0	0,0
7.	Length of model, mm	z	1016	1016
8.	Evaluation of deviation, mm	Δz	12,7	12,7
9.	The whole time, s	τ	0,0	2,0
10.	Coefficient of turbulent transfer	β	0,02	0,02
11.	Temperature, ^{2}Ñ	t	30	30

accounting longitudinal molecular and turbulent transfer by a momentum and heat in balance equations stipulates approximate results of calculation obtained by the programs COBRA-IIIC, THJ-3D, ASFRE, SABRE, DECOS. The increase of calculation accuracy is promoted by taking into account of longitudinal diffusion of momentum and heat. The full kind of balance equations for this case is given in the paper [4]. In this case set of equations becomes similar to a set of Navier-Stokes equations correctly circumscribing flows with strong disturbances.

2.3. Program UZU

The attempt to take into account of effect of longitudinal diffusion is made in the UZU program [11, 15]. Besides in the UZU code in mass and momentum balance equations the thermal expansion of sodium is taken into account.

Boundary conditions used in the UZU code is the following:

- at assembly inlet the pressure profile uniform, cross-sectional velocity component is absent;
- at assembly outlet the velocity and temperature distribution is steady-state;
- on a vertical plane of symmetry normal gradients of pressure, of longitudinal velocity and of temperatures are equal to zero;
- on surface of blockage the tangent stresses are substituted by force of friction. The normal velocity components disappear in case of rigid blockage. In case of porous blockage the axial components on the lower and upper surfaces correspond to velocities of fluid leakage through blockage.

The cross-sectional turbulent diffusion of a momentum $\left(\varepsilon_m^c\right)$ is represented by a ratio:

$$\varepsilon_m^c = c_{ij} w_{ij} \beta_{ij} \tag{1}$$

where c_{ij} - distance center to center of adjacent channels; w_{ij} - mean velocity in two adjacent channels; β_{ij} - coefficient of turbulent transfer assigned to the ratio Rowe and Angle [43]:

$$\beta_{ij} = \xi_c \frac{d_{\Gamma ij}}{\Delta s_{ij}} \mathrm{Re}_{ij}^{-\theta_c} \tag{2}$$

Here $d_{\Gamma ij}$, Re_{ij} - mean hydraulic diameter and the Reynolds number for two adjacent channels; ξ_c and θ_c - constant defined from experience.

The axial turbulent diffusion of momentum $\left(\varepsilon_m^a\right)$ is expressed by a ratio, implying from the Prandtl theory

$$\varepsilon_m^a = l_m^2 \left|\frac{\partial u}{\partial z}\right| \tag{3}$$

where length of a path of mixing is according to Nikuradze

$$\frac{l_m}{r} = 0{,}14 - 0{,}08\left(1 - \frac{y}{r}\right)^2 - 0{,}06\left(1 - \frac{y}{r}\right)^4 \tag{4}$$

From (4) it is possible to receive (average on the area), that

$$l_m = 0{,}04 L_m \tag{5}$$

The value L_m varies in an interval from d_Γ up to D_B (diameter of blockage). The resistance coefficient for longitudinal current is determined according to a Blasius ratio for round pipes. The resistance coefficient for cross-sectional flow $\left(f_c\right)$ is injected from a ratio Fishenden and Saunders (is quoted in [15]) for bundles of rods and has a kind:

$$f_c = \xi_c \left(\frac{l_p}{d} - \xi_c'\right) \mathrm{Re}_c^{-\theta_c} \tag{6}$$

where Re_c - local Reynolds number calculated from velocity of cross-sectional flow and diameter of a rod d; l_p - distance center to center of adjacent rods. The constants ξ_c, ξ_c' and θ_c are determined from an experimental data.

From paper [14, 15] it is visible that the results of calculations depend on size of assigned parameters:

- The increase of coefficients of intermixing results in more fast equalization of a velocity profile and decreasing of length of recirculating zone;
- The increase of a coefficient of axial diffusion also reduces length of recirculating zone.

A special problem is the analysis of calculation results of natural convection in locked assembly of rods. This problem is connected to a difference of temperatures between central and circumferential zones of assembly and taking into account the thermal sodium extension with temperature. It looks as follows by results of calculation of the author [14, 15].

At taking into account of the thermal extension of sodium it is visible (ðèñ.3, à), that at small distances z behind blockade (smaller, than 192 mm) sodium is accelerated in a central zone (where temperature higher) and is decelerated in a circumferential zone (where temperature lower).

The arising lift immedINPEly behind blockage ($z = 7{,}5$ mm - fig. 3, á) reduces intensity of recirculation, and peak of temperature becomes higher, than if the thermal extension of sodium is not taken into account. However at distances removed from blockage

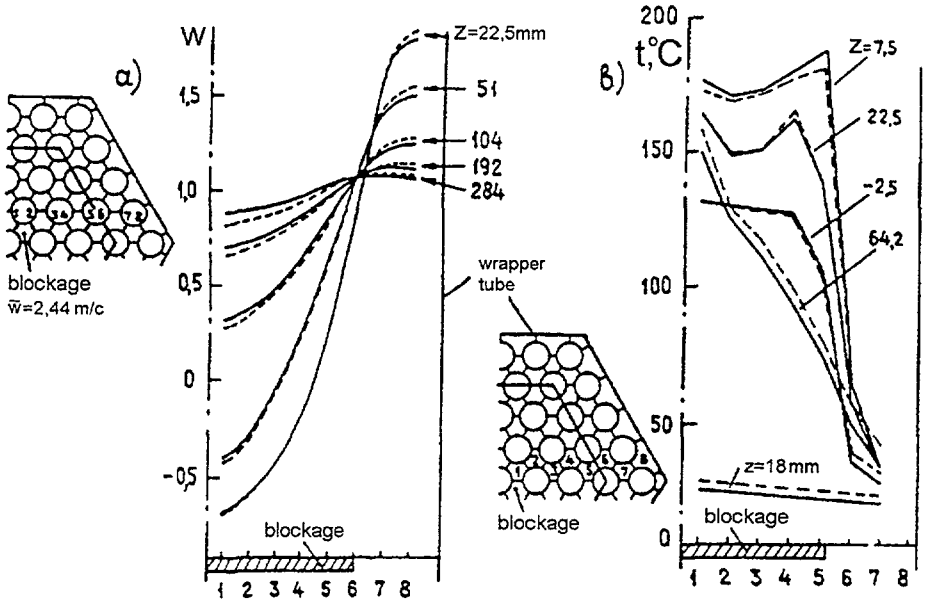

Fig. 3, а, б. Computational (UZU program [14, 15]) profiles of velocities (а) and temperature (б) of the coolant in a number of cross sections behind central blockage of assembly of fuel elements : —— - with allowance for dependence of density of the coolant from temperature, - - - - - for a constant density of the coolant [14, 15].

(z = 64,2 mm), as well as on segments before blockage (z = −18 mm), temperature becomes lower, than if the thermal extension of sodium is not taken into account, as main weight of a flow is accelerated.

In the total it is possible to conclude: the neglect in calculations by the thermal extension of sodium results in underestimation of peak of temperature in sodium and overestimate of sodium temperature at outlet) (far from blockage).

It is necessary to note., that the influence of natural convection is characterized by a Richardson criterion, which is determined as a measure of the ratio of gravity to force of inertia:

$$Ri = \frac{g\beta\left(T_{\max} - T_m\right)L}{\overline{w}^2} \qquad (7)$$

where $\overline{w}$ - mean-mixing flow velocity of the coolant; $T_{\max}$ - maximum temperature in a flow behind blockage; T_m - mean temperature in cross-section, where is maximum temperature (in a flow behind blockage); L - length of energy release behind blockage; β - thermal expansion coefficient of sodium; g - acceleration of gravity.

The calculations of Miyaguchi [15] were conducted for value of parameter $Ri = 1{,}27{*}10^{-2}$.

Let's consider the calculations of Miyaguchi, executed by the program UZU for case, when the central blockage (38 %) placed immedINPEly on the lattice, that for practice is quite probably [15].

It was shown, that in this case temperatures in sections $z/D_б$ = 0,64 and 9,49 are higher, than for blockage without lattices (fig.4, а).

Distributions of temperature on altitude of assembly in channels [1] 1,2,3,4 is characterized by peaks on the lattice with small displacement on a course of a flow (ðèñ.4, á).

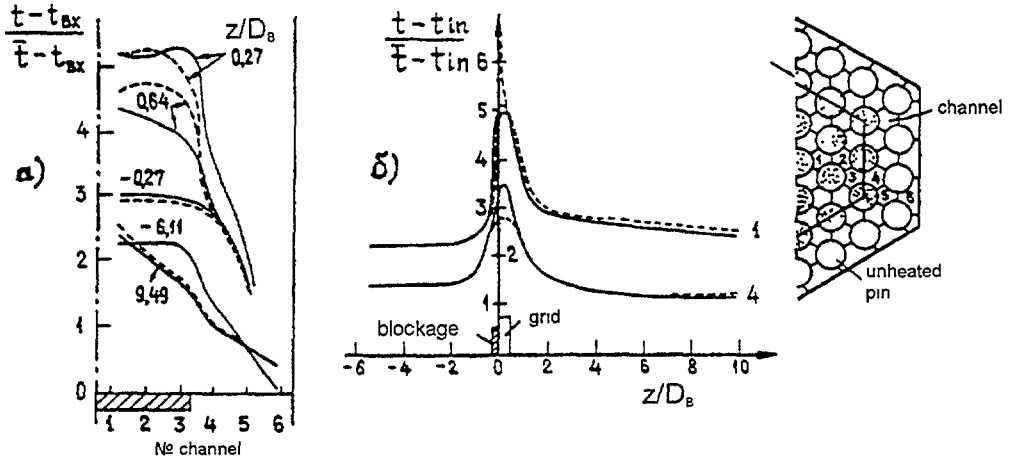

Fig. 4, а, б. Computational (UZU program [14, 15]) distribution of temperature in cross sections (а) and on length of channels № 1 and 4 (б) in assembly with 38 % central blockage: ——- without of a lattice; - - - - with a lattice.

The maximum temperatures take place in a channel ¹ 1, and the peak of temperature appears much above, than for blockade without a lattice.

Other results of calculations of the hydrodynamic and thermal characteristics (velocities, pressure, temperature), obtained by the program UZU, are shown in a fig. 5, à, á, â in a comparison with experimental data (the versions of blockage are shown on ðèñ.5, ã) [44]. It is necessary to note a whole satisfactory agreement of calculation results and experiment. The maximum deviation is no more of 10 %, can be explained by some imperfection of a computational model and accuracy of experiments. Besides the calculations are made for nominal geometry, and actually geometry of assembly can differ from nominal.

The deviation for a channel ¹ 1 between the computational and measured data (in a position Â - fig.5, â) the authors [44] explain much more actual leakage behind blockage, than it is supposed in calculations.

2.4. Thermohydraulic calculations of two-phase flows

The analysis of thermohydraulic processes in assembly of fuel elements at two-phase flow (boiling, availability of gas in the coolant), spent with the help of codes based on a subchannel technique represents the large interest. So the authors [26] have analyzed with the help of the SABENA-3D code sodium boiling in model assembly with blockage, and the authors [45] have considered process of an accumulation of gases behind blockage by the SABRE code.

Before to proceed to the analysis of these works it is expedient to illustrate, according to being available representations, general scheme of most important thermohydraulic appearances in a track behind the central blockage (ðèñ.6), and also processes of formation of a liquid (drainage) film and flow of vapor behind blockage in region of fuel element (in case of boiling of the coolant) - fig. 7. It will be useful for understanding a number of positions of papers [26, 45].

The black arrows on fig. 7 submit fluid, the white arrows - vapor or two-phase flow. The area of interface (especially in a zone À) is not constant, and is subject to random changes; in a zone Â a flow "comes across" to a surface of fuel element, partially merges with a main flow (impact current), and partially is directed in liquid (drainage) film and to reversible flow in a track.

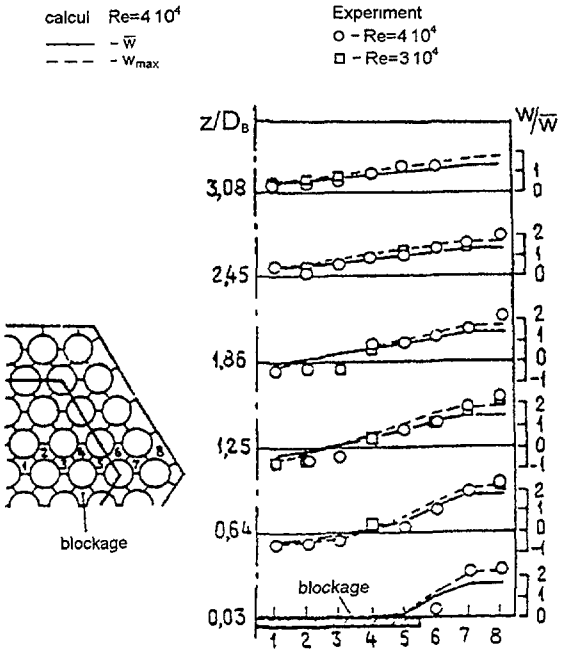

Fig. 5, a. A comparison of computational (by the program UZU) and of experimentally found profiles of velocity in cross-sections of model assembly with central 38 % blockage of cross-section [14, 15]

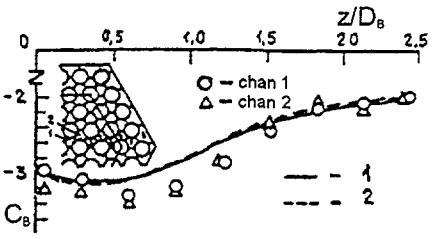

Fig. 5, б. A comparison of computational (by the program UZU) and of experimentally found distributions of pressure on length of channels № 1 and 2 [14] in assembly of rods with central 38 % blockage located on a lattice.

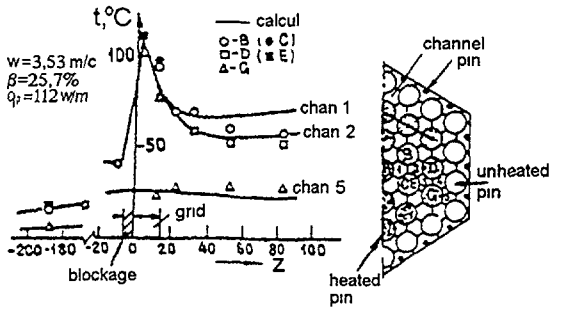

Fig. 5, с. A comparison of the computational and of experimentally found distributions of temperature on length of channels № 1, 2, 5 in 37-rods model assembly with 38 % central blockage located on a lattice: —— - calculation under the UZU program; □, o, Δ - experimental data.

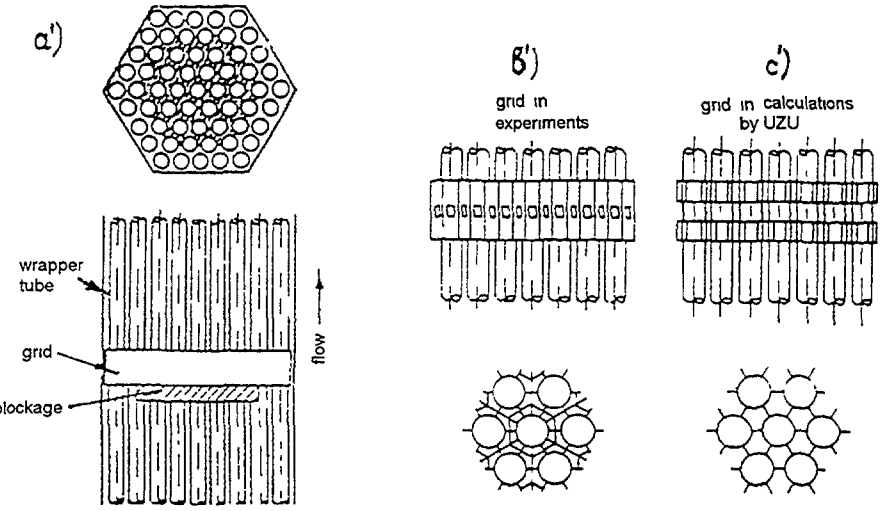

Fig. 5, г. A diagrammatic representation of assembly of fuel elements with central blockage before a lattice (а') and various kinds of lattices (б', в')

2.4.1. Calculations of sodium boiling in locked fuel assemblies by the SABENA code

In the paper [26] the analysis of processes of sodium boiling with reference to two experiments conducted with locked assembly of fuel elements is carried out. The first experiment (37WEB-143) concerns to model with partial (50 %) blockage consisting of 37 elements (the purpose of the analysis was to underline importance of processes of oscillations arising at steady-state boiling, and to consider process of transition to crisis of heat transfer); the second experiment is conducted on model consisting from 23 fuel elements at full blockage of cross-section, according to the international program SCARABEE (France), - experiment SCARABEE PI-A with researches of process of destruction of fuel elements clads and behavior of melted materials in conditions of formation of cracks both in fuel elements clads and in a cover of assembly (the important information on a problem of crisis of the first kind and destruction of fuel elements, connected with him, was obtained. It was the purpose of the analysis by the computational program SABENA-3D, constructed on two-liquid technique of calculation).

The description of the SABENA-3D program and results of calculation

The existence of cooled sodium around boiling area results in processes of evaporation and condensation representing key moments of an appearance (they result in instability in calculations also because of large gradients of temperature across the boundary between turbulent area behind blockage and area of main flow - fig. 6, 7).

In the SABENA-3D program, as in the rather universal program of the analysis of many problems connected to sodium boiling in parallel channels of fuel assembly, velocity of vapor condensation is calculated under the formula obtained because from the kinetic theory:

$$\Gamma_c = \lambda_c A_l \left(\frac{M}{2\pi R}\right)^{0,5} \left(\frac{P_{sat}}{\sqrt{T_f}} - \frac{P}{\sqrt{T_g}}\right), \tag{8}$$

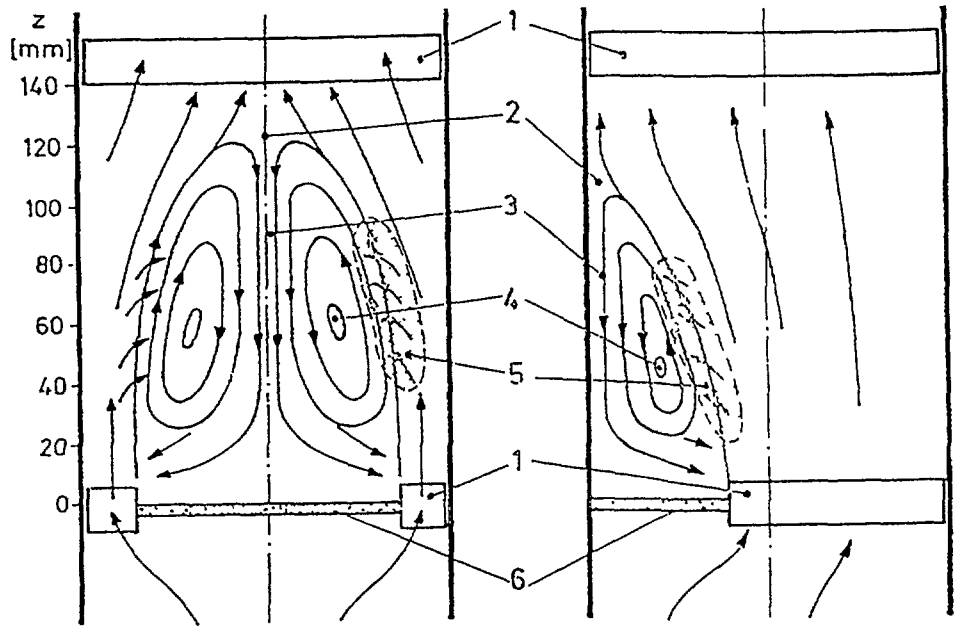

Fig. 6. A typical flow pattern behind of central and angular blockage.

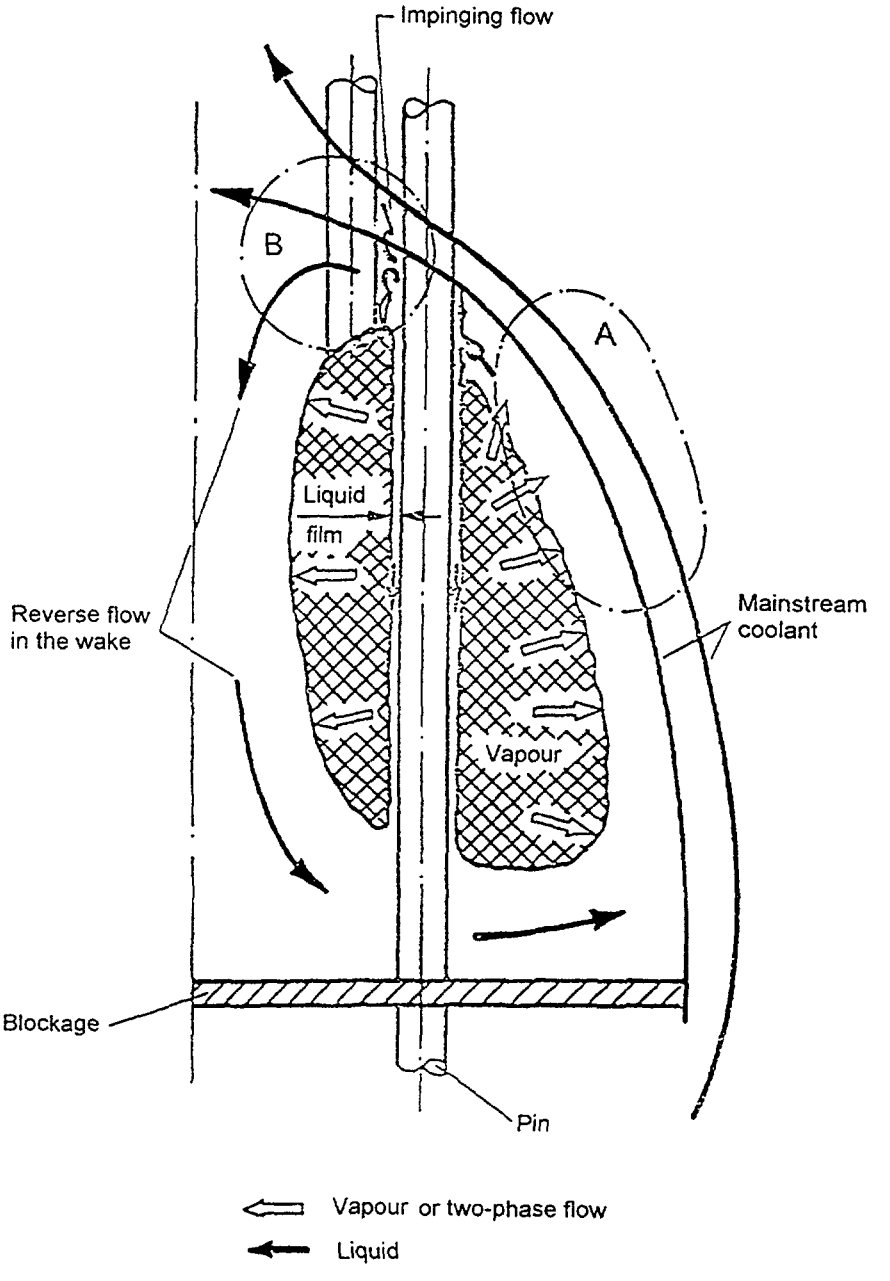

Fig. 7. The illustrating scheme of formation of a liquid drainage film and a vapour flow in assembly with blockage

where λ_c - coefficient of condensation; A_l - area of surface of single volume; M - molecular mass of sodium; R - gas constant; P_{sat} - pressure of saturation; P, T_f - pressure and temperature of fluid; T_g - temperature of vapor.

For calculation of boiling processes behind blockage it was necessary to have a rather small time step to avoid of excessive vapor condensation in area with large gradients of temperature.

The 37WEB-143 experiment was analyzed by the SABENA-3D program from a beginning of boiling before transition to crisis of heat transfer at the constant sodium flow rate through assembly and constant temperature at inlet.

Length of analyzable area was divided into 73 segments, near to blockage the interval of a partition was $0{,}005 \leq \Delta z \leq 0{,}04$ mm. Total of computational elements was $73 \times 44 = 3212$; the symmetry of assembly with respect to 180^0 was taken into account.

The results of calculations have shown, that in a condition before crisis the steady-state oscillations, characteristic for bubble boiling take place, and the process of propagation of boiling with consequent transition to crisis is accompanied significant in time leakage of vapor from area of local boiling to area of adjacent channels (fig.8, a): if at τ=9,63 s (q=138,2 W/cm^2) the area of boiling is small and is localized, then after 12 seconds (q=139,7 W/cm^2) sudden increase of vapor volume happens (fig. 8, á), the area of boiling extends, being spreaded on a turbulent zone after blockage; there is a mode of dehumidifying (fig.8, â), "pure" recirculating flow is upset (because of a great many of vapor; the oscillations is increased sharply, exceeding steady-state oscillations; the transition to crisis happens which is spreaded up to hexagonal cover; the mode of flow of a liquid phase is transformed (fig.8, ã).

The tendency, detected in calculation, of propagation of boiling and transition to crisis in general has agreement with experiment. Also, in general, results of calculations of process of oscillation of the flow rate at assembly outlet have agreement with experiment also: in calculation the oscillatory process began from τ=1,75 s, reached a maximum at τ=2,75 s (with amplitude 1,3 m^3/h); in experiment the beginning of oscillations was fixed at τ=1,8 s, the maximum was reached at τ=3,75 s, with amplitude 1,5m^3/h.

Thus program rather precisely predicted change of vapor volume in analyzable assembly. A little bit smaller, than in experiment, the values of characteristic times for process were, apparently, are connected to the insufficient taking into account in calculations of vapor condensation. At the same time coefficient of condensation λ_c was intentionally underestimated for preventing numerical instability.

The crisis of heat transfer for circumferential fuel elements came in experiment later, than for central fuel elements (approximately to the 13-th second after a beginning of boiling), the calculations have resulted in delay on a comparison with experiment on 0,2 - 0,7 seconds.

The extension of capabilities of the SABENA-3D program for calculation of process of covers melting and fuel melting in conditions of crisis is supposed. If for central area of fuel assembly this process can be described in two-dimensional statement $(r-z)$, for circumferential area it is necessary to take into account interaction of melted materials with a flat wall of the assembly.

2.4.2. Calculations of thermohydraulic of locked fuel assemblies in operational modes with entered gas by the SABRE code [45]

Fig. 9 show a degree of agreement experimentally obtained and calculated by the SABRE code of radial temperature profiles in sodium behind 49 % central blockage in a direction of a corner and plane of a fuel assembly cover on various distances from blockage (velocity of a main flow - 4ì/ñ). For 21 % angular blockage it can be seen from fig. 10.

The distributions of temperatures behind central and angular blockade (as isotherms) under the data of experiment and calculation are shown on fig.11 and fig.12.

3. CALCULATIONS OF VELOCITY AND TEMPERATURE FIELDS IN LOCKED ASSEMBLIES OF FUEL ELEMENTS, BASED ON MODEL OF A POROUS BODY

3.1. UGRA, PROTVA, COMMJX programs

The model of a porous body (or quasi-homogeneous model), is explicitly circumscribed, for example, in works [7, 46] and used in these works for development of a computational technique with a construction of the UGRA and PROTVA programs, allows to

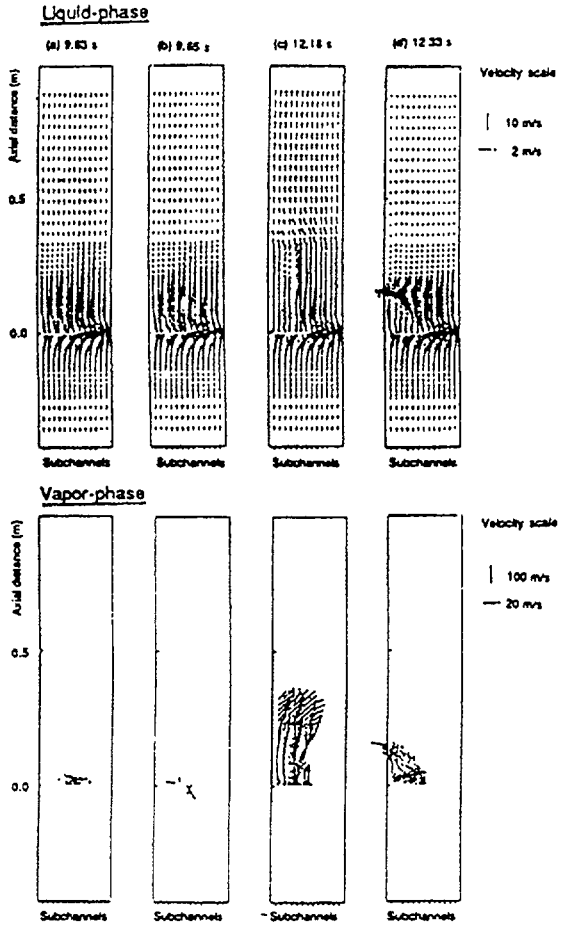

Fig. 8, а. Distributions of a liquid and steam phase velocities at 9.63, 9.65, 12.18 and 12.33 sec, calculated by SABENA 3D

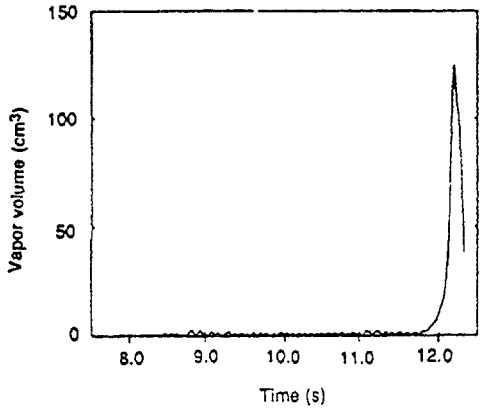

Fig. 8, б. Vapour volume (sm^3) during boiling calculated by SABENA 3D.

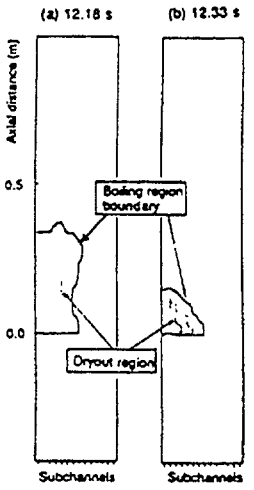

Fig. 8, в. Modes of boiling and dehumidifying at 12,18 and 12,33 seconds.

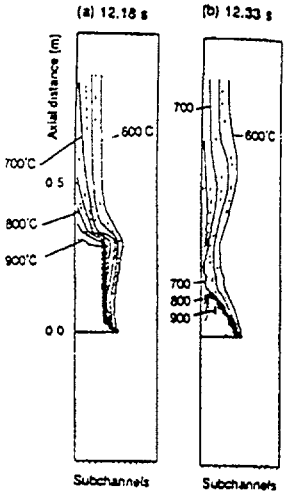

Fig. 8, г. Distributions of temperature in a liquid phase at 12,18 and 12,33 seconds.

calculate a mean velocity, pressure and temperature fields in assembly of fuel elements. The assembly of fuel elements, streamlined by the coolant, is simulated by solid medium with internal resistance and energy release.

The two-dimensional set of equations for porous medium is solved in [47, 48] at use of the following boundary conditions:

- velocity and temperature on the boundaries are set from experiments, the pressure is determined from an equation such as the Poisson;

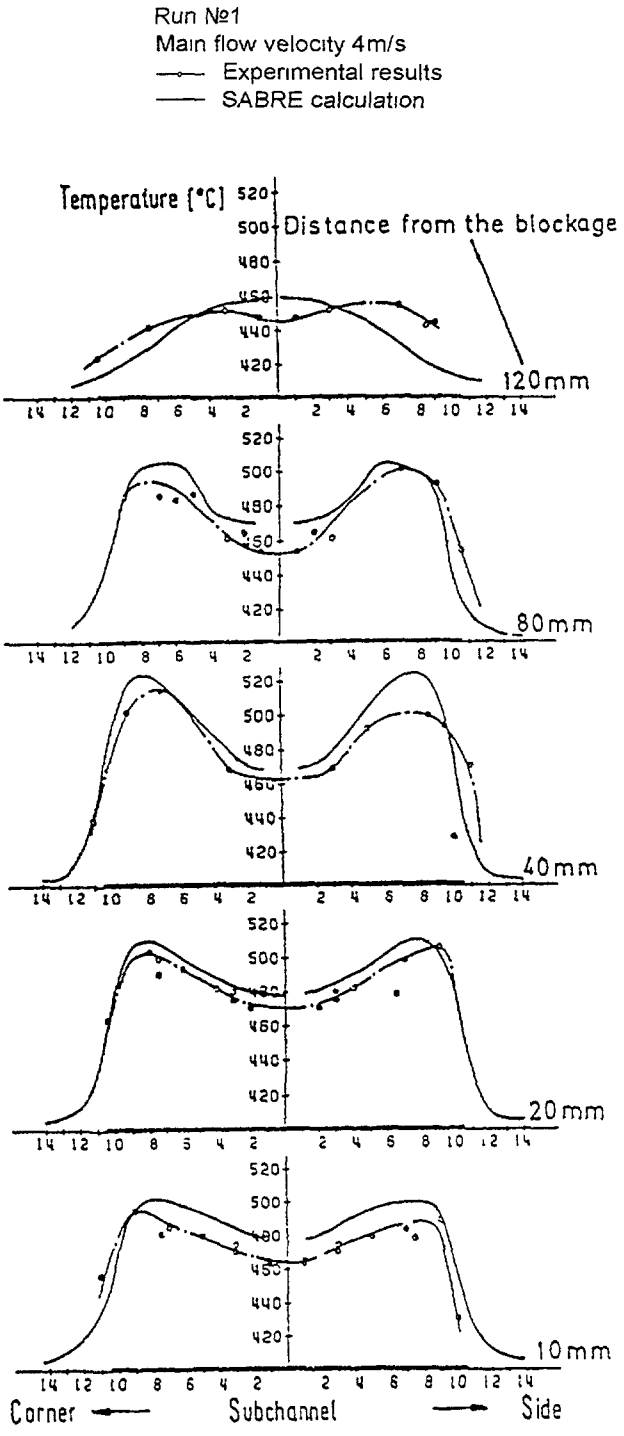

Fig. 9. 49 % central blockage, radial temperature profiles in sodium

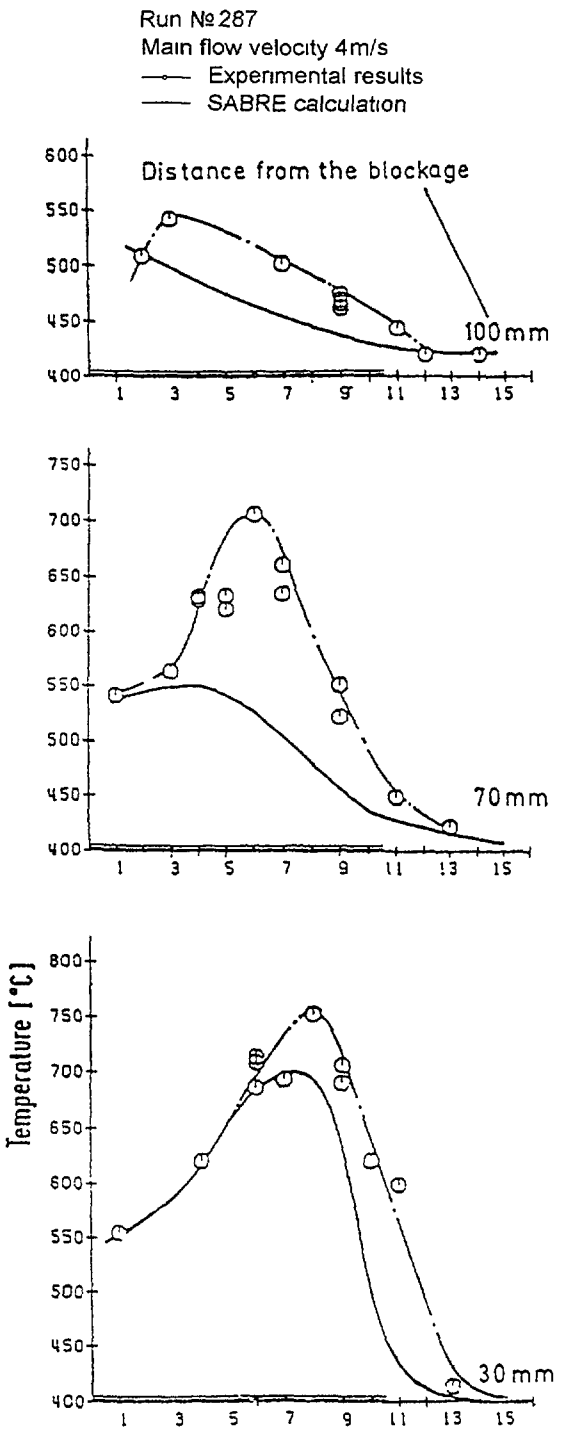

Fig. 10. 21 % angular blockage, radial profiles of temperature in sodium

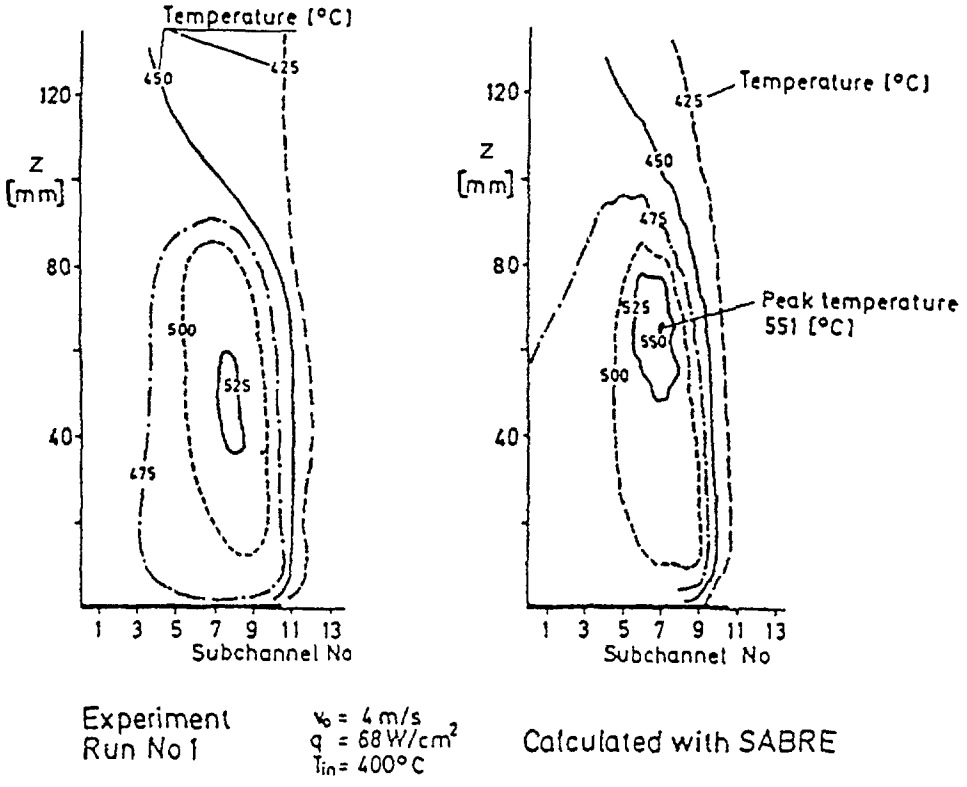

Fig. 11. 49 % central blockage, distribution of temperatures.

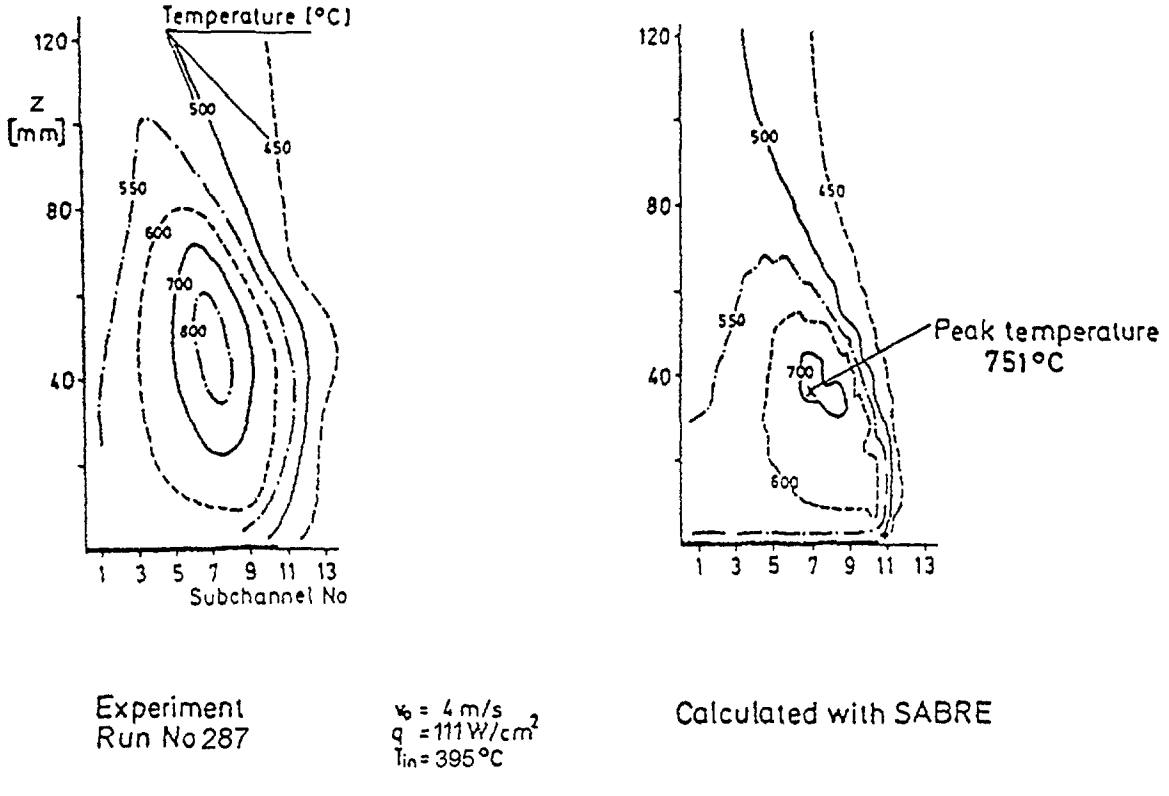

Fig. 12. 21% angular blockade, distribution of temperatures.

- on a line of a symmetry the flows of mass, momentum and heat are equal to zero;
- the rigid walls are impenetrable and adiabatic;
- the pressure is constant at inlet.

The comparison of calculation results of work [48] with the experimental data [49], [27] has resulted in introduction of correction to a technique [7, 46] for components of volumetric force of resistance dependent from a local angle of attack and coefficient of an anisotropy of resistance.

The accuracy of calculations by the program UGRA and PROTVA of a field of velocity at blockage is evaluated by the authors [7, 46] as 5 %, field of pressure as 15 %, field of temperature as 10 %.

The authors of the paper [48] offer the following computational formula for length of recirculating zone:

$$\frac{L}{d} = \frac{28(1+\beta)^{1,5} * \beta^{0,25}}{\xi_z(a_{rz} + 4\beta^{0,25})}\left(\frac{s}{d} - 1\right)^{0,2} * \left(\frac{s/d - 1}{s/d}\right)^{0,3} \qquad (9)$$

where s/d - relative step of fuel elements, β - degree of blockage , ξ_z, a_{rz} - coefficients.

For calculation of coolant overheating behind blockage the following formula is offered:

$$t^{max} - t_0 = \frac{q_F}{\rho c_p w_0} \mathrm{Re}^{0,28}\left[1 - \exp\left(-10,8\beta^{0,28}\right)\right], \qquad (10)$$

where q_F - heat flow from unit of a surface of a fuel element, w_0 - velocity before blockage.

The comparison of calculation results of a temperature field in locked assembly obtained by the COMMJX code [19] with experimental data for assembly with lateral blockade at screw wrapper of rods (wire wrappers) indicates, that the best agreement of results is reached at the taking into account in a computational model of convective transfer stipulated by wire wrappers (fig.13).

In case of porous blockage the axial leakage through blockage is calculated from a difference of pressure between two surfaces. The distribution of temperature within the limits of blockage can be calculated from heat conduction of a blockage material, from leakage in axial direction and at definition of heat transfer coefficient for a surface of blockage.

3.2. PORTER, TEMPER programs [23]

In the above-stated methods of calculation of three-dimensional flows and temperatures of the coolant in bundles of fuel elements with a strong disturbance of a velocity field (blockage) the finite difference approximation of equations on rectangular grids is implemented. Under the judgment of the authors [23], "it does not reflect geometry of a structure of a triangular lattice of fuel elements, hampers calculation of distribution of the coolant on cells of a bundle and complicates taking into account of existing systems of empirical constants on interchannel interaction". Besides the authors note[23], that majority of methods based on quasi-homogeneous model are devoted to calculation only of two-dimensional flows of the coolant.

The authors [23] emanate from a set of equations circumscribing three-dimensional flow of the coolant as in bundles of fuel elements, both in free areas, i.e. from a set of equations which is transient to finite difference approximation of equations of the Navier-Stokes on a triangular grid in case of free areas. This general statement of a problem is a doubtless virtue of work [23]. The properties of the given approach can be found in [50].

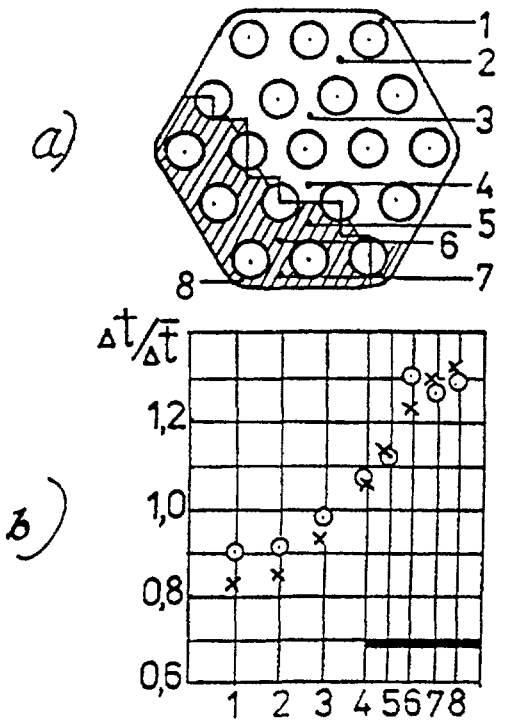

Fig. 13. Cross section of assembly with blockage (a) and distribution of coolant heating at assembly outlet (б). o- experiment [38], x - calculation [23].

The solution of a set of equations of momentum and mass conservation implements by the numerical method developed for the solution of three-dimensional equations of the Navier-Stokes [51].

With the purpose of the substantation of developed in [50] approaches realized in the program PORTER, the calculations of velocity and temperature fields of the coolant in experimental assembly of fuel elements with various blockage of cross-sections were executed. The calculated fields were compared to experimental data.

For calculation of three-dimensional fields of coolant temperature in assembly of fuel elements from calculated velocities fields the program (subprogram) TEMPER is developed. In it the algorithm of the numerical solution of equations of thermal energy balance obtained for triangular cells of a bundle of fuel elements is realized. In equations the diffusion and convective flows of thermal energy on all directions of a bundle are taken into account.

Calculation of a temperature field in 19-rods assembly with lateral blockage. The assembly was considered, for which the experimental data on distribution of fluid temperature at outlet [38] are obtained.

Some characteristics of assembly: diameter of fuel elements - d=5,84 mm, length of fuel elements - 1016 mm, relative step of fuel elements - s/d=1,24, step of wire wrapper - 304,8 mm, length of a heated segment - 457,2 mm, distance from a beginning of a heated segment before blockage - 101,6 mm; the coolant - sodium, velocity of the coolant - 6,93 m/s.

The temperatures of the coolant in cells of a bundle are measured in positions shown on fig. 14.

The values of diffusivities in momentum and energy equations reflecting an operation of interchannel intermixing (including through wire wrapper) were set pursuant to [6], and resistance coefficients in longitudinal and cross-sectional directions of a bundle - pursuant to

[6, 22]. At inlet and outlet bundle the rectangular distributions of axial component of velocity were assumed.

The bundle was divide into 26 computational sections on altitude with uniform step Δz=25,4 mm, the blockade placed at a level of the sixth cross-section.

As a whole, it is possible to consider, that the results of calculation were agreed with the computational data (fig.14): the deviation in heating has not exceeded 10 % from a mean heating, that has made no more 15^0C, and the maximum deviation had a place in area of near-a-wall cells, for which the geometric factor was insufficiently strictly taken into account.

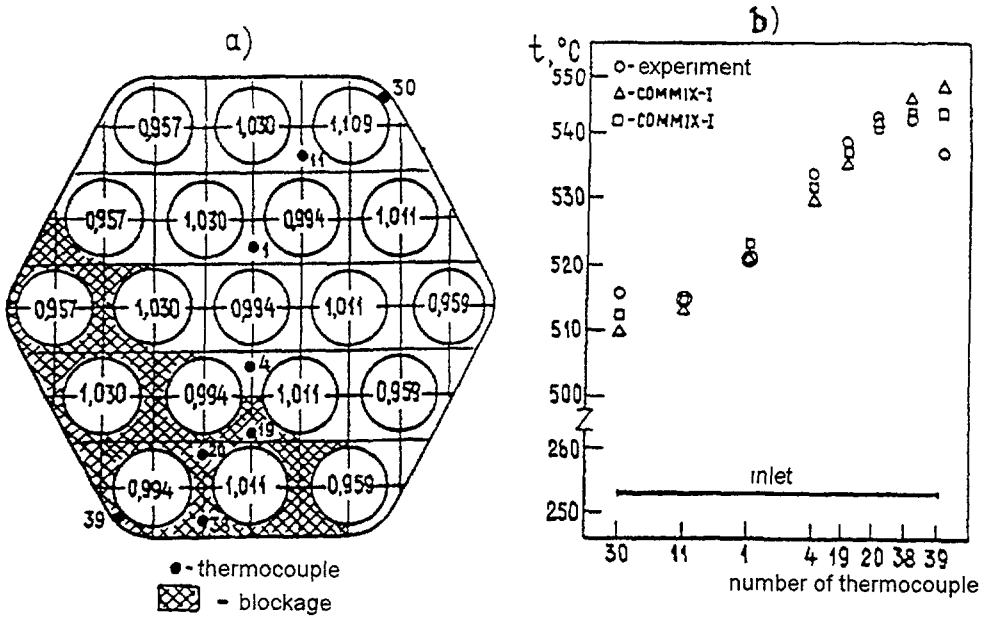

Fig. 14. A comparison of computational (program COMMIX-I) and of experimentally found distributions of temperature in cross section of model assembly with lateral blockage [38]:
Δ - withhout wire wrap, □ - with wire wrap

Calculation of velocity field in 61-rods assembly with central and lateral blockage. The degree of central blockage was 17 and 38 %, lateral - 50 %; the distributions of velocities and statistical pressure in assembly are obtained in experience of the authors [52, 14].

Some characteristics of assembly: diameter of rods - d = 26 mm, length of rods - 2000 mm, relative step of rods - s/d = 1,215, distance of arrangement of blockage from inlet bundle - 500 mm, coolant - water, Reynolds number in experience - Re=$2*10^4$; $2,9*10^4$; $3,9*10^4$.

The calculations are made by the program PORTER at Re=$3,9*10^4$ for 38 % central blockage and lateral blockage.

For reduction of volumes of calculations the length of assembly in calculation was taken equal 1000 mm, and position of blockage - on a distance of 200 mm from inlet bundle. It was supposed, that it can be made because of weak influence the postconditions and blockage against current to flow of the coolant. The rectangular distributions of velocities at input and output bundle were set. In calculations the difference of the form of cross-sections of circumferential cells from central was not taken into account.

The computational area of a bundle was divide into 50 sections on length with uniform step Δz=20 mm.

The computational and experimentally found distributions of axial component of velocity (referred to mean velocity w) on a radius of assembly on various distances from blockage $z/D_Б$ ($D_Б$ - diameter of blockage) were satisfactorily agreed one another in central area of assembly (fig. 15). However in circumferential cells the deviation reached 30 % (especially in section of arrangement of blockage), that is explained by a discordance of the actual sizes of these cells to the sizes adopted in calculation.

Calculated length of a recirculation zone (L_w = 336 mm) has appeared close to experimentally found (~ 410 mm) [52]. The computational distribution of axial velocity component in central channels in a recirculation zone also slightly differed from an experimental data (fig. 16). That is possible to tell about 50 % lateral blockage (fig. 17), though the computational values of velocities in a zone of recirculation lie a little bit below experimentally obtained (if the form of circumferential cells is not taken into account).

Let's mark, that in case of lateral blockage the more good agreement of calculated and experimentally measured distributions of velocity in section of a bundle at a level of blockage is obtained, that is connected to smaller influence of nonstandard circumferential cells to general flow, than in case of 38 % central blockage.

Calculation of velocity and pressure field in 19-rods assembly with 55 % central blockage. The hydrodynamics of the given assembly is investigated experimentally in IPPE by authors [53]. The assembly consists of smooth rods (d =19 mm, working length ~745 mm),

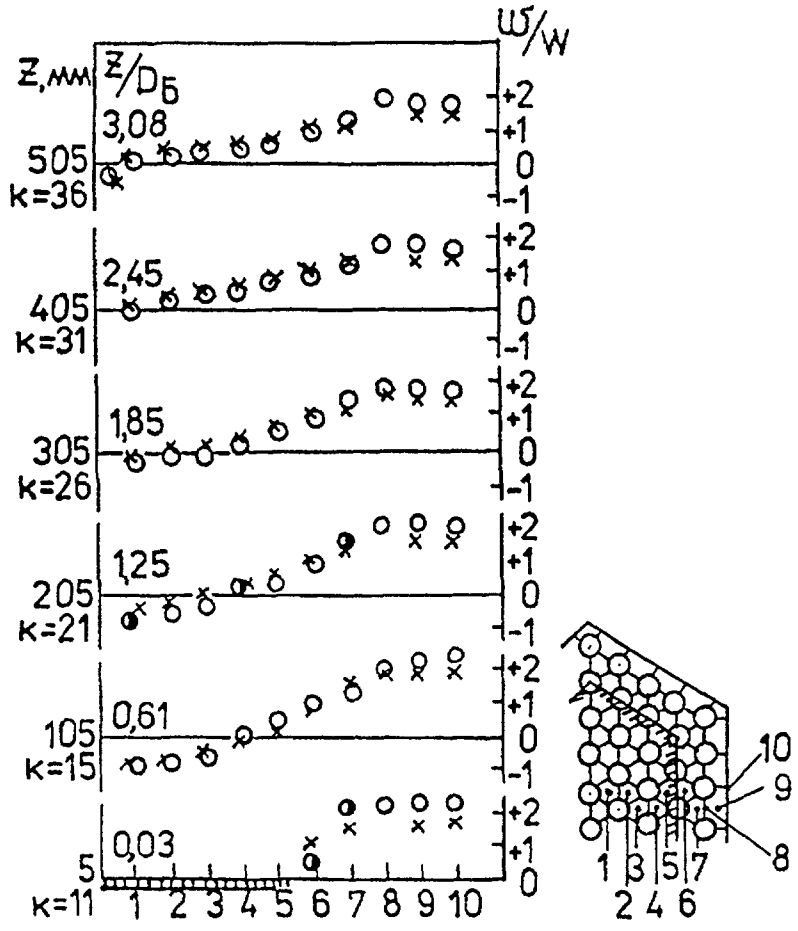

Fig. 15. A comparison of computational [23] and of experimentally found [14], [52] distributions of velocities behind 38 % central blockage of 61-rods assembly; x - calculation for Re = $3.9 \cdot 10^4$; o - experiment for Re = $3.9 \cdot 10^4$; ● - experiment for Re = $2.9 \cdot 10^4$.

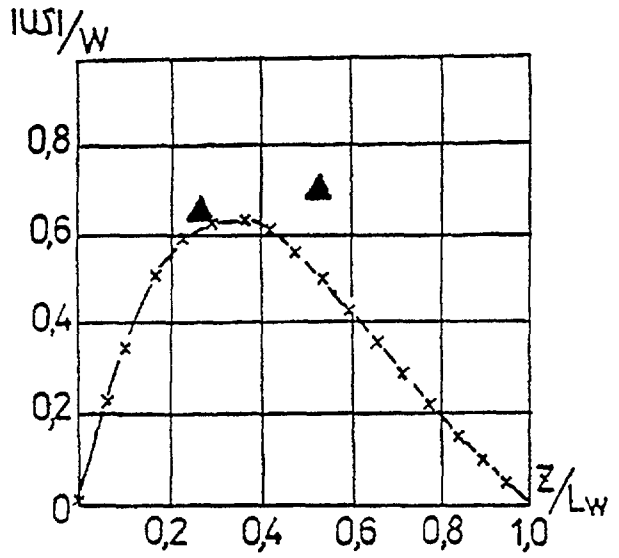

Fig. 16. Distribution of axial component of velocity on length of a zone of recirculation in central channels of assembly behind 38 % by central blockade; ▲- experiment [52], --x--x-- - - calculation [23].

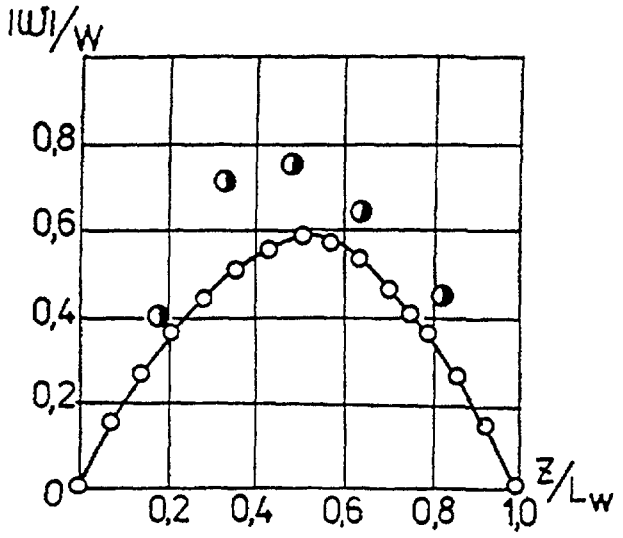

Fig. 17. Distribution of axial component of velocity on length of a zone of recirculation behind 50 % lateral blockade of 61-rods assembly in a channel with maximum velocity of a return flow; ◑ - experiment [14], --o--o-- - calculation [23].

located in hexagonal cover with a step s/d = 1,17 (geometry of fuel elements lattice of fast reactors). The blocking slice (thickness δ = 8 mm) placed on a distance 380 mm from inlet bundle of rods. The more in-depth data about assembly and results of researches see in [53].

For calculation the experimental mode with a maximum Reynolds number Re = 33000 is selected. As the blockage overlapped all standard cells of a bundle, leaving for pass of the coolant only nonstandart cells near a wall, in calculations the difference of cross-sections, resistance coefficients and coefficients of exchange of cells near a wall from standard triangular cells was taken into account.

The coefficient of effective viscosity defined through a coefficient of turbulent exchange is taken from the data [1]. For a considered Reynolds number it is $\nu_{эф}=2,5*10^{-4}m^2/s$.

On the fig.18 computational and experimentally found in work [53] distributions of axial velocity component in central cells on length of a bundle are compared. It is visible, that the calculated flow qualitatively corresponds to actual, but is characterized by almost twice smaller velocity of damping of non-uniformity in a track behind blockage.

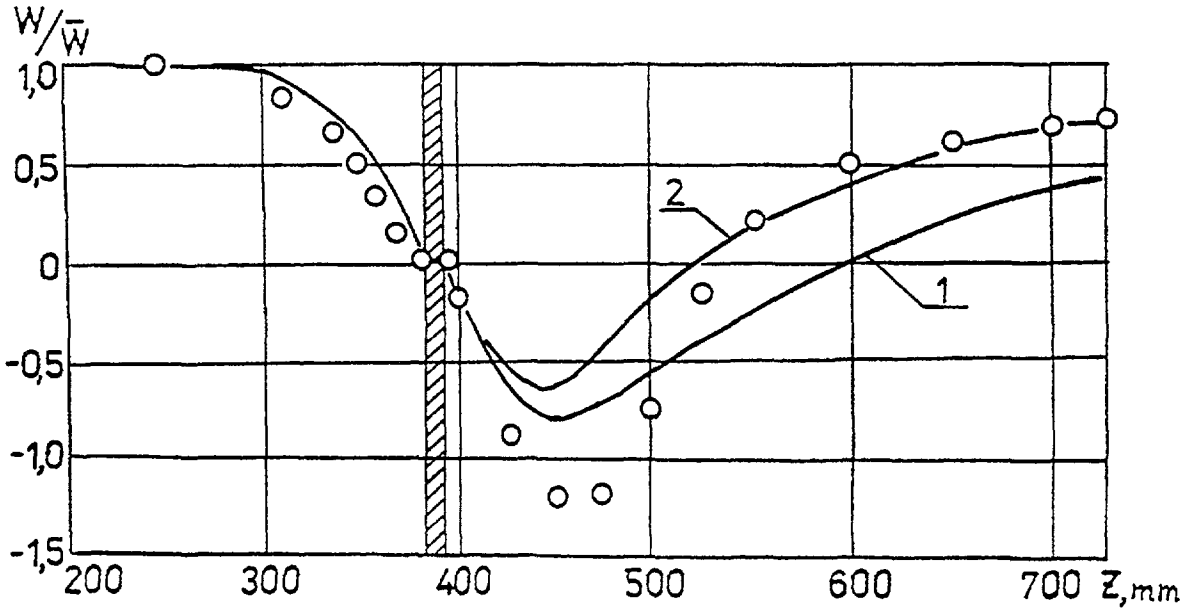

Fig. 18. Distribution of axial component of velocity on length of central cells of 19-rods assembly with central blockage; ----- - calculation [23]: 1 - $\nu_{эф}=2,5\cdot10^{-4}m^2/s$, 2 - $\nu_{эф}=2,5\cdot10^{-3}m^2/s$; o - experiment [53].

The supposition was made, that the deviation with experiment is connected to value of interchannel exchange coefficient, which for flow behind blockage in the given assembly considerably exceeds the value, adopted in calculation determined for stabilized flow. Therefore Additional calculation with a coefficient of the turbulent interchannel exchange exceeding in 10 times a coefficient of exchange for stabilized current (i.e. $\nu_{эф}=2,5*10^{-3}$ m^2/s) was executed. In this case damping of non-uniformity of velocity in a track and size of a recirculation zone have appeared close to experimentally measured (curve 2 on fig. 18). However maximum velocity of recirculation behind blockage twice has decreased on a comparison with the experimentally measured values. In this connection the authors [23] consider that calculation of perturbed flow of fluid, such as flow behind blockage, require a perfect system of constants (resistance coefficients, effective viscosity), taking into account instability of flow of the coolant.

Summing up results of calculation of thermohydraulics of locked fuel elements by the programs PORTER, TEMPER, it is possible to tell, that:

- the calculated velocity, pressure and temperature fields, in various assembly with blockage of the diverse form and size in comparison to approprINPE experimental data testify to applicability and satisfactory accuracy of the used method for calculation of complex three-dimensional flows with strong disturbances;

- for precise calculation of spatial coolant flow in bundles of fuel elements it is necessary further perfecting and extension of area of applicability of a system of constants (empirical resistance coefficients and interchannel exchange) for the non- stabilized currents.

3.3. "THEHYCO-3DT" program complex

The speech goes about verification on an experimental material of IPPE of a hydrodynamic module of a program complex "THEHYCO-3DT" (three-dimensional thermohydraulic code), created for modeling of three-dimensional non-stationary neutron-thermophysic processes in core of perspective nuclear power installation with fuel assemblies without covers [24].

In the THEHYCO-3DT code the mathematical model of complex thermohydraulic calculation of the reactor core (fig. 19) is used.

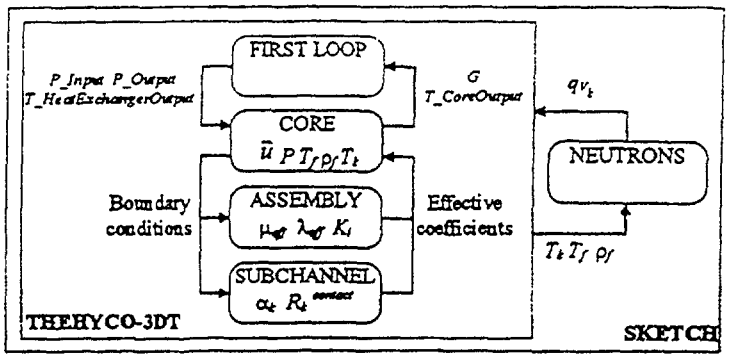

Fig. 19. Multi-stage model for core realized in the computational SKETCH code.

At a "Core" stage the equations of conservation and boundary conditions for incompressible viscous fluid in the supposition of model of a porous body are noted.

At a "Fuel assembly" stage the effective viscosity μ_{eff}, effective heat conduction λ_{eff} and crest coefficient K_i (for resistance) are set as empirical constants or are calculated previously with the help of subchannel codes of a type COBRA-IV, SABRE etc. [54] (these codes can be used in a code THEHYCO-3DT as auxiliary). The empirical constants are borrowed from [1] and [55].

In porous medium consisting of a bundle of rods, the effective coefficients are determined as:

$$K_i = \varepsilon_f \cdot \frac{\xi_i}{2d_\Gamma}, \tag{11}$$

$$\lambda_{eff} = \varepsilon_f \rho c |u_z| \frac{l_c}{d} \cdot \frac{A}{\frac{l}{d} - 1} \cdot \mu^T, \tag{12}$$

$$\mu_{eff} = \varepsilon_f \rho |u_z| \frac{l_c}{d} \cdot \frac{A}{\frac{l}{d} - 1} \cdot \mu^\Gamma, \tag{13}$$

where ξ_i - resistance coefficient in a direction i; μ^T, μ^Γ - coefficients of interchannel interaction by heat and momentum [1/m].

We shall mark, that the fact of separate use by the authors [24] in equations of energy and motion of coefficients of interchannel exchange by a heat (μ^T) and momentum (μ^Γ)

(μ^{Γ}, more correct, is a coefficient of exchange of mass, however it is possible to consider, that it is equal (the numerical value) to a coefficient of exchange by a momentum) and the drawing of numerical values of these coefficients from [1] answer to modern sights to a problem of interchannel interaction in fuel assemblies of reactors and correspond to developed in IPPE philosophy of interchannel interaction in lattices of fuel elements of cores of nuclear reactors.

At a stage "Inter-fuel-element channel" contact thermal resistance $R_K^{contact}$ is determined from a condition of heat transfer through a clad at use of empirical coefficients of heat transfer α_K [55] for quasi-stationary conditions.

For verification of a code the experimental data obtained on air model in IPPE by B.N.Gabrianovich with employees are used. The model (fig.20) consists from 563 wire-wrapped rods (d = 15 mm, l/d = 84 mm, step of wire wrapper T/d = 62), located in a triangular lattice with a relative step s/d = 1,13 (11 - 12 numbers till 49 rods in each). The velocity field (Re = 7900) was measured inside model in conditions 37 % blockage of cross-section of model at inlet or / and outlet model.

The results of calculations and experiments compared on the fig.21, 22 are agree one another.

The authors [24] underline a universality of applicability of the THEHYCO-3DT code, working both in core of the reactor, and in assembly at use of various coolant (air, liquid metal), however it is marked, that at any application of this code the effective coefficients (11) - (13) should be updated, and hereafter, for code verification with reference to liquid metal cooled reactors it is necessary to receive experimental data on liquid metal.

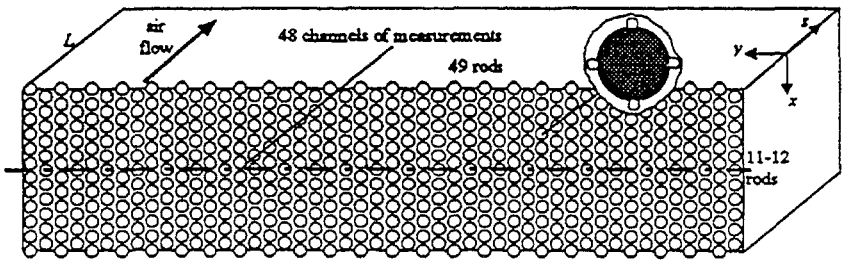

Fig. 20. Experimental assembly (d=15 mm, L/d =84, T/d = 62, s/d = 1.13); Re = 7900.

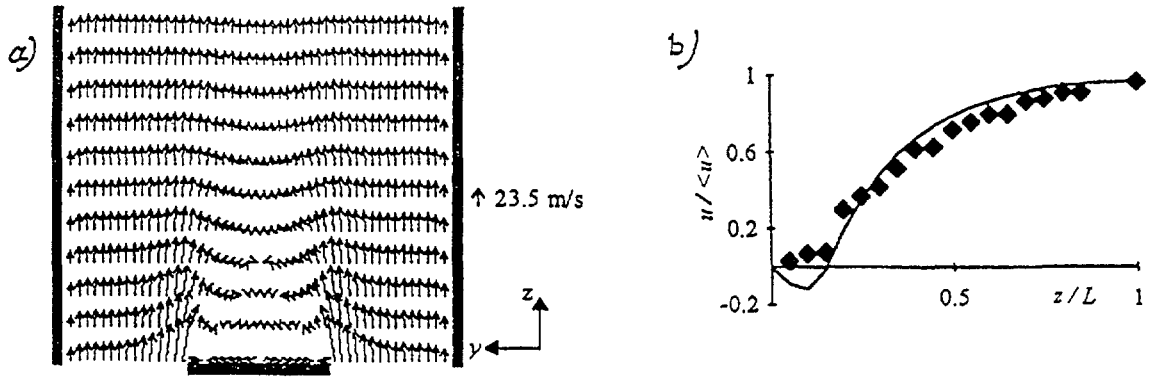

FIG. 21. A field of velocity behind central blockage at inlet (a) and axial velocity in a central channel (б); —— - calculation; ◆ - experiment.

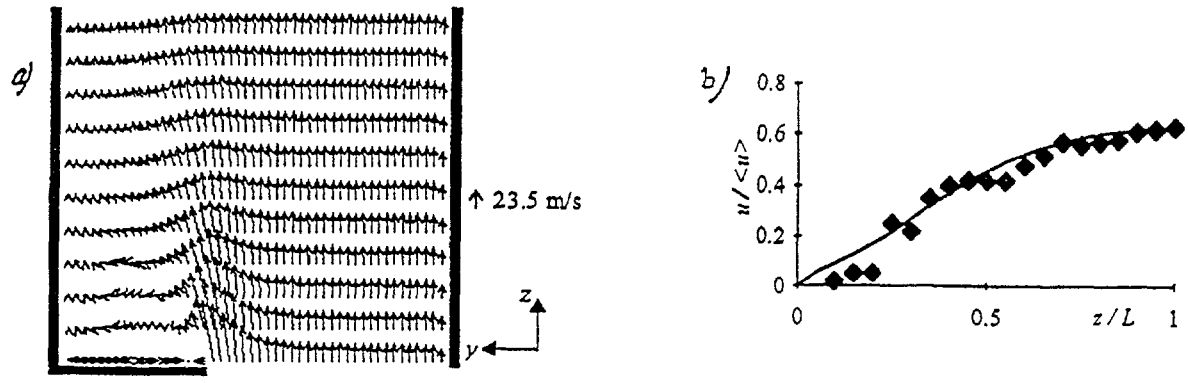

Fig. 22. A field of velocity for near-a-wall by blockage at inlet (a) and axial velocity in a central channel (б); —— - calculation; ◆ - experiment.

CONCLUSIONS

In addition to earlier published researches of the authors [56–58] of the analysis and generalization of results of experiments on study of velocity and temperature fields for fuel assemblies of fast reactors with partial blockage of cross-section under the coolant the analysis being available in the literature (known to the authors) works on numerical modeling of an indicated problem is conducted.

REFERENCES

[1] ZHUKOV A.V., KIRILLOV P.L., MATJUKIN N.M., SOROKIN A.P. et al. Thermogidraulic Account Fuel Assemblies of Fast Reactors With Liquid Metals Cooling // Ì: Energoatomizdat, 1985.

[2] ZHUKOV A.V., SOROKIN A.P., MATJUKIN N.M. Interchannel Exchange in Fuel Subassemblies Fast Reactors: the Settlement Programs and Practical Appendix // Ì: Energoatomizdat, 1991

[3] ZHUKOV A.V., SOROKIN A.P., HUDOSKO V.V. Influence Thermogidraulics the Factors on Safety Fuel Assemblies Fast Reactors // INPE, Obninsk, 1990.

[4] ZHUKOV A.V., KORNIENKO YU.N., SOROKIN A.P. et al. Methods and programs subchannel thermogidraulics of account fuel subassemblies in view of interchannel interaction of the heat-carrier // Analitical review. Obninsk, IPPE, ÎB-107, 1990, 82p.

[5] ZHUKOV A.V., SOROKIN A.P., USHAKOV P.A. et al. Subchennal Therogidraulic Account Fuel Subassemblies Nuclear Reactors // Atomic Energy, 1981, v.51, ¹ 5, p.307-311.

[6] SUBBOTIN V.I., IBRAGIMOV M.H., USHAKOV P.A., BOBKOV V.P., ZHUKOV A.V., YURIEV YU.S. Hydrodynamics and Heat Exchange on Nuclear Power Installations // Ì.Atomizdat, 1975, 408pp.

[7] GORCHAKOV M.K., KASTEEV V.M., KOLMAKOV A.P. et al. Application of Model a Porous Body to Thermogidraulics Accounts Reactors and Heat Exchenger // Termal-physics of high temperatures, 1978, ò.14, ¹4, p. 866-871.

[8] LEONCHUK M.P., SMIRNOVA N.S., SHVETSOV YU.E. Account of Fields of Speed and Temperature in Nuclear Reactorwith Integrated. // Industrial termal engineering, ¹6, 1984, p. 23-25.

[9] SCHERBAKOV S.I. Account of Current and Temperature Fields in Flowing Parts and Constructive Elements Heatengineering of the Equipment // Preprint IPPE -1368, Obninsk, 1982, p.12.

[10] SHA W. An Overview on Rod - Bundle Thermal - Hydraulic Analysis // Nuclear Engineering and Design, 1971, v .62, 1980, p.1-24.
[11] ROWE D.S.: COBRA-IIICA: A Digital Computer Program for Steady State and Transient Thermal - Hydraulic Analysis of Rod Bundle Nuclear Fuel Elements // BNWL-1965. 1973.
[12] SHA W.T., SCHMITT R., HUEBOTTER P.H.: Boundury - Value Thermal Hydraulic Analysis of a Reactor Fuel Bundle // Nuclear Science and Engineering, 1978, v.59, '2, p.140-160.
[13] WEISS E., MARKLY R.A., BATTACHARYYA A.: Open Duct Cooling - Concept for the Radial Blanket Region of a Fast Breeder Reactor // Nuclear Engineering and Design, 1971, v.16, '4, p.375-386.
[14] MIYAGUCHI K. Analysis of the Flow Temperature Fields in Locally Blocked LMFBR Fuel Subassemblies // JWGFR-29, 1979, p.152-163.
[15] MIYAGUCHI K. Analitical Studies on Local Flow Blockages in LMFBR Subassemblies, Using the UZU Code // Nuclear Engineering and Design, 1980, v.62, '1-3, p.25-38.
[16] ARAI M., HIRATE N. Analysis of the Central Blockage Wake in an LMFBR Subassembly // Nuclear Engineering and Design, 1976, v.45, '1, p.127-132.
[17] DEARING J.F. Calculated vs Experimental Temperature Distribution Behind Six - Channel Central Blockage // Transaction of the American Nuclear Society, 1977, v.27, p.566-567.
[18] CHELEMER H. åt. al. Thermal Hydraulic Analysis Method for Rod Bundle Cores // Nuclear Engineering and Design, 1977, v.41, '2, p.219-230.
[19] SHA W.T., DOMANUS H.M., SCHMITT R.C. Some Numerical Results Obtained From the Single Version of COMMJX Code // JWGFR/29, 1978, p.107-131.
[20] MENANT B., BASQUE G., CRAND D. Theoretical Analysis and Experimental Evidence of Thermohydraulic Incoherency in Indisturber Cluster Geometry // JWGFR/29, 1979, p.134-151.
[21] SIEGMANN E.R., GILBORTSON J.C. Assessment of local Blockages in Carbide Assemblies // Transaction of the American Nuclear Society, 1975, v.21, p.315
[22] GORCHAKOV M.K., KOLMAKOV A.P., YURIEV YU.S. Anizotropic of Friction Factor in Porous Bodies, Consisting of Bunches of Cores // Preprint IPPE-446, Obninsk, 1973, 18 pp.
[23] VEREMEEV À.À., KUMAEV V.YA., LEONCHUK Ì.P. Account of Spatial Current of the Heat-Transport Medium and Temperatures in Fuel Assembly on a Basis on Cell of the Approach // Preprint IPPE -1789, Obninsk, IPPE, 1986.
[24] KORSUN A.S., VITRUK S.G., USHAKOV P.A., GABRIANOVICH B.N. Verification of the Hydrodynamical Module of a Program Complex THEHVCO-3DT. Problems of Safety of Nuclear-Power Installations. The theses of the Reports IX Seminars on Problems of Physics Reactors, "Volga-95", Moscow, 4-8 september 1995, v.2, p.165-167 // Ì.: ÌEFI, 1995 -234p.
[25] ITOH K., SATOH K., ENDO H., HASHIGUCHI Y. Basic Study on Local Blockage in the FBR Fuel Subassembly. Proceedings of the Fifth International Topical Meeting on Reactor Thermal Hydraulic NURETH-5 "Towards the Next Generation of Nuclear Power Reactors", Sept.21-24, 1992 // Little America Hotel, Salt Lake City, UT, USA, v.VI, p.1529-1536.
[26] NINOKATA H., KONOMURA M. Thermohydraulics Analysis of Local Subassembly Accidents in Liquid Metal Cooled Breeder Reactors. Proceedings of the Fifth International Topical Meeting on Reactor Thermal Hydraulic NURETH-5 "Towards the

Next Generation of Nuclear Power Reactors", Sept.21-24, 1992 // Little America Hotel, Salt Lake City, UT, USA, v.VI, p.1537-1545.
[27] KIRSCH D. Investigations on the Flow and Temperature Subassemblies // Nuclear Engineering and Design, 1975, v.31, ¹2, p.266-279.
[28] OHTSUBO A., UKUWASHI S. Stagnat Fluid due to Local Flow Blockage // Nuclear Science and Technology, 1972, v.9, ¹7, p.433-434.
[29] ICHU M., CHAWLA T.C. A Termal Analysis of Hot Spots on Fast - Reactor Fuel Cladding Due to Deposition of Low - Conductivity Materials // Nuclear Science and Engineering, 1975, v.56, p.188-196.
[30] SMIDT D., SCHLEISIEK K. Fast Breeder Safety Against Propagation of Local Failures // Nuclear Engineering and Design, 1977, v.40, ¹3, p.393-402.
[31] NELSON P., NEIL C. Initial - Value Methods in a Simplified Subchannel Analysis of Flow - Blockages Problems // Transaction of the American Nuclear Society, 1980, v.34, p.294-295.
[32] NELSON P., NEIL C. Initial - Value Methods in a Simplified Subchannel Analysis of Flow - Blockages Problems // Nuclear Science and Engineering, 1980, v.76, p.366-370.
[33] ROWE D.S. Experimental Study of Flow and Pressure in Rod Bundle Subchannels Containing Blockages // BNWL - 1771, 1973.
[34] CREER J.M., BATES J.M., SUTEY A.M. Turbulent Flow in a Model Nuclear Fuel Rod Bundle Containing Partial Flow Blockages // Nuclear Engineering and Design, 1978, v.52, ¹1, p.15-33.
[35] BROWN W.D., KHAN E.U., TODREAS N.E. Prediction of Cross Flow due to Coolant Channel Blockages // Nuclear Science and Engineering, 1975, v.57, ¹2, p.164-174.
[36] LIN E.I.H., SHA W.T. Triangular Edge - Subchannel Wire - Wrap Function for Flow Blockage Analysis // Transactions of the ANS, 1978, v.30, p.529-530.
[37] LIN E.I.H., SHA W.T. Termal - Hydraulic Analysisof a Wire - Wraped 19-Rod Bundle with Edge Blockage // Transactions of the American Nuclear Society, 1978, v.28, p.539-540.
[38] WANTLAND J.L., et. al. Duct Wall Temperature due to a Heated - Zone Edge Blockage in a Sodium - Colled 19-Rod Bundle // Transactions of the American Nuclear Society, 1977, v.19, ¹ 1, p.245-248.
[39] ZHUKOV A.V., KOTOVSKIY N.À., KUDRYAVTSEVA L.Ê. et al. Interchannel Thermal Interaction in Bunches Smooth of Cores, Streamline Liquid Metals // Preprint IPPE-757, Obninsk, DSTI, IPPE, 1977.
[40] ZHUKOV A.V. et al. Fields of speeds in fuel assembly fast reactors at change of geometry of peripheral zones // In Heat-physical of research. Ì., Published VIMI, 1977, p.17.
[41] ZHUKOV A.V. et al. Researches of Interchannel Hashing in Lattices of Cores with Small Relative Steps and Generalization of an Actual Material for Systems with Remote Wire Coiling // Preprint IPPE-799, Obninsk, 1977.
[42] ZHUKOV A.V., SOROKIN A.P., MATJUKIN N.M. Interchannel exchange in fuel assemblies fast reactors :theoretical of a basis and physics of process // Ì.: Energoatomizdat, 1989.
[43] ROWE D.S., ANGLE C.W. Experimental Study of Mixing Between Rod Bundle Fuel Element Flow Channels During Boiling // Transactions of the American Nuclear Society, 1967, v.10, p.655.
[44] NAKAMURA H., MIYAGUCHI K., TARAHASHI J. Hydraulic Simulation Experiments with Simulated LMFBR Subassemblies unter Nominal and Non-nominal Operating Conditions // IWGFR/29, 1979, p.58-75.

[45] HUBLER F., PEPPLER W. Summary and Implications of Ont-of-pile Investigations of Local Cooling Disturbances in LMFBR Subassembly geometry unter Single // Phase and Boiling Conditiens. KfK 3927, May 1985.
[46] INSTITUTE FüR REAKTORENTWICKLUNG PROJEKT SCHNELLER BRUTER KERNFORSCHUNGSCENTRUM KARLSRUHE.
[47] VLADIMIROVA L.I., KOLMAKOV À.P., YURIEV YU.S. The Account Complexis Longitudinal - Cross Currents of a Liquid in Reactor Core and Heat Exchendger on the Basis of Model Anizotropic Porous Body // In :Questions of a nuclear science and engineering, series "Reactor design", № 4(18). Ì., CSII atom information, 1977, p.17-20.
[48] KOLMAKOV À.P. Account of a Field of Speed, Pressure and Temperature of the Heat-Carrier Behind Blockade in the Cartridge Fuel Elements // Preprint IPPE-930, DSTI, IPPE, 1979.
[49] USHAKOV P.A., YURIEV YU.S., KOLMAKOV À.P. Fields of speed, pressure and temperature in cartridges fuel elements of fast ðåàêòîðîâ at blocking through passage // In: Heat and masstransfer - VI, Minsk, IHME AS Belorussia Republic, 1980, v.8, p.173-180.
[50] GREEF C.P. Temperature Fluctuations: An Assessment of Their Use in the Detection of Fast Reactor Coolant Blockages // Nuclear Engineering and Disign, 1979, v.52, ¹1, p.35-55.
[51] KUMAEV V.YA., LEONCHUK Ì.P., DVORTSOVA L.I. Technique of numerical account of three-dimensional currents of the heat-carrier in bunches of cores // Preprint IPPE -1733, Obninsk, 1985, 32p.
[52] LEONCHUK Ì.P., SIVAK Z.V. Implicit method of the decision of the three-dimensional equation Novie-Stoks for a viscous incompressible liquid // Preprint IPPE-1325, Obninsk, 1982, 19p.
[53] NAKAMURA H., MIYAGUCHI K., TAKAHASHI J. Hydraulic Simulation of Local Blockage in a LMFBR Fuel Subassembly // Nuclear Engineering and Disign, 1980, v.62, ¹1-3, p.323-333.
[54] ZHUKOV A.V., MATJUKIN N.M., RIMKEVICH Ê.S. Influence of blocking of through passage section of model assembly of the cartridge fuel elements fast reactors on distribution of speed of the heat-carrier // Preprint IPPE -1479,Obninsk: IPPE, 1982.
[55] DUNN F.E., MALLOY D.J., MOHR O. Computer Code Abstract. Liquid-Metal-Cooled Reactor Thermal-Hydraulic Calculations in the United States, Nuclear Science and Engineering 100, p.558-563, 1988.
[56] KIRILLOV P.L., YURIEV YU.S., BOBKOV V.P. The Directory on Thermogidraulic to Accounts (Nuclear Reactors, Heat Exchander, Generators Pair) // Ì., Energoatomizdat, 1984.
[57] ZHUKOV A.V., SOROKIN A.P., MATJUKIN N.M. Research of Fields of Speed and Temperature in Fuel Assembly Reactors with Partial Blocking of Through Passage Section. Works of the International Conference "Heatphysics 98" - Heat physical aspects of safety VVER, Obninsk, 26-29 may 1998 // Obninsk: IPPE, v.1, p.115-131.
[58] ZHUKOV A.V., MATJUKIN N.M., SOROKIN A.P. Thermogidraulics of the Characteristic Model Reactors of Fuel Assemblie at Partial Blocking of Through Passage Section (Fuel Elements with Wire Coiling) // Nuclear power, News of higher educational institutions, Obninsk, INPE, 1997, ¹5, pp.65-73.
[59] ZHUKOV A.V., MATJUKIN N.M., SOROKIN A.P. Experimental and Settlement Researches of Fields of Speed and Temperature in Model Fuel Assemblies of Fast Reactors with Distance Fuel Element Wire Coiling at Partial Blocking of Through Passage Section; Safety NPS and Training of Personnel // V International conferences: the theses of the reports, Obninsk, INPE, 1998, p.10-12.

THE QUESTIONS OF LIQUID METAL TWO-PHASE FLOW MODELLING IN THE FBR CORE CHANNELS

D. YE. MARTSINIOUK, A.P. SOROKIN
State Scientific Centre of Russian Federation,
Institute of Physics and Power Engineering,
Obinisk, Kaluga Region, Russian Federation

Abstract

The two-fluid model representation for calculations of two-phase flow characteristics in the FBR fuel pin bundles with liquid metal cooling is presented and analysed. Two conservation equations systems of the mass, momentum and energy have been written for each phase. Components accounted the mass-, momentum- and heat transfer throughout the interface occur in the macro-field equations after the averaging procedure realisation. The pattern map and correlations for two-fluid model in vertical liquid metal flows are presented. The description of processes interphase mass- and heat exchange and interphase friction is determined by the two-phase flow regime. The opportunity of the liquid metal two-phase flow regime definition is analysed.

1. INTRODUCTION

The nuclear reactor heat removal with natural circulation origin in the reactor first contour, with coolant boiling, with consequent possible dryout in the core (the crisis of heat exchange), is one of the most unexplored and hardly predictable modes of the NPS accident situations. Now there is a rather large number of the machine codes for the analysis of similar processes for reactors with the cooling by water. The problem of modelling the non-stationary thermohydraulic processes in the fast reactor first contour in which the liquid metal is used as the coolant is in a more complicated position.

This paper is devoted to description of a two-fluid mathematical model of the heat exchange process in the fast reactor circulating contour under heat removal conditions. The presented system of constitutive relations is basically constructed on empirical relations and essentially depends on a two-phase flow regime. However adequate description of the boundaries between liquid metal two-phase flow regimes is hampered. That reduces to a problem of a experimental pattern maps creation which could be used in computer codes for calculation the non-stationary processes in the fast reactor first contour.

2. THE STATEMENT FOR A MODEL

The necessary assumptions for simplification of full statement for a model could be defined as follows:

(1) The phases pressure is equal.
(2) Phases velocities on the interface are equal.
(3) The force of joined masses is zero.
(4) The through passage section area function is continious.

With allowance for these assumptions the two-phase flow model will be named as a two-fluid model of unequal phases velocities and temperatures.

The conservation equations system has the following aspect:

$$\begin{cases} \dfrac{\partial}{\partial\tau}(\varphi_k\rho_k\omega)+\dfrac{\partial}{\partial z}(\varphi_k\rho_k w_k\omega)=\Gamma_{lk}\omega \\ \dfrac{\partial}{\partial\tau}(\varphi_k\rho_k w_k\omega)+\dfrac{\partial}{\partial z}(\varphi_k\rho_k w_k^2\omega)=\Gamma_{lk}w_l\omega-\varphi_k\omega\dfrac{\partial p}{\partial z}-s_{wk}\tau_{wk}\omega+s_l\tau_{lk}\omega \\ \dfrac{\partial}{\partial\tau}(\varphi_k\rho_k h_k\omega)+\dfrac{\partial}{\partial z}(\varphi_k\rho_k h_k w_k\omega)=\Gamma_{lk}h_l\omega+\varphi_k\omega\dfrac{\partial p}{\partial\tau}+w_k\varphi_k\omega\dfrac{\partial p}{\partial z}+ \\ \qquad\qquad +(w_k-w_l)p\omega\dfrac{\partial\varphi_k}{\partial z}+s_{wk}q_{wk}\omega+s_l q_{lk}\omega \end{cases} \tag{1}$$

$k = l, g.$

The conservation equations on the interface can be noted as follows:

$$\begin{cases} \sum\limits_{k=l,g}\Gamma_k=0 \\ \sum\limits_{k=l,g}(\Gamma_k w_{lk}-\tau_{lk})=0 \\ \sum\limits_{k=l,g}(\Gamma_k h_{lk}+q_{lk}-\tau_{lk}w_{lk})=0 \end{cases} \tag{2}$$

The system of six differential equations includes six unknowns: h_l, h_g, w_l, w_g, φ, p. The model is made for calculation of processes in a contour with natural circulation. Therefore mathematically propulsion can be found through a residual of contour segments weights. Thus, the pressure falls out of an unknown variables list and the initial conservation equations system undergoes the following modifications:

$$\begin{cases} \dfrac{\partial\rho_m}{\partial\tau}+\dfrac{\partial}{\partial z}(\rho_m w'_m)=0 \\ \dfrac{\partial}{\partial\tau}(\varphi_g\rho_g\omega)+\dfrac{\partial}{\partial z}(\varphi_g\rho_g w_g\omega)=\Gamma_{lg}\omega \\ \dfrac{\partial}{\partial\tau}(\varphi_k\rho_k w_k\omega)+\dfrac{\partial}{\partial z}(\varphi_k\rho_k w_k^2\omega)=\Gamma_{lk}w_l\omega-\varphi_k\omega\dfrac{\partial p}{\partial z}-s_{wk}\tau_{wk}\omega+s_l\tau_{lk}\omega \\ \dfrac{\partial}{\partial\tau}(\varphi_k\rho_k h_k\omega)+\dfrac{\partial}{\partial z}(\varphi_k\rho_k h_k w_k\omega)=\Gamma_{lk}h_l\omega+\varphi_k\omega\dfrac{\partial p}{\partial\tau}+w_k\varphi_k\omega\dfrac{\partial p}{\partial z}+ \\ \qquad\qquad +(w_k-w_l)p\omega\dfrac{\partial\varphi_k}{\partial z}+s_{wk}q_{wk}\omega+s_l q_{lk}\omega \end{cases} \tag{3}$$

That is, the momentum and energy conservation equations for each phase and mass equation for gas remain without modifications and instead of the mass equation for fluid the mass equation for a two-phase mixture is decided. In an outcome to a list from five unknowns sixth is added (w'_m): it is possible to describe as a two-phase mixture velocity modification owing to that the volumetric extension. It is obvious that in difference from the momentum conservation equations, in which the velocity of each phase is concerning the contour length, the value w'_m is of the rather pseudo-fixed coolant.

So, we have a system of six differential equations with six unknowns: h_l, h_g, w_l, w_g, φ, w'_m. We have a list of parameters derivatives from these unknowns: ρ_l, ρ_g, t_l, t_g, which are connected by the following relations:

$$t_k = {}^{h_k}\!/_{C_{pk}}; \tag{4}$$

$$\rho_k = \rho_{0k} - \beta_k \cdot t_k, \tag{5}$$

and also series of auxiliary magnitudes:

S_I – the interface boundary length;
w_I – the interface rate;
$\tilde{A}_{Il}$, $\tilde{A}_{Ig}$ – the mass exchange velocity on the interface;
τ_{Il}, τ_{Ig} – interphase shear stress of phases;
τ_{wl}, τ_{wg} – wall shear stress of phases;
q_{Il}, q_{Ig} – interphase heat flux;
q_{wl}, q_{wg} – wall heat flux.

2.1. Interface boundary length

The interface boundary length is directly through magnitude of the interphase area:

$$s_I = a_I \cdot \omega, \tag{6}$$

The analysis of calculation techniques data is submitted in [1].

The interphase area depends on a coolant flow pattern as follows:

Nucleate regime [2]:

$$a_I = \frac{3\varphi}{r_p} \tag{7}$$

where $r_p = 0.06147 \cdot \dfrac{We_{кр}}{(2\rho_m w_R)^2}$ – Characteristic size of bubbles;

$We_{êð} = 1.24$,

$w_R = w_g - w_l$.

Beam and turbulence regime [3]:

$$a_I = \frac{4.5}{d_\Gamma} \cdot \frac{\varphi - \varphi_{gs}}{1 - \varphi_{gs}} + \frac{3\varphi_{gs}}{r_p} \cdot \frac{1 - \varphi}{1 - \varphi_{gs}} \tag{8}$$

where φ_{gs} – Average steam fraction on a liquid fuse segment.

Annular and disperse-annular regime [3]:

$$a_I = \frac{4\xi_ш}{d_\Gamma} \cdot \sqrt{\frac{\varphi}{1 - \varphi_{ld}}} + \frac{3\varphi_{ld}}{r_p} \cdot \frac{\varphi}{1 - \varphi_{ld}} \tag{9}$$

where φ_{ld} – volumetric drops concentration in the steam kernel;

$\xi_ø$ – the grain parameter.

$$\varphi_{ld} = \frac{E^*(1 - \varphi)}{\varphi} \tag{10}$$

$$E^* = \frac{1}{1 - \left(1 - \dfrac{1}{E}\right)\dfrac{w_d}{w_l}} \text{ – volumetric drops concentration} \tag{11}$$

$$E = 1 - exp\left[-0.23\left(w_g - w_E\right)\right] \text{ – drops fraction} \tag{12}$$

$$w_E = 2.3\left[13\sigma \cdot \left(\frac{\rho_l - \rho_g}{\rho_g^2}\right)\right]^{0.25} \text{ – the drops ablation velocity} \tag{13}$$

Disperse regime [2]:

$$a_I = \frac{3(1-\varphi)}{r_p} \tag{14}$$

where $r_p = 0.06147 \cdot \frac{13 \cdot \sigma}{(2\rho_m w_R)^2}$

2.2. Interface velocity

The interface velocity is generally determined by the friction forces balance equation in couples vapour – interface and fluid – interface:

$$\xi_{Ig}\rho_g(w_g - w_I)^2 - \xi_{II}\rho_l(w_l - w_I)^2 = 0 \tag{15}$$

Which solution has the following aspect:

$$w_I = \frac{\left(\xi_{Ig}\rho_g w_g - \xi_{II}\rho_l w_l\right) - \sqrt{\xi_{Ig}\rho_g \xi_{II}\rho_l}\left(w_g - w_l\right)}{\xi_{Ig}\rho_g - \xi_{II}\rho_l} \tag{16}$$

As reasonable simplification it is possible to suppose that $\xi_{Ig}\rho_g = \xi_{II}\rho_l$. Then the interface velocity is equal:

$$w_I = \frac{w_g - w_l}{2} \tag{17}$$

2.3. Interface mass exchange

There are some various groups of constitutive relations intended for an evaluation of a mass flow through the interface used at a two-fluid models creation for known thermohydraulic codes:

RELAP5/MODL [4]

In a model the empirical relation for steam phase generation intensity in all range of steam fraction is used:

$$\Gamma_g = \frac{-6.45 \cdot 10^{-3}\left[(\rho w)_m + (\rho w)_0\right]^2 \sqrt{p}\left(x + 10^{-5}\right)(x - \tilde{x})}{\rho_g} \tag{18}$$

where $\tilde{x} = \frac{h_{in} - h_l}{r} + \frac{q\pi z}{\omega r}$ – quality;

$(\rho w)_0 = 3500\ kg/(m^2 s)$.

SABENA [5]

$$\tilde{A}_g = -\tilde{A}_l = \tilde{A}_e + \tilde{A}_c \tag{19}$$

where $\frac{p_s}{\sqrt{t_l}} - \frac{p}{\sqrt{t_g}} > 0$

$$\Gamma_e = \lambda_e a_I \varphi_g \varphi_l \left(\frac{M}{2\pi R}\right)^{1/2} \cdot \left(\frac{p_s(t_l)}{\sqrt{t_l}} - \frac{p}{\sqrt{t_g}}\right) \text{è } \tilde{A}_c = 0 \tag{20}$$

in case $\frac{p_s}{\sqrt{t_l}} - \frac{p}{\sqrt{t_g}} \le 0$

$$\Gamma_c = \lambda_c a_I \varphi_g \varphi_l \left(\frac{M}{2\pi R}\right)^{1/2} \cdot \left(\frac{p_s(t_l)}{\sqrt{t_l}} - \frac{p}{\sqrt{t_g}}\right) \text{è } \tilde{A}_e = 0 \tag{21}$$

where $\lambda_{\tilde{n}}$ è λ_e – condensation and evaporation coefficients accordingly.

THERMIT [6]

With allowance for relation (20):

$$\Gamma_e = a_l \begin{cases} 0, \ in \ case \ T_l \le T_d \\ q_w \dfrac{T_l - T_d}{T_s - T_d}, \ in \ case \ T_d < T_l < T_s \\ q_w, \ in \ case \ T_l \ge T_s \end{cases} \tag{22}$$

$$\Gamma_c = a_l \frac{k_l}{0.015 r_b}(t_l - t_w) \tag{23}$$

Where a bubble temperature t_d is calculated by relation:

$$T_s - T_d = \frac{q_w}{\alpha}, \ \alpha = 2.44 \frac{\lambda}{d_\Gamma}\left(\frac{Gd_\Gamma}{\mu}\right)^{1/3} Pr^{1/3}\left(\frac{h_{in}}{h_l}\right)^{1/3}\left(\frac{r}{h_l}\right)^{1/3}$$

There is very simple in a programming context formula for calculation of a mass exchange velocity on the interface [2]:

$$\Gamma_k = \left[(-1)^n \sum_{k=l,g} \alpha_{lk}(t_s - t_k)/r\right] \cdot \frac{s_l}{\omega} \tag{24}$$

where $n = 1$, *in case* $k = g$;
$n = 2$, *in case* $k = l$.

From a mass conservation equation on the interface follows:
$\tilde{A}_{ll} = -\tilde{A}_{lg}$ è $\tilde{A}_l = |\tilde{A}_{lg}|$.

2.4. Interface friction.

The interphase shear stress can be calculated by relation:

$$\tau_{lk} = \xi_{lk} \frac{\rho_k}{2}(w_k - w_l)^2 \tag{25}$$

The interface rate is determined under the formula (17). With allowance for it we have:

$$\tau_{lk} = \xi_l \frac{\rho_k}{8}(w_g - w_l)|w_g - w_l| \tag{26}$$

where ξ_l – the interface friction coefficient which depends on a coolant flow pattern and can be calculated by following relations.

Nucleate regime [7]:

$$\xi_l = \frac{24}{Re} + \frac{4}{\sqrt{Re}} + 0.4 \tag{27}$$

where $Re = \dfrac{2 r_p \rho_c (w_g - w_l)}{\mu_c}$

Slug regime [3]:

$$\xi_l = 9.8(1 - \varphi)^3. \tag{28}$$

Turbulence regime [3]:

$$\xi_l = 0.375(1-\varphi)^2 . \tag{29}$$

Annular regime [4]:

$$\xi_l = \begin{cases} \dfrac{64}{Re_{gl}}, \ in \ \ case \ \ Re_{gl} < 500 \\ \dfrac{64}{Re_{gl}}\left(\dfrac{1500 - Re_{gl}}{1000}\right) + \dfrac{Re_{gl} - 500}{1000} x^{\gamma} \ \ in \ \ case \ \ 500 < Re_{gl} < 1500 \\ 0.02\left[1 + 150\left(1 - \sqrt{\varphi}\right)\right] \ \ in \ \ case \ \ Re_{gl} > 1500 \end{cases} \tag{30}$$

where $Re_{gl} = \dfrac{2\rho_g \, Re(w_g - w_l)}{\mu_c}$;

$$Re = \sqrt{\varphi}\,\frac{d_\Gamma}{2}; \quad \gamma = 0\,02\left[1 + 150\left(1 - \sqrt{\varphi}\right)\right]$$

Disperse regime [8]:

$$\xi_l = \left(\frac{24}{Re} + \frac{4}{\sqrt{Re}} + 0.4\right) K_\varphi K_{wl} K_{Ma} \tag{31}$$

where $K_\varphi = (1-\varphi)^{-2\,7}$ – influence of a disperse phase concentration;

$K_{wl} = exp\left(0.03We_p^{1\,5}\right)$ – influence of a dispersible particles strain;

$K_{Ma} = 1 + exp\left(-\dfrac{0.427}{Ma_c^{4\,63}} - \dfrac{3}{Re_c^{0\,88}}\right)$ – influence of a carrying phase compressibility;

$Ìa_ñ$ – the Makh Number of a carrying phase.

2.5. Wall shear stress of phases.

Generally total two-phase flow friction force on a wall is determined by a relation:

$$\tau_w s_w = \sum_{k=l\,g} \tau_{wk} s_{wk} \tag{32}$$

and $\tau_{wk} = \xi_{wk} \dfrac{\rho_k w_k^2}{8}$

where s_{wk} – wall surface which is in contact with the phase k and relayted to a unit of flow volume.

$$s_{wk} = \frac{4\varphi_k}{D} \ (D - \text{an equivalent pipe diameter}). \tag{33}$$

The friction description for each phase on channel wall assumes evaluation of a total two-phase flow friction force on a wall and consequent separation of this force on component concerning to separate phases. Mechanical interaction of two-phase flow phases with channel walls is investigated very poorly and requires to accept some assumptions. As such an assumption it can be considered, that the vapour friction on a wall in nucleate, slug and disperse-annular regimes is equal to zero. Then the liquid phase friction on a wall is calculated by relations for a total friction force.

Pin bundles [9]:

$$\tau_w = \xi_w \frac{\rho_l w_0^2}{2d_\Gamma}, \tag{34}$$

where

$$\xi_w = \xi'_{wl}\,\psi\left[1 + x\left(\frac{\rho_l}{\rho_g} - 1\right)\right];$$

$$\psi = \left[1 + 0.57\left(\frac{1}{0.2 + k} - 5.2(s/d)^2\right)\cdot(s/d)^{0.125}\cdot\left(1 - (s/d)^2\right)\right]\cdot\left[1 + x\left(\frac{\mu_l}{\mu_g} - 1\right)\right]^{-0.2\,s/d};$$

$$k = \frac{w_0}{\sqrt{g d_r}}\frac{\rho_g}{\rho_l};$$

$w_0 = \frac{\rho w}{\rho_l}$ – circulating velocity;

ξ'_{wl} – the hydraulic resistance coefficient in a bundle for a single-phase flow.

The method of the two-phase flow friction definition on a wall by two-phase factor [2] is very much widespread also:

$$\tau_w = \tau'_l \cdot \Phi_l^2; \tag{35}$$

where τ'_l – wall shear stress of an initial single-phase fluid flow;

$\Phi_l^2 = 1 + \frac{20}{X} + \frac{1}{X^2}$ – two-phase factor;

X – The Martinelly-Lockart parameter which in case of turbulence flow of both fluid and gas can be found by the Blasius law:

$$X^2 = \left(\frac{\mu_l}{\mu_g}\right)^{0.25}\left(\frac{1-x}{x}\right)^{1.75}\frac{\rho_g}{\rho_l}.$$

Another path of approximate exposition of separate phases friction forces on a wall consists of reformulating the problem to appropriate phase flow in some equivalent pipe. In this case the two-phase flow regime is essential.

Disperse regime (nucleate, disperse-drop):

$Re_{ek} = \frac{\rho_k |w_k D}{\mu_k}$ – Reynolds Number for phase flows in equivalent pipes;

$$\xi^L_{wk} = \frac{64}{Re_{ek}} \text{ in case } 1 < Re_{ek} < 2000 \text{ [4]}; \tag{36}$$

$$\frac{1}{\sqrt{\xi^T_{wk}}} = 1.74 - 2\lg\left[\frac{2\varepsilon}{D} + \frac{18.7}{Re_{ek}\sqrt{\xi^T_{wk}}}\right] \text{ in case } Re_{ek} > 4000 \text{ [4]}. \tag{37}$$

In case $2000 < Re_{ek} < 4000$ the friction coefficient can be determined by the linear interpolation on variable $1 / Re_{ek}$ as follows:

$$\xi_{wk} = \left(2 - \frac{4000}{Re_{ek}}\right)\left(\xi^T_{wk} - \xi^L_{wk}\right) + \xi^L_{wk}. \tag{38}$$

Annular regime (slug, annular, disperse-annular):

The area of vapour phase contact with a wall is equal to zero. The Reynolds Number of an equivalent flow only for a liquid phase accordingly is:

$$Re_{el} = \frac{(1-\varphi)\rho_l |w_{l_1} D}{\mu_l};$$

And the calculation of friction factors is calculated by the equations (36) - (38).

2.6. Interface heat exchange.

The heat exchange intensity between phases and interface is characterised by interface heat exchange factors:

$$q_{Ik} = \alpha_{Ik} \cdot (t_I - t_k) \tag{39}$$

where it is possible to consider the interface temperature to be equal to the temperature of saturation ($t_I = t_s$).

The relations for the definition of interface heat exchange factor essentially depend on a two-phase flow pattern. Their analysis is submitted in [10].

Nucleate and slug regimes:

$$\alpha_{Ik} = \frac{Nu_{Ik}\lambda_k}{2r_p} \tag{40}$$

where for the liquid phase:

$$Nu_{II} = Nu_0 + 1.13Pe^2\left(\frac{1}{13Ja^{3.3} + Pe^{1.5}} - \frac{6Ja^{0.63}}{31Ja^{4.3} + Pe}\right);$$

$$Nu_0 = 3.9Ja\left[1 + 0.5\left(Ja \cdot \pi/6\right)^{2/3} + Ja \cdot \pi/6\right];$$

$$Nu_{II} = Pe\sqrt{\frac{4}{\pi}} \text{ in case } Ja << 1,\ Pe >> 1;$$

$$Nu_{II} = 2 + 2\varphi + 22.5\varphi^2 \text{ in case } Ja << 1,\ Pe << 1;$$

$$Pe = 2r_p\frac{|w_l - w_g|}{a_l};$$

$$Ja = \frac{1}{r}\frac{\rho_l}{\rho_g}C_{Pl} \cdot \left(t_l - t_g\right);$$

r_p – characteristic size of bubbles, of which calculation technique is reduced in item 1. for the vapour phase $Nu_{Ig} = 16$.

Disperse-annular regime:

$$\alpha_{II} = \frac{Nu_{II}\lambda_l}{\delta_l} \tag{41}$$

where $Nu_{II} = 1$.

$$\alpha_{Ig} = \frac{Nu_{Ig}\lambda_g}{R - \delta_g} \tag{42}$$

where

$$Nu_{Ig} = \frac{0.023\,Re_g^{0.8}\,Pr_g^{0.4}}{4\delta_l/d_\Gamma}\sqrt{\xi_{Iш}\frac{4\delta_l/d_\Gamma}{\xi_I}};$$

$$Re_g = \rho_g|w_g - w_{l|}\frac{2(R - \delta_l)}{\mu_g};$$

$\xi_{Iø}$ – the interface grain parameter;

δ_l – the fluid film thickness.

2.7. Heat exchange of phases with walls.

The calculation of heat exchange of phases with channel walls is produced by analogy to above mentioned calculation of friction forces that is the summarised heat flow between a wall and coolant is determined and then the distribution of a common flow between phases is:

$$q_w s_w = \sum_{k=l,g} q_{wk} s_{wk} \; ; \tag{43}$$

$$q_w = \alpha_w \cdot (t_w - t_l);$$

$$q_{wk} = \alpha_{wk} \cdot (t_w - t_k).$$

For calculation of the heat transfer coefficient from a wall to a two-phase mixture the following formula [9] can be used:

$$Nu = 0.017\, Re_{cм}^{0.8}\, Pr_w^{0.8}\, Y \tag{44}$$

where:

$$Re_{cм} = \left(\frac{\rho w d}{\mu_g}\right)\left[1 + x\left(\frac{\rho_l}{\rho_g} - 1\right)\right];$$

$$Y = 1 + 0.5\left(\frac{\rho_l}{\rho_g} - 1\right)^{0.8}(1 - x) \text{ in case } \frac{\rho_l}{\rho_g} < 450;$$

$$Y = 1 + 70(1 - x) \text{ in case } \frac{\rho_l}{\rho_g} > 450.$$

For the heat transfer to a vapour [11]:

$$Nu = 0.023\, Re_g^{0.8} \cdot Pr_g^{0.4}$$

2.8. Criteria of the two-phase flow regimes definition.

The calculation of some thermohydraulic characteristics such as length of the interface boundary, interface friction, interface heat exchange, friction of phases with walls is based on the two-phase flow regimes definition. The two-phase flow regimes definition depends on large number of parameters. Therefore, despite of rather large number of researches carried out, the problem of the two-phase flow regimes definition remains now appreciably unsolved. It is the only actual way to describe the boundaries between regimes with the help of approximate maps of pattern. The large number of parameters influencing to a flow regime and their complicated association from each other does not allow to construct a "universal" map of pattern and reduces in a population of pattern maps each of which describes a single class of two-phase flow.

For steam-water flows there is a series of maps used in calculations and empirically obtained relations for delimitation of two-phase flow regimes. In the contrary for a liquid metal two-phase flow there is no pattern map. Therefore it is necessary to investigate the following problem: whether the use of pattern maps obtained for water boiling in calculations of liquid metal two-phase flow characteristics is possible, or in view of the liquid metal boiling process specific feature the construction of a special pattern map is necessary?

As a basis at a construction the pattern map for calculation characteristics of vertical steam-water flows the Bennett pattern map is used [12]. The Bennett pattern map obtained for steam-water flows under high pressure conditions in vertical pipes and shown on fig. 1.

In [13] the pattern map for a vertical two-phase flow constructed on the basis of researches with the laser holography of steam-water flows structural performances is

presented. The pattern map was constructed under the following conditions: in a pipe by a diameter $d = 8.8\ mm$ at pressure $p = 1 \div 6.9\ MPa$, in an annular channel by a diameter $d = 5.5\ mm$ at pressure $p = 1 \div 9.8\ MPa$ (fig. 2).

There are also dimensionless relations for the regimes boundaries:

For the boundary between nucleate and slug regimes:

$$x = \pm 0.01; \tag{45}$$

For a upper bound of the slug regime:

$$x = (4.5 \pm 1.5) \cdot 10^{-2} \left(\frac{(\rho w)^2}{\rho_{l_s}^2 g d_l} \right)^{-0.25}. \tag{46}$$

In spite of the fact that both Bennett pattern maps (fig. 1) and Doroschuk pattern map (fig. 2) are obtained for water boiling under similar conditions of high pressure, the comparison shows their essential difference (fig. 3). It once again proves the statement about a complicated association of a two-phase mixture flow regimes from various thermophysic and hydrodynamic parameters. Though, it is necessary to note, that the Bennett map was constructed in 1965 when the computing tools could not supply necessary accuracy at handling of an experimental material, and the Doroschuk map (1985) was constructed by using the advanced technological developments.

Therefore it is necessary to modificate initial maps with the purpose of a release from an association of some regimes from the most essential defining parameters.

The modification of maps can be carried out in two directions. The first from them: whenever possible it is less deviating from a pre-image to facilitate use of a map in calculated codes by the realisation of the following operations:

- The passage from coordinates (ρW, x) to coordinates (ρW, φ), that probably will allow with smaller errors to describe boundaries between regimes not depending on pressure;
- Simplification of the regimes boundaries representation by direct lines;
- The unity of all regimes at large values φ to an annular regime at which all the fluid is considered to be concentrated in a liquid film on the wall.

The outcome of similar modification of a Bennett map is presented in [14] and is shown on fig. 4. In a similar way it is possible to conduct modification of a Doroschuk map. The problem is that the experimental data used at its construction are obtained for large scale of pressure ($p = 1 \div 9.8\ MPa$). As corollary specified interval of pressure corresponds broad interval of steam density on saturation line which in turn is one of the basic magnitudes at the definition true volumetric steam fraction φ from quality x. Therefore as shown in fig. 5 in an outcome of Doroschuk map modification regimes boundaries are mapped for various pressure ambiguously.

The second direction of modification differs by more significantly simplification of a pattern map rebuilt in coordinates (ρW, φ) and introduction of transitional zones between regimes.

In a fig. 6 and fig. 7 the pattern maps obtained by this method from a Bennett map ([4, 15]) are shown. The slug regime can appreciably be treated as transitional from nucleate to disperse-annular regime (as for example in [15]). Therefore in this case the transitional zone between nucleate and slug regimes is not necessary.

The researches in the liquid metal flows regimes definition are not so rich in experimental and theoretical data. It is enough to say that a pattern map of liquid metal adopted for use in calculated codes similar Bennett map does not exist yet. From experimental

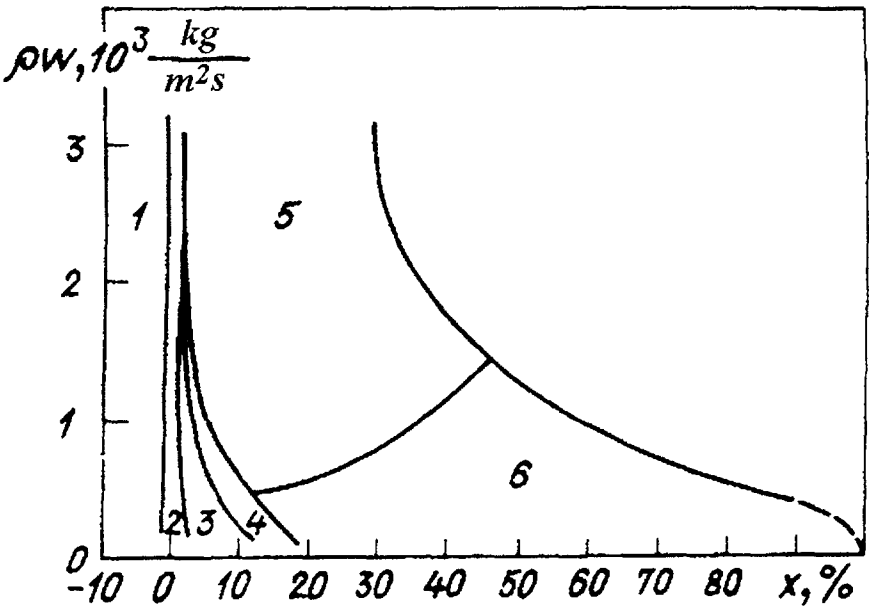

Fig. 1. Bennett pattern map. Regimes:
1 – single-phase flow, 2 – nucleate, 3 – slug, 4 – emulsion, 5– disperse-annular, 6 – annular.

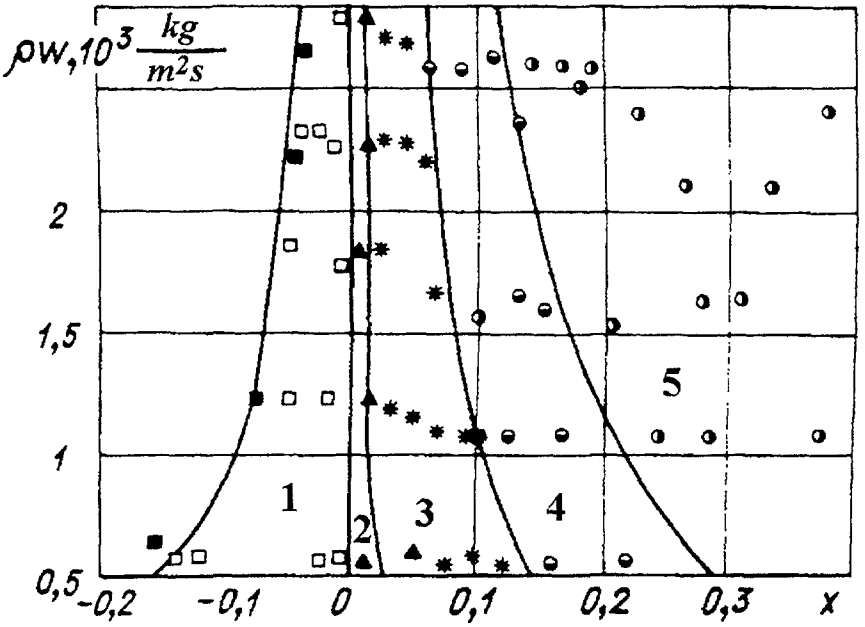

Fig. 2. Doroschuk pattern map. Regimes:
1 – nucleate, 2 – transitional zone, 3 – slug, 4, 5 – disperse-annular.

pattern maps obtained for liquid metal boiling it is possible to reduce a map presented in Yamaguchi paper [16] constructed for $\rho W < 250\ kg/m^2s$ (fig. 8) and a map constructed in IPPE [17] for a large interval of parameters on the basis of experimental data on eutectic alloy sodium-potassium (22%-78%) boiling conditions in the fast reactor core under the natural circulation conditions at pressure 0.6 bars (fig. 9). The comparison between them has shown a good coincidence (fig. 10).

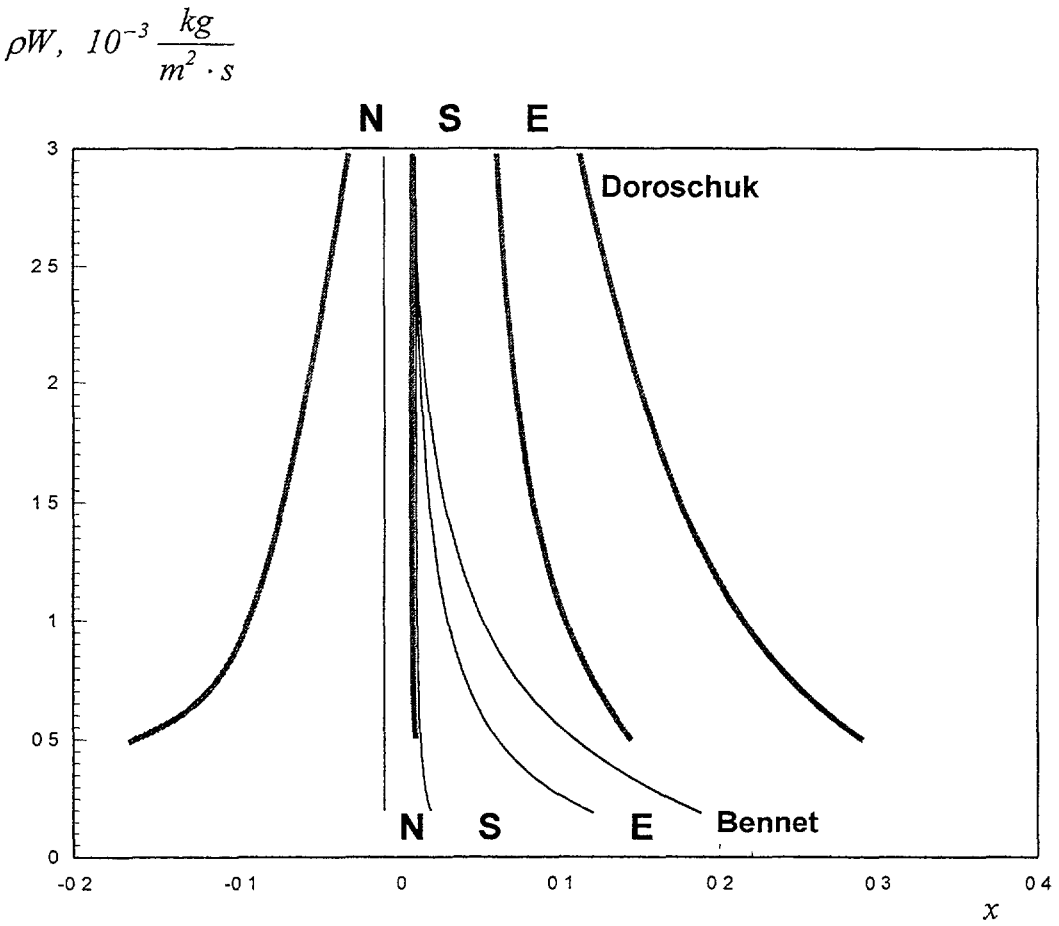

Fig. 3. The comparison of Bennett pattern map and Doroschuk pattern map.
N -- nucleate regime, S -- slug regime, E -- emulsion regime.

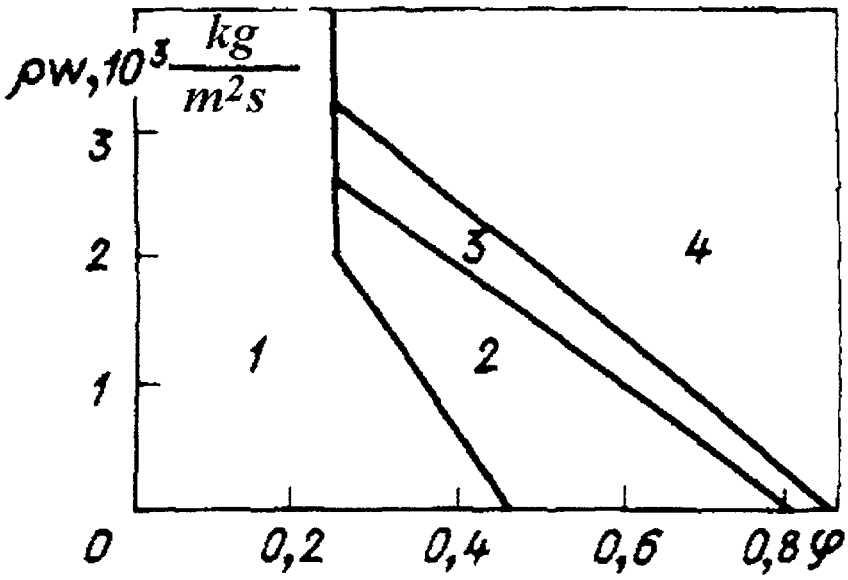

Fig. 4. The Bennett pattern map modified by the first method. Regimes:

1 – nucleate, 2 – slug, 3 – emulsion, 4 – annular.

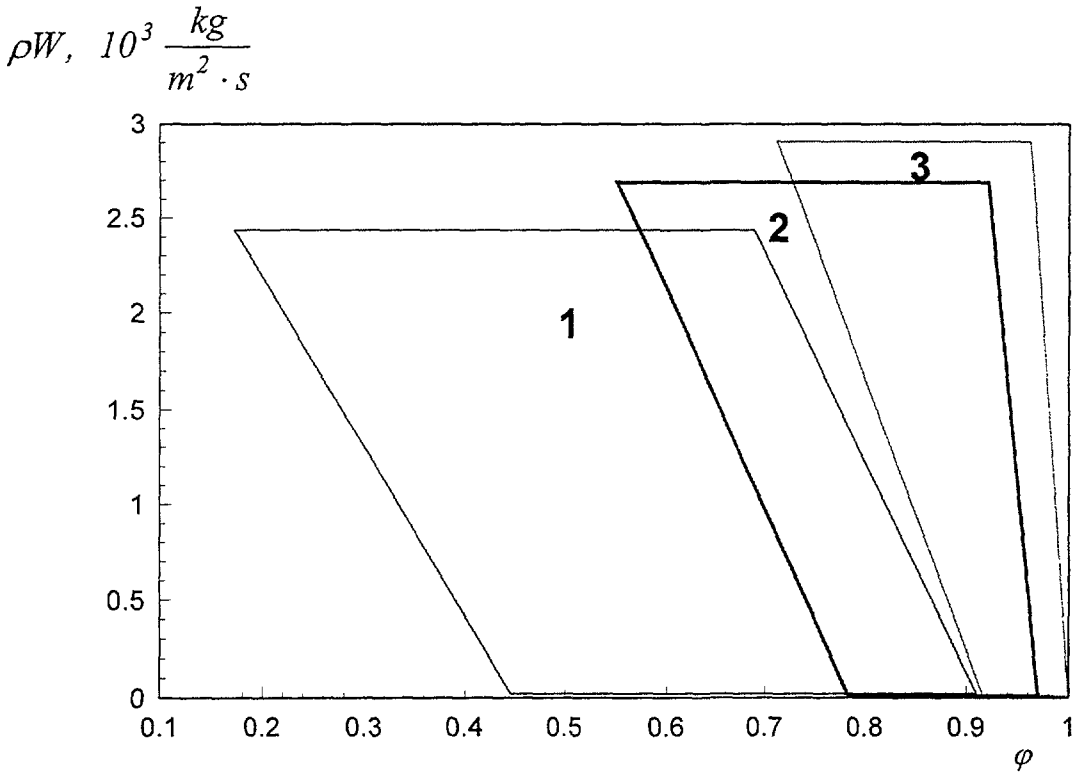

Fig. 5. The Doroschuk pattern map modified by the first method for different pressure magnitudes.
1 -- the boundary between nucleate and slug regimes;
2 -- the boundary between slug regime and disperse-annular regime with waves on the film;
3 -- the boundary between disperse-annular regime with waves on the film and disperse-annular regime with wave-likes on the film;

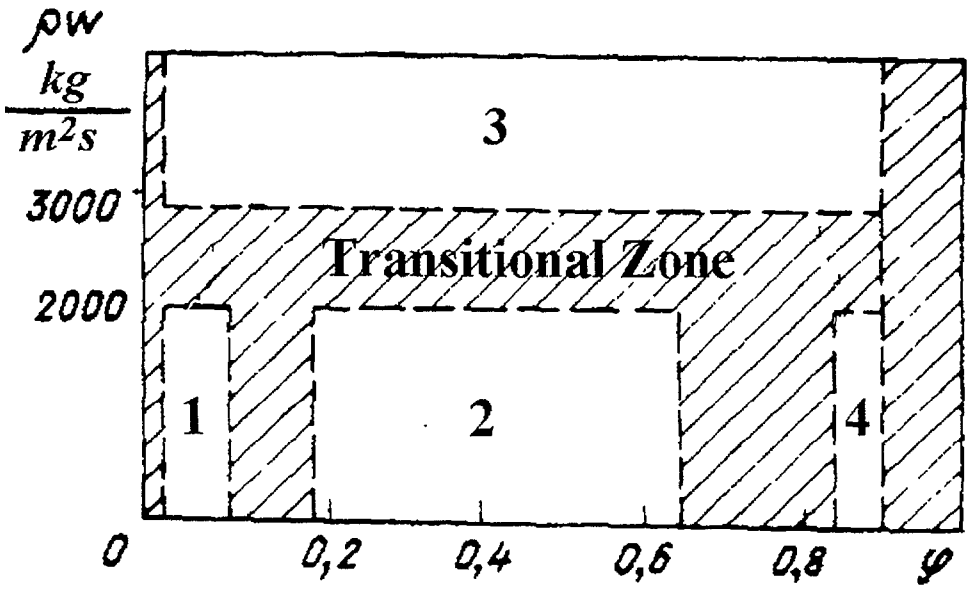

Fig. 6. The Bennett pattern map modified by the second method. Regimes:
1 – nucleate, 2 – slug, 3 – turbulence, 4 – annular.

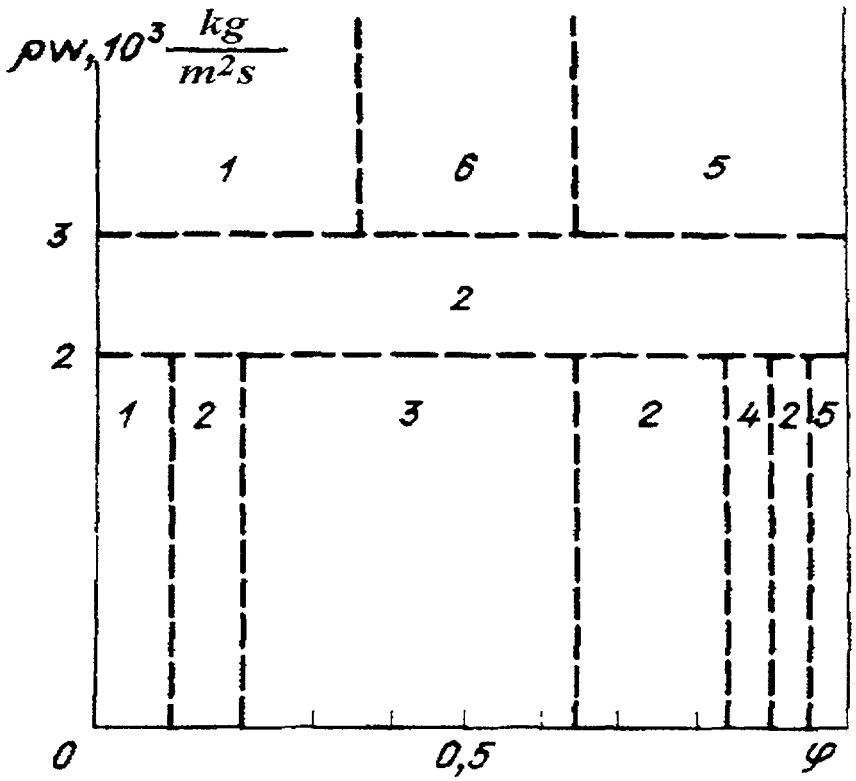

Fig. 7. The Bennett pattern map modified by the second method (for the interphase friction description). Regimes:
1 – nucleate, 2 – transitional zones, 3 – slug, 4 – annular, 5 – disperse, 6 – emulsion.

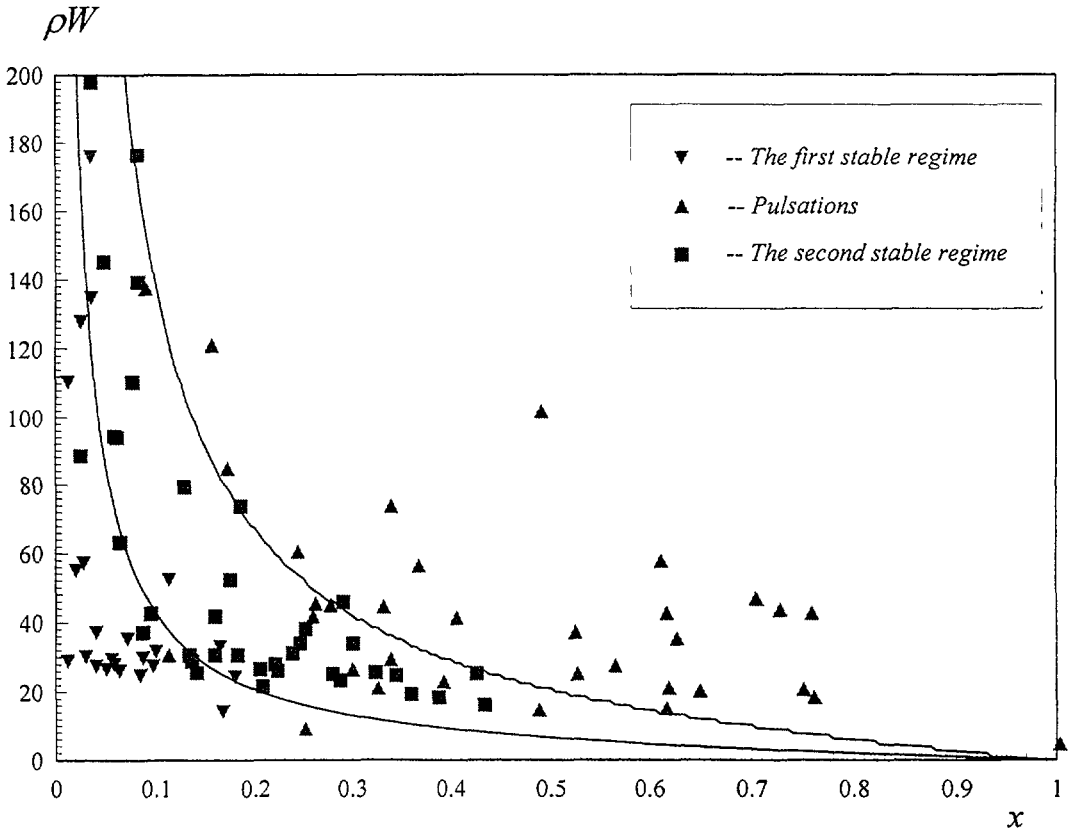

Fig. 8. Experimental pattern map constracted by Yamaguchi.

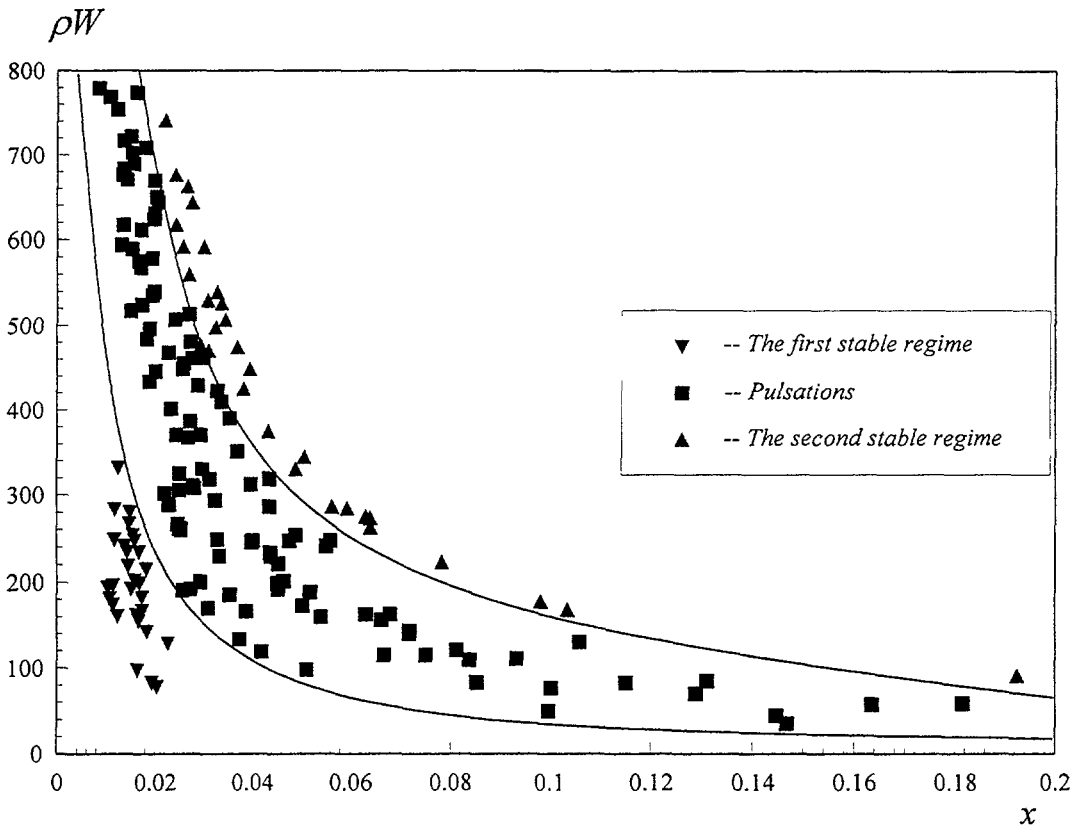

Fig. 9. Experimental pattern map, constracted in IPPE.

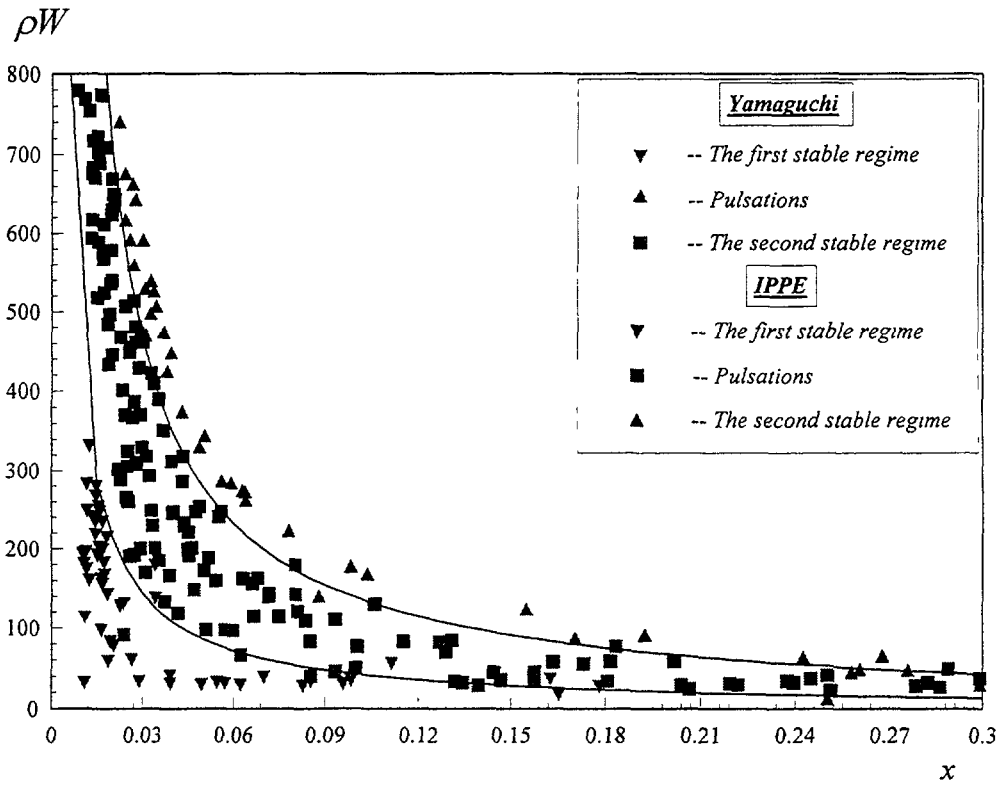

Fig. 10. The comparison of Yamaguchi pattern map and IPPE pattern map

It is necessary to note that the difficulty of regimes identification at realisation of experiments on liquid metals has reduced to the definition of flow regimes by two-phase flow stability criteria. It is known that in liquid metal two-phase flow there are the same regimes as in steam-water flows. In [18] in the analysis of experimental data on sodium boiling presented in [19] three basic boiling regimes are selected: nucleate (small steam fraction values and minor flow rate fluctuations), slug (significant fluctuations of the flow rate), disperse-annular (the drop of fluctuations and passage to stable flow is observed). Proceeding from this for a determinacy as the first approximation it is possible to put in the correspondence the first stable flow to the nucleate regime, unstable regime to the slug regime, the second stable regime to the transitional from slug to disperse-annular regime and disperse-annular regime.

Fig. 11 and 12 demonstrate the difference of Bennett and Doroschuk maps from Yamaguchi and IPPE pattern maps. It confirms the statement about essential association of regimes boundaries on many parameters, in this case from pressure and coolant properties. Hence comparison is necessary to realise on pattern maps modified by the first method and presented in coordinates (ρW, φ). The comparison of a modified Bennett map with an integrated Yamaguchi and IPPE modified map is shown on fig. 13. From fig. 13 it is visible that the modified Bennett map is not necessary for application in the liquid metal two-phase flow calculations. It is impossible adequately to modify a Doroschuk map (fig. 5) in a similar way. Therefore in a plan of calculations is it also unsuitable. Besides on fig. 14 it is shown that the approximating lines designed on the formulas (45), (46) also inadequately describe the liquid metal two-phase flow regimes boundaries.

Thus for calculation of a two-phase liquid metal flow it is necessary to use experimental pattern maps obtained just for liquid metal. We take into account the IPPE pattern map because it is obtained for the greater range of the flow rate and steam fraction magnitude than Yamaguchi pattern map. After excluding from reviewing experimental points

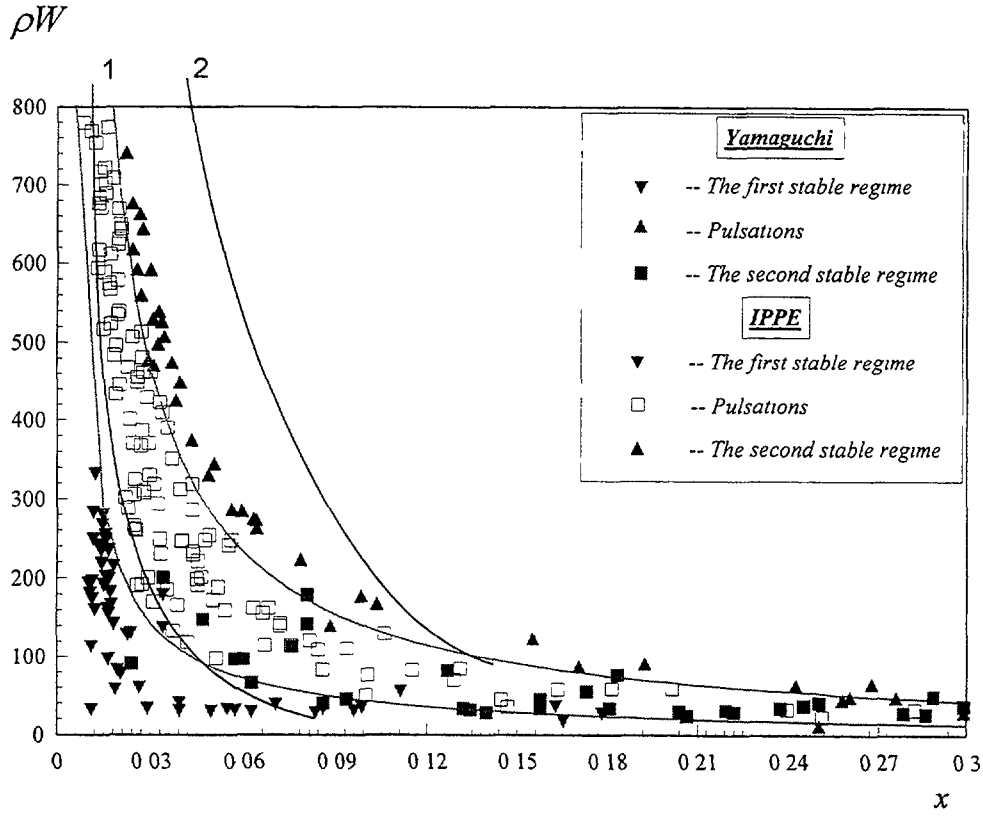

Fig. 11. The comparison of Bennett pattern map and Yamaguchi-IPPE pattern map.
1 -- the boundary between nucleate and slug regimes
2 -- the boundary between slug and emulsion regimes

with leaving only boundaries between regimes and presenting obtained map on the plot in coordinates (ρW, φ) we produce a new pattern map (fig. 15). It can be used in computer codes for calculation of the liquid metal two-phase flow characteristics at atmospheric pressure under the natural circulation conditions in the fast reactor core (heat removal conditions).

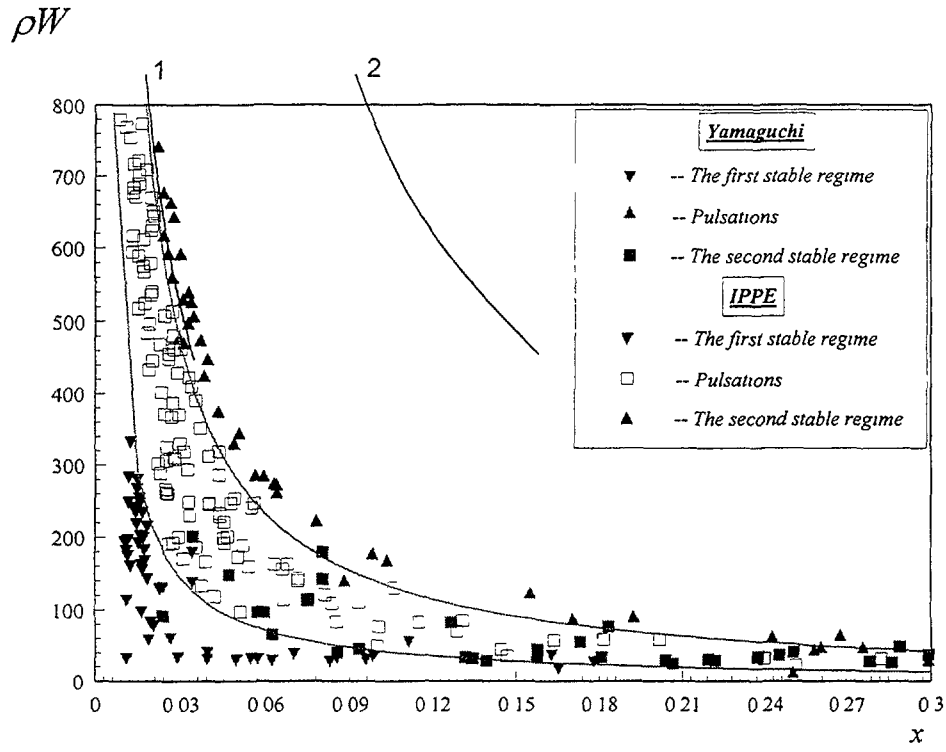

Fig. 12. The comparison of Doroschuk pattern map and Yamaguchi-IPPE pattern map.
1 -- the boundary between nucleate and slug regimes
2 -- the boundary between slug and disperse-annular regimes

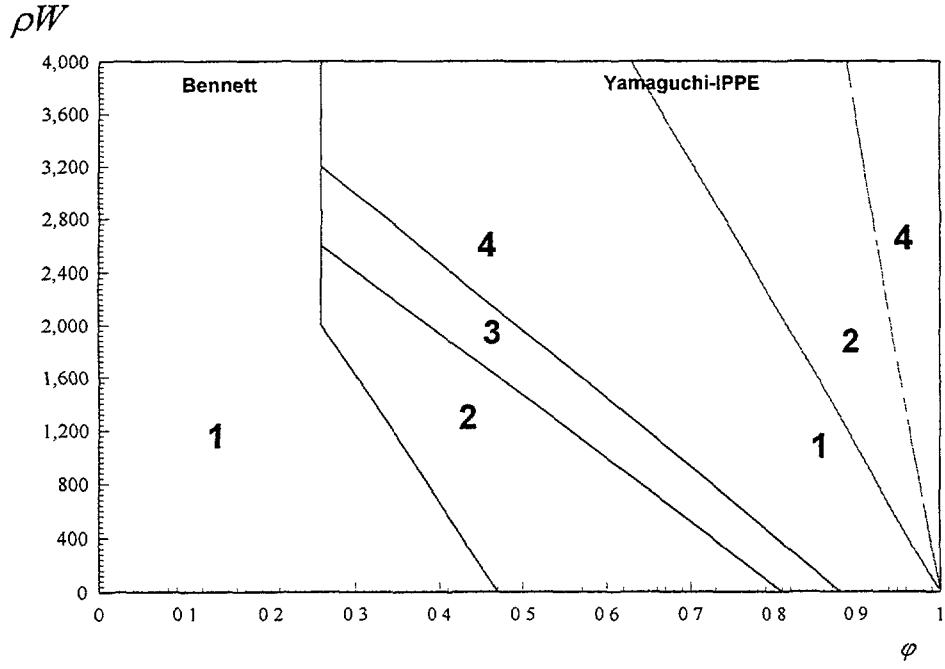

Fig. 13. The comparison of Bennett pattern map
and Yamaguchi-IPPE pattern map modified by the first method.
1 -- nucleate regime; 2 -- slug regime; 3 -- emulsion regime;
4 -- disperse-annular and annular regimes.

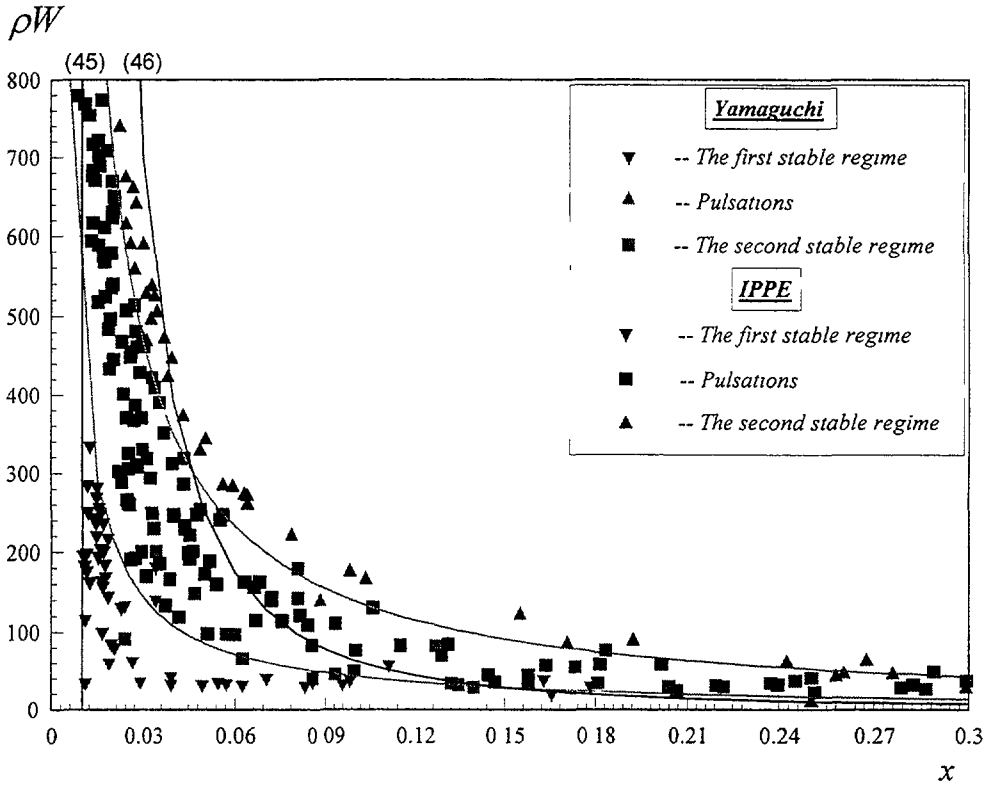

Fig. 14. The comparison of regimes boundaries calculated by formulas (45), (46), and regimes boundaries on the Yamaguchi-IPPE pattern map.

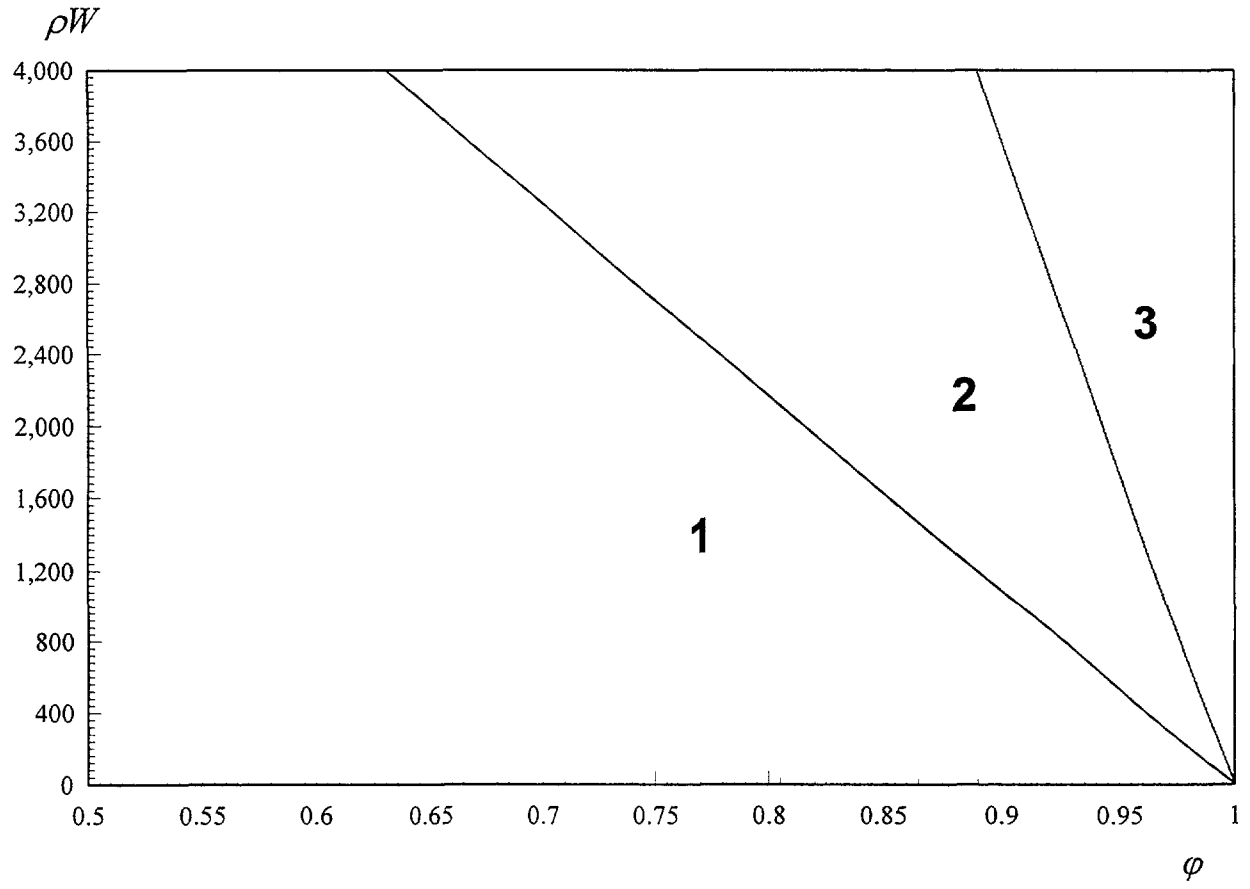

Fig. 15. The IPPE pattern map modified by the first method.
1 -- nucleate regime; 2 -- slug regime; 3 -- disperse-annular and annular regimes.

CONCLUSION

Due to detail phases interaction description and thermohydraulics of non-stationary conditions the two-fluid model is effective in calculations of non-stationary processes in nuclear reactors in various accident situations as compared, for example, with a homogeneous model. The statement of the problem presented in the paper in an approximation of equal pressure both unequal phases velocities and temperatures has the closed system of constitutive relations. This constitutive relations system is used in connection with an adjacent problem of a two-phase flow regimes boundaries definition (in this case for liquid metal flow). The difficulties in a construction of a two-fluid model for exposition of a liquid metal flow are connected basically with insufficient knowledge in the field of interphase interaction characteristics connections. It is necessary to select constitutive relations very accurately, correctly justifying their applicability for the appropriate conditions. Therefore the model presented in this paper requires the careful analysis and checking that it is possible to realise only by means of computer code creation on the basis of this model and its verification on experiments.

REFERENCES

[1] BOGOSLOVSKAYA G.P., BOGATYIRJEV I.L., ZHUKOV A.V., SOROKIN A.P., TITOV P.A. The Interphase Interaction in Two-Phase Gas-Liquid Flows in Channels. IPPE Preprint ¹ 2149, Obninsk, 1990, 43 ps (in Russian).

[2] KOUZNETSOV YU.N. Heat Exchange in the Nuclear Reactor Safety Problem. Moskow, Energoatomisdat, 1989, 296 ps (in Russian).

[3] ISHII M., MASHIMA K. Two-Fluid Model and Hydrodynamic Constitutive Relations // Nuclear Engineering and Design, 1984, v.82, ¹ 1-3, p. 107–126.

[4] RELAP5/MODL. Code Manual. v.1: System Models and Numerical Methods // NUREG/RCR – 1826, 1981.

[5] NINOKATA H., OKANO T. SABENA: Subassembly Boiling Evolution Numerical Analysis // Nuclear Engineering and Design, 1990, v.120, ¹ 3, p. 349–367.

[6] KELLY J.E., KASIMI M.S. Development of the Two-Fluid Multidimentional Code THERMIT for LWR Analysis // Heat Transfer, 1980, v.102, p. 149–162.

[7] NIGMATULLIN R.N. Fundamentals of a heterogeneous mediums mechanics. Moskow, Nauka, 1978 (in Russian).

[8] WALLIS G. One-Dimentional Two-Phase Flows. Moskow, Mir, 1972 (Translated from English to Russian).

[9] KIRILLOV P.L., YURIEV YU.S., BOBKOV V.P. The Hand Book on Thermohydraulic Clculations (nuclear reactors, heatexchangers, steamgenerators). Moskow, Energoatomisdat, 1990 (in Russian).

[10] BOGOSLOVSKAYA G.P., BOGATYIRJEV I.L., ZHUKOV A.V., SOROKIN A.P., TITOV P.A. The Two-Fluid Model for Calculation of Two-Phase Flows in Reactor Fuel Subassemblies (equations, the constitutive relations system). IPPE Preprint ¹ 2166, Obninsk, 1991, 38 ps (in Russian).

[11] BORISHANSKI V.M., KUTATELADZE S.S., NOVIKOV I.I., FEDYNSKI O.S. Liquid Metal Coolants. Moskow, Atomizdat, 1976, 328 ps (in Russian).

[12] BENNETT A.W. et al. Flow Visualisation Studies of Boiling Water at High Pressures // AERE-R4874, 1965.

[13] DOROSCHUK V.E., BOREVSKY L.JA., LEVITAN L.L. Holographic Investigation of Steam-Water Flows in Heated and Unheated Channels // Heat Transfer, Proc. VII Internat. Heat Transfer Conf., Munich, FRG, v. 5, p. 537–553.

[14] SOLBRIG C.W. et al. Heat Transfer and Friction Correlations Required to Describe Steam-Water Behavior in Nuclear Safety Studies // AIChE Symp. Ser. 1978, v. 74, ¹ 174, p. 100–128.
[15] TRAC-PD2. An Advanced Best-Estimate Computer Program for Pressurized Water Reactor Loss-of-Coolant Accident Analysis. // NUREG/CR-2054, 1981.
[16] YAMAGUCHI K. Flow Pattern and Dryout under Sodium Boiling Conditions. // Nuclear Engineering and Design, 1987, v. 99, p. 247–263.
[17] SOROKIN A.P., IVANOV YE.F., MALKOV V.L., KOLESNIK V.P., MARTSINIOUK D.YE., RYMKEVICH K.S., KORKHOV O.A. Experimental Investigations of the Heat Exchange and Stability of the Liquid Metal Boiling in the Natural Circulation Loop. IPPE Preprint ¹ 2631, Obninsk, 1997, 32 ps (in Russian).
[18] ZEIGARNIK YU.A., LITVINOV V.D. The Alcaline Metals Boiling in Channels. Moskow, Nauka, 1983 (in Russian).
[19] KIKUCHI J., HAGA K., TAKAHASHI T. Experimental Study of Steady-State Boiling of Sodium Flowing in a Single-Pin Annular Channel. // J. Nucl. Sci. and Technol., 1975, v. 12, ¹ 2, p. 83–91.

ON DEVELOPMENT OF ANALYTICAL CLOSURE RELATIONSHIPS FOR LOCAL WALL FRICTION, HEAT AND MASS TRANSFER COEFFICIENTS FOR SUB-CHANNEL CODES

Y. KORNIENKO
State Scientific Centre of Russian Federation,
Institute of Physics and Power Engineering,
Obinisk, Kaluga Region, Russian Federation

Abstract

The purpose has been to describe an approach suggested for constructing generalized closure relationships for local and subchannel wall friction, heat and mass transfer coefficients, with not only axial and transversal parameters taken into account, but azimuthal substance transfer effects as well. These constitutive relations that are primary for description of one- and two-phase one-dimensional flow models can be derived from the initial 3-D drift flux formulation. The approach is based on the Reynolds flux, boundary layer and generalized coefficient of substance transfer. One more task has been to illustrate the validity of the "conformity principle" for the limiting cases. The method proposed is based on the similarity theory, boundary layer model, and a phenomenological description of the regularities of the substance transfer (momentum, heat, and mass), as well as on an adequate simulation of the forms of flow structure by a generalized approach to build (an integrated in form and semi-empirical in maintenance structure) analytical relationships for wall friction, heat and mass transfer coefficients.

1. INTRODUCTION

A detailed understanding of the momentum, heat and mass transfer intensities is of great importance for the analysis of complex processes in the transient and abnormal nuclear reactor clustered rod bundles behavior. Also, it is an urgent problem for validation and verification of the closure relationships for such lumped parameters "best estimate" codes as RELAP, TRAC, COBRA, and so on. Averaged by area, the field equations obtained become one-dimensional. Therefore, the information on changes of variables in the direction normal to the main (axial) flow is actually lost. Thus, the transfer of momentum, energy and mass between the wall and fluid should be specified by closure relationships in forms of theoretical, semi-empirical, or empirical correlations.

In the nominal and steady state conditions, the package of friction, heat and mass transfer coefficients have been known well enough. However, as a rule, for complicated conditions (when there are several physical effects in an interaction), the knowledge of closure relationships leaves much to be desired. For example, in the low mass flux tube flow, the friction factor (by homogeneous model) the calculated results appear to be 500-1000% as small as experimental data (Nakorajkov et al, 1980) with saddle-shape void fraction profiles. Frequently rather than not, there appear limitations of experiments and/or lack of measured parameters necessary, that is why it is not possible to estimate individual effects of different phenomena. In particular, in LOCA experiments there were no simultaneous measurements of shear stresses and local void fraction. That is why the anomalous increasing effects of friction and heat transfer (Kornienko, 1997a) were not taken account in the "best estimate" codes. On the other hand, for clarifying such effects and developing the mathematical models for their closure relationships, it is necessary to create simple and appropriate method for description of such transversal profile effects.

It should be noted that a similar situation takes place in the evaluation of the gravity term of the momentum equation at mixed convection (Iannello et al, 1988). In order to properly evaluate this term, the spatially-averaged fluid density must be known. Typically, however, the bulk-averaged (mixing-cup) fluid properties are measured in experiments and

calculated by lumped parameter analysis codes. However, this is the case not only with the density term but also with ones inertial and spatial mass flux gradient ones. Moreover, this is also the case for energy and mass conservation equations. For low mass flux the bulk-averaged and spatially-averaged densities may significantly differ, and thus there is an inherent error introduced by using the bulk density to compute the gravity pressure gradient and other components. Alternatively (Iannello et al, 1988), this error can be eliminated by including a separate correction term in the momentum equation to account for this difference. Instead of correcting both the friction and gravity pressure gradient terms for mixed convection effects, the gravity correction term is included in the friction term. In doing so, a modified friction factor is defined which includes the gravity pressure gradient correction term. In a similar way consideration must be given to the Nusselt (Stanton) numbers for heat and mass transfer processes. The first attempts of such description were described in papers by Kornienko 1995, 1997b for round tube and flat channel, and for subchannel geometry, accordingly.

Moreover, it is important to take into account thermo-physical properties, the contribution of inner sources (sinks) of the substance, flows with injection (suction), two-phase flows and turbulent longitudinal flow through pin bundles. As a rule, the previous analytical descriptions and models (Petukhov, 1987; Novikov and Voskresensky, 1977; Kutateladze and Leont'ev, 1985; Lyon, 1951) were developed for solving certain specific problems and so they are limited by certain sets of assumptions which make possible applications more limited.

Of significant scientific and practical value is the extraction of the analytical and approximate solutions of these problems (or even revealing the conditions for existence of such solutions) that can be implemented only by a generalized formulation of the coefficients sought. Here, the use of the basic three dimensional drift flux model (Ishii, 1975) differential conservation law equations and boundary conditions provide the required completeness of the physical effects taking into account the analytical relationships sought for the above mentioned coefficients.

On the whole, the method proposed is a generalization of the Lyon's integral derivation not only for the heat transfer but for friction and mass-transfer coefficients as well. Besides, the approach expands of the above mentioned methods analytical descriptions with the account of the influence of additional effects, such as substance radial transfer mechanisms (injection and suction flows in their number), contributions of inner sources (or sinks) of the substance and two-phase flows (Kornienko, 1995, 1996, 1997b), effects of transient and azimuthal substance transfer.

The wall friction, heat and mass transfer coefficients local formulation is correlated with averaging of the variables within the boundaries of a small area normal to the channel wall. The local formulation is tightly bound to the subchannel geometry formulation. This work was performed to obtain standard and modified analytical description of the friction factor and Nusselt (Stanton) numbers with take into account the above mentioned separate effects. The general integral descriptions are obtained in non-dimensional forms in providing these results.

2. UNIFIED REPRESENTATION OF PARAMETER PROFILES IN CHANNEL AND SUBCHANNEL CROSS SECTION

Thermal hydraulic design studies of clustered rod bundles with axial flows are carried out using lumped parameter computer codes with segmenting the fuel assembly geometry into a large number of coolant subchannels, see Fig.1. The use of one-dimensional systems of the conservation law equations in such codes requires creating closure relationships for wall friction, heat and mass-transfer coefficients in a wide range of physical phenomena and

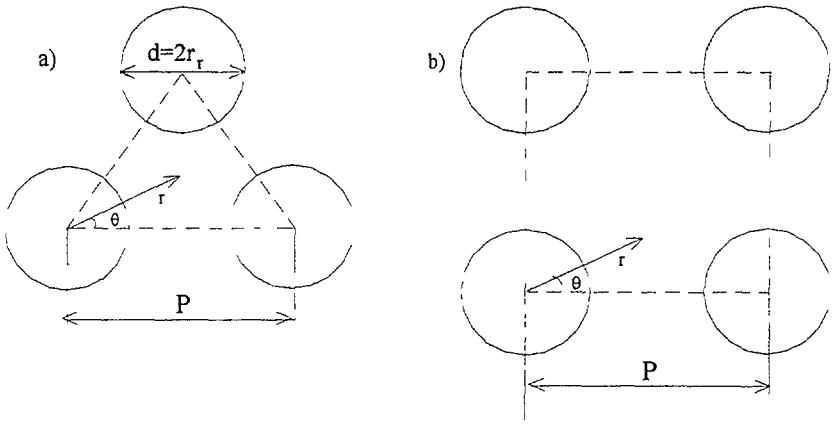

Fig1. Cross-section of an equilateral a) and square b) rod array. P - pitch, r_r - rod radius.

operation conditions for one- and two-phase coolant flows. These closure relationships appearing in the mathematical models depend on both molecular transport properties and the averaging procedures. In general, these terms will depend on the flow geometry, geometric arrangement of the phases, conventionally termed the flow regime, and thus criteria for flow regimes determination (based on predicted quantities) will also be needed.

Experimental data (Ibragimov et al, 1978; Bobkov et al, 1984 and others) shows that velocity and temperature distributions along the normal to wall (even for a complicated subchannel such as cell with dense packaging pin bundles all over) is described with good precision by relationships for round tube. Thus, the hypothesis is valid about universal velocity and temperature distributions in the complicated form channels in just the same way as the round tubes. Practically, one can define thermally and hydraulically interconnected channels (subchannels) connected to a particular fuel element and considering a cluster with an infinite number of fuel rods, see Fig.1.

According to the phenomenological theory of hydrodynamics, heat and mass transfer (Petukhov, 1987; Novikov and Voskresensky, 1977; Reynolds, 1974) used for describing substance, heat and momentum fluxes well-known Fick's, Fourier's and Newton's transfer gradient hypotheses are applied.

For longitudinal flows through unbaffled assemblies of fuel rods with constant cross-sections, the main flow characteristics vary both in axial, radial and azimuthal directions. In particular, flows in the frames of the boundary layer (see Fig.2.) various models may be considered for this type of problem. Then, for fully stabilized flows in channels with a constant cross-section, changes of local value of the S-variable (by which we mean axial velocity, enthalpy or concentration) prove to be identical at every normal to wall of the subchannel and at least linear along the channel, Reynolds (1974). The main assumption is the validity of gradient formulation of substance transfer along the normal to the wetted perimeter.

To unify the designations used and to reduce transpositions in deriving relationships for parameter profiles, as well as friction, heat and mass transfer coefficients, it is helpful to use the concepts of generalized substance transfer coefficients (see Reynolds, 1974) and the gradient transfer model. The mathematical similarity descriptions of the three transfer processes mentioned above (see the top line in TABLEI) make it possible to introduce a formally generalized equation, where the substance flux J is expressed by the transfer characteristic γ_T and the gradient of the transfer potential S normal to wall as:

$$J=\rho\gamma_T\frac{\partial S}{\partial y}, \qquad (1)$$

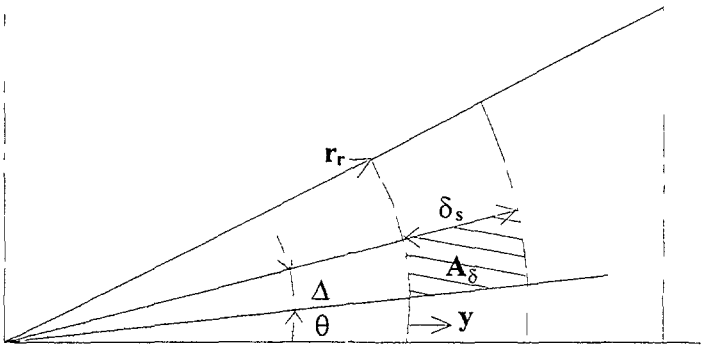

Fig2. Momentum, thermal (or concentrations) boundary layers near the rod of the bundle, not to scale.
r_r - rod radius, θ - azimuthal angle, Δ - increment of the azimuthal angle,
y - coordinate from rod surface and normal to it,
δ_s - substance (momentum, thermal (or concentration)) boundary layer thickness,
A_δ - annular cross sector area.

where $\gamma_T = \gamma + \varepsilon_t$ - total (molecular (γ) + molar (ε_t)) substance transfer characteristic (coefficient), namely, viscosity, thermal conductivity or diffusion coefficient (see the 1-st line in TABLE I). It should be emphasized that in accordance with Boussinesque's idea of expressing the turbulent friction formula in the form of Newton's laminar law, the turbulent heat and mass fluxes are recasted to the form which generalizes Fourier and Fick laws.

After scaling variables in equation (1) with respect to their wall values and after integrating along radius Y we can obtain the profile of variation for any of the potentials under consideration in the channel cross-section if the substance flux and (molecular + molar) transfer characteristics are known. This is expressed by the formula:

$$S_w^+ - S^+ = Pe_{s*} \int_0^Y \frac{\tilde{J}}{\tilde{\rho}\tilde{\gamma}_T} dY \qquad (2)$$

A detailed description of the substance fluxes and the key to decode the designations are quite obvious from the first six lines of TABLE I.

Using definitions in TABLE I, one can easily reconstruct specific relationships for the profiles of axial velocity, enthalpy (temperature) and concentrations from integral (2), see the 2-nd line.

They prove to be a generalization of the relationships obtained by Petukhov (1987) for velocity and temperature profiles that are not limited by assuming that viscous stress distribution is linear.

3. GENERALIZED SUBSTANCE TRANSFER COEFFICIENT

In accordance with the definitions of the wall friction factor and heat- and mass transfer coefficients (Petukhov, 1987; Reynolds, 1974) each of them is a function of the averaging pattern in the cross-section flow profile parameters (velocity, temperature, and concentration, see the 5-th line in TABLE I). For example, local heat-transfer coefficient is

$$\alpha = \frac{dQ_w}{(T_w - T_f)dF} = \frac{q_w}{T_w - T_f}, \qquad (3)$$

TABLE I. FORMULATIONS OF LOCAL SUBSTANCE TRANSFER FLUXES, NUMBERS AND COEFFICIENTS FOR SUBCHANNEL BOUNDARY LAYER MODEL

	Substance flux	Momentum flux	Heat flux	Mass flux
	$J=\rho\gamma_T\frac{\partial S}{\partial y}$	$\tau=\rho\nu_T\frac{\partial w}{\partial y}$	$q=-\rho k_T\frac{\partial h}{\partial y}$	$N=-\rho D_T\frac{\partial c}{\partial y}$
1	Transfer coefficient $\gamma_T=\gamma+\varepsilon_t$; $(\tilde{\gamma}_T=\gamma_T/\gamma_w)$	$\tilde{\nu}_T=\tilde{\nu}+\tilde{\nu}_t$	$\tilde{k}_T=k+\tilde{\nu}_t\ Pr/Pr_t$	$\tilde{D}_T=\tilde{D}+\tilde{\nu}_t\ Sc/Sc_t$
2 Variable S → (w, h, (T), c)	$S_w^+-S^+=\frac{S}{S_*}=Pe_{S_*}\int_0^Y\frac{\tilde{J}}{\tilde{\rho}\tilde{\gamma}_T}dY'$	$w^+=Re_*\int_0^Y\frac{\tilde{\tau}}{\tilde{\rho}\tilde{\nu}_T}dY'$, for $w_w=0$	$h_w^+-h^+=Pe_*\int_0^Y\frac{\tilde{q}}{\tilde{\rho}\tilde{k}_T}dY'$	$c_w^+-c^+=Pe_{D_*}\int_0^Y\frac{\tilde{N}}{\tilde{\rho}\tilde{D}_T}dY'$
3	Substance of friction $S_{*\theta}=J_{w\theta}/(\rho_{w\theta}w_{*\theta})$	$w_{*\theta}^2=\tau_{w\theta}/\rho_{w\theta}$	$h_{*\theta}=q_{w\theta}/(\rho_{w\theta}w_{*\theta})$	$c_{*\theta}=N_{w\theta}/(\rho_{w\theta}w_{*\theta})$
4	Transfer number $Pe_{s\theta}=\prec\rho w\succ\delta_s/(\rho_{w\theta}\gamma_{w\theta})$ $Pe_{s*\theta}=w_{*\theta}\delta_s/\gamma_{w\theta}$	$Re_\theta=\prec\rho w\succ\delta_\tau/(\rho_{w\theta}\nu_{w\theta})$ $Re_{*\theta}=w_{*\theta}\delta_\tau/\nu_{w\theta}$	$Pe_\theta=\prec\rho w\succ\delta_q/(\rho_{w\theta}k_{w\theta})$ $Pe_{*\theta}=w_{*\theta}\delta_q/k_{w\theta}$	$Pe_{D\theta}=\prec\rho w\succ\delta_N/(\rho_{w\theta}D_{w\theta})$ $Pe_{D*\theta}=w_{*\theta}\delta_N/D_{w\theta}$
5	Friction, heat or mass-transfer coefficient	$\zeta_\theta=\frac{\delta\tau_{w\theta}}{\prec\rho\succ(\overline{w}_\theta)^2}=\frac{\delta\tau_{w\theta}}{\prec\rho w\succ\overline{w}_\theta}$	$\alpha_\theta=q_{w\theta}/(\overline{T}_{w\theta}-\overline{T}_{f\theta})$; $St_\theta=\alpha_\theta/\prec\rho w\succ C_p$	$\alpha_{N\theta}=\frac{N_{w\theta}}{c_w-\bar{c}_\theta}$; $St_{D\theta}=\frac{\alpha_{N\theta}}{\prec\rho w\succ}$
6	Reynolds flux $Rm_{s\theta}=J_{w\theta}/\eta(S_{w\theta}-\overline{S}_\theta)$	for $w_w=0$, $Rm_{\tau\theta}=\tau_{w\theta}/\overline{w}_\theta$	$Rm_{q\theta}=q_{w\theta}/(\overline{h}_{w\theta}-\overline{h}_{f\theta})$	$Rm_{N\theta}=N_{w\theta}/(c_{w\theta}-\bar{c}_\theta)$
7	Substance number $Nu_{s\theta}=Pe_{s*\theta}/(\tilde{\eta}(S_{w\theta}^+-\overline{S}_\theta^+))$	for $w_w=0$, $\tilde{\eta}=1$, $\sigma=0$ $Nu_{\tau\theta}=Re_{*\theta}/\overline{w}_\theta^+=\zeta_\theta Re_\theta/8$	for $\sigma=1$, $\tilde{\eta}=C_{pw\theta}/\overline{C}_{p\theta}$ $Nu_{q\theta}=Pe_{*\theta}/((T_{w\theta}^+-\overline{T}_\theta^+)\tilde{\eta})$	for $\sigma=1$, $\tilde{\eta}=1$ $Nu_{N\theta}=Pe_{D*\theta}/(c_{w\theta}^+-\bar{c}_\theta^+)$
8	Stanton number $\frac{1}{St_{s\theta}}=\tilde{\eta}Pe_{s\theta}\int_\theta^{\theta+\Delta l}\int_0^1\frac{\rho w^\sigma}{\prec\rho w^\sigma\succ}\cdot\left[\int_0^Y\frac{\tilde{J}}{\tilde{\rho}\tilde{\gamma}_T}dY'\right](1+2\tilde{\delta}_s Y)dYd\theta$	for $w_w=0$, $\tilde{\eta}=1$, $\sigma=0$ $\frac{1}{\zeta_\theta}=\frac{Re_\theta}{8}\int_\theta^{\theta+\Delta l}\int_0^1\frac{\rho}{\prec\rho\succ}\cdot\left[\int_0^Y\frac{\tilde{\tau}}{\tilde{\rho}\tilde{\nu}_T}dY'\right](1+2\tilde{\delta}_\tau Y)dYd\theta$	for $\sigma=1$, $\tilde{\eta}=C_{pw\theta}/\overline{C}_{p\theta}$ $\frac{1}{St_{q\theta}}=\tilde{\eta}Pe_\theta\int_\theta^{\theta+\Delta l}\int_0^1\frac{\rho w}{\prec\rho w\succ}\cdot\left[\int_0^Y\frac{\tilde{q}}{\tilde{\rho}\tilde{k}_T}dY'\right](1+2\tilde{\delta}_q Y)dYd\theta$	for $\sigma=1$, $\tilde{\eta}=1$ $\frac{1}{St_{D\theta}}=Pe_{D\theta}\int_\theta^{\theta+\Delta l}\int_0^1\frac{\rho w}{\prec\rho w\succ}\cdot\left[\int_0^Y\frac{\tilde{N}}{\tilde{\rho}\tilde{D}_T}dY'\right](1+2\tilde{\delta}_N Y)dYd\theta$
9	Relative transfer laws $\tilde{St}_{s\theta}=\frac{St_{s\theta}}{St_{so\theta}}=\frac{Pe_{o\theta}}{Pe_\theta}\frac{Pe_{*\theta}}{Pe_{*_o\theta}}\frac{S_{wo\theta}^+-\bar{S}}{S_{w\theta}^+-\bar{S}}$	for $w_w=0$, $\sigma=0$, $\tilde{\eta}=1$. $\tilde{\zeta}_\theta=\frac{\zeta_\theta}{\zeta_{o\theta}}=\frac{Re_{o\theta}^2}{Re_\theta^2}\frac{Re_{*\theta}^2}{Re_{*_{o\theta}}^2}\frac{\prec\tilde{\rho}\succ}{\prec\tilde{\rho}\succ_o}$	for $\sigma=1$, $\tilde{\eta}=C_{pw}/\overline{C}_p$. $\tilde{St}_{s\theta}=$ $\frac{St_\theta}{St_{o\theta}}=\frac{Pe_{o\theta}}{Pe_\theta}\frac{Pe_{*\theta}}{Pe_{*_{o\theta}}}\frac{h_{wo\theta}^+-\bar{h}_{o\theta}^+}{h_{w\theta}^+-\bar{h}_\theta^+}$	for $\sigma=1$, $\tilde{\eta}=1$. $\tilde{St}_{D\theta}=$ $\frac{St_{D\theta}}{St_{Do\theta}}=\frac{Pe_{Do\theta}}{Pe_{D\theta}}\frac{Pe_{D*\theta}}{Pe_{D*_{o\theta}}}\frac{c_{wo\theta}^+-\bar{c}_{o\theta}^+}{c_{w\theta}^+-\bar{c}_\theta^+}$

quantities q_w and T_w are taken for surface element dF. But the Newton's law does not determine the selection of the calculation temperature of fluid T_f. In general case of heat transfer by convection the temperature of fluid varies in the space considered. This requires a conventional solution on the fluid temperature to be used for calculation purposes, i.e. to be used in the equation describing Newton's law. It is common practice to use various values of temperature in calculations. For instance, with fluid flowing in tubes, the mean (or bulk-averaged, in western terminology) fluid enthalpy (or temperature) over the cross-section of flow is used

$$\bar{T}_f = \frac{\int_0^A \rho w T dA}{\int_0^A \rho w dA} = \frac{\int_0^{\pi r}\int_0 \rho w T_f 2\pi r dr d\theta}{\int_0^{\pi r}\int_0 \rho w 2\pi r dr d\theta} = \frac{\int_0^{\pi l}\int_0 \rho w T_f 2\pi R dR d\theta}{\int_0^{\pi l}\int_0 \rho w 2\pi R dR d\theta} = \frac{<\rho w T_f>}{<\rho w>}. \tag{4}$$

This definition gives the following usual average heat-transfer coefficient

$$\bar{\alpha} = \frac{\bar{q}_w}{\bar{T}_w - \bar{T}_f}. \tag{5}$$

For local and subchannel geometry in boundary layer frame (see Fig.2) we may take into account the azimuthal coordinate effect by formula for mean (or termed bulk in western countries) fluid temperature over the annular sector

$$\bar{T}_{f\theta} = \frac{\int_0^{A_\delta} \rho w T_f dA}{\int_0^{A_\delta} \rho w dA} = \frac{\int_\theta^{\theta+\Delta}\int_{r_r}^{r_r+\delta_q} \rho w T_f 2\pi(r_r+y) dy d\theta}{\int_\theta^{\theta+\Delta}\int_{r_r}^{r_r+\delta_q} \rho w 2\pi(r_r+y) dy d\theta} = \frac{\int_\theta^{\theta+\Delta}\int_0^1 \rho w T_f (1+2\tilde{\delta}_q Y) dY d\theta}{\int_\theta^{\theta+\Delta}\int_0^1 \rho w (1+2\tilde{\delta}_q Y) dY d\theta} = \frac{\prec \rho w T_f \succ}{\prec \rho w \succ}, \tag{6}$$

where $\tilde{\delta}_q = \frac{\delta_q}{2r_r}$; $Y = \frac{y}{\delta_q}$, with definition of the local heat transfer coefficient

$$\bar{\alpha}_\theta = \frac{\bar{q}_{w\theta}}{\bar{T}_{w\theta} - \bar{T}_{f\theta}}, \tag{7}$$

and with the following relation between average and local heat transfer coefficients

$$\bar{\alpha}_\theta = \bar{\alpha}\frac{\bar{q}_{w\theta}}{\bar{q}_w}\frac{\bar{T}_w - \bar{T}_f}{\bar{T}_{w\theta} - \bar{T}_{f\theta}}. \tag{8}$$

Subscript θ denotes an azimuthal direction. The following nomenclature is used below for the sake of brevity: S - assumes the value of enthalpy - h (or temperature - T) and concentration - c, when σ=1.

$$S_{w\theta} - \bar{S}_\theta = \frac{\int_\theta^{\theta+\Delta}\int_{r_r}^{r_r+\delta_s} \rho w^\sigma (S_w - S) 2\pi(r_r+y) dy d\theta}{\int_\theta^{\theta+\Delta}\int_{r_r}^{r_r+\delta_s} \rho w^\sigma 2\pi(r_r+y) dy d\theta} = \frac{\int_\theta^{\theta+\Delta}\int_0^1 \rho w^\sigma (S_w - S)(1+2\tilde{\delta}_s Y) dY d\theta}{\int_\theta^{\theta+\Delta}\int_0^1 \rho w^\sigma (1+2\tilde{\delta}_s Y) dY d\theta} =$$

$$= \frac{\prec \rho w^\sigma (S_w - S) \succ}{\prec \rho w \succ} \tag{9}$$

The module of the $|S_{w\theta} - \bar{S}_\theta|$ is required for axial velocity w. The mean velocity of flux over the annular sector is

$$\prec \rho w \succ = \frac{\int_{\theta}^{\theta+\Delta}\int_{0}^{\delta_s} \rho w 2\pi(r_r + y)dyd\theta}{\int_{\theta}^{\theta+\Delta}\int_{0}^{\delta_s} 2\pi(r_r + y)dyd\theta} = \frac{1}{A_{\delta_s}} \int_{\theta}^{\theta+\Delta}\int_{0}^{1} \rho w(1 + 2\tilde{\delta}_s Y)dYd\theta , \tag{10}$$

where $A_{\delta_s} = \Delta(1 + \tilde{\delta}_s)$.

Thus when there is no sliding on the wall (for w_w=0) the weighted mean velocity is defined with a density-weighted value

$$\bar{w}_\theta = \frac{\prec \rho w \succ}{\prec \rho \succ}, \tag{11}$$

where mean density over the annular sector is

$$\prec \rho \succ = \frac{\int_{\theta}^{\theta+\Delta}\int_{0}^{\delta_s} \rho 2\pi(r_r + y)dyd\theta}{\int_{\theta}^{\theta+\Delta}\int_{0}^{\delta_s} 2\pi(r_r + y)dyd\theta} = \frac{1}{A_{\delta_s}} \int_{\theta}^{\theta+\Delta}\int_{0}^{1} \rho(1 + 2\tilde{\delta}_s Y)dYd\theta . \tag{12}$$

For the sake of uniformity of these definitions it is expedient to use the Reynolds (1974) flux concept (see, the 6-th line in TABLE I). Then, substance flux can be expressed, in a general form by the formula:

$$J_{w\theta} = \eta Rm_{s\theta}(S_{w\theta} - \bar{S}_\theta). \tag{13}$$

The choice of the sign depends on specific flow conditions, and it is considered to be positive by default. Multiplier η appears for the Reynolds heat flux as the averaged specific heat capacity of the flow for the heat transfer coefficient defined on the basis of Newton-Rikhman's law for friction and mass transfer coefficient considered to be η=1.

By definition the generalized substance transfer coefficient $St_{s\theta}$ is expressed by the relation

$$St_{s\theta} = \frac{Rm_{s\theta}}{\prec \rho w \succ}, \tag{14}$$

using axial velocity of flux $\prec \rho w \succ$.

Elimination of $Rm_{s\theta}$ from equations (13) and (14) results in the following relationship for the generalized substance transfer coefficient:

$$St_{s\theta} = \frac{J_{w\theta}}{\prec \rho w \succ \eta(S_{w\theta} - \bar{S}_\theta)} = \frac{J_{w\theta} \prec \rho w^\sigma \succ}{\prec \rho w \succ \prec \eta(S_{w\theta} - \bar{S}_\theta)\rho w^\sigma \succ}. \tag{15}$$

The physical meaning of $St_{s\theta}$ becomes clear from eq. (14) and (15), which define the generalized substance transfer coefficient (momentum, heat and mass), as a measure of radial-to-axial substance transfer ratio.

4. BASIC INTEGRAL RELATIONSHIP FOR GENERALIZED SUBSTANCE TRANSFER COEFFICIENT

As a result of scaling variables in equation (15), we obtain:

$$\frac{1}{St_{s\theta}} = \prec \tilde{\rho} w^+ \succ \tilde{\eta}(S_w^+ - \bar{S}_\theta^+), \tag{16}$$

where $\prec \tilde{\rho} w^+ \succ = \frac{\prec \rho w \succ}{\rho_{w\theta} w_{*\theta}} = \frac{Pe_{s\theta}}{Pe_{s*\theta}}$, $\quad \tilde{\eta} = \begin{cases} 1 - \text{for friction and mass transfer}, \\ C_{pw\theta} / \bar{C}_{p\theta} - \text{for heat transfer}, \end{cases}$

$$\bar{C}_{p\theta} = \frac{(h_{w\theta} - \bar{h}_{f\theta})}{(T_{w\theta} - \bar{T}_{f\theta})} = \int_{\bar{T}_\theta}^{T_{w\theta}} \frac{C_p dT}{(T_{w\theta} - \bar{T}_{f\theta})}. \tag{17}$$

Substituted integral relationship for the substance profile (2) taking account of eq. (9) or (11) into relationship (16) render the integral form of the generalized coefficient of substance transfer

$$\frac{1}{St_{s\theta}}=Pe_{s\theta}\tilde{\eta}\int_{\theta}^{\theta+\Delta 1}\int_{0\prec\rho w^{\sigma}\succ}^{1}\frac{\rho w^{\sigma}}{\left(\int_{0}^{Y}\frac{\tilde{J}}{\tilde{\rho}\tilde{\gamma}_{T}}dY'\right)}(1+2\tilde{\delta}_{s}Y)dYd\theta\,. \tag{18}$$

Thus $St_{s\theta}$ is expressed by means of the local substance flux J profile, local physical properties η, ρ, w, and total (molecular + molar) transfer characteristics γ_{T}. It should be stressed that eq. (18) is universal, i.e. inserting appropriate fluxes and substance characteristics transforms it into the friction, heat-and mass transfer coefficients. This can be easily verified by using definitions given in TABLE I.

However, unlike (Petukhov, 1987), integral relationships for the coefficients mentioned above (see 7-th and 8-th lines of TABLE I) are not limited by assuming a linear distribution of viscous stresses along the normal to wall.

Introducing the "standard" (reference) condition concept (the lower index "o"), one can construct a generalized relative integral form for the substance transfer coefficients considered, namely, wall friction, heat and mass transfer factors:

$$\frac{St_{s\theta}}{St_{so\theta}}\frac{Pe_{s\theta}}{Pe_{so\theta}}=\frac{\tilde{\eta}_{o}}{\tilde{\eta}}\int_{\theta}^{\theta+\Delta}\int_{0\prec\rho w^{\sigma}\succ_{o}/\prec\rho w^{\sigma}\succ}^{1}\frac{(\rho w^{\sigma})_{o}/(\rho w^{\sigma})}{\left(\int_{0}^{Y}\frac{\tilde{\rho}/\tilde{\rho}_{o}(\tilde{\gamma}_{T}/\tilde{\gamma}_{To})}{\tilde{J}/\tilde{J}_{o}}dY'\right)}(1+2\tilde{\delta}_{s}Y)dYd\theta\,. \tag{18a}$$

It is clear that in order to obtain a specific form for the particular transfer law one should have full information about the density distributions, mass velocity, the substance flux being transferred and also about turbulent transfer coefficients.

Relative laws of substance transfer can be written in an alternative form based on eq.(16):

$$\tilde{St}_{s}=\frac{St_{s}}{St_{so}}=\frac{\prec\tilde{\rho}w^{+}\succ\tilde{\eta}_{o}(S^{+}_{w\theta}-\bar{S}^{+}_{o\theta})}{\prec\tilde{\rho}w^{+}\succ\tilde{\eta}\,(S^{+}_{w\theta}-\bar{S}^{+}_{\theta})}=\frac{Pe_{o\theta}}{Pe_{\theta}}\frac{Pe_{*\theta}}{Pe_{*o\theta}}\frac{\tilde{\eta}_{o}}{\tilde{\eta}}\frac{S^{+}_{wo\theta}-\bar{S}^{+}_{o\theta}}{S^{+}_{w\theta}-\bar{S}^{+}_{\theta}}\,. \tag{18b}$$

The final expression of the wall friction, heat and mass transfer laws is given in the 9-th line of TABLE I.

5. SUBSTANCE FLUX DISTRIBUTION

To have a possibility to extend the method being developed to two-phase flows it is convenient to use the conservation laws in a form equally acceptable both for one-phase and two-phase flows. For this purpose it appears expedient to describe the two-phase flow on the basis of the drift flux model of Ishii (1975). TABLE II shows the drift flux model modified in accordance with the purposes of the present paper. The law of the light phase propagation is described by the convective diffusion equation. The conservation laws equations are used in a non-conservative form. Here for the sake of the two-phase flows conditions we should regard density ρ, mass velocity ρu and enthalpy h as their two-phase characteristics, defined in the right part of TABLE II. The terms with subscript "d" that take into account the light phase drift are added to the corresponding turbulent substance fluxes with the subscript "t". The additional acceleration due to vapor formation at the phase interface can be written together with the hydrostatic component. Thus we obtain the form which is identical both for the one-phase and two-phase flows.

TABLE II. NON-CONSERVATIVE (TRANSPORTABLE) FORMS OF CONSERVATION LAW EQUATIONS, TWO-PHASE FLOW DESCRIPTION IS BASED ON DRIFT FLUX MODEL OF ISHII (1975).

Field equations of:	Definitions of parameters
general form: $\rho\frac{\partial S}{\partial t}+\rho\vec{u}\cdot\nabla S=-\nabla\cdot(\tilde{\tilde{J}})+I_v$,	
mixture continuity: $\frac{\partial\rho}{\partial t}+\nabla\cdot(\rho\vec{u})=0$,	$\rho=(\varphi\rho)_g+(\varphi\rho)_f$; $\rho\vec{u}=(\varphi\rho\vec{u})_g+(\varphi\rho\vec{u})_f$; where $\varphi_g=1-\varphi_f$.
convective diffusion: $\rho\frac{\partial c}{\partial t}+\rho\vec{u}\cdot\nabla c=-\nabla\cdot(\vec{N}_T)+\tilde{\Gamma}$,	$C=(\varphi\rho)_g/\rho$, $\vec{N}_T=\vec{N}_t+\vec{N}_d$; $\vec{N}_d=c(\varphi\rho)_g\vec{u}_{gf}$; $\vec{u}_{gf}=\vec{u}_g-\vec{u}_f$.
mixture energy: $\rho\frac{\partial h}{\partial t}+\rho\vec{u}\cdot\nabla h=-\nabla\cdot(\vec{q}_T)+q_v$,	$h=[(\varphi\rho h)_g+(\varphi\rho h)_f]/\rho$; $\vec{q}_T=\vec{q}_t+\vec{q}_d$; $\vec{q}_d=c\rho_f\vec{u}_{gf}(h_g-h_f)$.
mixture momentum: $\rho\frac{\partial\vec{u}}{\partial t}+\rho\vec{u}\cdot\nabla\vec{u}=\nabla\cdot(\tilde{\tilde{\tau}}_T)-\nabla P+\rho\vec{g}_T$.	$\vec{u}=[(\varphi\rho\vec{u})_g+(\varphi\rho\vec{u})_f]/\rho$; $\tilde{\tilde{\tau}}_T=\tilde{\tilde{\tau}}_t+\tilde{\tilde{\tau}}_d$; $\tilde{\tilde{\tau}}_d=\frac{c}{1-\varphi}\rho_f\vec{u}_{gf}\vec{u}_{gf}$; $\rho\vec{g}_T=\rho(\vec{g}+\frac{\tilde{\Gamma}}{\rho}\vec{u}_{gf})$.

Further, we shall confine our to consideration to transient flow conditions for cylindrical coordinates (z-r-θ) geometry. Using the boundary layer approximation we can write the conservation law equations presented in TABLE II in a generalized and unified form by means of the single substance transfer equation:

$$\frac{1}{r}\frac{\partial}{\partial y}(rJ_{y\theta})=\rho w\frac{\partial S}{\partial z}+\rho v\frac{\partial S}{\partial y}+\rho v_\theta\frac{1}{r}\frac{\partial w}{\partial\theta}-\frac{1}{r}\frac{\partial J_\theta}{\partial\theta}-I_{v\theta}+\rho\frac{\partial S}{\partial t}, \tag{19}$$

where w - axial, v - radial, v_θ - azimuthal velocities, J_θ - azimuthal substance flux. In the present paper the source term $I_{v\theta}$ unites the pressure gradient and hydrostatic component in the motion equation, whereas in the energy and mass transfer equation it is the heat and mass source (sink).

After scaling the variables in eq. (19) we obtain

$$\frac{1}{1+2\tilde{\delta}_sY}\frac{\partial(1+2\tilde{\delta}_sY)\tilde{J}_{y\theta}}{\partial Y}=\tilde{\rho}w^+\frac{\partial S^+}{\partial\tilde{z}}+\tilde{\rho}v^+\frac{\partial S^+}{\partial Y}+\frac{\tilde{\rho}v_\theta^+}{1+2\tilde{\delta}_sY}\frac{\partial S^+}{\partial\theta}-\frac{1}{1+2\tilde{\delta}_sY}\frac{\partial\tilde{J}_\theta}{\partial\theta}-\tilde{I}_{v\theta}+\frac{\tilde{\rho}}{Sr_*}\frac{\partial S^+}{\partial\tilde{t}}, \tag{20}$$

where $\tilde{I}_{v\theta}=I_{v\theta}\frac{\delta_s}{J_{w\theta}}$, $\tilde{z}=\frac{z}{\delta_s}$, $\tilde{\delta}_s=\frac{\delta_s}{2r_r}$, $Y=\frac{y}{\delta_s}$, $\tilde{J}_\theta=\frac{J_\theta}{J_{w\theta}}$, $Sr_*=\frac{t_0W_*}{\delta_s}$, $\tilde{t}=\frac{t}{t_0}$,

$t_t<<t_0<t_{tr}$.

Here t_{tr} - transport time, t_t - turbulent pulsation period.

Having integrated the latter equation first with the variable upper limit Y and then up to the boundary layer Y=1 and having combined the integrals obtained we can derive the equation for the local substance flux:

$$\tilde{\tilde{J}}_{Y\theta}=\left[1-Y(1+\tilde{\delta}_sY)\left(\frac{1}{1+\tilde{\delta}_s}+\prec Sz\succ-\prec Sz\succ_Y+\prec Sn\succ-\prec Sn\succ_Y+\prec Si\succ-\prec Si\succ_Y+\right.\right.$$
$$\left.\left.\tilde{\delta}_s\left(\prec S\theta\succ-\prec S\theta\succ_Y+\prec\frac{\partial\tilde{\tilde{J}}_\theta}{\partial\theta}\succ-\prec\frac{\partial\tilde{\tilde{J}}_\theta}{\partial\theta}\succ_Y\right)-\prec\tilde{\tilde{I}}_{v\theta}\succ+\prec\tilde{\tilde{I}}_{v\theta}\succ_Y\right)\right]\frac{1}{1+\tilde{\delta}_sY}, \tag{21}$$

here we use the following designations for the sake of brevity:

$$\prec Sz \succ = \frac{1}{A_{\delta_s}} \int_{\theta}^{\theta+\Delta 1} \int_{0}^{1} \tilde{\rho} w^{+} \frac{\partial S^{+}}{\partial \tilde{z}} (1 + 2\tilde{\delta}_s Y) dY d\theta \tag{22}$$

$$\prec Sz \succ_Y = \frac{1}{A_Y} \int_{\theta}^{\theta+\Delta Y} \int_{0}^{Y} \tilde{\rho} w^{+} \frac{\partial S^{+}}{\partial \tilde{z}} (1 + 2\tilde{\delta}_s Y) dY d\theta , \tag{23}$$

$$\prec Sn \succ = \frac{1}{A_{\delta_s}} \int_{\theta}^{\theta+\Delta 1} \int_{0}^{1} \tilde{\rho} v^{+} \frac{\partial S^{+}}{\partial Y} (1 + 2\tilde{\delta}_s Y) dY d\theta , \tag{24}$$

$$\prec Sn \succ_Y = \frac{1}{A_Y} \int_{\theta}^{\theta+\Delta Y} \int_{0}^{Y} \tilde{\rho} v^{+} \frac{\partial S^{+}}{\partial Y} (1 + 2\tilde{\delta}_s Y) dY d\theta , \tag{25}$$

$$\prec S\theta \succ = \frac{1}{A_{\delta_s}} \int_{\theta}^{\theta+\Delta 1} \int_{0}^{1} \tilde{\rho} v_{\theta}^{+} \frac{\partial S^{+}}{\partial \theta} dY d\theta , \tag{26}$$

$$\prec S\theta \succ_Y = \frac{1}{A_Y} \int_{\theta}^{\theta+\Delta Y} \int_{0}^{Y} \tilde{\rho} v_{\theta}^{+} \frac{\partial S^{+}}{\partial \theta} dY d\theta , \tag{27}$$

$$\prec Si \succ = \frac{1}{Sr_* A_{\delta_s}} \int_{\theta}^{\theta+\Delta 1} \int_{0}^{1} \tilde{\rho} \frac{\partial S^{+}}{\partial \tilde{t}} (1 + 2\tilde{\delta}_s Y) dY d\theta , \tag{28}$$

$$\prec Si \succ_Y = \frac{1}{Sr_* A_Y} \int_{\theta}^{\theta+\Delta Y} \int_{0}^{Y} \tilde{\rho} \frac{\partial S^{+}}{\partial \tilde{t}} (1 + 2\tilde{\delta}_s Y) dY d\theta , \tag{29}$$

$$\prec \frac{\partial \tilde{\tilde{J}}_{\theta}}{\partial \theta} \succ = \frac{1}{A_{\delta_s}} \int_{\theta}^{\theta+\Delta 1} \int_{0}^{1} \frac{\partial \tilde{\tilde{J}}_{\theta}}{\partial \theta} dY d\theta , \tag{30}$$

$$\prec \frac{\partial \tilde{\tilde{J}}_{\theta}}{\partial \theta} \succ_Y = \frac{1}{A_Y} \int_{\theta}^{\theta+\Delta Y} \int_{0}^{Y} \frac{\partial \tilde{\tilde{J}}_{\theta}}{\partial \theta} dY d\theta , \tag{31}$$

$$\prec \tilde{\tilde{I}}_{v\theta} \succ = \frac{1}{A_{\delta_s}} \int_{\theta}^{\theta+\Delta 1} \int_{0}^{1} \tilde{\tilde{I}}_{v} (1 + 2\tilde{\delta}_s Y) dY d\theta , \tag{32}$$

$$\prec \tilde{\tilde{I}}_{v\theta} \succ_Y = \frac{1}{A_Y} \int_{\theta}^{\theta+\Delta Y} \int_{0}^{Y} \tilde{\tilde{I}}_{v} (1 + 2\tilde{\delta}_s Y) dY d\theta . \tag{33}$$

It should be remembered that $A_{\delta_s} = \Delta(1 + \tilde{\delta}_s)$; $A_Y = \Delta \cdot Y(1 + \tilde{\delta}_s Y)$.

Relationship (21) describing the radial distribution of the substance flux being transferred, and equations (2) and (18) enable us to calculate radial profiles and generalized substance transfer coefficients. As one can see from equation (21), the contribution of each of the effects under consideration (convective axial, radial and azimuthal directions transfer, inertial term, sources (sinks), etc.) to the substance flux being transferred can be described as a correction for the linear distribution. It is obvious that when the boundary layer is very thin, $\tilde{\delta}_s << 1$. Then, we see just a small correction for linear flux distribution $\tilde{\tilde{J}}_{y\theta}$ accounting for the influence of above-mentioned transversal profile terms.

6. ANALYTICAL RELATIONSHIPS FOR SUBCHANNEL WALL FRICTION FACTOR, HEAT AND MASS TRANSFER COEFFICIENTS

Assuming that the axial pressure gradient does not change in the annular sector, we can obtain the following relationship for the wall friction factor from equations (21) and (18):

$$\frac{8}{\zeta_{\theta}} = \mathrm{Re}_{\theta} \int_{\theta}^{\theta+\Delta 1} \int_{0}^{1} \frac{\rho}{\prec \tilde{\rho} \succ} \left(\int_{0}^{Y} \left\{ 1 - Y(1 + \tilde{\delta}_{\tau} Y) \left[\frac{1}{1 + \tilde{\delta}_{\tau}} - \frac{\prec \tilde{\rho} \succ}{Fr_{*\theta}} - \prec Wz \succ - \prec Vn \succ - \prec Wi \succ \right. \right. \right.$$

$$\left. \left. \left. - \tilde{\delta}_{\tau} \left(\prec V\theta \succ - \prec \frac{\partial \tilde{\tilde{\tau}}_{\theta}}{\partial \theta} \succ \right) \right. \right. \right. +$$

$$+\frac{\prec\tilde{\rho}\succ_Y}{Fr_{*\theta}}+\prec Wz\succ_Y+\prec Vn\succ_Y+\prec Wi\succ_Y+\tilde{\delta}_\tau\left(\prec V\theta\succ_Y-\prec\frac{\partial\tilde{\bar{r}}_\theta}{\partial\theta}\succ_Y\right)\Bigg]\Bigg\}\frac{dY}{\tilde{\rho}\tilde{v}_T(1+2\tilde{\delta}_\tau Y)}\Bigg)$$

$$(1+2\tilde{\delta}_\tau Y)dYd\theta \tag{34}$$

where integrals $\prec Wz\succ$, $\prec Vn\succ$, $\prec V\theta\succ$, $\prec Wi\succ$ are relationships (22)-(29) in substituting velocity for variable S and

$$\prec\tilde{\rho}\succ_Y=\frac{1}{A_Y}\int_\theta^{\theta+\Delta}\int_0^Y\tilde{\rho}(1+\tilde{\delta}_\tau Y)dYd\theta\,, \tag{35}$$

$$Fr_{*\theta}=\frac{\tau_{w\theta}}{\rho_{w\theta}\,g\,r_w}\,. \tag{36}$$

It is true to say that equation (34) generalizes the integral obtained by Petukhov-Popov (Petukhov, 1987) for the friction factor not only with respect to the functional way of taking into account the profile density. This equation takes into account the axial $\prec Wz\succ$, and radial $\prec Vn\succ$, and azimuthal $\prec V\theta\succ$, and inertial $\prec Wi\succ$ flow accelerations, generalizing at the same time two-phase flow model by Sato et al (1981).

Assuming as above that the axial enthalpy (and concentration) gradients are not the function of the radial coordinate, we can obtain the following expression from eq. (21) and (18):

$$\frac{1}{St_\theta}=Pe_\theta\tilde{\eta}\int_\theta^{\theta+\Delta}\int_0^1\frac{\rho w}{\prec\rho w\succ}\Bigg(\int_0^Y\Big[1+\prec Hn\succ_Y-\prec Hi\succ_Y-\prec\tilde{\bar{q}}_v\succ_Y+\tilde{\delta}_q(\prec H\theta\succ_Y+\prec\frac{\partial\tilde{q}_\theta}{\partial\theta}\succ_Y)-\big(1-\prec Hn\succ-\prec Hi\succ$$

$$+\prec\tilde{\bar{q}}_v\succ-\tilde{\delta}_q(\prec H\theta\succ+\prec\frac{\partial\tilde{q}_\theta}{\partial\theta}\succ)\Big)\int_0^Y\frac{\rho w(1+2\tilde{\delta}_q Y)dY}{\prec\rho w\succ}\Big]\frac{dY}{\tilde{\rho}\tilde{k}_T(1+2\tilde{\delta}_q Y)}\Bigg)(1+2\tilde{\delta}_q Y)dYd\theta\,, \tag{37}$$

where integrals $\prec Hn\succ$, $\prec H\theta\succ$, $\prec Hi\succ$ are identical to relationships (24)-(29) when h is substituted for S and

$$\prec\tilde{\bar{q}}_{v\theta}\succ=\frac{1}{A_{\delta_q}}\int_\theta^{\theta+\Delta}\int_0^1\tilde{\bar{q}}_{v\theta}(1+\tilde{\delta}_\tau Y)dYd\theta\,, \tag{38}$$

$$\prec\tilde{\bar{q}}_{v\theta}\succ_Y=\frac{1}{A_Y}\int_\theta^{\theta+\Delta}\int_0^Y\tilde{\bar{q}}_{v\theta}(1+\tilde{\delta}_\tau Y)dYd\theta\,. \tag{39}$$

The relationship for the mass transfer coefficient $St_{D\theta}$ is functionally fully identical to eq. (37), differing only by $\tilde{\eta}=1$ factor. The comparison of equation (37) obtained with the relationships found in references (Petukhov, 1987; Novikov and Voskresensky, 1977; Kutateladze and Leont'ev, 1985; Lyon, 1951) enables us to conclude that it is actually a generalization of Lyon's integral for flows with allowance for injection (suction), the inner heat sources (sinks), as well as azimuthal substance transfer effects. This is confirmed by the fact that the "conformity principle" is met including the limiting cases, for instance:

(1) when transient (or inertial) term $\prec Hi\succ\to 0$ the local time variation is excluded and we obtain Kornienko (1997a) type relationship, which describes the heat transfer for boundary layer model accounting for the azimuthal transfer effects;

(2) when $\prec Hi\succ\to 0$, $V_\theta\to 0$ or/and $\partial h^+/\partial\theta\to 0$, and $\partial q_\theta/\partial\theta\to 0$ ($\theta_{eff}\to 0$) the effect of azimuthal heat transfer is excluded and we obtain Kornienko (1995, 1996) type relationship, which describes the heat transfer for the flow in axial symmetry round tube;

(3) when $\prec Hi\succ\to 0$, $\theta_{eff}\to 0$ and $v\to 0$, the effect of the radial transfer is excluded, and we obtain Novikov and Voskresensky (1977) type relationship, which describes heat transfer for the flow with inner heat sources;

(4) when $\prec Hi \succ \to 0$, $\theta_{eff} \to 0$, $v \to 0$ and $q_v \to 0$ we obtain Petukhov-Popov's (Petukhov, 1987) relationship;

(5) when $\prec Hi \succ \to 0$, $\theta_{eff} \to 0$, $v \to 0$ and $q_v \to 0$ and the physical properties are constant, we obtain the classical Lyon's integral (Lyon, 1951).

The analytical expressions obtained above are nonlinear integral dimensionless equations. For their completion they require the relevant model representations for the physical phenomena included into consideration (beginning with the substance turbulent transfer models in one- and two-phase non-equilibrium flows up to the radial and axial transfer models). The analytical expressions concerned also require the development of corresponding numerical methods for solving equations like Sato et al (1981).

However, after several additional simplifications and assumptions eliminating nonlinearity it is possible to obtain quadrature solutions, retaining the generalized and heuristic properties of the integral forms obtained above, for example Kornienko (1997a).

7. EXAMPLES OF REDUCING GENERAL ANALYTIC RELATIONSHIPS TO PARTICULAR ONES

A detailed comparison of conclusions resulting from methods of closure relationships considered is very time and labour-consuming as it involves detailed descriptions of a numerous assumptions and a lot of additional extensive calculations, exceeding the frames of this work. That is why only some examples of obtaining new analytical relationships for wall friction and heat transfer coefficients are considered in this chapter; they are also compared with examples available from the literature.

The general idea is to introduce concepts, like (Kutateladze and Leont'ev, 1985), "standard" flow (subscribed by "o") and of a flow perturbed by some physical effect or process. Moreover, the conservation hypothesis of integral momentum and heat transfer characteristics in boundary layer zones and turbulent core is used for standard and perturbed flows.

7.1. Relative Laws for Friction and Heat Transfer

A relative law for the wall friction coefficient can be obtained from (18a) or directly from TABLE I (line 9, column 2) as follows:

$$\left(\frac{\zeta_\theta}{\zeta_{o\theta}}\right)_{\mathrm{Re}_{*\theta}=idem} = \left[\int_0^Y \frac{\tilde{\rho}_o}{\tilde{\rho}}\left(\int_0^Y \frac{\tilde{\rho}/\tilde{\rho}_o(\tilde{\nu}_T/\tilde{\nu}_{To})}{\tilde{\tau}_\theta/\tilde{\tau}_{o\theta}}dY'\right)(1+2\tilde{\delta}_\tau Y)dY\right]^2. \tag{40}$$

Following L. Prandtl's model for describing the turbulent viscous stresses results in a friction relative law generalization, which is close in form to Kutateladze-Leont'yev (1985) relationship. So it follows:

$$\tau_t = \rho\left(\ell\frac{dw}{dy}\right)^2. \tag{41}$$

Using our designations, it can be written:

$$\frac{\tilde{\nu}_T}{\tilde{\nu}_{To}} = \frac{\mathrm{Re}_{*\theta}}{\mathrm{Re}_{*_o\theta}}\frac{d}{dR}\left(\frac{w^+}{w_o^+}\right). \tag{42}$$

Then, using designation $\omega = w^+/w_o^+$, expression is obtained:

$$\left(\frac{\zeta_\theta}{\zeta_{o\theta}}\right)_{\mathrm{Re}_{*\theta}=idem} = \left[\int_\omega^Y \frac{\tilde{\rho}_o}{\tilde{\rho}}\left(\int_0^Y \frac{\tilde{\rho}/\tilde{\rho}_o\, d\omega}{\tilde{\tau}/\tilde{\tau}_o}\right)\right]^2 (1+2\tilde{\delta}_\tau Y)dY, \tag{43}$$

which reflects one of fundamental properties of turbulence, i.e. wall flow conservation when viscosity influence disappears.

It is clear that in so doing all the limiting transitions of Kutateladze-Leont'yev (1985) model are fulfilled and the limiting relative friction law depends only on parameters characterizing the compressibility and stress profile, being not dependent on Re.

Relative law for heat and mass transfer coefficients is derived from (11) or directly from TABLE I (line 8, column 3(4)) as follows:

$$\frac{St_\theta}{St_{o\theta}}\frac{Pe_\theta}{Pe_{o\theta}}=\frac{\widetilde{\eta}_o}{\widetilde{\eta}}\int_\theta^{\theta+\Delta}\int_0^1\frac{(\rho w)_o/(\rho w)}{\prec \rho w\succ_o/\prec \rho w\succ}\left(\int_0^Y\frac{\widetilde{\rho}/\widetilde{\rho}_o(\widetilde{k}_T/\widetilde{k}_{To})}{\widetilde{q}/\widetilde{q}_o}dY'\right)(1+2\widetilde{\delta}_q Y)dYd\theta\,. \tag{44}$$

Transformations with the heat conductivity relative coefficient $\widetilde{k}_T/\widetilde{k}_{To}$ under condition $k_w << \mathrm{Pr}/\mathrm{Pr}_t * v_w$ result in

$$\frac{\widetilde{k}_T}{\widetilde{k}_{To}}=\frac{Pe_{*\theta}}{Pe_{*_{o\theta}}}\frac{d}{dR}\left(\frac{w^+}{w_o^+}\right)\frac{\mathrm{Pr}_{to}}{\mathrm{Pr}_t}\,. \tag{45}$$

Then relative law of heat and mass transfer will be expressed follows:

$$\left(\frac{Nu_\theta}{Nu_{o\theta}}\right)_{\mathrm{Re}_{*\theta}=idem}=\frac{\widetilde{\eta}_o}{\widetilde{\eta}}\int_\theta^{\theta+\Delta}\int_0^1\frac{(\rho w)_o/(\rho w)}{\prec \rho w_o\succ/\prec \rho w\succ}\left(\int_0^Y\frac{\widetilde{\rho}/\widetilde{\rho}_o(\mathrm{Pr}_{to}/\mathrm{Pr}_t)d\omega}{\widetilde{q}/\widetilde{q}_o}\right)(1+2\widetilde{\delta}_q Y)dYd\theta\,. \tag{46}$$

In case there is a temperature and velocity fields similarity eq. (37) for σ=0 and η=1 turns into eq. (34). The relationship for the mass transfer relative law under the same assumptions has the form of equations (35) and (37) for η=1, σ=1 after substituting N for q and Sc for Pr.

7.2. Hydrostatic Force Effects on the Wall Friction Factor

If we neglect all the terms (except hydrostatic term) in the general relationship (21) in the shear stress form, we can take results in the following expression:

$$\tau_{zy\theta}=\tau_{zw\theta}\frac{1-\dfrac{Y(1+\widetilde{\delta}_\tau Y)}{1+\widetilde{\delta}_\tau}\left[1\mp\dfrac{1+\widetilde{\delta}_\tau}{Fr_{*\theta}}\left(\prec\rho\succ-\prec\rho\succ_Y\right)\right]}{1+2\widetilde{\delta}_\tau Y}\,. \tag{47}$$

For the thin boundary layer when $\widetilde{\delta}_\tau << 1$, we have

$$\widetilde{\tau}_{zy\theta}=1-Y\left[1\mp\frac{1}{Fr_{*\theta}}\left(\prec\widetilde{\rho}\succ-\prec\widetilde{\rho}\succ_Y\right)\right]. \tag{48}$$

The upper and lower signs at Froude number term in the both eqs. (47) and (48) should be used for upward and downward flows, respectively. Eqs. (47, 48) demonstrate the functional form and influence of density transversal variation on the linear distribution of shear stresses in the boundary layer approximation.

It is not difficult to derive specific relationships for friction factor and Stanton number (when $Pr\approx$1) similar to those published by Kornienko (1996, 1997a).

8. ON INTERPRETATION OF THE LOCAL CLOSURE RELATIONSHIP FORMULATIONS FOR FLOW IN ANNULAR CHANNEL

The relationships reported are useful as initial formulas in construction of the annular channel wall friction, heat and mass transfer coefficients taking into account additional (separate) effects represented by the integrals (22)-(33). However, as there is a large variety of the boundary conditions of the first and second kind on the inner and outer wall (from constant and equal to each other values up to periodical and unequal to each other values on every wall). They involve a large number of transpositions beyond the scope of this article. Therefore, it is appropriate at this point to bring only the brief interpretation of the above relationships for annular channels.

Relationship (21) for substance flux is suitable for its profile description in the inner and outer regions of annular channel. It is obvious that for annular channel the substance flux profile is non-linear even when we neglect all of the individual effects expressed by the integrals (22)-(33). This has an important influence on the local wall friction, heat and mass transfer coefficients introduced in the 8-th line of Table I.

Flow in concentric annulus and designations of appropriate variables are shown in Fig.3. For axial symmetry concentric annular channel we may neglect azimuthal transfer effects. The general ideas of the construction of the closure relationships for annular channels go back to Dwyer's (1963) method. But now we can take into account the number of separate effects from the list of integrals (22) - (33).

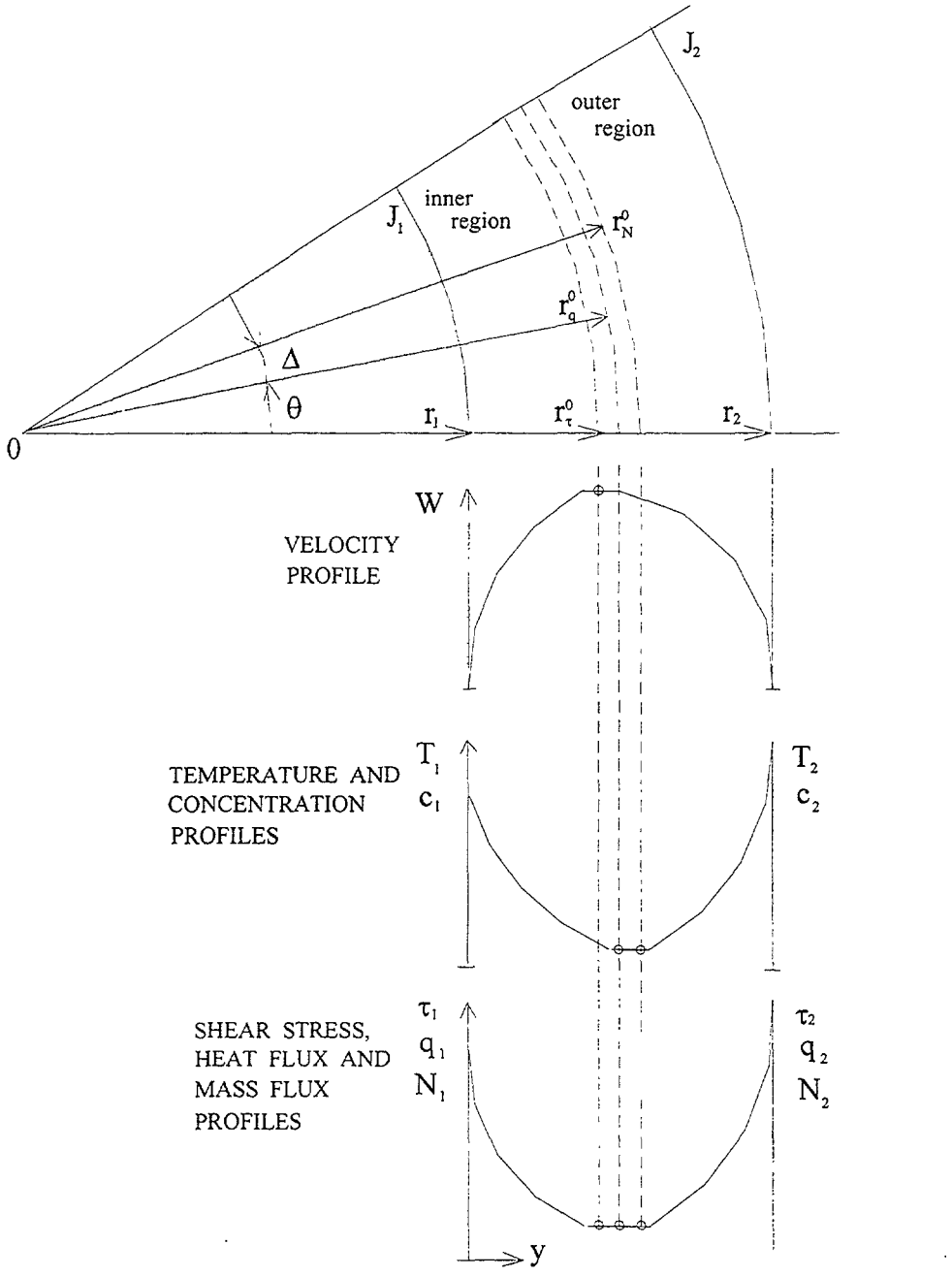

Fig.3. Graphical representation the case of unequal shear stresses, heat and mass fluxes from the walls of concentric annulus to fluid flowing therein.

Expression (47) is valid for the annular channel shear stress profile, taking into account the hydrostatic term. However, as the boundary layer thickness should be take the distance from the wall to the line of maximum velocity

$$\delta_\tau = r_\tau^0 - r_1 . \tag{49}$$

The heat flux profile has a similar form. The distance from the wall to the minimum temperature line is:

$$\delta_q = r_q^0 - r_1 . \tag{50}$$

Using the balance of the substance fluxes in general form, it is not difficult to derive the equation for boundary between the inner and outer region in the concentric annular channel

$$\tilde{r}_s^2 = \frac{A_{in}\tilde{r}_{12}^2 + A_{ou}F_s}{A_{in} + A_{ou}F_s}, \tag{51}$$

where relative extremum velocity (temperature or concentration) radius is:

$$\tilde{r}_s = \frac{r_s^0}{r_2} = \frac{r_1 + \delta_s}{r_2} = \frac{r_1(1+2\tilde{\delta}_s)}{r_2} = \tilde{r}_{12}(1+2\tilde{\delta}_s), \tag{52}$$

boundary parameters

$$F_s = \frac{J_1 r_1}{J_2 r_2} = \left\{ F_\tau = \frac{\tau_1 r_1}{\tau_2 r_2},\ or\ F_q = \frac{q_1 r_1}{q_2 r_2},\ or\ F_N = \frac{N_1 r_1}{N_2 r_2} \right\}. \tag{53}$$

Relationships A_{in} and A_{ou} - are integrals in the form of eqs. (22), (24), (26), (28), (30) and (32), for inner and outer regions of the annular channel.

In particular, we can derive from the momentum balance, neglecting all of the separate effects (excepting hydrostatic term), the following relationship for the boundary line between inner and outer velocity regions

$$\tilde{r}_\tau^2 = \frac{\left(\frac{dP}{dz} - <\rho>_{in} g\right)\tilde{r}_{12}^2 + \left(\frac{dP}{dz} - <\rho>_{ou} g\right)F_\tau}{\frac{dP}{dz} - <\rho>_{in} g + \left(\frac{dP}{dz} - <\rho>_{ou} g\right)F_\tau}. \tag{54}$$

From the heat balance, neglecting all of the separate effects (except that of inner heat sources), we have relationship for boundary line between inner and outer temperature region

$$\tilde{r}_q^2 = \frac{\left(<\rho w\frac{\partial h}{\partial z}>_{in} + <q_v>_{in}\right)\tilde{r}_{12}^2 + \left(<\rho w\frac{\partial h}{\partial z}>_{ou} + <q_v>_{ou}\right)F_q}{<\rho w\frac{\partial h}{\partial z}>_{in} + <q_v>_{in} + \left(<\rho w\frac{\partial h}{\partial z}>_{ou} + <q_v>_{ou}\right)F_q}. \tag{55}$$

It is not difficult to verify that these equations take the same form as the Dwyer's (1963) equations when we neglect the hydrostatic term in eq. (54) and inner heat sources in eq.(55).

Using methods Maubach (1972) and Kornienko (1997a) one can get the wall friction factor for annular channel in "two-zone model" approximations, as the harmonic mean form:

$$\zeta = \frac{1}{\left(\sqrt{\frac{<\rho>(\beta^2-\alpha^2)}{\zeta_1 <\rho>_{in}\alpha(1-\alpha)}}\frac{\beta^2-\alpha^2}{1-\alpha^2} + \sqrt{\frac{<\rho>(1-\beta^2)}{\zeta_2 <\rho>_{ou}(1-\alpha)}}\frac{1-\beta^2}{1-\alpha^2}\right)^2} \tag{56}$$

where Maubach designations are used for $\tilde{r}_{12}=\alpha$ and $\tilde{r}_\tau = \beta$.

CONCLUSION

A simple and descriptive approach to construct generalized three-dimensional integral relationships for local and subchannel wall friction, heat and mass transfer coefficients has

been suggested. This approach is based on the boundary layer approximations using Reynolds' flux concept and a generalized substance transfer coefficient.

With this approach, one can create integral analytical forms for the wall friction factor, heat and mass transfer coefficients accounting for the contribution of various complementary effects. It is precisely these transversal varied profiles that are complementary effects for the one-dimensional model. They include not only density (in the mixed convection problem), but also other components at the momentum, heat and mass transfer processes, as well as their sources and sinks in the channel flow cross section.

Unlike the well known Kutateladze-Leont'yev (1985) relationships for the limiting friction, heat and mass transfer laws, and unlike Petukhov-Popov's relationship (Petukhov, 1987), the integral forms deduced in this paper are typified by a more general character and are characterized by an additive form of notation of the effects under consideration. This is significant for the criteria assessments of the contribution of the effect in question. Besides, it is the weighted value-mean integral difference that is important, rather than the absolute value of this effect.

The general integral relationships developed are recommended as a basis for the construction of new phenomenological models of local and subchannel wall friction factor, heat and mass transfer coefficients.

NOMENCLATURE

C_p	specific heat capacity
C	concentration, $(\varphi\rho)_g/\rho$
D	diffusion coefficient
g	gravitational acceleration
h	specific enthalpy
k	thermal conductivity
N	mass flux, $\{\rho w\}$
P	pressure, pitch
q	heat flux
R	relative coordinate, r/r_w
r	radius, distance from axis
r_1	inner radius of annulus
r_2	outer radius of annulus
$\tilde{r}_{12}$	annulus radius ratio r_1/r_2
S	generalized variable, (w, h(t), c)
T	temperature
$\bar{u}$	local velocity
$\bar{u}_{gf}$	phase difference velocity
v	radial velocity
v_θ	azimuthal velocity
y	distance from the rod wall
Y	relative coordinate, y/δ_s
w	axial velocity
z	axial coordinate

Greek symbols

α	heat transfer coefficient
α_N	mass transfer coefficient
Γ	mass source
ν	kinematic viscosity
ρ	density, $\{\varphi\rho_g + (1-\varphi)\rho_f\}$
τ	shear stress
φ	void fraction
ζ	friction factor
θ	azimuthal angle
Δ	increment of an azimuthal angle
δ_s	boundary layer thickness

Subscripts, superscripts

D	diffusion,	s	substance transfer,
d	drift,	q	heat transfer,
f	fluid,	N	mass transfer,
g	gas{vapor},	τ	momentum transfer,
t	turbulent,	v	local sources,
T	total,	in	inner region
w,r	wall,	ou	outer region
Y	variable upper limit of integration		

Symbols

*	friction
+	friction scales
~	relative
-	weighted mean (bulk) value
< >	area average
⋖⋗	annular sector area average
≈	tensor

Dimensionless groups

Fr	Froude number
Pe	Peclet number
Pr	Prandtl number
Re	Reynolds number
St	Stanton number.

REFERENCES

[1] BOBKOV V.P., SAVANIN N.K., 1981, "The Local Heat Transfer Coefficient and its Use in the Calculations of the rod bundle temperature conditions." Atomnaya Energiya, v.51, N1, pp.12-16, in Russian.

[2] DWYER O.E., 1963, "Equations for Bilateral Heat Transfer to a Fluid Flowing in a Concentric Annulus." Nuclear Science and Engineering, No 15, pp.52-57.

[3] IANNELLO V., SUH K.Y., TODREAS N.E., 1988, "Mixed convection friction factors and Nusselt numbers in vertical annular and subchannel geometries." International Journal Heat Mass Transfer., V.31, No 10, pp.2175-2189.

[4] IBRAGIMOV M.KH., SUBBOTIN V.I., BOBKOV V.P. et al. 1978, "Turbulent Flow Structure and Heat Transfer Mechanism in the Channels." Atomizdat, Moscow, in Russian.

[5] ISHII M., 1975, "Thermo-Fluid Dynamic Theory of Two-Phase Flow", Eyrolles, Paris.

[6] KORNIENKO YU.N. 1995, "Generalized Integral Forms for Friction, Heat and Mass Transfer Coefficients." International Journal Heat Mass Transfer., V. 38, No 16, pp. 3103-3108.

[7] KORNIENKO YU.N., NEVINITSA A.N., 1996, "Development of generalized integral forms of closure relationships for wall friction, heat and mass transfer factors in non-homogeneous coolant flows for assessment of limits and capabilities of system codes.", Proc. of Conf. ICONE-4, Vol.1a, pp.217-229.

[8] KORNIENKO YU.N., 1997a, "Effect of saddle-shape transversal void fraction on low Reynolds number wall friction and heat transfer in bubble flows.", Proc. of Conf. ICONE-5, Paper N2433, Trac 1, Nice, France, 1997.

[9] KORNIENKO YU.N., 1997b, "Subchannel analytical formulation of the closure relationships for single and two-phase flow wall friction, heat and mass transfer", Forh Int. Seminar on Subchannel Analysis, Proc. of Seminar ISSCA-4, pp. 175-187. Tokyo, Japan, 1997.

[10] KUTATELADZE S.S. and Leont'yev A.I., 1985, "Heat, Mass Transfer and Friction in Turbulent Boundary Layer", Energoatomizdat, Moscow, in Russian.

[11] LYON R.N., 1951, "Liquid Metal Heat Transfer Coefficients." Chem. Eng. Progr., Vol.47, No.2, pp.75-79.

[12] MAUBACH K., 1972, "Rough annulus pressure drop- interpretation of experiments and recalculation for square ribs", Int. J. Heat Mass Transfer, V.15 pp.2489-2498.

[13] NOVIKOV I.I., VOSKRESENSKY K.D. 1977, "Applied Thermodynamics and Heat Transfer", Atomizdat, Moscow, in Russian.

[14] PETUKHOV B.S., 1987, "Heat Transfer Problems." Nauka, Moscow, in Russian.

[15] REYNOLDS A.J., 1974, "Turbulent Flows in Engineering", J. Wiley & Sons, London.

[16] SATO Y. et al, 1981, "Momentum and Heat Transfer in Two-Phase Bubble Flow." International Journal of Multiphase Flow, V.7, pp.167-177, Pergamon, London.

SETTLEMENT SUBSTANTIATION OF THE PASSIVE DEVICES SHUTDOWN FAST REACTORS BY TRIP THE ABSORBING ROD IN CASE OF ANTICIPATED ACCIDENT

A.G. PORTIANOY, E.N. SERDUN, A.P. SOROKIN, V.A. UHOV, V.S. EGOROV
State Scientific Centre of Russian Federation,
Institute of Physics and Power Engineering,
Obinisk, Kaluga Region, Russian Federation

Abstract

Results of improvement of the passive device shutdown fast reactors BN-600 (PDSR) are considered. The device works (lets off a neutron absorber) at increase of coolant temperature above 660 ^{0}C (650 ^{0}C). The PDSR working element represents a design of a sylphon-container type, filled with allumunium (magnesium) and operates (extended) under melting it at the expense of energy of a compressed high-temperature spring, and/or increases of a volume (6% of aluminium) at melting, and/or increases of a volume at further growth of a temperature. Account of the characteristics of PDSR working elements is carried out. Mathematical models, describing dependence of the basic of the characteristics (sluggishness, size of lengthening) from the constructive factors and modes of anticipated accident, are received. Is shown, that the PDSR characteristics provide an emergency stop of the reactor BN-600 in a case of a heaviest anticipated accident prior to the beginning sodium boiling in a core. The developed PDSR have a number of advantages before known, for example, magnetic with a Curie point, first of all, at the expense of significant efforts generation, multi-channels of operation and weak dependence on the operational factors, first of all, neutron fluence.

1. INTRODUCTION.

One of urgent problems of NPD safety level increase is decrease of probability of development heavy (out-of-design) accidents. Numerical estimations of out-of-design accidents development have shown that in fast reactor with sodium coolant, by its physical features, damages of the core can be obviated even during the most severe accidents being followed by attendant failure of active elements in emergency system, if the light action of passive means on reactivity will be provided [1]. Reactor, supplied by such a systems, acquires actually properties of internal inherent safety, as all means and effects of its protection are based on natural processes, proceeding in the core without any communication with external control systems or sources of energy. Function of the systems is controlling out-of-design accidents followed by a standard emergency system failure with the aim to except sodium boiling and severe accidents in reactor core.

The illustration of a role PDSR is served, for example, the results of work [2], which is shown, that the probability of development of heavy accidents for fast reactor DFBR, under input PDSR in NPD structure, is practically by two order reduced (from $8{,}2\cdot 10^{-8}$ to $9{,}4\cdot 10^{-10}$ 1/ (reactor year).

2. STATE OF DEVELOPMENT AND BASIC PDSR TYPES.

The spent analysis of technological and patent sources has shown, now days already it is offered more hundred of various devices, capable to carry out of PSDR function [1,3]. We shall stop in more detail on PDSR for fast reactor, working in heavier conditions. The considered devices can be used and on other types NPD.

Basic known PDSR on character of a feedback it is possible to divide on working on:

- to excess of fuel temperature;
- to decrease of the coolant charge;
- to increase of coolant temperature.

The work of the first type of devices is based on phase transition, for example, melting [2], sublimation [4] and moving of nuclear fuel. Apparently, given type of devices will allow to effectively supply fulfillment of safety function, but now days they are poorly technologically worked and their introduction should be preceded with a rather long and expensive stage of improvement.

On a high level there is the development of devices, working on decrease of a level or the charge (pressure) of the coolant:

- increase of neutron leakage (Japan, GEM) [2];
- hydrodynamic retention of absorber (Russia) [5].

The basic lack of the given type of devices is their low sensitivity to change of temperature (capacity) reactor.

Nowadays PDSR, operating on excess of temperatures are the most distributed. They can be divided into devices of gravitational and compulsory input of an absorber in an core.

As a rule, PSDR working elements with compulsory input of an absorber work in result of temperature expansion of a firm body or liquid [1,6]. During their use it is possible to lower probability wedging of an absorber when the core is deforming, but known devices are unwieldy, massive and, as a consequence, have essential sluggishness and bring appreciable changes in a design and material structure of reactor.

PSDR of a gravitational type are placed, as a rule, on an exit from core of nuclear reactor and them temperature-dependent element is washed by coolant. When the coolant temperature is higher extreme allowable there is the operation of an element and clearing of an neutron absorber, which is lowered under own weight in a core, translating it in subcritical condition. The given type of devices is sensitive to increase of temperature on an exit from core in all accident with unbalance of a ratio of capacity and charge and now days is developed the most heavily.

Nowadays PDSR, operating on excess of a temperatures are the most distributed. There are several groups of this devices: magnitude, including Curie point; expend on heating of firm body; effect of shape remember; melting; volume expend of fluid.

Now, the majority of perspective passive devices shutdown reactors PDSR use the working elements with fusible inserts and sylphons [1].

The interest to the technical decisions with fusible inserts is explained by a simplicity of construction and high operating reliability. Among defects, limiting their application, there is a great response time, stipulated by slow plastic deformation of the fusible element.

The wide using of sylphon working elements is explained by follow its advantage:

- sylphons are used in a different branches of industry, including atomic energetic, as a separator of media, packing elements, load-bearing units in medium, which does not result in corrosion of sylphon material;
- stainless steel sylphons are used in a wide temperature range and at temperature ~600 ^{o}C offer rather high resource of trouble-free operation (~10% of resource at 20 ^{o}C) [7].
- there are an extensive experimental data connecting sylphon characteristics (stroke, resource) with environmental parameters (temperature, pressure, neutron fluence) and parameters of sylphon by itself (diameter, number and thickness of the plies, number of corrugations).

The spent expert estimation of the characteristics of PDSR various types has shown, that now, with reference to fast reactors, sylphons with working substance, increasing volume at melting are one of the most perfect, as have properties of limiting, generation of significant efforts and multi-channel [7]. Based on the analysis of perspective passive emergency protection systems for reactor of BN-600 type the construction of the system, operating on several physical principles on an excess of limiting temperature of outlet sodium was

developed. Construction includes positive moments of existing systems of a similar type, first of all, sylphon and fusible ones.

PDSR is located in the subassembly head of passive accident protection (PAP) – simulator of fuel assembly and is washed by outlet sodium flow from the assembly (see Fig. 1). The PDSR construction is presented in Fig. 2.

The system consists on releasing device with grabs holding an neutron absorber, sylphon working element. PDSR works (lets off an absorber) at given increase of sodium temperature above nominal (570 – 600 ^{0}C). The PDSR operation should prevent boiling of sodium in reactor in conditions heaviest anticipated accident of reactor BN-600 (800) with a stop of 1 contour pumps, refusal of active protective systems and extraction of a absorbing rod by efficiency 0,24% ΔK/K c by the maximum speed with bottom position.

If environmental temperature exceeds the critical value (620-670 ^{O}C), system comes into action - the grab is pushed out from the case and releases neutron absorber. The system operates under action of the several independent factors:

- Temperature-sensitive substance melts (for example, aluminium, magnesium or antimony), first of all over sylphon contour, corrugations and ends of which are released, and under the effect of high-temperature spring the sylphon is extended by the length needed to open grabs and to discharge absorber to the core.
- Temperature-sensitive substance increases its volume due to interphase transition and volumetric temperature expansion.

The use of several independent passive force factors increases the operational reliability of the system, that allows reactor shut-down to be performed in the event of out-of-design accident and safety of Nuclear Power Plant to be improved.

3. PREDICTION OF MELTING TIME FOR WORKING BODY WITHIN SYLPHON

Sylphon under consideration is a complex geometrical area. Really, the hydrodynamics and heat transfer in such an area represent combined processes. In first approximation we shall consider heat transfer in a liquid, flowing between two coaxial cylinders (see Fig. 3).

As the length of sylphon is not large (~0,1 m), dependence of melting time on the height of sylphon system shall be ignored. Radius of corrugations is taken as external radius. The problem is to solve the set of heat conduction differential equations:

$$\rho_i c_{p_i} \frac{\partial T_i}{\partial \tau} = \frac{\lambda_i}{r} \frac{\partial}{\partial r} r \frac{\partial T_i}{\partial r} \qquad (1)$$

where i = 1, 2, 3, 4.

The indexes (1, 2, 3, 4) in equations concern, respectively, to the sylphon cladding, liquid and solid phases of melting material and insert. An index "5" - area of coolant flo, r_s - border between phases.

Initial temperature condition:

$$T|_{\tau=0} = T_0 \qquad (2)$$

where T_0 is the coolant temperature.

Boundary conditions are condition of conjunction :

$$T1|_{R_c} = T2|_{R_c} \qquad (3)$$

$$\lambda_1 \frac{\partial T1}{\partial r}\bigg|_{R_c} = \lambda_2 \frac{\partial T2}{\partial r}\bigg|_{R_c} \qquad (4)$$

$$T2|_{r_s} = T3|_{r_s} = T_{melt} \qquad (5)$$

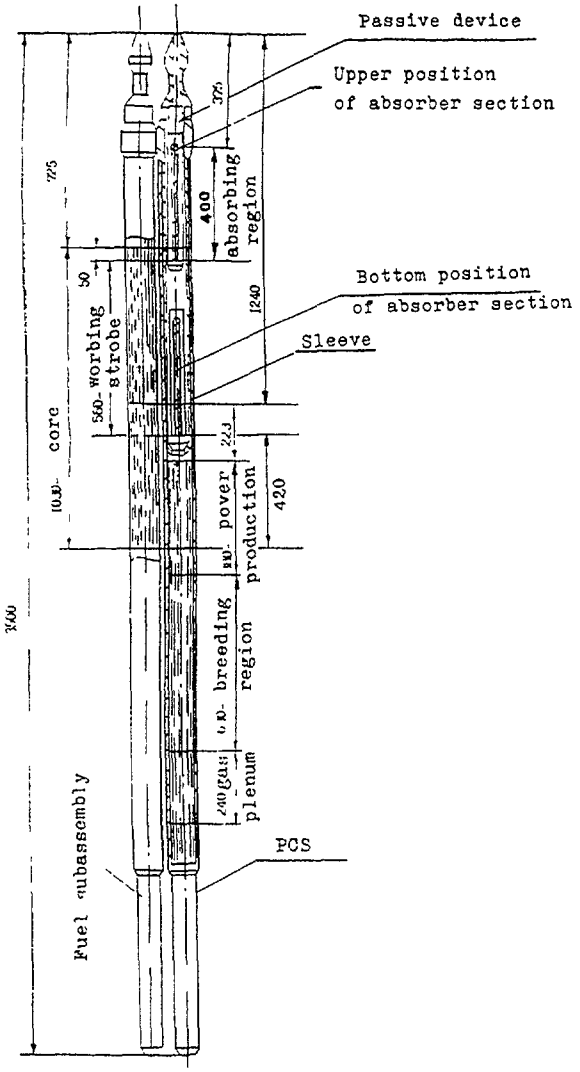

FIG. 1 Scheme of arrangement of passive device in the PAP

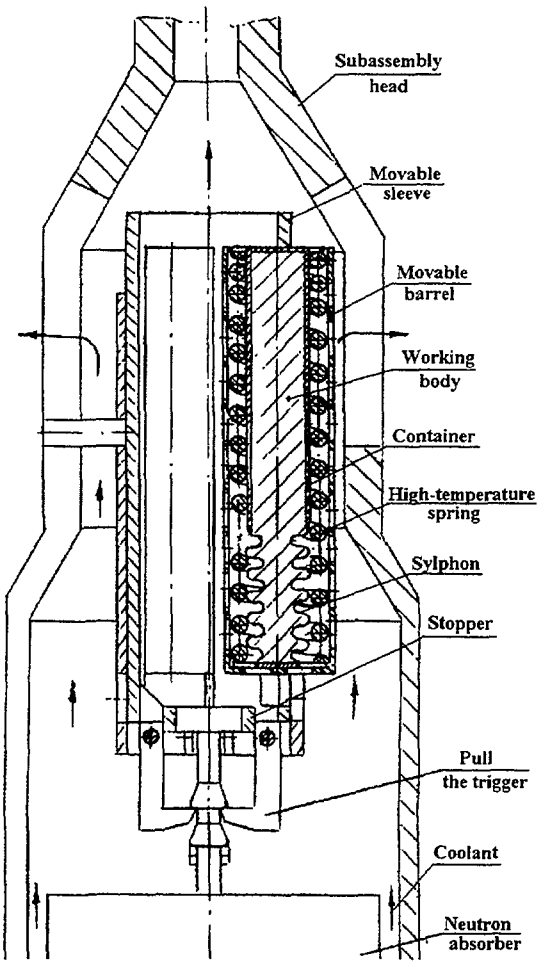

FIG. 2 Three-sylphon passive emergency protection sistem

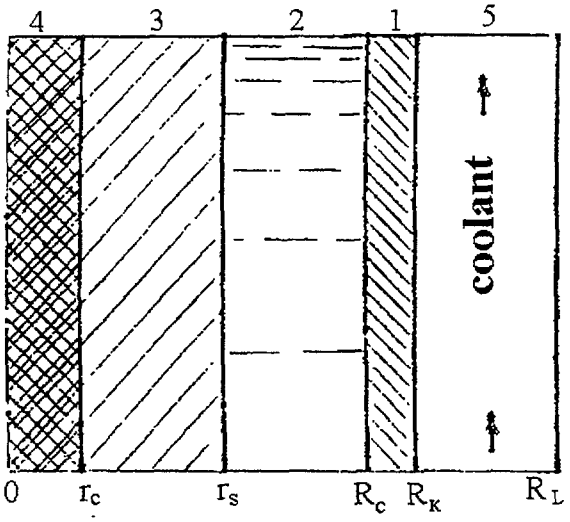

FIG.3 Scheme of calculated region

$$\lambda_2 \frac{\partial T_2}{\partial r}\Big|_{r_s} = \lambda_3 \frac{\partial T_3}{\partial r}\Big|_{r_s} + \rho q \frac{\partial r_s}{\partial \tau} \tag{6}$$

$$T_3\big|_{r_c} = T_4\big|_{r_c} \tag{7}$$

$$\lambda_3 \frac{\partial T_3}{\partial r}\Big|_{r_c} = \lambda_4 \frac{\partial T_4}{\partial r}\Big|_{r_c} \tag{8}$$

Boundary conditions

$$\lambda_4 \frac{\partial T_4}{\partial r}\Big|_{r=0} = 0 \tag{9}$$

$$-\lambda_1 \frac{\partial T_1}{\partial r}\Big|_{R_K} = \alpha\left(T_5 - T_1(R_K)\right) \tag{10}$$

were T_5 is the coolant temperature; q is the specific heat of phase transition.

Heat transfer coefficient is given by the relation:

$\alpha = Nu\lambda_5 / (R_L - R_k)$

Nu is defined according to the well-known relation unilateral heat transfer in liquid metal:

$Nu = 6.+0.02(Re\,Pr)^{0.8}$

where

$Re = \dfrac{(R_L - R_k)}{\nu} W$, Pr=0.0044

W – is the coolant velocity, ν – is the kinematic viscosity.

Ignoring heat capacity of solid phase and insert, and assuming, that the quasi-steady-state temperature distribution is realised in liquid during melting, we receive the following equation for the rate of interface motion:

$$q\rho \frac{\partial r_s}{\partial \tau} = \frac{(T_5(\tau) - T_{пл})}{2(R_c - r_s)\left[\dfrac{1}{2\alpha R_K} + \dfrac{(R_K - R_c)}{R_c \lambda_1} + \dfrac{1}{2\lambda_2} \ln\left(\dfrac{R_c}{R_c - r_s}\right)\right]} \tag{11}$$

with initial condition:

$$r_s\big|_{t=0} = R_c \tag{12}$$

Working out the (11) at T_5 = const, we receive relation for the melting time:

$$t(r_s) = \frac{q\rho}{(T_5 - T_{пл})}\left\{\left[R_c^2 - (R_c - r_s)^2\right]\left(\frac{1}{2\alpha R_K} + \frac{(R_K - R_c)}{R_c \lambda_1} + \frac{1}{4\lambda_2}\right) - \right.$$
$$\left. - (R_c - r_s)^2 \frac{1}{2\lambda_2} \ln\left(\frac{R_c}{R_c - r_s}\right)\right\} \tag{13}$$

Taking into account, that $r_{max} = (R_c - r_c)$, the relationship for melting time is the following one:

$$t_{пл} = \frac{q\,\rho}{(T_5 - T_{melt.})}\left\{\left[R_c^2 - r_0^2\right]\times\left(\frac{1}{2\alpha R_K} + \frac{(R_K - R_c)}{R_c\lambda_1} + \frac{1}{4\lambda_2}\right) - \frac{r_0^2}{2\lambda_2}\ln\left(\frac{R_c}{r_0}\right)\right\} \qquad (14)$$

In the event $r_c \to 0$, we have:

$$t_{melt} = \frac{q\rho}{(T_5 - T_{melt.})}\left(\frac{1}{2\alpha R_K} + \frac{(R_K - R_c)}{\lambda_1 R_c} + \frac{1}{4\lambda_2}\right) \qquad (15)$$

Analysis of the (13) - (15) has shown that melting time is in proportion to specific heat of phase transition and density of working body. Increase in temperature difference $(T_5 - T_{melt})$, thermal conductivity of a material of working body, coolant velocity results in reduction of melting time, i.e. reduction of response time of a working element. The dependence of melting time on geometry of sylphon system has more complex character, which can be defined by numerical calculation.

The set of differential equations (1) with boundary conditions (2) - (10) is approximated by finite differences, much as the approach represented [10]. Algebraic system is solved by sweep method.

4.CALCULATING RESULTS OF DYNAMIC CHARACTERISTICS OF SYLPHON WORKING ELEMENTS

The analysis performed has shown, that with consideration for requirements on the melting temperature of a working body of PDSR sylphon elements ($670^oC > T_{melt} > 620^oC$) attention must be given to aluminum, magnesium and antimony. Some main parameters of these substances are indicated in Table I.

TABLE I. SOME PARAMETERS OF PERSPECTIVE SUBSTANCES TO USE AS A WORKING BODY IN PDSR [11,12,13]

Material	T_{melt} (^oC)	ρ (g/cm^3)	q (kJ/mol)	$\rho \cdot q$ (kJ/cm^3)	γ_{melt}	λ (W/m·K) Ò=1000Ê	β (10^{-6} K^{-1}) Ò=1000Ê
Al	660,2	2,69	10,8	1.08	0,048...0,071	93	113
Ìg	650	1,74	8,56	0.61	0,034...0,041	84	380
Sb	630,5	6,69	20,1	2.64	-0,009...0,015	27	122

The choice of characteristic parameters is explained by the following circumstances:

- the melt time of working substance $t \sim q \cdot \rho$ and decreases with growth λ;
- size of lengthening $h \sim \gamma_{melt}$, where $\gamma_{melt} = \left(\frac{\Delta V}{V}\right)_{melt}$;
- speed of lengthening $\frac{dh}{dt} \sim \gamma_{melt}/q\rho$.

Coefficient β characterizes intensity of inclusion of the following operation channel, connected to temperature volumetric expansion of liquid substance. We shall note fact, that meanings γ_{melt} for aluminium, magnesium and the antinomies on various sources much differ. At further estimations average meanings – 0,060 for aluminium and 0,037 for magnesium are accepted.

From results in Table 1 given in view of a ratio (2) it is necessary to expect, that the elements with magnesium will have smaller sluggishness, and elements with aluminium –

large lengthening; the speed of lengthening for both substances is about identical. Elements with antimony it will be essential to concede on the basic characteristics.

The settlement estimations of size of sylphon lengthening were carried out at the following assumptions:

- sylphon is completely filled by liquid metal;
- size shrinkage porosity of aluminium 0,3 %, linear shrinkage 1,8 % [14];
- the change of substance volume at melt occurs only at the expense of increase of length sylphon.

Under the above-stated conditions the settlement lengthening sylphon in length 100 mm with aluminium at γ_{melt}=0,06 has made size ~ 4 mm, if to accept, that shrinkage at magnesium same as well as aluminium, lengthening sylphon with magnesium will make ~ 1,6 mm.

The maximum effort, generated sylphon at lengthening was estimated proceeding from allowable internal pressure and, for example, for sylphon 16–20–0,16×2 STD 21744–83 has made size ~ 37,5 kg.

In Table II results of accounts of melt time of a working body in sylphon are resulted. The account was carried out for the linear law of temperature change of the coolant, that corresponds to a mode of anticipated accident. The variants of account got out according to the mathematical theory of experiment planning (orthogonal two-level two-factor plan with a control point).

TABLE II. THE MELT TIME IN THREE-PLIES SYLPHON (Δ = 0,48MM), D = 18 MM, SINCE THE ANTICIPATED ACCIDENT ARISING

dT/dt (K/c)	W (m/s)	Time (s)			
		Aluminium		Magnesium	
		r=0	$r_{internal}$ = 6mm	r = 0	$r_{internal}$= 6 mm
30	2	8,5	5,3	6,5	4,4
20	10	10,2	6,5	7,9	5,4
20	2	11,0	7,1	8,5	5,9
25	6	9,1	5,6	7,0	4,7

The beginning time of the sodium melt in the case of the most anticipated accident BN-600 reactor ($\frac{dT}{dt} = 30$ K/c) is ~ 12.6 c. The melting time of substance in corrugations is r=$r_{internal}$, r=0 – the complete melt of substance in sylphon.

The equation of regression are identical and have a form:

for aluminium:

$$\tau_{melt,Al}(r = 0) = 9.0 - 1.2x_1 - 0.3x_2, \quad (16)$$
$$\tau_{melt,Al}(r = 6) = 5.7 - 0.8x_1 - 0.2x_2;$$

for magnesium:

$$\tau_{meltMg}(r = 0) = 7.1 - 0.9x_1 - 0.2x_2, \quad (17)$$
$$\tau_{meltMg}(r = 6) = 4.8 - 0.7x_1 - 0.2x_2,$$

were

$$x_1 = \begin{cases} +1, \text{при } \dfrac{dT}{dt} = 30\,{}^{K}/_{c}, \\ -1, \text{при } \dfrac{dT}{dt} = 20\,{}^{K}/_{c}; \end{cases}$$

$$x_2 = \begin{cases} +1, \text{при } W = 10\,{}^{м}/_{c}, \\ -1, \text{при } W = 2\,{}^{м}/_{c}. \end{cases}$$

From data resulted in Table II follows, that for various anticipated accident time of PDSR operation will be essential (almost twice) less time of a beginning of sodium boiling. However, the data resulted in Table II have estimated character and experimental confirmation of operation time and size of a sylphon course of PDSR working elements is necessary.

The experimental study of the sylphon characteristics of working elements was spent on specially made liquid-metal installation (see Fig. 4).

In experiments at the first cycle lengthening of 2,4 mm was observed, that is close settlement meaning (2,8 mm). Beginning from the second cycle after sylphon cooling up to 450 ^{0}C sylphon was shortened up to an initial condition and stably was extended at repeated cycles (15 cycles) on 1,8 mm. The time of achievement of the maximum sylphon lengthening made 5 s, the lengthening speed about constant.

Comparing experiments results with account data on sluggishness and the sylphon lengthening can make a conclusion, that despite of a number of initial data γ_{melt} were not define, they are in the satisfactory consent and the developed techniques can be used for estimated accounts of developed devices.

After tests the sylphon was visually surveyed. Leakage of aluminium and corrosion traces is not found out. Residual axial deformation of sylphon is marked.

The spent researches have confirmed serviceability of the offered technical decision and have allowed to reveal lacks of a design – first of all axial deformation and small size of a working course, that complicates development simple and reliably working PDSR.

The carried out studies have shown expediency of transition from the sylphon working element to a design as "sylphon–container". The basic advantage of the latter is large size of a working course at melt of substance and its further temperature volumetric expansion. The given design represents also opportunity of regulation of a working course by change of the relation of sylphon and container volumes.

The "sylphon–container" design has much higher axial stability. In an offered design easier questions of accommodation of a high-temperature spring are decided. The PDSR circuit with three working elements as "sylphon–container" is resulted on Fig. 2. Presence of three working elements allows to use substances with different melt temperature and raises reliability of operation.

For account of the elements type as "sylphon–container" characteristics a technique of account of sylphon working elements was modernized. The complex geometry was replaced by system of coaxial cylinders. The account of lengthening was made from a ratio of volumes balance. Thus it was supposed, that sylphon does not begin to be extended up to complete melt of substance in corrugations. The text of the program is written in language a Fortran and realizes the numerical decision of system of the equations (1).

Study of dependence of the characteristics (sluggishness, size of a working course) working elements from geometry (diameter, length of sylphon and container) and operational factors (speed, rate of growth of temperature of the coolant) is spent. Mathematical models, describing dependence a testimonial from geometry of design are received.

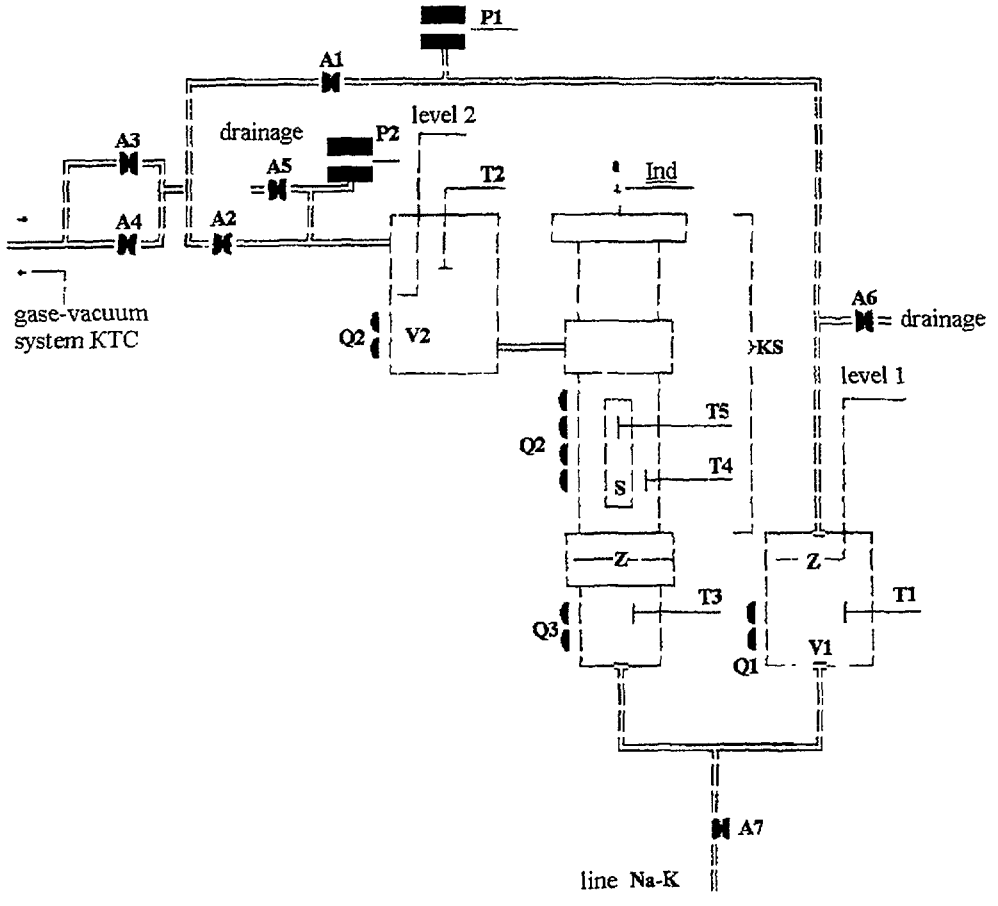

FIG.4 Scheme of liquid metal experiment installation for PDSR test

The mathematical models for aluminium are adequate and look like:

$$\tau\,(h=2\text{ mm})=3{,}71+0{,}22\cdot x_1-0{,}78\cdot x_2-0{,}33\cdot x_3+0{,}07\cdot x_1\cdot x_2+0{,}24\cdot x_1\cdot x_3-0{,}18\cdot x_2\cdot x_3-$$
$$-\,0{,}49\cdot x_1\cdot x_2\cdot x_3 \qquad (18)$$

$$\tau\,(h=5\text{ mm})=7{,}03+0{,}96\cdot x_1-1{,}38\cdot x_2-1{,}00\cdot x_3+0{,}22\cdot x_1\cdot x_2+0{,}20\cdot x_1\cdot x_3-0{,}27\cdot x_2\cdot x_3-$$
$$-\,0{,}53\cdot x_1\cdot x_2\cdot x_3 \qquad (19)$$

$$h_{max}=12{,}1-3{,}20\cdot x_1+5{,}10\cdot x_2+2{,}60\cdot x_3-1{,}70\cdot x_1\cdot x_2-1{,}10\cdot x_1\cdot x_3+1{,}70\cdot x_2\cdot x_3-0{,}50\cdot x_1\cdot x_2\cdot x_3, \qquad (20)$$

where

$$x_1=\begin{cases}+1,\ D_s=16\text{mm},\\ -1,\ D_s=11\text{mm};\end{cases}$$

$$x_2=\begin{cases}+1,\ D_c=28\text{mm},\\ -1,\ D_c=16\text{mm};\end{cases}$$

$$x_3=\begin{cases}+1,\ l_c=80\text{mm},\\ -1,\ l_c=40\text{mm}.\end{cases}$$

The accounts are carried out at $\gamma_{melt}=0{,}06$, $l_s+l_c=100$ mm, $dT/dt=30$ K/s and $W=2$ m/s.

The adequacy of models is checked by comparison with data of accounts in zero points of the plan: 3,7 and 3,8 with, 7,0 and 7,1 with, 12,1 and 12,4 mm, accordingly.

The experimental substantiation of lengthening size is carried out on breadboard models working elements as (D_s=16 mm, l_c=44 mm, D_c=28 mm, l_s=50 mm). Improvement of technology of manufacturing of working elements as "sylphon–container" has allowed to reduce influence of shrinkage at crystallization. By warming up breadboard models was made in the furnace. The comparison results of the given experiments with results of estimations on model (7) are resulted on Fig. 5. We shall note the good consent of the given measurements and modeling, that proves applicability of developed techniques and mathematical models for estimated accounts of the characteristics of PDSR working elements.

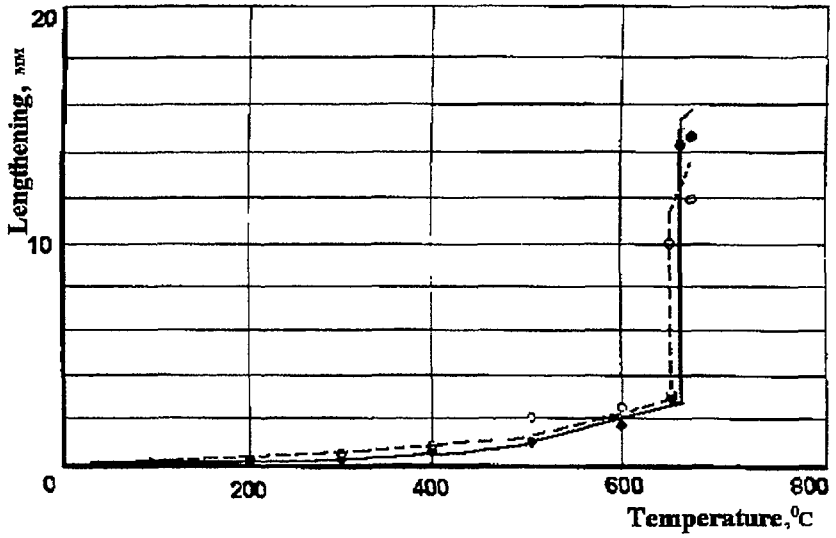

FIG.5 Independent PDSR lengthening of temperature

●, ——— **Aluminium (experiment, calculation)**

○, - - - **Magnesium (experiment, calculation)**

CONCLUSIONS.

Is reasonable perspective to use the effect of volume increase at melt of substance for creation of accident protection devices on a level of temperature, including passive devices of an emergency stop nuclear reactor.

PDSR of an offered type have a number of advantages before known: threshold character of operation, generation of significant efforts, low sensitivity to the operational factors (including a neutron fluence), reliability of operation and simplicity of a design.

Carried out calculated and experimental research in a substantiation of PDSR for reactor BN-600 have shown, that:

- in quality of temperature-sensitive substance expediently to use aluminium or magnesium;
- corrosion stability of steel sylphon under PDSR operating conditions is experimentally reasonable;
- techniques of account sluggishness and lengthening of working elements as sylphon and "sylphon-container" are developed, mathematical models for an estimation of the element characteristics are received;
- serviceability of a sylphon design is experimentally shown, demonstrated that the small influence will complicate creation of PDSR with elements of the given type;
- carried out calculated and experimental study of characteristics of the working elements as "sylphon-container" has shown, that they have number of advantages beforesylphon, first

of all greater size and variable of a working course, and also opportunity to use the substances with small increase of volume at melt;

- the characteristics of perspectiv working elements (time of operation 3÷8 with at a course 2÷5 mm) provide a passive emergency stop of reactor in a case of the heaviest script of development of anticipated accident prior to the beginning of sodium boiling.

ACKNOWLEDGEMENT

The authors are grateful to Maltsev V.G., Novicov A.Ye., for help in realization of experiments, Portianoy G.A. for "know-how" in making for the device, Stepanov I.A for participation in the development of a technique of account, Bagdasarov Yu.E., Buksha Yu.K., Voznesenski R.M., Poplavski V.M. for their support and discussion of the received results.

REFERENCES

[1] VOZNESENKI R.M., EGOROV V.S., LISITSA V.G., et al. Development and study of the characteristics of the passive device emergency protection for fast reactor, working on several physical effects on excess of temperature leaving from core sodium. // Preprint IPPE-2549, 1996, 27 p.

[2] ÎKADA K., TARUTANI K., SHIBATA Y., et al. The Design of a Backup Reactor Shutdown System of DFBR//IAEA IWGFR Technical Committee Meeting, 3-7 July, 1995, Obninsk, Russia. IAEA-TECDOC-884, 1996, p.113-125.

[3] IONAITIS R.R., SWEDOV N.L. Directly operating emergency protection // Atomic engineering abroad, 1988, ¹ 1, p.10-16.

[4] PATENT USSR ¹423 394,24.02.72

[5] BAGDASAROW YU.E., BUKSHA YU.K., VOSNESENSKY R.M., et al., Development of Passive Safety Devices of Sodium-cooled Fast Reactors //IAEA IWGFR Technical Committee Meeting, 3-7 July, 1995, Obninsk, Russia. IAEA-TECDOC-884, 1996, p.97-106.

[6] PATENT USA ¹ 5051229, 24.09.91

[7] STD 21744-83 Multy-layer metal sylphon. Common specifications.

[8] PORTIANOY A.G, VOZNESENKI R.M., EGOROV V.S., LUZIN V.P., MALTSEV V.G., SERDUN E.N., SOROKIN A.P. An expert estimation of the characteristics of passive devices emergency shutdown fast reactor// Preprint IPPE - 2609, 1997, 16 p.

[9] PATENT RU ¹ 2096009, 21.12.94

[10] BOGOSLOVSKAYA G.P., MATJUKHIN V.I., MIKHIN V.I., SOROKIN A.P., STEPANOV I.A. Transitive Thermal Hydraulic processes in fast reactor core// Atomic Energy, 1996, v. 80, ¹1, p. 11-15.

[11] PHYSICAL SIZES: Directory // Babichev A.P., et al. Ì.: Energyatomizdat, 1991, 1232 p.

[12] ALUMINIUM: PROPERTIES AND PHYSICAL METALLURGY, Ì.: Metallurgy, 1989, 422 p.

[13] THE DIRECTORY OF THE CHEMIST, v. 1, L-Ì, 1963, 1072 p.

[14] LIPCHIN T.N. Structure and properties of colour alloys, hardening under pressure. Ì.: Metallurgy, 1994, 128 p.

MODELING PROBLEMS OF EMERGENCY NATURAL CONVECTION HEAT REMOVAL IN THE UPPER PLENUM OF FAST REACTORS USING WATER

P.A. USHAKOV, A.P. SOROKIN
State Scientific Centre of Russian Federation,
Institute of Physics and Power Engineering,
Obinisk, Kaluga Region, Russian Federation

Abstract

The problem of clearly defined purposes of modeling is posed. Conditions for an approximate modeling developed by the Japanese researchers are analyzed. Problems of modeling are considered *in the events of different Euler criteria in liquid metal cooled reactor and in the water model; in* deciding on structure of simulating heat exchanger etc. It is emphasized that there's no way to simulate the overall transient process from the moment of reactor shutdown up to an establishment of natural convection in the same model.

Analysis of the results obtained in water experiments carried out in Japan and independently in the State Scientific Center of Russian Federation IPPE has shown, that violating the modeling rules is observed at small Peclet numbers in laminar flow because of strong dependence of hydraulic resistance from Reynolds number.

It is proved that transient process may be simulated by the methods acceptable for the stable natural convection. Also it is shown, that modeling reactors with lead-bismuth alloy cooling (similar reactors are discussed at present as perspective ones) can be done easier, than in sodium cooled reactors.

The lines of future researches are proposed as a contributory points for development of the natural convection modeling theory.

1. THE BASIC EQUATIONS FOR A NATURAL CONVECTION [3, 4]

Assumptions:

- Bussinesk approximation.
- Reactor core, heat exchangers are «black boxes» at $Eu = idem$ (area with $\Omega^* = 1$).
- Uniform volumetric heat generation (heat consumption) instead of heat injection and heat rejection.
- The influence of a thermal capacity of constructions is not taken into account
- Thermal property are fixed.

$$\frac{\partial u_i^*}{\partial x_i^*} = 0,$$

$$\frac{\partial u_i^*}{\partial \tau^*} + u_j^* \frac{\partial u_i^*}{\partial x_j^*} = \left(\frac{1}{Re}\right)\frac{\partial^2 u_i^*}{\partial x_j^{*2}} - (Ri)T^*\delta_{1,3} - \frac{\partial p^*}{\partial x_i^*} + (Eu)\Omega^*,$$

$$\frac{\partial T^*}{\partial \tau^*} + u_j^* \frac{\partial T^*}{\partial x_j^*} = \left(\frac{1}{Pe}\right)\frac{\partial^2 T^*}{\partial x_j^{*2}} + \left(\frac{Q}{\rho c V \Delta T L^2}\right)\Omega^*.$$

x_i - coordinate, τ - time, u_i - component of a velocity,

$t - t_o$ - temperature counted from reference temperature,

ρ - pressure, Q - power, $\delta_{1,3}$ - delta-factor of Kronecker

Dimensionless values:

$$x_i^* = \frac{x_1}{L}, \qquad T^* = \frac{t - t_o}{\Delta T}, \quad u_i^* = \frac{u_1}{V}, \qquad p^* = \frac{p}{pV^2}, \qquad \tau^* = \frac{\tau V}{L} = H_o.$$

The criterions of a similarities presented in the equations, include characteristic values.
Similarity criterions system:

$$Ri = \frac{g\beta\Delta TL}{u^2}, \qquad Eu = \frac{\Delta p}{\rho V^2} = \frac{\xi}{2}, \qquad N = \frac{Q}{\rho cV\Delta TL^2},$$

$$Pe = \frac{VL}{a}, \qquad Re = \frac{uL}{v}, \qquad Ho = \frac{\tau V}{L} = \tau^*.$$

The characteristic values are in criterions.

2. VALUES SCALES IN THE REACTOR AND WATER MODEL, TAKING INTO ACCOUNT THE INFLUENCE OF Re ON *Eu*.

Conditions: Ri = Eu [6]

$$2Eu = \xi = \frac{A}{Re_\xi^n}, \qquad A_p = A_M, \qquad N_p = N_M.$$

System of value scales

$$\left(\frac{V_p}{V_M}\right)_\xi \approx \left(\frac{\beta Q}{v^n \rho c L^{1-n}}\right)_p^{\frac{1}{3-n}} \cdot \left(\ \dots\ \right)_M^{-\frac{1}{3-n}}$$

$$\left(\frac{\Delta T_p}{\Delta T_M}\right)_\xi \approx \left[\frac{v^n Q^{2-n}}{\beta(\rho c)^{2-n} L^{5-n}}\right]_p^{\frac{1}{3-n}} \cdot \left(\ \dots\ \right)_M^{-\frac{1}{3-n}}$$

$$\left(\frac{\Delta P_p}{\Delta P_M}\right)_\xi \approx \frac{\rho_p}{\rho_M}\left(\frac{\beta Q}{v^n \rho c L^{1-n}}\right)_p^{\frac{2}{3-n}} \cdot \left(\ \dots\ \right)_M^{-\frac{2}{3-n}}$$

$$\left(\frac{\tau_p}{\tau_M}\right)_\xi \approx \left(\frac{v^n \rho c L^{2(2-n)}}{\beta Q}\right)_p^{\frac{1}{3-n}} \cdot \left(\ \dots\ \right)_M^{-\frac{1}{3-n}}$$

$$\left(\frac{Pe_p}{Pe_M}\right)_\xi \approx \left(\frac{\beta L^2 Q}{v^n \rho c a^{3-n}}\right)_p^{\frac{1}{3-n}} \cdot \left(\ \dots\ \right)_M^{-\frac{1}{3-n}}$$

The boundary condition $(Pe_P)_\xi = (Pe_M)_\xi$ gives exact value of power scale

$$\left(\frac{Q_p}{Q_M}\right)_{Pe,\xi} \approx \left[\frac{v^n a^{3-n}}{L^2}\left(\frac{\rho c}{\beta}\right)\right]_p \left[\ \dots\ \right]_M^{-1}; \qquad \left(\frac{Q_p}{Q_M}\right)_\xi \approx \frac{1}{m_\xi}\left(\frac{Q_p}{Q_M}\right)_{Pe,\xi}$$

m_ξ - factor entered in practice at a power model choice

In (8) - (13) for laminar current $n = 1$, for turbulent - $n = 1/4$

3. VALUES SCALES IN THE REACTOR AND WATER MODEL AT $Eu_p = Eu_м = const$

Conditions: $Ri_p = Ri_м$, $N_p = N_м$, at $n = 0$ In (15) - (20).

Scales from papers [3,4]

$$\frac{V_p}{V_м} \approx \left(\frac{\beta Q}{\rho c L}\right)_p^{1/3} \cdot (\ldots)_м^{-1/3},$$

$$\frac{\Delta T_p}{\Delta T_м} \approx \left[\frac{Q}{\beta(\rho c)^2 L^5}\right]_p^{1/3} \cdot (\ldots)_м^{-1/3},$$

$$\frac{\Delta p_p}{\Delta p_м} \approx \left[\rho^3\left(\frac{\beta Q}{\rho c L}\right)^2\right]_p^{1/3} \cdot (\ldots)_м^{-1/3}$$

$$\frac{\tau_p}{\tau_м} \approx \left(\frac{\rho c L^4}{\beta Q}\right)_p^{1/3} \cdot (\ldots)_м^{-1/3}$$

$$\frac{Pe_p}{Pe_м} \approx \left(\frac{\beta L^2 Q}{\rho c a^3}\right)_p^{1/3} \cdot (\ldots)_м^{-1/3}$$

$$\frac{Re_p}{Re_м} \approx \frac{Pe_p}{Pe_м} \cdot \frac{Pr_м}{Pr_p}$$

$$\left(\frac{Q_p}{Q_м}\right)_{Pe} \approx \left(\frac{\rho c a^3}{\beta L^2}\right)_P \cdot (\ldots)_м^{-1},$$

Thus $m = m_\xi \left(\frac{Pr_м}{Pr_p}\right)^n$.

4. INFLUENCE OF A SYSTEM SCALES CHOICE

Their differences can be characterised by factors K, equal to ratio of scales with dependency and without dependancy of resistance from a Reynold's number. As a result of transformations, it is possible to get relations

$$K_{\Delta T} = K_\tau = \frac{1}{K_V} = \frac{1}{K_{Pe}} = \left(\frac{1}{K_{\Delta p}}\right)^{1/2} = \left[\frac{1}{m}\left(\frac{Pr_м}{Pr_p}\right)^3\right]^{\frac{n}{3(3-n)}},$$

where $K_{\Delta T} = \left(\frac{\Delta T_p}{\Delta T_м}\right) \Big/ \left(\frac{\Delta T_p}{\Delta T_м}\right)_\xi$, $K_\tau = \left(\frac{\tau_p}{\tau_м}\right) \Big/ \left(\frac{\tau_p}{\tau_м}\right)_\xi$ etc..

The values of factors are presented on fig.2 for different values «m» in function of an extent «n» at a Reynold's number in the formula for resistance coefficient.

These data concern to geometrically similar systems of model and reactor having the same resistances relaition from a Reynold's number.

As $m = m_\xi \left(\frac{Pr_м}{Pr_p}\right)^n$, the formula (14) can be noted as follows:

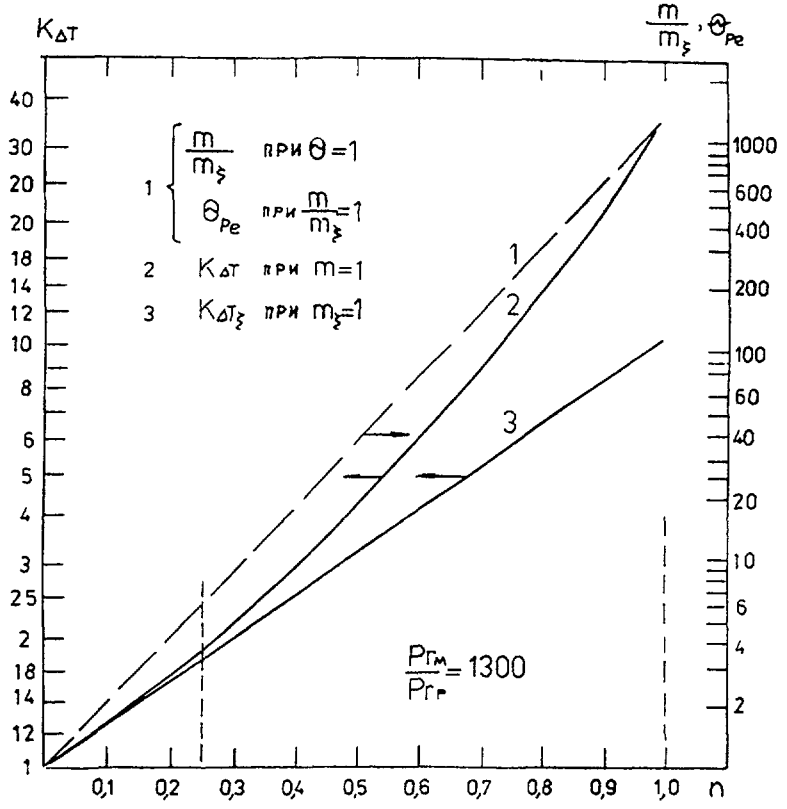

Fig. 1. Dependence of predicted characteristic on a degrec at Reynolds number (n) under conditions of natural convektion.

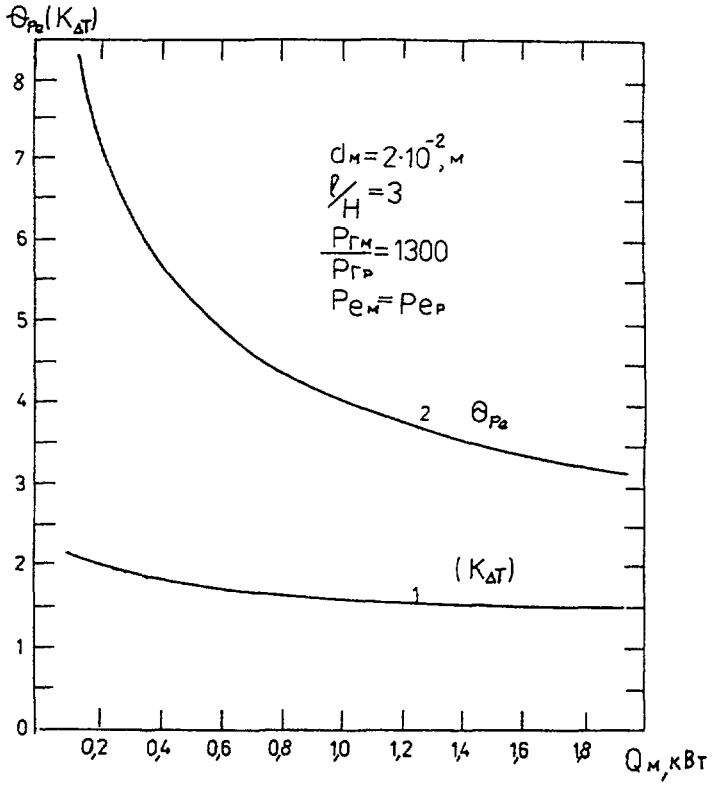

Fig. 2. Power dependence of characteristic of the model under conditions of natural convection.

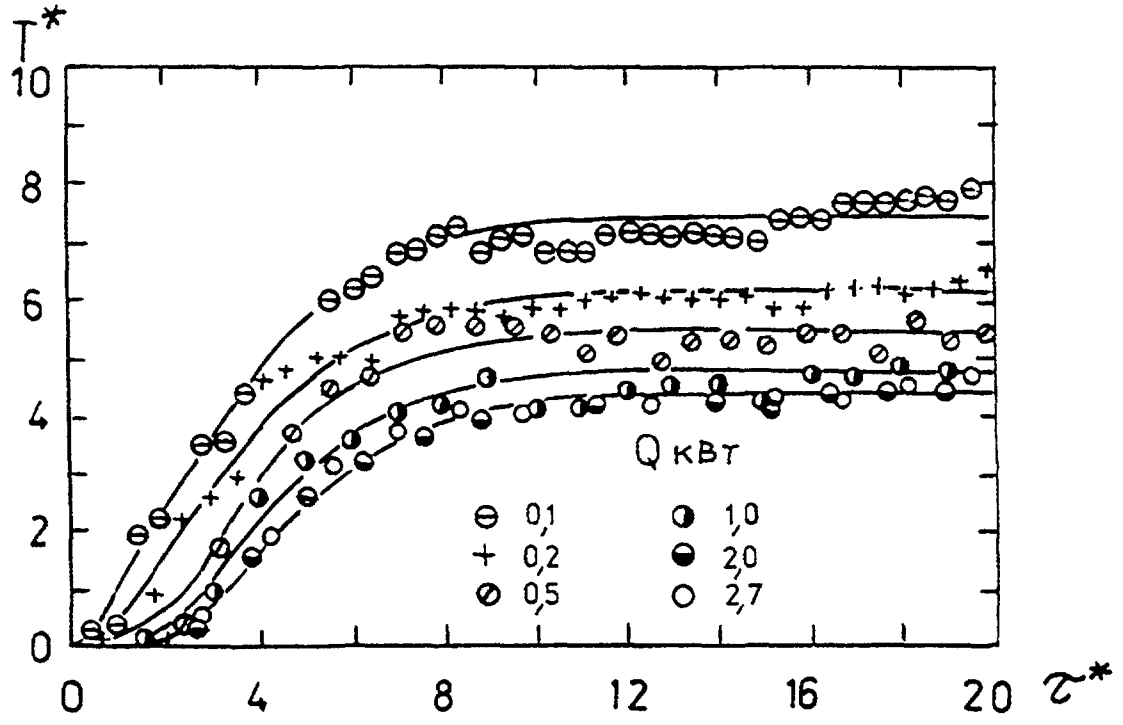

Fig. 3. Time dependence of dimensionless temperature in the flat water model.

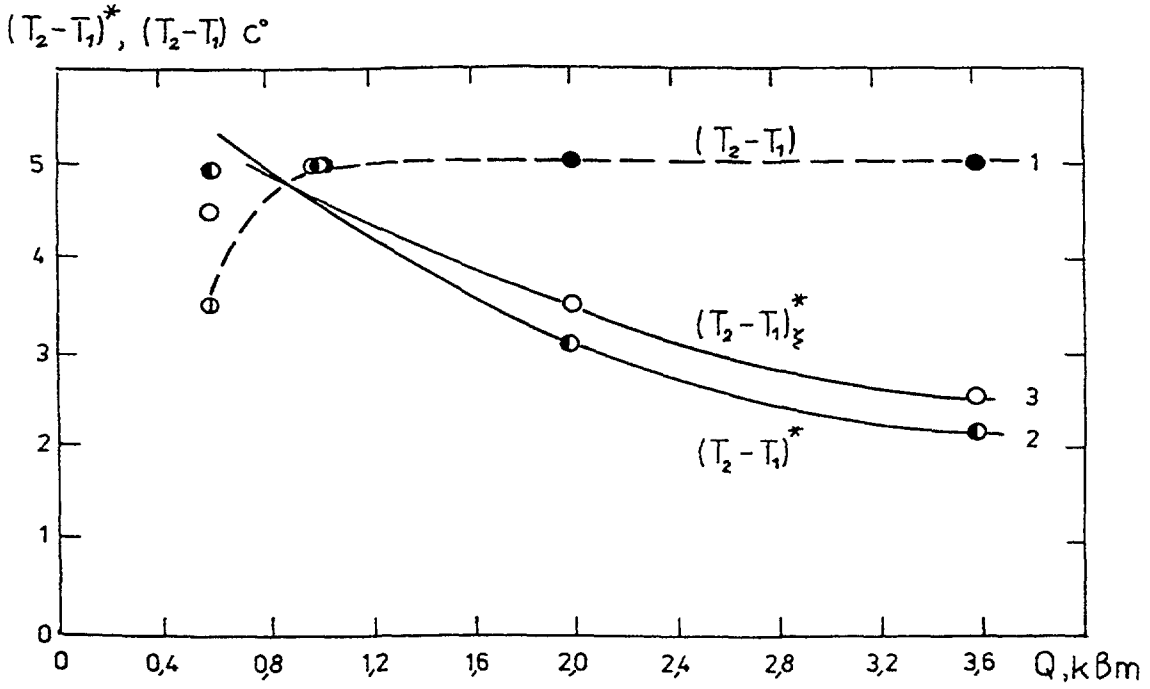

Fig. 4. Power dependence of temperature difference in the upper chamber of the Ramona loop.

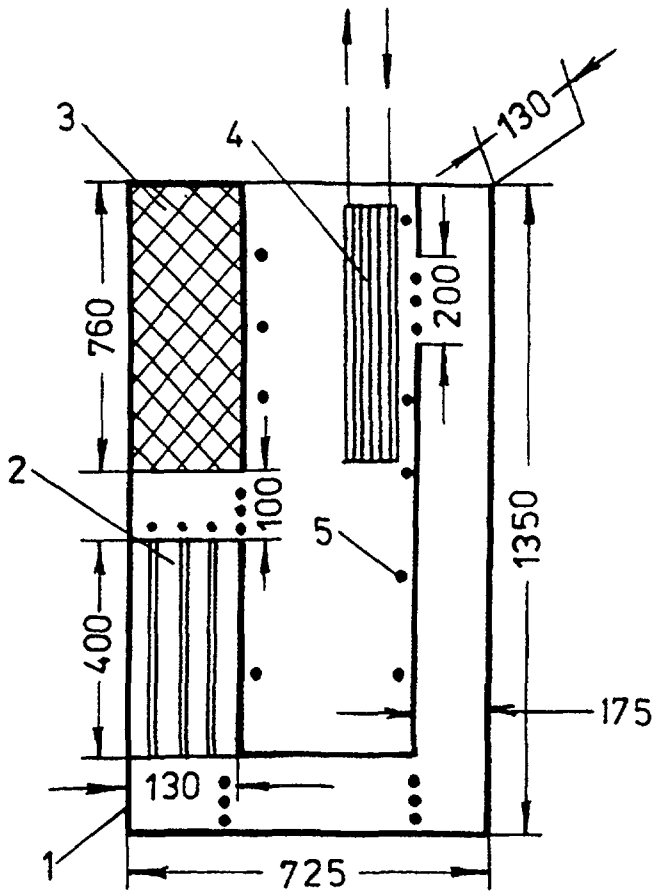

Fig. 5. Schematic of IPPE flat transparent model
1-clad, 2-bundle of heated pins, 3-displacer, 4-immersed heat exchanger, 5-thermocouples

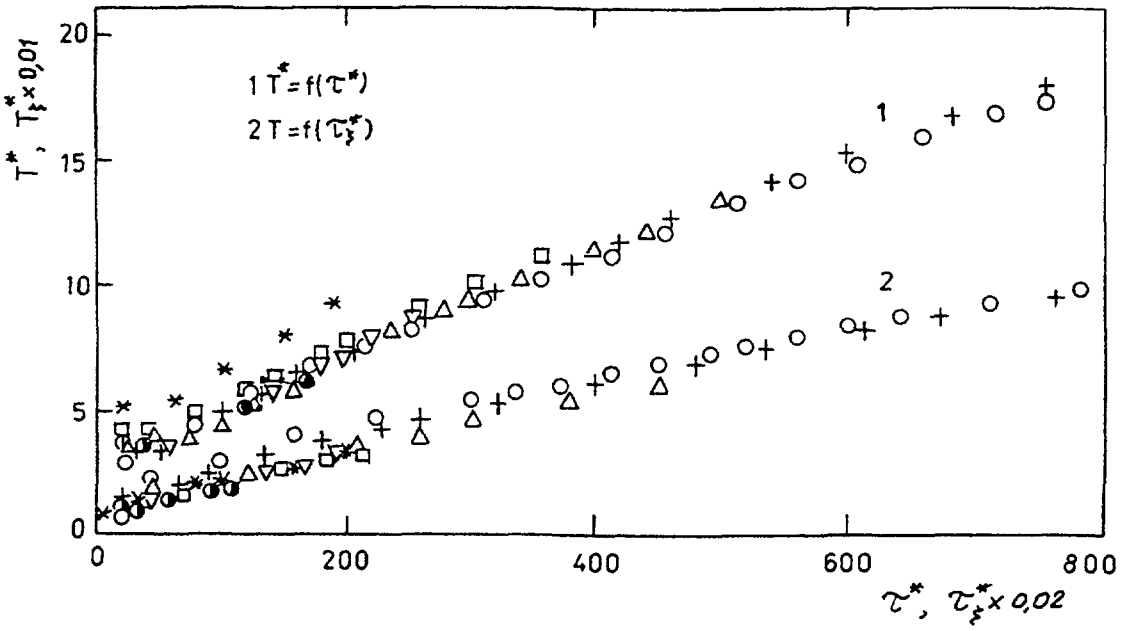

Fig. 6. Dimensionless temperature as a function of dimensionless time at various processing of experimental data obtained at the IPPE

$$K_{\Delta T_\xi} = \left[\frac{1}{m_\xi} \left(\frac{Pr_M}{Pr_p} \right)^{3-n} \right]^{\frac{n}{3(3-n)}}$$

$$K_{\Delta T} = K_{\Delta T_\xi} \text{ at } \frac{Q_M}{Q_p} = \text{idem}$$

The necessity of introduction of factor m follows from a Table I.

TABLE I. VALUES SCALES IN A WATER MODEL AT $\frac{Ri_p}{Ri_M} = \frac{N_p}{N_M} = \frac{Pe_p}{Pe_M} = \frac{Eu_p}{Eu_M} = 1$

$M = \frac{L_M}{L_p}$	$\left(\frac{Q_M}{Q_p}\right)_{Pe}$,10^{-6}	$\left(\frac{\Delta T_M}{\Delta T_p}\right)_{Pe}$,10^{-3}	$\left(\frac{V_M}{V_p}\right)$,$10^{-3}$
1/3	0,5	0,2	6,8
1/4	1,1	0,5	9,1
1/5	1,7	0,9	11
1/6	2,4	1,6	14
1/8	4,2	3,8	18
1/10	6,6	7,4	23

5. THE PROBLEMS TO BE SOLVED FOR DEVELOPMENT OF PRINCIPLES OF NATURAL CONVECTION MODELING

- The further development of numerical codes for prediction mixed, transitive and established natural convection
- Analysis and selection of the data available, for verification of codes
- Development of a problem of natural convection heat removal, as from fuel elements within subassembly and in the intersubassly gap
- Development of experimental techniques taking into account heat capacity of the reactor units
- Numerical experiments for simple models of influence of various criteria of similarity, including for imaginary of coolants
- The prove an opportunity of experimental identification of the processes transient mixed convection with steady state natural convection
- Development of the reasonable principles of a choice of models emmersed heat exchendger and methods of operative regulation of their power
- Developmen of simple approximate measurement of local velocity of water in models under conditions natural convection

REFERENCES

[1] INTERNATIONAL ATOMIC AGENCY, IWGFR/88. Specialists' Meeting on "Evaluattion of Decay Heat Removal by Natural Convection". 22-23 Feb.1993. Oarai Ång. Center, PNC, JAPAN.

[2] EGUCHI Y., YAMAMOTO K., KOGA T., TAKEDA H., SASAKI K., KAJIWARA H., TODA M., Maekàwa I. Experimental and Computational Study on Prediction of Natural Circulation in Top-entry Loop-type FBR // Loîk at [1], pp. 86-96.

[3] EGUCHI Y., TAKEDA H., KOGA T., TANAKA N., YAMAMOTO K. Quantitative Prediction of Natural Circulationin in an LMFR with a Similarity law and a Water Test // Nuclear Engineering Design 178 (1997), pp. 295-307.

[4] TAKEDA H., KOGA T. Study on Similarity Rule for Natural Circulation Water Test of LMFBR // Look at [1], pp.58-66.

[5] USHAKOV P.A., SOROKIN A.P. Influence of a Reynold's number at modelling of a natural convection in liquid metals // Atomic Energy, in a seal.

[6] USHAKOV P.A., SOROKIN A.P. Problems of modelling on water of an emergency tap of residual heat release by a natural convection. Preprint IPPE // 2585, Obninsk, 1997.

[7] WEINBERG D., HOFFMANN H., OHIRA H., SCHNETGKE G. The status of Studies Using RAMONA and Neptun Models on Decay Heat Removal by Natural Convection for European Fast Reactor // Look at [1], p.56

FAST REACTOR CORE THERMAL-HYDRAULIC ANALYSES DURING TRANSITION FROM FORCED TO NATURAL CIRCULATION

M. NISHIMURA, H. OHSHIMA, H. KAMIDE
O-arai Engineering Center,
Power Reactor and Nuclear Fuel Development Corporation,
O-arai, Ibaraki-ken, Japan

ABSTRACT

The modeling for inter-subchannel mixing effects was presented to simulate the fast reactor transition from rated to natural circulation decay heat removal conditions which was usually accompanied by all flow regimes: forced, mixed and natural convection. The model was constructed based on correlations for mixing and pressure drop coefficients developed at MIT. This correlation was originally proposed for steady states subchannel analyses. In the present study, application of the mixing correlation was extended to unsteady multi-dimensional analyses by introducing a threshold function. The function enabled to switch the correlations adequately with change of the flow regimes, depending on Richardson number which is an index of buoyancy effect on the flow field. The modeling was validated through calculation of sodium experiments featuring 37, 61 and 169-pin bundle subassemblies. Comparisons of the experimental and numerical results revealed that the modeling was capable of predicting the core thermal-hydraulic field under wide spectrum of flow rate and heating conditions.

1. INTRODUCTION

The prediction of temperature distribution in the fuel subassembly is one of the most important issues for the reactor safety assessment. Temperature distributions thus the maximum cladding temperature in the subassemblies are interactively affected by inter-subassembly heat transfer and cooling capability of an inter-wrapper flow. To take account of the interactions among these phenomena in the core, computational simulations should calculate whole core region. And in some cases an upper plenum region should be also included in the modeling. In order to treat these interactive and complex phenomena in the reactor, a multi-dimensional thermal hydraulic analysis is one of the most promising methods. Therefore a modeling was developed for the multi-dimensional analysis to predict the thermal-hydraulic field in the subassembly. In the present modeling, a staggered half pin mesh arrangement[1] and the inter-subchannel mixing coefficient[2],[3] were employed. The staggered half pin mesh has a similar feature to the subchannel analysis, in which each mesh accommodates only 1 subchannel in its horizontal cross section. The inter-subchannel mixing, which is caused by wire sweeps, turbulence, and thermal plumes due to heating, is one of the most important parameters predominating temperature profiles inside the subassembly. The mixing correlation developed at MIT for the subchannel analysis was applied to the diffusion terms of the conservation equations in the multi-dimensional thermal hydraulic code AQUA. Basque had used this mixing correlation in a multi-dimensional code to predict the thermal hydraulic fields of coolant in the single spent fuel subassembly[4]. His prediction gave fairly good agreement with experiments in natural and mixed convection regimes.

In the present study, the usage of this modeling was extended to transient analyses, and its applicability was examined. A threshold function[5] was proposed to control the usage of mixing factors and enabled to handle the all flow regimes continuously; forced, mixed and natural convection, appeared in the reactor transient conditions.

A comparison of the multi-dimensional analysis and the subchannel analysis was also made to examine the consistency of formulations between the two analytical methods. Because MIT's correlation was derived for the subchannel analysis but not for the multi-dimensional analysis.

The code was validated through the analysis of the sodium experiments; 37-pin, 61-pin, and 169-pin subassembly steady state experiments. The first two tests accompanied by the inter-subassembly heat transfer. The simulation capability was also examined for 7-subassembly sodium tests under transition from forced to natural circulation conditions simulating scram transient to natural circulation decay heat removal (NC/DHR) in the real reactor with and without inter-subassembly heat transfer.

2. COMPUTATIONAL TECHNIQUES

2.1 Governing equations

A porous body model[1] was used to simulate the thermal hydraulic field in the fuel pin bundles, in which volume porosity and surface permeability of the fluid were used. The differential conservation equations of mass, momentum, and energy for the flow in porous medium can be written as the following forms.

Conservation of mass:

$$\gamma_v \frac{\partial \rho}{\partial t} + \frac{\partial \left(\gamma_i \rho U_i\right)}{\partial x_i} = 0. \tag{1}$$

Conservation of momentum in the *i*-direction:

$$\gamma_v \frac{\partial \rho U_i}{\partial t} + \frac{\partial \left(\gamma_j \rho U_i U_j\right)}{\partial x_j} = -\gamma_v \frac{\partial p}{\partial x_i} + \frac{\partial}{\partial x_j}\left(\gamma_j \rho \Gamma_m \frac{\partial U_i}{\partial x_j}\right) + \gamma_v g_i(\rho - \rho_0) + R_f . \tag{2}$$

Conservation of energy:

$$\gamma_v \frac{\partial \rho h}{\partial t} + \frac{\partial \left(\gamma_j \rho U_j h\right)}{\partial x_j} = \frac{\partial}{\partial x_j}\left(\gamma_j \rho \Gamma_e \frac{\partial h}{\partial x_j}\right) + q_{rod} . \tag{3}$$

where,

$$\Gamma_m = Pr_t \times (\varepsilon_l + \varepsilon_M) + \kappa\nu \text{ : total diffusivity of momentum,} \tag{4}$$

$$\Gamma_e = \varepsilon_l + \varepsilon_M + \kappa \frac{\lambda}{\rho c_p} \text{ : total diffusivity of energy,} \tag{5}$$

$$Pr_t = 1 \text{ : turbulent Prandtl number.} \tag{6}$$

These conservation equations were discretized to finite difference form by integrating over each control volume of computational mesh. In the code, a thermal structure model was also employed to take into account of heat capacity and conduction inside the heater pins.

2.2 Mixing correlations for the fuel subassemblies

A systematically formulated correlation was constructed at MIT for the mixing factor which is applicable to all flow regimes[2],[3]. Cheng and Todreas[2] reported that under the forced convection, the mixing due to swirl flows generated by wrapped wire spacers on the pins plays key role. While the mixing induced by thermal plumes prevails in the mixed convection flow regime. And the inter-subchannel mixing plays minor role under the natural convection condition. Because an inter-

subchannel flow redistribution is predominant in determining temperature profiles inside the subassemblies. From these context and as in equations (4) and (5), diffusivity was divided into three terms regarding there physical effects as follows.

2.2.1 Mixing effect due to wire spacer sweep and turbulence

The effective diffusivity representing wire spacer sweep and turbulence mixing were defined as follows.

$$\varepsilon_l = \varepsilon_{l\eta}^{*} \cdot V_i \cdot \eta \tag{7}$$

where,

$\varepsilon_{l\eta}^{*}$: non-dimensional effective diffusivity for wire spacer sweep and turbulence mixing which depends on geometrical parameters of the pin bundle and local Reynolds number Re_i.

$$Re_i = \frac{V_i\, De_i}{\nu} \tag{8}$$

V_i : axial velocity component

η : distance between the subchannels under consideration

subscript,

i = 1 : refers to interior subchannel
= 2 : refers to edge subchannel.

In MIT's correlation, above non-dimensional effective diffusivities were individually defined for interior and edge subchannels. According to reference [2], the non-dimensional effective diffusivity for the interior subchannel were derived from Reynolds number range from 400 to 1.0×10^6. In this correlation, Reynolds numbers were based on the averaged velocities within the same category of subchannel : interior or edge. Though, local, mesh-wise velocities were referred for the definition of Reynolds number in AQUA. Since, local difference may occur when the inter-subassembly heat transfer is large, which causes a steep temperature gradient across the bundle and even a reverse flow at a cold side.

For the surrounding subassemblies, factor of 0.2 was multiplied to $\varepsilon_{l\eta}$ to fit the calculation to the experiment. Since the surrounding subassemblies consisted of 7- pin bundles, which had only one layer of the inner subchannels, making more difficult to establish a consistent formulation compared to bundles with more than 19 pins.

2.2.2 Mixing effect due to thermal plumes

The effective diffusivity for the mixing effect of thermal plumes were defined similarly as $\varepsilon_{l\eta}$.

$$\varepsilon_M = \varepsilon_{\eta M}^{*} \cdot V_i \cdot \eta \tag{9}$$

$$\varepsilon_{\eta M}^{*} = 0.1 \cdot \left(\frac{c}{D}\right)^{-0.5} \left(\frac{Gr_{\Delta T}}{Re_b}\right) \tag{9.a}$$

where,

$\varepsilon_{\eta M}^{*}$: non-dimensional effective diffusivity for thermal plumes mixing which depends on geometrical parameters of the pin bundle and non-dimensional parameter $Gr_{\Delta T} / Re_b$,

$Gr_{\Delta T}$: Grashof number based on axial temperature gradient proposed by Engel et al.[6], defined as follows,

$$Gr_{\Delta T} = \frac{g\beta\left(\frac{\Delta T_b|_0^L}{L}\right)De_b^4}{\nu^2} \tag{10}$$

Re_b : Bundle averaged Reynolds number,

$$Re_b = \frac{V_b De_b}{\nu}. \tag{11}$$

This correlation was derived from data under the following conditions[3],

$$170 \le Gr_{\Delta T} \le 650 \quad ; 520 \le Re_b \le 4400$$
$$0.06 \le Gr_{\Delta T} / Re_b \le 0.73 ; 1.08 \le P/D \le 1.25.$$

In the above expressions, $Gr_{\Delta T}$ is defined at the top end of the heated section. In other words, it is based on the averaged axial temperature gradient within the heated length. This definition encounters no inconsistency as far as concerning a single subassembly. And Cheng and Todreas[2] used $Gr_{\Delta T}$ which was resulted in an averaged $\varepsilon_{\eta M}$ within the heated length. On the other hand, for multi subassemblies with inter-subassembly heat transfer, variation of the axial temperature gradient exists. Therefore, a local axial temperature gradient was introduced for $Gr_{\Delta T}$ denoted by $Gr^*_{\Delta T}$:

$$Gr^*_{\Delta T} = \frac{g\beta\frac{\Delta T_b}{\Delta z}\Big|_K De_b^4}{\nu^2} \tag{12}$$

where K is an index of axial node number of a computational mesh. In AQUA, $Gr^*_{\Delta T}$ and axially local $\varepsilon_{\eta M}$ were used.

2.2.3 Thermal conduction with geometric effect of the subchannel

The geometric effect depends on bundle arrangements only. The shape factor in Eq. (4) is introduced for the bare bundles as follows,

$$\kappa = 0.66\left(\frac{P}{D}\right)\left(\frac{c}{D}\right)^{-0.3}. \tag{13}$$

Cheng and Todreas[3] suggested that the above correlation is also applicable to the wire-wrapped pin bundles. Since the relative importance of conduction is not significant compared to the other three : the flow redistribution in the low Reynolds number range, the thermal plume mixing in the mixed convection condition, and the wire sweep under the condition $6000 < Re$.

2.3 Threshold function for the flow regime changing

We introduced a threshold function to cut off the diffusivity of thermal plumes under inertia dominated conditions. This function goes from 1 to 0 when Richardson number decreasingly passes

through value of 0.1, since no thermal plumes were observed under the condition with Richardson number below 0.1, in the results of existing studies[2],[7]. The function is defined as follows :

$$fx_{pl} = \max\left[0,1-10^{\{-6\cdot(Ri-0.1)\}}\right] \tag{14}$$

$$Ri = \frac{Gr}{Re_i^2} \tag{15}$$

$$Gr = \frac{g\beta\Delta T_b|_0^L De_b^3}{\nu^2} = Gr_{\Delta T}\frac{L}{De_b}. \tag{16}$$

We assumed that this threshold of Ri is applicable to a local state, as well as an average condition of the heated length. Namely,

$$\Delta T_b|_0^L = \left.\frac{\Delta T_b}{\Delta z}\right|_K \cdot L \tag{17}$$

$$Gr = Gr^*_{\Delta T}\frac{L}{De_b}. \tag{18}$$

Figure 1 shows a curve of fx_{pl} versus Ri.

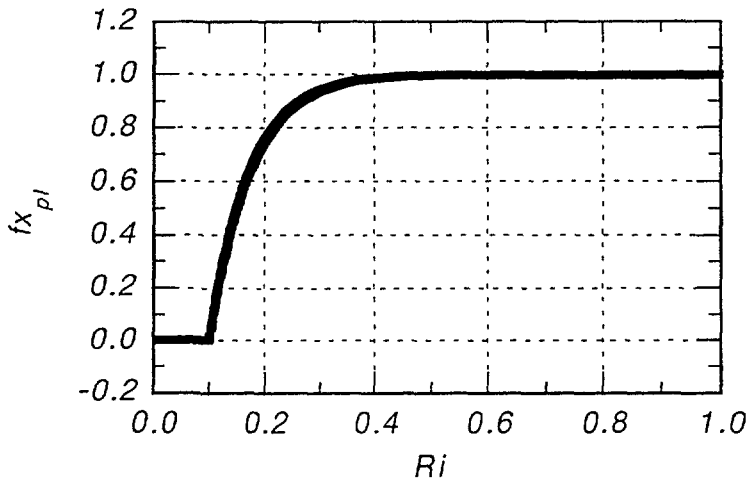

FIG. 1 Curve of the threshold function for the diffusivity of thermal plume mixing

2.4 Computational algorithms

Calculation conditions are summarized in Table 1. A first upwind scheme was applied to this calculation with which error caused by numerical diffusivity was suggested in some cases. In the pin bundles though, the flow resistance term R_f is predominant in the momentum equation (2). Therefore, the numerical diffusion is relatively negligible.

TABLE 1 CALCULATION CONDITIONS

Numerical Method	
Algorithm	: SIMPLEST-ANL[8]
Linearization	: Iterative Method
Matrix Solver	: MICCG[9] (for p eq.)
	Point SOR (for all the other eqs.)
Discretization Scheme	
Convection Term	: 1st-order Upwind
Diffusion Term	: 2nd-order Central Differential
Time Integration	: Implicit Euler
Physical Models	
Porous Body Model	: COMMIX type[1]
Flow Resistance Model	: correlation of Cheng and Todreas[3]
Heat Transfer Mode l	: correlation of Sabbotin

The axial component of the flow resistance was modeled by the correlation of Cheng and Todreas[3]. While no correlation was used for the cross flow component assuming that the relative magnitude of this component was much smaller than the axial component.

Inter-subassembly heat transfer between two neighboring subassemblies were taken into account by using a thermal structure model. One-dimensional conduction equation was solved in the normal direction to the wrapper tube face. The sodium coolant in the inter-wrapper gap was assumed to be stagnant. Thus the steel-sodium-steel composite slab was formed in each thermal structure model. Heat transfer coefficients inside the wrapper tube were calculated with Subbotin's correlation for the pin surface and the inner surface of the wrapper tube:

$$Nu = 5.0 + 0.025Pe^{0.8}. \tag{19}$$

The uniform profile inlet velocity and temperature were specified to each subassembly as boundary conditions. For momentum equations, velocity components normal to the outlet boundary surfaces were specified to satisfy the mass conservation law concerning the outlet control volumes. For energy equation, adiabatic condition was applied at the outlet. And constant pressure condition was given to the outlet control volumes, as a Dirichlet pressure boundary condition.

3. THE EXPERIMENTS AND MODELING

For validation of the code, various sodium experiments were simulated. Firstly, the calculation were performed on the steady state tests. And the test of transition from forced to natural circulation was also calculated. For simulation of transitions, the correlations used in the code are needed to simulate the change of flow regimes continuously .

3.1 The 61-pin bundle with inter-subassembly heat transfer

A schematic diagram of core component test loop (CCTL-CFR)[10] and its test section are shown in FIG. 2. The test section is consisted of a 61-pin bundle and two 19-pin bundles, simulating the driver and blanket subassemblies respectively. Each bundle is such bounded by solid steel slab to the others that the heat flux due to the inter subassembly heat transfer is measurable using thermocouples attached on the slab surfaces. A cooling channel was also equipped in 61-pin bundle behind the wrapper wall opposite to the 19-pin bundle side to provide various thermal boundary conditions simulating the inter-subassembly heat transfer. Table 2 shows specifications of the test rigs simulated in the present code validation. The staggered half pin mesh arrangement were used to simulate the fuel pin bundles as illustrated in FIG. 3.

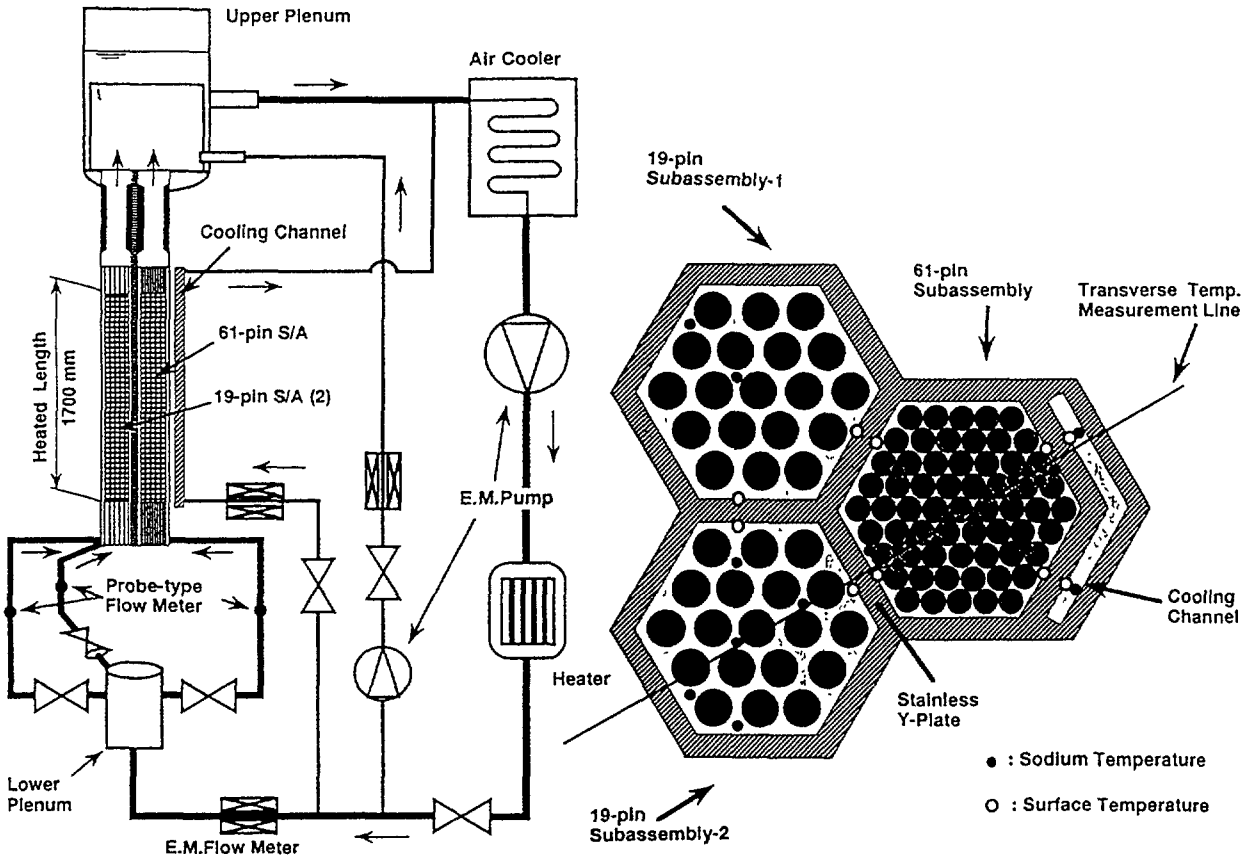

FIG. 2 Schematic diagram of core component test loop (CCTL-CFR) and its test section

In the simulation, symmetry of thermal-hydraulic field was assumed based on the geometry and boundary conditions of the test section. And one half of the cross section was taken into account of the computational region. The cross sectional computational region was divided in two domains: one is for 61-pin and another is for 19-pin bundles. Because the dimension of pin diameter and pitch was different from 61-pin and 19-pin bundles, it was impossible to apply the staggered half pin mesh arrangement in unique computational domain and coordinate. These two domains, i.e. bundles, ware thermally connected by using a thermal structure model representing the wrapper tube (Y-plate) wall.

TABLE 2 SPECIFICATIONS OF SODIUM TEST SUBASSEMBLIES

		CCTL-CFR		169-pin	PLANDTL-DHX	
		Driver	Blanket		Center	Surrounding
Number of Subassemblies		1	2	1	1	6
Number of Pins		61	19	169	37	7
Pin Diameter	(mm)	16.0	25.0	6.5	8.3	20.8
Pin Pitch	(mm)	17.4	30.2	7.86	9.9	22.4
Spacer Wire Diameter	(mm)	1.4	5.2	1.26	1.5	1.5
Spacer Wire Lead	(mm)	200	700	306	165	165
Wrapper Tube Inner Flat to Flat Distance	(mm)	140.0		104.6	63.0	
Inter-wrapper Gap Width	(mm)	0		-	7	
Wrapper Tube Thickness	(mm)	15		3	4	
Heated Length	(mm)	1700		930	1000	
Axial Power Profile		Uniform		Uniform	Chopped Cosine	

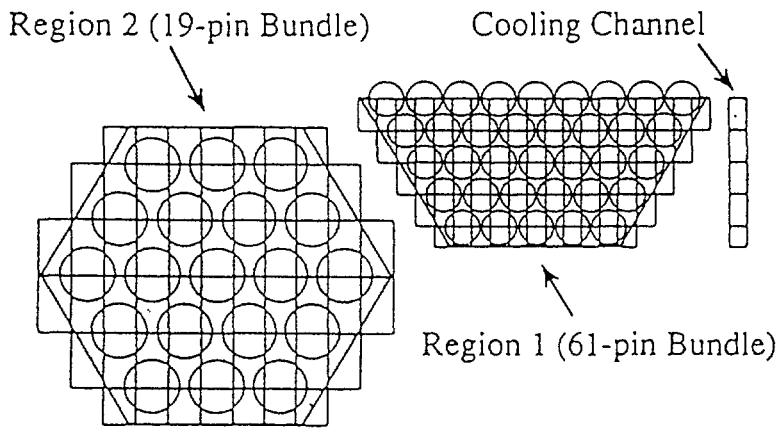

FIG. 3 Mesh arrangement in the horizontal plane for CCTL-CFR

TABLE 3 TEST CONDITIONS OF CCTL-CFR

Case No.	Heater Power (kW/Ass.)		Flow Rate (ℓ/min/Ass.)			Inlet Temperature (℃)			Heat Transfer To 61pin Bundle
	61 pin Bundle	19 pin Bundle	61 pin Bundle	19 pin Bundle	COOLING CHANNEL	61 pin Bundle	19 pin Bundle	COOLING CHANNEL	
61A	14.5	33.5	10.3	13.1	1.0	251.3	252.1	247.2	heated
61B	15.3	7.8	29.4	13.5	0.0	251.2	252.2	-	isothermal

Test conditions of CCTL-CFR used in the code validation were shown in Table 3. In Case-61A, 61-pin bundle was heated by the 19-pin bundles and cooled by the cooling channel featuring heat flux crossing the 61-pin bundle. While 61-pin bundle was under almost adiabatic wrapper wall condition in Case-61B.

3.2 The sparsely heated 169-pin subassembly

This test rig had a 169-pin fuel subassembly model in which heater pins were installed sparsely. Specifications of the test rig are listed in Table 2. The capability of each heater pin was 300 W/cm. FIG. 4 shows the mesh arrangement for this bundle together with positions of the heater pins. Test conditions cited for the code validation is listed in Tale 4. Reynolds numbers in Case-169A and Case-169B were 5.5×10^4 and 2.7×10^3 respectively corresponding forced and natural circulation conditions.

TABLE 4 TEST CONDITIONS OF 169-PIN BUNDLE

Case No.	Heater Power (kW)	Flow Rate (ℓ/min)	Inlet Velocity (m/s)	Inlet Temperature (℃)
169A	122.90	1220.0	5.56	394.4
169B	6.86	59.8	0.27	392.5

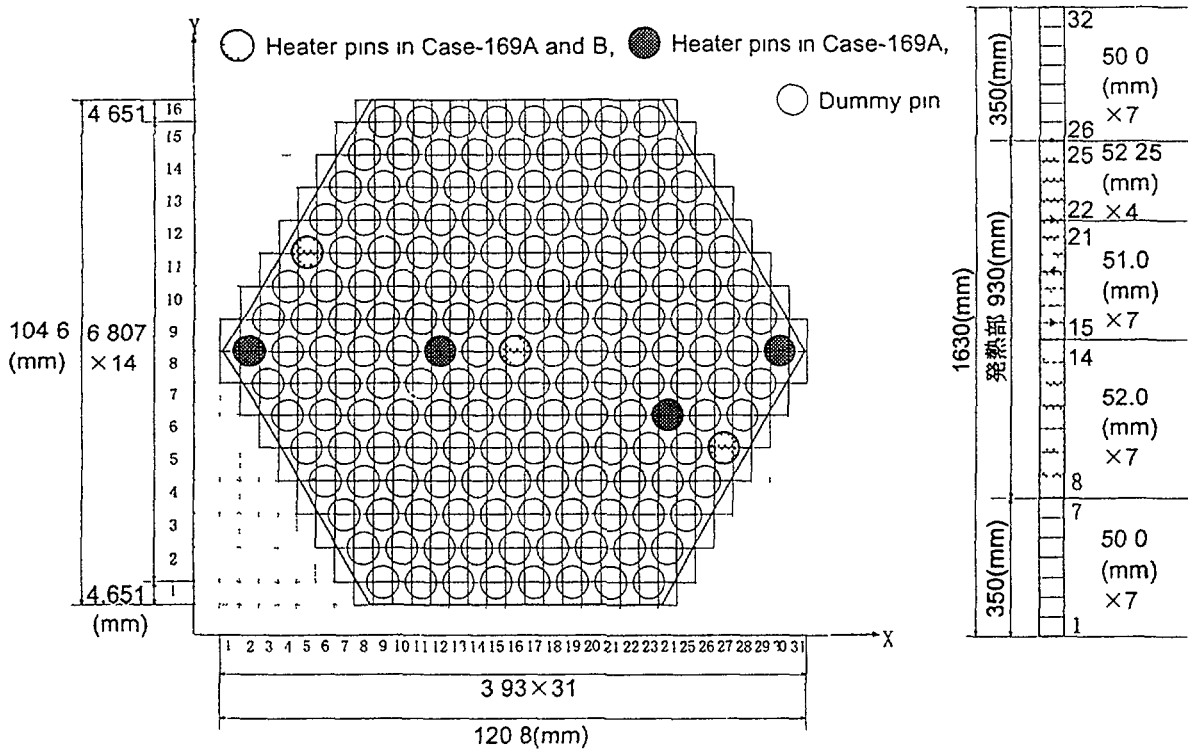

FIG. 4 Mesh arrangement for 169-pin subassembly with positions of heater pins

3.3 The 7-subassembly under transition from forced to natural circulation

3.3.1 The facility and its modeling

To simulate the complex phenomena in the reactor, a core model composed of seven subassemblies was installed in the sodium test loop PLANDTL-DHX. A schematic flow diagram of PLANDTL-DHX is shown in FIG. 5. The core model's horizontal cross section is illustrated in FIG. 6, and Table 2 shows specifications of it. The core model was connected to the upper plenum in which DHX of a direct reactor auxiliary cooling system (DRACS) was immersed to remove the decay heat. The inter-wrapper gaps filled with sodium were also connected to the upper plenum. The primary circuit had IHX equipped with primary reactor auxiliary cooling system (PRACS), a pump, and a

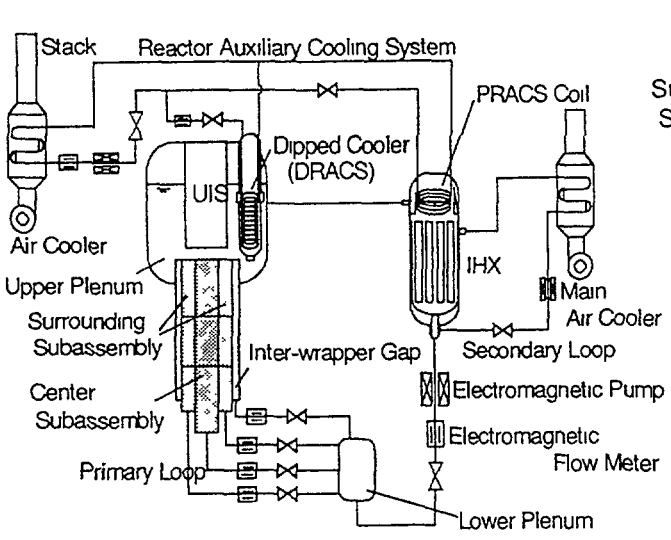

FIG. 5 Flow diagram of PLANDTL-DHX

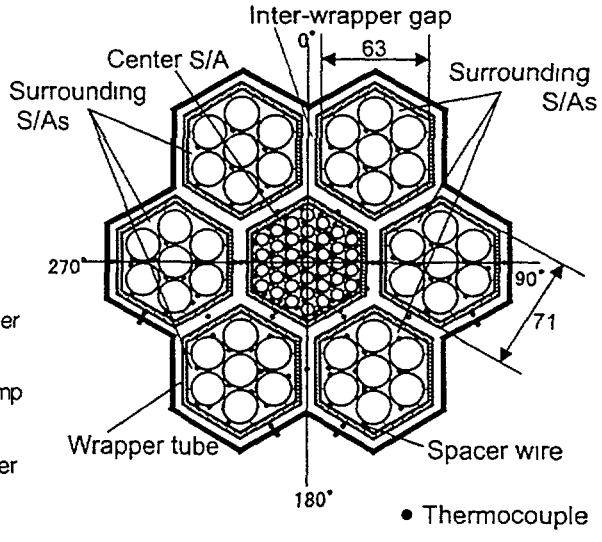

FIG.6 Horizontal cross section of the core model

lower plenum. Sodium coolant flow was fed by three lines respectively to the center subassembly, the three surrounding subassemblies ranging in one side, and the opposite side. The flow rate in each line of the three was controlled individually. The secondary circuits of the IHX and the two reactor auxiliary cooling systems had air coolers and pumps. This facility could simulate transitions from forced to the NC/DHR conditions in the primary and decay heat removal systems of FBRs.

The center subassembly consisted of a 37-pin bundle. And each surrounding subassembly had a 7-pin bundle. Every pin was heated by electrical heater. The pin bundle in the center subassembly simulated a core fuel pin of a large FBR in full scale. The flat to flat distance of the subassembly was about 1/2 of that of large size FBRs which contains 217 or 271 fuel pins.

Coolant temperatures of the core model were measured by K-type thermocouples of 0.3 or 0.5 mm in diameter. The positions of thermocouples were also shown in FIG. 6. The signal of temperature, flow rate, and electric power of heater pins were recorded at a sampling interval of 0.096 seconds using a mini-computer system.

Symmetry respect to the vertical center plane of the core model was assumed on the thermal hydraulic field regarding the geometry and the boundary conditions. Again the staggered half pin mesh arrangement was applied to the core model of PLANDTL-DHX. In vertical direction, each subassembly was divided into 29 meshes for the total length of 2825 mm. And the mesh widths in the heated length were 82.5 mm or 87.5 mm. A transient calculation was also performed using finer mesh with half width in vertical direction; i.e. 41.25 mm or 43.75 mm in the heated length. However, no apparent difference was obtained compared to the reference mesh.

3.3.2 Test cases

IHX was used as a heat sink of the primary system to suppress inter-wrapper flow for both steady state and transient experiments. IWF is also suppressed if the PRACS were applied as a heat sink. Therefore, the experiments bellow were characterizing NC/DHR with IHXs or PRACSs.

A. Steady state experiments

Steady state experiments were carried out regarding two parameters: the flow rate and the heater pin power in the center subassembly. We show test conditions of the simulated experiment in TABLE 5. Case-ST43 featured forced convection. While Case-ST70,72 and 80 were corresponded to mixed convection flow regime imposing adiabatic, cooled and heated inter-subassembly heat transfer conditions respectively to the center subassembly.

TABLE 5 TEST CONDITIONS OF PLANDTL-DHX FOR STEADY STATE CALCULATIONS

Case No.	Heater Power (kW/ass.)		Flow Rate (ℓmin/ass.)		Inlet Temperature (℃)	Δ T Center-Surround (℃)	Heat Transfer To Center Bundle
	Center	Surr.	Center	Surr.			
ST43	144.3	144.3	49.0	49.0	298.5	298.5	Isothermal
ST70	24.0	23.0	8.0	7.7	300.0	0	Isothermal
ST72	24.0	15.9	8.0	7.7	300.0	-50	Cooled
ST80	24.0	27.5	8.0	7.7	300.0	+30	Heated

For Case-ST43 a comparison was made on multi-dimensional and subchannel analyses to examine consistency of correlation formulations. The subchannel analysis code ASFRE[11] was used as a counterpart. And same correlation for friction and mixing factors were used in the calculation with ASFRE.

In TABLE 5, ΔT is an adiabatic inter-subassembly temperature difference at the outlet. The "adiabatic" means that no heat transfer was assumed between the bundles, e.g. 30 °C is a difference of temperature rises between the center and surrounding subassemblies, calculated from the heater power and the flow rate. Therefore, actual temperature differences were less than 30 °C in the experiments due to the inter-subassembly heat transfer.

B. Transition experiments

Transient behaviors in the multi subassemblies were studied under the conditions with and without inter-subassembly heat transfer. In the experiment of Case-TR43, a transient condition was given as follows. Initially, the facility was operated at 12% power and forced flow velocity corresponding to the rated condition of the real reactor. Then scram shutdown was imposed to reach 2% forced flow rate which simulated the NC/DHR condition. Time trends of power and flow rates are shown in FIG. 7. During the transition, the flow rates and the heater powers in the all subassemblies were controlled to kept identical with one another. In this condition, therefore, no inter-subassembly heat transfer could occur. Slight offset however existed between the heater powers of the center and the surrounding subassemblies in the fast transient phase (20 - 60 sec.).

In Case-TR49, all test conditions were set similar as that of Case-TR43 except the initial heater powers of the surrounding subassemblies. They were set lower than the center subassembly to make the surroundings outlet temperature lower by 30 °C than the center if adiabatic wrapper walls were assumed. Thus the inter-subassembly heat transfers were occurred in Case-TR49.

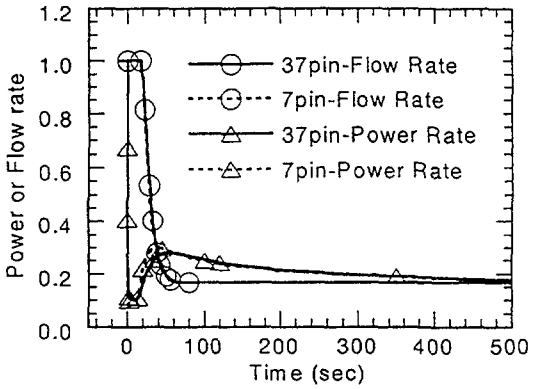

FIG. 7 Power and flow rate time trend of transition experiments

4. RESULT AND DISCUSSION

4.1 The 61-pin bundle with inter-subassembly heat transfer

Comparisons of the experimental and numerical temperature distributions are shown in FIG. 8. The difference of temperature between the experiment and the prediction is less than 3 °C. In Case-61A prediction reproduced temperature gradient imposed by the heat flux crossing the 61-pin bundle from 19-pin bundle side to the cooling channel. Temperature difference at the cooling channel implies uncertainty of the flow rate measurement of this channel. Normalized temperature profiles in 61-pin bundle are plotted in FIG. 9. A definition of the normalized temperature is as following equation:

$$T^* = \frac{T - T_{in}}{T_{ave} - T_{in}}. \tag{20}$$

Contents of the total thermal diffusivity is also shown in this figure. Result of the prediction with the mixing model showed slightly better agreement with the test data than that without the mixing model in Case-61A. And contribution of the mixing coefficients to the total diffusivity is more than 50 %. On the other hand in Case-61B, the mixing model presented enhancement in the computational accuracy, despite of its less contribution to the total diffusivity compared to Case-61A. The difference of effect of the mixing factor on the calculated results is attributed to influence of flow regimes.

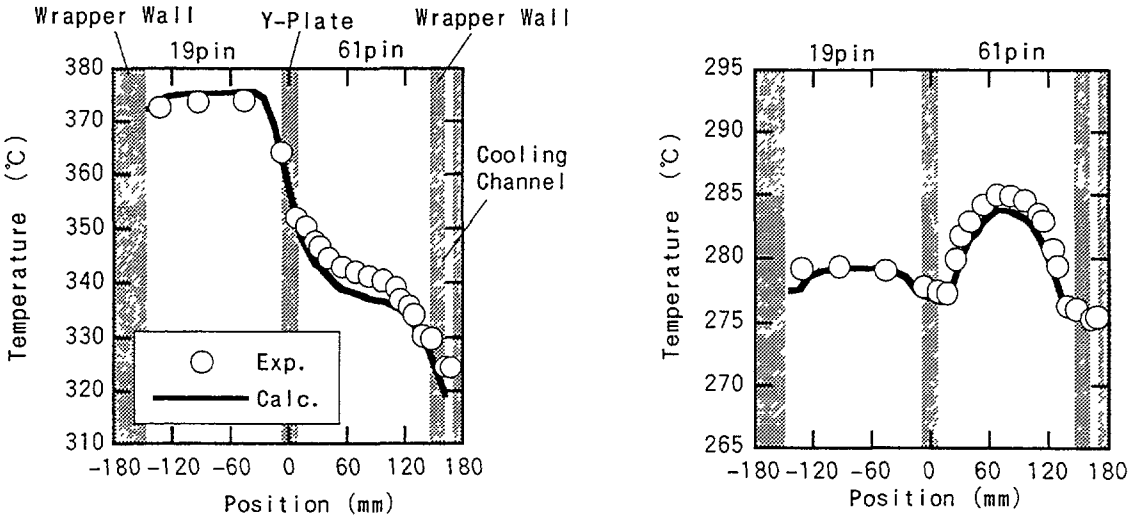

FIG.8 Comparisons of temperature profiles in CCTL-CFR

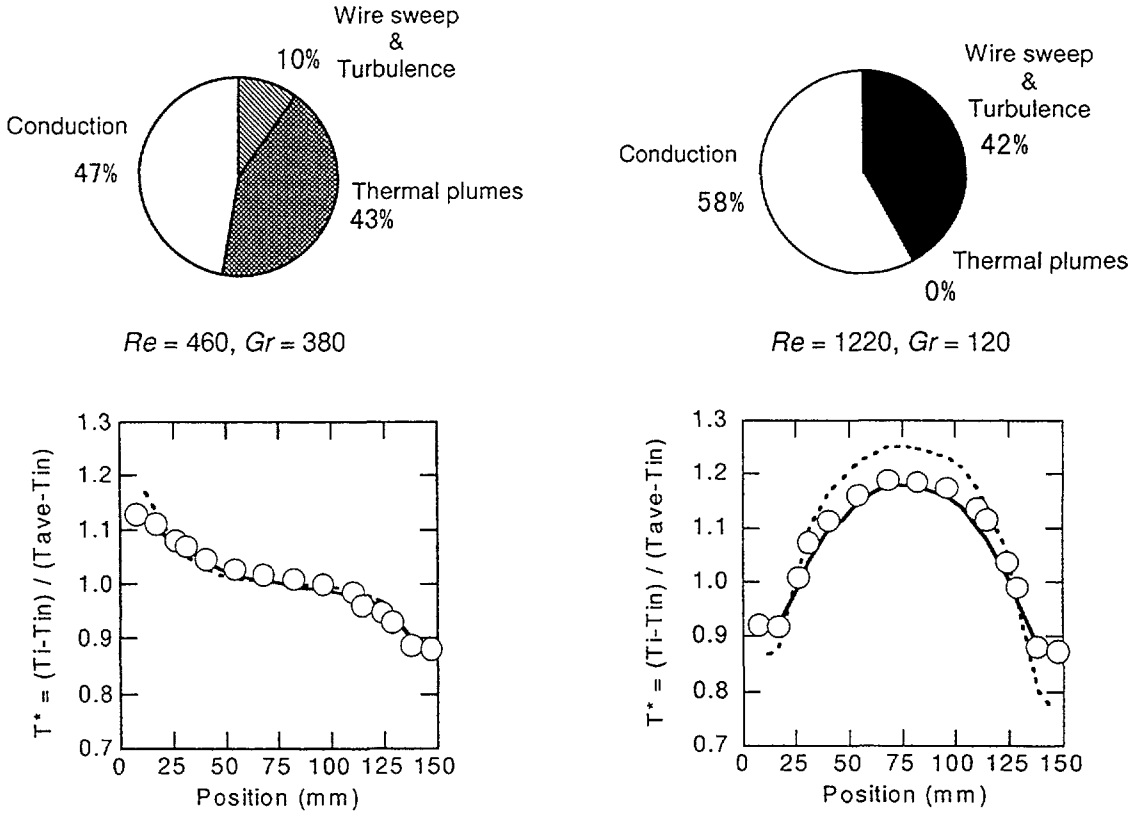

FIG. 9 Contents of total diffusivities and normalized temperature profiles in 61-pin bundle

Flow field in Case-61A was corresponded to the natural convection at such low Reynolds number and relatively high Grashof number that inter-subchannel flow redistribution due to predominant buoyancy forces played key role in determining temperature profile. Thus the thermal diffusivity had second order importance in Case-61A prediction. While inertia is the most active force in Case-61B featuring the effect of the diffusivity on temperature distribution. From the results above, it was shown that the present model is capable of predicting thermal-hydraulics in the subassemblies under forced and natural circulation conditions.

4.2 The sparsely heated 169-pin subassembly

Temperature distributions in transverse direction at the top end of the heated section are shown in FIG. 10. A sparsely heated condition may be quite difficult to predict for numerical simulation codes though, the calculations with the mixing model shows good agreement with the experiment in both cases. On the other hand, calculations without the mixing model over-predicted the temperature showing invalidity of the thermal diffusivity. The error concerning temperature rise from the inlet to the maximum value was almost 100% in the calculation without the mixing model. This magnitude of the error was decreased to less than 1/3 when the mixing model was applied. And the error may diminished much more in the predictions of real bundles in which all pins are the heat sources. Thus the mixing model showed its applicability to real sized subassemblies with large numbers of pins.

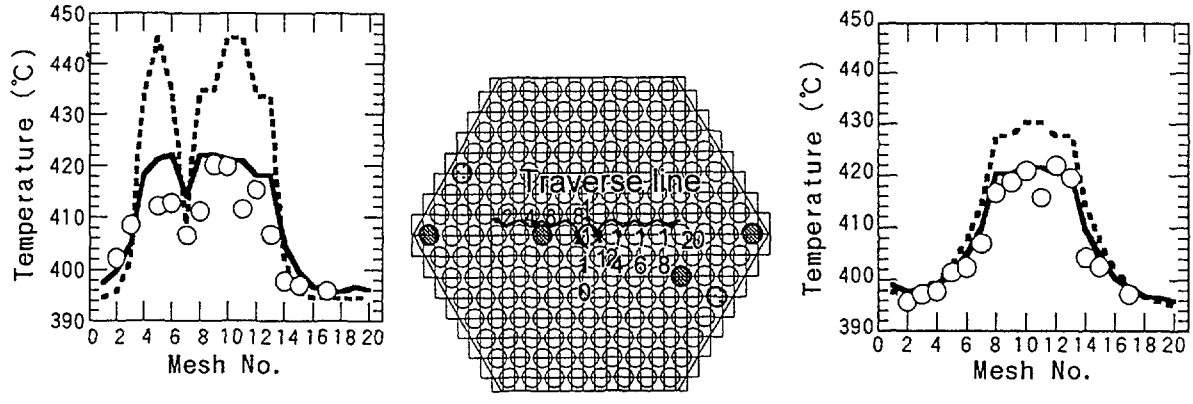

FIG. 10 Comparison of temperature profiles in 169-pin bundle at the top end of the heated section

4.3 The 7-subassembly under transition from forced to natural circulation

A. Steady state experiments

Firstly we take a look at a comparison between multi-dimensional and subchannel analyses to examine the consistency of mixing modeling formulations between the two analytical methods. Figure 11 shows comparison of temperature profiles. As no mixing correlation used, an influence of difference in mesh structure is featured between the two analysis methods. In this case both prediction agreed very well. Of course, both analyses over-predicted the maximum temperature compared to the experiment due to omission of the mixing effect. When the mixing model ware applied, both analyses showed good agreement with the experiment. While slight differences were seen between the predictions. However this difference was so small, less than 5 % of temperature rise (about 170 °C) in the subassembly, corresponding to measurement uncertainties, that the results from both analyses agreed each other substantially. And this result reflect validity of Ro's[1] recommendation of using the staggered half pin mesh in the multi-dimensional pin bundle analyses.

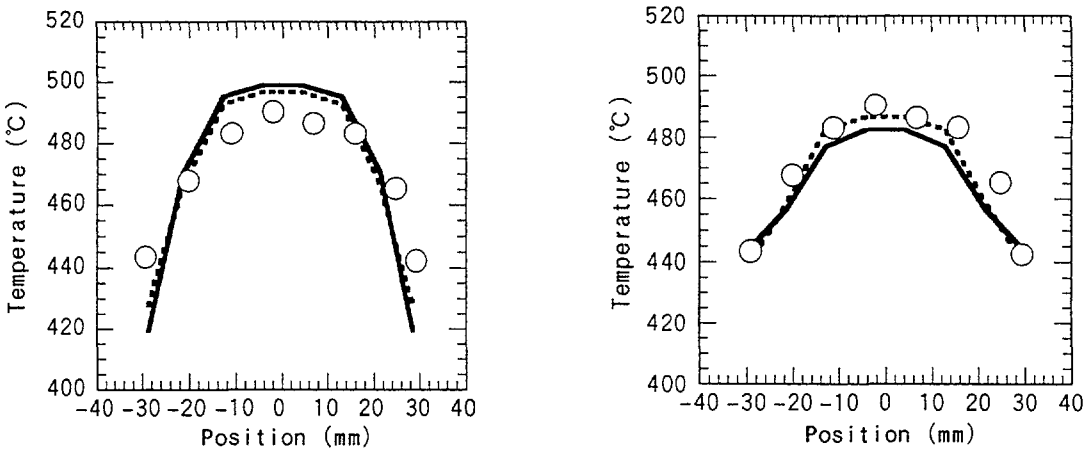

(a) Cal. without mixing model *(b) Cal. with mixing model*

FIG. 11 Comparison of temperature profiles among experiment, subchannel and multi-dimensional analyses

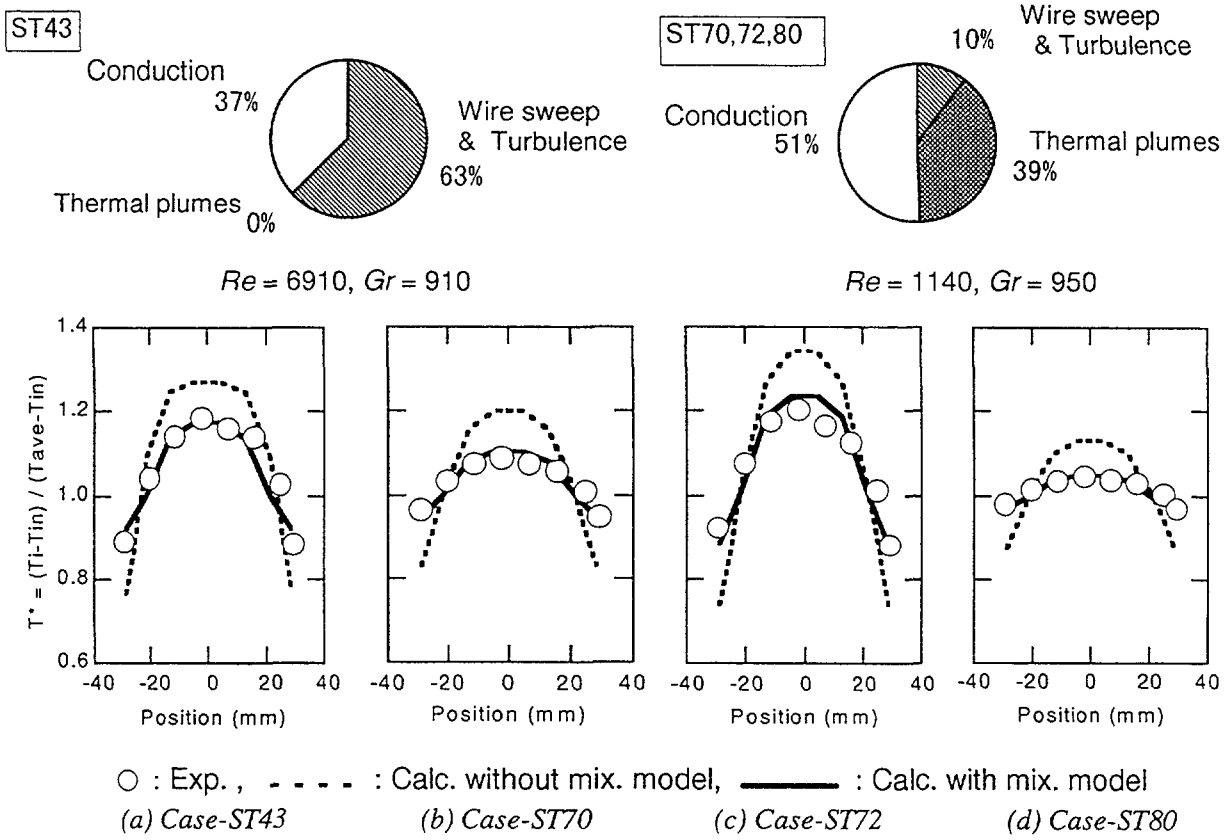

(a) Case-ST43 *(b) Case-ST70* *(c) Case-ST72* *(d) Case-ST80*

FIG. 12 Normalized temperature profiles in 37-pin subassembly and contents of total diffusivity at steady states

Figure 12 presents normalized temperature profiles and contents of total diffusivity in 37-pin subassembly. The calculations with the mixing model gave much better agreement with the experiment compared to the results without the mixing model for the all cases: isothermal, cooled and heated inter-subassembly heat transfer conditions respect to 37-pin bundle. Wire sweep and turbulence mixing is predominant in Case-ST43 under forced convection condition. In Case-ST70, ST72 and ST80, mixing due to thermal plumes showed major contribution in the total diffusivity, featuring mixed convection flow regime. And it is noted that influence of thermal plume mixing is more remarkable on temperature profile in mixed convection compared to in natural convection (see FIG. 9 (a), Case-61A).

B. Transition experiments

Time trend of temperature variations are presented in FIG. 13 at the center subchannel in the center subassembly where peak temperatures were observed. The maximum temperatures in space and time were occurred at the top end of the heated section and around 150 sec. in both cases. The numerical results over-predicted the maximum temperatures by 15 to 20 °C. Otherwise the calculations showed good agreement with the experiments.

Figure 14 shows variations of horizontal temperature profiles at the top end of the heated section. The predicted temperature profiles agreed well with the experiment in both cases at the start of the scram (t = 0 sec). After 50 seconds from the scram, predicted temperatures were 15 to 20 °C higher than the experiments in the surrounding subassemblies. And at 150 seconds, the predicted maximum temperatures were over-estimated by 15 to 20 °C both in the center and the surrounding subassemblies. Temperatures in the inter-wrapper gaps also gave large deviation between the predictions and the experiments. This deviation causes the over-prediction of the maximum temperature. In the calculations, sodium in the inter-wrapper gaps was assumed to be stagnant. Although, these experimental results suggested existence of inter-wrapper flows which was neglected in the calculations. Actually, temperature differences about 25 °C were seen between the center and outer inter-wrapper gaps at 150 sec in the experiments of both cases. These temperature differences may cause a inter-wrapper flow in reality. At 400 seconds, the predictions gave good agreements with the experiments of both cases.

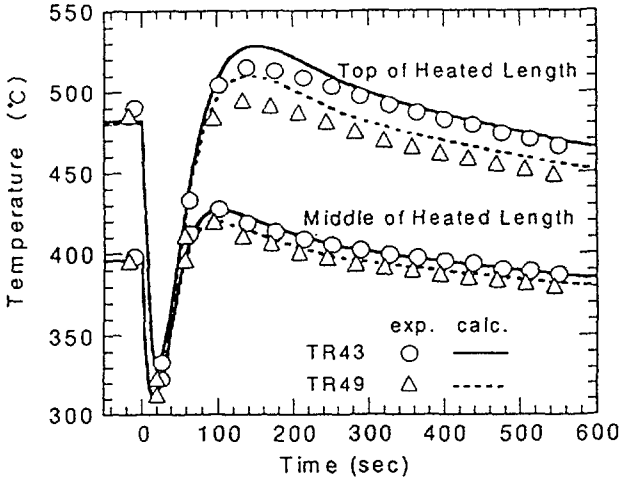

FIG.13 Time trend of temperature variations at the center subchannel in the center subassembly

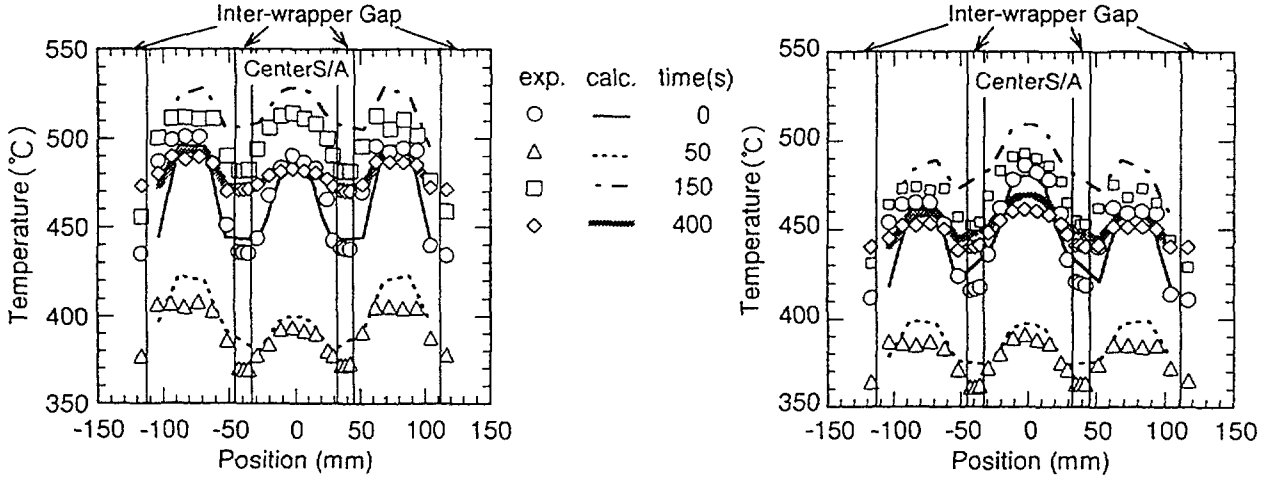

(a) Iso-temperature rise (Case-TR43) *(b) Inter-subassembly heat transfer (Case-TR49)*

FIG. 14 Variation of horizontal temperature profiles at the top end of the heated section

Normalized temperature profiles are presented in Fig. 15 regarding the top end of the heated section in the center subassembly. The predicted results almost perfectly traced the experimental data even for the peak temperature at 150 seconds despite of the difference in the absolute value just seen before. The errors of the spatial peaking factors at 150 seconds were less than 1 %. From this result, it is confirmed that the effective diffusivity, i.e. mixing factor is valid, while the error of the absolute temperature might be caused by the boundary condition of the inter-wrapper gap. The errors of the spatial peaking factors were less than 1.5 % after the peaks (t=150 sec) in the transitions of both cases.

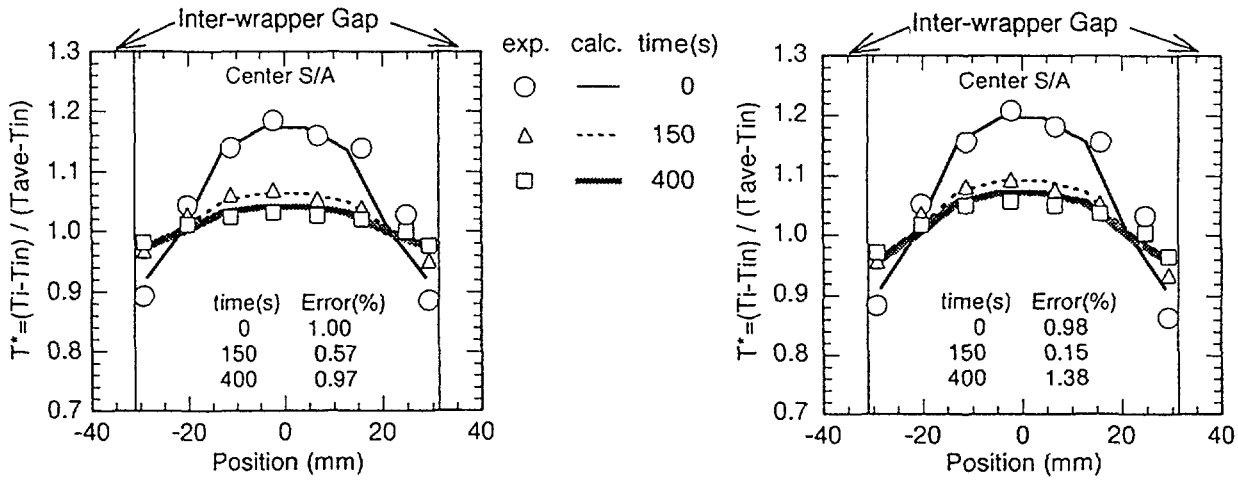

(a) Iso-temperature rise (Case-TR43) *(b) Inter-subassembly heat transfer (Case-TR49)*

FIG.15 Variation of normalized temperature profiles in 37-pin bundle

5. CONCLUSION

The prediction of the maximum cladding temperature in the fuel subassembly is one of the most important issues for the reactor safety assessment. To predict thermal-hydraulics in the core accurately, some important phenomena are existed to be modeled adequately: the inter-subchannel mixing, the intra/inter-subassembly flow redistribution, the inter-subassembly heat transfer and inter-wrapper flow. Among these important phenomena, inter-subchannel mixing is the most influential to the maximum cladding temperature as well as temperature distribution within the fuel pin bundle. In the present study, modeling of inter-subchannel mixing based on MIT's correlation was implemented to the multi-dimensional thermal-hydraulic analysis code AQUA. Also a threshold function, which controlled mixing coefficient of thermal plumes, was proposed to treat all flow regimes continuously: forced, mixed and natural convection, appeared in the reactor scram transition.

The code was validated through the analysis of the sodium experiments; 37-pin, 61-pin, and 169-pin subassembly steady state tests. The simulation capability was also examined for 7-subassembly sodium tests under transition from forced to natural circulation conditions with and without inter-subassembly heat transfer.

The analysis succeeded to predict the experimental temperature distributions. The errors of temperature rise from inlet to maximum values were comparable to measurement uncertainties in the steady state experiments of 37-pin ant 61-pin subassemblies. For 169-pin subassembly, the error was reduced to less than 1/3 magnitudes by using the mixing factors, compared to those of analyses without the mixing factors. The simulation slightly over-predicted the maximum temperature in 7-subassembly transition experimental analysis. This error was attributed to existence of the inter-wrapper flow in the experiment. Because prediction treated sodium in the inter-wrapper gaps as stagnant. The prediction traced the experimental normalized temperature profiles perfectly in 37-pin subassembly during the transition. This indicated that the mixing coefficient for thermal plumes were controlled adequately by the threshold function as the flow regime was changed. Finally, numerical

results with subchannel and multi-dimensional analyses agreed well showing consistency of the formulations in both mesh structures. Thus the computational method using multi-dimensional code has been established for thermal-hydraulics inside the subassembly under various conditions in geometry, dimensions, and flow regimes except for pin bundle deformations.

ACKNOWLEDGEMENT

The authors are grateful to Dr. Maekawa of Kawasaki Heavy Industries Ltd. for his technical advice. And the authors appreciate Mr. Miyake of NDD Co. for his support for performing calculations and technicians of Joyo Sangyo Co. for their technical and engineering supports for the experiments.

NOMENCLATURE

c : gap width between neighboring to pins (m)
c_p : specific heat {J/(kgK)}
D : pin diameter (m)
D_{ei} : hydraulic diameter for the subchannel category i (m)
D_{eb} : bundle averaged hydraulic diameter (m)
fx_{pl} : threshold function for the eddy diffusivity of thermal plumes defined by Eq. 14 (-)
g : gravitational acceleration in z (vertical) direction (m/s^2)
g_i : gravitational acceleration in i coordinate direction (m/s^2)
Gr : Grashof number for the threshold function defined by Eq.18 (-)
$Gr_{\Delta T}$: Grashof number introduced by Engel et al.[6] defined by Eq. 10 (-)
$Gr^*_{\Delta T}$: Grashof number based on axial temperature gradient defined by Eq. 12 (-)
h : specific enthalpy (J/kg)
L : heated length (m)
Nu : Nusselt number (-)
P : pitch of pins in the bundle (m)
p : static pressure (Pa)
Pr : Prandtl number (-)
Pe : Peclet number ($= Re_i \times Pr$) (-)
q_{rod} : heat flow per unit volume of coolant from the pins (W/m^3)
$q''_{wall/pin}$: ratio of heat fluxes on the wrapper tube wall and on the pin surface
R_f : flow resistance (Pa/m)
R_i : Richadson number defined by Eq. 15 (-)
T : temperature (℃)
t : time (sec)
T_{ave} : flow area weighted average temperature within a horizontal cross section of the bundle (℃)
T_{in} : inlet temperature of the subassembly (℃)
ΔT_b : difference of bulk temperature between two levels (℃)
U_i, U_j : velocity component in i and j coordinate directions (m/s)
V_b : average vertical velocity component (m/s)
V_i : vertical velocity component (m/s)
x_i, x_j : coordinates in i and j directions
z : vertical coordinate (m)

Greek Symbols

β : volumetric expansion coefficient (1/K)
γ_i : surface permeability in i direction (-)
γ_v : volume porosity (-)
ε_t : diffusivity of mixing due to wire sweep and turbulence (m^2/s)
ε_M : diffusivity of mixing due to thermal plume (m^2/s)
η : subchannel centroid to centroid distance (m)
κ : shape factor for conduction in provided by Eq. 13 (-)

λ : thermal conductivity {W/(mK)}
ρ : density of the coolant (kg/m^3)
ρ_0 : reference density of the coolant (kg/m^3)
ν : kinematic viscosity (m^2/s)

REFERENCES

[1] T. S. Ro et al, "Porous Body Approach for Wire-wrapped rod bundle analysis", Proc.3rd International Topical Meeting on Nuclear Power Plant Thermal Hydraulics and Operations, Seoul, South Korea, Nov.,(1988).

[2] Shih-Kuei Cheng, Tae Sun Ro and N. E. Todreas, "Energy Transfer Mechanism Under Mixed Convection Conditions in LMFBR Wire-Wrapped Bundles", Proc. of the 3rd Int. Topical Mtg. on Reactor Thermal Hydraulics, Newport USA, Oct. (1985).

[3] Shih-Kuei Cheng and Neil E. Todreas, "Hydrodynamic Models and Correlations For Bare and Wire-Wrapped Hexagonal Rod Bundles - Bundle Friction Factors, Subchannel Friction Factors and Mixing Parameters", Nuclear Engineering and Design, Vol. 92, pp.227-251, (1986).

[4] G. Basque, "3D computation of thermal-hydraulics in a wire-wrapped rod bundle in the natural and mixed convection regimes using the TRIO VF code", Proc. of NURETH-4, Karlsruhe F.R.Germany, p.1346, Oct. (1989).

[5] M. Nishimura, H. Kamide, K. Hayashi and K. Momoi, "Inter-subassembly Heat Transfer During Natural Circulation Decay Heat Removal - Experimental Transient Behavior from Forced to Natural Circulation and its Multi-dimensional Analysis with Mixing Model -", Proc. of NURETH-8, Kyoto Japan, p.903, Oct. (1997).

[6] F. C. Engel, R. A. Markley, and A. A. Bishop, "The effect of radial heat flux gradients and flow regimes on the peak sodium temperature rise in wire wrapped bundles", Proc. of NUREG/CP-0034, vol. 2, 566 -582, New York, Sept. (1982).

[7] J. M. Bates and E. U. Khan, "Investigation of combined free and forced convection in a 2 x 6 rod bundle during controlled flow transients", AIChE Symposium Series, Heat Transfer, Orlando, (1980).

[8] H. M. Domanus, "A new implicit numerical solution scheme in the COMMIX-1A computer program", ANL 83-64, NUREG/CR-3435, (1983).

[9] T. Murata, et al., "Super computer", (in Japanese), Maruzen, (1985).

[10] H. Kamide, et al., "Inter-subassembly heat transfer during natural circulation decay heat removal of FBRs", Proc. of ICONE-3, Kyoto, Japan, S101-3, April (1995).

[11] H. Ohshima and H. Ninokata, "Analysis of Thermal-Hydraulic Behavior in a Fast Reactor Fuel Subassembly with Porous Blockages," International Meeting on Advanced Reactor Safety (ARS'97), Orlando USA, (1997).

NATURAL CONVECTION AS THE WAY OF HEAT REMOVAL FROM FAST REACTOR CORE AT COOLDOWN REGIMES

A.V. ZHUKOV, J.A. KUZINA, V.A. UHOV, G.A. SOROKIN
State Scientific Centre of Russian Federation,
Institute of Physics and Power Engineering,
Obinisk, Kaluga Region, Russian Federation

XA0055068

Abstract

The problems of thermohydraulics in fast reactors at cooldown regimes at heat removal by natural convection are considered The results of experiments and calculations obtained in various countries in this area are presented. The special attention is given to heat removal through inter-assembly space in the core and also to problems of thermohydraulics in the upper plenum.

1. INTRODUCTION

The problems of natural and mixed convection in fuel assemblies of reactor cores represent a large practical significance from a point of view of reactors cooling in unnominal and emergency regimes of operation [1 - 3].

At natural convection in installation there are series of thermohydraulic phenomena which are not inherent to forced flow. So, at natural convection velocities and local directions of flow depend on distribution of temperature of the coolant, while at forced convection the velocity determines temperature distribution. The conditions with natural and mixed convection are characterized by thickening of hydrodynamics of a stream: there are reverse flows in fuel assemblies, owing to what there can be additional nonuniformities of temperature and hot spots, increase coefficients of a hydraulic resistance etc.

At the same time experimental and calculated researches of natural convection processes in a core and vessel of the fast reactor undertaken per last years, testify to positive influence of natural convection on processes of heat removal in conditions of fast reactor cooldown. In particular, concept of heat removal by natural convection originating in inter-assembly space of the nuclear reactor at use of let-down heat exchangers in a emergency cooldown system is successfully developed [4, 5].

As to calculated codes intended for estimations of temperature regimes with natural convection, they are verified on an experimental material and to the present time are advanced with reference to thermohydraulic processes in the upper plenum of the reactor, and in core fuel assemblies (inter-assembly space).

For the upper plenum of the reactor the following codes are most advanced: DYANA / ATTICA [6] - one-dimensional and two-dimensional code; TRIO [7], ASTEC [8], FLUTAN [9], AQUA [10] - three-dimensional codes developed in France, England, Germany, Japan; the two-dimensional NECTAR code [11] developed in IPPE etc.

The development of calculated codes for fuel assemblies of reactor cores is founded on two approaches: subchannel technique and model of a porous body. First from them is based to solution of the equations of impulse, mass and energy conservation in channels (cells) formed by adjacent fuel rods, second - on representation of a bundle of rods by an anisotropic porous medium with heat release distributed on volume (a quasi-homogeneous model).

In the report some information about developed in IPPE codes based on a subchannel technique (MID, TEMP, TEMP-M, MIF etc.) is given, and the brief outcomes of calculation obtained by these codes with allowance for heat interaction of core fuel assemblies (coolant leakage in inter-assembly space) are represented. It is necessary to consider enough explicitly

the methods of calculation of temperature fields in fuel assemblies of reactors at cooling through inter-assembly space in cooldown conditions, when approprINPE circulation circuits with natural convection appear (researches in ÎÊBÌ - Russia, in PNC - Japan; the calculated method based on models of a porous body is demonstrated in the latter case).

The problem on calculated research of thermohydraulics at natural convection in the reactor upper plenum conducted in IPPE by the NECTAR code is considered

Largely this report is devoted to exposition of experimental data on natural convection in fuel assemblies obtained in IPPE, as the base data for improvement of calculated codes.

2. EXPERIMENT AS A RESOURCE OF BASE CONSTANTS FOR IMPROVEMENT OF CALCULATED CODES UNDER THE ANALYSIS OF NATURAL CONVECTION PROCESSES IN FAST REACTORS

The evaluation of work of systems with natural convection is much more complicated than with forced flow, and the development of the calculated approaches is hampered because of a great many of parameters defining thermohydraulics in considered cases. Therefore experimental study of dynamics of temperature perturbations in systems with natural convection for concrete situations is necessary. By results of the analysis of base constants obtained in experiments, it is possible to update theoretical methods of the prognosis and evaluation of development of natural convection processes.

Thus it is necessary:

- To understand an essence of thermohydraulic phenomena accompanying natural convection processes;
- To develop a technique of effectiveness estimations of a emergency cooldown system of the fast reactor based on use natural convection; to generalize obtained experimental data used in these evaluations as empirical relations with the purpose of their further use in calculated codes.
- To select the basic direction in development of emergency cooldown systems, distinguished by an increased potency and safety at maintenance, i.e. to optimize a heat removal system connected with natural convection.
- To create a rigorous (high capacities) data base for development and debugging of calculated codes.

With the purpose to study operating regimes of nuclear power installation in conditions of natural circulation the reactor experiments will be carried out, for example [12 - 14]. The obtained data also are a test material for calculated codes of circulation circuit, collected of modules approximately circumscribing a conditions of heat and mass transfer in the circuit elements (core, mixing cameras, heat exchangers, pumps etc.). Thus the improvement of the calculated scheme for concrete arrangement of an equipment, for example [12] is fulfilled. The error of fulfilled calculations, certainly, is determined largely by error of exposition of hydrodynamics and heat transfer of the elements of a circuit, and also of selected common scheme of circulation. The heat and mass transfer processes in the elements of circulation circuit at natural convection conditions are determined by geometry of area, boundary conditions (availability and disposition of heat transfer surfaces), properties of the coolant, availability of free surfaces and other factors. The data retrieval for operation in NC conditions of such important component of the circuit , as the reactor core, is one of primal problems of the substantation of safety of nuclear power installation. The obtained data can also be used for a construction (improvement) of approximate models of calculation in separate modules of calculated codes at the analysis of operation of whole nuclear power installation.

The programs of researches of natural and mixed convection are realized in various centers of science of a series of countries, for example, in Grenoble (France) [15], in Richland (USA) [16], in Germany, England [17], PNC (Japan) [5] etc.

The solution of the task includes:

- Development of problems on modeling of processes with natural and mixed convection in assembly of cylindrical rods (fuel rods);
- Realization of experimental researches of thermohydraulics on models of fuel assemblies in conditions with natural and mixed convection;
- Development of a technique of calculation including mathematical statement with a solution of a boundary problem, system of constants (closing relations), method of numerical solution and creation of calculated code;
- Code testing by an experimental material;
- Realization of calculated researches with consequent generalization of outcomes;

The available work on thermohydraulics at natural convection in rod assemblies testify to two approaches in statement of experiments: the separate channel of rods bundle [18] is reproduced or the experiences are carried out on the whole bundle of rods [19].

Results of experimental researches obtained in IPPE on that and other technique are considered below. In the first case the cell of dense packing of smooth rods was reproduced, in the second case fuel assemblies of cores and shields of fast reactors BOR-60, BN-350, BN-600, BN-800 were simulated (the relative pitch of fuel assemblies simulators varied in an interval $1.04 < s / d < 1.24$).

At the first stage the development of the constants system for the solution of equations of thermohydraulics in regimes with natural and mixed convection in core fuel assemblies of reactors [20] was executed. The realization of experimental researches of temperature fields in model fuel assemblies in indicated modes ($Re \leq 2 \cdot 10^3$) is the second stage.

3. EXPERIMENTAL DATA OBTAINED ON MODEL FUEL ASSEMBLIES OF FAST REACTORS IN CONDITIONS OF COOLANT FLOW WITH LOW VELOCITIES AND AT NATURAL CONVECTION

3.1 Basic performances of model fuel assemblies

Model fuel assemblies of fast reactors consist from 37 fuel elements (simulators of fuel elements), located in a triangular lattice with a relative pitch $1.04 < s / d < 1.24$ and made in hexagonal cover. The assemblies with $s / d = 1.04; 1.062; 1.10; 1.15; 1.24$ were used. In the fig. 1. as an example the cross-section of the model fuel assembly of the BOR-60 reactor ($s / d = 1.10$) is shown. Model fuel assemblies of other reactors have a similar construction. The heating of the elements is carried out from nichromium heaters ensuring a constant heat flow on an interior surface of the elements and on length of energy release. The central, side and angular elements are made out rotary. On their surface are fixed till 12 Cr - Al thermocouples in covers from steel Õ18Í9Ò (diameter of a cover is 0.8 õ 0.5 mm, diameter of thermal electrodes is 0.2 mm), measuring the surface temperature of elements.

Coolant temperature is measured in collectors of models, and also in each cell at bundle outlet. The Cr - Al thermocouple in covers ∅ 0.8 õ 0.5 mm are used for it.

In the table I the geometric performances of model fuel assemblies of the BOR-60 reactor are represented.

In the table II the distances l from a beginning of energy release are given, on which the junctions of thermocouples for the same model are fixed.

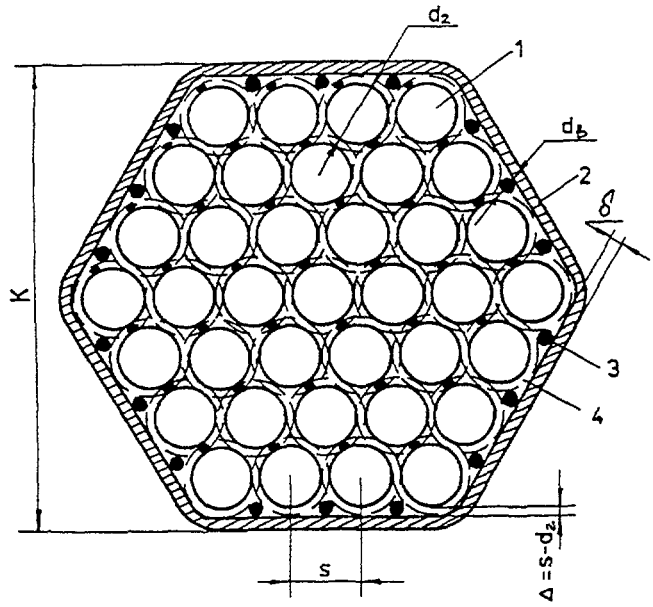

Fig.1. Cross section of the model fuel assembly BOR-60: 1 - simulator of fuel element; 2 - barrel; 3 - cylinder ; 4 - wire wrapper.

TABLE I. THE GEOMETRIC PERFORMANCES OF MODEL FUEL ASSEMBLY OF THE BOR-60 REACTOR

1	Name	Label	Dimen-sionality	Numerical value
1.	Exterior diameter of fuel element simulator clad	d = 2R	mm	17.4
2.	Interior diameter of fuel element simulator clad	d_1	mm	13.0
3.	Relative pitch of disposition of fuel element simulators	s / d	-	1.1
4.	Length of energy release	l_0	mm	900
5.	Distance between face lattices	L	mm	950
6.	Wire wrapper pitch	h	mm	317
7.	Diameter of the wrapping wire	d_1	mm	1.5
8.	Interior size of the barrel "on a turn-key basis"	b	mm	119
9.	Thickness of a barrel wall	δ′	mm	2
10.	Diameter of cylinders	$d_â$	mm	4.5
11.	Area of cross-section of cells:			
	central	ω_o	mm^2	38.9
	side	ω_a	mm^2	64.0
	angular	$\omega_ó$	mm^2	11.5
12.	The moistened perimeter of cells:			
	central	$Ð_ò$	mm	19.6
	side	$Ð_â$	mm	62.9
	angular	$Ð_ó$	mm	11.0
13.	Hydraulic diameter of cells:			
	central	$d_{ãò}$	mm	5.23
	side	$d_{ãa}$	mm	4.07
	angular	$d_{ãó}$	mm	4.2

TABLE II. THE DISTANCES FROM A BEGINNING OF ENERGY RELEASE OF ROTARY FUEL ELEMENT SIMULATORS, ON WHICH JUNCTIONS OF THERMOCOUPLES ARE FIXED ($D_Ã$ - HYDRAULIC DIAMETER OF CENTRAL CELLS)

[1] thermocouples of fuel element simulators			l	l / $d_ã$
angular	side	central	mm	($d_ã$=5.2 mm)
1	38	20	5	0.96
2	39	21	85	16.4
3	40	22	165	31.2
4	41	23	245	47.0
5	42	24	325	62.5
6	43	25	405	78.0
7	44	26	485	93.0
8	45	27	565	109
9	46	28	645	124
10	47	29	725	140
11	48	30	805	155
12	49	31	885	170

3.2. Experimental model

The experimental model is installed on a sodium or sodium - kalium circuit of a bench 6Á [21, 22].

Circulation of liquid metal (sodium, an sodium - kalium alloy: 22 % Na + 78 % K) is carried out by the electromagnetic pump of an alternating current by efficiency ~ 150 m^3/h (construction see in [22]).

The heat removal released in a model, is carried out in the heat exchanger metal - water with an intermedINPE cavity, completed helium or working under vacuum. A construction of the heat exchanger also see in [22].

The regulation of flow rate of liquid metal is carried out by the electromagnetic pump or valves (by silphon - alloy Na - K; with frozen compacting - sodium).

3.3. Technique of realization of experiments

In steady-state operation of the circuit the temperature fields of the characteristic elements (central and near a wall), and also coolant temperature in each cell of a bundle are measured. The turn of the elements in an interval of angles 0 - 360^0 through $\Delta\varphi$~5 - 10^0 is carried out.

The measurements are carried out with use of a measuring device IS-200 permitting to produce sequential pick up of information from 200 sensors.

In experiences a force of current, voltage and electrical power of each element of a model are measured. The measuring complex Ê-50 is used.

For smoothing loads of heaters the additional resistance including in a circuit of each heater is used.

In a table III the performances of experiences conducted on the BOR-60 model assembly are represented.

TABLE III. THE CHARACTERISTICS OF EXPERIMENTAL MODES

№	Velocity $\overline{w}$ m/s	Flow rate G m^3/h	Temperature at assembly outlet $t_{вых}$ ^0C	Heating of the coolant Δt ^0C	Power of the simulator of fuel element $N_{им}$ kW	Thermal Flow $\overline{q}$ $kcal/m^2h$	The Reynolds number* Re	The Peclet number* Pe
1	0,0279	0,335	285	135	0,41	7160	294,9	1,75
2	0,0416	0,497	241	91	0,41	7160	439,7	2,60
3	0,0576	0,688	214	64	0,40	7000	608,8	3,60
4	0,0848	1,014	199	48,9	0,45	7870	896,3	5,30
5	0,112	1,339	187	37	0,45	7870	1183,7	7,0
6	0,140	1,673	180	30	0,45	7870	1479,7	8,75
7	0,154	1,84	177	27	0,45	7870	1627,6	9,6
8	0,168	2,00	174,7	24,8	0,45	7870	1775,6	10,5
9	0,197	2,35	171	21,1	0,45	7870	2082,1	12,3

* - The Reynolds and Peclet numbers are calculated on mean speed of the coolant on cross-section of assembly (u) and hydraulic diameter of central cells ($d_{ãö}$)

3.4. Results of experiments and their analysis

3.4.1. Some effects in model fuel assemblies of reactors connected to natural convection

Assuming that maximum nonuniformity of temperature of a wall on a perimeter of fuel elements near a wall $\Delta T_W^{max} = \frac{t_w^{max} - t_w^{min}}{\bar{q}R}\lambda_f$ (the fig. 2) is determined by a difference of heating of the coolant in approprINPE channels, and making simple balance relations for adjacent streams of the coolant in channels in the assumption, that between streams the fluid is not intermixed and does not exchange a heat, we shall receive an inversely proportional assotiation between a difference of heating of the coolant in channels and the Peclet number:

$$\frac{\Delta t_{III} - \Delta t_{II}}{\bar{q}R}\lambda_f = \pi l_i\left(\frac{d_{rIII}}{Pe_{III}\omega_{III}} - \frac{d_{rII}}{Pe_{II}\omega_{II}}\right) = \frac{\pi l_i}{Pe}\left(b\frac{d_{rIII}}{\omega_{III}} - c\frac{d_{rII}}{\omega_{II}}\right) \quad (1)$$

Here Δt_{III} and Δt_{II} - average heating of the coolant in central (III) and near-a-wall (II) channels of fuel elements assembly (it is supposed, that in channels II the coolant is not heated up on comparison with channels III) l_i - current distance from a beginning of energy release; d_{aIII}, d_{aII}, ω_{III}, ω_{II} - hydraulic diameters and cross-sectional areas of channels III and II; $Pe_{III} = \frac{w_{III}d_{rIII}}{a}$, $Pe_{II} = \frac{w_{II}d_{rII}}{a}$, $Pe = \frac{\bar{w}d_{rIII}}{a}$ - the Peclet numbers calculated at mean speeds in channels III and II and at mean speed on section of fuel assembly ($\bar{w}$); b and c - factors connecting speeds w_{III}, w_{II} and $\bar{w}$.

The increase of nonuniformity of temperature near-a-wall fuel elements with decreasing Pe can not be boundless because of heat transfer between channels, which is proportional to difference of heating in channels. In the field of low speeds the natural convection promoting intermixing of fluid between channels and reducing temperature

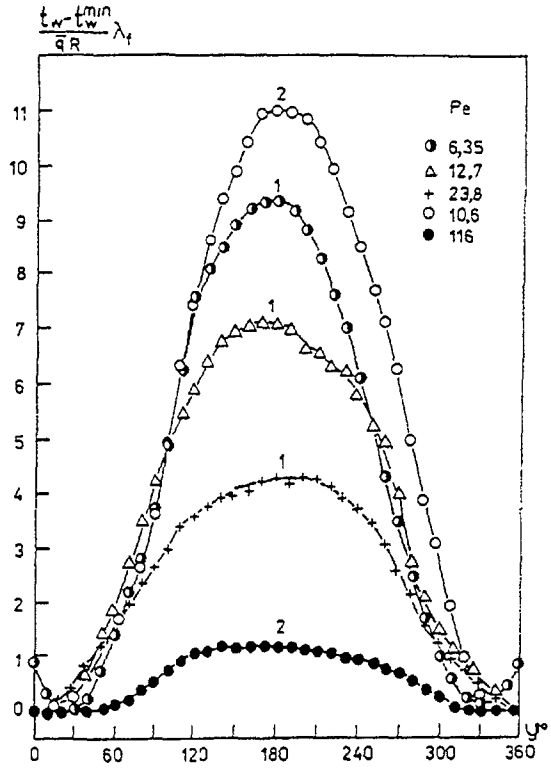

Fig. 2. The temperature fields of near-a-wall wire-wrapped (1) and smooth (2) simulators of fuel elements of the model fuel assembly BOR-60.

nonuniformity is exhibited. It determines peaks in regularities $\Delta T_w^{max} = f(Pe, Re)$ at some Peclet (Reynolds) numbers - fig. 3, 4 [23 - 25].

Position and size of peaks depend on geometry of a channel, physical properties of the coolant, the distances from a beginning of energy release and other factors. At fixed geometry of a channel the numerical values of peaks are about identical on various distances from a beginning of energy release, but the displacement of peaks to area of increased Ðå (fig. 3) happens at increasing $l/d_э$. Decreasing of peaks at the end of a zone of energy release (fig. 4) is probably also.

The influence of natural convection has an effect for character of behavior of temperature nonuniformities of fuel elements on length of energy release (fig. 5). For example, in model fuel assembly of the BOR-60 reactor the temperature nonuniformity of fuel elements is increased linearly on length of energy release at large Peclet numbers (Ðå ≥100); in the field of small Ðå the tendency to stabilization is exhibited, at some Ðå the stabilization comes, and at the very small Peclet regularities lose monotone character because of influence of natural convection.

Let's consider the data on distribution of coolant heating in channels of model fuel assembly at small Peclet numbers. P.A. Ushakov has shown, that [26]: if there is no natural convection, with decreasing of the Reynolds number the temperature nonuniformity of fluid on radius of assembly should be aimed to constant value characteristic to the given kind of fluid and given geometry of assembly. Really, by assuming, that two fluid flows with flow rates v_{III} è v_{II} ($v_{III} < v_{II}$) flow past, not mixing up among themselves, in central (III) and side (II) channels of fuel assembly, and heat transfer exists between channels by means of heat conduction of fluid, we shall receive distribution of mean temperatures of flows on length z as:

$$t_{f\,III} - t_{f\,II} = c_1\left(1 - e^{-c_2 \frac{z}{d_{r\,III} Pe}}\right), \qquad (2)$$

where $c_1 = \frac{qh}{\lambda}\left(\frac{1-\beta}{1+\beta}\right)$, $c_2 = (1+\beta)\frac{4d_{r\,III}}{h}$, $\beta = \frac{v_{III}}{v_{II}}$, $Pe = \frac{\overline{w} d_{r\,III}}{a}$; h - the characteristic size in a plane, perpendicular axis z.

It is visible that at Ðå → ∞ the difference of temperature $t_{f\,III} - t_{f\,II}$ aims to zero, and at decreasing the Peclet (Pe → 0) - to a constant $\tilde{n}_1$.

From results of experience follows that in the field of small Reynolds numbers (Peclet) with decreasing Re in assembly equalization of temperature of fluid happens(fig. 6), that is connected to development of natural convection. In moved apart assembly of rods (s / d = 1.24) conditions for development of natural convection are better, than in tight assembly (s / d = 1.062; 1.15) - the equalization happens at bigger Re (smaller heating). The origin of peaks in tight assembly is possible only in area very small Re: in model assembly of shields of reactors (s / d = 1.04; 1.062) peaks are not observed even at very small Reynolds numbers.

In assembly of wire-wrapped rods a condition for a development of natural convection it is worse, than in assembly of "smooth" rods (the part of cross section of assembly is overlapped by edges), - the equalization happens at smaller Re (bigger heating).

With decreasing of the Prantl number peaks displace in area of smaller Reynolds numbers (see data for sodium and alloy of a sodium - kalium on the fig. 6).

In a regime of transient current (1000≤Re≤4000) the redistribution of the flow rate of the coolant on cross-section of fuel elements assembly can happen, if the channels of assembly have various geometry [25 - 27]. It is stipulated by that the flow in such channels is with various Reynolds numbers. By assuming, that in central ("ö") channels of fuel assembly

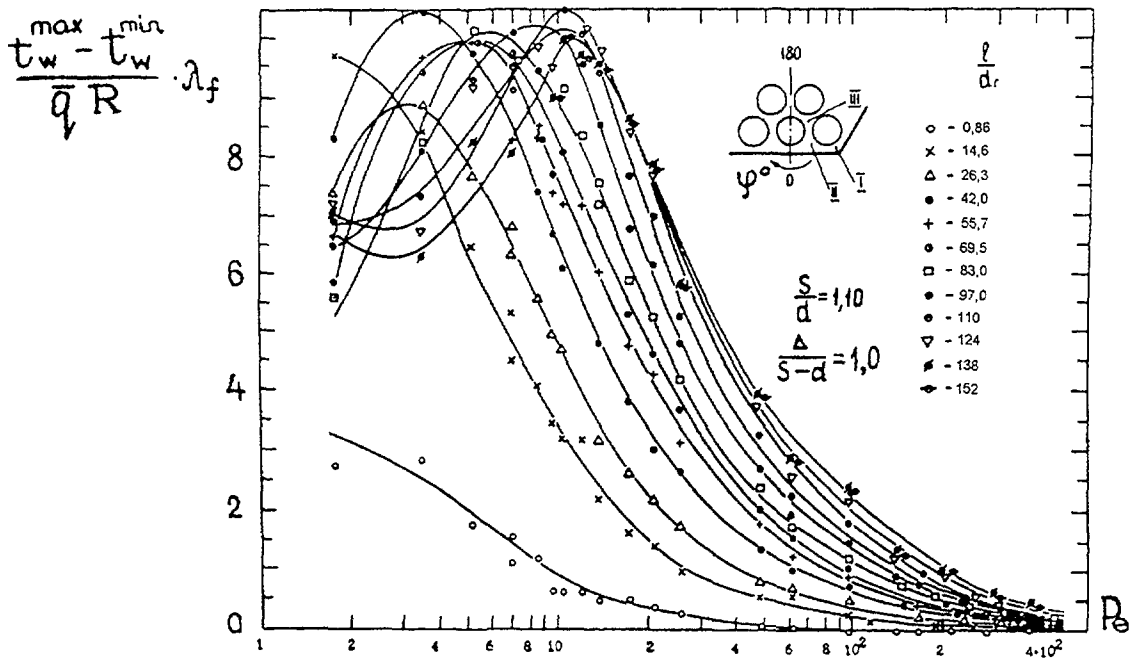

Fig. 3. Change of maximum nonuniformities of temperature of the lateral fuel element simulator of the model fuel assembly BOR-60 from the Peclet number.

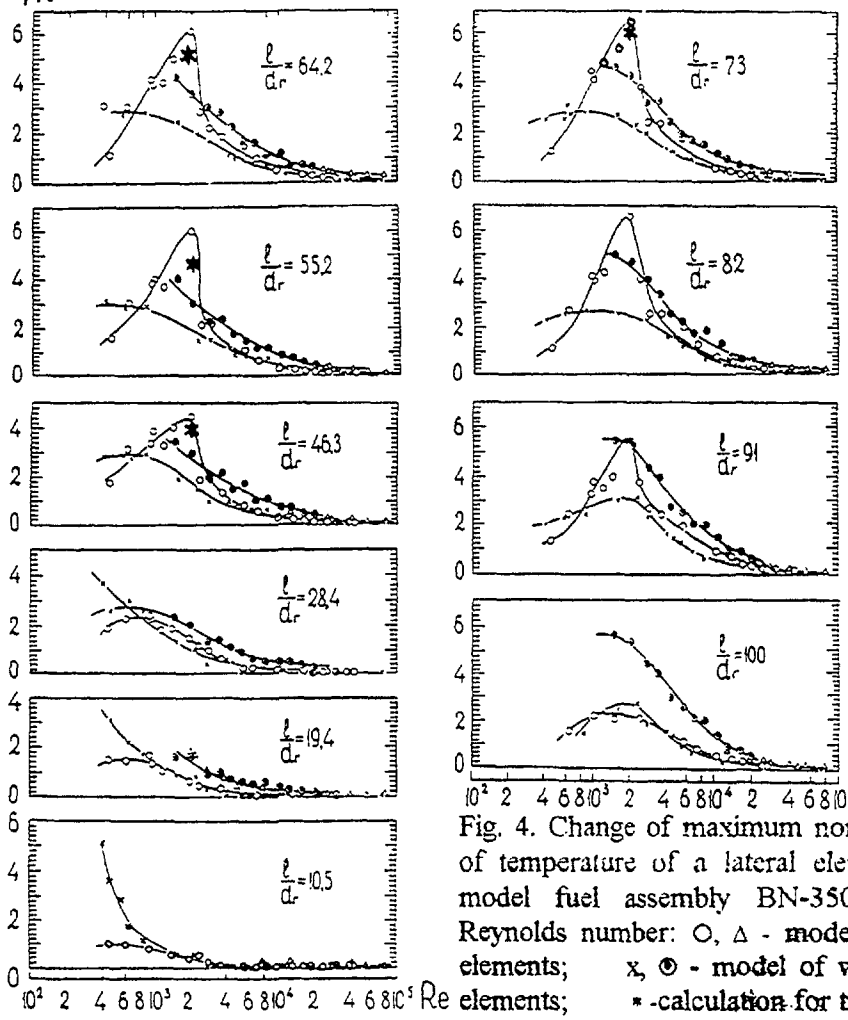

Fig. 4. Change of maximum nonuniformities of temperature of a lateral element of the model fuel assembly BN-350 from the Reynolds number: ○, △ - model of smooth elements; x, ⊙ - model of wire-wrapped elements; * -calculation for transient flow regime.

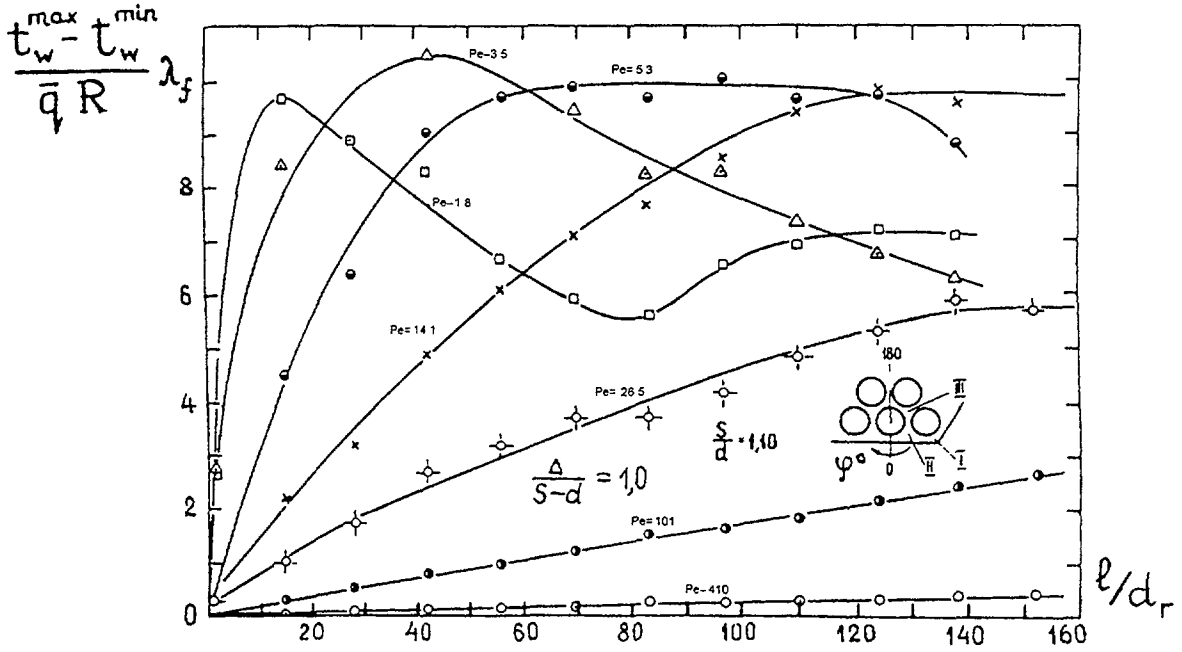

Fig. 5. Change of maximum nonuniformities of temperature on length of the near-a-wall smooth simulator of the fuel element of the model fuel assembly BOR-60.

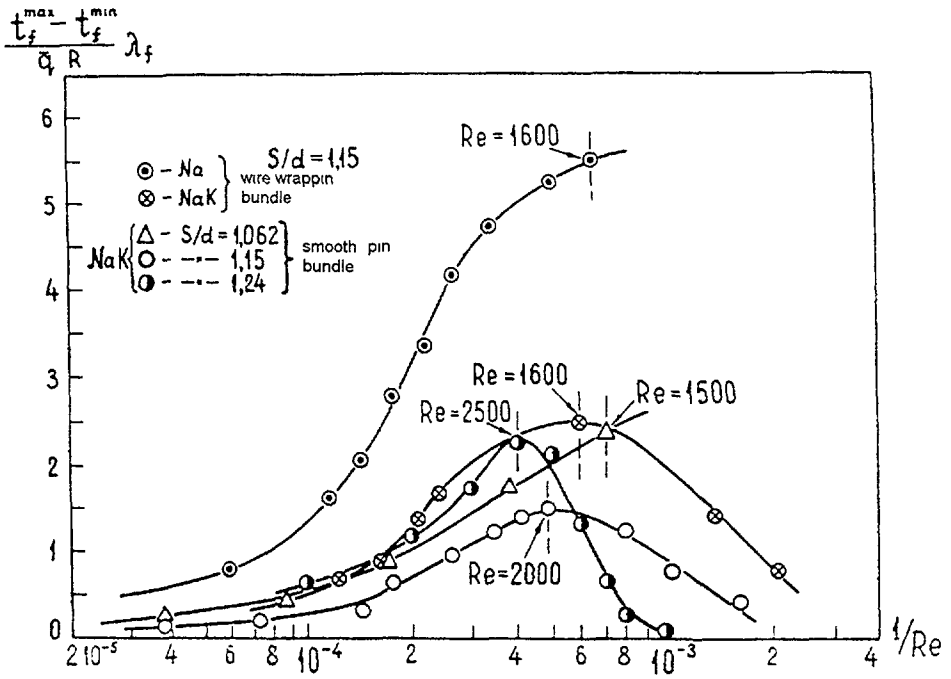

Fig. 6. Change of maximum nonuniformities of temperature of fluid in cross-sections of a model fuel assembly in a function 1 / Re.

turbulent current has a place, and in circumferential (" ï ") - laminar at general transient current in fuel assembly, we shall receive a nude fact, that the redistribution of speed is connected to a measure of difference of hydraulic resistance at turbulent ("ò") and laminar ("ë") currents of the coolant:

$$w_n = w_u \sqrt{\frac{d_{гп}}{d_{гц}}} \cdot \sqrt{\frac{\xi_{цт}}{\xi_{пл}}} \qquad (3)$$

Above mentioned calls additional nonuniformity of temperature in fuel assemblies. For example at model fuel assembly outlet of the BN-350 reactor temperature of fluid varies in such manner that the maximum heating of fluid are observed not in center of assembly but on some distance from center (fig. 7). Temperature of fuel elements located near to a cover of fuel assembly exceeds temperature of central fuel elements. These fuel assemblies have the greatest nonuniformity of temperature on a perimeter also, as fuel elements are under influence of the greatest gradients of temperature in fluid.

The calculation of distribution of flow rate of the coolant on channels of assembly in transient area of current by using a hypothesis of isobaric cross-section (Δp=idem) should take into account various regimes of flow in adjacent channels, while at a homogeneous regime of flow on cross-section of assembly usually relations are correct:

$w \sim d_г^{0.714}$ for a turbulent mode of flow,

$w \sim d_г^2 / A$ for a laminar mode of flow.

À - the coefficient dependent on the form of a channel.

Evaluations of temperature nonuniformities of fuel elements and fluid in fuel assembly of fast reactors in regimes with small Peclet numbers the including regimes with natural convection, is necessary to make with use of the above-stated graphic relations. The marked effects connected to natural convection, should be taken into account at development of approprINPE computational codes.

3.4.2. Analysis of effects connected to natural convection in fuel assembly of reactors, with the help of the modified Grashof criterion

At Pr << 1 (liquid metal coolant) significant influence of a molecular thermal conduction at natural convection is spreaded far from area of a near-a-wall stratum. In this case at the analysis of experimental data it is expedient to use a criterion $GrPr^2$ [28]. This criterion is recommended by Kutateladze S.S. for natural convection of liquid metals from the fact of significant influence of molecular heat transfer.

By entering for our case the modified Grashof number

$$Gr^* = \frac{g\beta q_w l^4}{\lambda_f \nu} \qquad (4)$$

(here g - acceleration of gravity, β- coefficient of the volumetric extension, q_w - density of heat flow on a surface of the fuel element (of the simulator), l - axial coordinate counted from a beginning of energy release; λ_f, ν - thermal conductivity and kinematic viscosity of the coolant accordingly), Matjuhin N.M. has made attempt to analyze with the help of criterion Gr^*Pr^2 experimental data explained in section 2.4.1.

In the fig. 8. the local values Gr^*Pr^2 found on q_w and l in twelve cuts on length of a zone of energy release (see approprINPE values $l / d_г$ in tables II) are shown. Two zones are chosen there: zone A - range of a modification Gr^*Pr^2 in experiences of the authors [19] and zone Á - range of a modification Gr^*Pr^2 in experiences of the authors [18].

With use of local values of a parameter Gr^*Pr^2 the relations ($\Delta T_w^{max} = f(Gr^*Pr^2)$) for wire-wrapped (fig. 9) and smooth (fig. 10) elements of model assembly BOR-60 are constructed at various values of the Peclet number.

In relations $\Delta T_w^{max} = f(Gr^*Pr^2)$ the following singularities take place:

- At Đå < 100 for wire-wrapped side elements (fig. 9) and Đå < 10 for the smooth side elements (fig. 10) two ranges of modification ΔT_w^{max} in function of growth Gr^*Pr^2 are observed - at first the magnification ΔT_w^{max} up to some "limiting" value, characteristic for fixed Đå, and then - falling ΔT_w^{max} at large values of Gr^*Pr^2 parameter;
- In accordance with magnification of the Peclet number a displacement of a "limiting" value ΔT_w^{max} to area of bigger values Gr^*Pr^2 happens; and at Đå = 370 for the wire-wrapped elements (fig. 9) and Đå = 26.5; 100 for the smooth elements (fig. 10) limiting values ΔT_w^{max} are not reached in an investigated interval of modification of the Gr^*Pr^2 parameter.

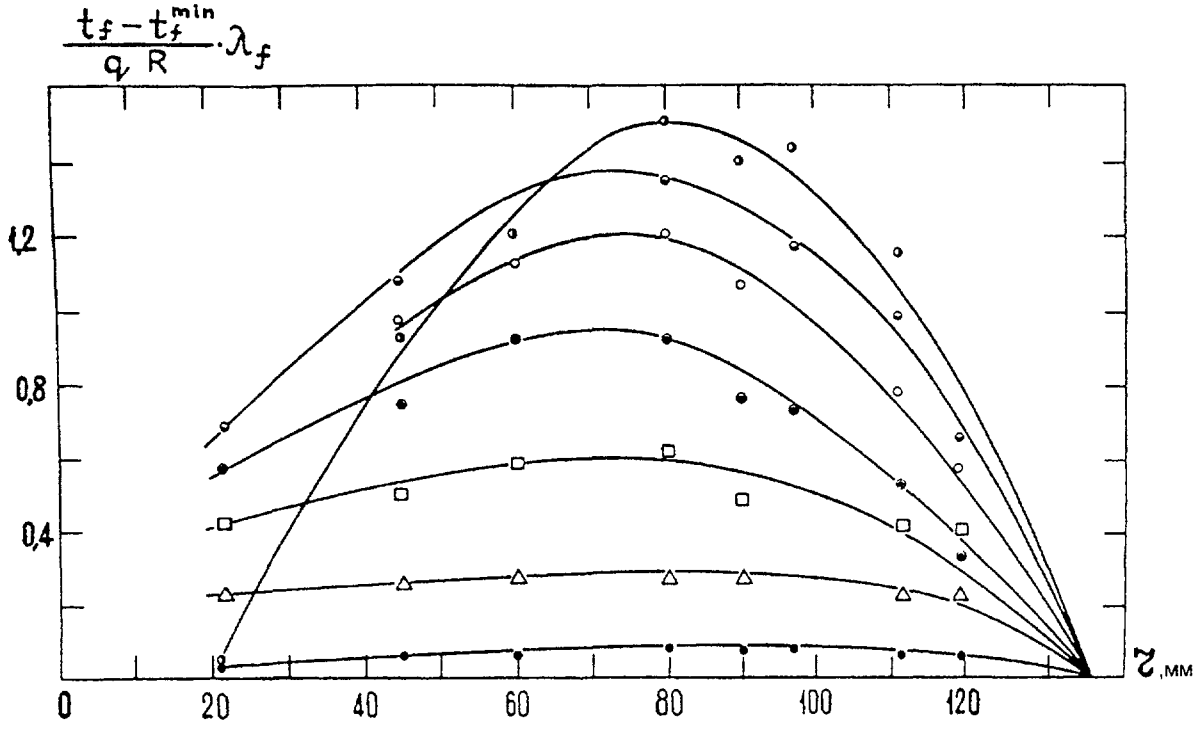

Fig. 7. Radial distributions of fluid temperature in a model fuel assembly BN-350: O, Δ, □, O, O, O, O - Pe = 568, 179, 141, 104, 80, 67, 53 accordingly.

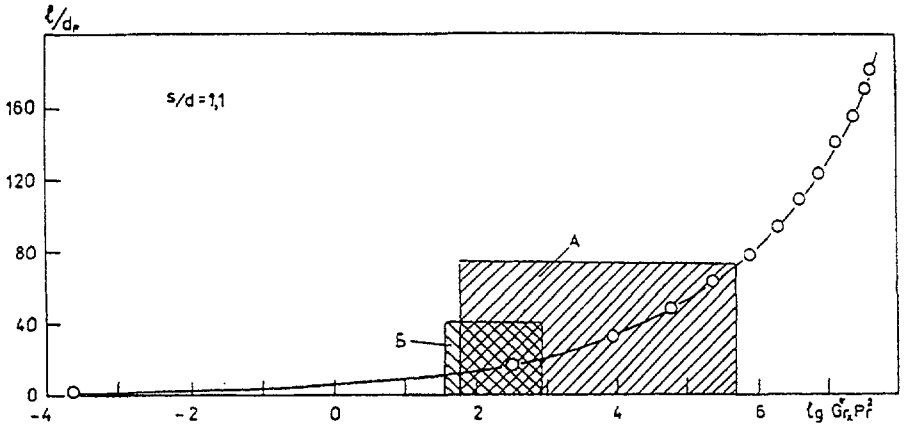

Fig. 8. Values Gr^*Pr^2 on length of a segment of energy release of the fuel element simulator of the model fuel assembly BOR-60.

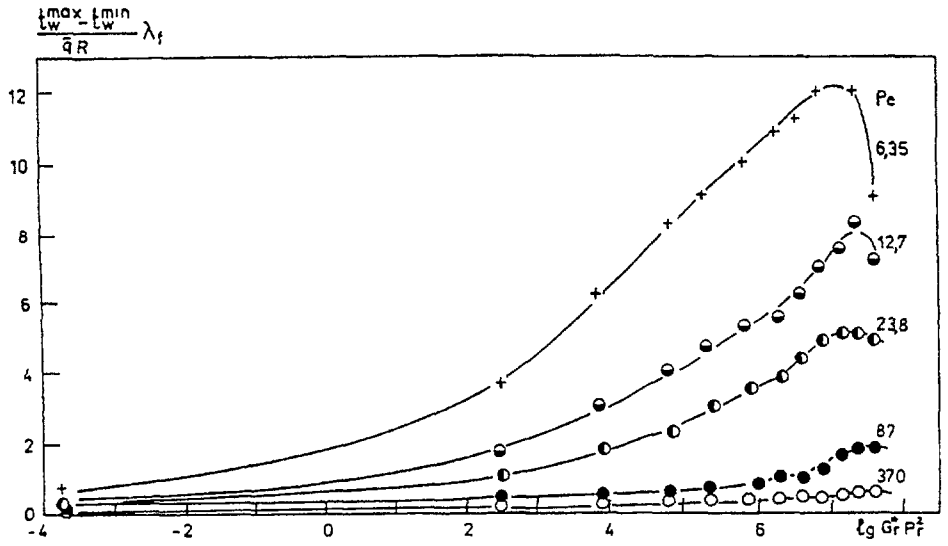

Fig. 9. Relation of maximum temperature nonuniformity of the near-a-wall simulator of fuel element of the model fuel assembly BOR-60 from Gr^*Pr^2.

– The limiting values ΔT_w^{max} are about identical to the smooth side elements for various numbers Ðå and they are $\Delta T_w^{max} \approx 10$ (fig. 10).

4. ABOUT SOME RESULTS OF RESEARCHES OF HEAT TRANSFER TO AN ALLOY SODIUM-KALIUM IN A CELL OF DENSE PACKING OF RODS AT MIXED CONVECTION IN IPPE [18]

In light of the above-stated data for natural convection in model fuel assembly of reactors we shall mark some results of thermal researches obtained by V.I.Koljaskin, L.Ê. Êudrjavtceva and P.À.Ushakov at natural convection in a cell of dense packing of rods and treated in function of the $GrPr^2$ parameter (for a defining size in the Grashof criterion the hydraulic diameter of the channel $d_ã$ is adopted, for a defining difference of temperatures - temperature pressure wall - fluid). These results correspond with the above-stated data in some measure.

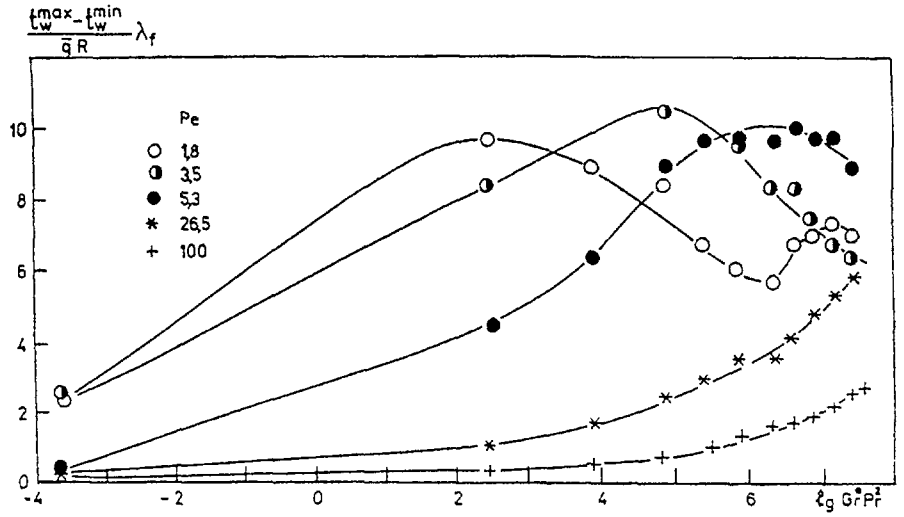

Fig. 10. Relation of maximum temperature nonuniformity of the near-a-wall simulator of fuel element of the model fuel assembly BOR-60 from Gr^*Pr^2.

So the dimensionless nonuniformity of temperature of a wall of the channel $\Delta T_w^{max}=(t_w^{maax}- t_w^{min})\lambda_f / \bar{q}R$ decreases with magnification $GrPr^2$ at a parallel mixed convection on the average on 20 %, at counter - on 35 % (fig. 11), and the temperature fields in a coolant flow react to natural convection a little more. This fact corresponds to zones of ΔT^{max} diminution in the fig. 9, 10 in experiences with model fuel assembly of reactors.

The significant growth of heat transfer is obtained at parallel mixed convection with magnification $GrPr^2$ at numbers Ðå < 100 (fig. 12). At Ðå > 100 influences of natural convection sharply decrease, and at Ðå > 400, as the authors [18] mark, becomes commensurable with an exactitude of experiments.

5. NATURAL CONVECTION IN INTER-ASSEMBLY GAPS OF FAST REACTORS CORES

5.1.Calculated researches in OKBM [4]

At power failure of installation in the fast reactor the stopping of pumps of the first and second loops happens, the channels of system of emergency reactor cooldown are

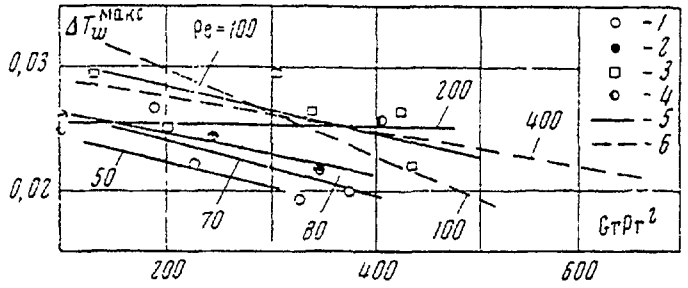

Fig. 11. Influence of natural convection to dimensionless temperature nonuniformity on a perimeter of a channel. Pe : *1* - 70; *2* - 80; *3* - 100; *4* - 190; *5* and *6* - accordingly for parallel and counter mixed convection.

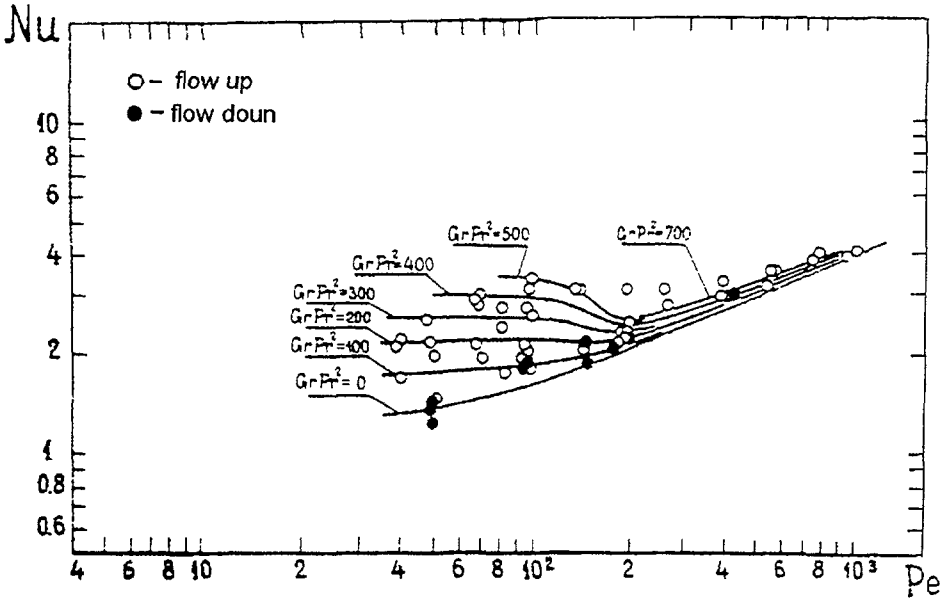

Fig. 12. Heat transfer in a channel of densely-packed bundle of rods.

included and the "cold" sodium with outlet temperature from let-down heat exchanger $t_{âûõ} \approx 350^0$Ñ (for system of emergency reactor cooldown with let-down heat exchangers for the project of the upgraded fast reactor BN-600Ì [4]) merges in the bottom of "hot" cavity of the plenum and begins to fill in inter-assembly space. Sodium in inter-assembly space is heated up because of higher temperatures inside fuel assembly (especially in case of small flow rate inside fuel assembly), a circuit of natural circulation appears: the let-down heat exchanger inlet - the let-down heat exchanger outlet - bottom of "hot" plenum - inter-assembly space - space between heads of fuel assembly and the above core construction - the heat exchanger inlet.

The less flow rate of sodium inside fuel assembly, the bigger role the flow rate in inter-assembly space plays in relation to temperature field inside fuel assembly, cooling sodium and fuel elements of fuel assembly. The moment can occur, when the coolant flow rate inside fuel assembly will become less, than in inter-assembly space, then the role of natural circulation through inter-assembly space will be defining.

If to consider a limiting case of blockage of the coolant input to fuel assembly, inside fuel assembly the regime of U-figurative flow called in the literature "thermosiphon" (fig. 13) will take place. This regime was analysed and calculated by V.À.Sobolev, according to which brief exposition of physics of a considered appearance is given below.

If there is heat release in fuel assembly and leakage of sodium in inter-assembly space the gradient of temperature on a radius of fuel assembly (in a center of fuel assembly temperature is higher, than on a rim) is created, owing to what there is a pressure of natural convection: the sodium in a center of fuel assembly floats up, leaving through orifices in the head of fuel assembly, and to it place a more cold sodium through the bottom of windows of the head of fuel assembly goes(from inter-assembly space, from a let-down heat exchanger after rise of a level "cold" sodium up to heads of fuel assembly; the flows mix up), being lowered along walls of fuel assembly. The lowered pole of sodium is warmed up from a hotter flow in a center of fuel assembly. However heating is not too great because of good heat transfer through a wall of fuel assembly and a big sodium flow rate in inter-assembly space , exceeding the sodium flow rate in a "thermosiphon" circuit($G_{ïîñ} > G_{òðàí}$).

The calculations are carried out at reviewing by one fuel assembly of core with allowance for flow rate of natural circulation in inter-assembly gaps: the part of fuel assembly on a height from a beginning of energy release zone to absorber rods bundle outlet is selected, the cut of a chosen part of fuel assembly is devided into 12 parts in a transversal plane; the task includes 619 elements (sodium, a cover of a fuel element, fuel cores, a cover of an absorber rod, cores of absorber rods). The task of searching of temperature field is solved at specific heating rate, component 2 % from nominal, both specific temperature and sodium flow rate on inter-assembly space inlet.

5.2. Researches in IPPE

In IPPE calculated and experimental researches of temperature fields with reference to fuel assemblies of fast reactors under nonadiabatic conditions on covers of fuel assemblies (model assemblies), stipulated by leakage of the coolant in inter-assembly space, including at natural convection were carried out [26, 29]. The subchannel technique of thermohydraulic calculation of fuel assemblies (groups of interacting fuel assemblies by means of inter-assembly space) was developed, calculated codes was verified by means of obtained experimental material.

5.2.1. Subchannel technique and calculated codes

The subchannel technique of calculation of temperature regimes of fuel assemblies is published in a series of papers, in particular in [29, 30], therefore there is no necessity in it

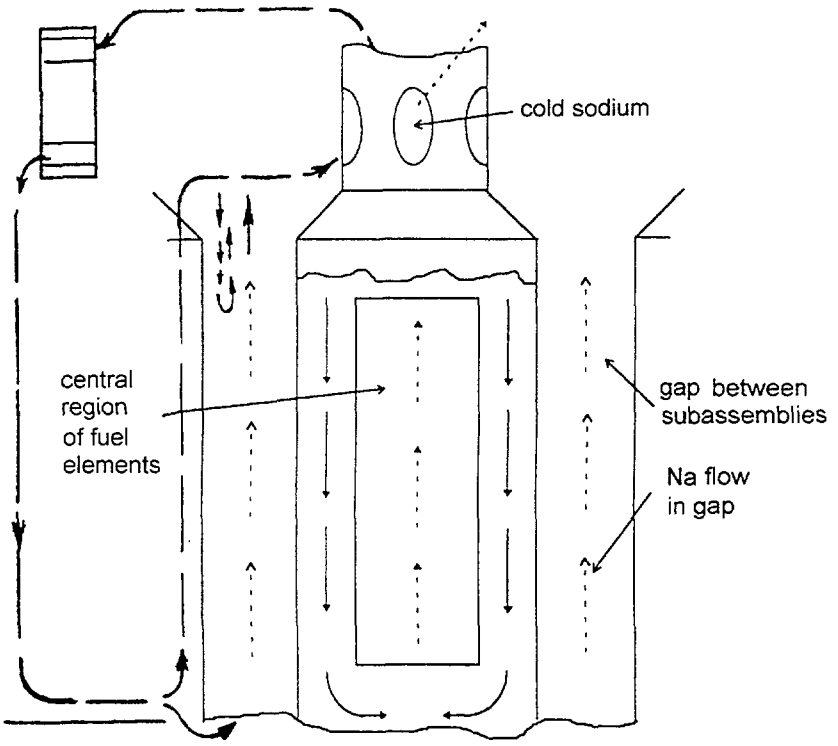

Fig. 13. The scheme of "thermosyphon" flow at blockage of fuel assembly inlet of the fast reactor.

reviewing. Let's mark only, that the whole population of channels in fuel assembly and in inter-assembly space (fig. 14, 15) is considered at an approprINPE solution of the balance equations. Such channels are: interior (fig. 14, á); interior, contiguous to peripheral (fig. 14, â); side, angular; channels in gaps between fuel assemblies (fig. 15). In assembly the interchannel exchange happens because of wire wrapper (fig. 16) and of other mechanisms of transfer.

As an example we shall consider an energy balance equation for channels in inter-assembly gaps (index ξ) in case of the stabilized flow of the coolant at wire-wrapped fuel elements by indirectional wire wrapper within the framework of integral model of interchannel exchange:

$$\frac{d}{dZ}\left(W_\xi T_\xi \Omega_\xi\right) = \sum_{i=1}^{2} \mu_{i\xi}^{T} L(T_i - T_\xi) + \sum_{i=1}^{2} \frac{\delta_{\text{заз}} / s}{Pe}\left(T_i - T_\xi\right) \qquad (5)$$

Here $Z = \frac{z}{L}$, $W_\xi = \frac{w_\xi}{\overline{w}}$, $T_\xi = \frac{t_\xi c_p \rho \overline{w} d_{r0}}{4\overline{q}L}$, $T_i = \frac{t_i c_p \rho \overline{w} d_{r0}}{4\overline{q}L}$, $\Omega_\xi = \frac{\omega_\xi}{\omega_0}$; $Pe = \frac{\overline{w} d_{r0}}{a}$;

z - longitudinal coordinate, L - length of energy release, w_ξ - speed in a channel of an inter-assembly gap, $\overline{w}$ - mean on section of fuel assembly speed of the coolant, d_{a0} - hydraulic diameter of central channels, $\overline{q}$ - mean heat flow from a surface of fuel elements; ω_ξ- cross-sectional area of a central channel, $\delta_{çàç}$ - width of an inter-assembly gap, s - distance center to center of fuel elements; $ñ_ô$, ρ, à and - thermal capacity, density, temperature conductivity of the coolant.

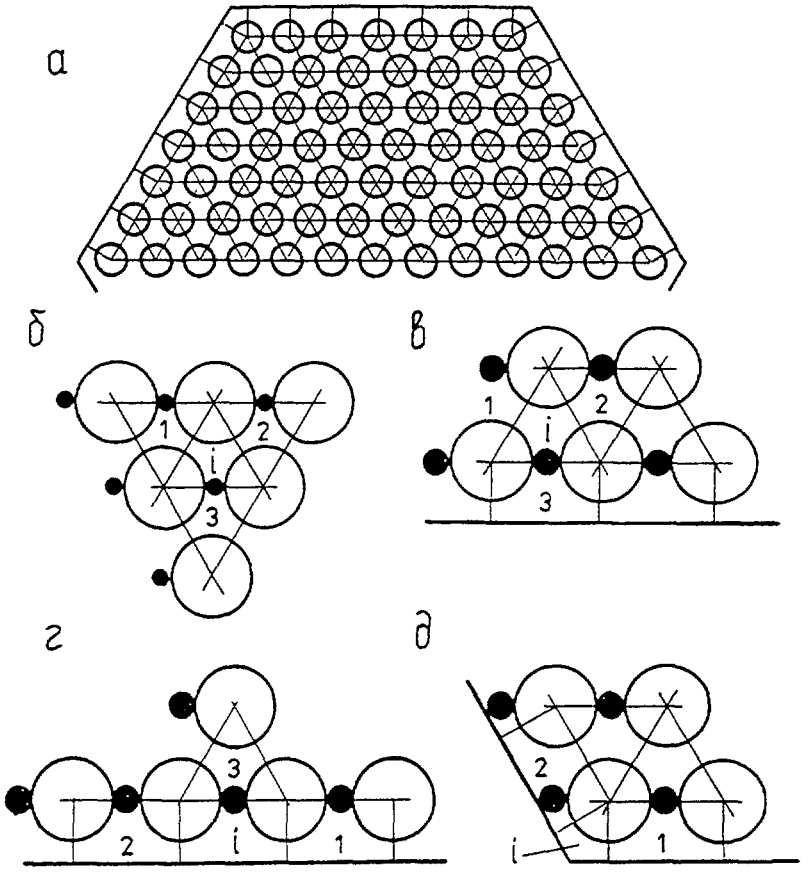

Fig. 14. The scheme of breakdown of cross section of hexagonal fuel assembly (а) on characteristic channel banks (б, в, г, д).

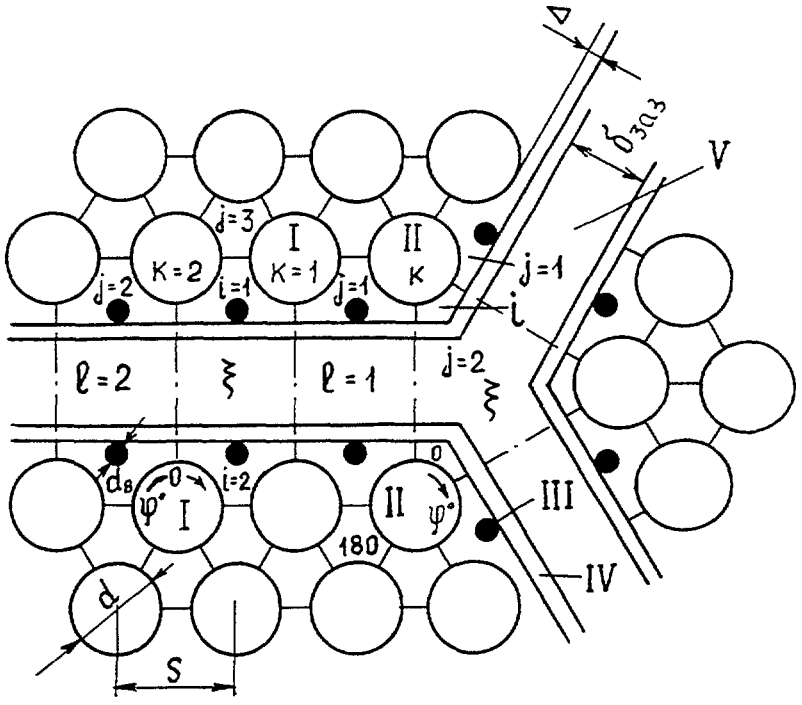

Fig. 15. The scheme of fuel elements arrangement in circumferential zones of adjacent fuel assemblies and breakdown of zones on characteristic channels: I - lateral fuel element, II - angular fuel element, III - cylinder , IV - cover of fuel assembly, V - inter-assembly gap.

The coefficient of interchannel exchange by heat through a cover of fuel assembly, $м^{-1}$, is determined by relation:

$$\mu_{i\xi} = \frac{8}{\pi} \frac{k_{i\xi} s / d}{\lambda_f Pe}, \qquad (6)$$

where the heat transfer coefficient through a cover of fuel assembly is calculated with allowance for of heat conduction of a cover and coefficients of heat transfer in channels of a near-a-wall zone of fuel assembly and inter-assembly space (about coefficients of heat transfer in different categories of channels of fuel assemblies more in detail see in [29]).

The set of equations (5) is decided together with similar equations for other categories of fuel assembly channels at definition of a system of interchannel exchange constants in fuel assembly. The system of these constants is completed in experiments and is explained in [31, 32].

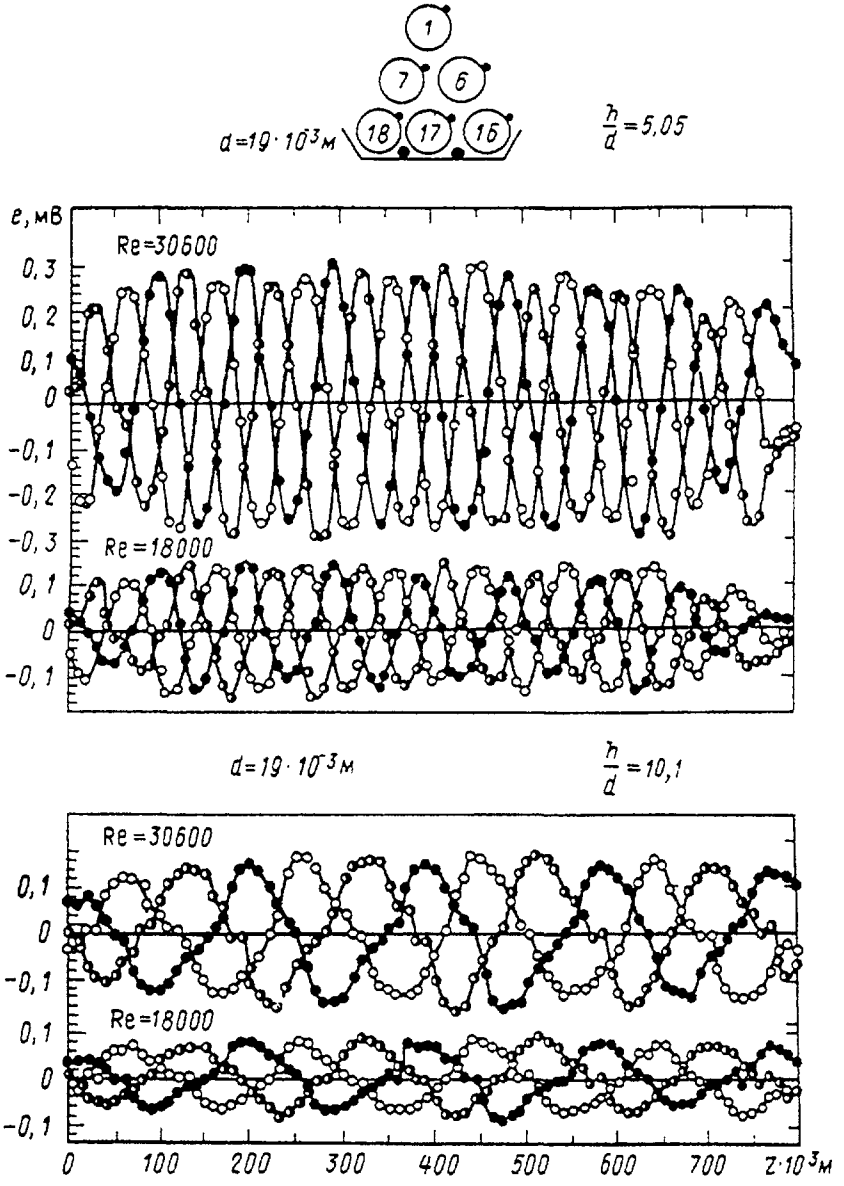

Fig. 16. Change cross-sectional leakage of the coolant (in mW of the sensor) on length of gaps in lattices of wire-wrapped fuel elements of a type "an edge on an cover".

With use of the subchannel technique are developed the following computational thermohydraulic program: GID, TEMP, TEMP-M, MIF, ÌID (non-stationary case). Their detailed definition see in [26, 32].

5.2.2. Results of calculation, comparison to experiment

In general case the effect of non-adiabatic boundary conditions on covers of fuel assembly to temperature field is determined by geometry of fuel assembly, intensity of interchannel exchange in fuel assembly and heat transfer between fuel assemblies, size inter-assembly leakage of the coolant, and also character of energy release field.

The thermal exchange between fuel assemblies can increase or reduce temperature non-uniformity of circumferential fuel elements depending on character of fuel assemblies interaction.

The solution of a set of energy balance equations for group interacting fuel assemblies of the reactor BN-600 with irregular energy release in cross section shows, that the increase of heating of the coolant in adjacent fuel assemblies has a place in the field of low energy release at small leakage of the coolant in gaps between fuel assemblies ($g_{i\delta} \le 2\%$) together with some drop of a peak level of coolant heating in area with high energy release. The drop of coolant heating in circumferential areas of fuel assembly (fig. 17) happens because of leakage increase of the coolant in inter-assembly gaps.

At low intensity of heat transfer through a cover of fuel assembly ($\mu^{\dot{O}}_{i\xi} < 1\ i^{-1}$) or at small coolant leakage ($g_{i\delta} << 1\%$) heat transfer to the inter-assembly gap unsignificantly influences on a temperature field of fuel assembly. At high intensity of inter-assembly heat transfer ($\mu^{\dot{O}}_{i\xi} > 2\ i^{-1}$) and at large coolant leakage in an inter-assembly gap ($g_{i\delta} > 1\%$) the drop of coolant heating on a rim of fuel assembly appears essential. It considerably increases non-uniformity of temperature on a perimeter of circumferential fuel elements. At the same time the heat transfer through a cover of fuel assembly acts on a temperature field of maximum three - four numbers of fuel elements, contiguous to a cover, and can render essential effect on

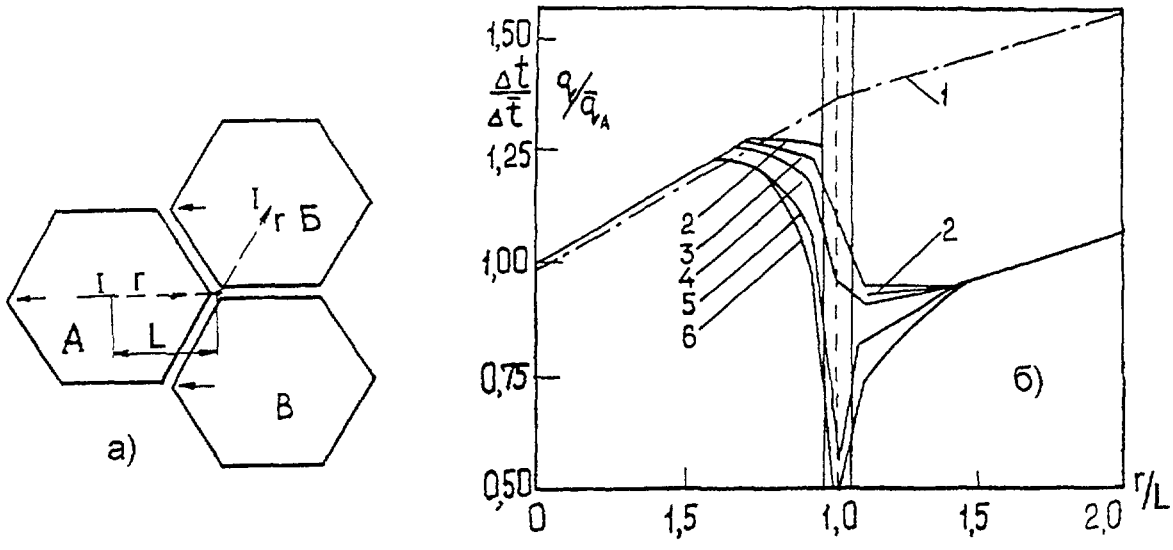

Fig. 17. Distribution of energy release (1) and heating of the coolant in cross section of two interacting fuel assemblies: 1 - calculation disregarding of inter-cartridge heat transfer; 2 - 6 - calculation with allowance for of inter-cartridge heat transfer at the coolant flow rate in inter-cartridge gaps, component 0; 0,02; 0,04 of coolant flow rate through fuel assembly and equal ∞ accordingly; а) - arrangement of adjacent fuel assemblies; б) - results of calculation in a direction r.

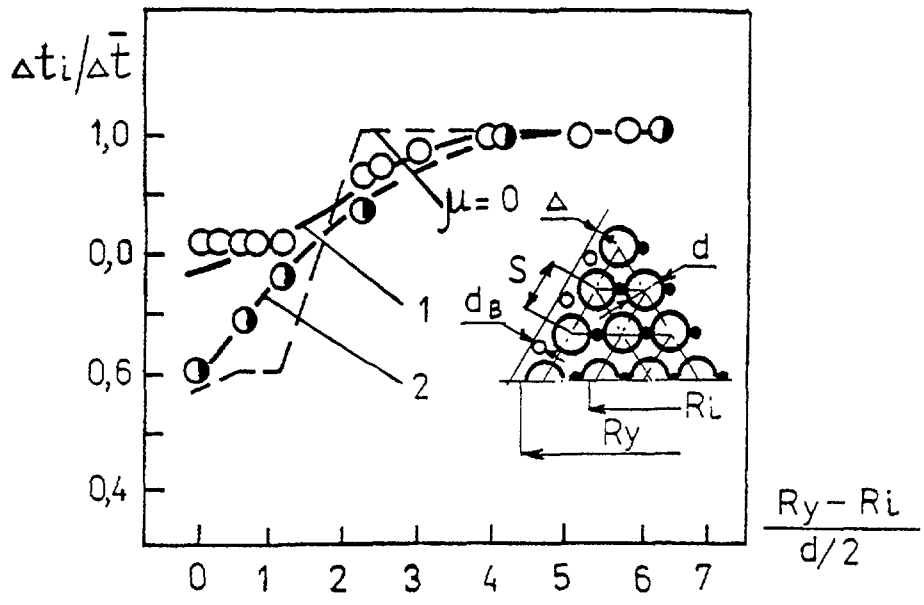

Fig. 18. Distribution of coolant heating on a radius of model fuel assembly of the BOR-60 reactor under adiabatic conditions on a cover (1) and on a radius of thermometric package of fuel elements of the reactor in conditions inter-assembly leakage, equal 4% (2); ○, ◑ - experimental data [23, 24] and [33] accordingly; - - - - - - calculation disregarding of interchannel heat transfer.

a level of temperature of fuel assembly with small number of elements. The experimental data obtained on a thermometric bundle of fuel elements of the BOR-60 reactor [33] (fig. 18) and on the assembly of 19 simulators of fuel elements, simulating the fuel assembly of the BN-350 reactor (fig. 19) [29] testify to it.

5.3. Researches in Japan

The Japanese experts [5, 34 - 36] are engaged in problem of decay heat removal from cores of fast reactors through inter-assembly space of fuel assemblies in conditions of reactors cooldown per the last years.

5.3.1.Experimental researches

The problem on experimental researches of an indicated problem in Japan leaves for frameworks of the given report. Let's indicate only, that in Japan the extensive program of researches [34] is developed, the unique experimental base (fig. 20, 21) is created, series of experiments are conducted by using sodium as the coolant. For familiarity of the reader with some obtained results it is possible to recommend papers [5, 36].

We shall stay on a computational technique used recently by the Japanese experts for the analysis of experimental data in more detail.

5.3.2. Computational researches [35]

The numerical method of the analysis is based on use of approximation of a porous body [37]. The equations of mass, moment and energy conservation for flow in porous environment are noted in the final differential form (non-stationary case) for internal and external channels of assembly. It is supposed that the full diffusion of momentum

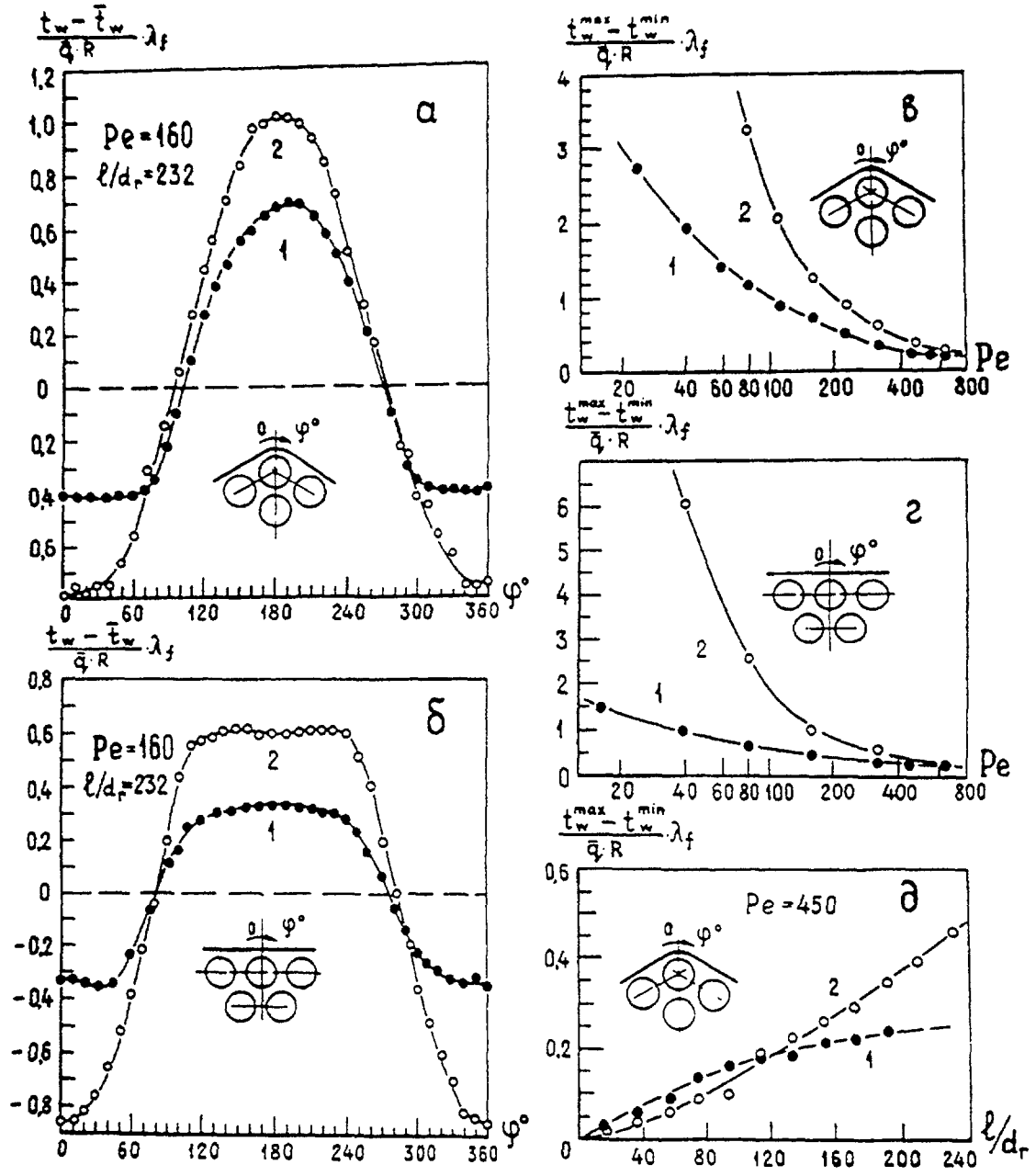

Fig. 19. Temperature fields of angular (а) and lateral (б) simulators of fuel elements of the model fuel assembly of the БN-350 reactor at adiabatic (1), non-adiabatic (2) conditions on a cover of assembly and regularity of change of maximum nonuniformities of temperature from the Peclet number (в, г) and from length of energy release (д).

$$\tilde{A}_m = \varepsilon_e + \varepsilon_M + k\nu \tag{7}$$

and energy

$$\tilde{A}_e = Pr_t(\varepsilon_e + \varepsilon_M) + k\frac{\lambda}{\rho c_p} \tag{8}$$

consist from heat transfer by means of wire wrapper (ε_e), thermal vortexes (ε_M) and molecular transfer ($\nu, \frac{\lambda}{\rho c_p}$).The coefficients of turbulent intermixing undertake from S.K.Cheng and

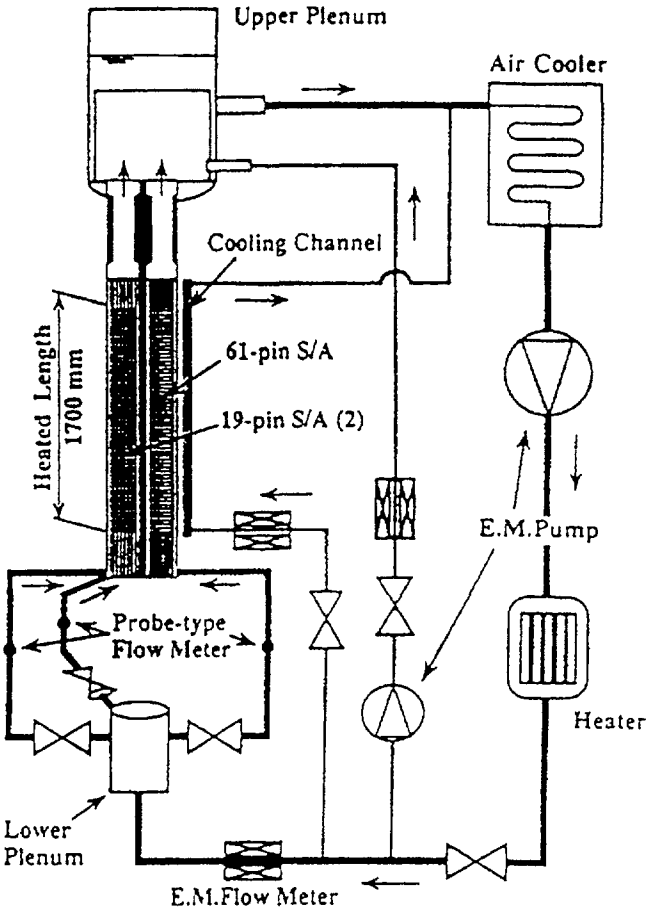

Flow Diagram of the CFR Test Section installed in the CCTL

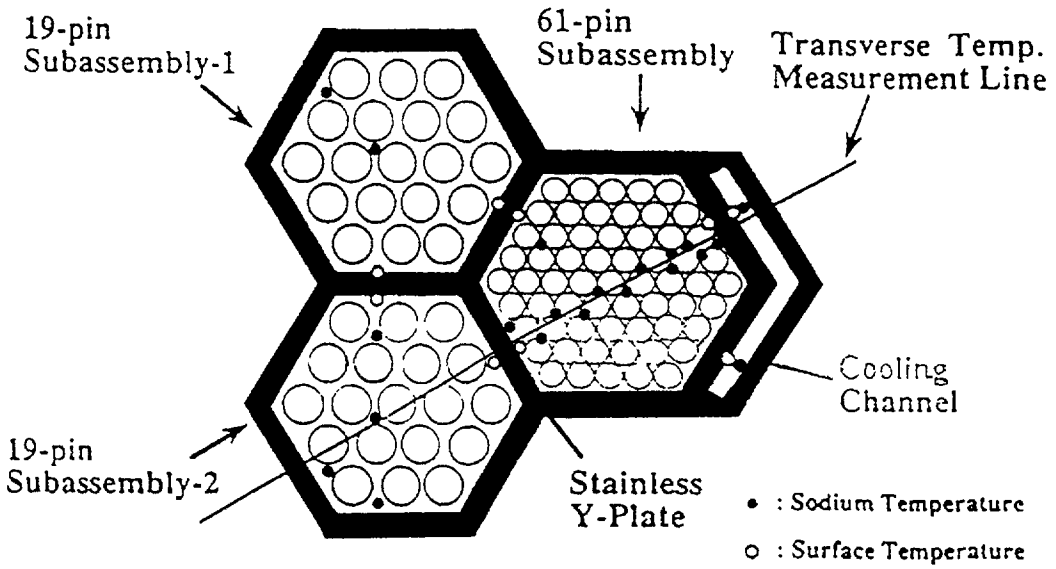

Cross Section View of CCTL-CFR Subassemblies

Fig. 20. CCTL-CFR experiment.

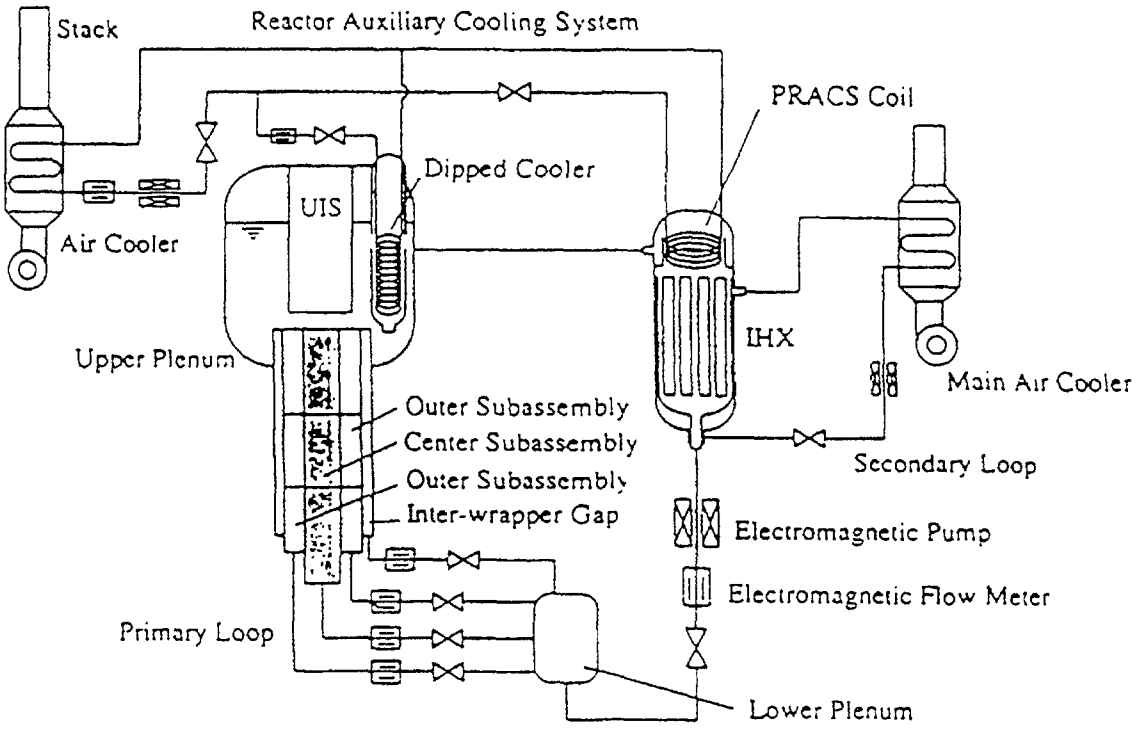

Flow Diagram of PLANDTL-DHX

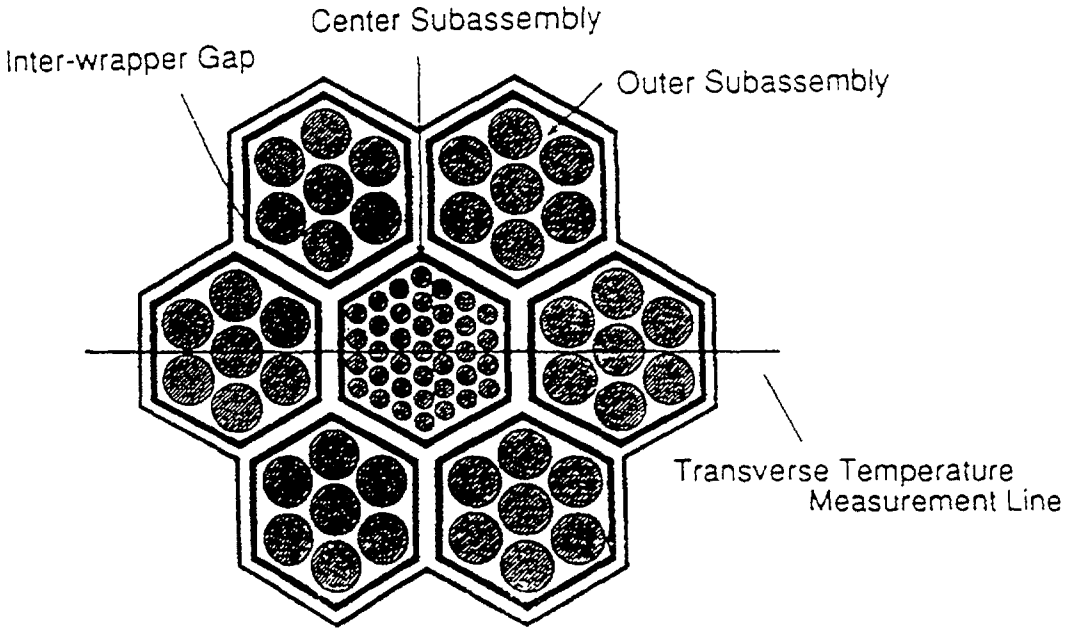

Cross Section View of PLANDTL-DHX Subassemblies

Fig. 21. PLANDTL-DHX experiment.

N.E.Todreas [38, 39], and coefficients of exchange by means of wire wrapper - from [40, 41].

The turbulent Prantl number is supposed equal 1. The coefficient k, taking into account geometric factor in molecular exchange, is calculated from Cheng and Todreas [39]:

$$k = 0.66\left(\frac{P}{D}\right)\left(\frac{C}{D}\right)^{-0.3} \tag{9}$$

Here P - distance center to center of rods, D - diameter of rods, C - gap between adjacent rods. It is supposed, that the relation (9) is fair and for wire-wrapped rods.

It is marked, that the role of a thermal conduction is insignificant on a comparison with intermixing through thermal curls in conditions of convective mixing, by means of wire wrappers and redistribution of flow in the field of low values of Reynolds numbers.

The inter-assembly heat transfer is taken into account. It is marked, that if it is great, it can be the reason of large temperature gradients across a bundle and even of an inverse flow.

The Grashof number according to Engel etc. is introduced [42].

$$Gr_{\Delta T} = \frac{g\beta \dfrac{\Delta T_b\big|_0^L}{L} D_{eb}^4}{\nu^2}, \tag{10}$$

where D_{eb} - hydraulic diameter of a bundle of rods, L - length of energy release, $\Delta\dot{O}_b$ - difference of mean-mixing (index "b") temperatures between two levels.

As it is visible from (10) $Gr_{\Delta T}$ is determined from average longitudinal temperature gradient in limits of length of energy release.

As in an ensemble of assemblies with inter-assembly heat transfer the modification of an axial gradient of temperature happens, the modified Grashof criterion is used

$$Gr^*_{\Delta T} = \frac{g\beta \left.\dfrac{\Delta T_b}{\Delta z}\right|_k D_{eb}^4}{\nu^2}, \tag{11}$$

where k - number of an axial knot of a calculated grid.

Local on an axes $Gr^*_{\Delta T}$ numbers are used in a calculated code AQUA.

The resistance coefficients for longitudinal flow are calculated from relation of Cheng and Todreas [38]. The resistance in transversal direction is supposed much smaller, than in longitudinal.

The threshold function eliminating effect of a diffusion through thermal curls at the Richardson number $Ri \le 0.1$ is introduced into reviewing, about what the data of [39, 43] testify.

This function varies from 1 up to 0 and looks as follows (fig. 22):

$$fx_{pl} = \max\left[0.1 - 10^{\{-6(Ri-0.1)\}}\right] \tag{12}$$

$$Ri = \frac{Gr}{Re_i^2} \tag{13}$$

$$Gr = \frac{g\beta\Delta T_b\big|_0^L D_{eb}^3}{\nu^2} = Gr_{\Delta T}\frac{L}{D_{eb}} \tag{14}$$

It is supposed, that the threshold on Richardson (Ri) is applicable as for local and for average conditions, i.e.

$$\Delta T_b\big|_0^L = \left.\frac{\Delta T_b}{\Delta z}\right|_k \cdot L \tag{15}$$

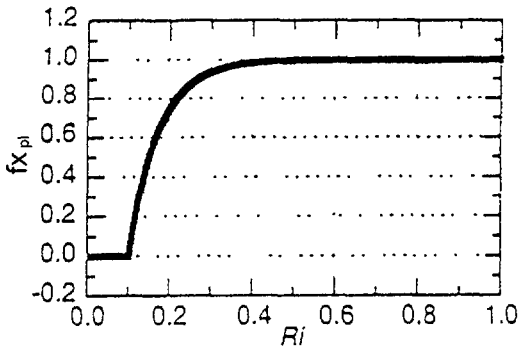

Fig. 22. A curve of a threshold function for diffusion at mixing of thermal vortexes.

$$Gr = Gr^{*}_{\Delta T}\frac{L}{D_{eb}} \tag{16}$$

The relations for coefficients of interchanging are obtained for the following intervals of a modification of defining parameters: $170 \le Gr_{\Delta T} \le 650$; $520 \le Re_b \le 4400$; $0.6 \le Gr_{\Delta T} / Re_b \le 0.73$; $1.08 \le P / D \le 1.25$.

Here $Re_b = \frac{v_b D_{eb}}{\nu}$ - average on a bundle the Reynolds number.

The calculated grid is selected according to Ro and Todreas [37]. On a vertical the assembly is devided into 29 knots at overall length of 2825 mm. The interval between knots on length of energy release makes 82.5 mm or 87.5 mm. The non-stationary calculations are fulfilled at use of a more small-sized grid with a half distance between knots on a vertical, i.e. 41.25 mm or 43.75 mm.

The coefficients of heat transfer inside a cover of assembly, and also on an interior surface of a cover are calculated on a relation Subbotin V.I.

$$Nu = 5.0 + 0.025\ Pe^{0.8} \tag{17}$$

The sodium in an inter-assembly gap is supposed fixed (the first stage of calculations); the one-dimensional heat conduction equation in perpendicular direction to a surface of a cover is decided.

The numerical method is used according to [44]. The characteristic results of calculation of relative heating of the coolant on a cut of model assembly are represented in the fig. 23.

The rather in-depth account of methodical side of research [35] in the report is connected to importance of an analyzable problem and with necessity of comparison of results of this work with earlier obtained data in IPPE on a considered problem [26, 29, 31, 32].

6. THERMOHYDRAULICS IN THE UPPER PLENUM OF THE FAST REACTOR IN COOLDOWN CONDITIONS

6.1 Processes defining thermohydraulics at natural convection in the upper plenum of the reactor

Creation of thermohydraulic codes of various assigning, various volume and content, passes already more than 20 years. The calculated codes, their architecture and content are determined mainly by population of problems, which are before the scientists and designers investigating nominal and abnormal processes of existing nuclear reactors. Per last years it is problems connected to safety of nuclear reactors.

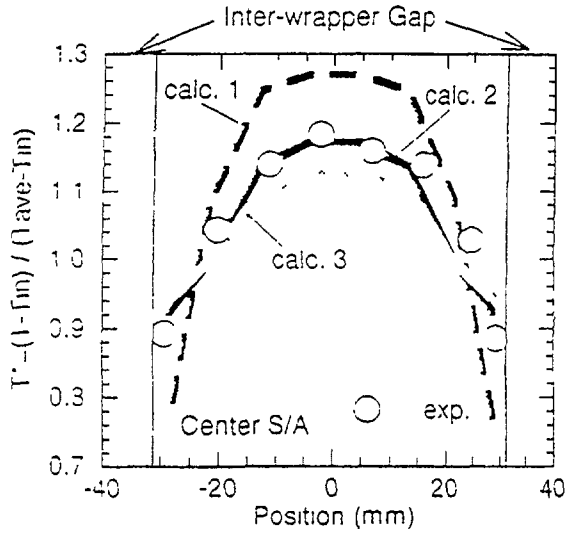

Calculation	The factor of intermixing	Threshold function
1	is not used	is not used
2	is used	is used
3	is used	is not used

$Re_B = 6912$, $Gr_{\Delta T} = 913$, $Gr = 2{,}27 \cdot 10^6$, $Ri = 0{,}005$

Fig. 23. A normalized temperature profiles on the upper of a heated zone at initial Condition-1.

The basic place among thermohydraulic processes takes heat transfer in bundles of rods of a core and in the upper plenum of the reactor. In a core it is possible to mark researches of temperature fields in a condition with blockage of a part of cross section of fuel assembly, role of stringers and other researches partially considered above.

One from major problems of thermohydraulics of the upper plenum of the fast reactor, especially in the cooldown process, is the definition of velocity and temperature fields for various variants of removal of thermal power. These temperature and high-speed fields depend on phenomenon of temperature striping which have a place in liquid metal reactors. Let's mark some from them: thermal stratification, thermal striping, core - plenum interaction, free surface sloshing.

6.1.1. Thermal stratification

Thermal stratification phenomenon appears in large volume of upper plenum after scram due to relatively cold temperature fluid being continuously supplied with low velocity into the upper plenum at decay heat power level. The interface between hot (upper) and cold (lower) fluid regions in the upper plenum will oscillate slowly and largely under certain conditions. Such a large oscillatory motion of the stratification interface, which has a large temperature difference, causes severe thermal stress to the reactor vessel and reactor components.

6.1.2. Thermal striping

Thermal striping phenomena characterized by random temperature fluctuations inevitably occur in the mixing regions of hot and cold coolant, e.g., the area between the core outlet and the upper core structure. In the region around the core outlet, the interaction of cold sodium flowing out of a control rods assembly and hot sodium flowing out of adjacent

fuel assemblies causes the thermal striping and might give high-cycle fatigue to the in-vessel components located in this region. Therefore it is necessary to evaluate influenced area and characteristics of the random thermal process and to protect the corresponding components from high-cycle fatigue.

6.1.3. Free surface sloshing

In the heat transport system of liquid-metal reactors, free surfaces exist for absorbing the coolant thermal expansion when the temperature rises. As it gives large temperature difference to attached structures, the free surface must be kept stable not to cause sloshing and rapid shrinkage during various operating conditions.

6.1.4. Core - plenum interaction

From the viewpoint of passive safety, it is desirable that the decay heat could be removed only by natural circulation when the pony motor could not be operated. During the operation of cooling system, relatively cold temperature fluid from the heat exchangers directly immersed in a hot plenum flows down to the core outlet region and may repeat to penetrate into some subassemblies under a certain natural circulation condition. This phenomenon, which is called the core-plenum interaction, is probable to influence not only structure material but also the natural circulation head which determines core flow rate and therefore affects the core coolability.

6.2 Codes used for natural convection research and some results of researches

Let's mark some system codes used for natural convection research and partially mentioned in introduction. It is codes AQUA, TRIO-VF, FLUTAN, ASTEC, SSC-L, DINUS-3, NECTAR. The SSC-L code deals with various accidents and transients such as natural circulation. But in the given code for the upper plenum the two-dimensional model is used. It is not enough of it, since the natural convection has a three-dimensional character. With the help of the ASTEC code thermohydraulics of installation RAMONA was simulated. The comparison of computed and experimental results shows that following the pump rundown transient the core inlet and outlet temperatures, and hence the core flow rate, recover faster than the experimental data show. The similar code on the given problem is the German FLUTAN code, which also allows to analyze thermohydraulic phenomena including a system of passive cooling of the reactor. The French TRIO-VF code are used to compute the characteristics of temperature fluctuations occurring in a tee mixing hot and cold sodium pipe flows. In this case in the given code the model of a turbulence LES (modeling of large curls) is applied.

But the most characteristic and universal code for natural convection research, under the judgement of the authors, is the Japanese code AQUA.

A general purpose multi-dimentional thermohydraulic analysis code AQUA was developed at PNC (Japan) and was improved in order to evaluate thermal stratification phenomena including large oscillatory motions of the stratification interface. AQUA is based on the finite difference method and is characterized by the incorporation of advanced turbulence models, higher-order discretization schemes for the convection terms, treatment of time-dependent terms with second-order accuracy.

AQUA is applied to simulate both the water and sodium experiments. To accurately model the buoyancy effects, two kinds of turbulence models were implemented to AQUA: the $k - \varepsilon$ model with Pr_t being dependent on the local Richardson number and the algebraic stress model (ASM). Model ASM gives good results for sodium experiments.

For the evaluation of the temperature fluctuation intensity, $k - \varepsilon - \theta$ model and the Reynolds stress model (RSM) as well as ASM were incorporated into AQUA. ASM is the

most suitable turbulence model because it shows the better prediction accuracy and uses much less computational time.

Similar AQUA code developed in Japan is the DINUS-3 code. The direct simulation code DINUS-3 is the code without any turbulence models The basic purpose of the code is to investigate temperature fluctuations in the core outlet region and in the upper plenum of fast reactors

As it was marked above, in IPPE the two-dimensional NECTAR code is developed. Let's present as an example the results calculations of process of decay heat removal by natural convection which are carried out on this code The scheme of installation is shown in the fig. 24 The standard set of Navier-Stokes and energy equations was decided by a finite difference method of Patankar.

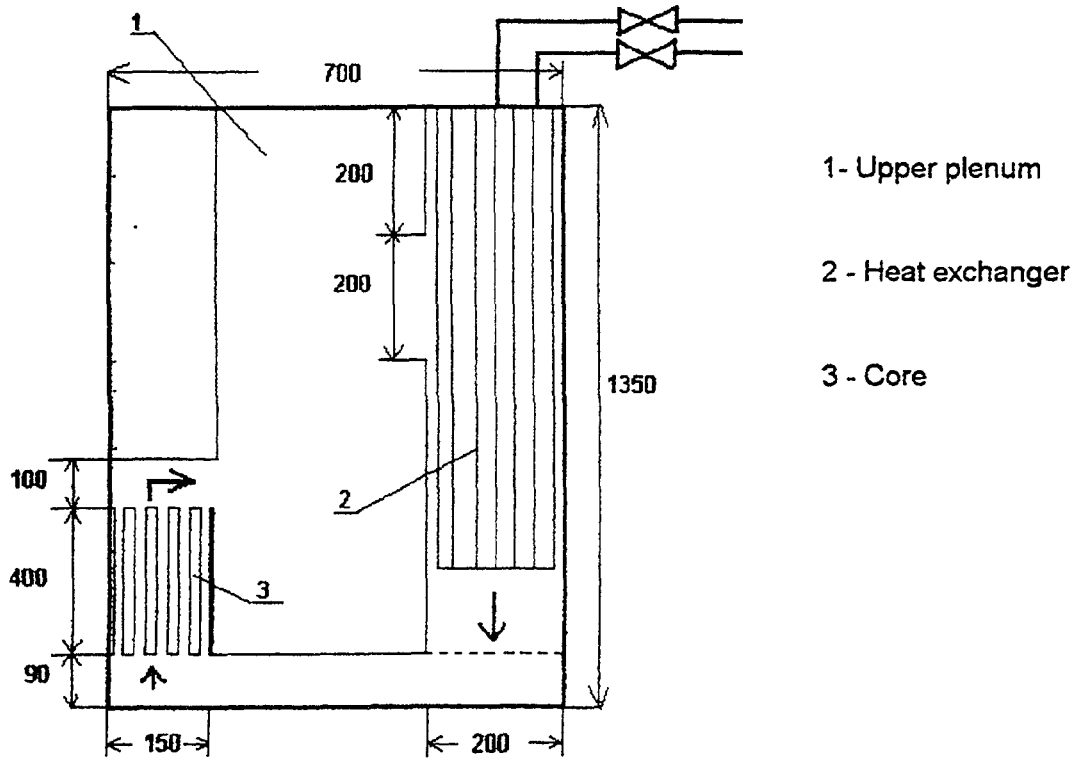

Fig. 24. The scheme of the installation for calculations by the NECTAR code.

In the fig. 25 the modification of temperature of the coolant (sodium) at core outlet in time is shown. The thermal power, Q, assigned as a parameter, varied from 0.1 kW up to 10 kW. For all values Q there is a growth of temperature for all considered slice of time. These results have a preliminary character, for reliable simulation of system of emergency cooldown the in-depth study of influence of a thermal power Q, geometry of a model, performances of the heat exchanger is necessary.

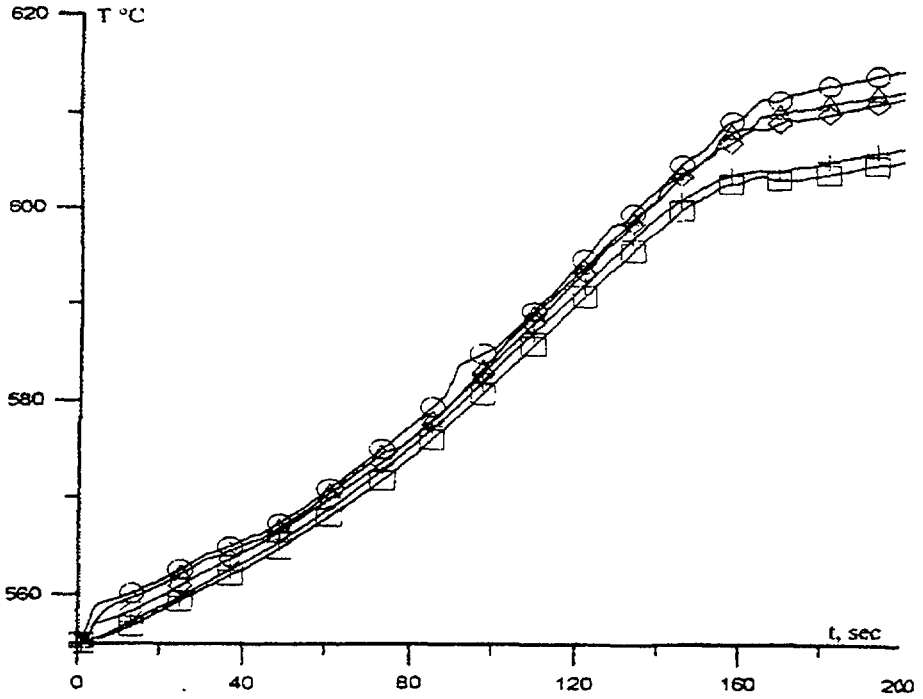

Fig. 25. Change of the coolant temperature (sodium) at outlet core in time at various powers: □ - 0.1 kW, + - 1 kW, ◊ - 2 kW, Δ - 4 kW , ○ - 10 kW.

REFERENCES

[1] IAEA / IWGFR / 88, Specialists Meeting on "Evaluation of Decay Heat Removal by Natural Convection", 22-23 February 1993 // Oarai Engineering Center, PNC, Japan.

[2] ZHUKOV A.V., SOROKIN A.P., KUZINA J.A Removal of Residual Heat Natural Convection at Emergency Cooldown Fast Reactors: the Concepts and Results of Researches The report on V international conferences "Safety NPS and training of personnel", OINPE, Obninsk, 2-5 February 1998. The theses of the reports // OINPE, Obninsk, 1998.

[3] ZHUKOV A.V., SOROKIN A.P., KUZINA J.A. Results of Decay Heat Removal Researches for Fast Reactors on Problems of Emergency Reactor Cooldown (Review of Studies) // Meeting 4-th working groups on fast reactors technology, IPPE, June 15-20, 1998, Obninsk, Russia.

[4] THE AGREEMENT ON FAST REACTOR BETWEEN COMMISSARIAT ON AN ATOMIC ENERGY ON FRANCE AND MINATOM OF RUSSIA ON 1994-1995.

[5] SOBOLEV V.A., VORONOV V.N., KUZAVKOV N.G. Analysis of Decay Heat Removal from the Core Using Passive Cooling System // Sodium Cooled Fast Reactor Safety, International Topical Meeting, Obninsk, Russia, October 3 - 7, 1994, Proceedings, v. 4, p.p. 6-12 - 6-23.

[6] KAMIDE H., IEDA Y., TODA S., ISOZAKI T., SUGAWARA S. Multi-bundle Sodium Experiments for Thermohydraulics in Core Subassemblies during Natural Circulation Decay Heat Removal Operation // IAEA / IWGFR / 88, Specialists Meeting on "Evaluation of Decay Heat Removal by Natural Convection", 22-23 February 1993, Oarai Engineering Center, PNC, Japan.

[7] ERTEL V., REINDERS R. Development and Application of Thermohydraulic System Code DYANA/ATTICA // Proc. Intern. Conf. On Fast Reactor Safety, Juersy, GB, 1986.

[8] GRAND D. et al. The Dimensional Computations of Thermalhydraulic Phenomena in Reactor Vessel // Advanced in Mathematics, Computations and Reactor Physics, Int. Meeting, Pittsburg, USA, April 28 - May 2, 1991.

[9] GEORGEOURA S.E., KEETON J.A. A three Dimentional Simulation of a Pool Type Fast Reactor Model using the ASTEC Code // NURETH-5, Sept. 21 - 24, 1992, Salt Lake City, USA.

[10] BORGWALDT H., BAUMANN W., WILLERDING G. FLUTAN, Input Specification (related to family of COMMIX codes) // KfK 5010, Kernforschungszentrum Karlsruhe, Germany, May 1992.

[11] MAEKAVA I., Numerical diffusion in single-phase multidimensional thermal-hydraulic analysis // Nucl. Engrg. Des. 120 (1990), 323.

[12] KUZINA J.A., SOROKIN A.P., UKHOV V.A. The Status of Thermohydraulic Codes for Reactors on Fast Neutrons / Meeting 4-th working groups on fast reactors technology, IPPE, June 15-20, 1998, Obninsk, Russia.

[13] THE AGREEMENT ON FAST REACTOR BETWEEN COMMISSARIAT ON AN ATOMIC ENERGY ON FRANCE AND MINATOM OF RUSSIA ON 1996-1997.

[14] MITENKOV F. M., BAGDASAROV YU.YE., BUKSHA YU.Ê. et al. Engineering methods of the analysis of modes with natural circulation in installations of a type BN // Atomic Energy, 1987, v. 62, № 3, p. 147 - 152.

[15] YAMAGUCHI A., et al. Plant-wide Thermal Hydraulic Analysis of Natural Circulation Test at JOYO with MK-Ï Irradiation Core // NURETH-4, v.1, p. 398 - 404.

[16] SATON K., et al. Study of Decay Heat Removal by Natural Circulation // NURETH-4, v. 1, p. 378 - 383.

[17] AUBRY S., LAMBERT M. Thermal-Hydraulic Study of LMFBR Fuel Assemblies under Accident Cooling Conditions during Internal Storage or Handling // Science and Technology of Fast Reactor Safety, BNES, London, 1986, p. 219, 223.

[18] FORT J.A., et al. Investigation of Flow Recirculation in Rod Bundle during Natural Convection Flow and Power Transient // Second International Topical Meeting on Nuclear Reactor Thermal-Hydraulics, Santa Barbara, California, USA, Jan. 11 - 14, 1983.

[19] WYDLER P., SIGG B., DUTTON P. Studies of Decay Heat Removal by Natural Convection using the SONACO Sodium-Cooled 37-Pin Bundle // Science and Technology of Fast Reactor Safety, BNES, London, 1986, p. 185 - 190.

[20] KOLYASKIN V.I., KUDRYAVTSEV L.K., USHAKOV P.A. Heat Transfer to an Alloy Sodium -êàëèé in a Cell of Dense Packing of Cores at Mixed Convection ÒÂÒ, ò.11, ¹ 4, 1973, p. 781 - 787.

[21] DATTON, UELTY. Experimental Research Natural Convection about a Lattice of the in Regular Intervals Heated up Vertical Cores at Small Prandtl Numbers // Heat Transfer, ¹ 3, 1975, p. 57 - 63.

[22] BOGATIRJOV I.L. et al. System of Constants for Subchanals Thermogidraulics of Account of Modes the Operations Subassemblies Reactors with Natural and Mixed Convection // Preprint IPPE-2238, Obninsk, 1992.

[23] THE CATALOGUE OF STANDS, REACTORS OF ZERO CAPACITY AND OTHER EXPERIMENTAL INSTALLATIONS // Published by CEC, CSTC 1-2, 1978, p. 20 - 22.

[24] ZHUKOV A.V., SOROKIN A.P., SVIRIDENKO YE.YA., HUDASKO V.V. Experimental and Settlement Modeling Thermogidraulic Heat Transfer of Devices NPP. Model Assembly, Gauges, Technique. Liquid Metal the Stand. The Manual for the Students of Courses of Improvement of Qualification and Special Faculty // ÎINPE, Obninsk, 1992 ã., p. 59 - 76.

[25] SUBBOTIN V.I., ZHUKOV A.V., PASHEK M. et al. Experimental Study on Model of the Operating Temperature Regimes of the Fuel Elements of a Bor-60 Reactor // Preprint IPPE - 137, Obninsk, 1969.

[26] SUBBOTIN V.I., ZHUKOV A.V., PASHEK M. et al. Experimental Study on Model of the Operating Temperature Regimes of the Fuel Elements of a Bor-60 Reactor // Heat Transfer, Soviet Research, 1971, v.3, ¹ 5, p. 15 - 26.

[27] ZHUKOV A.V., KUDRYAVTSEVA L.K., SVIRIDENKO YE.YA. et al. Experimental Research on Models of Temperature Heat Removel Elements // Liquid Metals, Ì., Atomizdat, 1967, p. 170 - 194.

[28] ZHUKOV A.V., SOROKIN A.P., KIRILLOV P.L. et al. The Methodical Instructions and Recommendations on Thermogidraulic to Account of Fast Reactors Core // RTM–1604.008-88, Obninsk, Published by DSTI, IPPE, 1989.

[29] SUBBOTIN V.I., USHAKOV P.A., ZHUKOV A.V. et al Temperature Fields of Fuel Elements in Fast Reactors Core with Liquid Metal Cooling // Atomic Energy, 1967, v.22, № 5, p. 372–378.

[30] KUTATELADZE S.S. Bases of the Theory of Heat Exchange // "Nauka", Novosibirsk, 1970.

[31] ZHUKOV A.V., KIRILLOV P.L., MATJUKIN N.M., SOROKIN A.P., et al Thermogidraulic Account in Fuel Subassemblies Fast Reactors with Liquid Metal Cooling // Ì: Energoatomizdat, 1985.

[32] ZHUKOV A.V., SOROKIN A.P., USHAKOV P.A. et al Thermogidraulic Account in Fuel Subassemblies Fast Reactors with Liquid Metal Cooling // Atomic Energy, 1981, v.51, p. 307 - 311.

[33] ZHUKOV A.V., SOROKIN A.P., MATJUKIN N.M. Interchannel Exchange in Fuel Subassemblies Fast Reactors; Theoretical Bases and Physics of Process // Ì: Energoatomizdat, 1989

[34] ZHUKOV A.V., SOROKIN A.P., MATJUKIN N.M. Interchannel Exchange in Fuel Subassemblies Fast Reactors: the Settlement Programs and Practical // Ì: Energoatomizdat, 1991.

[35] GRYAZEV V.M., ASEEV N.A., MARKIN S.A et al. Calculated-experimental researches Heat of physics and hydrodynamics of packages of an reactor core Bor-60 // In Heat physics and hydrodynamics of an core and generators pairfor of fast reactors. Prag, DSTI, Atomic Energy Commette, 1978, v.1, p. 182 - 209.

[36] IEDA Y., KAMIDE H., OHSHIMA H., SUGAWARA S., NINOKATA H. Strategy of Experimental Studies in PNC on Natural Convection Decay Heat Removal // IAEA / IWGFR / 88, Specialists Meeting on "Evaluation of Decay Heat Removal by Natural Convection", 22-23 February 1993, Oarai Engineering Center, PNC, Japan.

[37] NISHIMURA M., KAMIDE H., HAYASHI K., MOMOI K.: Inter-Subassembly Heat Transfer During Natural Circulation Decay Heat Removal - Experimental Transient Behavior from Forced to Natural Circulation and its Multi-dimensional Analysis with Mixing Model // Eighth International Topical Meeting on Nuclear Reactor Thermal-Hydraulic, Kioto, Japan, September 30 - October 4, 1997., Proceeding, vol.2, p. 903 - 913.

[38] KAMIDE H., HAYASHI K., MOMOI K. Experimental Study of Core Thermogydraulics in Fast Reactors During Transition from Forced to Natural Circulations - Influence of Inter-Wrapped Flow // NURETH-8, New Horizonns in Nuclear Reactor Thermal-Hydraulics, Eighth International Topical Meeting on Nuclear Reactor Thermal-Hydraulic, Kyoto, Japan, September 30 - October 4, 1997., Proceeding, vol.2, p. 922 - 931.

[39] RO T.S., TODREAS N.E. Porous Body Analysis of Vertical Rod Bundles under Mixed Convection Conditions // Ph.D.Thesis, Department of Nuclear Engineering, M.I.T, (1983).

[40] CHENG S.K., TODREAS N.E. Hydrodynamic Models and Correlation for Bare and Ware-Wrapped Hexagonal Rod Bundles // Subchannel Friction Factor and Mixing Parameters", Nucl. Engrg. And Des., 92, 227 - 251, 1986.

[41] CHENG S.K., TODREAS N.E. Energy Transfer Mechanism under Mixed Convection Conditions in LMFBR Wire-Wrapped Bundles // Proc. Of the 3-rd Int. Topical Mtg. On Reactor Thermal Hydraulics, Newport, USA, p 16 - E1, Oct.1985.

[42] NINOKATA H., EFTHIMIADIS A., TODREAS N.E. Distributed Resistance Modeling of Wire-Wrapped Rod Bundles // Nuclear Engireeng and Design, 1987, v. 104, p. 93 - 102.

[43] GEORGE T.L., BASEHORE K.L., et al., COBRA-WC: a Version of COBRA for Single-Phase Multiassembly Thermal Hydraulic Transient Analysis // PNL-3259, Battelle Pacific North West Laboratory, 1980.

[44] ENGEL F.S., MARKLEY R.A., BISHOP A.A. The Effect of Radial Heat Flux Gradients and Flow Regimes on the Peak Sodium Temperature Rise in Wire Wrapped Bundles // Proc. Of NUREG / CP-0034, vol. 2, 566 - 582, New York, Sept, 1982.

[45] BATES J.M., KHAN E.U. Investigation of Combined Free and Forced Convection in a 2 x 6 Rod Bundle During Controlled Flow Transients // AIChE Symposium Series, Heat Transfer, Orlando, 1980.

[46] DOMANUS H.M. A New Implicit Numerical Solution Scheme in the COMMIX-1A Computer Program // ANL 83-64, NUREG/CR-3435, 1983.

LIST OF PARTICIPANTS

Coste, P.
CEA, DRN/DTP/SMTH
17 rue des Marturs
38054 Grenoble Cedex, France

Every, D.
BNFL
Springfields, Preston
PRA OXJ, UK

Ivanov, Ye.F.
Institute of Physics and Power Engineering
Bondarenko sq.,1,
249020, Obninsk, Kaluga region
Russian Federation

Kim, Young - Gyun
Korea Atomic Energy Research Institute
P.O. Box 105, Yusung, Taejon,
305-600, Republic of Korea

Kirillov, P.L.
Institute of Physics and Power Engineering
Bondarenko sq.,1,
249020, Obninsk, Kaluga region
Russian Federation

Kornienko, Yu.
Institute of Physics and Power Engineering
Bondarenko sq.,1,
249020, Obninsk, Kaluga region
Russian Federation

Kozlov, F.A.
Institute of Physics and Power Engineering
Bondarenko sq.,1,
249020, Obninsk, Kaluga region
Russian Federation

Kriventsev, V.
Tokyo Institute of Tecnology
2-12-1 O-okayama, Meguro-ku,
Tokyo 152-8550, Japan

Martsiniouk, D.Ye.
Institute of Physics and Power Engineering
Bondarenko sq.,1,
249020, Obninsk, Kaluga region
Russian Federation

Michin, V.I.
Institute of Physics and Power Engineering
Bondarenko sq.,1,
249020, Obninsk, Kaluga region
Russian Federation

Ninokata, Hisashi
Tokyo Institute of Tecnology
2-12-1 O-okayama, Meguro-ku,
Tokyo 152-8550, Japan

Nishimura, Motohiko
O-arai Engineering Center
Pover Reactor and Nuclear Fuel
Development Corporation
O-arai, Ibakari - Ken, 311-1393, Japan

Rineiskii, A.A.
Scientific Secretary,
IAEA, Wagramer Strasse 5
P.O. BOX 100, A-1400
Vienna, Austria

Roychowdhury, D.G.
Indira Gandhi Centre For Atomic Research
Kalpakkam - 603102, India

Serdun, E.N.
Institute of Physics and Power Engineering
Bondarenko sq.,1,
249020, Obninsk, Kaluga region
Russian Federation

Shvetsov, Yu.Ye.
Institute of Physics and Power Engineering
Bondarenko sq.,1,
249020, Obninsk, Kaluga region
Russian Federation

Sorokin, A.P.
Institute of Physics and Power Engineering
Bondarenko sq.,1,
249020, Obninsk, Kaluga region
Russian Federation

Sorokin G.A.
INPE, Studencheskiy Gorodok,
249020, Obninsk, Kaluga region
Russian Federation

Sourkova, I.
Institute of Physics and Power Engineering
Bondarenko sq.,1,
249020, Obninsk, Kaluga region
Russian Federation

Portianoy, A.G.
Institute of Physics and Power Engineering
Bondarenko sq.,1,
249020, Obninsk, Kaluga region
Russian Federation

Tuchkov, A.
Beloyarsk Nuclear Power Plant (BN-600)
624051 Zarechny, Sverdlovsk region,
Russian Federation

Ushakov, P.A.
Institute of Physics and Power Engineering
Bondarenko sq.,1,
249020, Obninsk, Kaluga region
Russian Federation

Valentin, Bernard
CEN Cadarache
DEC/SECA/LTEA
13108 Saint Paol Lez Durance, France

Zhimin, Yang
China Institute of Atomic Energy (CIAE)
P.O. Box 275(95), Beijing 102413, China

Zhukov, A.V.
Institute of Physics and Power Engineering
Bondarenko sq.,1,
249020, Obninsk, Kaluga region
Russian Federation